

Surface chemistry of cellulose nanocrystals

Elena Sîrbu MSc

Thesis submitted to the University of Nottingham for the degree of Doctor of Philosophy

December 2015

If we knew what it was we were doing, it would not be

called research, would it?

Albert Einstein

Abstract

Chemical surface modification of cellulose nanocrystals has had a fast development and increased interest from the scientific community as cellulose is the most abundantly available renewable polymer with many advantages such as nanoscale dimensions, high specific strength and modulus, high surface area, unique optical properties and the extraordinary modification potential to increase the application field. This thesis is aimed at expanding and improving upon the current knowledge in order to unlock new applications. Four esterification techniques were applied to the formation of cellulose nanocrystal esters of acrylic acid and methacrylic acid. The degree of surface substitution reached two to three surface hydroxyl groups (the maximum number) available for functionalization and this degree of substitution is very much dependent on the chosen esterification methodology.

Two new fluorescently modified cellulose esters based on carbazole-9-yl-acetic acid and coumarin-3-carboxylic acid were synthesised using *p*-toluenesulfonyl chloride/pyridine and carbodiimide esterifications methods. Absorption and fluorescent properties were also measured and showed fluorescence proportional to the extent of surface functionalization. The maximum theoretically attainable degree of substitution could be reached while still maintaining the crystal structure of cellulose.

Cationic cellulose nanocrystals were produced with a high positive surface charge when compared with the literature. The synthesis procedure was attempted in two steps and in a single step. The degree of modification for pyridinium acetate cellulose and methyl imidazolium acetate cellulose was found to depend significantly on the selected pathway. The cationic nature of the modifications was verified using zeta potential measurements and through adsorption of an anion dye.

Synthesised cellulose acrylates and methacrylates were used in Thiol-Ene click reactions in which very mild and environmentally friendly reaction conditions proved to work from 10 min reaction times. Four different thiols were added, with and without hexylamine catalyst. In addition, an amidine functionalised

cellulose nanocrystal was synthesised based on previously click-modified cellulose in a 2-hour reaction. Furthermore, the switchable behaviour of the synthesised nanoparticles was demonstrated by reverse bubbling with CO_2 and Ar.

Acknowledgements

Firstly, I am indebted to my supervisor Dr Wim Thielemans for his support throughout this research project. His intelligence and experience along with helpful guidance, mentoring and encouragement were a source of continuous motivation along my PhD studies. In addition, I am grateful for his patience with me whenever I needed more time to understand my work and when writing this thesis that I could not have finished without his help. Secondly, I am grateful to all my past colleagues especially to Dr Samuel Eyley who trained me in different experimental procedures and instruments specifically at the beginning of my PhD. Furthermore, I am grateful to Dr Lindy Heath for her kind advices and to Latifah Jasmani for discussing work related problems and life in general, making the lab experience more pleasant. Emily Smith deserves special thanks for running the XPS instrument for surface chemical analysis for all my samples present in the thesis, including training on the instrument and software processing, and for her help in solving unusual XPS related issues. Also, I would like to thank Dr Stephen Davies for allowing me to use fluorimeter, to Dr Chen Xinyong for running the AFM analysis and to Mr. Nigel Neate for running TEM analysis based on previous sample preparation performed by my supervisor and also to Dr Enrique Pérez Gutiérrez at Group of Optical Properties of Materials, Mexico, for the help with OLEDs fabrication. For elemental analysis performed during this work I am grateful to Dr Lee Stevens, especially for running sulfur analysis when highly needed, to Dr Tong Liu for all C, H and N elements and to Dr Ian Blakeley and Mrs. Tanya Marinko-Covell from Leeds University for the analyses that could not be performed at The University of Nottingham (halogens). It would be careless of me not to mention the technical staff support in the School of Chemistry notably to Mr. Mark Guyler, Mr. Clive Dixon and Mr. Neil Barnes for the design, manufacture and maintenance of much of the equipment used during my PhD. I must also thank The University of Nottingham for awarded me the European Union Excellence Research Scholarship. Last but not least, I would like to thanks to my family and friends and especially to my grandmother for her love and support and to whom I dedicate this thesis.

Table of Contents

1 Introduction 1

1.1 Thesis overview 1

1.2 Cellulose 2

1.3 Chemical structure of cellulose 3

1.4 Supramolecular structure of cellulose 7

1.5 Morphology 11

1.6 Cellulose nanocrystals 13

1.7 Chemical modification of cellulose nanocrystals 16

1.7.1 Noncovalent surface modification of CNCs 19

1.7.2 TEMPO-mediated oxidation 20

1.7.3 Cationization 21

1.7.4 Polymer grafting 24

1.7.5 Esterification 25

1.7.6 Etherification 31

1.7.7 Fluorescence Labelling 32

1.7.8 Thiol-Ene click chemistry 34

1.8 Aims of the thesis 37

2 Characterization of cellulose nanocrystals 40

2.1 Crystal model and surface chain ratio 41

2.2 Powder X-ray diffraction 43

2.3 Infrared Spectroscopy 49

2.4 Elemental Analysis 50

2.5 X-ray photoelectron spectroscopy 56

2.6 Atomic Force Microscopy 62

2.7 Transmission Electron Microscopy 64

2.8 UV-Vis and Fluorescence Spectroscopy..... 65

2.9 Zeta potential measurement 67

3 Cellulose nanocrystal esters 70

3.1 Carbodiimide mediated esterification for cellulose acrylate nanocrystals synthesis 71

3.2 Carbodiimide mediated esterification for cellulose methacrylate nanocrystals synthesis 75

3.3 Tosyl Chloride/Pyridine esterification for cellulose acrylate nanocrystal synthesis 80

3.4 Tosyl Chloride/Pyridine esterification for cellulose methacrylate nanocrystal synthesis 84

3.5 Tosyl Chloride/Triethylamine esterification for cellulose acrylate nanocrystal synthesis 90

3.6 Acryloyl Chloride/Triethylamine esterification for cellulose acrylate nanocrystal synthesis 94

3.7 Conclusions..... 99

4 Fluorescently labelled materials based on cellulose nanocrystals..... 101

4.1 *9H*-Carbazole and carbazole-9-yl-acetic acid 101

4.2 Coumarin and coumarin-3-carboxylic acid..... 104

4.3 Esterification reaction for the synthesis of carbazole-9-yl-acetate cellulose nanocrystals through carbodiimide-mediated coupling..... 105

4.4 Esterification reaction for the synthesis of carbazole-9-yl-acetate cellulose nanocrystals through TsCl/Py..... 109

4.5 Esterification reaction for the synthesis of coumarin-3-carboxylate cellulose nanocrystals 116

4.6 TEM and AFM characterization 120

4.7 Absorption and Fluorescence characterization 122

4.8 OLEDs preparation procedure 136

4.9 Conclusions 139

5 Cationized materials based on cellulose nanocrystals 142

5.1 Introduction to cationized materials 143

5.2 Two steps synthesis towards cationized nanoparticles 146

5.2.1 Pyridinium acetate cellulose bromide 150

5.2.2 Methyl imidazolium acetate cellulose bromide 154

5.3 Modification of the two step cationic nanoparticles synthesis 158

5.4 Influence of the solvent 162

5.5 One-pot reaction towards pyridinium cationized nanoparticles 165

5.6 One-pot reaction towards methyl imidazolium cationized nanoparticles 169

5.7 One-pot synthesis towards pyridinium cationized cellulose nanoparticles using TsCl/Py conditions 173

5.8 Adsorption of dye on the cationized cellulose nanoparticles 178

5.9 Conclusions 182

6 Thiol-Ene click chemistry based on cellulose nanocrystals 184

6.1 Click chemistry applied to cellulose nanocrystals 184

6.2 Thiol-Ene click modified cellulose nanocrystals 188

6.3 Thiol-Ene click chemistry conclusions 212

6.4 Surface Charge-Switchable Nanoparticles based on cellulose nanocrystals (Switch-CNC) 215

6.5 Switchable cellulose nanoparticles characterization 217

6.6 Conclusions on switchable nanoparticles synthesis 224

7 Experimental 225

7.1 Materials 225

7.2 Cellulose nanocrystals 226

7.3 Synthesis of cellulose acrylate through the DIC/DMAP methodology... 227

7.4 Synthesis of cellulose methacrylate through the DIC/DMAP methodology 227

7.5 Synthesis of cellulose acrylate through the TsCl/Py methodology . 228

7.6 Synthesis of cellulose methacrylate through the TsCl/Py methodology …….228

7.7 Synthesis of cellulose acrylate through the TsCl/Et_3N methodology….. 229

7.8 Synthesis of cellulose acrylate with acryloyl chloride through the Et_3N/DMF methodology 229

7.9 Synthesis of methyl 2-(9*H*-carbazol-9-yl) acetate 230

7.10 Synthesis of carbazole-9-yl-acetic acid 230

7.11 Synthesis of carbazole-9-yl-acetate cellulose through carbodiimide coupling 231

7.12 Synthesis of carbazole-9-yl-acetate cellulose through the TsCl/Py methodology 231

7.13 Synthesis of coumarin-3-carboxylate cellulose through the TsCl/Py methodology 232

7.14 Synthesis of bromoacetate cellulose 232

7.15 Synthesis of pyridinium acetate cellulose bromide - 1[Br][PyAc]-g-CNC… 233

7.16 Synthesis of methyl imidazolium acetate cellulose - 1[Br][MeImAc]-g-CNC 234

7.17 Synthesis of bromoacetate cellulose in THF 234

7.18 Synthesis of bromoacetate cellulose in Et_3N 235

7.19 Synthesis of pyridinium acetate cellulose bromide 2[Br][PyAc]-g-CNC… 235

7.20 Synthesis of methyl imidazolium acetate cellulose bromide 2[Br][MeImAc]-g-CNC 236

7.21 Synthesis of pyridinium acetate cellulose bromide 3[Br][PyAc]-g-CNC… 236

7.22 Synthesis of cellulose 2-methyl-3-((3-trimethoxysilyl)propyl)thio) propanoate 237

7.23 Synthesis of cellulose 3-((3-trimethoxysilyl)propyl)thio) propanoate… 238

7.24 Synthesis of cellulose 3-((2-mercaptoethyl)thio) propanoate 238

7.25 Synthesis of cellulose 3-((2-aminoethyl)thio) propanoate hydrochloride 239

7.26 Synthesis of cellulose 3-((2-aminoethyl)thio) propanoate in acetone…. 240

7.27 Synthesis of cellulose 3-((2-aminoethyl)thio) propanoate in DMF/DMSO/H_2O 240

7.28 Synthesis of cellulose 3-((2-aminoethyl)thio) propanoate in DCM 241

7.29 Synthesis of switchable nanoparticles based on cellulose nanoparticles – 3-(2-(*N*,*N*-dimethylacetimideamide)ethylthio) propanoate cellulose nanoparticles 242

8 Conclusions and Future Work 243

9 References 253

10 Appendix 271

10.1 Appendix for chapter 3 271

10.2 Appendix for chapter 4 282

10.3 Appendix for chapter 5 290

10.4 Appendix for chapter 6 308

Abbreviations & Acronyms

at%	Atomic percent
AA	Acrylic acid
ACNC	Cellulose acrylate
AFM	Atomic Force Microscopy
AGU	Anhydroglucose unit
Alq3	Tris(8–hydroxyquinoline)–aluminium)
BE	Binding Energy
BrAcCNC	Bromoacetate Cellulose Nanocrystals
[Br][MeImAc]-*g*-CNC	Methyl imidazolium acetate cellulose bromide
[Br][PyAc]-*g*-CNC	Pyridinium acetate cellulose bromide
CB	Chlorobenzene
CNC	Cellulose Nanocrystals
Co-c-CNC	Coumarin-3-carboxylate Cellulose Nanocrystals
CuAAC	Copper-catalysed azide/alkyne cycloaddition
Cz	9*H*-Carbazole
Cz-a-CNC	Carbazole-9-yl-acetate cellulose
DCM	Dichloromethane
DIC	*N,N'*- diisopropylcarbodiimide
DMAP	4-Dimethylaminopyridine
DMF	*N*,*N*-Dimethylformamide
DMSO	Dimethyl sulfoxide

DS	Degree of substitution
DS_{surf}	Surface degree of substitution
DT-CNC-DCM	Cellulose 3-((2-mercaptoethyl)thio)propanoate in DCM
EA	Elemental Analysis
EML	Emissive Layer
Et_3N	Triethylamine
ETL	Electron Transporting Layer
EtOH	Ethanol
FT-IR	Fourier Transform Infrared Spectroscopy
FWHM	Full Width at Half Maximum
FTO	Fluorine doped Tin Oxide
HTL	Hole Transporting Layer
ITO	Indium Tin Oxide
MAA	Methacrylic Acid
MACNC	Cellulose methacrylate
MeOH	Methanol
MFC	Microfibrilated Cellulose
MS	Mass Spectroscopy
NMR	Nuclear Magnetic Resonance
OLEDs	Organic Light Emitting Diodes
PDOT	Poly(3,4-ethylenedioxythiophene)
PSS	Polystyrene sulfonate

Py	Pyridine
Switch-CNCs	3-(2-(*N*,*N*-dimethylacetimideamide)ethylthio)propanoate cellulose nanoparticles
T-24-CNC-DCM	cellulose3-((3-trimethoxysilyl)propyl)thio)propanoate in DCM
tBu-PBD	2-(4-tert-Butylphenyl)-5-(4-biphenylyl)-1,3,4-oxadiazole
TCNC-Acetone	cellulose 3-((2-aminoethyl)thio)propanoate in acetone
TCNC-DCM	cellulose 3-((2-aminoethyl)thio)propanoate in DCM
TCNC-DMF	cellulose 3-((2-aminoethyl)thio)propanoate in DMF
TCNC-DMSO	cellulose 3-((2-aminoethyl)thio)propanoate in DMSO
TCNC-EtOH	cellulose 3-((2-aminoethyl)thio)propanoate hydrochloride in EtOH
TCNC-H_2O	cellulose 3-((2-aminoethyl)thio)propanoate in H_2O
TEC	Thiol-Ene Chemistry
TEM	Transmission Electron microscopy
THF	Tetrahydrofuran
TsCl	*p*-toluenesulfonyl chloride
UV-Vis	Ultra Violet – Visible spectroscopy
XPS	X-ray Photoelectron Spectroscopy
XRD	Powder X-ray Diffraction
ε	Molar absorption coefficient
χ_C^R	Crystallinity index by Rietveld refinement

PART I

INTRODUCTION

1 Introduction

1.1 Thesis overview

Cellulose is the most abundantly available renewable natural polymer.[1] This ubiquitous polymer has been used in chemistry as fibres or derivatives for almost 150 years and was adopted by humans since the time of the Egyptians in the form of papyrus.[1] Annually, almost half of the world production of biomass by weight is represented by cellulose which serves as a building material of cell membranes in higher plants or as a mechanical support and protection in algae, tunicates and bacteria. Annual cellulose production is estimated at $1.5 \cdot 10^{12}$ tons.[2,3]

Chemical treatment and functionalization of cellulose allows adapting cellulose to a wide variety of new applications. Among these, of great importance in the current focus on nanotechnology, is the acid hydrolysis of native cellulose fibres which results in nano-sized particles, i.e. cellulose nanocrystals (CNC), with excellent mechanical properties.[4,5] Initially, due to their high mechanical properties, abundance, low weight and biodegradability, these nanocrystals were investigated as reinforcements for polymers through the fabrication of nanocomposites. To improve the interactions of CNC with the polymer matrix, the modification of nanocrystals surface is generally required for hydrophobic polymers, while at the same time the crystal structure needs to be preserved to retain the mechanical properties. Based on previous knowledge, the aim of this thesis is to broaden the diversity of cellulose nanocrystal surface modifications in order to expand the applications of these materials beyond the nanocomposites field. Therefore, this work develops the fields of fluorescent materials, cationized nanoparticles and click-chemistry modified CNC.

This thesis is divided into three parts. The first part presents fundamental knowledge of cellulose together with the synthesis, description and properties of CNC followed by a review of the current modification methodologies for cellulose surface. This part further defines the main objectives proposed for this thesis (Chapter 1). Chapter 2 presents the cellulose nanocrystal preparation employed in this project and introduces the main experimental techniques used during cellulose characterization in order to determine the degree of modification. The second part presents the research carried out that contributed to the development of know-how of modified CNC esters. In light of previous research, Chapter 3 describes esterification methods of cellulose in order to introduce small molecules and investigates and compares different methods. The CNC esters were synthesised to optimize the reactions and to introduce new molecules that extend the applications of CNC. Chapter 4 contributes to the extension of fluorescently labelled cellulose by the introduction of two new fluorescent molecules onto CNC. Cationized nanoparticles with ion-exchange capacity synthesised in this project are investigated in Chapter 5. As thiol–ene coupling is emerging as a very attractive click chemistry process, Chapter 6 comes with new developments and optimizes this click reaction for use on CNC. Furthermore, this methodology is used to prepare precursors for a further reaction step resulting in nanoparticles with switchable surface charges upon flushing with CO_2 and Ar in a reversible process. The last part, Chapter 8 outlines the results of the work performed in this thesis and proposes routes for further investigation.

1.2 Cellulose

Cellulose is considered the most ubiquitous polymer on the planet produced by nature. Nowadays, it has boundless industrial uses as it had in the past, such as timber for housing, paper, ropes and sails. The most exploited natural resource that contains cellulose is certainly wood. Other plants that consist of a significant amount of cellulose are cotton, ramie, jute, flax and hemp but

cellulose is also found in some non-plant sources such as algae, bacteria and tunicates.[6]

The first isolation from plants and determination of the chemical formula of cellulose was carried out by the French chemist Anselme Payen in 1838 while the people used cellulose since the time of the Egyptians in the form of papyrus and cotton.[7] Nowadays, despite its abundance, cellulose is mostly used as a raw material in the paper industry but also for further chemical processing for use in textiles, medicine, cosmetics, hygiene products, food industry, and pharmaceutical applications, yet only 2% of cellulose is used for the production of fibres, films of regenerated cellulose and cellulose ethers and esters synthesis.[8-16]

1.3 Chemical structure of cellulose

Cellulose (Figure 1.3.1) is derived from the condensation of β-D-glucopyranose units (also named anhydroglucose units (AGU)), linked together by β-1,4-glycosidic bonds. These result in a high molecular weight, linear and relatively rigid homopolymer, in which every AGU is corkscrewed 180 degrees with respect to the previous AGU. Two neighbouring AGU's form a cellobiose unit.[1,17]

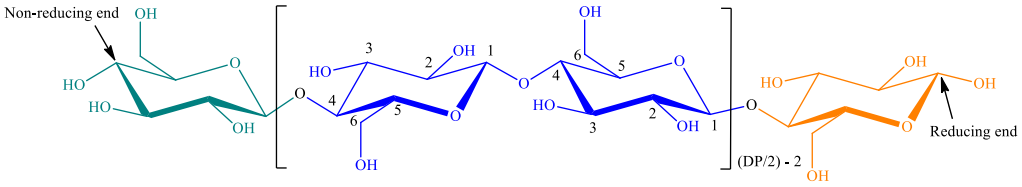


Figure 1.3.1 Molecular structure of cellobiose repeating unit with the carbon atoms numbering, the reducing end in orange and the non-reducing end in green

The degree of polymerization (DP) for native cellulose is very closely related to the origin of the polymer and the extraction procedure. Deposition of cellulose in the primary cell walls of plants occurs together with hemicellulose, pectin and structural proteins.[18] Traditional wood pulps with 40–50 % cellulose

content have a DP with values in the range of 300 – 1,700 whereas cotton with 95 – 99 % cellulose content has a DP that ranges between 800 and 10,000, influenced by the treatment protocol.[3]

Figure 1.3.1 shows the repeat unit of the cellulose macromolecule with the conventional numbering of the carbon atoms in the pyranose ring where two oxygen atoms are attached to C_1 followed by two hydroxyl groups substituents at C_2 and C_3, another oxygen atom bound to carbon C_4 and one hydroxymethyl group at the C_5 position.[17] The inter-unit link is achieved at the 1 and 4 positions through a glycosidic bond. O_1 is the oxygen atom that forms part of the glycosidic bond while O_5 is the one that forms part of the pyranose ring. O_2 and O_3 are the oxygen atoms of the secondary hydroxyl groups and O_6 is the one of the primary hydroxyl group. C_1 is the acetal centre functionality throughout the entire chain except for the last AGU where it becomes a hemi-acetal centre with inherent reducing properties.[17]

Each polymeric chain is delimited by two endings, one being a chemical reducing functionality, i.e. the hemi-acetal reducing end, while the other is a pendant hydroxyl group, denominated as the non-reducing end.[17] The AGU has a chair conformation, designated $^4C_1$ (Carbon 4 high and C1 low) with all the hydroxyl groups and hydroxymethyl (CH_2OH) substituents in the equatorial position. The large number of hydroxyl groups present on each cellulose chain contributes to the formation of an inter- and intra-chain hydrogen bonding network which determines the position of chains in the macroscopic structure and confers cellulose its unique properties of chemical stability and mechanical strength.

As specified earlier, the monomer of cellulose, β-D-glucopyranose, is the six-membered heterocyclic form of glucose. Glucose is one of the three common "single" sugars (glucose, fructose and galactose), and as an aldohexose with the formula $C_6H_{12}O_6$, glucose contains four asymmetric centres as becomes clear in the Fisher projection. By convention, D-enantiomers are represented with the hydroxyl group bonded to the right of the asymmetric centre at the

bottom chiral carbon, C_5. D-glucose is the naturally occurring form of glucose.[17]

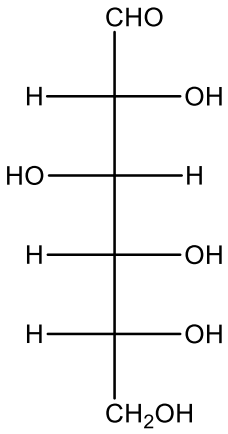


Figure 1.3.2 Fisher Projection in linear form of D-Glucose

The cyclization of D-glucose by reaction of the hydroxyl group on C_5 with the aldehyde functionality, results in the formation of a six-membered pyranose ring where the asymmetric carbon C_1 is called the anomeric carbon and becomes the centre of a hemiacetal functional group. Two anomers, α and β, can be formed during ring closure. Both configurations have a $^4C_1$ chair conformation with respect to the reference plane containing the ring atoms C_2, C_3, C_5 and O_5 while C_4 and C_1 are out of the plane. For the β anomer configuration of glucose, the hydroxyl group of C_1 is placed in the equatorial position or in the mean plane of the ring, in the chair conformation, whereas for the α anomer, the hydroxyl group is axial or perpendicular to the mean plane of the ring (Figure 1.3.3).

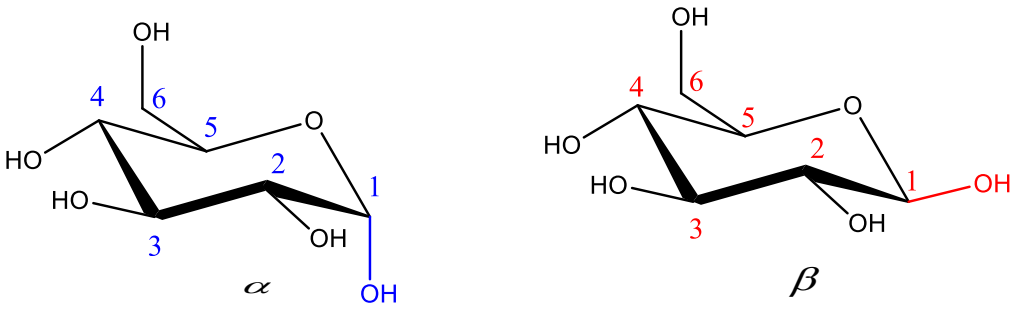


Figure 1.3.3 The α and β configurations of glucopyranose in the chair conformation

Considering the equatorial orientation of the hydroxyl group, the β configuration of the ring could be considered more stable purely based on steric effects (the other two hydroxyl groups occupy equatorial positions on the pyranose ring) but the α anomer and therefore the α configuration is stabilized by the so call endo-anomeric effect which is a charge delocalization manifestation from the oxygen atom of the acetal group (lone pair of electrons on the endocyclic oxygen) towards the anomeric carbon (σ× antibonding orbital of the exocyclic C–O bond) inducing an energy reduction of the system (Figure 1.3.4). The exo-anomeric effect on the other hand is based on the stabilization induced by the donation of electrons that may proceed from the exocyclic oxygen to the antibonding orbital of the bond between the ring oxygen and anomeric carbon (endocyclic C–O bond). This effect is stronger for substituents in the equatorial position.[19]

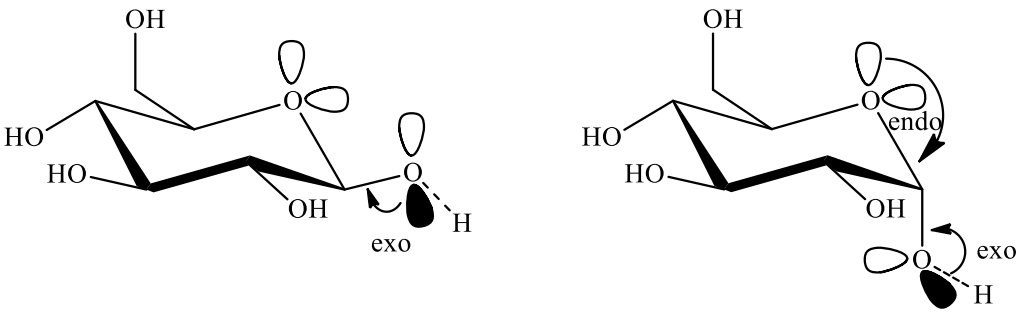


Figure 1.3.4 The α and β configurations of glucopyranose with schematic representation of the exo and endo anomeric effect[19]

Also, the solvent seems to influence the exo and endo-anomeric effect. Thus, the endo-anomeric effect is stronger than the exo-anomeric effect in non-polar solvents and therefore the α anomer is the favoured conformation. In polar solvents, the β anomer is preferred based on hydrogen bonding to the anomeric hydroxyl group which increases the electron density on the oxygen and therefore increases the exo-anomeric effect.[19] In addition to solvent effects, for glucoses and other pyrans, with C_1 substituted with an electronegative element, the endo-anomeric effect is almost always stronger and therefore results in the axial anomer being the preferred formation.[19,20]

The reaction of the C_1 hydroxyl group on one glucose molecule with the C_4 hydroxyl group of another glucose molecule, results in the formation of glycosides bridged via a glycosidic bond. Therefore, the β configuration of the anomeric form comprises the formation of equatorial linkages whereas for α anomer, the axial linkage is formed.[17] As it was earlier mentioned, each glucose molecule is linked to the next one through the anomeric bond into the equatorial position (glycosidic bond) and therefore the bond between the C_1 and the other end of the following molecule C_4, with all the anomeric bonds being equatorial.[20] Thus, the cellulose molecule is linear in general and it is made rigid by extra hydrogen bonds between the ring oxygen atoms and the C_3–OH hydroxyl group, as shown in Figure 1.3.5.

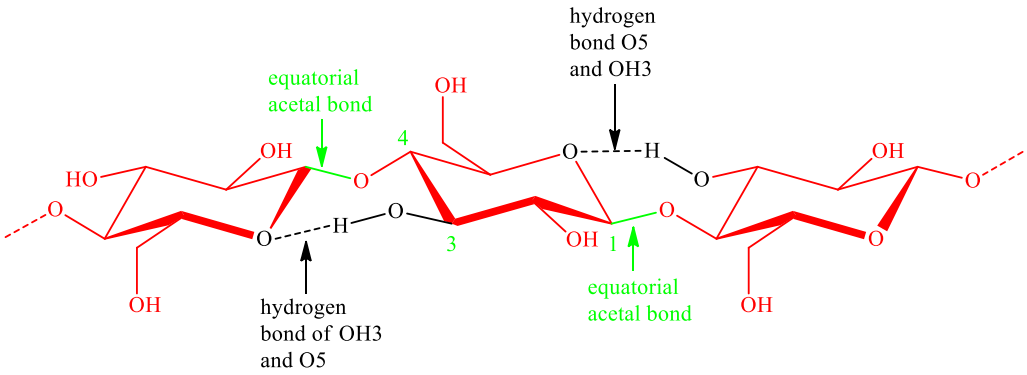


Figure 1.3.5 Cellulose structure of β configuration with the equatorial acetal bond and the hydrogen bond between O_5 and OH_3 of the next AGU highlighted[20]

1.4 Supramolecular structure of cellulose

The supramolecular structure of cellulose characterises the crystal structure, molecular structure and the hydrogen-bonding network within the cellulose.

In 1913, the first X-ray diffraction patterns of cellulose were generated from wood, hemp and bamboo samples and these patterns represent the first scientific proof of highly ordered crystalline regions with a rod-like shape.[21] Chemical composition, conformation of the cellulose chains and the intra- and intermolecular hydrogen-bonding network are accountable for cellulose's tendency to form a highly ordered crystalline structure. Several different

crystalline polymorphs were identified for pure cellulose: cellulose I, II, III and IV, with each polymorph having different unit cell parameters. Normally, irrespective of the cellulose source, native cellulose has a higher crystallinity than man-made celluloses. With only a few exceptions, all native cellulose consist of cellulose I, and its unique crystallinity lattice occurs in two allomorphs I_α and I_β.[22] I_α is metastable and can easily and entirely be converted in I_β by a hydrothermal treatment using low concentration NaOH.[23]

Celluloses that have been either treated with a concentrated alkaline swelling agent and washed with water (mercerization) or dissolved and precipitated (regeneration) consist of cellulose II which is thermodynamically more stable than cellulose I, and results thus in an irreversible transformation of cellulose I to cellulose II.[24] Fairly stable allomorphs, cellulose III_I and III_{II} are obtained from cellulose I and II respectively, by swelling with amines and liquid ammonia and subsequent removal of the swelling agents.[25] The cellulose IV polymorph is normally obtained by annealing cellulose III in glycerol and has two allomorphs IV_I and IV_{II} depending on whether the starting material is cellulose III_I or III_{II} respectively.[26]

In 1984 by solid-state ^{13}C cross-polarization/magic angle spinning (CP-MAS) nuclear magnetic resonance (NMR) spectroscopy, it was established that Cellulose I existed as sub allomorphs called I_α and I_β.[1] Cellulose I_α exists only in celluloses from algae and bacteria while both I_α and I_β can be present in higher plants. Atalla and Vander Hart concluded through solid state NMR studies that higher plant celluloses contain a minor amount of I_α sub allomorph and the I_α/I_β ratio is less than 0.25.[27] The cellulose found in *Valonia* algae (90 % crystallinity range) and cellulose produced by bacteria (40-63 crystallinity range) is rich in I_α cellulose and the family of ramie and cotton, predominantly being I_β (50-80 %).[28] Tunicin, derived from tunicates which are sea animals, belongs to the I_β allomorph and is a highly crystalline material (80 %) which consists only of I_β.

The I_α allomorph corresponds to a single chain triclinic unit cell and I_β has a monoclinic unit cell formed by two parallel chains as was identified by electron diffraction studies in 1991 by Sugiyama *et al.* (Figure 1.4.1).[23,29]

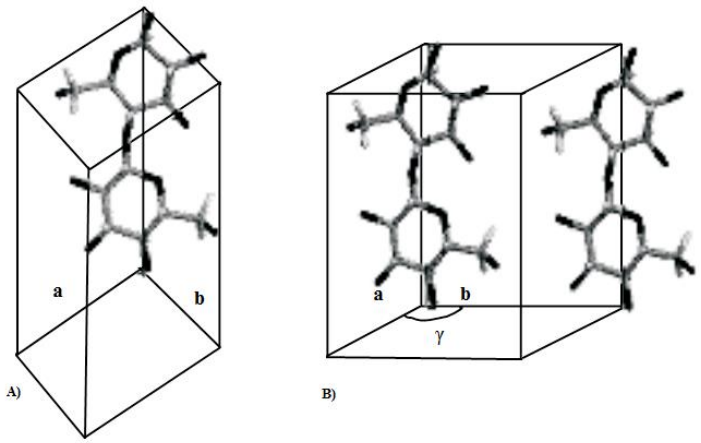


Figure 1.4.1 Schematic representation of the chain packing mode of cellulose I with A) Triclinic unit cell and B) monoclinic unit cell. Reproduced from the work of Koyama *et al.*[30]

In the one chain triclinic structure (I_α), all the chains are packed parallel within the crystals and are organised in sheets along the (110) planes by inter-chain hydrogen bonding with the β-(1-4) glycosidic bond propagating down the c axis of the unit cell (the fibre axis) by a quarter of the c axis between one sheet and the next one. By contrast, the unit cell of cellulose I_β contains two independent chains, one referred to as at the origin (corner) and the other one as the centre chain of the cell, based on their position in the unit cell. Therefore, this crystal structure contains alternating hydrogen bonded sheets with structures determined by origin and centre chain, parallel packed, while the centre chain contained sheets offset from those in the origin chain by a quarter of the c axis.

Therefore the main difference between I_α and I_β is the position of the adjacent chains by a quarter of the c axis in order to result in either a diagonally shifted I_α or a staggered I_β packing of the cellulose unit cells (Figure 1.4.2).[23]

The hydrogen bond network in I_α and I_β is represented by relatively strong intramolecular O_3–H···O_5 hydrogen bonds that are well organized and with slightly different geometries (H···O distance and OH···O angle) between the two conformational distinct chains for I_β and between adjacent chains for I_α. Opposite to this, the rest of the intra- and intermolecular partially occupied hydrogen bonding involving the hydrogen atoms linked to O_2 and O_6 appear

disordered and can be explained by the existence of two mutually exclusive hydrogen bonding networks in both cellulose I_β and I_α. In a I_β, a network is formed between intra-chain O_2–H···O_6 and inter-chain O_6–H···O_3 hydrogen bonds that are found in both sheets and a second network contains an inter-chain hydrogen bond formed between O_6–H and O_2 in a three centre hydrogen bond in the centred sheet while in the origin sheet O_2–H can also form a weak three-centred hydrogen bond arrangement with O_1 (Figure 1.4.3).

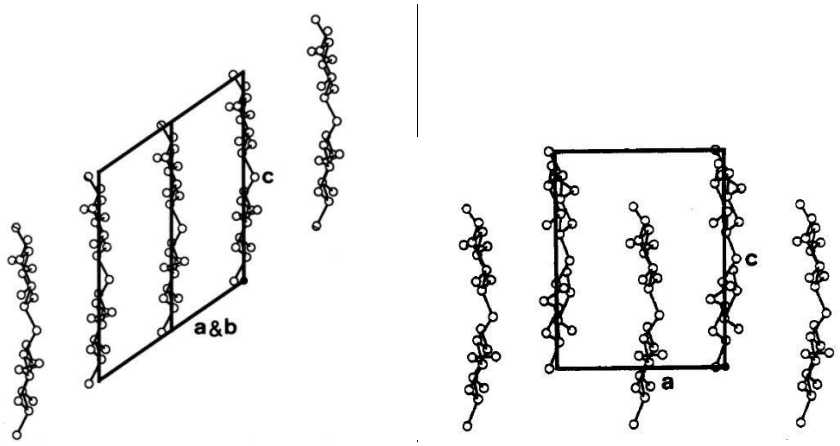


Figure 1.4.2 Schematic drawing of cellulose chains parallel to (110) planes of the triclinic unit cell (left) and the monoclinic unit cell (right) as represented by Sugiyama *et al.*[31]

These two networks may be found at certain places in the sample or they may reflect a different relative occupancy for the two allomorphs. Local hydrogen bond geometries can also change in both position and time with I_β considered to have a more favourable geometry and therefore a stronger hydrogen bonding network. There is no inter-sheet O–H···O hydrogen bond formed in either allomorph and the weaker, relative hydrophobic C–H···O hydrogen bonds that are more present in I_β than in I_α, together with the van der Waals interactions hold together the hydrogen-bonded sheets.[22,32] The hydrogen bond strength is less than 40 kJ/mol, which is much weaker than the covalent bond energy (>400 kJ/mol) but at the same time is still significantly stronger than van der Waals interactions (~4 kJ/mol).[33] The other polymorphs of cellulose differ by inter- and intra-hydrogen bonding and they are not discussed here in detail as the purpose of this thesis concentrated only on cellulose I, and I_β in particular.

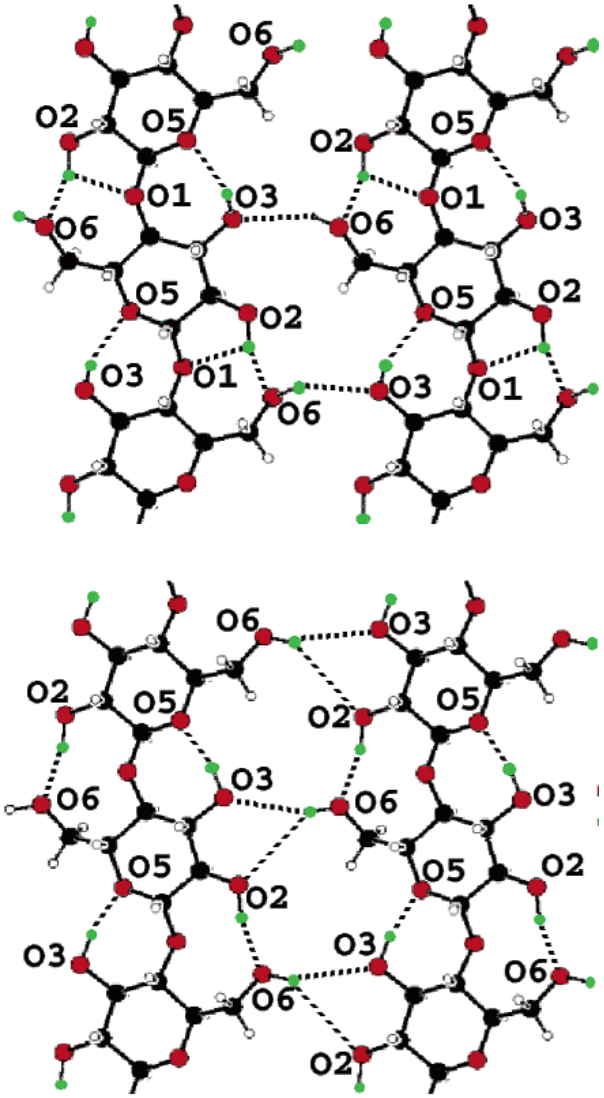


Figure 1.4.3 Schematic representation of the hydrogen bonds of cellulose I_β in the origin (top) and centre (bottom) sheets as represented by Nishiyama *et al.*[32]

1.5 Morphology

The morphological structure describes the organization of the crystals into microfibrils, layers, cell wall, fibrils, tissues or other cellulose morphologies. Native cellulose occurs in general as fibres, a term that is used to designate different kinds of fibres that are naturally produced by plants, animals and minerals.[34] Other forms of cellulose such as regenerated cellulose can be obtained as fibres, films or other products with a completely different morphology than native cellulose. Basically, natural fibres are composed of

cellulose, lignin and hemicellulose and therefore, natural fibres are also referred to as cellulosic or lignocellulosic fibres. Other components such as pectins, pigments and extractives are found in lower quantities. Figure 1.5.1 presents the detailed schematic of cellulose molecules organized in cellulose crystals which are hydrogen bonded to form microfibrils that are organized in fibrils and together with the other components form the cell wall of the plant cell.

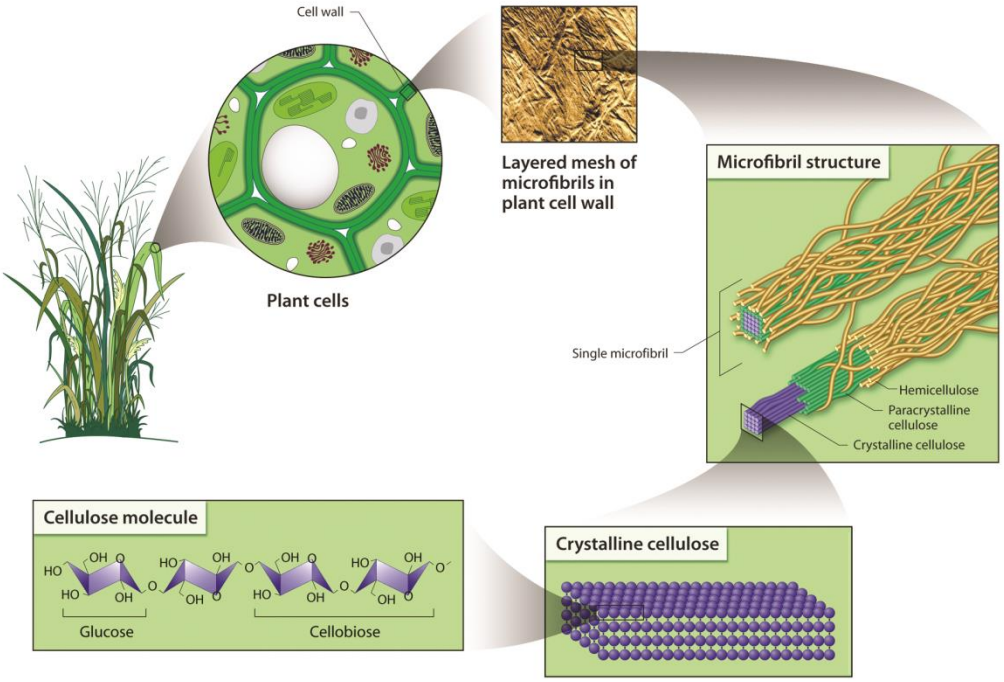


Figure 1.5.1 Cellulose from plant cells to the molecule (reprinted with acknowledgements to U.S. Department of Energy Genomic Science Programs, *http://genomics.energy.gov.*

Essentially, each fibre is a composite of rigid cellulose microfibrils (biosynthesized by a number of different living organisms) embedded in a soft matrix mainly composed of lignin and hemicellulose.[34,35] The mechanical properties of natural fibres are directly dependent on the cellulose type due to the fact that each type of cellulose has its own crystalline organization.[34] Mainly, there are two families of nanosized cellulosic particles: CNC and microfibrilated cellulose (MFC).[36,37] However, different terminologies are used to characterize cellulose nanoparticles (cellulose nanowhiskers, nanocrystals, nanofibres, nanocrystalline cellulose, microfibrilated cellulose, cellulose

crystallites, etc.) and hence there exist some misunderstandings in the (especially older) literature. Generally, the raw fibres are milled and alkali treated and bleached in order to remove the lignin and hemicellulose. Then, the bleached fibres are hydrolysed (acid hydrolysis) which will lead to nanocrystalline cellulose or disintegrated (mechanically shearing under high pressure) resulting in microfibrilated cellulose.[38]

1.6 Cellulose nanocrystals

Initially described in 1949 by Rånby *et.al.*, the procedure in which native cellulose is subjected to acid hydrolysis to induce glycosidic bond hydrolysis (acetal hydrolysis) is used to produce individual crystalline particles referred to as cellulose nanocrystals or nanowhiskers (CNC).[39,40] It is well known that acid hydrolysis of native cellulose with strong acids, e.g. sulfuric or hydrochloric acid, leads to a decrease in the degree of polymerization of cellulose which after a certain time stays constant for longer periods even under prolonged hydrolysis.[41] During acid hydrolysis, long cellulose chains are longitudinally cleaved preferentially in the non-crystalline domains/amorphous regions of native cellulose due to free volume effects, thereby releasing short crystalline objects as a Level-off Degree of Polymerization (LODP) is reached.[42,43] It is these short crystalline objects that are referred to as CNC. As it was reported by Araki *et al*., hydrochloric acid hydrolysis leads to limited dispersibility of cellulose whiskers and the nanocrystals show a tendency to flocculate in aqueous environment.[44] If sulfuric acid is used, the acid reacts also with the surface hydroxyl groups resulting in a limited amount of sulphate half-esters on the surface that upon deprotonation induce very good dispersion properties and give rise to non-flocculating suspensions.[41] The disadvantage of sulfuric acid hydrolysis is represented by the fact that these sulphate moieties are rather labile, being easily removed from the surface of the nanowhiskers under mild alkaline conditions and so removing the dispersion and non-flocculation properties.[41] The nanowhiskers/nanocrystals are rigid rods with a rectangular cross-section consisting in crystalline regions and amorphous regions, that can

be regularly distributed or could be without periodic structural defects, as in the case of *Valonia* and bacterial cellulose and consequently they do not present a distinct LOPD.[45] The dimensions of the resulting acid hydrolysis nanocrystals are dependent on the cellulose source used as starting material (Table 1.6.1).

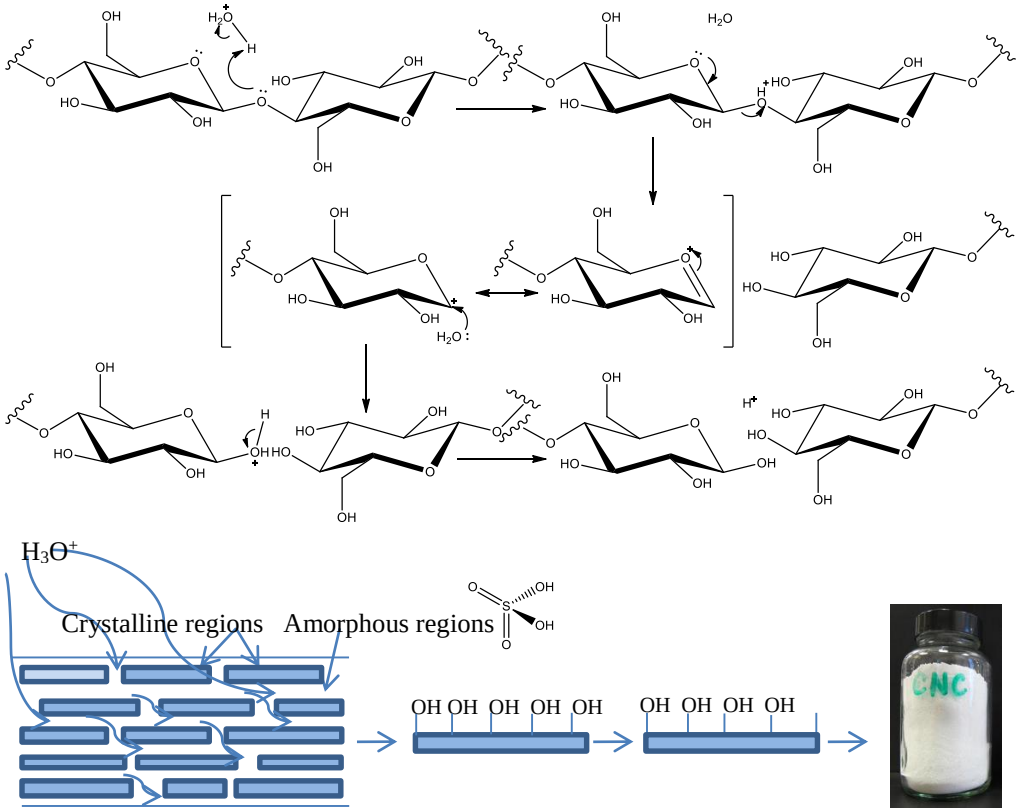
Table 1.6.1 Cellulose nanocrystals dimensions reported in the literature, originating from different sources

Cellulose source	Length/nm	Cross-section diameter/nm	Ref
Cotton	70-300	5-30	45-49
Tunicates	100-few μm	5-30	45,49-51
Sisal	150-300	3-6	52,53
Ramie	150-250	6-8	54,55
Wood	100-300	3-5	56
Valonia algae	>1000	10-20	57
Bacterial	100-2 μm	20-50	58,59

Although the cellulose source is very important in the determination of the cellulose nanocrystal dimensions, acid strength or prolonged hydrolysis times are also decisive in the final crystallite size.[45] Thus, Elazzouzi Hafraoui *et al*. have investigated the influence of sulfuric acid hydrolysis temperature on the cellulose nanocrystal (cotton, Avicel and tunicin) shape and size distribution.[45] It was concluded that increasing of temperature led to a decrease in the nanocrystal length without being correlated with the width of the nanocrystals.[45] Strictly related to the shape of the cellulose source is the morphology of the initial microfibril cross-section that is determined by the shape of the terminal complex during cellulose biosynthesis, although the directly accepted model for the majority of CNC is considered an almost square cross section, except for tunicates which have a parallelogram-shaped cross section.[60] The morphology of the cellulose nanocrystal along the crystal axis is also dependent on the source of the nanocrystal. As can be seen in Atomic Force Microscopy (AFM) and Transmission Electron Microscopy (TEM), bacterial[61] and tunicates[45] CNC were reported to have a ribbon–like shape with twists with half-helical pitches of 600-800 nm (*Micrasterias*

dendriculata) and 1.2-1.6 μm, respectively. However, these effects were not clearly identified on CNC derived from higher plants, which are considered to be flat with uniplanar-axial orientation.[1,45,61] Preferential aggregation of the nanocrystals along the nanocrystal length represents drawbacks in differentiating between a single nanocrystal (formed of multiple elementary crystals with rectangular cross section) and multiple (square) side by side nanocrystals by microscopy techniques such as AFM and TEM.[45]

Acid hydrolysis of CNC is most often done with sulfuric acid (Figure 1.6.1) followed closely by hydrochloric acid as it was previously mentioned.[1,62] Furthermore, hydrobromic acid was also used for acid hydrolysis by Filpponen *et al.* in a similar procedure to that used for hydrochloric acid.[46,63]



Acid hydrolysis →Rapid dilution → Centrifugation →Dialysis → Filtration → Sonication →Ion Exchange → Freeze Drying → Ethanol Soxhlet Extraction→ Vacuum Drying

Figure 1.6.1 Schematic representation of acid hydrolysis reaction and the main steps of CNC obtaining process (detailed in Chapter 2) adapted after the work of Morandi *et al.* and Eyley. [64,65]

The properties of the resulting CNC are influenced by the acid selection and so the nanocrystals isolated by sulfuric acid hydrolysis present a negative surface charge due to the introduction of a number of sulfate half esters at the surface

of CNC thus inducing good electrostatic stabilization of the nanocrystals in aqueous suspension.[66,67] By comparison, the hydrochloric and hydrobromic acid catalysed hydrolysis promotes unmodified surface hydroxyl groups and so reduced suspension stability.[1,68]

1.7 Chemical modification of cellulose nanocrystals

Cellulose reactivity is given by the large number of hydroxyl groups and by the glycosidic bonds. Cellulose reactions can be carried out either homogeneously by first dissolving the cellulose in a solvent system or heterogeneously on the fibre or cellulose nanocrystal as it is studied in this thesis. Homogeneous reactions present the advantage of better reaction control, selectivity control and a more complete modification whereas heterogeneous modification of cellulose represents the traditional route to cellulose functionalization when low functionalization and original fibre or crystal structure retention is required to be maintained for specific applications.

In cellulose chemistry, there are two categories of reagents. The first category can penetrate only the amorphous regions, thus causing only intercrystalline swelling while the second class induces both intercrystalline and intracrystalline swelling. Sodium hydroxide is the most studied intracrystalline swelling agent in cellulose technology and has the potential to penetrate and fully disrupt the cellulose crystals. Other intracrystalline representative agents are some inorganic acids and salts, some amines, ammonia and hydrazine. The dissolution of cellulose is essential for the production of regenerated cellulose products such as rayon. Another classification of solvents exists: derivatizing solvents and non-derivatizing solvents. Non-derivatizing solvents include systems that dissolve cellulose by intermolecular interaction only to deliver a solution of unmodified cellulose. These systems are usually transition metal amines complexes. The derivatizing solvents are systems in which cellulose dissolution takes place accompanied by the formation of an unstable ester, ether or other cellulose derivatives. The two categories of solvents include both aqueous and non-aqueous media.[17] The great number of hydroxyl groups present at the surface determines the behaviour of cellulose and therefore the

majority of reactions carried out on cellulose require electrophilic reagents. The most important industrially produced cellulose esters (organic and inorganic) and ethers were reviewed by Heinze and Liebert and are presented in Table 1.7.1.[69]

Cellulose ethers and esters presented are generally produced in heterogeneous reaction conditions. Cellulose acetate is the most industrially significant cellulose ester of an organic acid, a cellulose derivative with a large number of applications from membranes to coatings and films.[70] Cellulose nitrate, commonly called nitrocellulose, with a high nitro-content was one of the most important explosives. This cellulose derivative was also one of the first polymeric materials used as "plastic" under the name of Celluloid. Currently, cellulose nitrate is the only inorganic cellulose ester with commercial applications.[71] Other cellulose products such as methyl-, ethyl-, hydroxyethyl ethers or cellulose acetate with combination of various functional groups are still important. Ionic cellulose derivatives of which carboxymethyl cellulose ether is the most known since its preparation in 1918, are commercially produced in large quantities for diverse applications.

Mainly, the cellulose derivatives properties are determined by the functional groups present and they can be significantly modified by tailoring the degree of functionalization and the degree of polymerization of the polymer backbone.[69] Current research focuses on new cellulose polymers specifically polymers with more than one functional group or combinations of different functional groups (lipophilic or hydrophilic) or new functionality such as fluorophores, chromophores, redox active groups, and special magnetic and optical substituents or with biological activity.[69]

Table 1.7.1 The most important industrially produced cellulose esters and ethers from Heinze and Liebert[69]

Product	Worldwide	Functional	DS[a]	Solubility

	production kt/year	Group		Examples
Cellulose acetate	900	$–C(O)CH_3$	0.6-0.9	Water
			1.2-1.8	2-Methoxy ethanol
			2.2-2.7	Acetone
			2.8-3.0	Chloroform
Cellulose acetate propionate	-[b]	$–C(O)CH_3$/ $–C(O)CH_2CH_3$	2.4/0.2	Acetone Ethyl acetate
Cellulose acetate butyrate	-[b]	$–C(O)CH_3$/ $–C(O)(CH_2)_2CH_3$	0.2/2.7	Acetone, Diisobutyl ketone
Cellulose nitrate	200	$–NO_2$	1.1/1.6	Acetone
			1.8-2.0	Ethanol
			2.0-2.3	Methanol, acetone, methylethyl ketone
			2.2-2.8	Acetone
Cellulose xanthate	3200	–C(S)SNa	0.5-0.6	$NaOH_{(aq)}$
Carboxymethyl cellulose	300	$–CH_2COONa$	0.5-2.9	water
Methyl cellulose	150	$–CH_3$	0.4-0.6	4% $NaOH_{(aq)}$
			1.3-2.6	Water
			2.5-3.0	Organic solvents
Ethyl cellulose	4	$–CH_2CH_3$	0.5-0.7	4% $NaOH_{(aq)}$
			0.8-1.7	Water
			2.3-2.6	Organic solvents
Hydroxyethyl cellulose	50	$–CH_2CH_2OH$	0.1-0.5	4% $NaOH_{(aq)}$
			0.6-1.5	Water

[a] Degree of substitution (number of functionalized hydroxyl groups per glucopyranose unit)
[b] no production numbers available

Considering the abundance of hydroxyl groups at the surface of CNC, a wide variety of chemical modifications have also been carried out in cellulose nanocrystal research, including oxidation, etherification, esterification, silylation, polymer grafting and cationization.[1,41,72] Also, attempts to non-

covalently modify the nanocrystal surface through the use of adsorbing surfactants and polymer coatings were performed.[73,74]

1.7.1 Noncovalent surface modification of CNCs

Noncovalent surface modification is a simpler method than chemical grafting as there is no chemical reaction involved. It is usually done through physical interactions, by adsorption of small molecules or macromolecules onto the surface. Thus, the surface of cellulose nanowhiskers can for example be tuned with surfactants. Surfactants are amphiphilic organic compounds (containing hydrophobic groups referred to as the "tail" and hydrophilic groups usually named the "head"). The hydrophilic end of the surfactant may be adsorbed onto the surface of the cellulose nanoparticles while the hydrophobic end will then point out affording a non-polar surface and decreasing the surface tension of the nanoparticles. As a consequence, the surfactant-coated nanocrystals are more readily dispersed in non-polar organic media. This path was initially introduced by Heux *et al.* who introduced surfactants containing mono- and di-esters of phosphoric acids bearing alkylphenol tails on cotton and tunicin nanocrystals[73,75] and later on cotton linters[45]. Detailed analysis provided by Small Angle Neutron Scattering (SANS) showed that a thin layer of about 15 Å was formed at the surface of CNC.[76] Bondeson *et al.*[77] used an anionic surfactant to enhance the dispersion of CNC in poly(lactic acid). Non-ionic surfactants were used by Kim *et al.*[78] and Rojas *et al.*[78] to disperse the CNC in polystyrene-based composites. The main drawback of this approach is the relatively weak interface at the surfactant-CNC interaction plane. A new approach was recently reported by Zhou *et al.*[79] who surface-modified CNC by adsorption of saccharide-based amphiphilic block copolymers. Imitating lignin-carbohydrate copolymers, they adsorbed xyloglucan oligosaccharide–poly(ethylene glycol)– polystyrene triblock copolymers onto the CNC surface. The modified CNCs presented excellent dispersion properties in non–polar solvents.

1.7.2 TEMPO-mediated oxidation

TEMPO-mediated oxidation is a surface modification method used to convert the hydroxymethyl groups to their carboxylic form by using a (2,2,6,6-tetramethyl)piperidine-1-oxyl-mediator (or TEMPO-mediator). Generally, the oxidation uses a catalytic amount of TEMPO and another oxidant such as sodium hypochlorite or sodium chlorite to recycle the TEMPO although sodium bromide is quite often used to increase the rate of oxidation through formation of sodium hypobromite (Figure 1.7.1).[80-82]

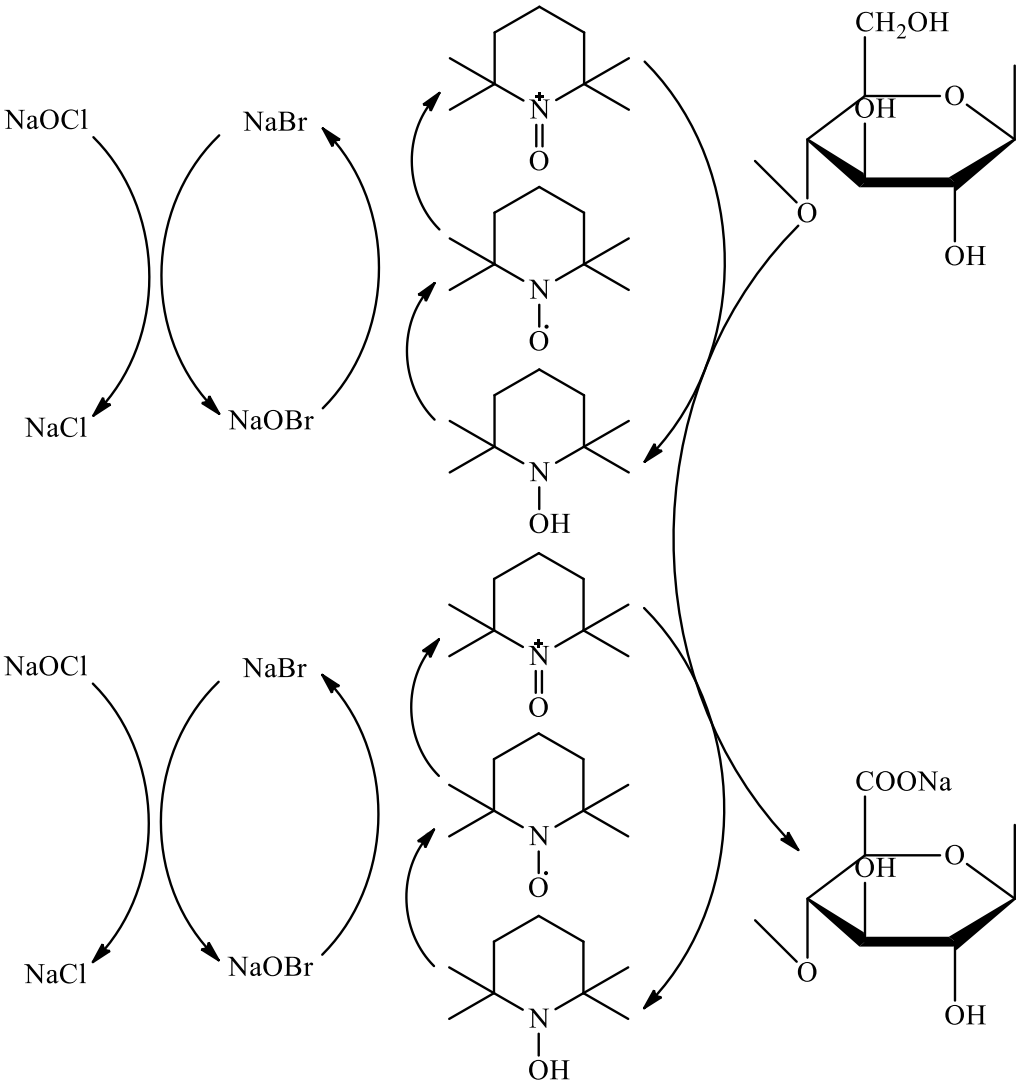


Figure 1.7.1 TEMPO-mediated oxidation mechanism schematic representation adapted from ref [1]

First introduced by De Nooy *et al.*[83] and many times reported since then, this method showed a selective oxidation of only primary hydroxyl groups of

polysaccharides. Actually, in the TEMPO-mediated oxidation of CNC, the secondary hydroxyl groups remain unaffected mainly because of the two-fold screw axis of the cellulose chain which promotes the accessibility of hydroxymethyl groups while the secondary hydroxyl groups are buried inside the sheets. The TEMPO oxidation of native cellulose fibres results in the oxidation of the surface of crystalline region but also oxidation of the amorphous sections.[84] Therefore, depolymerisation occurs in the amorphous sections while retaining cellulose crystallinity, thus making it possible to isolate nanocrystalline cellulose by this methodology.[85,86] When TEMPO oxidation was carried out on cellulose fibres isolated using HCl hydrolysis, the resulting nanocrystals maintained their initial morphological integrity and formed a homogeneous suspension through electrostatic stabilization when dispersed in water because the newly grafted carboxyl groups that impart negative charges to the cellulose surface.[44] Similar results were reported by Montanari *et al.* who also observed a reduction of the crystal size upon excessive TEMPO-oxidation as a consequence of partial surface cellulose chain exfoliation.[86] Thus, based on these studies, it was demonstrated that different degrees of oxidation can be obtained as a function of primary oxidizing agent amounts (NaOCl). When these TEMPO-oxidized or carboxylated CNC are suspended in water, they display birefringence patterns and do not flocculate or sediment.[41] Currently, TEMPO-oxidised nanocrystals are used as a precursor for further surface functionalization.[46,47]

1.7.3 Cationization

Cationization of cellulose represents the grafting of positive charges to the CNC surface. Cellulose fibres are negatively charged due to $–O^-$ or $–COO^-$ resulting from the deprotonation of hydroxyl groups and/or carboxylic acids present at the surface. These anionically charged surfaces will repel other anionic materials such as anionic dyes or inorganic fillers.[87] Consequently, cationized cellulose is used to ease the dispersion of anionic fillers and dyes which are extensively used in paper-making and the textile industry.[88,89] Also, cationized cellulose is extensively used in conditioners and moisturisers in the cosmetics industry.[90] Furthermore, cationic cellulose bearing quaternary

ammonium groups is used for its antibacterial properties or its therapeutic potential as promising gene carriers.[91,92]

All the applications of cationic cellulose mentioned above refer to homogeneously modified cellulose. Extending this work towards nanocrystals has only been reported a few times in the literature, in part because the required conditions generally result in destruction of the crystallinity of the nanoparticles. Making the conditions more benign tends to results in a very low degree of substitution. Therefore, developing strategies to reliably cationize CNC to a high extent and without loss of crystallinity is of great importance.

The first mentioned method by Hasani e*t al.* involves the surface cationization of H_2SO_4 hydrolysed CNC by using epoxy-propyltrimethylammonium chloride (EPTMAC) to introduce quaternary ammonium salts.[93] The method involved a mild alkaline surface activation with NaOH, before introduction of EPTMAC, in order to remove the sulphate groups introduced through acid hydrolysis, while preserving the crystalline morphology and cellulose nanocrystal dimensions. In spite of a successful cationization, this method led to a modest decrease in the total surface charge density as compared to the initial charge density of sulphated CNC. Meanwhile, this modification did lead to stable aqueous suspensions of the nanocrystals which exhibit unexpected gelling and rheological properties. The degree of substitution (DS) was found to be 0.02 per bulk anhydroglucose units and a surface charge density of 0.26 e nm^{-2} (+ charge) as compared to 0.41 e nm^{-2} (- charge) for the starting sulphated CNC.

A second method developed by Eyley *et al*. consists in the azidation of initially chlorinated nanocrystalline cellulose in order to synthesise an imidazolium salt by reacting the azidated cellulose with an alkyne terminated ionic liquid through a copper(I) mediated azide-alkyne cycloaddition. This synthesis route involves 3 steps and could be considered difficult for commercial applications. Nonetheless, this pathway gave a surface DS of 0.36, significantly higher than the previously reported route (DS = 0.02). This degree of substitution corresponds to a high extent of modification of the primary hydroxyl group and at the same time the cationized surface charge increased significantly up to

0.56 *e* nm^{-2}. This method provided the opportunity to synthesise a wide diversity of ion exchange systems or catalysts having CNC as a support medium.[94]

A comparable method to that adopted by Hasani *et al.* was reported by Zaman *et al.*, where the cationic surface modification was performed using glycidyltrimethylammonium chloride (GTMAC) based on a semi-dry method.[95] The most recently reported method by Jasmani *et al.* describes a one-pot route to produce pyridinium-grafted CNC using 4-(1-bromoethyl/ bromomethyl) benzoic acid (Figure 1.7.2).[96]

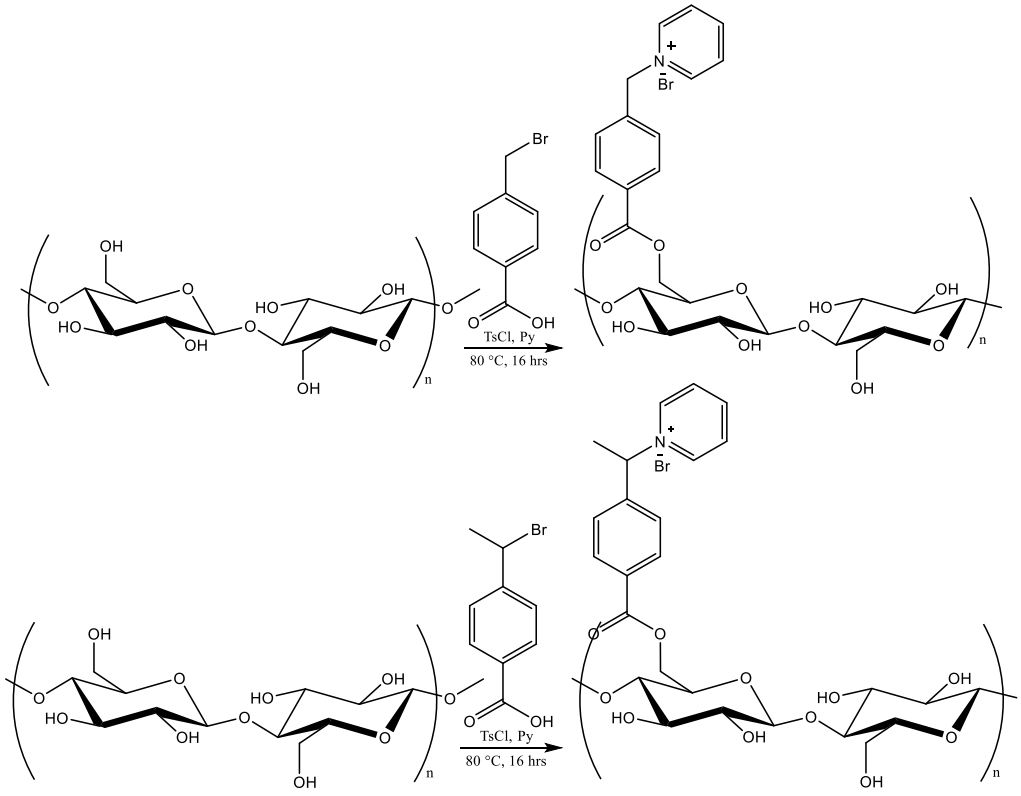


Figure 1.7.2 Cationization reaction of CNC with 4-(1-bromoethyl/ bromomethyl) benzoic acid adapted from Jasmani *et al.*[96]

Two reactions occur at the same time in the reaction vessel: the esterification of the benzoic acid with the nanocellulose surface hydroxyl groups and a nucleophilic attack of pyridine, used as a solvent, onto the alkyl-bromide bond of the aromatic ring substituent forming a pyridinium ion. The reported method led to a high grafting density (DS_{surf} up to 1.1, close to the maximum

achievable DS without loss of crystallinity) when compared to any of the previously published methods while also retaining the cellulose crystallinity.

1.7.4 Polymer grafting

Polymer grafting on the CNC surface has been conducted by two main strategies, namely the "grafting onto" and "grafting from" approaches.[97] The first strategy involves the attachment of pre-synthesised polymer chains to the hydroxyl groups at the surface of cellulose by using a coupling agent. The "grafting from" approach involves the *in situ* surface-initiated chain polymerization from immobilized initiators on the substrate.[1] The "grafting onto" was applied by Ljungberg *et al.* on tunicated cellulose nanowhiskers by their modification with a maleated polypropylene (PPgMA)[98] as it was initially applied by Felix *et al.* onto their cellulose fibres.[99] When dispersed in atactic polypropylene, the resulting grafted CNC proved to have very good compatibility and a high adhesion. Amine-terminated polymer grafting onto the surface of TEMPO-mediated oxidized CNC by using a peptide coupling process and catalysed by a carbodiimide derivative in water, was studied by Araki *et al.*[59] and Vignon *et al.*[100]. Other "grafting onto" attempts include the grafting of DNA oligomers on the CNC surface[101], grafting of polycaprolactone (PCL) with different molecular weights on CNC surface by using isocyanate-mediated coupling[44] with a high enough grafting that PCL chains were able to crystallise at the surface of cellulose and grafting of presynthesised water-borne polyurethane polymers through isocyanates.[102] The surface crystallization determined a co-crystallization of the respective polymer matrices upon the preparation of nanocomposites with modified nanocrystals with improved interfacial adhesion and resulting in nanocomposites with improved mechanical strength.

Habibi et al. was the first who reported the "grafting from" strategy in the grafting of polycaprolactone from the surface of CNC via a ring opening polymerization (ROP).[54] In order to enhance the grafting efficacy, other similar grafting reactions were carried out under microwave irradiation[103,104] or at elevated temperatures[105]. Surface-initiated atom transfer radical polymerization was a method to synthesise polystyrene grafts with good control of length and

composition when ethyl 2-bromoisobutyrate was used as an initiator.[64,106] In the same manner, other monomers (mainly acrylic) such as N-isopropyl-acrylamide were also polymerized from CNC surface with applications in thermo responsive substrates.[107,108] *In situ* polymerization of aniline through an oxidative polymerization using ammonium peroxydisulfate as an initiator onto CNC in hydrochloric aqueous solution resulted into grafting of polyaniline from CNC.[109]

1.7.5 Esterification

Esterification is a functionalization pathway used in this thesis and special attention will be given to it. Mainly, esterification produces cellulose esters with very wide industrial applications, of which cellulose acetate is the most important organic cellulose ester and this can be synthesised homogeneously and heterogeneously. Sassi and Chanzi have studied the acetylation of cellulose through these two pathways by using a dry mixture of **acetic anhydride** and acetic acid catalysed by a small amount of sulfuric or perchloric acid.[110] The presence of a non-swelling or swelling solvent dictates the acetylation mechanism pathway. Addition of solvents such as toluene, benzene or pentyl acetate results in the production of insoluble cellulose acetate without changes of the core fibre.

In the "homogeneous" process where no solvent was used, the cellulose acetate is solubilized in the reaction medium upon its production and therefore, substantial morphological modification occurs during acetylation and results in complete dissolution. Thus, it is presumed that the reaction mechanism proposed by them can be applied to other heterogeneous esterifications of cellulose fibres and CNC. However, acid anhydrides were extensively used in heterogeneous esterification, for low molecular weight aliphatic acids and formation of cellulose acetates with high degree of substitution.[111,112] These can only induce the surface acetylation of CNC when acetic anhydride in anhydrous pyridine is used.[113] Pyridine plays both the role of solvent but also of activating agent as is presented in Figure 1.7.3, although studies have indicated 4-dimethylamino pyridine (DMAP) to be a more efficient catalyst.[114,115]

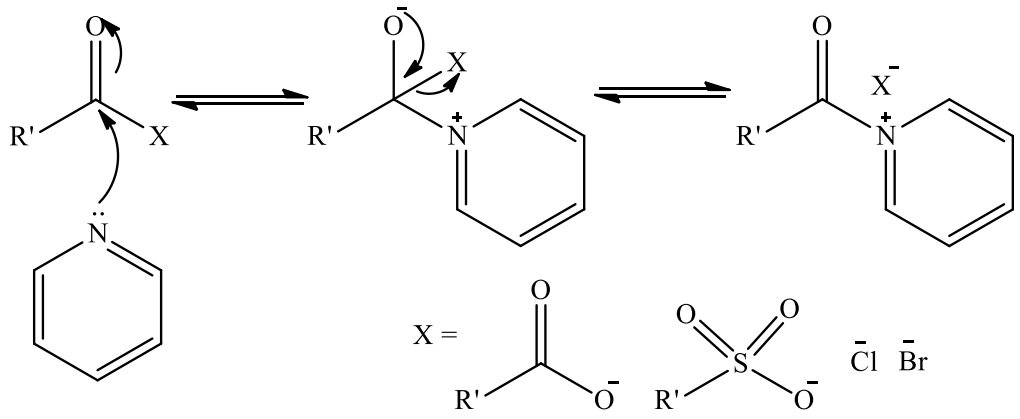


Figure 1.7.3 Reaction mechanism of anhydrides activation with pyridine to form a highly reactive acyl pyridinium intermediate, which is also applied to acyl halides and other nitrogen bases[65,114]

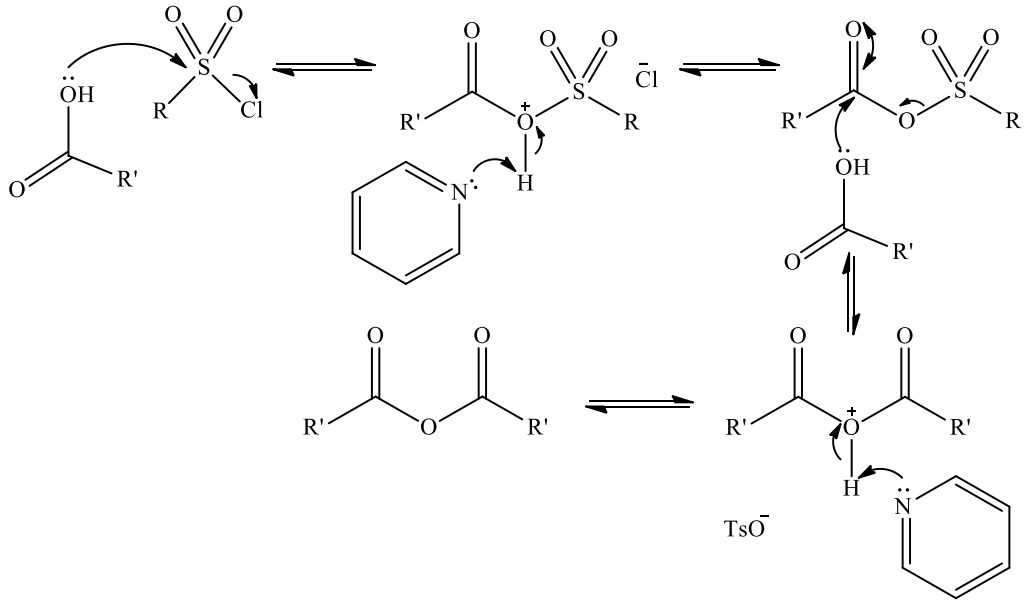


Figure 1.7.4 Reaction mechanism for the formation of symmetric and mixed anhydrides through the reaction of tosyl chloride with carboxylic acids in pyridine. R=tosyl, R'=alkyl or aryl.[20,65,116]

For synthesising cellulose esters of linear fatty acids, reactions can make use of in-situ formation of the anhydride by the use of *p*-toluenesulfonyl chloride (TsCl, tosyl chloride) [117,118] or of acetic anhydride [115,119] co-reactant as dehydrating agent that acts as a solvent in heterogeneous modifications[115,118] or as a reagent in homogeneous modifications.[117] Considering the acid and dehydrating agent concentrations, one produces either a mixed or a symmetric

anhydride, which will further react with the hydroxyl groups of cellulose (Figure 1.7.4).[116,120]

Another esterification procedure of cellulose makes use of **acyl halides** together with amine bases. This methodology is well known for the production of fatty acid cellulose esters. In comparison with the anhydride methodology, the powerful reagent produces aggressive HCl, as a by-product, that can either be released from the reaction as a toxic gas by applying a nitrogen gas stream[121] or vacuum,[122] or it can be mopped up by the amine base such as pyridine[123] and triethylamine[124] through formation of a salt complex. Similar to the previous esterification method, this procedure can be applied either homogeneously in a non-derivatizing solvent[125] or heterogeneously on the fibre[126-128] or on the nanocrystals.[64,106,129,130] When the esterification makes use of amine bases, two reaction mechanisms can be conceived depending on the nucleophilicity of the amine. If a nucleophilic amine such as pyridine or DMAP is used, the mechanism involves the formation of a charged reactive intermediate that drives the reaction forward, while in the case of a non-nucleophilic amine such as triethylamine, it will only behave as a catalyst of the esterification reaction (Figure 1.7.5).[131]

In the esterification of CNC with acyl halides, special attention has to be given to the grafting of bromoisobutyryl bromide (BiB) as it is commonly used to introduce initiating sites for atom transfer radical polymerization (ATRP) from the surface of nanocrystals. ATRP provides good control of the polymer graft length and composition.[64] Yi *et al.* modified CNC by this method and they observed the thermal and liquid crystalline properties of the grafts which showed birefringence above the melting temperature of the side chains, being the first instance of spontaneous formation of a chiral-nematic phase by CNCs as a result of thermotropism.[106] Although, there is no clear indication about the degree of substitution, the group used a moderate excess of bromoisobutyryl bromide (21mmol/g CNC) with DMAP and triethylamine in a molar ratio of 1.15:1:1 reacted in dry tetrahydrofuran (THF) for 24 hours at room temperature.[132] On the contrary, Morandi *et al.* studied the reaction conditions and concentration of BiB on the esterification and their maximum conversion

translated into a DS_{surf} = 1.05, achieved when a 420 mmol BiB/g CNC for 24 hours at 70 °C in dry *N*,*N*-dimethylformamide (DMF) was used.

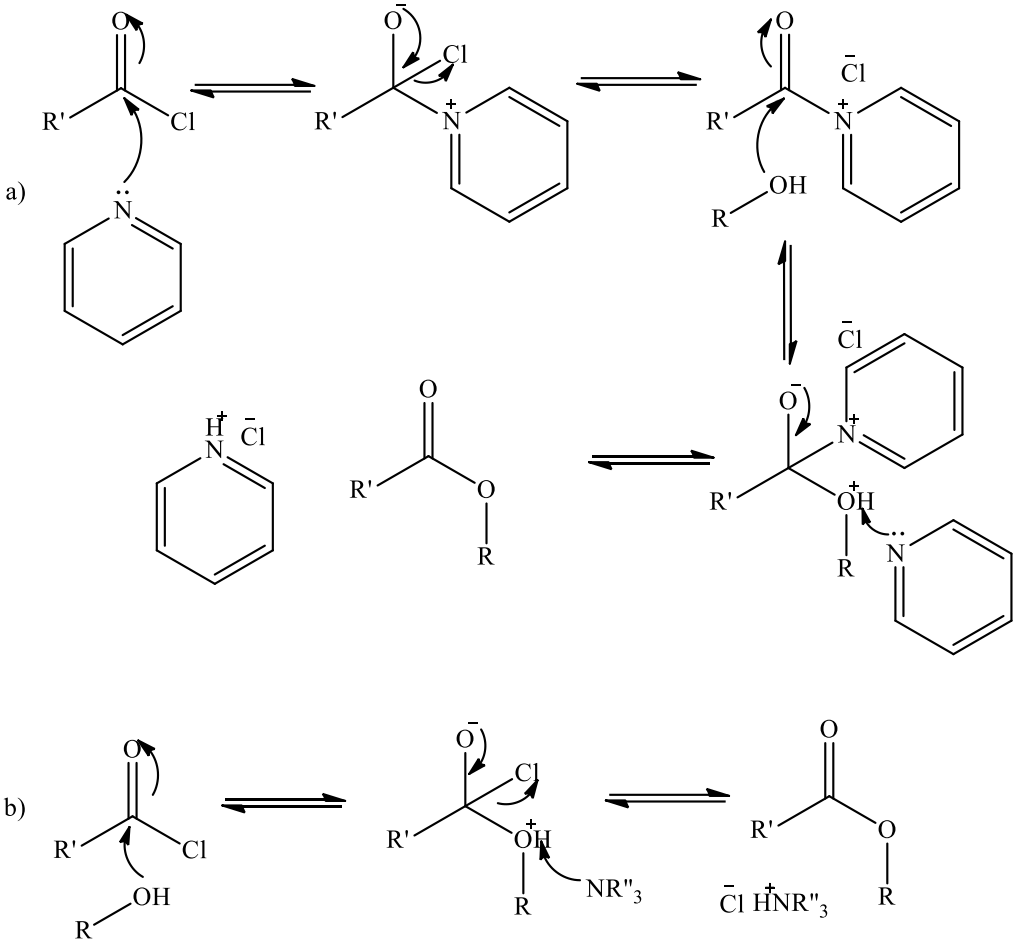


Figure 1.7.5 Reaction mechanism of esterification with acid halides using (a) a nucleophilic and (b) a non-nucleophilic amine base (b)[65]

It is worth mentioning that despite this high molar excess, the CNC maintained their crystalline integrity determined by powder X-ray diffraction (XRD) and the DS was directly proportional with the reaction time, temperature and BiB concentration.[64]

Majoinen *et al.* and Berlioz *et al.* applied chemical vapour deposition (CVD) to modified CNCs with tunicin whiskers and BiB, and bacterial cellulose micro-fibrils with palmitoyl chloride respectively. Although the first group claims a 58 % increase in modification over the previously published method by Morandi *et al.*, they did not consider the difference size of the nanocrystals used (CNC from filter paper) which produces a greater surface area and hence

resulted in a smaller actual increase, while also having a longer reaction procedure.[133] Berlioz *et al.* reported an extensive modification (DS = 2.7) while retaining the original morphology, explained by the method itself as the reaction is carried out in the absence of a swelling agent.[130] The cellulose tripalmitate is formed by CVD of palmitoyl chloride reaction with hydroxyl groups under a continuous slow nitrogen flow to remove the hydrogen chloride formed.[130] However, while the original morphology is retained, the crystallinity will be affected as this high DS does remove a significant amount of hydrogen capability, necessary to retain the crystalline structure.

Coupling agents used in the esterification represent a relatively new approach. *N*,*N*'-dicyclohexylcarbodiimide (DCC) (Figure 1.7.6) and 1,1'-carbonyldiimidazole (CDI) recently followed by benzotriazolyl esters and Mukaiyama reagents were applied in the modification of cellulose in solution.[124,134,135] DCC is a common condensation agent to convert carboxylic acids into anhydrides and is rarely used with the polymers, and was the first used in cellulose homogeneous modification to allow the synthesis of cellulose esters with low degree of substitution which is controlled by reagent stoichiometry and the applied reaction conditions.[124,134]

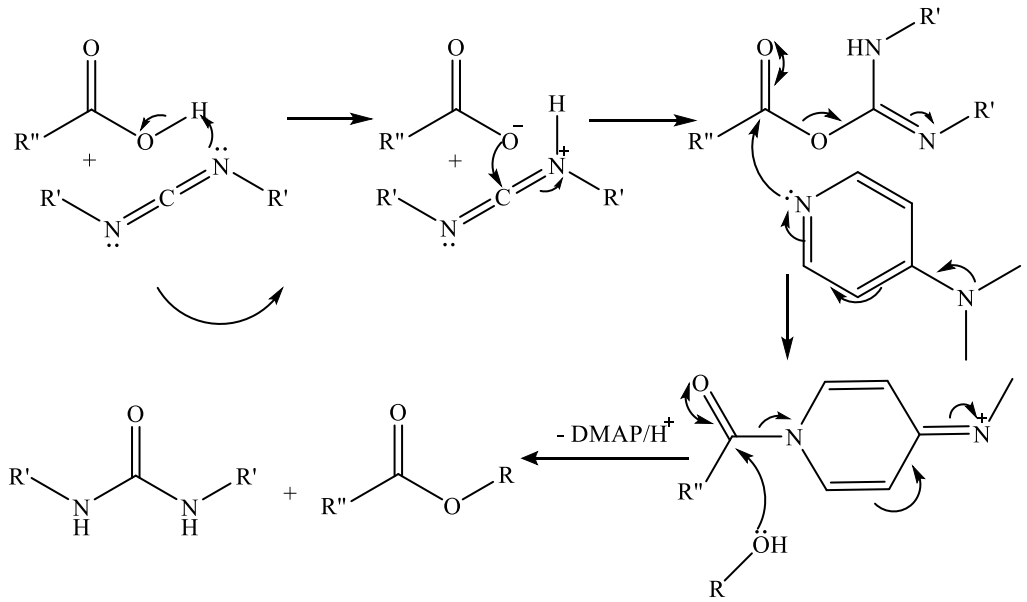


Figure 1.7.6 Reaction mechanism of DMAP reaction in carbodiimide-mediated esterification or Steglich esterification.[65,136]

Compared with the traditional esterification methods with acid anhydride and acid halides, DCC can be involved in esterifications with acids using only a low molar excess with respect to the cellulose. The esterification reaction mechanism consists in the activation of the acid by the carbodiimide with elimination of urea followed by acyl transfer to a base such as DMAP and then to the alcohol.[136]

Sulfonic acid esters of cellulose (tosylates) are formed by the reaction of cellulose with a specific sulfonyl halide, heterogeneously or homogeneously, with a small amount of chlorodeoxy functionalities formed. These derivatives are of considerable interest as an intermediate that serves as a leaving group or as a protecting group in further modifications of the remaining free OH groups.[137-140] The reaction mechanism is dictated by the structure of the sulfonyl halide and hence there are two different reaction mechanisms (Figure 1.7.7).[65,141,142] The presence or not of an α hydrogen atom results in a mesylation or a tosylation which are the most popular reactions.

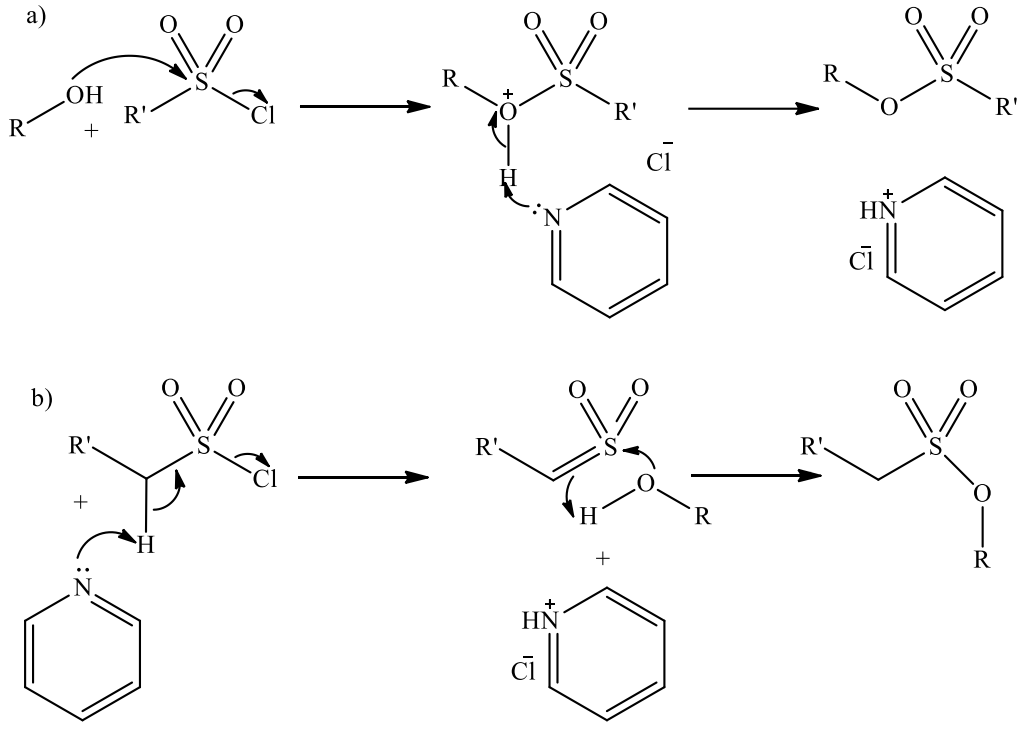


Figure 1.7.7 Reaction mechanism of esterification with (a) aryl[141] sulfonyl halides and (b) with alkyl[142] sulfonyl halides.[65]

As a consequence of steric hindrance, when 3 tosyl groups are attached onto one glucose unit, the mesylation offers a higher substitution even if tosyl chloride is generally the most applied sulfonic acid ester.[140] Heterogeneous tosylation performed on mercerized cellulose fibres in pyridine showed a DS ≤ 2 and an increase in the reaction temperature promotes the formation of chlorodeoxycellulose rather than tosylated cellulose.[137] The studies of McCormick *et al.* on reactions carried out in DMAc/LiCl (so a homogeneous reaction) indicate that the use of triethylamine or DMAP, instead of pyridine as a base, result in the minimization of the chlorination side reaction and offers a route to cellulose tosylates with varying DS that can be influenced by the molar ratio of tosyl chloride to cellulose.[139] Recently, Gericke *et al.* showed that chlorination can be prevented even with the use of pyridine, when tosylation of cellulose in ionic liquids (IL) is carried out at room temperature.[143] Strictly, the tosylation of CNC in pyridine at room temperature, for two days was confirmed by IR spectroscopy in the group of Argyropoulos *et al.* although detailed characterization was not given to determine the ratio of sulfonate to chlorine.[144]

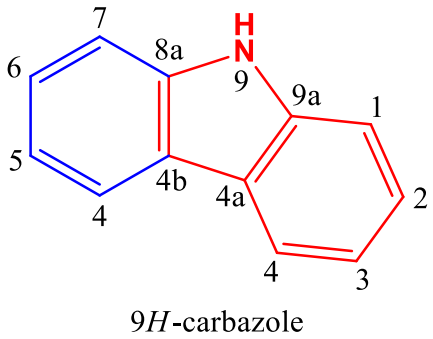
1.7.6 Etherification

Cellulose ethers are a very important class of cellulose derivatives prepared by heterogeneous modification of cellulose. Traditionally, they are prepared by reacting cellulose swollen in alkali solutions with alkyl halides. As a disadvantage, the alkaline system leads to a crystal structure modification from cellulose I to cellulose II upon recrystallization.[145] As it was mentioned in the cationization of CNC section reported by Hasani *et al.*[93], the positive charge grafting was carried out by an etherification reaction with a derivative of a complex salt such as epoxy-propyltrimethylammonium chloride (EPTMAC) or glycidyltrimethylamonium chloride (GTMAC) reported by Zaman *et al.*[95]. Initial modification of CNC with GTMAC resulted in very low degree of substitution (DS = 0.02 for cotton CNC and DS = 0.04 for wood CNC) for a reaction carried out in 1.75 M sodium hydroxide and heated for a few hours. Substantial functionalization of CNC was achieved by Zaman *et al.* (DS = 0.35) when CNC were ground with powdered sodium hydroxide followed by

suspending into a small amount of DMSO/water followed by heating and sonicating for a few hours.[95] Although TEM images confirmed retention of morphology, there were no XRD or SS-NMR data given to indicate whether there was a loss of crystalline integrity or change of the polymorph state of cellulose I to cellulose II. CNCs derived from tunicates have been silylated with derivatives of alkyldimethylchlorosilanes. It was proven that the silylated cellulose whiskers with a DS between 0.6-1 maintained their morphological crystallinity and due to their surface modification they become readily dispersible in solvents with low polarity (such as THF). The stable suspensions also showed birefringent behaviour. Upon a modification that induces a DS > 1, the nanowhiskers core becomes silylated, leading to the disintegration of the nanocrystals and, the loss of the original morphology.[146]

1.7.7 Fluorescence Labelling

Fluorescent cellulose is a new class of important functional materials with increased interest considering their promising applications in the field of sensors[147], fluorescent probes[148,149], optoelectronic materials[150,151] or biotechnology.[152,153] Between these fluorescent molecules, carbazole and coumarin have attracted huge interest for their applications. 9*H*-Carbazole is an aromatic heterocyclic organic compound with a tricyclic structure consisting of indole (Figure 1.7.8) as the base structure on which is fused in positions 8a and 4b a second benzene ring. Carbazole and its derivatives are mainly used as intermediates in the synthesis of pharmaceuticals, agrochemicals, dyes, pigments and other organic compounds.



9*H*-carbazole

Figure 1.7.8 Carbazole structure[154]

Coumarin, (Figure 1.7.9) a natural product with a sweet odor extracted from tonka beans, is extensively used as a precursor of a number of natural anticoagulant pharmaceuticals[155,156], rodenticide[157], food flavourings[158] or with clinical value as oedema modifier.[159]

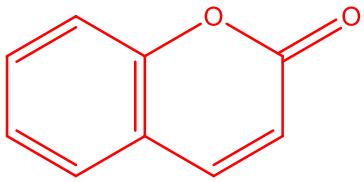


Figure 1.7.9 Coumarin structure

Organic Light-Emitting Diodes (OLEDs) based on carbazole-substituted cellulose have already been reported by Karakawa *et al*. in homogeneous reaction.[160] In order to induce optical and semi-conducting properties needed for OLEDs applications, fluorescent cellulose derivatives such as 6-*O*-*p*-methoxytrityl cellulose were homogeneously modified with carbazole groups. Also, Karakawa and his group have reported on the memory effect of carbazole-substituted cellulose, the first report on this characteristic for cellulose-based polymers.[161] Zhang *et al*. have homogeneously synthesised carbazole–substituted hydroxyethyl cellulose (HEC) where, by increasing the carbazole degree of substitution on the cellulose, the fluorescence lifetime was increased.[162] The fluorescence intensity of carbazole-substituted hydroxyethyl cellulose was also found to be stronger than for the carbazole derivative itself.

Properties such as photoconductivity of carbazole as a an electron donor[163], electron transfer quenching accompanied by highly efficient energy migration in Langmuir-Blodgett (LB) films assembly of carbazole chromophore[164], and inter layer energy transfer [165] have been reported for LB films incorporating carbazole. The LB films based on cellulose derivatives were of very high interest in applications including ultrathin membranes production[166], protein immobilisation at high density[167] and preparation of films with non-linear optical properties[168]. Lijun Mao and Anna M. Ritcey have prepared LB films of cellulose ethers containing carbazole as a side chain substituent through a

two-step alkylation procedure while varying reaction conditions and carbazole content.[169]

Also, coumarin derivatives are important fluorescent dyes with high photoluminescence quantum efficiencies, applications in optoelectronic materials, while they also display anti-tumoral, anti-coagulant, and anti-oxidant properties.[170-174] Fillponen *et al.* have covalently linked an azide-bearing fluorescent molecule in a three step reaction including, TEMPO mediated oxidation followed by propargylamine grafting by carbodiimide-mediated formation of an amide linkage followed by Copper(I) – catalysed Azide-Alkyne Cycloaddition (i.e. azide-alkyne click reaction) with azidocoumarin and azidoanthracene resulting in fluorescent compounds but only with a 0.1 degree of substitution.[63] Another modification with responsive fluorophores involving coumarin derivatives (7-hydrozino-4-methylcoumarin and 7-amino-4-methylcoumarin) was claimed by Huang *et al.* and was well characterised by spectroscopic and imaging techniques.[175] As the grafting consisted in the modification of the anhydroglucose units accessible at the reducing end of the nanocrystals that are in hemiacetal form, available to react with amino or hydrazo group, the resulting degree of substitution was obviously low. Another very recent paper reported on the design of light-responsive mechanically adaptive nanocomposites based on CNC that were modified with 7-coumaryl-(6-isocyanothohexyl) carbamate, without any indication about the amount of modification.[176] This work used the property of coumarin derivatives to undergo photo-dimerization to form a cyclobutane ring through cycloaddition upon UV light irradiation at a wavelength > 300 nm while the corresponding reverse reaction occurs at a wavelength < 280 nm.

1.7.8 Thiol-Ene click chemistry

In 2001, K. Barry Sharpless *et al.* introduced the concept of facilitation of organic reactions, the main idea behind "click chemistry". Click chemistry denotes the development of a set of powerful, highly reliable, in both small and large applications, and selective reactions that do not yield side products, for the rapid synthesis of useful new compounds through heteroatom-links (C-X-C).[177] The click reactions must be characterised by the followings: they must

be modular, wide in scope, giving very high yields with only inoffensive by-products that can be removed by non-chromatographic methods, and they must be stereospecific. With respect to the characteristics of the process, reaction conditions need to be simple, as much as possible insensitive to oxygen and water, using easily available starting materials and reagents, making use of no solvent or a benign solvent which can also be readily removed, and the product has to be easily isolated.[177]

Being the quintessential example of click chemistry, the copper-catalysed azide/alkyne cycloaddition (CuAAC) reactions have had an impressive impact on the field of macromolecular engineering with applications in biomedical polymers, especially materials that are located at the interface of biological, microelectronic and chemical polymers, new materials for solar cells and biomembranes.[178] Other applications of this reaction include the construction of linear polymers, dendrimers, networks, dendritic, hydrophilic, hydrophobic, amphiphilic and, block-co-polymers, and Si particle polymer hybrids, polymers for solar cell materials and many others.[179-181]

The reactions of sulphur-containing compounds with alkenes are dated back to the mid-19th century when Charles Goodyear discovered how to preserve and enhance the properties of crude rubber (poly(*cis*-isoprene)) by using sulphur and heat in a vulcanization process. Basically this was the beginning of classical Thiol-Ene Chemistry (TEC) – the radical addition of thiols across non-activated carbon-carbon double bonds (Figure 1.7.10).[182,183] Nowadays, most authors use the term Thiol-Ene to describe the reactions of thiols with a wide range of unsaturated functional groups such as maleimides, acrylates or norbornenes.[184-186] In some cases, the reaction mechanism can involve the classical radical addition or a Michael-type nucleophilic addition.[187]

Previously, the main purpose of Thiol-Ene chemistry was the formation of cross-linked networks and currently this concept is applied to hydrogels with distinctive properties such as cell delivery materials, thin films with a uniform cross-linked matrix with desired properties such as flexibility, and lithographic applications.[188-190]

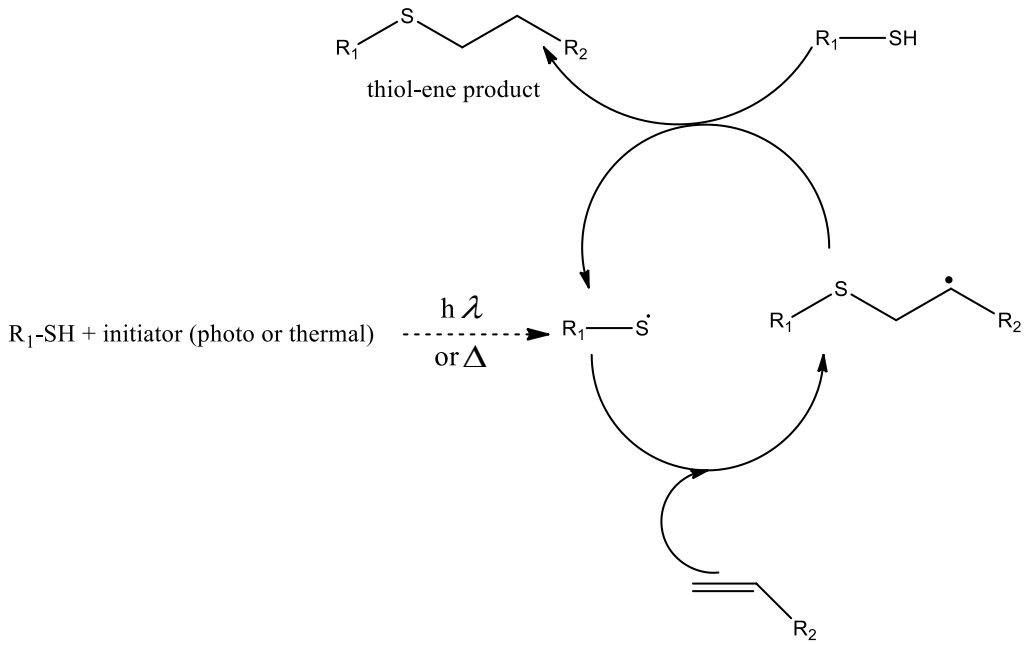


Figure 1.7.10 Mechanism of radical Thiol-Ene coupling[183]

The efficiency and homogeneous derivatization of dissolved polysaccharides has been reported many times but has been less studied for the surface modification of solid polysaccharides such as cellulose. However, direct, inexpensive, technically simple, environmentally friendly and modular modifications of solid carbohydrates are highly desirable for industrial applications of natural fibres, even if it is a difficult challenge because of the reduced reactivity of the cellulose surface.[191]

The first attempt to apply ”click" chemistry by using the copper-catalysed Huisgen reaction on polysaccharide cellulose was performed by Liebert *et al.* in 2006, who functionalized a cellulose surface by the introduction of functional groups using a triazole-spacer in a chemoselective and highly modular route.[192] Other applications of this reaction were performed in our group in order to synthesise cationized CNC as a support medium for a wide variety of ion exchange systems and catalysts, and for electron-conducting surface modified CNC.[193]

In comparison to copper-catalysed azide/alkyne reactions, the main advantage of Thiol-Ene ”click” coupling is the fact that it does not require the use of a metal catalyst to promote the reaction. Another advantage of the Thiol-Ene

click reaction is given by the activation way (thermally and photochemically) being dependent on the starting materials and it does not require a solvent. Therefore, these advantages make this reaction potentially green and highly efficient. It can also be carried out under acid/base or nucleophilic catalysis or without catalyst in a polar solvent.[194-196]

In 2010, Zhao *et al*. reported the first example of environmentally friendly benign heterogeneous modification of cellulose in its native solid state by Thiol-Ene click chemistry activated by an organocatalyst being described as highly modular and completely metal-free.[191] Firstly, they performed the esterification reaction with 9-decenoic acid or with 2-(oct-7enyl)oxirane, both catalysed by (S)-tartaric acid in order to obtain the corresponding modified cellulose (ester and ether) as paper samples. Their Thiol-Ene click reactions include thiols with long chains and aromatic structures and the reactions were UV irradiated for 1 hour. The purification was performed by Soxhlet extraction to remove the unreacted thiols. The successful Thiol-Ene derivatization was identified through UV fluorescence and with the FT-IR analysis which indicated the presence of covalently attached thiols. Similar research from our group also published in 2010 modified cellulose nanowhiskers using a Michael type addition resulting in attachment of analyte-sensitive fluorophores with applications in pH-sensing materials.[197]

1.8 Aims of the thesis

The aim of this thesis is to develop new methodologies for the surface modification of CNC in which already existing grafting techniques are adapted to give new reaction products and new methodologies are proposed for the preparation of new cellulose nanocrystals derivatives. Chapter 3 focuses on the use of esterification methods that mainly have not been applied to cellulose nanocrystals previously to form modified CNC with esters on the surface that can support further functionalizations. Starting from one esterification reaction described in the literature between methacrylic acid and CNC, Chapter 3

investigates in detail acrylate and methacrylate CNC considering three precursors and implicitly four esterification methodologies.

Considering the current state of the art of fluorescently labelled cellulose, Chapter 4 presents the synthesis of a new class of carbazole and coumarin derivatives, formed as CNC esters functionalized with these two well-known molecules. Thus, in this chapter, a new modification procedure for the grafting of CNC with carbazole and coumarin through esterification is developed, with the aim of improving the reliability of the modification reactions, increasing the attainable degree of substitution, and investigating the properties of the grafted nanocrystals.

The applications of cationic cellulose mentioned in the earlier literature review refer mainly to homogeneously modified cellulose and the extension towards nanocrystals has only been reported a few times in the literature, given the required conditions to introduce the cationic grafts. Therefore, developing strategies to reliably cationize CNC to a high degree and without loss of crystallinity will be developed in Chapter 5. Two well know ionic liquid precursors with high reactivity (pyridine and 1-methylimidazole) are used in order to enlarge the variety of grafted molecules and methodologies. Therefore, the cationization reaction of the cellulose nanoparticles is proposed to be carried out at the same time as the esterification step, comparable to the work by Jasmani *et al.*[96], or could be done sequentially to the esterification. The desired modification should be as easy and straightforward as possible, ideally in one-step. However, in order to find the optimum reaction conditions with the highest reaction yield, the two-step synthesis was also investigated as it allows intermediate characterisation. The first method includes a single step in which the esterification and nucleophilic attack happens simultaneously in the vessel to create the desired cationized cellulose nanoparticles. The second pathway investigated involves a two-step procedure with sequential esterification and nucleophilic attack, in which the initially synthesised bromoacetate cellulose is used in a separate cationization reaction with pyridine or 1-methylimidazole. Based on Jasmani *et al.*'s[96] work, the third esterification attempt optimised the

one-step method involving the esterification of bromoacetic acid and pyridinium formation in one reaction using a TsCl/Py system.

The alkene-functionalized cellulose nanocrystal derivatives synthesised in Chapter 3 (cellulose acrylate and cellulose methacrylate) are further functionalized with a range of alkyl thiols in order to promote these newly functionalized materials for different applications through Thiol-Ene click chemical modification in Chapter 6. CNC are mixed with the respective thiols and suspended in solvent under air atmosphere, for a specified amount of time and at room temperature, followed by purification. Moreover, the aim of the thesis is to extend the research beyond the synthesis of the new products through click chemistry itself, towards testing them in applications such as switchable nanoparticles at the end of chapter 6.

Throughout the thesis, considerable attention will be given to cellulose crystal structure preservation in order to retain their mechanical properties and high aspect ratio morphology and therefore, the modification strategies will be adapted to prevent crystalline structure deterioration or destruction.

2 Characterization of cellulose nanocrystals

Cellulose nanocrystals used as a starting material in this research were produced from cotton wool. This was done because of the availability of bleached cotton wool as a commercial product, thus significantly reducing the preparation steps involved in the nanocrystal extraction (other unbleached cellulose sources need to be bleached to remove residual lignin). Sulfuric acid was used as a hydrolysing agent to separate the CNC from the fibres following an adapted method described by Elazzouzi-Hafraoui *et al.*[45]

Cotton wool was introduced in a 64 % sulfuric acid bath heated to 45 °C for 35 minutes under continuous stirring. The resulting nanowhiskers suspension was diluted with deionized water and purified by several centrifugation cycles. Dialysis of the nanowhiskers suspension to neutrality of the eluent against tap water for 2 days was performed to remove residual free acids. The nanowhiskers suspension was then homogeneously dispersed by sonication and filtered to remove aggregated nanocrystals and unhydrolysed cellulose before treatment with a mixed-bed ion-exchange resin to replace surface cations with protons. The stable suspension was filtered and sonicated once again, flash-frozen in liquid nitrogen and freeze-dried to isolate the CNC as a dry powder. Based on the previous research performed in our group, it was concluded that Soxhlet extraction with ethanol (EtOH) was needed in order to effectively remove the absorbed low molecular weight organic compounds, thus improving the reproducibility of the reactions performed at the nanocrystal surface.[198] The removed impurities were cellulose hydrolysis products and lignin fragments not part of pure cellulose. Thus, a 48h Soxhlet extraction with EtOH was performed in order to purify the CNC before any further surface modification reactions were carried out. After Soxhlet extraction, the

nanowhiskers were dried *in vacuo* and were used as such. This chapter describes the characterization of the CNC products, before and after modification, with specific information given on how techniques were used and how information was derived from the characterisation results.

2.1 Crystal model and surface chain ratio

The size and shape of cellulose nanocrystals are often determined with transmission electron microscopy (TEM) or atomic force microscopy (AFM).[1,45,66] The disadvantage of these methods lies in the small sample size considered in the measurement of average dimensions. In addition, the effect of negative staining on the size distribution, used in sample preparation for TEM, may induce aggregation of the nanoparticles which can also occur as a direct result of sample drying during preparation.[45] The cellulose plant source and hydrolysis conditions both influence the length of the nanocrystals while the width of the nanocrystal is dependent on the cellulose plant source only.[1] Eyley and Thielemans have designed a cellulose nanocrystal model (Figure 2.1.1) using the dimensions for a batch of CNC produced under the same hydrolysis conditions as those used in this thesis.[72] A cellulose nanocrystal is usually defined by the crystallographic planes (110) and $(1\bar{1}0)$, facing the lateral sides of the crystal. In the model, the blue boxes represent cellulose chains ends coming out of the plane. The variables L_1, L_2 and L_3 represent the height, width and the length of the nanocrystal respectively.[72]

The chains exposed at the nanocrystal surface relative to the total number of chains (R_c) can be calculated by equation 2.1.1 and is usually around 0.3.[41]

$$R_c = \frac{Surface\ chains}{Total\ chains} = \frac{2\left(\frac{L_1}{d_{(110)}}\right)+2\left(\frac{L_2}{d_{(1\bar{1}0)}}\right)}{\left(\frac{L_1 \times L_2}{d_{(110)} \times d_{(1\bar{1}0)}}\right)} \qquad (2.1.1)$$

The number of surface chains is calculated by dividing the height (L_1) and width (L_2) by the plane spacing of each of the crystal planes that are perpendicular to the crystal faces ($d_{(110)}$ and $d_{(1\bar{1}0)}$). The area of the end face of

the crystal divided by the area within the crystal planes give the total number of chains.

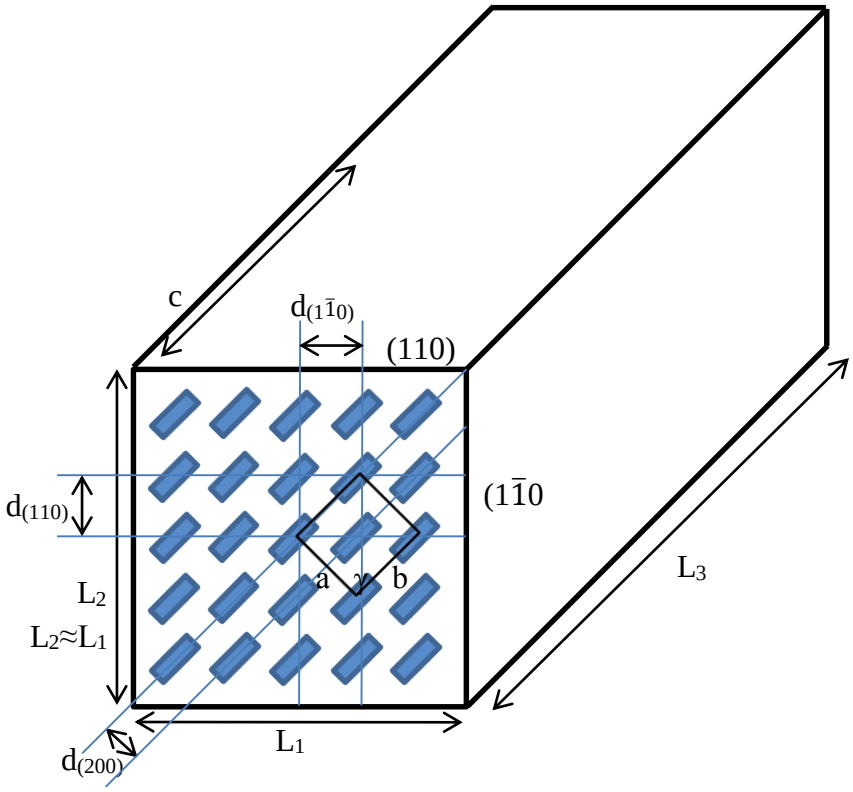


Figure 2.1.1 A model of a cellulose nanocrystal adapted from the work of Eyley *et al.*[72] that considers the crystal dimensions

Eyley and Thielemans also suggested a formula to calculate the number of hydroxyl groups per gram found at the surface of CNC (N_{OH} in moles/g) as indicated in equation 2.1.2:[72] n_1 is the number of primary hydroxyl groups facing (110) (or $(1\bar{1}0)$) in the unit cell, n_2 is the number of secondary hydroxyl groups facing (110) (or $(1\bar{1}0)$) in the unit cell, N_A is the Avocado's number, ρ is the crystalline cellulose I_β density, c is the unit cell dimension and the other parameters are the ones depicted in the cellulose nanocrystal model (Figure 2.1.1).[72] The second part of the equation $(2\left(\rho N_A L_3 d_{(110)} d_{(1\bar{1}0)}\right)^{-1})$ represents secondary hydroxyl groups, placed at the end of the cellulose chains and thus at the ends of the nanocrystals. This correspond to only a small percentage of the total number of the hydroxyl groups and is the only parameter that is length-dependent.[65]

$$N_{OH} = \frac{n_1+n_2}{\rho N_A L_1 L_2\ c}\left(\frac{L_1+L_2}{d_{(110)}} + \frac{L_1+L_2}{d_{(1\bar{1}0)}}\right) + 2\left(\rho N_A L_3 d_{(110)} d_{(1\bar{1}0)}\right)^{-1} \quad (2.1.2)$$

If one considers the cellulose nanocrystal dimensions as determined by Elazzouzi-Hafraoui *et al.*[45] (6 nm × 6.1 nm) and the unit cell dimensions and plane spacing determined by Nishiyama *et al.*[32](*a*(Å) = 7.784, *b*(Å) = 8.201, c(Å) = 10.380 and γ(°) = 96.5 and d-spacing (110) = 0.532 and (1$\bar{1}$0) = 0.588), we obtain the resulting N_{OH} = 2.99 mol/g of which only 46 μmol/g are found at the extremities of the nanocrystal. This represents a mere 2% of the total surface functionality.[32,45,65] Given the low number of C_1 and C_4 hydroxyl groups located at the cellulose chain ends, these will not be considered in this thesis when discussing the number of surface hydroxyl groups per gram. This is in line with common practice in the cellulose literature which generally quantifies the number of hydroxyl groups based on the C_2, C_3 and C_6, at the surface of the nanocrystals, thus disregarding the ends of the CNC.

2.2 Powder X-ray diffraction

In this thesis, powder X-ray diffraction (XRD) is used to collect information on the crystallinity of the cellulose nanocrystals and on the size of the crystallites. The CNC diffractogram displays clear diffraction peaks as a result of the cellulose crystal structure as shown in Figure 2.2.1 (a typical X-ray diffractogram of CNC prepared during this study). In general, XRD is a rapid analytical technique designed to probe the crystal structure of crystalline materials and to determine the crystallite size.[199,200] Determination of the crystallinity of cellulose nanocrystals, similar to the determination of crystallinity of all polymers, is complicated by the varying dimensions of their crystalline domains. Metallic and ceramic crystals are held together by metallic and ionic bonds, which are much stronger bonds than the weaker hydrogen bonds and Van der Waals interactions holding together polymer crystal domains. In addition, polymers are generally partially crystalline instead of achieving full crystallinity due to entropy.

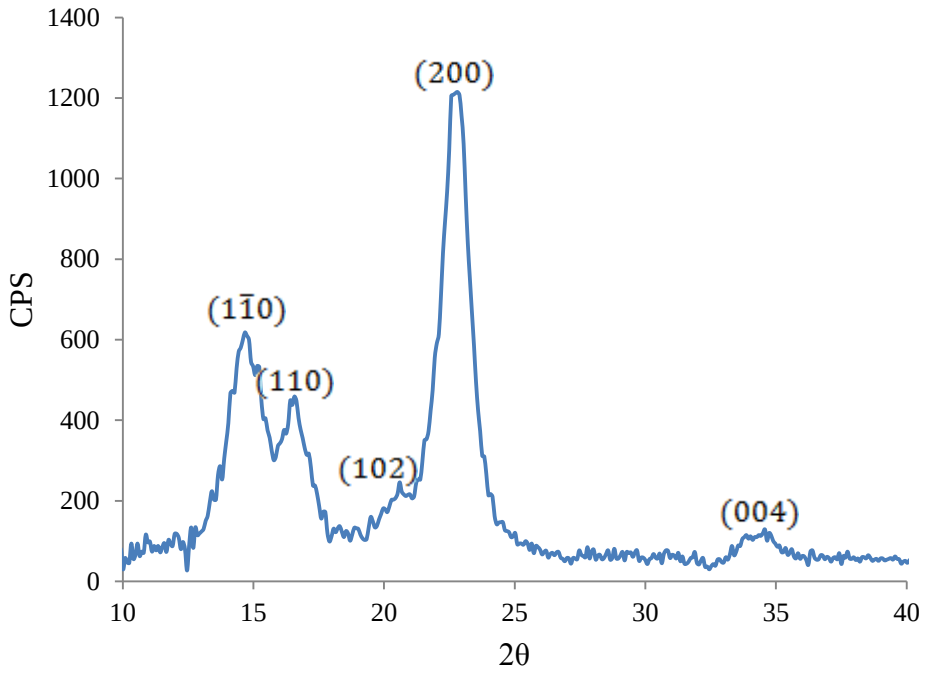


Figure 2.2.1 X-ray diffractogram of cellulose nanocrystals with peaks identified for corresponding diffracting planes

Shortly, in 1912, Max von Laue, discovered that the interaction of X-rays with a crystalline substance produced a distinctive interference pattern. By striking a pure anode of usually Cu with high energy electrons in a sealed vacuum tube, X-rays are generated which may be used in X-ray diffraction. The strongest monochromatic Cu radiation (Kα) wavelength is approximately 1.54 Å, 40 kV, 40 mA. A series of parallel plates and several scattering and receiving slits are used to create an incident beam of X-rays that are approximately parallel.[201-203] Scattering of X-rays on the sample will create diffracted beams of X-rays which are related to inter planar spacing characterising the crystalline powder according to Bragg's law:

$$n\lambda = 2dsin\theta, \tag{2.2.1}$$

where n is an integer, λ is the wavelength of the X-rays (Å), d is the inter planar spacing generating the diffraction (Å) and θ is the diffraction angle. This preferential diffraction from crystalline phases can be used to probe the crystalline state of the sample under investigation.

Powder X-ray diffraction of CNC gives rise to well identified crystalline peaks but these are also superimposed onto an amorphous contribution. The amorphous scattering contribution shows up as a softly rising and decreasing background, normally referred to as an amorphous halo. This complicates determination of the cellulose crystallinity as the contribution of the amorphous part must be reliably separated from the pure crystalline part in the powder diffraction pattern. When a well-crystallized sample with large enough crystallites is analysed, this will consequently give sharp diffraction peaks which can be easily isolated from the amorphous background. However, for cellulose with very small crystallites in the range of 20-50 Å in cross-section, this will cause considerable peak broadening and serious peak overlap.[200] As a result, the separation of the crystalline from the amorphous scattering signals is more difficult. Therefore, X-ray diffraction is used to determine the X-ray diffractogram of CNC after which software calculations will be used to determine the crystallite cross-section based on the width of the peaks representing the directions perpendicular to the fibre axis which have high intensity ((110) ($1\bar{1}0$) and (200) planes) with the crystallite length determined from the width of the peaks with reduced intensity (due to the preferred orientation determined by the alignment of the nanocrystals along the fibre axis), i.e. the directions parallel with the fibre axis ((102) and (004) plane).[200]

X-ray Powder Diffraction spectra were taken using a Panalytical X'pert PRO Multi-Purpose Device (Figure 2.2.2) operated in a flat-plate configuration with a "zero background" single crystal silicon plate, and under monochromated copper $K_{\alpha 1}$ radiation. The spectra were analysed using X'Pert HighScore Plus software.

The most common technique to determine the crystallinity of CNC is the Segal method (1959) based on the signal intensity determined at two points in the diffractogram.[204] This method consist in the measurement of the intensity of the (200) diffraction peak at $2\theta = 22.7°$ which represents both crystalline and amorphous cellulose, and the intensity measured at $2\theta = 18°$, the minimum between the (200) and (110) peaks, considered to represent the amorphous

scattering signal from the sample. The calculated percentage of crystalline material, the "crystallinity index" (χ_c), is then expressed as (equation (2.2.2)):



Figure 2.2.2 Panalytical X'pert PRO Multi-Purpose Device

$$\chi_c = \frac{I_{(200)} - I_{18^0}}{I_{(200)}} \qquad (2.2.2)$$

The crystallinity calculated for the CNC presented in Figure 2.2.1 after background subtraction using this method is calculated as χ_c = 0.909. The crystallinity determination was applied for three other cellulose batches and led to an average value of χ_c = 0.881 ± 0.0489 for all four batches. However, Segal's method considers that all the intensity at 18° is caused by amorphous scattering and that there is no influence coming from CNC or air scattering, which is a too significant simplification.[200] In addition, the determined amount of crystallinity is highly dependent on the positioning of the background which will be operator and sample dependent.

A more accurate recent method for crystal determination of cellulose that has many advantages over the traditional crystallinity determination used by Segal method, is based on Rietveld refinement that uses the recently published crystal structure of cellulose I_β followed by integration of the crystalline and amorphous (background) parts as shown by Thygesen *et al.*[200,205]

In comparison with Segal's method, Rietveld refinement, which was used for the crystallinity determination throughout this thesis allows a more accurate determination of the crystal structure from powder diffraction patterns and can even be used for quantitative phase analysis of chemical mixtures.[206] The refinement consists in fitting a known powder pattern from a crystal structure to an experimental powder pattern in a least-squares fitting procedure. Simultaneously, unit cell, crystal structure, peak profile parameters and background are fitted using the equation introduced by Rietveld for neutron diffraction data and this method is the current dominant method for obtaining structural information from powder diffraction data.[65,200,206]

Rietveld refinement was applied to CNC using High Score Plus software by fitting of the cellulose I_β pattern determined by X-ray and neutron fibre diffraction by Nishiyama *et al.* between 2θ = 10-40°.[32] The reliability of the procedure was verified in our group by Samuel Eyley during his PhD work.[65] Applying this method to the same crystallographic data to which Segal method was applied (Figure 2.2.1), I obtained a crystallite size of L = 6.65 nm and a crystallinity index of χ_c = 0.883. Rietveld refinement was applied to another three batches of cellulose giving an average χ_c = 0.813±0.123 (for the four batches) giving a smaller crystallinity than with the previously calculated method but more accurate.

Throughout this thesis, X-ray diffraction measurements were used to verify the state of the cellulose nanocrystal crystallinity before and after chemical modification. For modified cellulose nanocrystals, X-ray diffraction is used to confirm the retention of the cellulose I_β allomorph and that no other possible polymorph (e.g. cellulose II) is formed as a result of the reaction conditions. Application of Rietveld refinement is then used to determine any potential

decrease of crystallinity as a result of the introduction of an amorphous graft which can be compared with the expected loss of crystallinity determined using Elemental Analysis, as discussed in section 2.4 and described in the work of Eyley.[65]

Regarding the decrease of crystallinity, in 2007, Ifuku *et al.* worked on unmodified and modified cellulose fibres such as non-acetylated and acetylated fibres and the crystallinity decreases from 78 to 69 % for fibres and acetylated fibres respectively, while the crystallinity proportion of nanofibres drops from 81 to 74 %. The decrease of crystallinity is expected and explained by the degradation of the cellulose crystalline structure in the time of acetylation reaction.[207] As the acetylation reaction progresses, the surface cellulose chains are acetylated and therefore become soluble, being removed from the surface and thus exposing other new cellulose chains from the cellulose crystal which therefore further decreases the crystallinity of the remaining chains within the cellulose fibres upon acetylation continuation.[110]

In 2012, Salajkova stated in her work that X-ray diffraction measurements performed to verify any crystallinity alterations due to chemical reaction (different hydrolysis time) of cellulose nanocrystals, TEMPO oxidised nanofibrils or wood pulp displayed the characteristic patterns of cellulose I crystalline structure and the crystallinity of the cellulose nanocrystals was 78 – 80 % which was greater than the TEMPO modified nanofibrils and the original softwood pulp as a consequence of non-crystalline region degradation by HCl hydrolysis.[208] As stated by O'Sullivan *et al.*, another way of inducing amorphous structures except mechanical refining, which mechanically damages particles, roughens surfaces and causes surface chains disorder in the surface region, it is the existence of a surface as compared to the bulk, thus, any surface grafted molecules will contribute to the amorphous percentage increasing and consequently, crystallinity decreasing.[28,209] Furthermore, Solid-state NMR spectroscopy showed that the conformation of the cellulose chains at the surface and at the interior are different, with only the interior chains being truly crystalline.[210,211] Moreover, using molecular modelling, it was proved that hydrogen bonding configuration is different for the surface chains

and the interior chains and the mobility of the surface chains permits them to shift outside the lattice of cellulose I.[211,212] Therefore, the interior/exterior chain ratio may have influence on the crystallinity percent, with a contribution that is dependent on the cross-sectional of the given particle.[62]

2.3 Infrared Spectroscopy

Fourier Transform Infrared (FT-IR) spectra were collected on a Nicolet 380 FT-IR spectrometer (Thermo Electron Corporation) operated by OMNIC Version 7.2, in transmission mode using 1-2 mg of dry CNC sample in 200 mg of anhydrous KBr pellets.

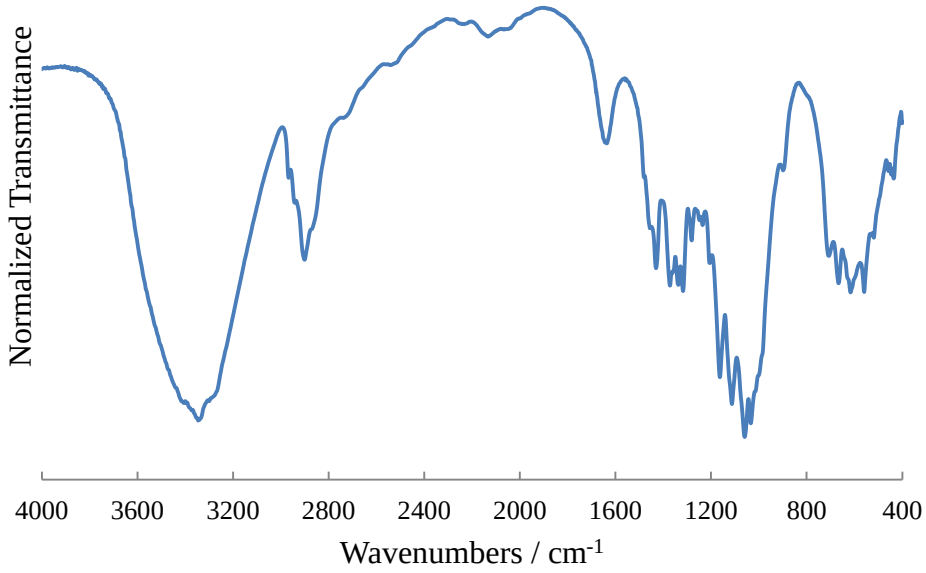


Figure 2.3.1 FT-IR spectrum of purified cellulose nanocrystals in a KBr disk

The KBr disks were prepared by physically mixing the sample with the KBr salt in an agate pestle and mortar followed by subjecting the powder to 10 t pressure using a laboratory press and anvil to cast a translucent disk for spectrum acquisition. The transmission spectra were recorded in infrared spectral width of 400 to 4000 cm^{-1}, with a resolution of 4 cm^{-1} and an accumulation of 16 scans, with KBr background subtraction. A purified CNC FT-IR spectrum is presented in Figure 2.3.1.

FT-IR spectrum band assignment of cellulose I_β was previously carried out by Maréchal and Chanzy:[213] $\bar{\nu}_{max}$ (KBr) / cm^{-1} 3345 ν(O−H), 2900 ν(C−H), 1636 δ(H_2O), 1430 δ(C−O−H), 1337 δ(C−O−H), 1317 δ(C−O−H), 1205 ν(C−O−C, glycosidic), 1163 ν(C−O−C, glycosidic, asym.), 1112 ν(C_2−OH), 1059 ν(C_3−OH), 1033 ν(C_6−OH), 707 ω(C-OH), 666 ω(C−OH), where ν is the stretching mode, δ is the bending mode and ω is attributed to the out-of-plane bending.[213] The broadening effect of cellulose bands is based on the H-bonding between the hydroxyl groups within the crystal structure, mainly ν(O−H).[213] Considering the large number of bands present in the spectrum, the correct identification of the modified CNC could be complicated by overlap of already existent bands associated with the nanocrystals characteristic vibrations and the specific bands correlated with the modification vibrations. FT-IR spectroscopy is thus only used qualitatively throughout this thesis.

2.4 Elemental Analysis

Elemental analysis (EA) of CNC provides the gravimetric composition and is used to calculate the degree of substitution of grafts on the CNC surface. EA helps to establish the empirical formula of the analysed compound and is commonly used to determine sample purity if heteroatoms are present.

Elemental analysis (C, H, N) was carried out by the University of Nottingham Department of Chemistry EA Service using a Model Elemental Analyser CE-440 CHN manufactured by Exeter Analytical. EA requiring sulfur determination (C, H, N, S) was carried out at the University of Nottingham, Faculty of Chemical and Environmental Engineering on a Thermo Scientific 1112 Flash EA. EA also requiring halogen determination was carried out by the University of Leeds Elemental Analysis Service. All samples were run thrice and the accepted deviation for the EA results was 0.4 %.

The method consists in combusting ca. 2 mg sample in a high temperature furnace (975 °C) in pure oxygen gas. A flow of helium gas is carrying the combustion products through the analytical system. The products are

completely oxidised by suitable reagents in the combustion tube and the by-products (sulfur, phosphorus or halogen gases) are also removed. The reduction tube is used to convert nitrogen oxides to molecular nitrogen and residual oxygen is removed. Subsequently, homogenization of the sample gases takes place after which they go through thermal conductivity cells. The absorption trap placed between the first pair of thermal conductivity cells removes the water from the sample gas. The differential signal read before and after water removal is used to determine the water content and thus the hydrogen content in the original sample. Similarly, the signal output difference is measured between the second pair of thermal conductivity cells where carbon dioxide is removed in between to determine the carbon content. Helium and nitrogen then remain and pass through the third thermal conductivity cell where the output signal is compared to a pure helium reference cell to determine the nitrogen concentration.[214]

The degree of substitution for CNC (initially mentioned in section 1.7) represents the number of functionalized hydroxyl groups per anhydroglucose unit. It is an important parameter used in the characterization of the extent or efficiency of the reactions of cellulose. As specified when describing the chemical structure of cellulose and CNC (Figure 1.3.1), there are one primary hydroxyl group per one AGU and two secondary hydroxyl groups on the next AGU, pointing upwards and available at the nanocrystal surface, and therefore three reactive hydroxyl groups per cellobiose unit on the surface of the CNC. This results in an average of 1.5 hydroxyl groups per AGU on the cellulose surface and thus, the maximum surface hydroxyl groups available for modification, equivalent with a maximum degree of substitution (DS_{surf}) = 1.5 which may be slightly influenced by the polydispersity of the nanoparticles in length and cross-section. When the secondary hydroxyl groups react is most likely to be the C_2–OH group as this is less involved in hydrogen bonding on the nanocrystal surface. Modification of the C_3–OH that is required for the hydrogen bonding that instills the rigidity in the cellulose chain usually results in a decrease of the CNC crystallinity due to dissolution of the surface chains.[215] As a result, when a DS_{surf} of 1 is achieved, this is generally

considered a very high degree of surface substitution which does not affect the CNC crystallinity. If the reaction takes place only at the primary hydroxyl group, this results in a maximum DS_{surf} = 0.5. The degree of substitution for cellulose modified in homogeneous reactions, where all the hydroxyl groups are available for modification, without any of them being trapped in a crystalline core, it ranges between 0 and 3 and the maximum value of 3 indicates that all three hydroxyl groups are substituted per AGU along the chain of cellulose.

When we consider the empirical formula of pure cellulose ($C_6H_{10}O_5$) with a molecular weight of an AGU of 162.081 g/mol, this results in the theoretical chemical composition presented in Table 2.4.1. The C, H and N contents determined by elemental analysis is slightly lower due to bound water which is consistent with the $\delta(H_2O)$ at 1636 cm^{-1} in the FT-IR spectrum and this has been confirmed in the literature to range between 3.5-5 %.[65]

Table 2.4.1 Elemental analysis results for pure cellulose nanocrystals

	C (%)	H (%)	N (%)
Theoretical	44.43	6.21	0
Determined	41.96	6.00	0

The determination of the degree of surface modification is influenced by the accuracy of EA (max 0.4 % standard deviation), by the purification of the product, which in this thesis was always done by Soxhlet extraction and by different experiments of the same modification. Thus, it is difficult to give an error in the DS calculations. EA results given for each modification in this thesis is an average of three measurements. Therefore, for unmodified cellulose presented in Table 2.4.1 the EA with the standard deviation is C (%) = 41.96 ± 0.19 and H (%) = 6.00 ± 0.04.

The calculation of the surface degree of substitution (DS_{surf}), or the number of hydroxyl groups that are modified per AGU, is carried out by making use of the theoretical composition of cellulose (resulted from the formula $C_6H_{10}O_5$) and the elemental composition as determined by EA. For example, equations 2.4.1 – 2.4.4 are used to calculate the values for C, H, O and X, which are

going to be used further, and are valid for esterification reactions between an acid and the hydroxyl groups, during which H_2O is removed from the combined composition of cellulose and the graft ((*p*-2), when H is determined in equation 2.4.2, and (*q*-1) for O determination in equation 2.4.3. For reactions with acyl halides, only one H atom is removed.

$$C(\%) = \frac{(6+n\times DS)\times 12.001}{MW+[12.001\times n+1.008\times(p-2)+15.999\times(q-1)+r\times A_r]\times DS}\times 100 \quad (2.4.1)$$

$$H(\%) = \frac{[10+(p-2)\times DS]\times 1.008}{MW+[12.001\times n+1.008\times(p-2)+15.999\times(q-1)+r\times A_r]\times DS}\times 100 \quad (2.4.2)$$

$$O(\%) = \frac{[5+(q-1)\times DS]\times 15.999}{MW+[12.001\times n+1.008\times(p-2)+15.999\times(q-1)+r\times A_r]\times DS}\times 100 \quad (2.4.3)$$

$$X(\%) = \frac{r\times DS\times A_r}{MW+[12.001\times n+1.008\times(p-2)+15.999\times(q-1)+r\times A_r]\times DS}\times 100 \quad (2.4.4)$$

where *n* is the number of carbons in the grafted molecule on the cellulose, *p* is the number of hydrogens in the grafted molecule, *q* is the number of oxygens in the grafted molecule, *r* is the number of atoms of an element X in the grafted molecule which is not present in cellulose, MW is the molecular weight of AGU, A_r is the atomic mass of the element X, and DS is the total degree of substitution.

In equation (2.4.1), C (%) is the number of C atoms found in cellulose plus the number of carbons found in the grafted molecules multiplied by the total degree of substitution and the molecular mass of carbon, everything divided by molecular weight of an AGU and individual products between the atomic mass of each element and the number of atoms for each element found in the modification everything multiplied by 100. The equation also applies for H, O and X (N, S or halogen (Cl, Br)). The schematic representation of the entire calculations is given in Figure 2.4.1.

As it was mentioned earlier, the determined composition of unmodified cellulose contains some water traces and therefore the small % difference between the theoretical C(%) calculated in one AGU (Table 2.4.1) and the carbon determined by EA (Table 2.4.1) (e.g. 44.43 – 41.96 = 2.47) will be

subtracted from the previously calculated C(%) (Equation 2.4.1) for the modification.

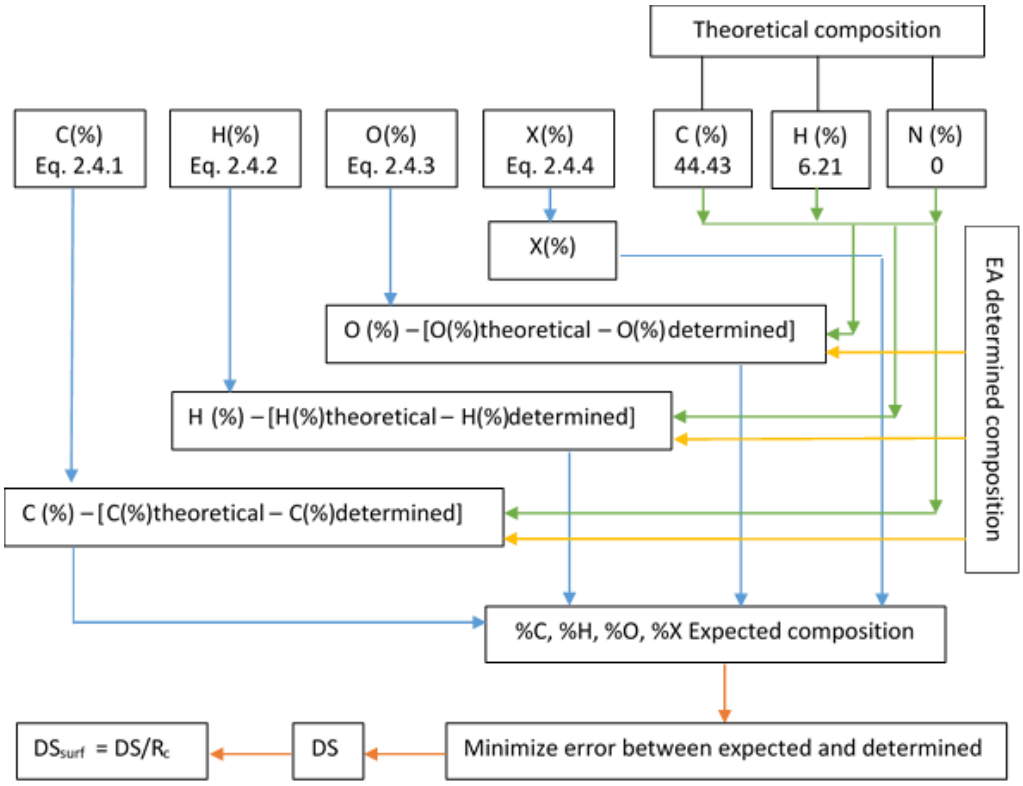


Figure 2.4.1 Schematic representation of the entire DS_{surf} calculations

This subtraction is applied also to O and H only, as can be seen in formulas 2.4.5-2.4.7 and to be distinguished from the previous calculations for modified cellulose, these C, O, H and X elements are called expected. The element X is left unaffected as this appears only in the modification and is not affected by the water found in the cellulose core (equation 2.4.8).

$$C(\%)\ expected = C(\%) - (C(\%)_{theoretical\ cellulose} - C(\%)_{determined\ in\ cellulose}) \quad (2.4.5)$$

$$H(\%)\ expected = H(\%) - (H(\%)_{theoretical\ cellulose} - H(\%)_{determined\ in\ cellulose}) \quad (2.4.6)$$

$$O(\%)\ expected = O(\%) - (O(\%)_{theoretical\ cellulose} - O(\%)_{determined\ in\ cellulose}) \quad (2.4.7)$$

$$\%X\ expected = \%X \quad (2.4.8)$$

$$DS = R_c \times DS_{Surf} \quad (2.4.9)$$

By the minimization of the error between the values calculated by equations 2.4.5-2.4.7 and the value of the elements given by EA for the modified cellulose, using an iterative method, the degree of substitution will be brought up by the mathematical calculations (Excel software, What if Analysis, Goal Seek which will find the right input when it is indicated the value of interest (DS)). In section 2.1, the chain ratio was calculated. Therefore, using the chain ratio value (R_c) (~0.3, calculated with X'Pert HighScore Plus software, for each modified cellulose) the surface degree of substitution (DS_{surf}) results (Equation 2.4.9).[65] This calculation method was used for all the modification presented in this thesis, using the specific EA composition for the CNC as determined experimentally.

Link between XRD and EA

The following example will be used to describe how EA and XRD results will be crosschecked for improved accuracy. Take for example a carbazole modified CNC with the experimentally determined EA of the carbazole-9-yl-acetate cellulose product: C (%) = 47.31, H (%) = 5.77 and N (%) = 0.88. The crystallinity of unmodified CNC used for this modification had a χ_C^R = 0.796 while carbazole-9-yl-acetate cellulose had a χ_C^R = 0.668, with both crystallinities determined by XRD and Rietveldt refinement. Thus, the crystallinity difference between the starting material and the modified material is 0.128, i.e. a loss of crystallinity of 12.8 %. For this modification, EA gives a 0.88 % of N, which relates to a DS_{surf} = 0.39. With the nitrogen content of nitrogen in carbazole-9-yl-acetate ($C_{14}H_{10}NO^-_2$) 6.25 %, the mass percentage of the modification (the graft) in the cellulose sample can be calculated as 0.88/6.25 = 14.08 %. This value for the mass % of the graft is very close to the loss of crystallinity in the overall sample as determined by XRD as would be expected since the graft is non-crystalline and thus introduces a non-crystalline contribution equal to its mass % in the overall sample. By comparing these results, XRD and EA can be used to cross-verify their results independently.

2.5 X-ray photoelectron spectroscopy

In 1960s Kai Siegbahn and his group developed an analysis method which initially was known as Electron Spectroscopy for Chemical Analysis (ESCA), and currently gets referred to more commonly as X-ray Photoelectron Spectroscopy (XPS).[216] XPS is a surface sensitive spectroscopic method based on the photoelectric effect which refers to the fact that electrons are emitted from the surface of a material when the material is irradiated with small wavelength visible light, UV-light or X-rays, due to absorption of energy. The electrons emitted in this manner are referred to as photoelectrons and their kinetic energy depends on the wavelength of the electromagnetic radiation as well as the characteristics of the spectrometer (Equation 2.5.1):[217-219]

$$E_k = h\nu - E_b - \varphi \qquad (2.5.1)$$

E_k = kinetic energy of the electron; h = Plank's constant; ν = frequency of the excitation radiation; E_b = binding energy of the photoelectron, i.e. the energy required to remove an electron from the orbital to the Fermi level, and φ = the work function of the spectrometer (the energy required to remove an electron from the Fermi level to the vacuum level).

Thus, the kinetic energy of the photoelectron is the energy of the X-ray photon minus the energy needed to extract the electron from the core orbital and minus the work function.[220] In other words, the binding energy can also be considered as the energy difference between initial state and final state of the electron as a consequence of photoemission and a schematic representation of the photoelectric effect is given in Figure 2.5.1.

Basically, XPS measures the binding energy (BE) of the electrons emitted from a sample which is ionised *in vacuo* by monoenergetic soft X-ray radiation.[221] XPS gives information on the relative concentration as well as on the chemical and electronic environment of elements. The penetration power of the photons in a solid is limited to approximately 1-10 nm, dependent on the sample composition and the angle of X-ray incidence. The XPS experiments require UHV (ultra-high vacuum) to ensure a near collision free environment that

provides a free path for photoelectrons emitted from the sample to the detector, free from scattering by inelastic collisions with gas molecules. During the experiment, the removal of photoelectrons leaves behind a positively charged surface and in the case of conducting samples these holes are quickly filled with electrons flowing through between the spectrometer and the sample surface through electric contact between the material and the spectrometer.

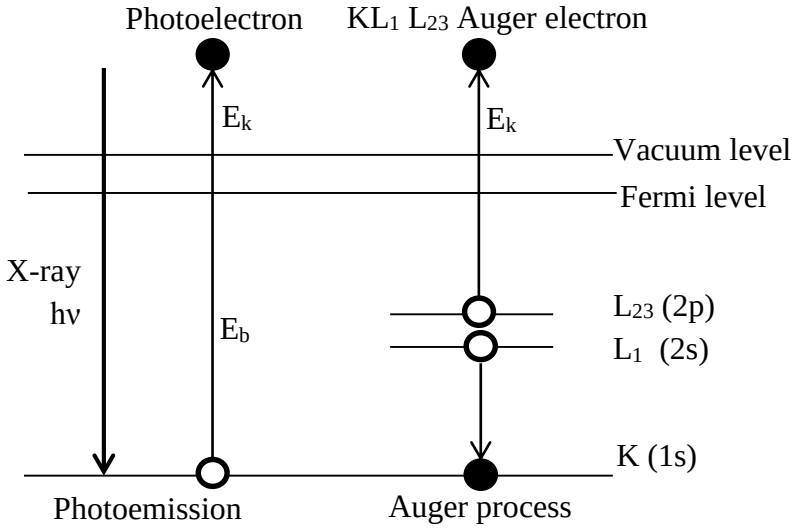


Figure 2.5.1 Schematic representation of photoelectric effect, the principles of XPS. An X-ray photon (hν) causes the ionization of a core electron on the sample surface and a photoelectron is emitted with the kinetic energy (E_k) equal to hν minus the binding energy (E_b) and the work function (φ). The created empty hole left by the photoelectron is filled up by an electron from a superior energy level ($L_1 \rightarrow K$), concomitant with the releasing of an Auger electron due to the relaxation energy emitted (L_{23} → Auger). Schematic representation adopted after Niemantsverdriet.[217]

As a result, the alignment of Fermi levels and the spectrophotometer are achieved with a constant work function (≈4.5 eV). If an insulating or a poorly conducting sample such as cellulose is exposed to X-rays, the positive charges add to the surface and are not inherently neutralised by electron flow from the spectrometer. This alters the energy of the Fermi level and hence the magnitude of the working function. As a result, the BE of the photoelectron peaks would be higher than the expected values.[220] In order to counterbalance

this unwanted variation due to this charging effect, charge neutralization of the sample is carried out during the experiment with low energy electron insertion onto the sample.[222] One must be careful as electron insertion can also exceed the charging effect resulting in a measured lower BE. During these experiments careful charge neutralization was applied, in addition to calibration of the whole spectrum by referencing it to a photoelectron peak of known BE process, also known as charge correction, in agreement with common procedures.[223-225]

The samples in this work were analysed using a Kratos AXIS ULTRA (Figure 2.5.2) with a monochromated Al kα X-ray source (1486.6 eV) operating at 10-15 mA emission current and 10-12 kV anode potential at 100-180 W. During analysis, the samples are mounted onto the XPS standard bar using double sided low silicone tape. For each sample, three different points were analysed and the values presented in the thesis are an average of the elements composition at these three points.

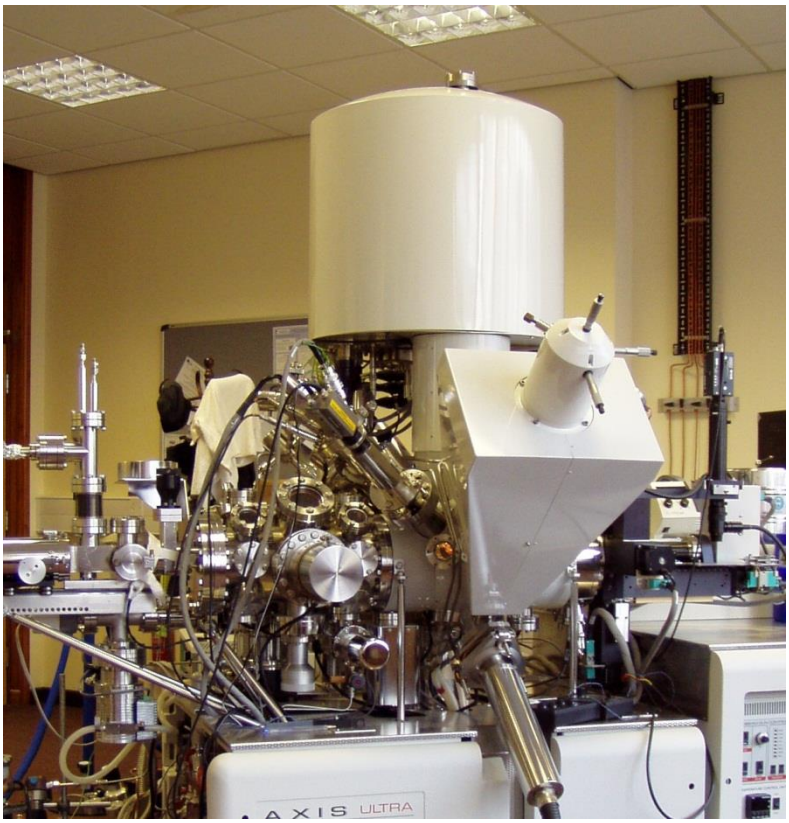


Figure 2.5.2 Kratos AXIS Ultra used for X-ray Photoelectron Spectroscopy

There are two types of spectra that were recorded: a wide (survey) scan covering all or a wide range of binding energies, and a high resolution scan which focuses only on a particular energy region surrounding the binding energy of a specific atom. The calibration of the spectrograms (charge correction) was done using the main C1s peak at 285 eV. Quantification of the relative atomic fractions of each element in the sample surface was carried out using atom-specific sensitivity factors, as each atom energy band has a specific sensitivity to electron emission.[224] XPS data analysis was carried out using CASAXPS software with Kratos sensitivity factors, specific to the XPS spectrometer, in order to determine relative atomic percent (at%) values from the peak areas. High resolution peaks that enable quantification of the atomic environment of the investigated atom were decomposed/deconvoluted using pseudo-Voigt peaks (line profile that results from the convolution of a Gaussian and a Lorentzian profile) together with an asymmetric correction taking into account the vibrational modes of covalent bonds. Covalent bond vibrations induce peak broadening at higher binding energies as a consequence of absorption of photon energy by vibrational transitions in the bonds connected to the atoms of interest.[65,220,226]

Figure 2.5.3 presents a typical wide scan for purified CNC in which C1s and O1s are present along with the O2s and also Auger lines, C KLL and O KLL. The S2p spectrum is given as a detail insert image as it is not readily visible in the larger spectrum. Sulfur is present because sulphate half esters are introduced during sulfuric acid hydrolysis of cellulose. The relative atomic percent concentrations of carbon, oxygen and sulfur are 56.34 at%, 43.57 at% and 0.08 at%, respectively. Atomic percentage composition run for three cellulose nanocrystals batches revealed the following average vales with corresponding standard deviation: 56.86 ± 2.21 % C1s, 42.88 ± 2.03 % O1s and 0.12 ± 0.04 % S2p.

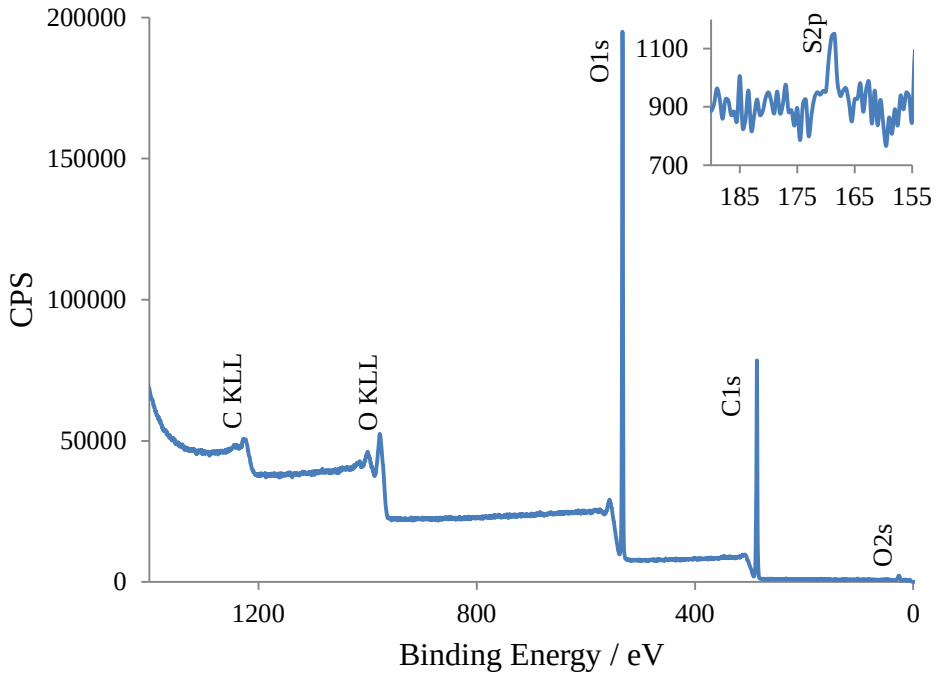


Figure 2.5.3 XPS wide scan of cellulose nanocrystals identifying the main peaks, C1s and O1s along with O2s and Auger Transitions C KLL and OKLL. Inserted spectrum presents a zoomed in image of the S2p signal.

Although the referencing of the spectrograms is generally done relative to the main C1s peak at 285 eV, the C1s high resolution scan (Figure 2.5.4 a) was calibrated at 286.50 eV which corresponds to the C–O environment.[224] At this position are found the C–O–C and C–OH contributions with a mean chemical shift of 1.5 eV relative to the saturated hydrocarbon (C1s = 285.00 eV). This signal is the largest for pure cellulose as it corresponds to the chemical environment for five atoms in the cellulose AGU.[227] The small contribution at 284.9 eV corresponds to the C–C environment with a magnitude of 8.1 at%. As can be seen in Table 2.5.1, the relative areas of C–O, O–C–O and O–C=O are 76.42 %, 14.2 % and 1.28 % eV. There is a minor difference between the ratio of C–O and O–C–O from the expected theoretical 5:1 ratio (5.38:1) and a possible explanation for this difference could be due to the insufficient averaging of information depth of environments in bulk cellulose. The peak identified at 288.1 eV corresponds to a carbon with two bonds to oxygen (O–C–O/C=O) of which there is only one atom per AGU. The component at 289.9 eV consists of to a carbon triply bonded to oxygen (O–C=O) corresponding to

a small fraction of oxidation as a results of the sulfuric acid hydrolysis. The O1s high resolution spectrum (Figure 2.5.4 b) is composed of two oxygen environments with a 1.09 FWHM, with an intensity ratio of 2:3 as expected from the chemical structure of cellulose, corresponding to O–C–O and C–OH at binding energies of 533.21 eV and 532.61 eV respectively, in agreement with the literature.[228] The separation of the two contributions was constrained to 0.6 eV also in line with the literature.

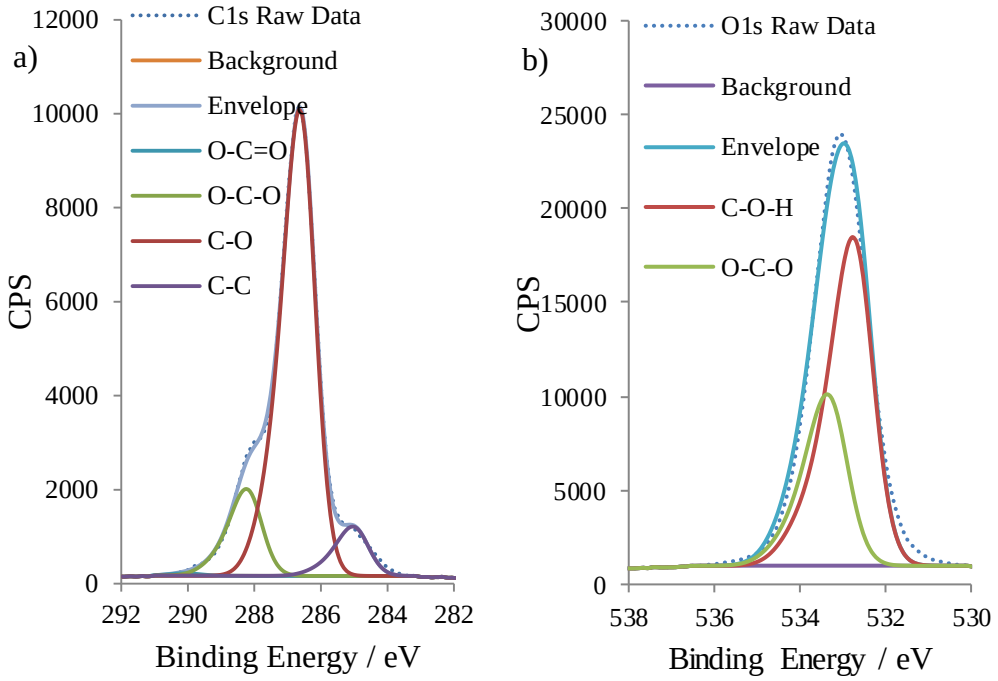


Figure 2.5.4 a) C1s and b) O1s high resolution of cellulose nanocrystals identifying the components peaks

The XPS data displayed in Table 2.5.1 are in broad agreement with the expected values for the stoichiometry of cellulose. This is as expected since for CNC the surface has the same composition as bulk cellulose. This will not be the case for modified CNC where the size of the crystal relative to the analysis depth does not provide precise quantification of the surface species.[229] Yet, the technique supplies important data on the chemical state of the species found on the surface of modified CNC.

Table 2.5.1 Detailed XPS data of cellulose nanocrystals

Orbital	Component	BE /eV	FWHM	Rel. A / % [a]	at%
C1s	C–C	284.90	1.08	8.1	4.56
	C–O	286.50	1.08	76.42	43.06
	O–C–O	288.11	1.08	14.2	8.00
	O–C=O	289.97	1.08	1.28	0.72
				100	56.34
O1s	C–O–H	532.61	1.09	66.68	29.05
	O–C–O	533.21	1.09	33.32	14.52
				100	43.57
S2p	S 2p 3/2	168.95	1.38	66.69	0.05
	S 2p 1/2	170.21	1.38	33.31	0.03
				100	0.08

[a] Relative area = component area×100/sum area of same

XPS of modified cellulose nanoparticles may also involve the analysis of heteroatoms such as S2p, N1s, Br3d and F1s. All the high resolution spectra of these heteroatoms were referenced to the C1s peak with a maximum at a binding energy of 286.5 eV. Peak fittings were done using peaks at expected positions for potential functional groups that could occur in the products, as referenced in literature. Also, the peak area for each element is constrained to the expected p- or d-orbital ratio such as 2:1 for S p-orbitals and 3:2 for Br3d d-orbitals all of them being fitted to the same FWHM for each individual deconvoluted peak in one high resolution element spectrum.

XPS can have an error of up to 5% close to the detection limit. Consequently, the errors become more important for small levels of modification. However, XPS coupled with other analysis techniques substantially contributes to the final product identification.

2.6 Atomic Force Microscopy

A direct observation method for particle dimensions and shape of cellulose nanocrystals is microscopy. Atomic force Microscopy (AFM) allows the observation of nanocrystals through height and modulus differences relative to

a flat support. The preparation of the samples for AFM imaging was performed according with the method used by Lahiji *et al.* in which few drops of a solution of 1.2 wt % suspension of CNC were placed on 1 cm × 1 cm freshly cleaved mica. The samples were rinsed with deionized water before drying and blown dry with Ar.[230] AFM measurements were performed by Dr. Xinyong Chen at University of Nottingham, Laboratory of Biophysics working on a 3100 AFM (Bruker) with a NanoScope IIIa Controller (Digital Instruments) in tapping mode. The manipulation of the AFM images was performed using Gwyddion 2.32 software.

The AFM imaging consisted in bringing a very fine sharp tip to either be at a very close distance to or come in contact with the sample. The dimensions of the tips are between few microns long and less than 100 Å in diameter. The tip is attached at the free end of a cantilever that is up to 200 μm long. The sample is scanned in tapping or contact mode beneath the tip which in function of the surface forces can be attracted or repealed. The topographical representation of the sample is the resulting image of all the deflections that are registered and analysed by the imaging software.

Figures 2.6.1. and 2.6.2 are AFM images of a CNC sample in which can be seen that the lengths of the CNC used here are between 100 nm up to 300 nm and an approximate width of 10 nm which corresponds with the literature values for CNC.[45]

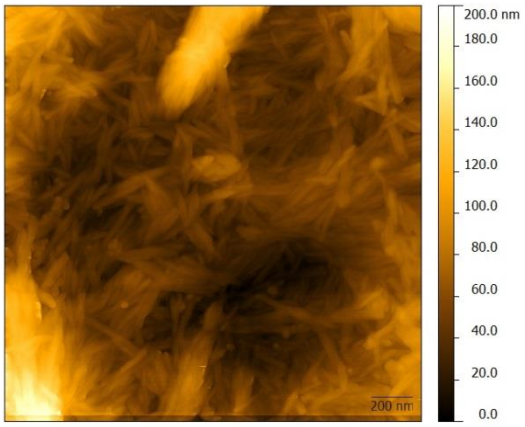


Figure 2.6.1 AFM image of Cellulose nanocrystals obtained in tapping mode over 2 μm

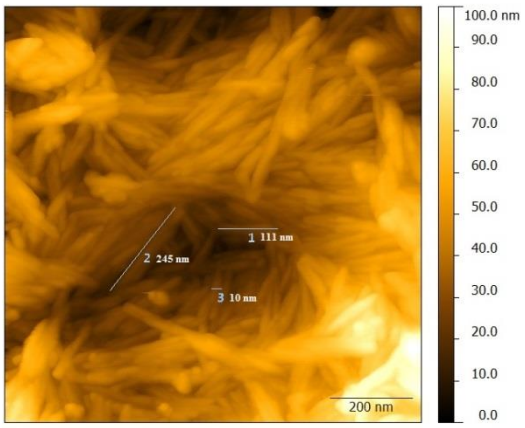


Figure 2.6.2 AFM image of Cellulose nanocrystals obtained in tapping mode over 1 μm 2 D image

2.7 Transmission Electron Microscopy

The second method used to observe the shape and dimensions of cellulose nanocrystals is Transmission Electron Microscopy (TEM). Drops of cellulose nanocrystal suspension of 0.001wt % were deposited on a carbon-coated Cu electron microscope TEM grid (Grid S160H) which was previously cleaned and partially oxidised using a Plasma Cleaner, Model 1020 operating under 25% oxygen atmosphere. After complete drying, the specimens were negatively stained with 2% uranyl acetate and observed using a JEOL JEM - 2000FXII Scanning Transmission Electron Microscope operated by Mr. Nigel Neate, at an accelerating voltage of 80 kV. The negative films were digitized and used for analysis.

Figure 2.7.1 illustrates a typical TEM image in which the elongated nanoparticles prepared by acid hydrolysis with sulfuric acid are well dispersed, their lengths vary between 100 to 300 nm with an average width of 10 nm and have a whisker-like morphology.[45]



Figure 2.7.1 TEM Micrograph of negatively stained individual cellulose nanocrystals

2.8 UV-Vis and Fluorescence Spectroscopy

Considering the aims of this thesis, characterization of the cellulose nanoparticles discussed here will also include cellulose modified with fluorescent grafts. Therefore, it is necessary to give a brief description of absorption and fluorescence properties.

Absorption spectra were measured on a PerkinElmer Lambda 25 UV-Vis Spectrometer operated by Lambda 25 software and using quartz cell with a path length of 1 cm in the 190 – 700 nm range with 1 nm resolution. The Beer–Lambert Law (Formula 2.8.1) relates the absorption of light (A) to the properties of the material: concentration (c), absorptivity (ε) and path length (l); thus, the molar extinction coefficient/absorptivity is a measure of the strength of a substance to absorb light at a specific wavelength.

$$A = \varepsilon c l \tag{2.8.1}$$

Furthermore, fluorescence measurements were carried out on a Varian Cary Eclipse Fluorescence Spectrophotometer, using a Xenon flush lamp, operated

by Cary Eclipse software. The measurements were performed in a 1 cm path length clear faced quartz cuvette.

Fluorescence is the process in which an electron of a fluorescent molecule absorbs a photon of excited light at a specific wavelength followed by the promotion of the electron from its ground state to an excited state. During the short excitation state (lifetime), a small part of energy is lost by molecular collisions or transferred to another molecule while the rest of the energy is emitted as a photon when the electron returns to the ground state (Jablonski diagram, Figure 2.8.1).

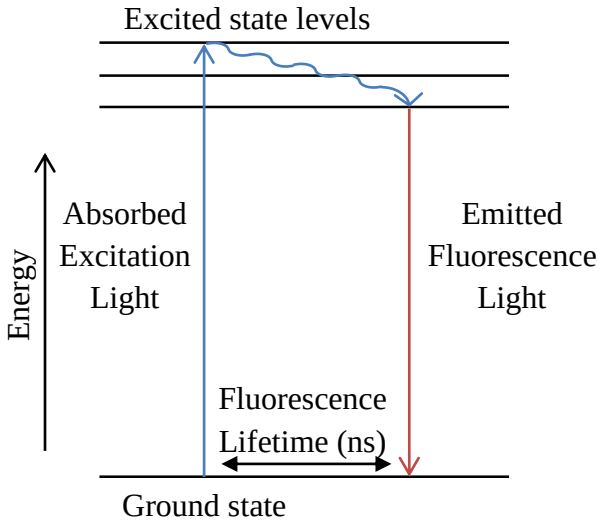


Figure 2.8.1 Jablonski energy diagram of fluorescence adapted from ref[231]

The fluorophore and the chemical environment of the fluorophore influence the amount and the wavelength of the emitted energy. Fluorophore compounds are also named as chromophores; however, the difference between them is that chromophores absorb light while fluorophores also emit light. The used term for light emission is luminescence, while fluorescence actually measures the transition from higher to lower singlet states of molecules where the life time is in the range of nanoseconds.[232]

The amount of fluorescent molecules can be mathematically determined (Equation 2.8.2) as the ratio of fluorescent cellulose concentration (from a calibration curve of the respective molecule for the corresponding absorption) and the known amount of modified cellulose suspended in the solvent.

$$fluorescent\ molecule\ \frac{mol}{g} = \frac{conc.\,of\ fluorescent\ (\frac{mol}{L})}{known\ conc.\ of\ grafted\ \ cellulose\ (\frac{g}{L})} \qquad (2.8.2)$$

Both, absorption and fluorescence will be applied in Chapter 4 and absorbance in Chapter 5 as well.

2.9 Zeta potential measurement

In this thesis, the stability of the cellulose nanocrystals suspensions before and after modification, as well as the cationic nature of the developed products was examined by measurement of zeta potential (ζ). Zeta potential is the scientific term for electro kinetic potential in colloidal dispersions.[233] Theoretically, zeta potential is the electric potential in the double layer (DL) interface localized in the slipping plane relatively to an outside bulk point (Figure 2.9.1).

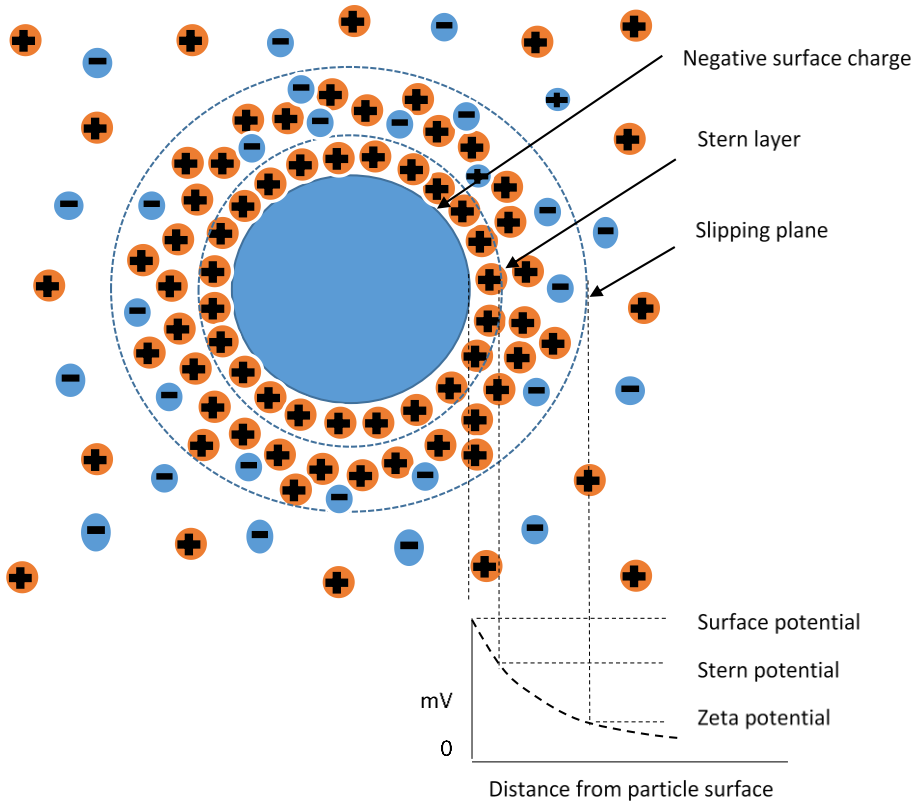


Figure 2.9.1 Diagram indicating the concentration of ions and ζ-potential as a function of distance from the negatively charged surface of a particle suspended in a dispersion environment

The potential is calculated using Smoluchowski equation which considers spherical particles morphology. Thus, the meaning of ζ-potential magnitude for this case cannot be used for quantitative analysis but only for qualitative comparison.[234] Being a key indicator of the stability of the nanoparticles, the magnitude of zeta potential shows the degree of electrostatic repulsion between neighbouring similar nanoparticles in a colloidal environment. Thus, colloids with high zeta potential (> 30 mV negative or positive) present a moderate to excellent stability while the one with low potential (< 30 mV negative or positive) tend to flocculate.[235,236]

The ζ-potential was recorded on a ZetaSizer Nano from Malvern and the value considered here are an average of 10 measurements.

PART II

CELLULOSE FUNCTIONALIZATION

3 Cellulose nanocrystal esters

The introduction chapter presented the wide range of methodologies that can be used to modify the surface of cellulose nanocrystals, with a strong focus on the synthesis of esters. Based on the previously synthesised cellulose esters discussed in the literature including esters that are industrially produced (please see Section 1.7, Table 1.7.1), this chapter will develop and enlarge the esterification procedures already in existence and will present new esterification products that will serve as building block for further functionalization as will be presented.

The discussion in this chapter starts from one esterification reaction of cellulose nanocrystals with methacrylic acid, initially developed in our group as a simple method for the grafting of carboxylic acids which generally gave a low degree of substitution. This esterification path is based on a literature procedure in which carbodiimide is used as a coupling agent in a Steglich esterification.[136] The acids used in this esterification procedure were acrylic and methacrylic acid, chosen because they are simple and small molecules, and because of their carbon-carbon double bond functionality that will be used for click-chemistry modification in Chapter 6.

The investigations are then extended to the different esterification methods mentioned in the introduction section (*p*-toluenesulfonyl chloride/pyridine or *p*-toluenesulfonyl chloride/triethylamine and esterification with acryloyl chloride). Each of the acids will be esterified using two esterification paths (carbodiimide mediated esterification and *p*-toluenesulfonyl chloride/pyridine or *p*-toluenesulfonyl chloride/triethylamine) while acryloyl chloride will only be studied under specific conditions with a very high molar excess as required. This work will allow a more structured investigation of all of these different

esterification strategies of cellulose nanocrystals which is still lacking in the current literature.

3.1 Carbodiimide mediated esterification for cellulose acrylate nanocrystals synthesis

The first methodology used for the esterification of surface hydroxyl groups of CNC with carboxylic acids such us acrylic and methacrylic acid was the use of a carbodiimide as a coupling agent. This methodology was developed based on a previous reaction carried out in our group in which methacrylic acid was used and final product had a DS_{surf} = 0.28.[65] Based on literature data, the selected coupling agent was *N*,*N*-diisopropylcarbodiimide (DIC) in the presence of DMAP as a base, as it was used in the esterification of Wang resins, a cross-linked polystyrene resin functionalized with benzyl alcohol.[237] This methodology will also be used later in this thesis (Chapter 4, section 4.5) for the cellulose nanocrystal surface modification with carbazole-9-yl-acetic acid.

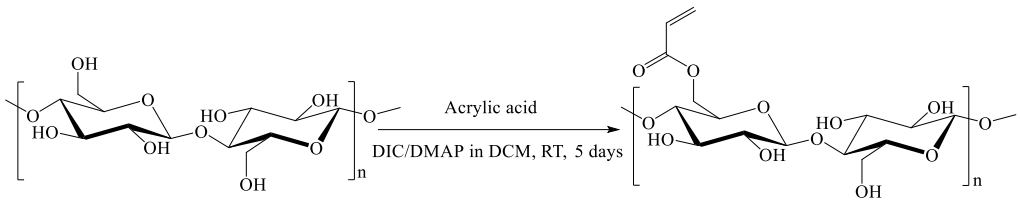


Figure 3.1.1 Esterification of cellulose nanocrystals with acrylic acid using DIC/DMAP

CNCs were thus esterified with equimolar amounts of acrylic acid, DIC and DMAP (Figure 3.1.1) in a ratio of 1:5.5:5.5:0.01 [OH]:[AA]:[DIC]:[DMAP] (with CNC displaying 3 mmol/g OH groups) in dry DCM under inert atmosphere, for 5 days at room temperature. Samples were subsequently purified by Soxhlet extraction with DCM for 24 hours and with EtOH for a further 24 hours followed by drying *in vacuo* before characterization. The resulting white nanocrystals were fully characterised in order to understand the reaction pathway and the extent of functionalization. The infrared spectrum of the esterified CNC (Figure 3.1.2) presents a well resolved sharp band at

1726 cm^{-1} that corresponds to a carbonyl stretching vibration band characteristic for esters, and also another band at 1636 cm^{-1} corresponding to the C=C bond stretching vibration in addition to another peak at 809 cm^{-1}. According to the data published by the Spectral Database for Organic Compounds, the C=O group in acrylic acid is found at 1705 cm^{-1}, in methyl acrylate at 1732cm^{-1} and in ethyl acrylate at 1728 cm^{-1} and C=C vibrations in acrylic acid are found at 1637, at 1636 cm^{-1} in methyl acrylate and at 1638 cm^{-1} in ethyl acrylate.[238] Thus, the infrared spectra of modified cellulose acrylate presents bands in the same spectral range as the methyl and ethyl acrylates where the presence of ester functionality necessitates a higher energy to vibrate and therefore resulting in a higher wavenumber in comparison with the unbound acrylic acid. Furthermore, the band at 809 cm^{-1} is due to =C–H and $=CH_2$ out-of-plane bending.[239] FT-IR for three repetitions of the reaction indicate the carbonyl frequency for the modified product occurs at an average value of 1727.63 ± 4.69 cm^{-1}. Therefore, the reaction product could be confirmed as cellulose acrylate (1-ACNC).

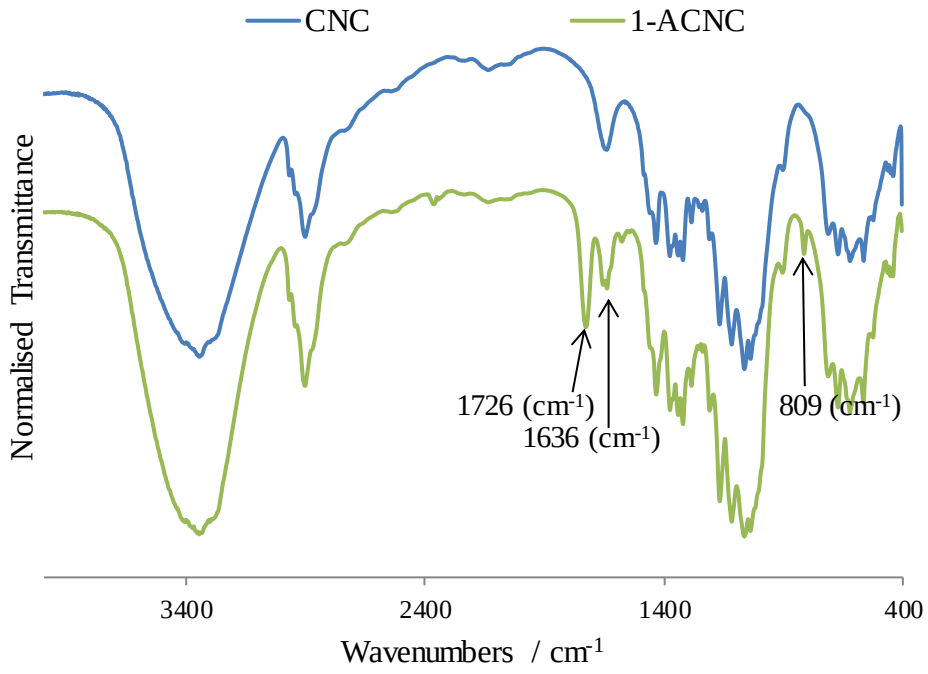


Figure 3.1.2 FT-IR spectrum of CNC and cellulose acrylate (1-ACNC) synthesised by the DIC/DMAP methodology

As this reaction product contains the same elements as the initial starting material, the calculation of the degree of modification based on EA is slightly more difficult as no heteroatoms can be used, and thus needs to be based on the carbon content. EA results (Table 3.1.1) show an increase of 2.02 % C relative to the initial CNC carbon content, which indicates the presence of a larger amount of carbon on the surface, corresponding to a DS_{surf}(C) = 0.94. This agrees with the modification of the primary hydroxyl group and almost one secondary hydroxyl group on each AGU (most likely the C_2–OH group as this is less involved in hydrogen bonding than the C_3-OH on the nanocrystal surface) on the surface of the nanocrystals. A DS_{surf} of 1 is generally considered close to the maximum DS_{surf} before the crystal structure is affected as modification of the C_3–OH removes the hydrogen bonding possibility of this OH which is required for chain rigidity along the cellulose backbone.

Table 3.1.1 Elemental analysis results for CNC and cellulose acrylate (1-ACNC)

Sample	C (%)	H (%)	N (%)	DS_{surf}(C)
CNC	41.95	5.99	0	
1-ACNC	43.97	5.96	0.15	0.94

The integrity of the crystalline structure was determined by X-ray diffraction (Chapter 3 Appendix, Figure 10.1.1) and after applying Rietveld refinement to the XRD diffraction pattern, the crystallinity index was determined to be χ_C^R = 0.775, representing a crystallinity drop of 10.8 % compared to the initial unmodified CNC (χ_C^R = 0.883). From EA (and a DS_{surf} of 0.94), the mass of introduced modification (which is amorphous) calculated based on the carbon content is ~4 %. This value, which is not calculated on a heteroatom but on carbon also found in the cellulose backbone, only shows slight agreement with the loss of crystallinity determined by XRD (4% *vs.* 10%) but still falls within the confidence interval for the Rietveld method ($\chi_C^R \pm 0.06$)[200] and so the disagreement can be considered to be just within the margin of error. Also, EA indicates a very small nitrogen content (0.15 %). This nitrogen could be found in the chemical composition of the secondary reaction product, diisopropylcarbodiimide. Therefore, this percentage contributes to the

amorphous content in the sample. The increase in the amorphous content would then be influenced by the mass of the modification in the sample and also this remaining secondary product. By dividing the EA nitrogen percentage by the percentage of nitrogen in the diisopropylcarbodiimide (19.42 %), it increases the amorphous content determined from EA from ~4% to about 5% %, bringing EA and XRD results closer together.

The XPS wide scan (Chapter 3 Appendix, Figure 10.1.2) of this reaction product showed carbon and oxygen as expected but also very small peaks of nitrogen and fluorine. The fluorine is believed to be due to contamination in the instrument as the reaction product was never in contact with fluorinated products and the XPS service is used to investigate fluorine-containing ionic liquids. The nitrogen signal however could be related to the reaction by-product, which, despite the 48 h Soxhlet extraction, is still present in a very tiny amount (0.25 at.% in XPS and 0.15 % in EA).

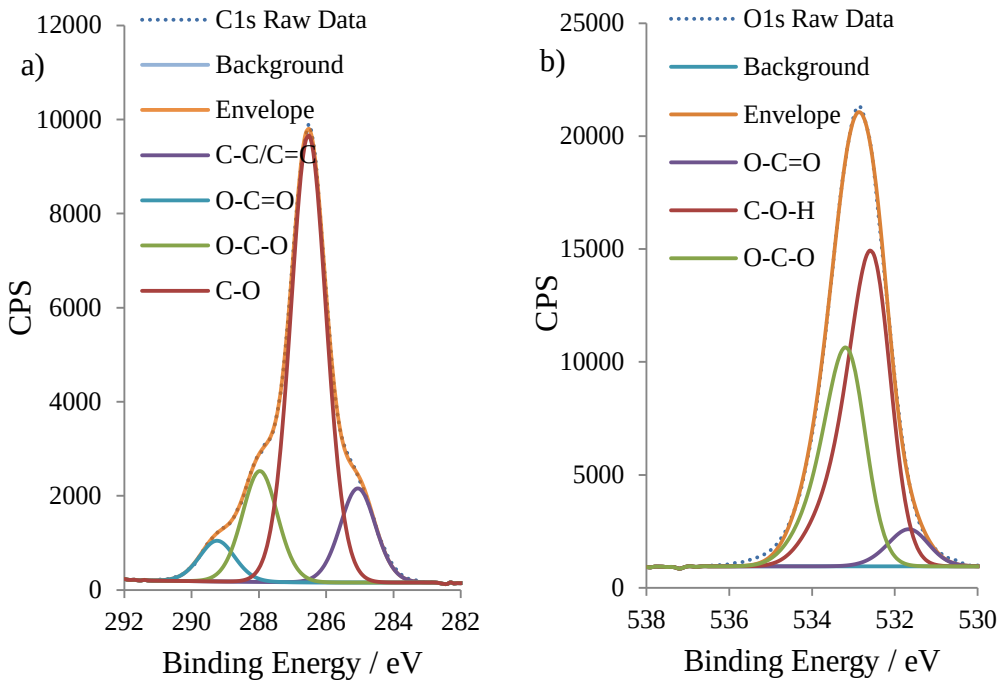


Figure 3.1.3 a) C1s high resolution spectrum of cellulose acrylate (1-ACNC) synthesised by the DIC/DMAP methodology; b) O1s high resolution spectrum of cellulose acrylate (1-ACNC) synthesised by the DIC/DMAP methodology

Deconvolution of the high resolution scans of C1s (Figure 3.1.3 a) and O1s (Figure 3.1.3 b) show the presence of O–C=O environment at 289.38 eV and at 531.34 eV respectively, indicating successful esterification. Also, if the C–C environment (BE = 285.07 eV in Table 3.1.2) is compared with the initial C–C component in cellulose, an increase from 4.52 to 10.03 at% is observed. This difference is attributed to the C=C environment in the grafted acrylate which occurs at almost the same BE as C–C, with the mean value of the C=C environment BE being 0.27 eV lower shifted.[240]

Table 3.1.2 Detailed XPS data of cellulose acrylate (1-ACNC) synthesised by the DIC/DMAP methodology

Orbital	Component	BE /eV	FWHM	Rel. A / % [a]	at%
C1s	C–C/C=C	285.07	1.17	16.53	10.03
	C–O	286.50	1.17	67.61	41.01
	O–C–O	288.18	1.17	12.32	7.47
	O–C=O	289.38	1.17	3.54	2.15
				100.00	60.66
O1s	O–C=O	531.54	1.12	5.84	2.26
	C–O–H	532.45	1.12	56.51	21.90
	O–C–O	533.05	1.12	37.65	14.59
				100.00	38.75
N1s	-[b]	400.5	1.62	100.00	0.25
F1s	-[b]	689.5	2.47	100.00	0.34

[a] Relative area = component area×100/sum area of same orbital
[b] Data available from low resolution wide scan

3.2 Carbodiimide mediated esterification for cellulose methacrylate nanocrystals synthesis

The same methodology was applied to the esterification of methacrylic acid onto CNC (Figure 3.2.1). Similar to the esterification of CNC with acrylic acid, the CNC were mixed with methacrylic acid, DIC and DMAP in a ratio of 1:5.5:5.5:0.01 [OH]:[MAA]:[DIC]:[DMAP] (assuming 3 mmol/g OH groups) in dry DCM under argon atmosphere for 5 days at room temperature, followed

by Soxhlet extraction with DCM for 24 hours and EtOH for a further 24 hours. The samples were then dried *in vacuo* to give a white powder.

FT-IR characterization (Figure 3.2.2) indicates the presence of an absorption band at 1714 cm^{-1} attributed to ester formation: ν(C=O). A band at 1636 cm^{-1} is indicative of water absorption on cellulose surfaces but also can be attributed to the C=C absorption frequency of methacrylates. Another band identified at 811 cm^{-1} present in the reaction product of methacrylic acid with cellulose can be attributed to some out-of-plane bending vibrations of methacrylate functionality.

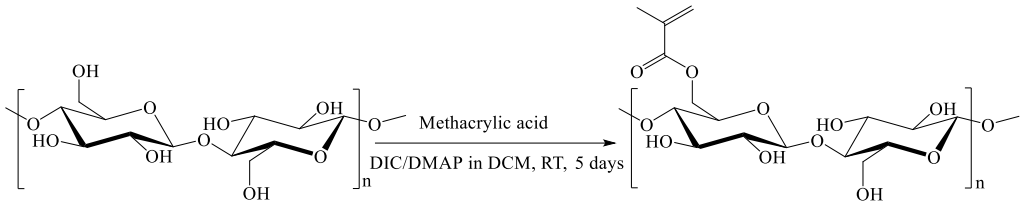


Figure 3.2.1 Esterification reaction of cellulose nanocrystals with methacrylic acid in DIC/DMAP conditions

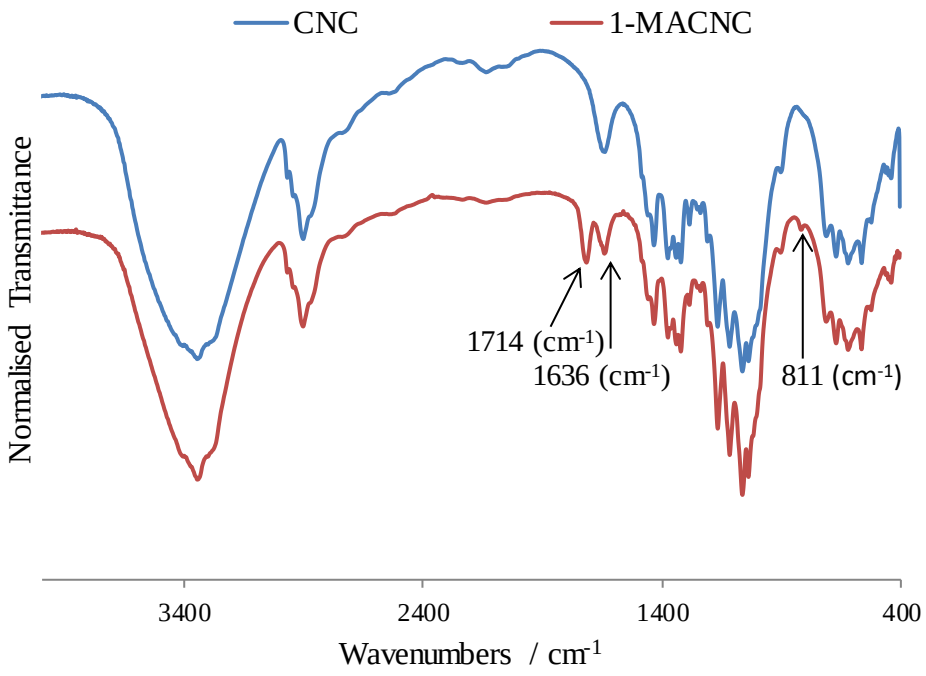


Figure 3.2.2 FT-IR spectrum of CNC and cellulose methacrylate (1-MACNC)

In the work published by Liang *et al.*, the methacrylic acid monomer is compared with stearyl methacrylate, in which case the C=O bond was

identified at 1720 cm^{-1} while the C=O in carboxylic acid was identified at 1705 cm^{-1}.[241] Relatively similar identification of the methacrylic acid carbonyl band is given by Chowdhury *et al.* where they found the C=O to occur at 1699 cm^{-1}.[239] Also, bands ranging from 780-995 cm^{-1} were assigned to =C–H and $=CH_2$ out-of-plane bending, while the symmetric C=C bonding of methacrylic acid monomer peak was identified at 1634 cm^{-1}.[241] Thus, the infrared spectra of modified cellulose methacrylate presents absorption bands in the same spectral range as stearyl methacrylate, where the presence of an ester functionality necessitates a higher energy to vibrate and therefore a higher wavenumber in comparison with the unbound methacrylic acid which is found at lower frequency as it is also confirmed by the data published by the Spectral Database for Organic Compounds where the C=O group in methacrylic acid is found at 1697 cm^{-1}, in methyl methacrylate at 1726 cm^{-1} and in ethyl methacrylate at 1720 cm^{-1}.[238] Moreover, the absorption bands at 1715 and 1637 cm^{-1} were identified by Marsano *et al.* exactly on cellulose methacrylate synthesised in a dimethylacetamide (DMAc)/5% LiCl and methacryloyl chloride homogeneous reaction which confirms the formation of cellulose methacrylate as well in the present research.[242] The average value for carbonyl vibration of two FT-IR repetitions for this product is 1714.65 ± 0.49 cm^{-1}.

EA gives a clear indication that in the case of CNC esterified with methacrylic acid, the functionalization is less pronounced with a DS_{surf} (C) = 0.52 which represents the functionalization of one hydroxyl group per AGU (Table 3.2.1). Even so, the current degree of esterification is higher when compared with the same modification performed by Eyley *et al.* (DS_{surf} = 0.28).[65] One possible explanation could be given by the higher molar ratio used here compared with 1:3.5:3.5:0.01 [OH]:[MAA]:[DIC]:[DMAP] in his work.

The XRD pattern (Figure 3.2.3) corresponds to the cellulose I_β allomorph and after applying Rietveld refinement, the calculated crystallinity of the reaction product was χ_C^R = 0.763 which represents a 12 % loss of crystallinity with respect to the starting cellulose crystallinity of χ_C^R = 0.883.

Table 3.2.1 Elemental analysis results for CNC and cellulose methacrylate (1-MACNC)

Sample	C (%)	H (%)	N (%)	DS_{surf}(C)
CNC	41.95	5.99	0	
1-MACNC	43.60	6.02	0.08	0.52

In agreement with the carbon content increase through functionalization (1.65 wt. %), the calculated expected reduction in crystallinity based on the EA data is ~3 % which would give a χ_C^R = 0.853, which is higher than the determined XRD crystallinity. Comparable to the previous modification, the drop of crystallinity can be attributed to the extent of modification, where the difference between the expected crystallinity from EA data and the actual crystallinity determined from XRD are due to remaining contamination from the by-product but also the error attributed to the calculations of DS from EA based on the same element (carbon) which represent a disadvantage of performing this analysis for this particular modification.

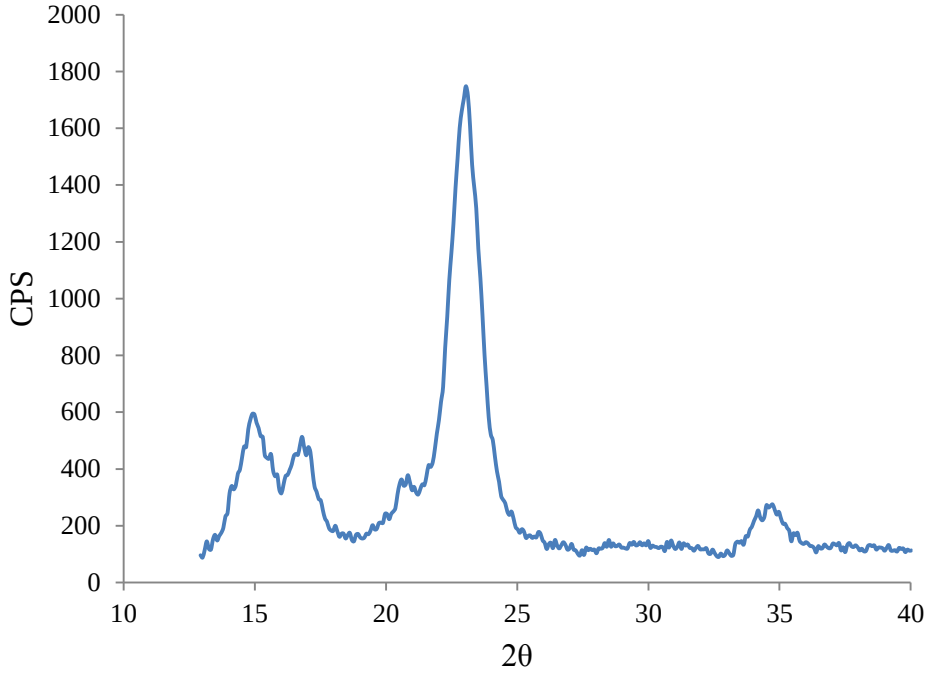


Figure 3.2.3 X-ray diffractogram of cellulose methacrylate (1-MACNC) synthesised by the DIC/DMAP methodology

The XPS wide scan (Figure 3.2.4 a) of the prepared cellulose methacrylate indicates only the presence of carbon and oxygen as expected and a trace amount of sulfur at a BE of S2p 3/2 = 168.75 eV. Sulfur is identified with the sulphate groups available on the CNC surface as a consequence of acid hydrolysis (Chapter 3 Appendix, Figure 10.1.4).

Further proof of esterification comes from the C1s (Figure 3.2.4 b) and O 1s high resolution scans (Chapter 3 Appendix, Figure 10.1.3) (with detailed XPS values in Appendix for Chapter 3, Table 10.1.1) where the O–C=O chemical environment is identified at a BE of 289.09 eV and 531.78 eV respectively.
In addition, the C–C/C=C peak intensity in 1-MACNC is also notably smaller when compared to the acrylate modification in accordance with the observations from FT-IR and EA.

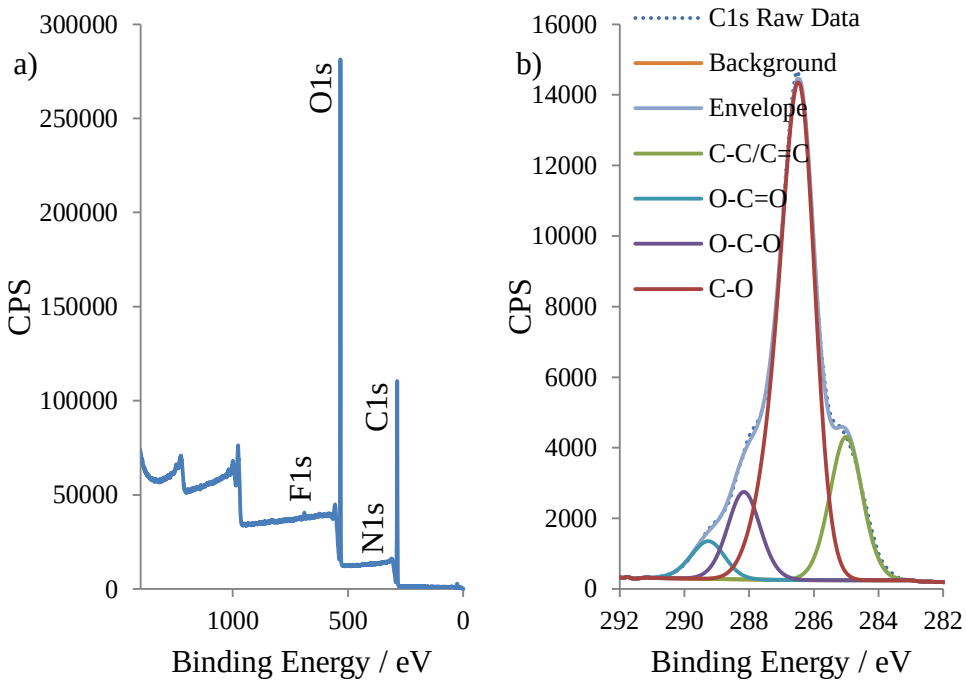


Figure 3.2.4 a) XPS wide scan of cellulose methacrylate (1-MACNC) synthesised by the DIC/DMAP methodology; b) C1s High resolution spectrum of cellulose methacrylate (1-MACNC) synthesised by the DIC/DMAP

Thus, it can be concluded that DIC/DMAP methodology using mild reaction conditions (room temperature) results in a white powder product of modified CNC with an esterification efficacy that depends on the molar excess used and

on the acid nature. It is obvious that the DS_{surf} = 0.94 for cellulose acrylate is almost double the DS_{surf} = 0.52 determined for methacrylate cellulose. Hence, the more reactive acrylic acid with a pKa = 4.25 reacts faster in CNC esterifications then methacrylic acid with pKa = 4.65.

3.3 Tosyl Chloride/Pyridine esterification for cellulose acrylate nanocrystal synthesis

The second methodology used for the esterification of CNC is based on the use of *p*-toluenesulfonyl chloride (TsCl) and pyridine (Py) for the acrylation and methacrylation of CNC as adapted from Brewster and Ciotti[120] and Heuser *et al*.[243] The methodology consists in the initial formation of an acid anhydride that will further react towards the formation of the cellulose ester. This method is also used later in this thesis for esterification with carbazole-9-yl-acetic acid (chapter 4, section 4.6) and bromoacetic acid (chapter 5, section 5.7). First, CNC were reacted with tosyl chloride and acrylic acid in dry pyridine, in a molar ratio of 1:2:2 OH:Acid:TsCl (considering 3 mmol/g OH groups), at 80 °C for 24 hours (Figure 3.3.1).

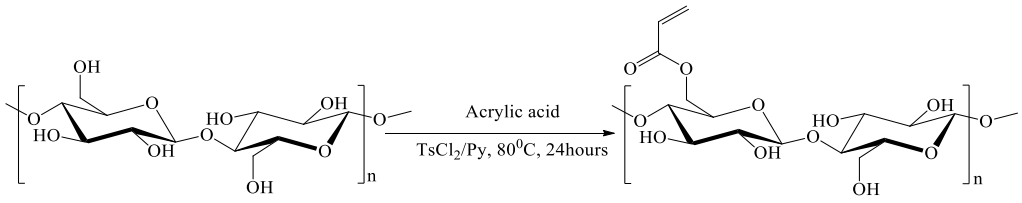


Figure 3.3.1 Esterification reaction of cellulose nanocrystals with acrylic acid in TsCl/Py conditions

The orange-red reaction product was purified by Soxhlet extraction with DCM for 24 hours and with EtOH for a further 24 hours. The product was dried *in vacuo* to result in an off-white powder.

At first glance, the FT-IR spectrum (Figure 3.3.2) indicates the presence of the ester linkage through a carbonyl absorption band at ν(C=O) at 1723 cm^{-1} and another sharp peak with a maximum at 1635 cm^{-1}, attributed to C=C bond

specific to acrylate as discussed for cellulose acrylate in section 3.1. So, the product was named cellulose acrylate (2-ACNC). The average value for carbonyl vibration of three FT-IR repetitions for this reaction was 1727.75 ± 5.44 cm^{-1}.

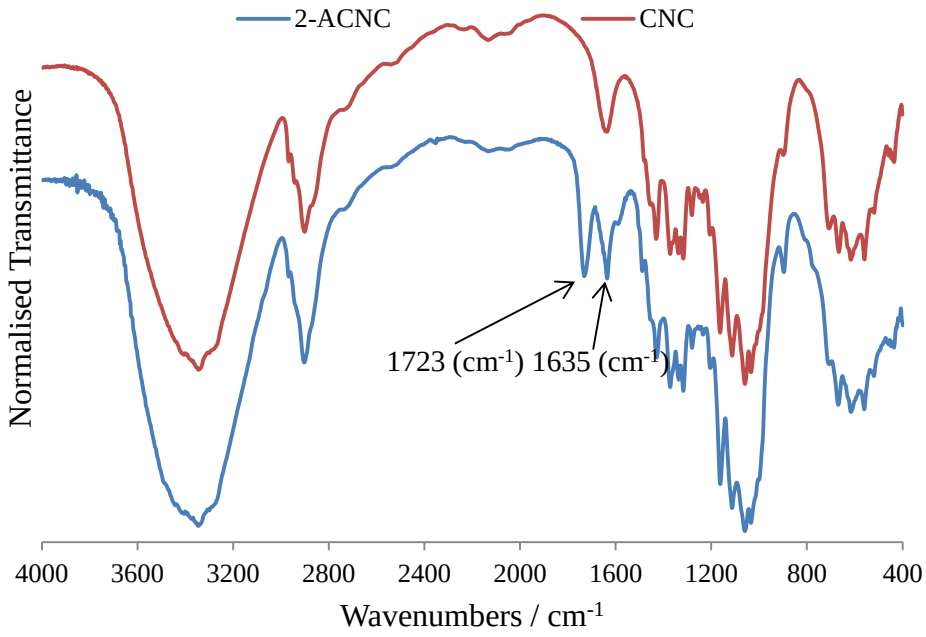


Figure 3.3.2 FT-IR spectrum of CNC and cellulose acrylate (2-ACNC)

EA results (Table 3.3.1) show that the extent of modification of CNC with acrylic acid by the TsCl/Py methodology, gave a $DS_{surf}(C) = 1.10$, a value that indicates modification of slightly more than two hydroxyl groups per AGU. According to the calculated DS_{surf}, the TsCl/Py methodology provides a higher modification than the DIC/DMAP esterification ($DS_{surf}(C) = 0.94$) for the same acid. Although unexpected, the EA also shows a small nitrogen content that will be discussed further below with the help of XPS analysis.

Table 3.3.1 Elemental analysis results for cellulose nanocrystals and cellulose acrylate (2-ACNC)

Sample	C (%)	H (%)	N (%)	$DS_{surf}(C)$
CNC	41.29	6.20	0	
2-ACNC	43.25	6.17	0.56	1.10

The integrity of the cellulose acrylate (2-ACNC) was assessed by powder X-ray diffraction (Chapter 3 Appendix, Figure 10.1.5). Rietveld refinement and subsequent determination of amorphous content showed a drop to χ_C^R = 0.738 that corresponds to a 5.8 % loss of crystallinity with respect to the initial cellulose crystallinity of χ_C^R = 0.796 (note that the crystallinity of these initial CNC is lower than those used in Section 3.1. It is thus paramount to record the initial crystallinity for each batch of CNC). In agreement with the carbon content increase through functionalization (EA) (1.96 wt. %), the calculated expected reduction is 3.86 % which would give a χ_C^R = 0.757, thus a crystallinity difference of 3.9 % between calculated and determined. Using the nitrogen content found in EA and knowing that the nitrogen content in pyridine (which possibly is adsorbed onto the surface) is 17.71%, this would result in a contribution to amorphous content of 3.16 %, in good agreement with the difference of 3.9 %.

The wide XPS scan of cellulose acrylate (2-ACNC) (Chapter 3 Appendix, Figure 10.1.6), indicates the presence of carbon and oxygen as expected and trace amounts of nitrogen (Chapter 3 Appendix, Figure 10.1.7), sulfur (Chapter 3 Appendix, Figure 10.1.8) and chlorine (Chapter 3 Appendix, Figure 10.1.9).

Thus, the presence of these elements indicate possible tosylation and chlorination side reactions that may have happened.[65] Esterification of cellulose is confirmed by the presence in the C1s high resolution spectrum (Figure 3.3.3 a) of a O–C=O carbonyl environment present at 289.4 eV BE.

The O–C=O oxygen environment is found at a BE of 531.34 eV in the O1s high resolution spectrum (Figure 3.3.3 b) as further confirmation of esterification of cellulose nanoparticles with acrylic acid. An increase in the C=C bond contribution from 12.61 at% for 2-MACNC to 14.06 at% for 2-ACNC is also seen as further proof (Table 3.3.2).

The N1s peak identified at a BE of 402.4 eV can correspond to a positively charged nitrogen (Chapter 3 Appendix, Figure 10.1.17). This may be due to some pyridinium chloride by-product still adsorbed onto the cellulose surface and confirms the assumption made for the source of nitrogen present in EA.

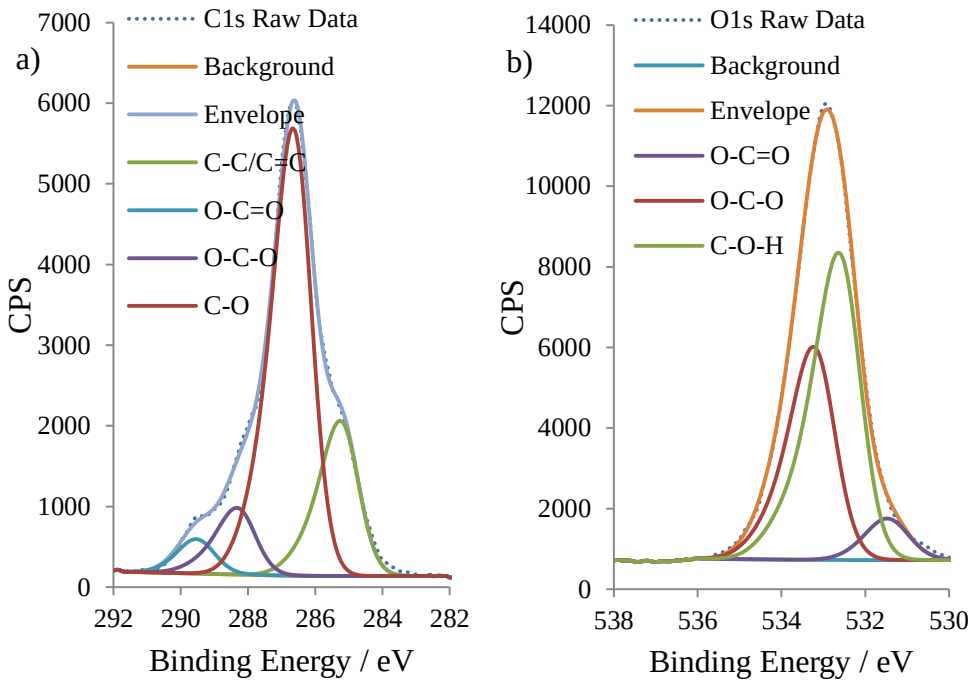


Figure 3.3.3 a) C1s high resolution spectrum of cellulose acrylate (2-ACNC) synthesised by the TsCl/Py methodology; b) O1s high resolution spectrum of acrylate cellulose (2-ACNC) synthesised by the TsCl/Py methodology

Despite intense Soxhlet extraction, this positively charged pyridine could not be fully removed from the surface. A second nitrogen environment identified at a BE of 399.9 eV could also be attributed to some pyridine absorbed on the surface, as the pyridine is the only nitrogen containing compound in contact with the reactants. The S2p and Cl2p signals could be due to tosylation and chlorination of a small fraction of surface hydroxyl groups as it is indicated by the position at which they were found: S2p 3/2 present at a BE of 168.41 eV and Cl2p 3/2 identified at a BE of 197.73 eV.[65]

Table 3.3.2 Detailed XPS data of acrylate cellulose (2-ACNC) synthesised by the TsCl/Py methodology

Orbital	Component	BE /eV	FWHM	Rel. A / % [a]	at%
C1s	C–C/C=C	285.10	1.27	22.17	14.06
	C–O	286.50	1.27	63.86	40.49
	O–C–O	288.17	1.27	9.50	6.02
	O–C=O	289.40	1.27	4.47	2.83
				100.00	63.41
O1s	O–C=O	531.34	1.20	6.65	2.33
	C–O–H	532.49	1.20	56.02	19.59
	O–C–O	533.09	1.20	37.33	13.05
				100.00	34.97
N1s	C–N=	399.93	1.31	29.70	0.29
	(C_4)–N^+	402.47	1.31	70.30	0.68
				100.00	0.97
S2p	3/2	168.41	1.40	66.69	0.21
	1/2	169.51	1.40	33.31	0.11
				100.00	0.32
Cl2p	3/2	197.73	1.41	66.69	0.22
	1/2	199.49	1.41	33.31	0.11
				100.00	0.33

[a] Relative area = component area×100/sum area of same orbital

3.4 Tosyl Chloride/Pyridine esterification for cellulose methacrylate nanocrystal synthesis

Continuing along the same line as with the previous synthesis (Figure 3.4.1), CNC, TsCl and methacrylic acid were incorporated in dry Py under argon atmosphere, in molar ratio of 1:1.83:1.83 [OH]:[TsCl]:[MA] (assuming 3 mmol/g OH groups). The reaction was left under stirring at 80 °C for 16 hours. The purification of the orange-red reaction product was carried out by Soxhlet extraction with DCM for 24 hours and for a further 72 hours with EtOH. The reaction product was dried *in vacuo* in order to result in off-white solid nanoparticles.

Figure 3.4.2 shows the FT-IR spectrum of the cellulose reaction product with methacrylic acid under TsCl/Py reaction conditions. It displays an absorption band at 1714 cm^{-1} attributed to the carbonyl stretch vibration and is found

exactly at the same wavenumber as it was found for cellulose methacrylate synthesised in the carbodiimide mediated esterification. Another broad band found at 1636 cm^{-1} is a composite peak of bound water and the C=C vibration similar with the findings for methacrylate cellulose as previously mentioned.

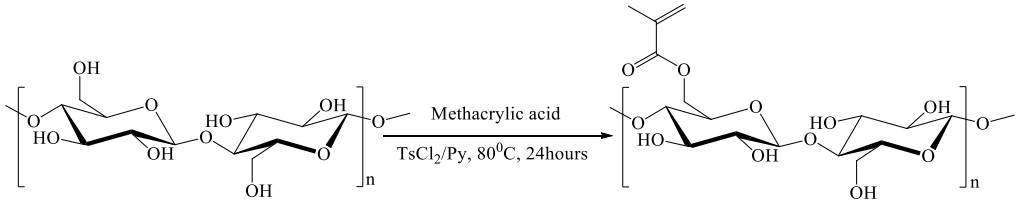


Figure 3.4.1 Esterification reaction of cellulose nanocrystals with methacrylic acid under TsCl/Py conditions

As well, the small absorption band found at 813 cm^{-1} is a result of =C–H and $=CH_2$ out-of-plane bending vibrations. The 1714 cm^{-1} band is clearly sharper when compared to the carbodiimide mediated esterification product, indicating successful modification. By comparing these peaks intensities with the one displayed by 1-MACNC, it is visibly clear that these intensities are higher and so an increased esterification is expected.

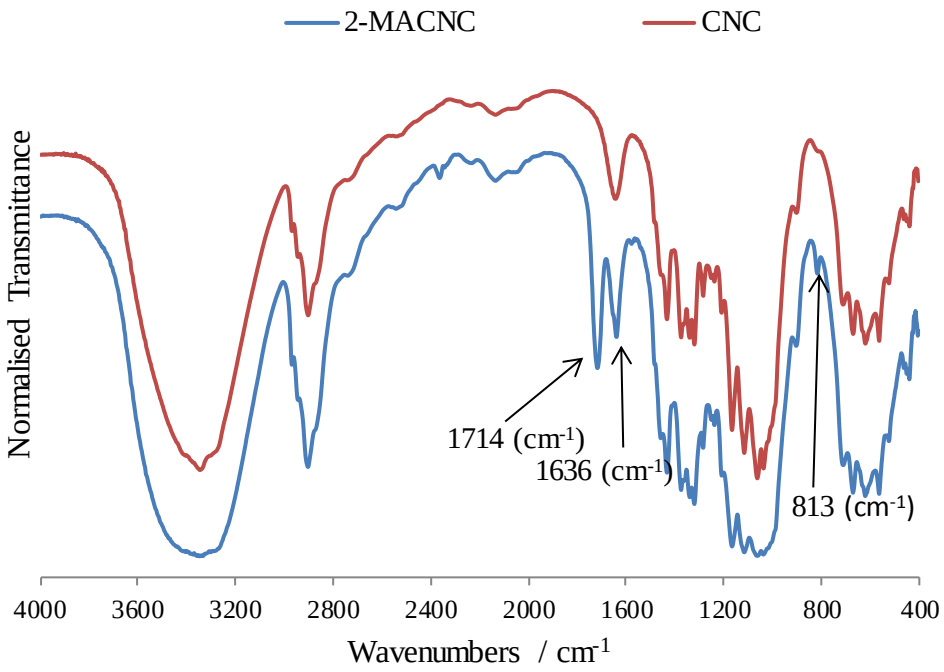


Figure 3.4.2 FT-IR spectrum of CNC and cellulose methacrylate (2-MACNC)

Some repetitions of the reaction indicated the appearance of carbonyl stretch vibration at a higher wavelength (1734 cm^{-1}) and therefore a possible dimerization of the methacrylic acid may rationalize this shift and this would obviously be avoided. The dimerization could be caused by the elevated temperature at which the reaction takes place, an assumption that is confirmed by the aspect of the reaction product: a yellowish solid sticky material instead of white nanoparticles.

EA comes to support the FTIR observation and a higher degree of substitution is determined, $DS_{surf}(C)$ = 0.95, which suggests that almost two hydroxyl groups per AGU were modified (Table 3.4.1).

Table 3.4.1 Elemental analysis results for CNC and cellulose methacrylate (2-MACNC)

Sample	C (%)	H (%)	N (%)	$DS_{surf}(C)$
CNC	41.77	5.91	0	
2-MACNC	43.97	5.96	0.15	0.95

Beyond the high modification calculated with EA, the diffraction pattern of this reaction product (Figure 3.4.3) confirms the retention of the cellulose I_β allomorph and the crystallinity calculated indicate a χ_C^R = 0.696, representing a crystallinity loss of 10 % with respect to the unmodified cellulose crystallinity (χ_C^R = 0.796). Even with this high modification achieved, this substantial decrease of crystallinity could be due to the use of pyridine, a swelling cellulose solvent, that could have favoured the reactants penetration into the CNC exterior sheets, resulting in an increased extent of modification but also a reduction in the overall crystallinity of cellulose methacrylate and hence increasing the amorphous background on the XRD pattern.[65]

Considering the amount of carbon added through modification (2.2 wt.%), the crystallinity reduction is expected to be ~ 4%, significantly lower than the determined crystallinity reduction from XRD. In this situation, it has to be underlined that errors can appear in the expected crystallinity based on EA calculations as it is considered an element that is also found in CNC.

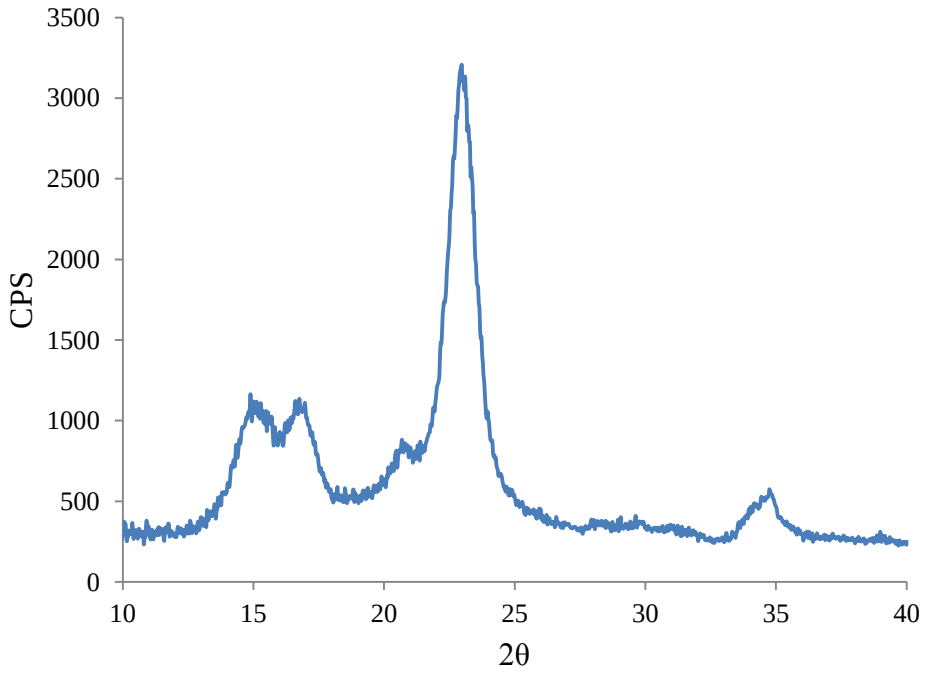


Figure 3.4.3 X-ray diffractogram of methacrylate cellulose (2-MACNC) synthesised by the TsCl/Py methodology

In comparison with the previous esterification, the drop of crystallinity can only be attributed to the amorphous content coming from absorbed pyridine to a small extent as this would give only a 0.84 % crystallinity reduction. Therefore, it could still be attributed to possible tosylation and chlorination secondary reactions (EA unavailable for Cl and S) that would bring some amorphous contributions as well.

However, it seems like a small fraction of the surface chains have become more mobile as a result of the modification as indicated by the 5% crystallinity reduction beyond what can be explained by the amorphous graft and pyridine contamination of the product. Figure 3.4.4a presents the XPS wide scan of cellulose methacrylate (2-MACNC) in which carbon and oxygen are identified as expected but also very small peaks of nitrogen are seen as an impurity, chlorine that is introduced by a chlorination side reaction or as counter ion to pyridinium, and sulfur that could be due to tosylation of the surface considering the tosyl chloride in the reaction mixture or from a tosylate counter ion to pyridinium.[65]

All of the heteroatoms occur in very low at% as shown in Table 3.4.2. Connecting the high esterification modification confirmed through EA to the C1s (Figure 3.4.4 b) and O1s high resolution spectra (Chapter 3 Appendix, Figure 10.1.10), the peaks found at a BE of 289.33 eV and 531.59 eV (Table 3.2.4) correspond to O–C=O components in the respective spectra. The C–C/C=C chemical environment in the C1s spectrum, at a BE of 285.25 eV, is also more than double (12.61 at%) the corresponding peak for the same methacrylate cellulose synthesised by DIC/DMAP (4.82 at%), in agreement with the degrees of substitution calculated from EA.

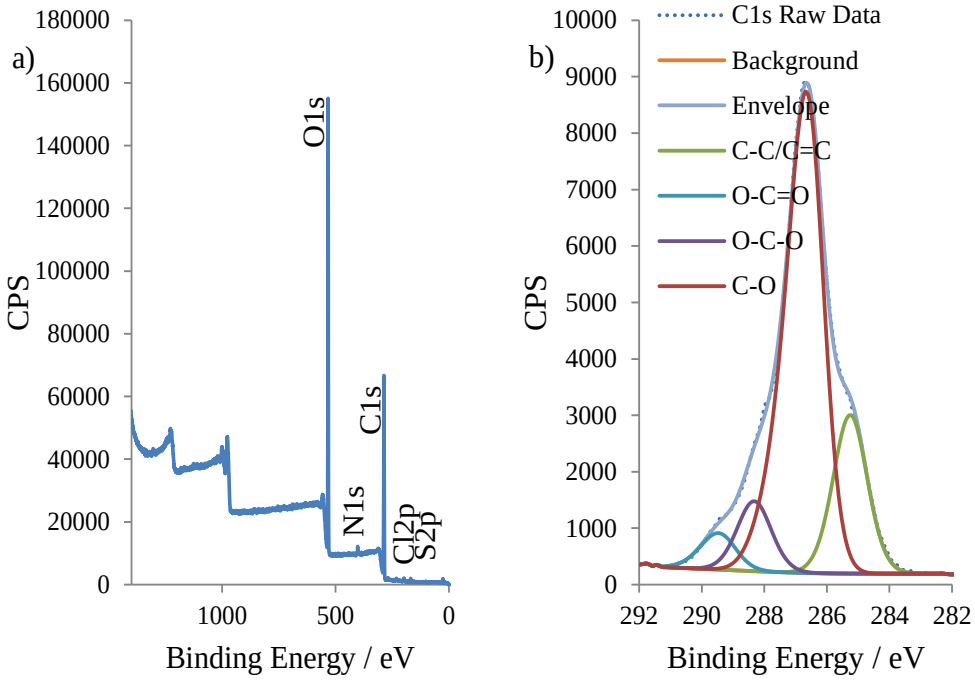


Figure 3.4.4 a) XPS wide scan of methacrylate cellulose (2-MACNC) synthesised by the TsCl/Py methodology; b) C1s high resolution spectrum of methacrylate cellulose (2-MACNC) synthesised by the TsCl/Py methodology

The S2p high resolution spectrum (Chapter 3 Appendix, Figure 10.1.11) suggests that a very small amount of tosylation may have occurred as a side reaction to the esterification. This observation is supported by the presence of a small Cl2p peak in the low resolution scan as a negatively charged ion, which requires tosylation as activation. At the same time, a N1s peak was identified at a BE of 402.6 eV corresponding to a positively charged nitrogen (Chapter 3

Appendix, Figure 10.1.12).[244] It might be possible that some pyridinium chloride/tosylate by-product still remains adsorbed onto the cellulose surface despite intense Soxhlet extraction purification. The second nitrogen environment present at a BE of 399.8 eV could be attributed to adsorbed pyridine and hence a very small at% of neutral nitrogen present at the surface.[65]

This second methodology (TsCl/Py) applied to the esterification of methacrylic acid with the surface hydroxyl groups of CNC thus resulted in a substantial increase of functionalization on the cellulose surface, from $DS_{surf}(C) = 0.52$ to $DS_{surf}(C) = 0.95$, when compared to the DIC/DMAP methodology.

Table 3.4.2 Detailed XPS data of cellulose methacrylate (2-MACNC) synthesised through TsCl/Py methodology

Orbital	Component	BE /eV	FWHM	Rel. A / % [a]	at%
C1s	C–C/C=C	285.25	1.28	19.55	12.61
	C–O	286.50	1.28	67.24	43.36
	O–C–O	288.32	1.28	8.58	5.53
	O–C=O	289.33	1.28	4.63	2.99
				100.00	64.49
O1s	O–C=O	531.59	1.21	7.28	2.46
	C–O–H	532.63	1.21	61.82	20.88
	O–C–O	533.23	1.21	30.90	10.43
				100.00	33.77
N1s	C–N=	399.86	1.35	15.66	0.09
	$(C_4)–N^+$	402.60	1.35	84.34	0.46
				100.00	0.55
S2p	3/2	168.43	1.88	66.71	0.39
	1/2	169.46	1.88	33.29	0.19
				100.00	0.58
Cl2p	- [b]	197.5	4.62	100.00	0.62

[a] Relative area = component area×100/sum area of same orbital
[b] Data available from low resolution wide scan

3.5 Tosyl Chloride/Triethylamine esterification for cellulose acrylate nanocrystal synthesis

In order to avoid the formation of secondary by-products in the methodology involving TsCl/Py, it was decided to try the esterification of CNC with acrylic acid where pyridine was replaced with a less nucleophilic amine, i.e. triethylamine. The reaction procedure in which CNC, TsCl and acrylic acid in a ratio of 1:1.83:1.83 OH:AA:TsCl (considering 3 mmol/g OH groups) were mixed in dry Et_3N under argon atmosphere, is identical with the procedure used for 2-MACNC where the reaction mixture was stirred at 80°C for 24 hours followed by filtration of the yellow-orange suspension and purification by Soxhlet extraction with DCM for 24 hours and EtOH and for a further 24 hours. The product was dried *in vacuo* to yield a white powder.

The FT-IR of the resulting nanocrystals (Figure 3.5.1) displays an absorption band at 1727 cm^{-1} that corresponds to a carbonyl stretching vibration and therefore confirms ester formation and consistency with the previously synthesised cellulose acrylates. Another band representative of the reaction product is evident in a sharp absorption signal with its maximum at 1634 cm^{-1} attributed to C=C bonds and a small band at 808 cm^{-1} due to =C–H and $=CH_2$ out-of-plane bending vibrations, both confirming the newly formed cellulose acrylate (2-ACNC(Et_3N)).

EA of the product gave an increase of 1.18 wt% of carbon corresponding to a degree of modification of $DS_{surf}(C)$ = 0.56 (Table 3.5.1). This value indicates that approximately one hydroxyl group is modified on each AGU at the surface of cellulose.

Table 3.5.1 Elemental analysis results of cellulose nanocrystals and cellulose acrylate (2-ACNC(Et_3N))

Sample	C (%)	H (%)	N (%)	$DS_{surf}(C)$
CNC	41.77	5.91	0	
2-ACNC(Et_3N)	42.95	6.10	0.48	0.56

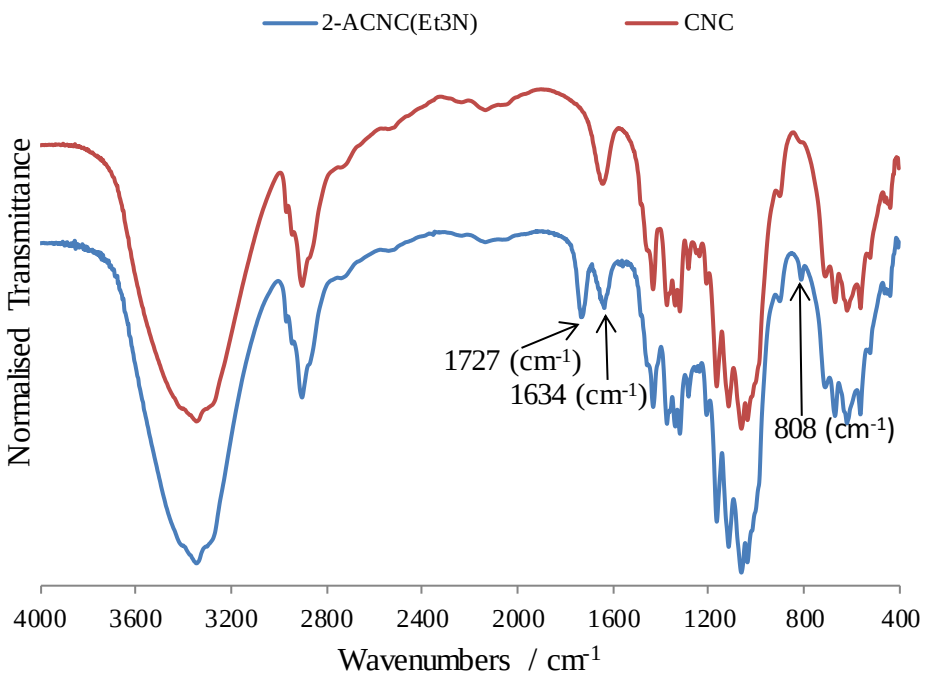


Figure 3.5.1 FT-IR spectrum of CNC and acrylate cellulose (2-ACNC(Et_3N)) synthesised by the TsCl/Et_3N methodology

When comparing this reaction with the previous one in which pyridine was used as solvent and catalyst, the degree of substitution is only half that achieved in pyridine in the case of triethylamine. Although the purpose of this reaction was to avoid as much as possible the secondary products, EA still shows the presence of nitrogen yet slightly lower when compared to the earlier 2-ACNC synthesis but higher when compared to 2-MACNC. This nitrogen presence will be further investigated through XPS analysis. Crystal structure integrity was verified (Chapter 3 Appendix, Figure 10.1.13) and the crystallinity index was determined to be χ_C^R = 0.74 representing a crystallinity loss of 5 % when consider the initial cellulose crystallinity (χ_C^R = 0.796). The amount of modification calculated based on EA indicate an expected modification of 2.32 % which would result in a χ_C^R = 0.772. The small disagreement between the two crystallinities can be covered by a small fraction of possible triethylamine ammonium chloride contamination, that would bring some extra amorphous material on the surface and it will be investigated with the XPS analysis. By comparing with the previous reactions in pyridine, the

esterification of cellulose acrylate in triethylamine has resulted in a lower decrease of crystallinity that could indicate that triethylamine is less of a swelling solvent for crystalline cellulose, as expected.

Carbon and oxygen are present in the XPS wide scan (Chapter 3 Appendix, Figure 10.1.14) as expected with also some traces of sulfur, nitrogen and fluorine. There was no presence of chlorine. The presence of fluorine indicates a possible contamination with a bistriflimide anion with its representative components, a contamination that is common in the XPS spectrometer used as bistriflimide ionic liquids are investigated in this apparatus and contamination of the analysis chamber may have occurred. As XPS is highly sensitive to fluorine, only trace amounts are necessary. Fluorine signals have also been seen to fluctuate on the same samples depending on when they were analysed. Fluorine cannot come from the reaction as the sample has never been in contact with fluorine-containing products.

The nitrogen identified at a BE of 399.8 eV of only 0.08 at.% could be assigned for the negative nitrogen as in bistriflimide.
The second nitrogen environment present at a BE of 401.83 eV could be explained in the same way as in the case of the previous esterification of 2-ACNC and so, some protonated triethylamine appears to be still present, therefore confirming the previous assumption made about the triethylamine hydrogen chloride contamination that would contribute to the amount of amorphous material at the cellulose surface.
In the C1s spectrum (Figure 3.5.2 a), the O–C=O chemical environment is clearly visible at a BE of 289.22 eV and a prominent C=C peak at a binding energy of 284.94 eV (Table 3.3.2).

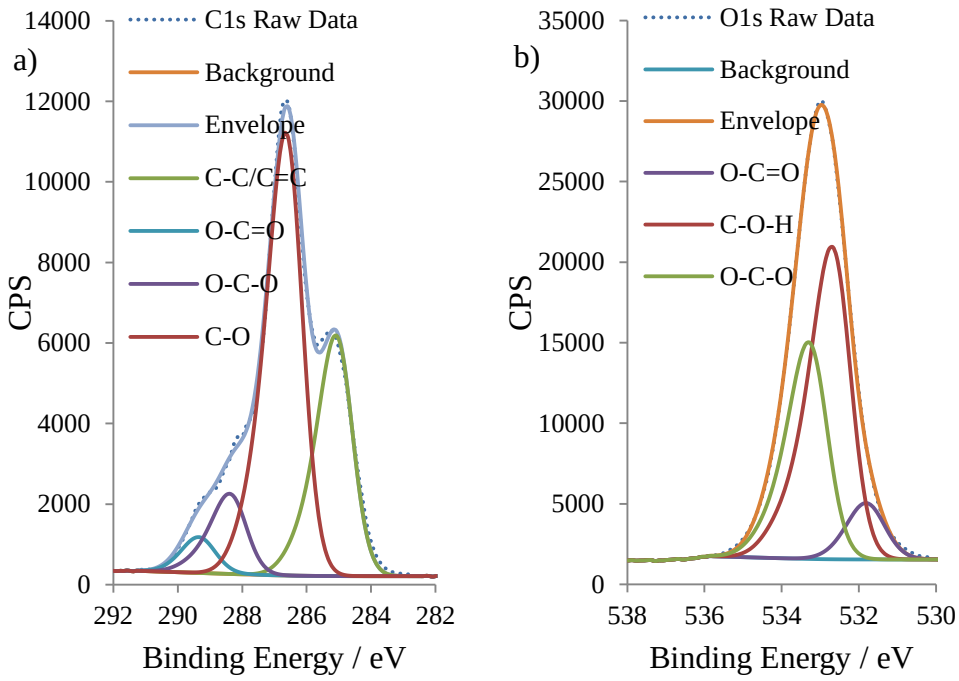


Figure 3.5.2 a) C1s and b) O1s high resolution spectra of acrylate cellulose (2-ACNC(Et_3N)) synthesised by the TsCl/Et_3N methodology

Table 3.5.2 Detailed XPS data of cellulose acrylate synthesised by the TsCl/Et_3N methodology

Orbital	Component	BE /eV	FWHM	Rel. A / % [a]	at%
C1s	C–C/C=C	284.94	1.21	30.28	20.01
	C–O	286.50	1.21	55.60	36.74
	O–C–O	288.24	1.21	10.04	6.63
	O–C=O	289.22	1.21	4.08	2.70
				100.00	66.08
O1s	O–C=O	531.59	1.13	8.68	2.91
	C–O–H	532.56	1.13	54.80	18.38
	O–C–O	533.16	1.13	36.52	12.25
				100.00	33.54
N1s	$–N^-$	399.88	1.22	58.92	0.08
	$(C_4)–N^+$	401.83	1.22	41.08	0.05
				100.00	0.13
S2p	3/2	168.39	1.57	66.70	0.09
	1/2	169.32	1.57	33.30	0.04
				100.00	0.13
F1s	-	689.5	2.02	100.00	0.12

[a] Relative area = component area×100/sum area of same orbital
[b] Data available from low resolution wide scan

3.6 Acryloyl Chloride/Triethylamine esterification for cellulose acrylate nanocrystal synthesis

Another esterification methodology, based on previous work by Morandi *et al.*[64] in our research group, consisted in the esterification of CNC with acryloyl chloride, a very highly reactive derivative of acrylic acid, in *N*,*N*-dimethylformamide (DMF) and catalysed by triethylamine (Et_3N) (Figure 3.6.1). The same esterification methodology of CNC with Et_3N in DMF but using bromoacetyl bromide is developed in Chapter 5 section 5.2.

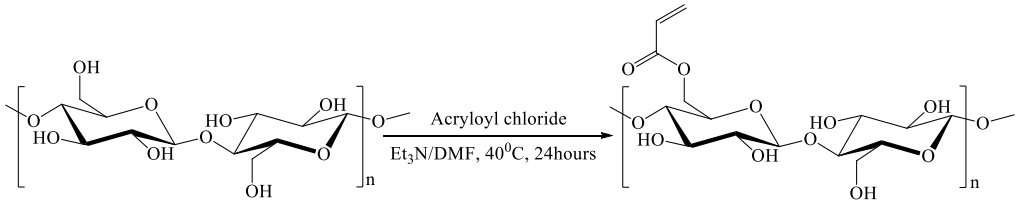


Figure 3.6.1 Esterification reaction of cellulose nanocrystals with acryloyl chloride

The first stage of the reaction involves the nucleophilic attack of one of the lone pairs on the oxygen of the cellulose hydroxyl group on the electropositive carbon atom in the acryloyl carbonyl group as it is showed in the schematic representation of the reaction mechanism (Figure 3.6.2). This attack requires hydrogen bonding on the nanocrystal surface to be weakened, hence the choice of DMF as the solvent. The second stage of the reaction takes place in two steps: First, the carbon oxygen double bond is reformed and the chlorine anion is removed. The second step consists in removing the hydrogen ion by a base, in this case triethylamine, in order to form the desired ester and triethylamine hydrogen chloride. A molar ratio of 1:66.66:76.66 OH:Cloride:Et_3N was used in the esterification reaction. The procedure consisted in the addition of Et_3N first into CNC suspended in DMF followed by dropwise addition of acryloyl chloride under an inert atmosphere with the entire setup placed into an ice bath. Once the acryloyl chloride was added the reaction was brought to room temperature and left to react for 24 hours at 40 °C.

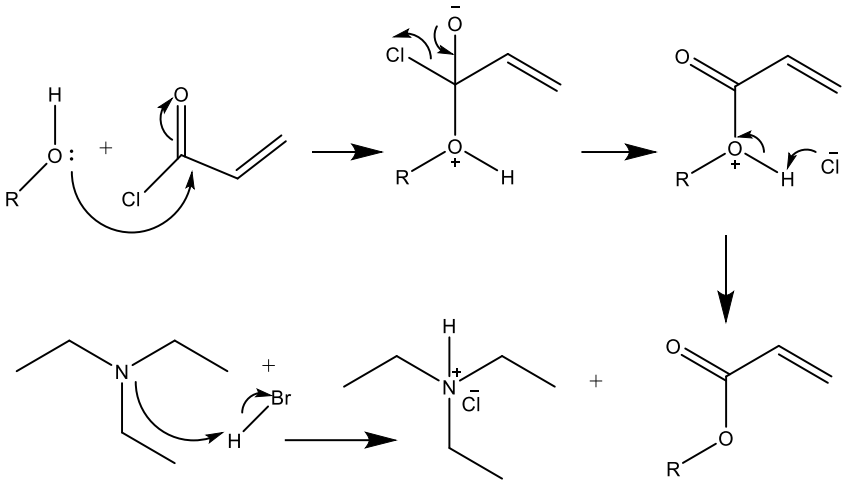


Figure 3.6.2 Schematic representation of hydroxyl nucleophilic attack on acryloyl chloride reaction mechanism

A molar ratio of 1:66.66:76.66 OH:Cloride:Et_3N was used in the esterification reaction. The procedure consisted in the addition of Et_3N first into CNC suspended in DMF followed by dropwise addition of acryloyl chloride under an inert atmosphere with the entire setup placed into an ice bath. Once the acryloyl chloride was added the reaction was brought to room temperature and left to react for 24 hours at 40 °C. The purification of the reaction product consisted in acetone and water centrifugation/washing steps and Soxhlet extraction with EtOH for 24 hours and DCM for a further 24 hours. The modified nanocrystals were then dried *in vacuo* to give a yellow solid powder. Considering the very high reactivity of acryloyl chloride and the molar excess used in the reaction, the reaction product was expected to have a very high degree of modification.

Table 3.6.1 Elemental analysis results for CNC and cellulose acrylate (3-ACNC) synthesised in acryloyl chloride/Et_3N/DMF system

	C (%)	H (%)	N (%)	DS_{surf}(C)
CNC	42.31	6.15	0	
3-ACNC	46.45	5.95	0.27	2.11

EA confirms this prediction as it indicates a DS_{surf}(C) = 2.11, a degree of substitution that exceeds the theoretical maximum degree of surface substitution of 1.5. Using the wt% carbon difference between unmodified and

the modified CNCs (4.14 %), the weight fraction of the modification in the final product can be calculated to be 8.16%, a value that is lower than the crystallinity drop of 21 % (the initial crystallinity is χ_C^R = 0.796) calculated from Rietveld refinement applied to the XRD diffraction pattern (Chapter 3 Appendix, Figure 10.1.17). Therefore, the loss of crystallinity can be attributed on one the hand to the very high extent of modification and therefore the increase of non-crystalline material from the surface of cellulose, but on the other hand, this modification also resulted in modification of some internal hydroxyl groups effecting a reduction in the crystallinity of the cellulose core (at least partial solubilisation of the surface chains).

The infrared spectrum confirms the EA modification results by showing the formation of the ester through the appearance of a very intense carbonyl band at ν(C=O) = 1728 cm^{-1} and another intense absorption band at 1634 cm^{-1} attributed to ν(C=C). This modification pathway thus provides a 3rd route to prepare cellulose acrylate (3-ACNC, Figure 3.6.3). The average value for carbonyl vibration of three FT-IR repetitions for this reaction is 1726.83 ± 1.36 cm^{-1}.

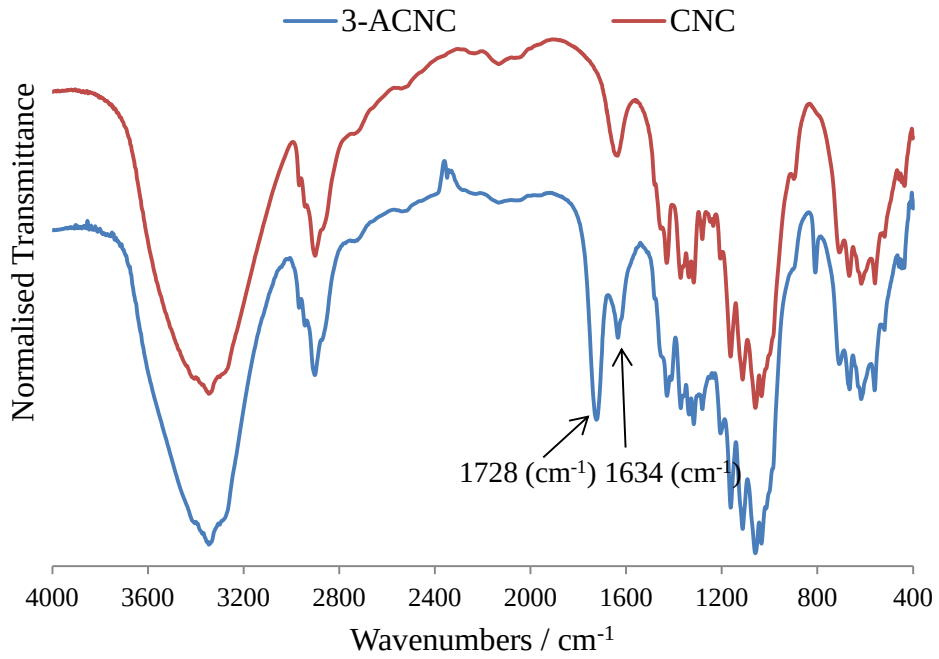


Figure 3.6.3 FT-IR spectrum of cellulose nanocrystals and cellulose acrylate (3-ACNC) synthesised by alkylation of acryloyl chloride on the CNC surface

Further characterization of 3-ACNC by XPS (Chapter 3 Appendix, Figure 10.1.18) shows the presence of carbon and oxygen as expected but also trace amounts of nitrogen, chlorine and silicon. As there is no silicon compound used in the reaction, the only probable source of silicon found in the XPS analysis is attributed to the silicone adhesive tape used to fix the modified CNC powder onto the XPS sample bar. This can occur if the layer of nanocrystalline cellulose powder is either not thick enough or if there are small holes in the deposited powder.

More confirmation is given by the decreased O–C–O environment from 8 at% in unmodified cellulose or 6.02 at% in 2-ACNC to 4.74 at% in this modification which can be attributed to the fact that internal cellulose becomes less visible by the XPS technique and so the O–C–O signal bond will inherently decrease in the C1s high resolution scan (Figure 3.6.4a).

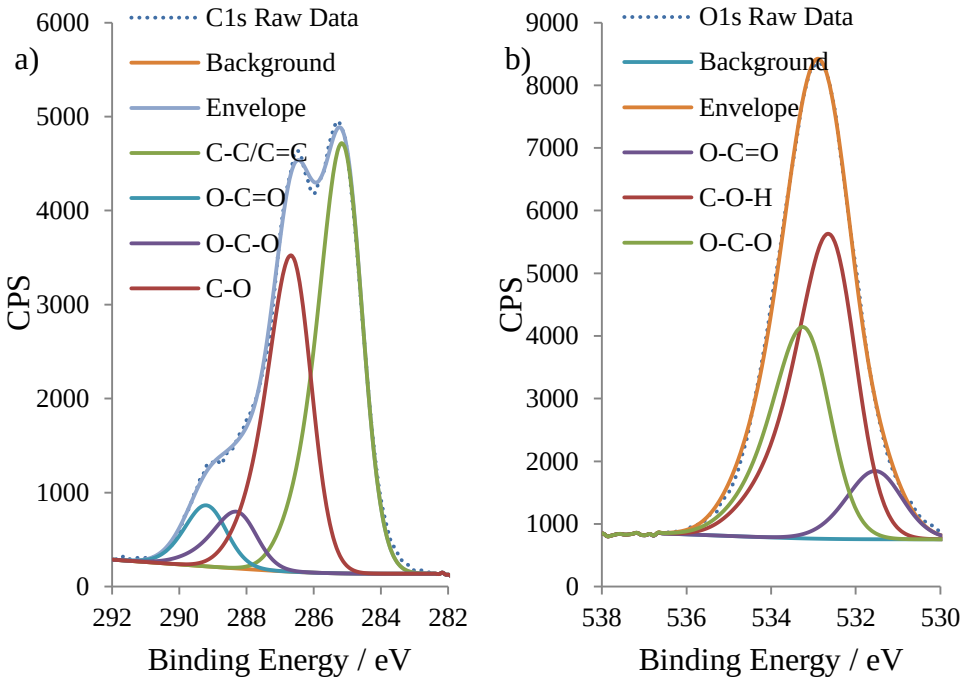


Figure 3.6.4 a) C1s and b) O1s high resolution spectrum of acrylate cellulose (3-ACNC) synthesised by the alkylation of acryloyl chloride in DMF, catalysed by Et_3N

The O1s high resolution spectrum (Figure 3.6.4b) agrees with these results. The O–C–O contribution shows a decrease of 4.85 at% while the C–O–H

decreased by half compared to the unmodified cellulose, which is very significant, as expected from the high extent of modification.

The N1s high resolution spectrum (Chapter 3 Appendix, Figure 10.1.19) presents two nitrogen environments. The first one at a BE of 402.43 eV corresponds to positively charged nitrogen that can be attributed to the triethylamine hydrogen chloride present in a small at% (0.39 %). The second nitrogen environment present at a BE of 400 eV could be attributed to physically absorbed triethylamine (Table 3.6.2).

Table 3.6.2 Detailed XPS analysis for cellulose acrylate modified with acryloyl chloride catalysed by triethylamine in DMF

Orbital	Component	BE /eV	FWHM	Rel. A / % [a]	at%
C1s	C–C/C=C	284.98	1.42	50.12	35.98
	C–O	286.50	1.42	36.81	26.42
	O–C–O	288.13	1.42	6.60	4.74
	O–C=O	289.05	1.42	6.47	4.64
				100.00	71.78
O1s	O–C=O	531.38	1.49	10.55	2.85
	C–O–H	532.46	1.49	53.68	14.52
	O–C–O	533.06	1.49	35.77	9.67
				100.00	27.04
N1s	C–N=	399.96	1.52	50.84	0.41
	$(C_4)–N^+$	402.43	1.52	49.16	0.39
				100.00	0.80
Cl2p	3/2	200.65	1.47	66.69	0.03
	½	202.08	1.47	33.31	0.02
				100.00	0.05
Si2p	-[b]	103	1.85	100.00	0.33

[a] Relative area = component area×100/sum area of same orbital
[b] Data available from low resolution wide scan

Despite the purification of the reaction product with extensive acetone and water washing followed by Soxhlet extraction with EtOH for 24 hours and DCM for a further 24 hours, there were still some traces on the cellulose surface. It might be that some of these impurities are trapped inside the amorphous layer around the crystalline cellulose core, making it impossible for them to be removed. These small impurities are thus inherent consequences of

the fact that the reaction is carried out at a very high molar ratio, in order for the reaction to be carried out to a high extent of modification. Later in this thesis (chapter 5) it will be described that a similar reaction was carried out with much lower molar ratio, resulting in a much lower extent of modification (DS_{surf}(Br) = 0.15), showing that a high excess is necessary to get sufficient modification.

3.7 Conclusions

Four main methodologies were examined for their capacity to esterify cellulose nanocrystals with acrylic/methacrylic acid and acryloyl chloride: activation by DIC/DMAP, anhydride formation via TsCl/Py and TsCl/Et_3N and the traditional acyl chloride methodology, all of these showing new modifications of CNC starting from one methodology presented in the literature. Table 3.7.1 indicates that TsCl/Py proved to be the most efficient methodology for the esterification of CNC with carboxylic acids (acrylic and methacrylic acid). The advantage of this methodology is given by the low molar excess of acrylic/methacrylic acid to functionalize the surface of cellulose in contrast with the traditional acyl halide methodology used to esterify the CNC with acryloyl chloride.

Table 3.7.1 Summary of Chapter 3

	Modified Surface	Acid	Molar ratio CNC:Acid:TsCl	Reaction Conditions			DS_{surf}(C)
1	CNC	Acrylic	1:5.5:5.5:0.01	DIC	DMAP	DCM	0.94
2	CNC	Methacrylic	1:5.5:5.5:0.01	DIC	DMAP	DCM	0.52
3	CNC	Acrylic	1:2:2	TsCl	Py		1.10
4	CNC	Methacrylic	1:1.83:1.83	TsCl	Py		0.95
5	CNC	Acrylic	1:1.83:1.83	TsCl	Et_3N		0.56
6	CNC	Acryloyl chloride	1:66.66:76.66	Et_3N	DMF		2.11

The synthesised esters produced by TsCl/Py are slightly coloured (white-cream) while the cellulose acrylate from acryloyl chloride/Et_3N methodology is yellowish. Although the degree of modification is half that of TsCl/Py, the cellulose acrylate resulting from TsCl/Et_3N (DS_{surf} = 0.56), presents a clear

white colour and therefore this methodology can also be recommended whenever the application requires a white product.

Using the DIC/DMAP methodology, which uses mild reaction conditions (room temperature), white powder CNC are obtained with an esterification efficiency that is dependent on the molar excess used and on the acid nature. The DS_{surf} = 0.94 for cellulose acrylate is almost double the DS_{surf} = 0.52 calculated for methacrylate cellulose for DIC/DMAP methodology. Thus, this methodology is also recommended when the application dictates the use of a white product despite the slightly lower substitution compared to TsCl/Py. Considering the less reactive nature of methacrylic acid then the corresponding acrylic acid as a result of electron-donating effect and the steric hindrance of α-methyl group, the difference between cellulose acrylate and cellulose methacrylate substitution degrees is unsurprising.

EA results for esterification of CNC with acrylic acid by TsCl/Py show that the extent of modification gave a $DS_{surf}(C)$ = 1.10, thus a higher modification than the DIC/DMAP esterification ($DS_{surf}(C)$ = 0.94) for the same acid. The TsCl/Py methodology applied to the esterification of methacrylic acid with the surface hydroxyl groups of CNC resulted in a substantial increase of functionalized cellulose surface from $DS_{surf}(C)$ = 0.52 for DIC/DMAP methodology to $DS_{surf}(C)$ = 0.94. However, a minor disadvantage of TsCl/Py methodology and especially acryloyl chloride/Et_3N is the fact that despite intensive purifications involved, the reaction products still contain some traces of by-products. Therefore, further purification methods are still required to be investigated. In all cases, the crystallinity of the product was influenced by the mass of modification introduced on the surface and the highest loss of crystallinity was encountered in the case of cellulose acrylate synthesised in acryloyl chloride/Et_3N conditions with a DS_{surf} = 2.11 and therefore it is supposed that some core hydroxyl groups were modified as well. All the reaction products synthesised by DIC/DMAP, TsCl/Py and Acryloyl chloride/Et_3N will be used in chapter 6 as ene-containing CNC for click chemistry.

4 Fluorescently labelled materials based on cellulose nanocrystals

Based on the fluorescently labelled cellulose described in the introduction, this chapter will develop new methodologies to prepare fluorescently labelled cellulose nanocrystals. Chapter 4 applies the previously developed esterification methodologies for the synthesis of two new compounds with fluorescent behaviour, i.e. CNC grafted with carbazole and coumarin. As it was detailed in section 1.7.7, carbazole and coumarin are small molecules very well-known for their fluorescent properties and wide applications, and therefore were considered the perfect candidates for their grafting onto the surface of cellulose nanocrystals.[162,245,246] In order to be grafted, their conversion into suitable acids was considered. As coumarin-3-carboxylic acid is almost 28 times cheaper than 2-(carbazole-9-yl) acetic acid, it was procured and used as received while 2-(carbazole-9-yl) acetic acid was synthesised in the laboratory, as will be detailed below. Thus, carbazole-9-yl-acetic acid and coumarin-3-carboxylic acid are grafted onto CNC through TsCl/Py and carbodiimide mediated esterification. Absorption and fluorescence properties together with microscopic characterization will also be detailed. In addition, fluorescent cellulose-based OLEDs preparation was attempted and this is presented towards the end of this chapter.

4.1 *9H*-Carbazole and carbazole-9-yl-acetic acid

Carbazole alkylation is of interest for the present research as carbazole-9-yl-acetic acid can be synthesised in two steps and this was the chosen acid for the

esterification of CNC. Alkylation of carbazole leads to the formation of an ester which can then be converted into an acid as described below.

If potassium hydroxide powder and carbazole are fused together at 220-260 °C, potassium salts of carbazole are obtained and can then be utilized in a hydrocarbon solvent. It has been proven that potassium hydroxide powder was better to obtain carbazole salts than strong aqueous sodium hydroxide.[247]

Considering the above findings, the selected method for the N-alkylation of this heterocyclic compound in order to prepare methyl 2-(9*H*-carbazole-9-yl)acetate, $C_{15}H_{13}NO_2$, (Figure 4.1.1) was based on the methodology described by Conn *et al*. which involves the nucleophilic aliphatic substitution of the carbazole salt with an alkylating agent in a polar aprotic solvent to speed up the reaction.[248] For this, carbazole is stirred with dry K_2CO_3 in dry DMF under inert conditions in order to synthesise the potassium salt of carbazole before methyl bromoacetate was added in aliquots. The reaction product was purified and the yield was calculated to be 86 %. The second step in the reaction towards the acid synthesis was the conversion of the previously obtained ester, methyl 2-(9*H*-carbazol-9-yl)acetate, into the corresponding acid, carbazole-9-yl-acetic acid, $C_{14}H_{11}NO_2$, (Figure 4.1.2) based on the method described by Guo *et al.*.[249]

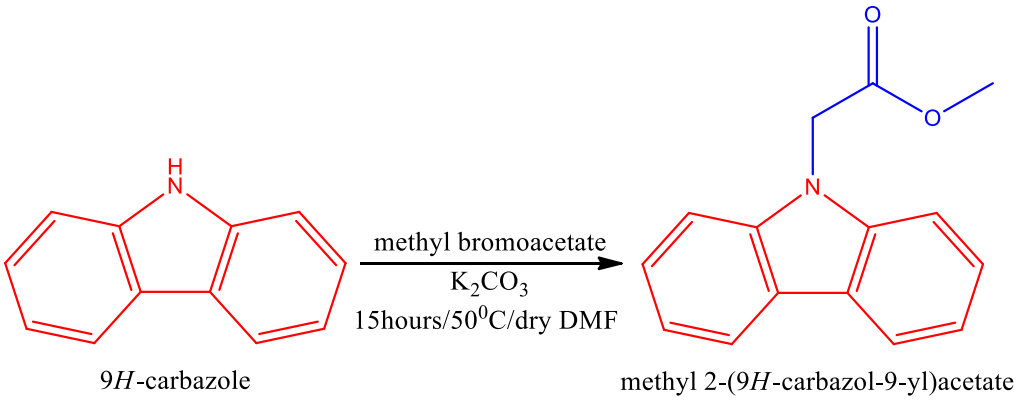
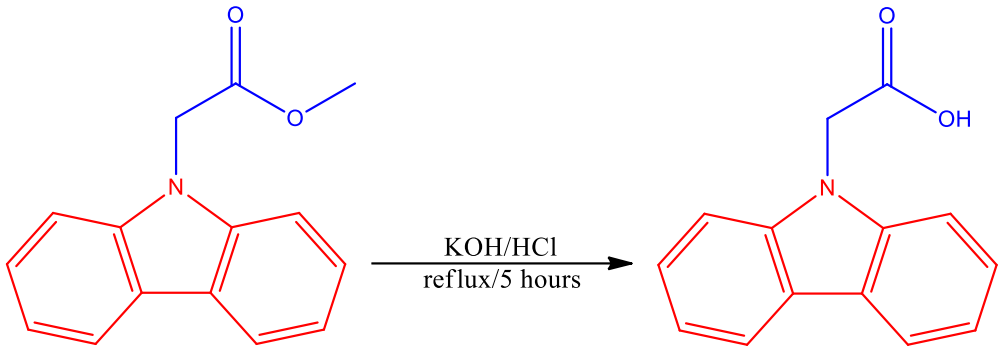


Figure 4.1.1 Synthesis of Methyl 2-(9*H*-carbazole-9-yl) acetate

Initially, the synthesis of carbazole-9-yl-acetic acid took place after the same method described by Conn *et al.*,[248] i.e. the formation of the carboxylic acid salt in MeOH by addition of KOH followed by neutralization with HCl to form the acid, but the yield of the reaction was relatively low.



methyl 2-(9*H*-carbazol-9-yl)acetate Carbazole-9-yl-acetic acid

Figure 4.1.2 Synthesis of Carbazole-9-yl-acetic acid

With this in mind, the synthesis methodology was altered to the method of Guo *et al.* in which methyl 2-(9*H*-carbazole-9-yl)acetate and KOH solution are heated and refluxed, followed by quenching and dilution with cold water and neutralization with a diluted solution of HCl to a pH of 2, followed by filtration of the white precipitate and washing with water. The yield increased from 64 % to 75 %.

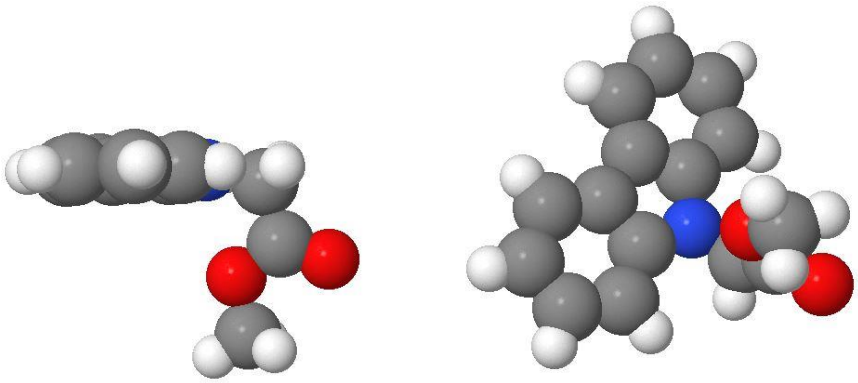


Figure 4.1.3 3D images of methyl 9H-carbazole-9-acetate as shown in Acta Crystallographica Section E[250]

The orientation of grafted molecules on cellulose can be predicted based on the crystal structure of the attached molecules. Figures 4.1.3 and 4.1.4 are pictures of the 3D structures of methyl 9H-carbazole-9-acetate and of 2-(carbazole-9-yl)acetic acid respectively.[250,251] Both molecules have a monoclinic structure in which the carbazole ring is essentially planar with a dihedral angle between the two benzene rings of 2.8 (5)°. The methyl acetate exists in a fully extended

conformation and the mean plane forms a dihedral angle of 93.5 (7)° with the carbazole mean plane[252,253] while in 2-(carbazole-9-yl)acetic acid, the pyrrole ring plane and the carboxylic acid plane forms a torsion angle of 88.5 (1)°.

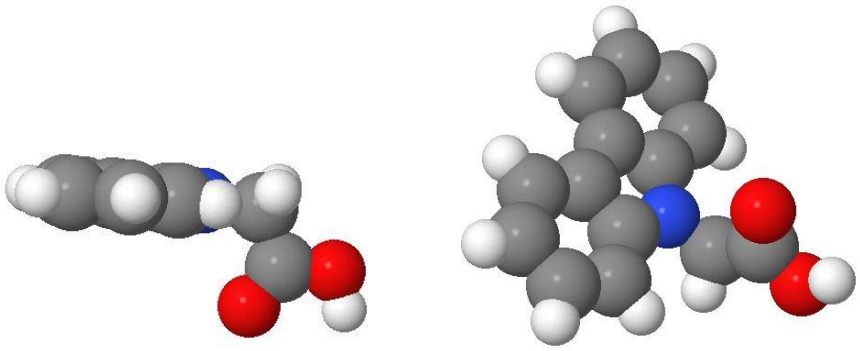


Figure 4.1.4 3D image of 2-(carbazole-9-yl)acetic acid (right) as it is shown in Acta Crystallographica Section E[251]

Both crystal structures present weak C–H···O hydrogen bonding. Hydroxyl groups are found in a perpendicular position on the surface of the cellulose. Therefore, the orientation of the grafted molecule is more likely to be in the same position as in the case of methyl 9H-carbazole-9-acetate. Thus, the grafted molecules create a planar layer of carbazole units nearly parallel to the surface of cellulose and linked to it through the ester linkage.

4.2 Coumarin and coumarin-3-carboxylic acid

Coumarin-3-carboxylic acid (Figure 4.2.1.) is based on coumarin. Initial synthesis of coumarin-3-carboxylic acid dates back to 1886 as mentioned by Dobson *et al*. based on the reaction between salicyl aldehyde and malonic acid.[254]

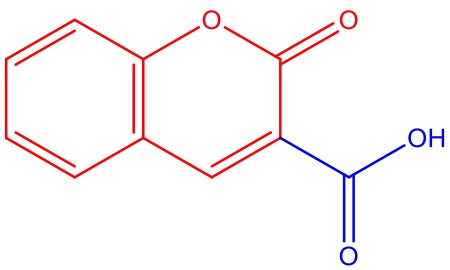


Figure 4.2.1 Coumarin-3-carboxylic acid

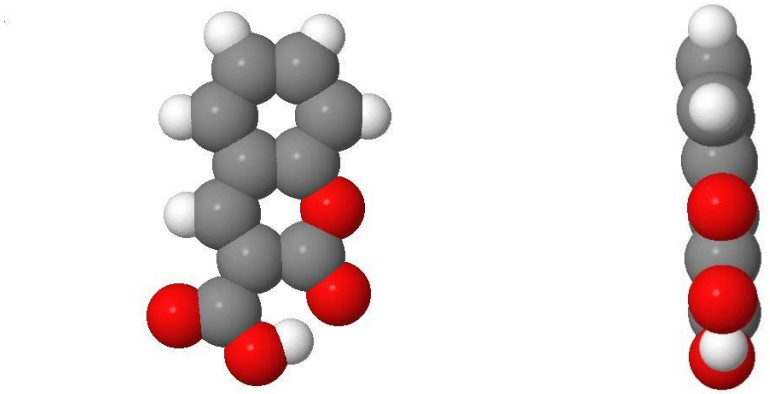


Figure 4.2.2 represents the 3D image of Coumarin-3-carboxylic acid as it is shown in Acta Crystallographica Section C.[254]

The molecule is nearly planar with a dihedral angle between the plane of the coumarin and the plane of the carboxyl group of 4.2 (1)°.[254]

4.3 Esterification reaction for the synthesis of carbazole-9-yl-acetate cellulose nanocrystals through carbodiimide-mediated coupling

The synthesis of carbazole-9-yl-acetate cellulose was first attempted by using a methodology in which a carbodiimide was used as the coupling agent. As described in Chapter 3 in the synthesis of acrylate/methacrylate cellulose, the methodology involving DIC as a coupling agent was also applied here in order to obtain the desired modification. CNC together with carbazole-9-yl-acetic acid (Cz-ac-a), DIC, DMAP with a molar ratio of 1:5.5:5.5:0.03 and 1:3:3:0.03 OH:Acid:DIC:DMAP (ratios calculated relative to the amount of hydroxyl groups per cellulose surface of 3 mmol/g) were flushed with argon and suspended in dry DCM for 5 days in room temperature, before purification by Soxhlet extraction with DCM for 24 hours and EtOH for further 72 hours and drying *in vacuo* (Figure 4.3.1 1st methodology).

The synthesised product is a white crystalline powder very similar to the original CNC. Looking at the infrared spectrum of the CNC and the two

modified products (figure 4.3.2.), it can be noticed that a carbonyl stretch vibration becomes visible at 1744 and 1746 cm^{-1} respectively, and vibrations characteristic for C=C bond at 1638 and 1646 cm^{-1} respectively albeit with a small intensity increasing from the modification with 1:3:3:0.03 ratio to the 1:5.5:5.5:0.03 OH:Acid:DIC:DMAP ratio. Yet, it still confirms the formation of the ester at the surface of CNC.

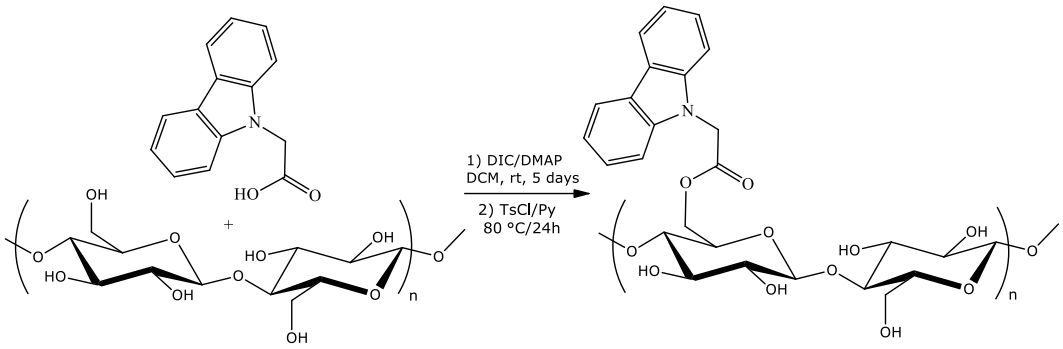


Figure 4.3.1 Carbazole acetate cellulose synthesis by two methodologies: 1) carbodiimide mediated esterification and 2) TsCl/Py methodology

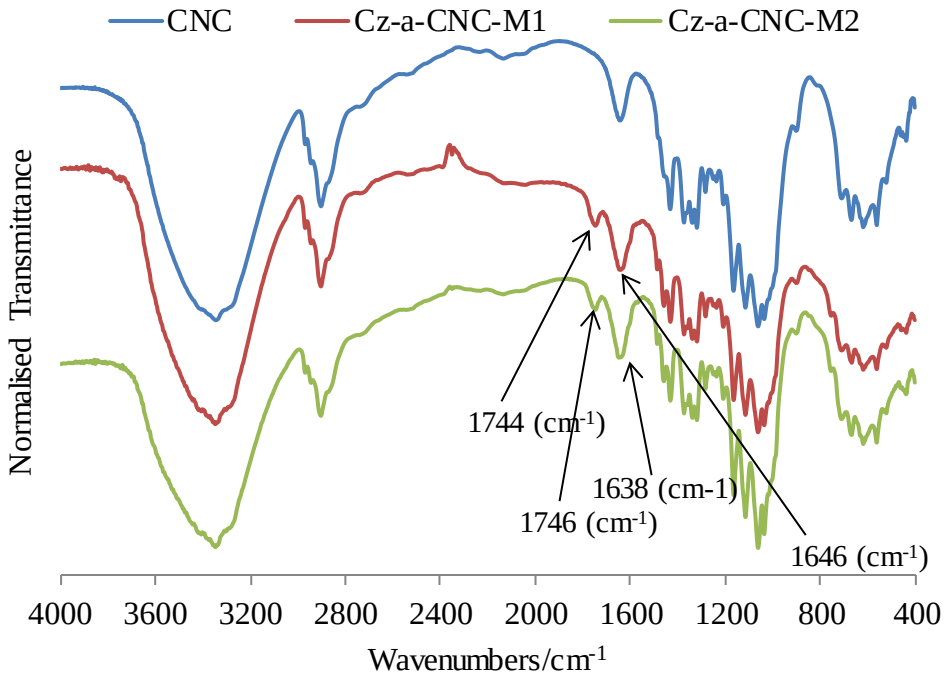


Figure 4.3.2 FT-IR Spectrum of CNC and carbazole-9-yl-acetate cellulose synthesised by carbodiimide-mediated coupling

Using EA, the surface degree of substitution was calculated and found to have a low value, in agreement with the small intensities of the C=O vibrations. For the two modified products, increasing the equimolar ratio of acid and DIC to CNC from 1:3:3 to 1:5.5:5.5 resulted in no significant difference in the final EA with a N % of 0.23 and 0.25, which corresponds to a DS_{surf} = 0.09 and 0.10 respectively (Table 4.3.1). The XPS wide scan for Cz-a-CNC-M2 (1:5.5:5.5:0.03 OH:Acid:DIC:DMAP ratio) (Chapter 4 Appendix, Figure 10.2.1) shows only carbon, oxygen and nitrogen elements on the surface, as expected. A closer insight into the XPS C1s high resolution scan revealed the presence of a peak at 289.43 eV, corresponding to ester carbonyl carbons (Figure 4.3.3.).[228]

Table 4.3.1 Elemental analysis results for CNC and of the two modifications carbazole-9-yl-acetate cellulose using DIC/DMAP methodology

Sample	Molar ratio OH:Acid:DIC:DMAP	C (%)	H (%)	N (%)	DS_{surf}(N)
CNC		41.77	5.91	0	
1 Cz-a-CNC-M1	1:3:3:0.03	43.67	5.86	0.23	0.09
2 Cz-a-CNC-M2	1:5.5:5.5:0.03	43.56	5.84	0.25	0.10

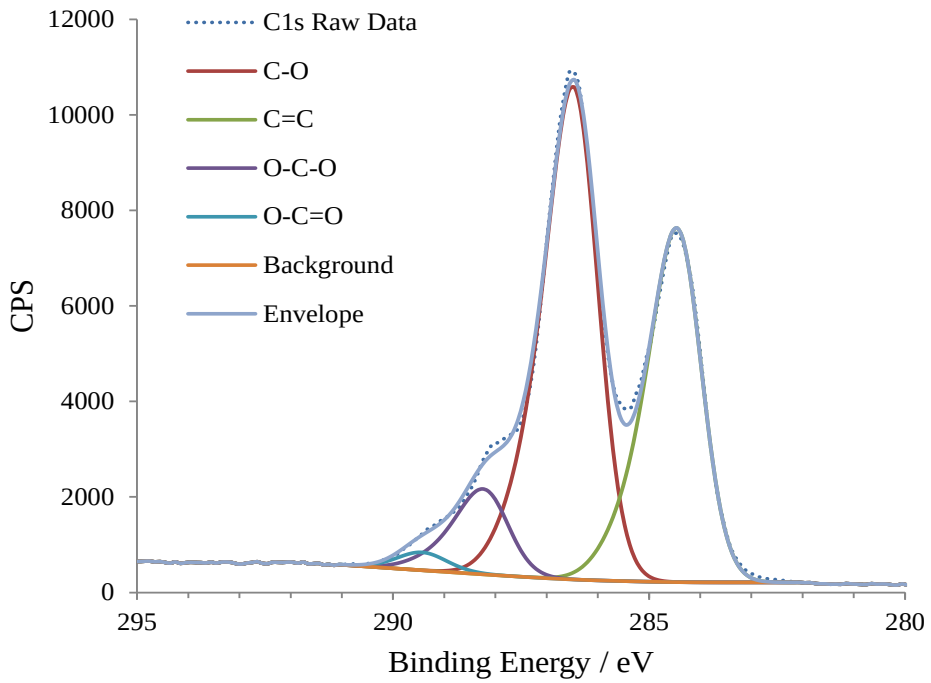


Figure 4.3.3 C 1s high resolution of carbazole-9-yl-acetate, Cz-a-CNC-M2, synthesised by DIC/DMAP, identifying the components peaks

Also, the presence of a very prominent peak at a BE of 284.32 eV, attributed to C=C bonds in the carbazole aromatic rings, shows success of modification (Table 4.3.2). Furthermore, a high resolution scan of N1s shows the presence of nitrogen at a BE of 400.1 eV which corresponds to nitrogen bound singly to three carbons as in tertiary amines (Chapter 4 Appendix, Figure 10.2.2).[255]

Table 4.3.2 Detailed XPS data for carbazole-9-yl-acetate cellulose, Cz-a-CNC-M2, synthesised through DIC/DMAP (results similar with Cz-a-CNC-M1)

Orbital	Component	BE /eV	FWHM	Rel. A / % [a]	at%
C1s	C=C	284.32	1.14	37.42	25.98
	C–O	286.34	1.14	51.96	36.07
	O–C–O	288.10	1.14	8.97	6.23
	O–C=O	289.43	1.14	1.65	1.15
				100	69.43
O1s	C–O–H	532.59	1.19	60.01	17.16
	O–C–O	533.19	1.19	39.99	11.44
				100	28.6
N1s	C–N=	400.11	1.06	100.00	1.97
				100	1.97

[a] Relative area = component area×100/sum area of same orbital

To determine the crystallinity of the modified CNC, powder XRD was used. After applying Rietveld refinement, the current batch of CNC used for this esterification presented an initial crystallinity index of χ_C^R = 0.796, whereas the final product Cz-a-CNC-M2 presented a loss in crystallinity of 4.84 %, thus displaying a crystallinity of χ_C^R = 0.747, (Chapter 4 Appendix, Figure 10.2.3). Using the nitrogen content from EA (0.25 %) and nitrogen content in carbazole-9-yl-acetic acid ($C_{14}H_{11}NO_2$) (6.22 %), the amount of modification (non-crystalline) in the sample is 4 %, very close to the observed crystallinity loss. The crystallinity loss can thus be attributed to the increase in non-crystalline material from the surface modification.

4.4 Esterification reaction for the synthesis of carbazole-9-yl-acetate cellulose nanocrystals through TsCl/Py

The second methodology applied to the heterogeneous esterification reaction to prepare carbazole-9-yl-acetate cellulose is carried out using the TsCl/Py system as described in section 4.3 (Figure 4.3.1 methodology 2). CNC, together with carbazole-9-yl-acetic acid and TsCl were flushed with argon and combined in pyridine at 80 °C for 24 hours before purification by Soxhlet extraction and *in vacuo* drying of the white-off carbazole-9-yl-acetate cellulose (Cz-a-CNC) product. The reaction was performed with increased molar ratios of CNC relative to equimolar amounts of carbazole-9-yl-acetic acid and TsCl in the following ratios: 1:0.66:0.66; 1:1.33:1.33; 1:2:2; 1:2.66:2.66; 1:3.33:3.33 for CNC:Acid:TsCl. The different molar excesses were used to determine the optimum for this esterification method in which carbazole-9-yl-acetic acid was used.

At a first glance, the infrared spectrum revealed the appearance of an increasingly prominent signal at 1744.5, 1748.6, 1748.7 1750.5, and 1750.8 cm^{-1} respectively, which corresponds to the carbonyl stretching vibration for each of the modified celluloses (Figure 4.4.1). Also, multiple aromatic C=C stretching vibrations at 1627, 1599, 1485, and 1456 cm^{-1} make their appearance. The band at 1356 and 1324 cm^{-1} could be attributed to carbon nitrogen C–N vibrations while bands at 751 and 722 cm^{-1} can be attributed to an out-of-plane C–H di–substituted aromatic systems as in the case of the two benzene rings that are fused together on the pyrrole ring.[256] To further confirm the presence of carbazole and the grafted carbazole-9-yl-acetic acid, an FT-IR spectrum was recorded for 9*H*-Carbazole and Carbazole-9-yl-acetic acid (Figure 4.4.2). The 9*H*-Carbazole presents very sharp absorption bands characteristic for N-H at 3418 cm^{-1}, C=C at 1625 and 1610 cm^{-1}, and specific aromatic vibration at 1485 and 1458 cm^{-1}. Out-of-plane C–H di–substituted aromatic vibrations can also be identified at 748 and 725 cm^{-1}. These values are mainly observed in the carbazole-9-yl-acetic acid spectrum but without the N-H vibration which is replace by the vibration of the hydroxyl group of the acid identified at 3050 cm^{-1} and the appearance of the carboxyl vibration is

identified at 1720 cm^{-1}. Consequently, the identification of the specific peaks of carbazole in carbazole modified cellulose is relatively straightforward and represents the confirmation of successful esterification for the 5 reactions.

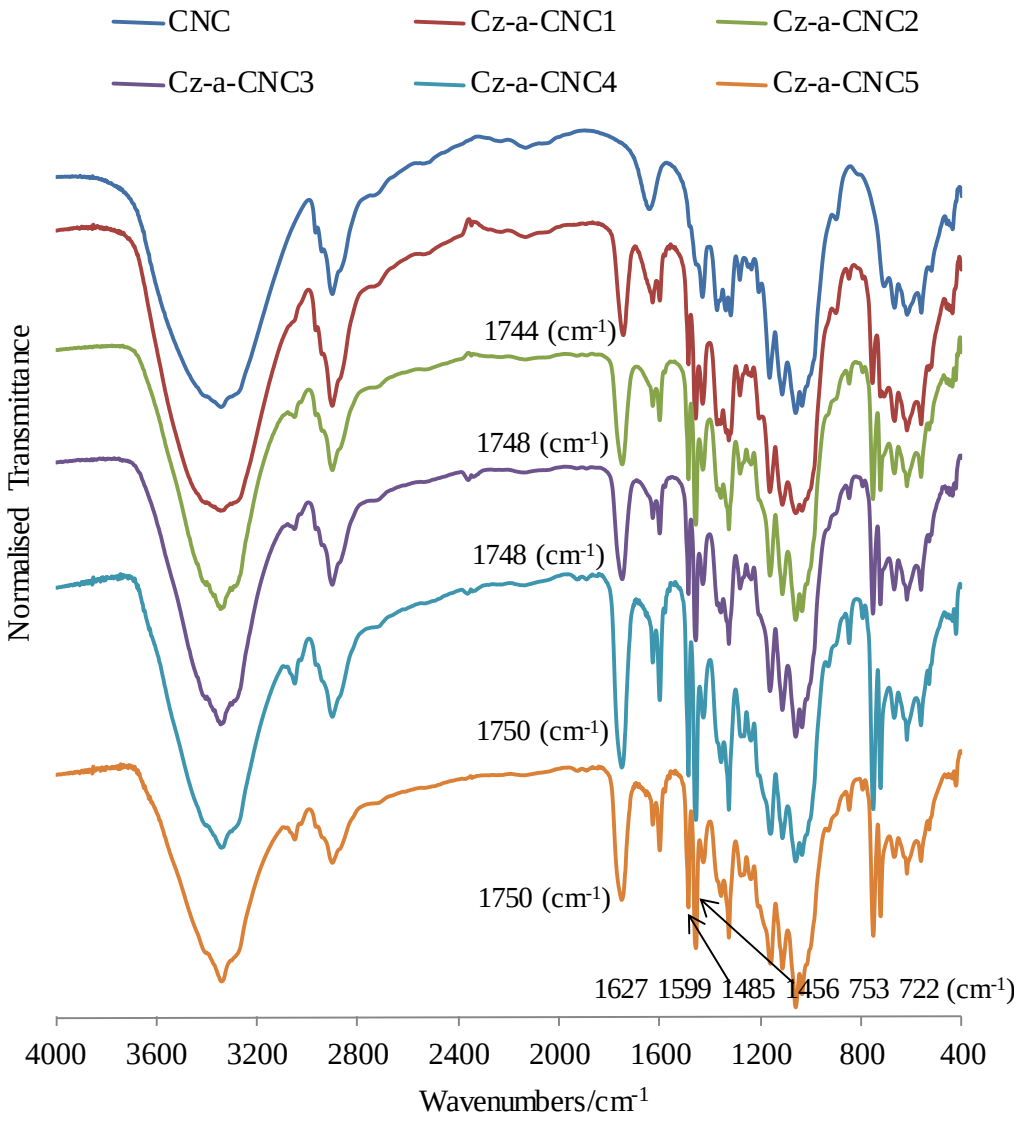


Figure 4.4.1 FT-IR Spectrum of CNC and Cz-a-CNC synthesised by TsCl/Py with the molar excess 1:0.66:0.66; 1:1.33:1.33; 1:2:2; 1:2.66:2.66; 1:3.33:3.33

EA of all five modified celluloses confirms the very high substitution revealed by FT-IR (Table 4.4.1). The increasing intensities of the absorption bands are proportional to the calculated DS_{surf} with the exception of the last absorption intensity that is correlated with a DS_{surf} = 1.55 which still can be considered the maximum given the possible error in the calculations and the polydispersity of

the nanoparticles in length and cross-section. Increasing the molar ratio, OH:Acid:TsCl, lead to a DS_{surf} that increases up to the maximum of hydroxyl groups available on the surface of nanocrystals for the last two modifications.

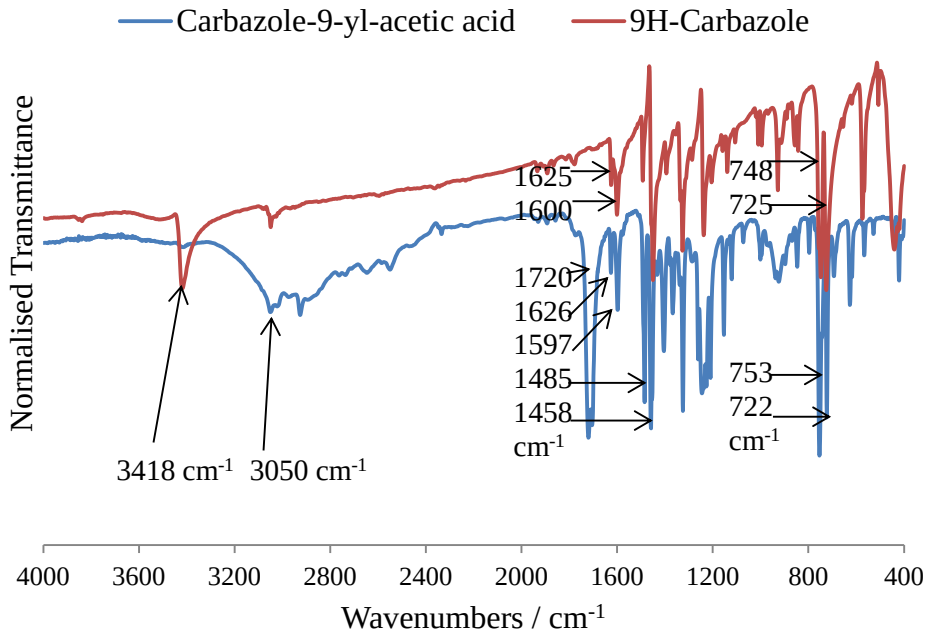


Figure 4.4.2 FT-IR Spectrum of 9*H*-Carbazole and Carbazole-9-yl-acetic acid

Table 4.4.1 Elemental analysis results for CNC and of the five modifications carbazole-9-yl-acetate cellulose using TsCl/Py

Sample	Molar ratio OH:Acid:TsCl	C (%)	H (%)	N (%)	DS_{surf}(N)
CNC		42.31	6.15	0	
Cz-a-CNC1	1:0.66:0.66	47.31	5.77	0.82	0.39
Cz-a-CNC2	1:1.33:1.33	51.42	5.65	1.57	0.72
Cz-a-CNC3	1:2:2	53.80	5.52	1.97	1.03
Cz-a-CNC4	1:2.66:2.66	57.34	5.30	2.55	1.6
Cz-a-CNC5	1:3.33:3.33	57.75	5.36	2.56	1.55

If all the hydroxyl groups were accessible for modification, the maximum DS_{surf} = 1.5. Therefore, the DS_{surf} = 1.55 and DS_{surf} = 1.60 for Cz-a-CNC5 and Cz-a-CNC4 modifications could be understood by the fact that due to the higher molar excess then the first 3 modifications, there may still be some unreacted carboxyl-9-yl-acetic acid, stuck on the surface and packed with the

grafts and therefore difficult to be removed. Although purification was carried out with DCM for 24 hours and with EtOH for further 72 hours, still appears to be insufficient. The carbazole-9-yl-acetic acid solubility in EtOH and DCM was tested in laboratory and therefore intensive purification was applied based on these good solubilities, especially in EtOH. Previous DS_{surf} calculations could be correlated with the FT-IR interpretation where the slight increase of carbonyl absorption wavelength could indicate the presence of some unreacted acid. Another possible explanation is the fact that the exceeding values are very close to the theoretical maximum value of surface degree of modification. Therefore, these values can stay in the experimental error or as it was mentioned in the Characterization Chapter, the theoretical maximum surface degree of modification is slightly influenced by the polydispersity in length and cross section of the nanocrystals and thus, slight variation.

The crystallinity of the modified CNC was determined by powder XRD followed by Rietveld refinement (Chapter 4 Appendix, Figure 10.2.4). Table 4.4.2 presents the values of the crystallinity index, χ_C^R, for the unmodified cellulose and the modified samples, N% from EA, the loss of crystallinity, $\Delta\chi_C^R$, and the calculated expected modification based on elemental analysis C_{modif}.

Table 4.4.2 Crystallinity index values, crystallinity loss, elemental analysis N % and the expected amount of modification

	CNC	Cz-a-CNC1	Cz-a-CNC2	Cz-a-CNC3	Cz-a-CNC4	Cz-a-CNC5
$\boldsymbol{\chi_C^R}$	0.796	0.668	0.584	0.574	0.474	0.476
$\boldsymbol{\Delta\,\chi_C^R}$		0.127	0.211	0.221	0.322	0.320
N %	-	0.82	1.57	1.97	2.55	2.56
C_{modif}		0.13	0.25	0.31	0.40	0.41

The calculated values for modification based on the amount of nitrogen agree well with the loss of crystallinity for the first two modifications. For the last three modifications, the amount of possible modification is higher than the value resulting from the loss of crystallinity, which could be explained by an excess of acid not grafted to the surface. The correlation between the expected

modification and the loss of crystallinity stays consistent. Thus, it is recommended that the optimum esterification molar excess would be 1:2:2 for carbazole-9-yl acetic acid, as this molar ratio results in the functionalization of two hydroxyl groups per AGU and thus maintaining the crystalline integrity.

XPS was used to further analyse the modifications and for all the five modifications, the wide scan XPS revealed the presence of carbon, oxygen and nitrogen and some trace amount of sulfur as expected for reactions involving TsCl (Chapter 4 Appendix, Figure 10.2.5). More than these, the XPS carbon high resolution scan gave even more significant evidence of esterification for all five modifications (Figure 4.4.3 a, Appendix for Chapter 4, Figure 10.2.6 – 10.2.9). Figure 4.4.3 a represents the decomposition of the C1s of Cz-a-CNC3 being the middle in the sequence of the five and having a DS_{surf} = 1.03 which means that on every AGU two hydroxyl groups are modified and so on every AGU there are two carbazole molecules facing outwards as described in section 4.1.

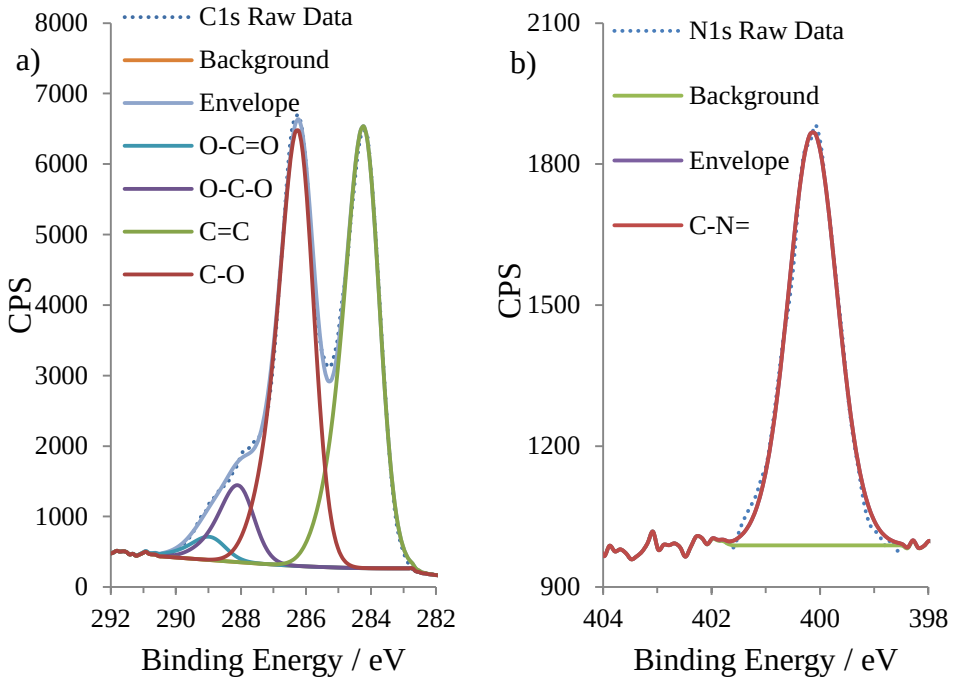


Figure 4.4.3 a) XPS high resolution spectrum of C1s peak of Carbazole-9-yl-acetate, Cz-a-CNC3 cellulose synthetized by TsCl/Py methodology; b) N1s high resolution scan of Cz-a-CNC3, synthesised by TsCl/Py

It is seen an increasing surface area of the O–C=O and large C=C for Cz-a-CNC1 up to Cz-a-CNC5 (Chapter 4 Appendix, Figure 10.2.6 – Figure 10.2.9). The decrease of the C–O relative peak intensity from the first modification to the last is partially explained by increased esterification of the hydroxyl groups by their conversion into esters, and so increased the O–C=O carbon environment, which may also include ungrafted acid. In addition, the C–O reduction is correlated with the XPS signal sensitivity which decreases as the bond becomes more embedded inside the structure. As for the carbazole-9-yl-acetate cellulose synthesised through this methodology, the nitrogen high resolution scan for these modifications shows a single peak at the same BE of 400.1 eV that corresponds to the C–N chemical environment found in carbazole (Figure 4.4.2 b). Table 4.4.3 gives further insight into the surface composition based on the wide scan spectra and the deconvoluted carbon composition from the high resolution scans for CNC and the five modified CNC through the discussed methodology.

The O/C ratio for unmodified cellulose, calculated from the relative peaks areas in wide scan, was found to be 0.74, lower than the theoretical value (0.82), which can be explained by surface contamination as a result of exposed to air and commonly attributed to adventitious carbon.[65] Upon modification, the O/C ratio decreased from 0.74 to 0.32 indicating that the surface became much richer in carbon atoms when compared to the unmodified cellulose, due to the grafted carbazole moieties. The decrease in O/C ratio is based on significant changes in the relative O and C atomic concentrations as the molar ratio of the reactants was increased. All the information gleaned from XPS agrees with the previous characterization techniques, FT-IR, EA and XRD, and underlines once again that full substitution of the hydroxyl groups is achieved as the molar ratio is varied in order to find the optimum value.

By comparing the two methodologies developed for carbazole-9-yl-acetate cellulose synthesis based on infrared spectroscopy and EA, the second methodology gives clearly superior degrees of substitution and a faster reaction time although the first methodology offers more friendly reaction conditions, such as room temperature reaction.

Table 4.4.3 XPS wide scan elemental surface composition and quantification of carbon chemical environments from C1s high resolution scan

	Surface composition (at. %)				Carbon composition (at. %)				
	C1s	O1s	N1s	O/C	C–C/ C–H	C–O	O–C–O	O–C=O	C=C
CNC	57.43	42.57		0.74	8.2	77.41	14.39		
Cz-a-CNC1	64.89	33.81	1.3	0.52		62.46	10.62	1.03	25.88
Cz-a-CNC2	68.66	29.56	1.78	0.43		49.77	8.92	2.4	38.92
Cz-a-CNC3	71.18	26.91	1.91	0.38		44.58	7.84	2.37	45.21
Cz-a-CNC4	73.36	23.88	2.76	0.33		41.69	6.12	3.51	48.68
Cz-a-CNC5	73.92	23.8	2.28	0.32		37.52	4.91	4.4	53.18

Similar to the observations from chapter 3, the two esterification strategies displayed reaction products with different coloration. The carbazole-9-yl-acetate cellulose synthesised by TsCl/Py showed an ecru colour while the DIC/DMAP product was clear white.

4.5 Esterification reaction for the synthesis of coumarin-3-carboxylate cellulose nanocrystals

The procedure to graft the second fluorescent molecule selected to label cellulose was based on the results obtained for the two esterification methodologies used for the carbazole-9-yl-acetate cellulose synthesis. Thus, the synthesis of coumarin-3-carboxylate cellulose was performed using the TsCl/Py methodology and only for molar ratios of 1:1.83:1.83 and 1:2.66:2.66. This was also in agreement with results obtained by research colleagues in our lab at the same time for the TsCl/Py methodology.[96] Thus cellulose nanoparticles, together with coumarin-3-carboxylic acid and TsCl, were flushed with argon and dispersed in pyridine, This mixture was then reacted at 80 °C for 16 hours before purification by Soxhlet extraction with DCM for 24 hours and EtOH for a further 72 hours, followed by *in vacuo* drying to yield coumarin-3-carboxylate cellulose (Co-c-CNC) shown in the reaction scheme presented in Figure 4.5.1.

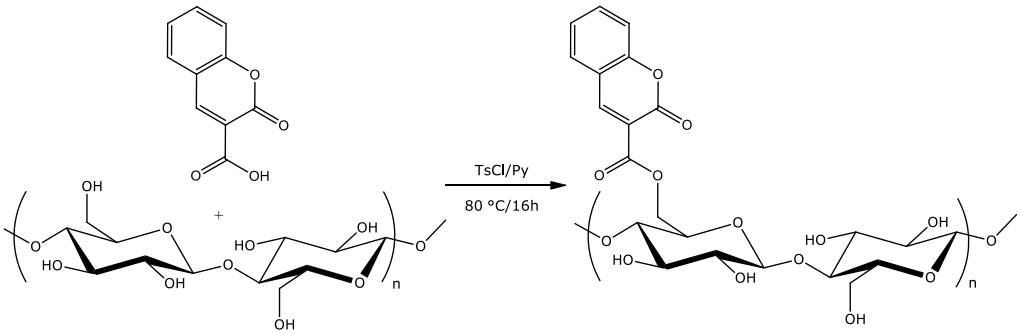


Figure 4.5.1 Coumarin-3-carboxylate cellulose synthesis by the TsCl/Py methodology

The infrared spectrum of the synthesised coumarin-3-carboxylate for the two molar ratios, Co-c-CNC1 and Co-c-CNC2, shows the clear presence of the

carbonyl stretching vibrations at 1762 and 1766 cm^{-1} for the first and second modifications respectively (Figure 4.5.2). Analogous to the previous esterification, a shift to a higher absorption wavelength is seen and hence possible un-grafted acid presence could be expected Also, compared with the unmodified CNC spectra, multiple aromatic C=C stretching vibrations at 1609, 1566, 1485, and 1455 cm^{-1} become visible. The bands at 1242 and 1209 cm^{-1} are attributed to carbon oxygen C–O–C ether stretching vibration bands while the signals present at 795 and 763 cm^{-1} can be attributed to an out-of-plane C–H di–substituted aromatic system as in the case of the benzene ring part of the coumarin molecule.

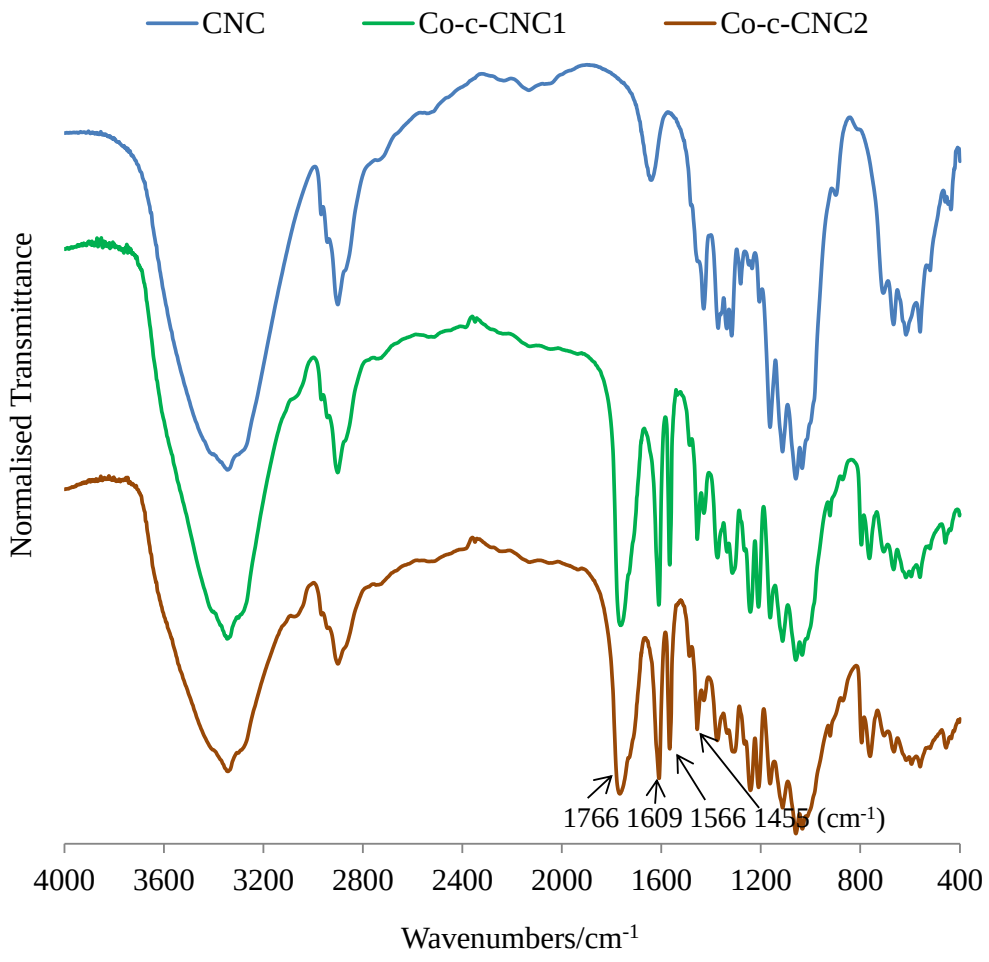


Figure 4.5.2 FT-IR Spectrum of CNC and coumarin-3-carboxylate cellulose, Co-c-CNC1 and Co-c-CNC2 synthesised by the TsCl/Py methodology

EA confirms the complete esterification of the starting nanocellulose. Based on the calculations of DS_{surf} = 1.33 for Co-c-CNC1 and DS_{surf} = 1.56 for Co-c-CNC2 with a molar ratio of 1:1.83:1.83 and 1:2.66:2.66 respectively, these represent the conversion of two to three hydroxyl groups. Yet, the second modification slightly exceeds the theoretical calculations but it could also be within the error of the calculation. The FT-IR observations agree with the EA finding that there might be some unreacted acid.

Table 4.5.1 Elemental analysis results for CNC and of the two modifications coumarin-3-carboxylate cellulose using TsCl/Py

Sample	Molar ratio OH:Acid:TsCl	C (%)	H (%)	DS_{surf}(C)
CNC		41.77	5.91	
Co-c-CNC1	1:1.83:1.83	50.00	4.89	1.33
Co-c-CNC2	1:2.66:2.66	50.97	4.74	1.56

Comparing the reaction products Cz-a-CNC4 (DS_{surf} = 1.6) and Co-c-CNC2 (DS_{surf} = 1.56) for the same molar ratio used in the reaction, 1:2.66:2.66, they resulted in having almost equal degrees of substitution, while Cz-a-CNC3 (1:2:2) with DS_{surf} = 1.03 and Co-c-CNC1 (1:1.83:1.83) DS_{surf} = 1.33 are slightly different. An explanation for this is their reactivity, the pKa of coumarin-3-carboxylic acid is 1.5 and is greater than the one of carbazole-9-yl-acetic acid which is 3.5 and even higher than the one of acrylic acid that is 4.25.

Considering these very high surface degrees of substitution, the integrity of the crystals might be significantly influenced. The determined crystallinity indexes for the two reaction products are χ_C^R = 0.654 and χ_C^R = 0.465 indicating a loss of crystallinity of 14.2 % and 33.1 % when compared with the unmodified CNC (χ_C^R = 0.796) (Chapter 4 Appendix, Figure 10.2.10 – 11). The calculated expected loss of crystallinity is 13.03 and 14.56 %, respectively. If the first value is almost only 1% difference and stays in the margin of error, the second modification has a much larger discrepancy. So, this high loss of crystallinity is assumed to a peeling off of the chains from the crystal core, opening up more hydroxyl groups for reaction and hence, a higher degree of substitution, which

also gives a reduction in overall sample crystallinity. As the reaction product Co-c-CNC1, satisfies the conditions for being the optimum reaction product, it will be further analysed. In addition to EA, XPS gives further indications on the formed product but only based on the presence of carbon and oxygen as these are the only elements that come from coumarin-3-carboxylic acid. The wide scan spectra (Chapter 4 Appendix, Figure 10.2.12) confirm the presence of only carbon and oxygen while the high resolution scans confirm the presence of trace amounts of sulfur attributed to the sulphate groups on the CNC from acid hydrolysis, considering that the amounts were significantly low, as sulphur peak couldn't be identified in the wide scan.

Further analysis of the product by XPS C1s high resolution (Figure 4.5.3) and O1s high resolution (Figure 4.5.4) scans reveals successful esterification through the existence of a component at a BE of 289.08 eV which is attributed to the O–C=O component expected for ester in C1s and at 531.54 eV in O1s (visible only due to the very high degree of substitution). Esterification was also confirmed by the peak corresponding to C=C identified at 285.02 eV.

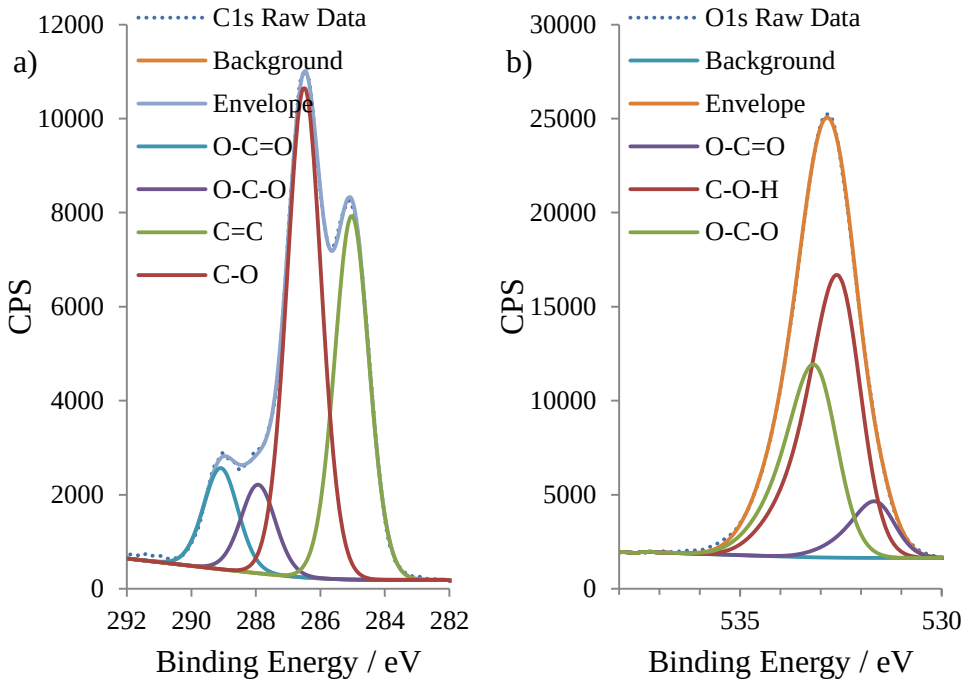


Figure 4.5.3 XPS high resolution spectrum of C1s a) and O1s b) peak of Coumarin-3-carboxylate cellulose, Co-c-CNC1 synthetized with the TsCl/Py reaction methodology

Table 4.5.2 Detailed XPS data for coumarin-3-carboxylate cellulose Co-c-CNC1, synthesised by TsCl/Py

Orbital	Component	BE /eV	FWHM	Rel. A / % [a]	at%
C1s	C=C	285.03	1.26	34.92	24.07
	C–O	286.50	1.26	46.96	32.37
	O–C–O	287.93	1.26	8.47	5.84
	O–C=O	289.08	1.26	9.65	6.65
				100	68.94
O1s	O–C=O	531.54	1.185	9.34	2.90
	C–O–H	532.43	1.352	54.5	16.91
	O–C–O	533.03	1.352	36.26	11.26
				100.00	31.06

[a] Relative area = component area×100/sum area of same orbital

The theoretical peak ratios from the stoichiometry of coumarin-3-carboxylate cellulose O–C=O:C=C are 2:7 (1:3.5) while the calculated one based on relative components area are 9.65:34.93 (1:3.61), thus showing good agreement (Table 4.5.2). All these analysis techniques show that the TsCl/Py methodology is highly effective for the surface esterification of CNC by acid-functionalised fluorescent molecules.

4.6 TEM and AFM characterization

The TEM and AFM images were recorded in order to check the morphological features of CNC after modification. Figures 4.6.1 are TEM micrographs of: a) unmodified Cellulose Nanocrystals; b) Carbazole-9-yl-acetate Cellulose (Cz-a-CNC3); and c) Coumarin-3-carboxylate cellulose (Co-c-CNC1). Mainly, the rod-like nanocrystal shape of the unmodified CNC is maintained upon modification, as well as the distribution of dimensions of the nanoparticles. When comparing the initial length and width values of cellulose whiskers (lengths between 100 and 300 nm and widths ranging 5 to 15 nm) with the modified ones, similar lengths of the nanocrystals with values between 100 to 300 nm while the average width is maintained around 10 nm are observed. In agreement with the TEM, the three-dimensional images of the surface for: a)

Cellulose nanocrystals; b) Carbazole-9-yl-acetate Cellulose (Cz-a-CNC3); c) Coumarin-3-carboxylate Cellulose (Co-c-CNC1), obtained in tapping mode collected by AFM (Figure 4.6.2) prove once again that the morphology of the cellulose nanowhiskers is not affected by the grafting and the shape and size are maintained.

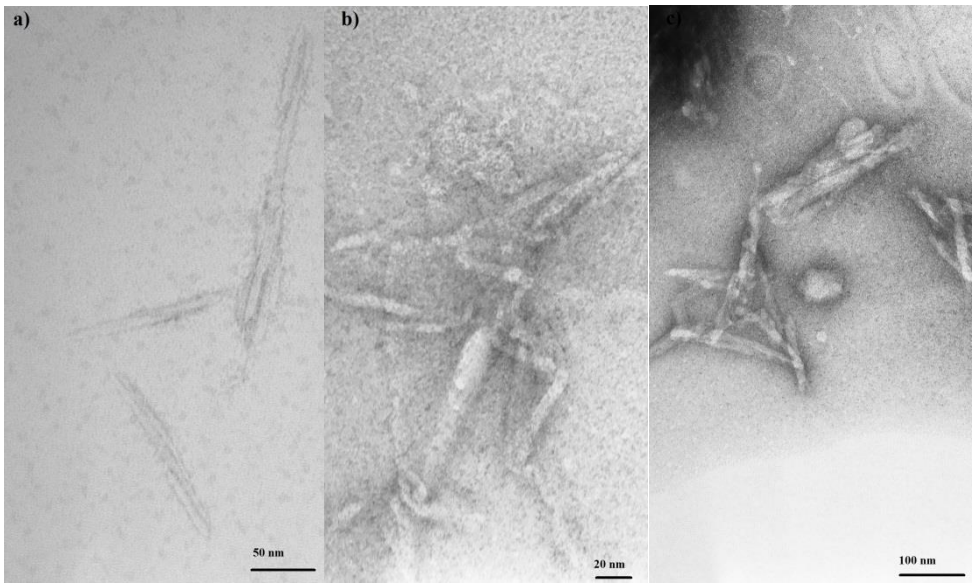
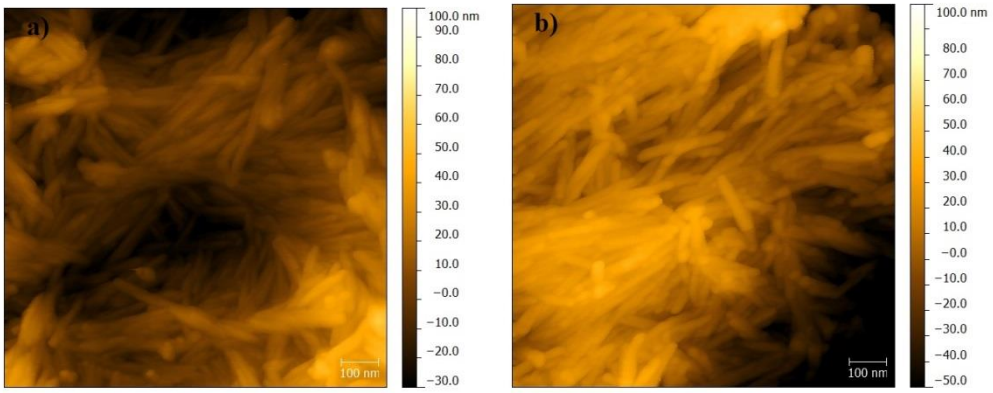


Figure 4.6.1 TEM Micrograph of a) Cellulose Nanocrystals; b) Carbazole-9-yl-acetate Cellulose (Cz-a-CNC4); c) Coumarin-3-carboxylate cellulose (Co-c-CNC1) (Negative – Staining with Uranylacetate)



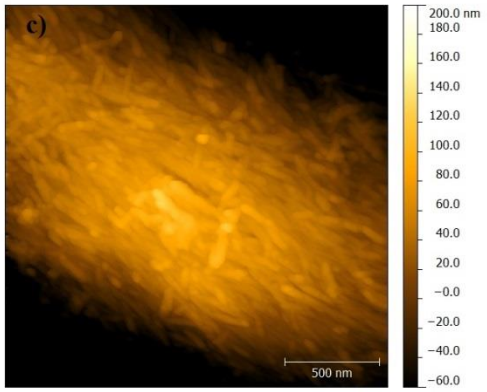


Figure 4.6.2 AFM images of a) Cellulose nanocrystals; b) Carbazole-9-yl-acetate Cellulose (Cz-a-CNC3); c) Coumarin-3-carboxylate Cellulose (Co-c-CNC1), obtained in tapping mode

4.7 Absorption and Fluorescence characterization

In order to use cellulose nanoparticles as fluorescent probes to obtain sensing nanomaterials, both UV-Vis spectroscopy and fluorescence measurements was applied to test the optical properties. First, the absorption properties of the fluorescent molecules were tested and UV-Vis measurements of carbazole and coumarin solutions respectively were carried out, in DMSO within the concentration range 5 – 54 μM for carbazole and 1– 100 μM for coumarin-3-carboxylic acid (Chapter 4 Appendix, Figure 10.2.13 and Figure 10.2.14). Second, the absorbance of each solution at their maximum (for carbazole at 294 and for coumarin-3-carboxylic acid at 293) was plotted against the concentration of the solution and linear regression was carried out to determine the extinction coefficient using the Beer–Lambert Law (Chapter 4 Appendix, Figure 10.2.15 and Figure 10.2.16). The resulting extinction coefficient is ε = 16780 $mol^{-1}dm^{-3}cm^{-1}$ for carbazole and ε = 11282 $mol^{-1}dm^{-3}cm^{-1}$ for coumarin-3-carboxylic acid (R^2 = 0.999 for carbazole and R^2 = 0.997 for coumarin-3-carboxylic acid) compared with 16000 $mol^{-1}dm^{-3}cm^{-1}$ (λ = 294) for carbazole in DMF (to the best of my knowledge, the extinction coefficient in DMSO is not reported in the literature) and 9378 $mol^{-1}dm^{-3}cm^{-1}$ (λ = 294) in DMSO for coumarin-3-carboxylic acid reported in the literature.[257,258]

The amount of grafted carbazole and coumarin respectively was determined by suspending a certain amount of modified and unmodified cellulose in a known volume of solvent followed by a determination of the absorption spectra of these samples (Figure 4.7.1 and 4.7.2). The amount of fluorescent molecules, mathematically determined as specified in section 2.8 (Equation 2.8.2), are presented in table 4.7.1. All the calculations were done only after subtraction of cellulose absorption from the modified cellulose spectra. Furthermore, the amounts of fluorescent molecules (0.376 mmol/g, 0.426 mmol/g, 0.576 mmol/g, and 0.930 mmol/g for carbazole-9-yl-acetate cellulose and 0.755 mmol/g for coumarin-3-carboxylate cellulose, respectively) were used to calculate the DS_{surf} considering the numbers of moles of modification per gram of product by using the equation (4.7.1) proposed by Eyley *et al*.[72]

$$DS_{surf} = \frac{1.5\, N_{mod}}{X_{cell} N_{OH}} \qquad (4.7.1)$$

The DS_{surf} is therefore the fraction between the product of the number of accessible hydroxyl groups per AGU at the surface (1.5) and the number of moles of modification (N_{mod}), and the product between the mass fraction of cellulose (X_{cell}) and number of moles of hydroxyl group per gram on the surface of cellulose nanocrystals (N_{OH}). The resulting values of DS_{surf} are 0.19, 0.22, 0.30, 0.49 for carbazole-9-yl-acetate cellulose and 0.39 for coumarin-3-carboxylate cellulose, and these values are significantly lower than those found by elemental analysis as indicated in Table 4.4.1 and Table 4.5.1.

The poor agreement between the two methods of DS_{surf} determination could be due to the fact that the extent of modification determined from optical properties which is less than the values determined by elemental analysis is due to a possible quenching effect causing significant reduction in absorption properties. This would therefore result in a final lower amount of modification determined on the surface. This will be further studied later on in this section in order to elucidate this possible influence on the final degree of substitution calculated using the number of moles of modification.

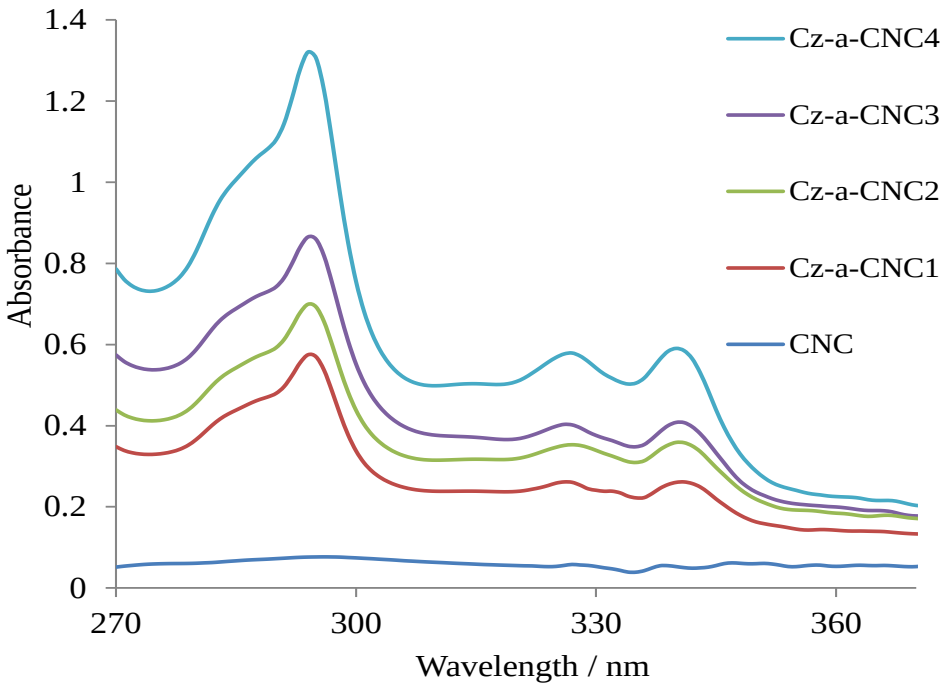


Figure 4.7.1 UV-vis spectrum of CNC and carbazole modified cellulose in DMSO (2mg/25 mL)

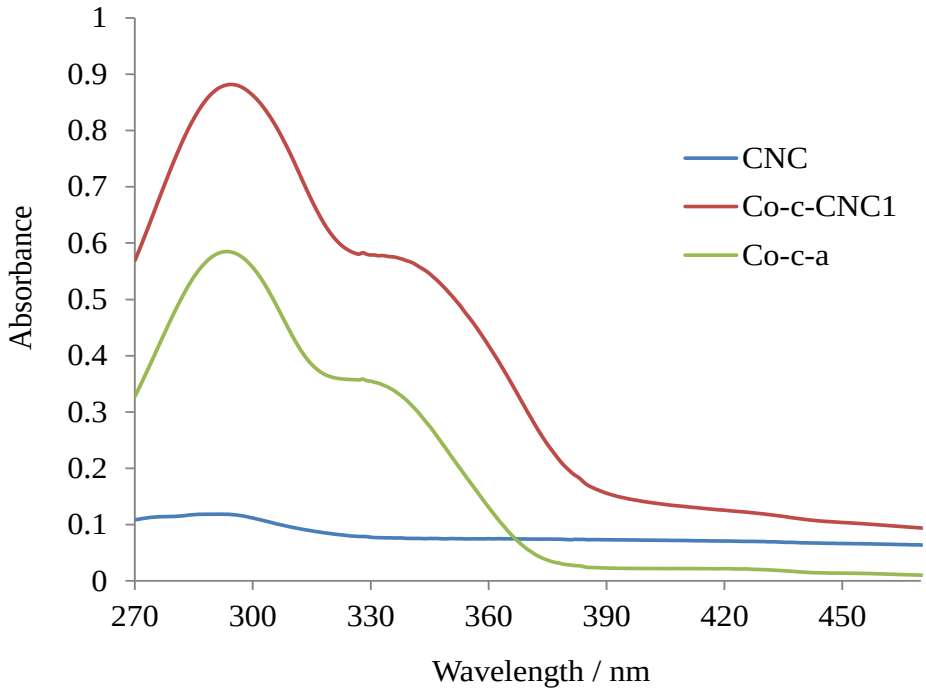


Figure 4.7.2 UV-vis spectrum of CNC, coumarin-3-carboxylate cellulose nanocrystals (Co-c-CNC1) and coumarin-3-carboxylic acid in DMSO with λ_{max}Co-o-a = 293, λ_{max} Co-c-CNC1 = 294 nm and another peak λ Co-c-a = 330 and λ Co-o-CNC1 = 335nm.

Table 4.7.1 Results of the absorption experiments of CNC and carbazole and coumarin modified CNC

	Mass /mg	Vol /mL	A	ΔA	C mmol/L	g/L	mmol/g	DS_{surf}
CNC	2.06	25	0.076					
Cz-a-CNC1	1.98	25	0.575	0.499	0.030	0.079	0.376	0.19
Cz-a-CNC2	2.18	25	0.699	0.623	0.037	0.087	0.426	0.22
Cz-a-CNC3	2.04	25	0.865	0.789	0.047	0.082	0.576	0.30
Cz-a-CNC4	1.99	25	1.321	1.245	0.074	0.080	0.930	0.49
CNC	2.01	25	0.118					
Co-c-CNC1	2.11	25	0.880	0.762	0.064	0.084	0.755	0.39

The resulting figures represent very high amounts of dye grafted onto the surface of cellulose when compared with the work published by Nielsen *et al.* with an amount of 10.4 μmol/g 5-(and-6)-carboxyfluorescein succinimidyl ester (FAM-SE), 4.7 μmol/g 5-(and-6)-carboxytetramethylrhod-amine succinimidyl ester (TAMRA-SE) and 7.3 μmol/g Oregon Green carboxylic acid, succinimidyl ester OG-SE.[147]

Fluorescence of carbazole-modified cellulose nanocrystals

The samples were dispersed in DMSO as this solvent offers good modified cellulose nanoparticles dispersibility, and for the excitation wavelength was chosen the maximum absorption wavelength from the absorption spectra. Initial fluorescence measurements were made to determine the best excitation wavelength that would give the highest intensity. Therefore, the fluorescence emission of Cz-a-CNC3 was determined at room temperature in DMSO with a width slit of 2.5 nm for excitation and for emission (Figure 4.7.3). The absorption spectra of the Cz-a-CNC3 presented in Figure 4.7.1 exhibited three absorption bands at around 294, 327 and 339 nm, thus the emission spectra for this compound were recorded for these excitation wavelengths. In figure 4.7.3, the emission maxima at 347 and 362 nm for excitation at 294 nm is double in intensity when compared with the other two emission intensities when excited

at 327 and 339 nm while the emission peak positions were maintained at the same wavelength.

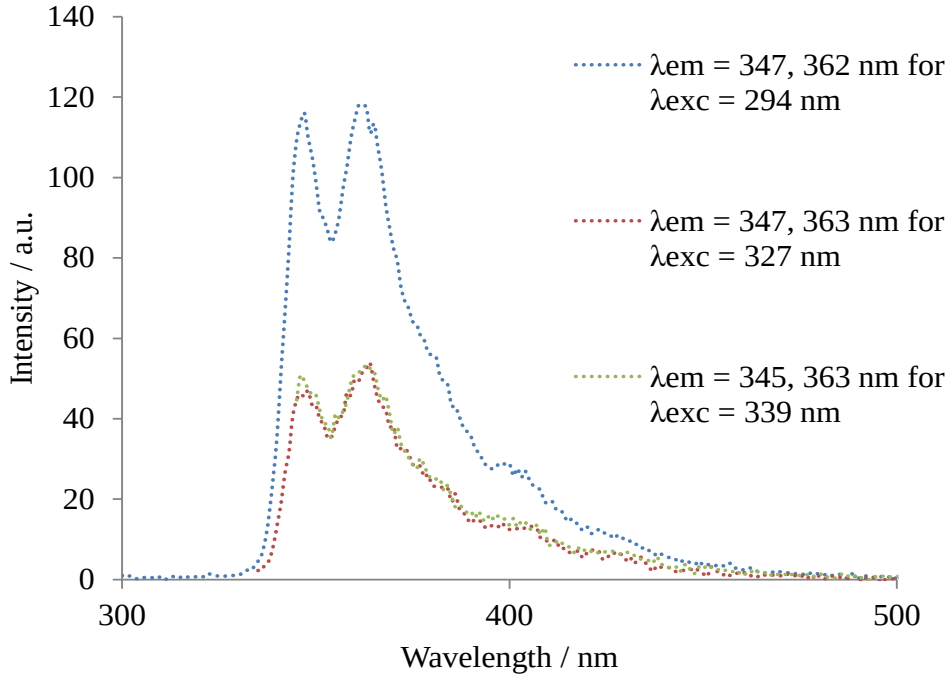


Figure 4.7.3 Fluorescence emission spectrum of Cz-a-CNC3 (0.01 mg/mL) in DMSO when excited at the three absorption wavelengths

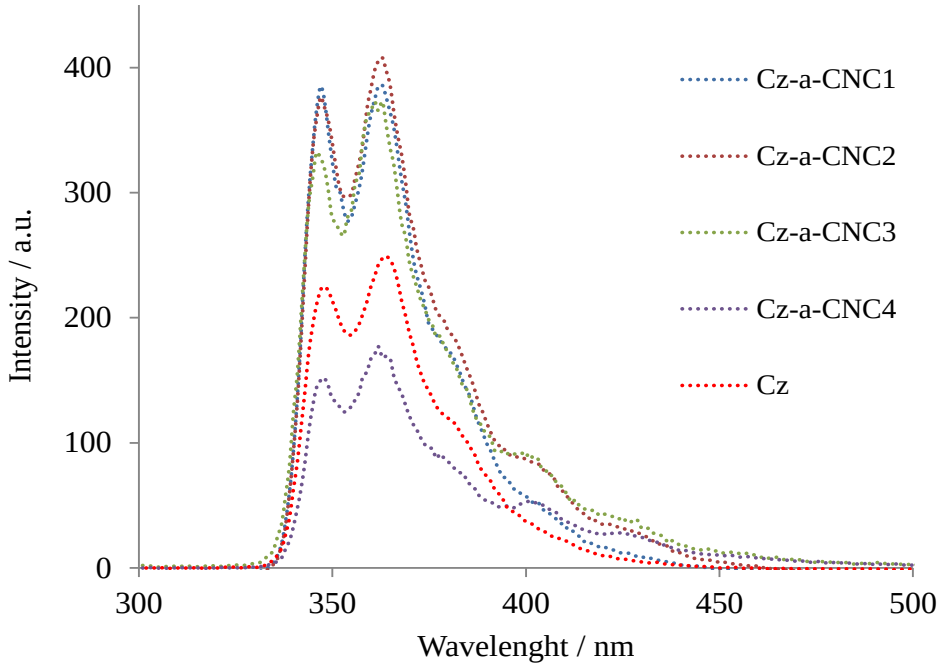


Figure 4.7.4 Fluorescence emission spectrum of carbazole modified cellulose (0.08 mg/mL) and *9-H*-carbazole (0.001 mg/mL) when excited at 294 nm

The Cz-c-CNC3 displayed an intense emission between 335 – 450 nm with a maximum peak at λ_{max} = 347 and 362 nm located in the ultraviolet spectral range. Consequently, the fluorescence emission spectra of the other three modifications of carbazole-9-yl-acetate cellulose were recorded for an excitation wavelength of 294 nm. So, the spectra of all four carbazole-9-yl-acetate celluloses for a concentration of 0.08 mg/mL and carbazole (0.001 mg/mL) were measured as presented in Figure 4.7.4.

Similar to the emission spectra of Cz-a-CNC3, the emission spectra for the other modified CNC showed an emission at 347 and 362 nm, consistent with the emission spectra of carbazole (red dash line in Figure 4.7.4) with its peak maxima at 348 and 364 nm. The carbazole derivatives used in these studies retain the characteristics of parent 9-*H*-carbazole.

In a solvent with a low cut-off such as acetonitrile the other signals visible from 200 nm onwards are also revealed (Figure 4.7.5). According to the literature, the absorption bands at around 260 and 295 nm are attributed to the intra-molecular transitions π–π^* and the absorption bands at around 325 and 340 nm were assigned to n–π^* transitions of the carbazole.[259] The π–π^* transitions are slightly red shifted and n–π^* are blue shifted in derivatives of carbazole as compared to the parent 9-*H*-carbazole when measured in the same solvent. Also, in Figure 4.7.4 it can be noticed that for the same concentration of modified cellulose in a solvent, the first three of them have approximately the same intensity while the forth modification, Cz-a-CNC4, present a less than half emission intensity as compared with the other three and considering the fact that this has the highest apparent degree of substitution. A possible explanation for this result is based on the quenching phenomenon that takes place due to the number of fluorescent molecules in the environment and not because of the number of nanoparticles present.

Therefore, quenching studies similar to the one performed by Zhang *et al.*[162], were proposed for the determination of the concentration of self-quenching properties. Thus the fluorescence properties of carbazole-9-yl-acetate CNC and coumarin-3-carboxylate CNC, respectively, dispersed in DMSO, were

measured for an increased concentration of nanoparticles. Figure 4.7.6 shows the fluorescent emission of Cz-a-CNC3 with increased concentration when excited at 294 nm.

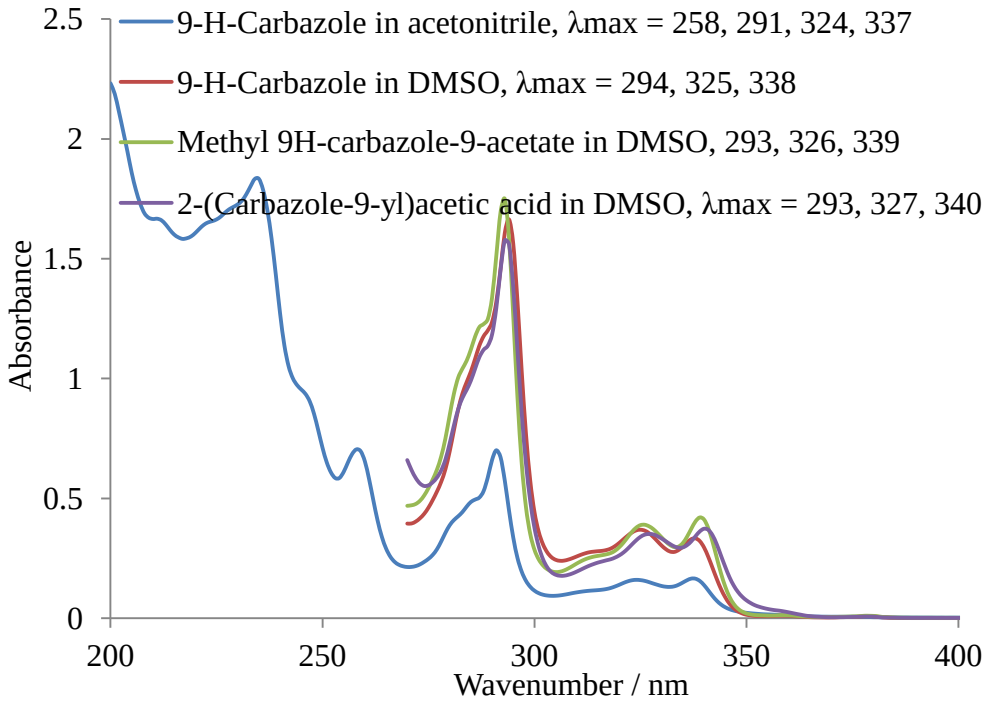


Figure 4.7.5 Absorption spectrum of 9-*H*-carbazole and carbazole derivatives in Acetonitrile and DMSO

The maximum emission wavelength was found at about 347 and 362 nm and the fluorescence intensity increased upon the concentration increase from 0.001 to 0.100 mg/mL (Figure 4.7.6 a). For further concentration increased from 0.100 to 0.500 mg/mL (Figure 4.7.6 b), a decrease in intensity was noticed confirming the fluorescence quenching effect in this concentration domain, as it was previously considered. Upon increasing the concentration up to 0.100 mg/mL the distance between fluorescent carbazole decreases, but still, the fluorescence emission occurs without interference between carbazole moieties. Above a concentration of 0.1 mg/mL, the carbazole groups could start to interact with each other because of the decrease in distance between the molecules with a decrease in fluorescence emission as a result.

Aside from the fluorescence emission measurements for modified CNC, the fluorescence behaviour of *9-H*-carbazole itself was compared with that of

modified cellulose and was found to show a similar concentration–dependent fluorescence evolution.

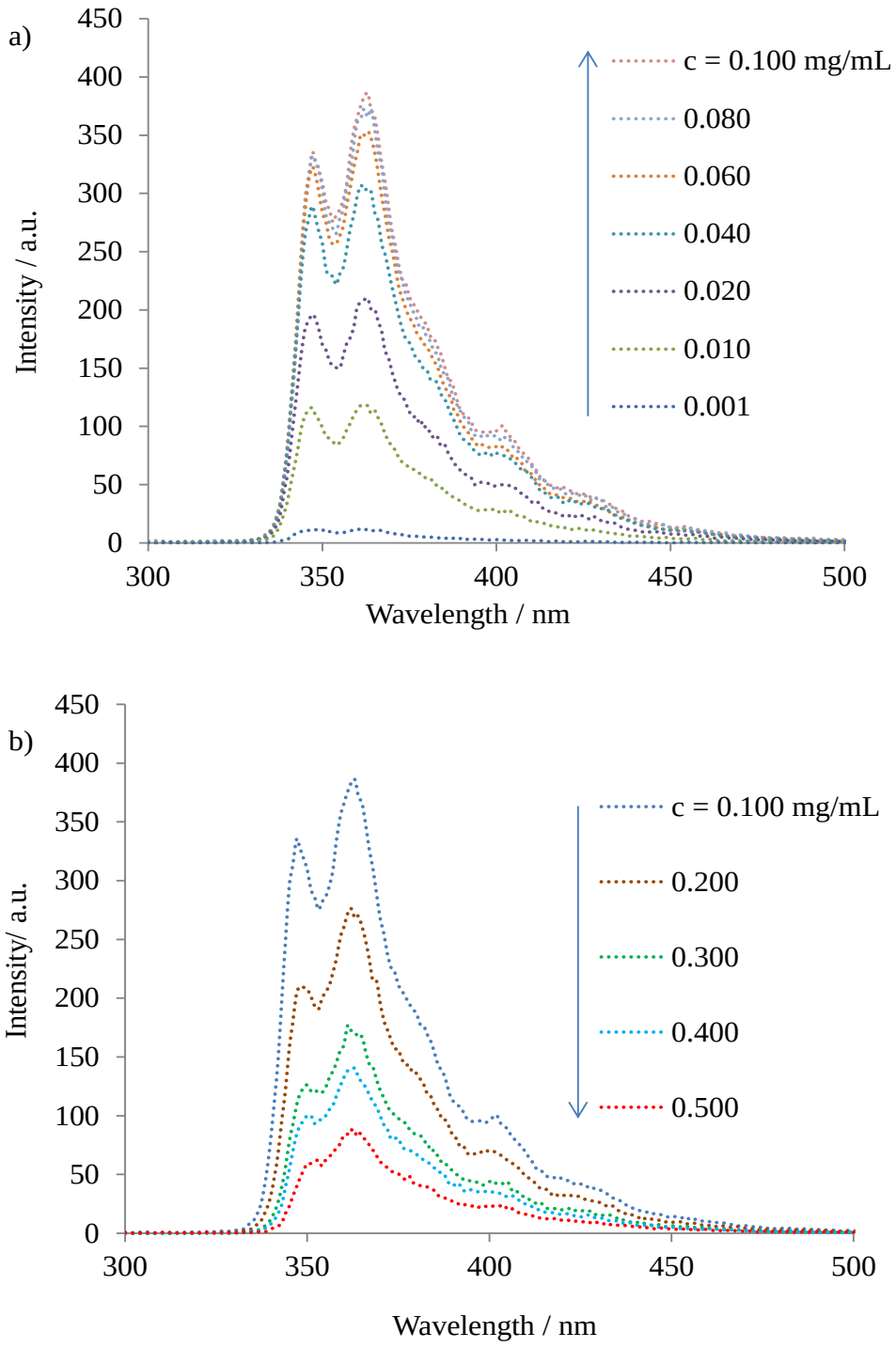


Figure 4.7.6 Fluorescence spectrum of Cz-a-CNC3 in DMSO with increasing concentration and emission intensity increasing (a) and emission intensity decreasing (b)

Figure 4.7.7 presents the evolution for all the 4 modified cellulose together with the *9-H*-carbazole fluorescence evolution, shows that the fluorescence shift happens at a much lower concentration (0.01 mg/mL) for *9-H*-carbazole. Once the *9-H*-carbazole molecules are grafted on CNC, the fluorescence shift happens at a higher concentration.

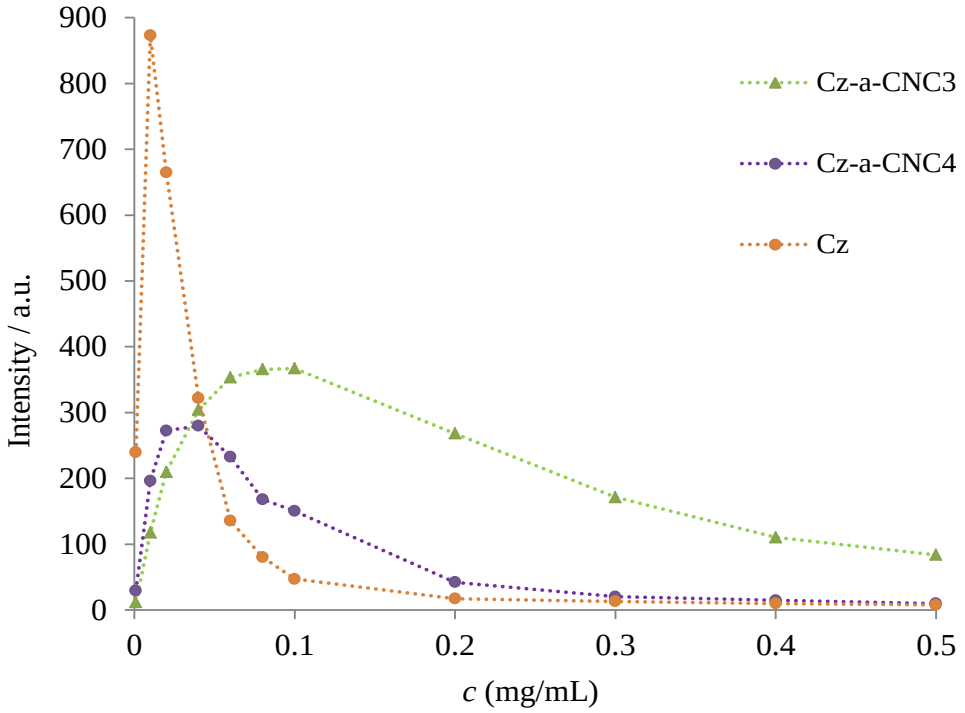


Figure 4.7.7 Fluorescence intensity of carbazole acetate cellulose and carbazole at the peak 363 nm in DMSO

In the work of Zhang *et al.* the carbazole-substituted hydroxyethyl cellulose (Cz-Hec) homogeneously synthesized presented the fluorescence intensity of the modified cellulose higher than for 9-*H*-carbazole. The behaviour of carbazole modified cellulose is very similar with the one of current cellulose modification and a possible explanation for the fluorescence intensity decrease for the modified CNC is given by the CNC presence in the solvent which may scatter the incident beam.[162]

Upon increasing the substitution degree from Cz-a-CNC3 to Cz-a-CNC4, the concentration to the highest intensity decreases and thus a decrease from 0.1 to 0.04 mg/mL for the highest substituted modifications is the result of the closer distance between carbazole groups. This will lead to fluorescence quenching at an even lower concentration.

In the carbazole derivative structure, the presence of the N electron donor group promotes a charge transfer phenomenon in the presence of an electron acceptor. Only under certain irradiation conditions, the weak electron donor and acceptor is excited, and the excited donor/acceptor can form an exciplex by charge transfer interactions with the acceptor/donor.[162] Therefore exciplex formation is confirmed by fluorescence measurements with fluorescence quenching upon increasing the quencher amount. Thus, a compound that contains a vinyl monomer, i.e. a carbon-carbon double bond electron acceptor, can behave as a quencher and therefore acrylonitrile was chosen, similarly to the work of Zhang *et al.* for easier comparison.[162]

In order to follow the interactions between carbazole modified cellulose and the acrylonitrile donor acceptor, carbazole-9-yl-acetate cellulose (Cz-a-CNC3) at the concentration that gives the highest fluorescence intensity (0.1 mg/mL) was excited at 295 nm in DMSO upon increased addition of acrylonitrile. Figure 4.7.8 shows the emission spectra of Cz-a-CNC3 where upon addition of quencher (acrylonitrile), the emission intensity visibly decreases.

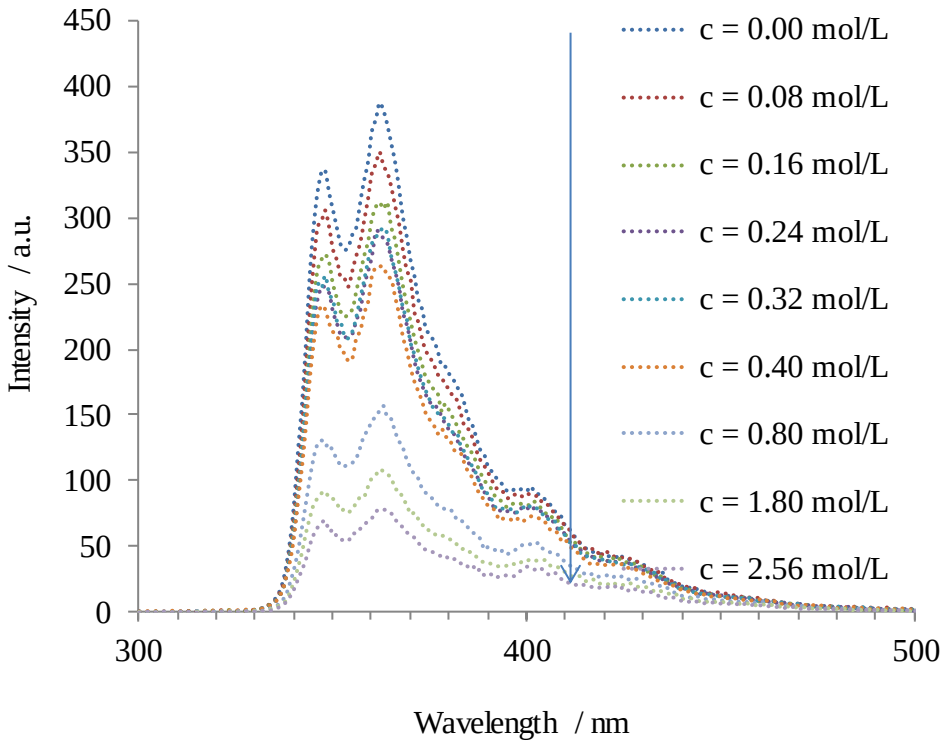


Figure 4.7.8 Fluorescence spectrum of Cz-a-CNC3 0.1 mg/mL in DMSO with increasing concentration of acrylonitrile from 0.00 mol/L to 2.56 mol/L

Comparing with the work of Zhang, the loss of intensity in the present case (38 a.u. for the 0 to 0.08 mol/L acrylonitrile) is approximately half the loss in intensity shown in their work for the same concentration of modified cellulose (0.1 mg/mL). Yet, the same shape and position of the emission spectra are maintained. Therefore, even higher amounts of quencher were used until the intensity almost reaches the detection limit, thus proving the quenching capacity of the quencher.

Fluorescence quenching refers to any process that reduces fluorescence and this can happen in two ways: static quenching through the formation of a ground state complex, and collisional or dynamic quenching. Both quenching mechanisms happen through electron/energy transfer from the emitter to the quencher and a quantitative description of each of them can be carried out through the Stern-Volmer equation which involves the use of lifetime measurements. [260] Although it is not a compulsory determination and the life time measurements could not be carried out during this thesis work, it would have been interesting to determine what type of quenching behaviour was happening in the present fluorescently modified cellulose nanocrystals. Therefore, it is part of the future work to determine what kind of molecular interaction determines the quenching of modified cellulose and at the same time the acrylonitrile quenching. In conclusion, the quenching effect did indeed occur and therefore it can exhibit a significant influence on the determination of the degree of substitution through optical methods.

Fluorescence of coumarin-modified cellulose nanocrystals

By comparison, the same fluorescence characterization was performed for coumarin-modified cellulose. The room-temperature fluorescence emission spectrum of coumarin-3-carboxylate cellulose (Co-c-CNC1) is presented in Figure 4.7.9. The absorption spectra (Figure 4.7.2) exhibited two absorption bands at 293 and at around 335 nm. The emission spectra were thus recorded under these excitation wavelengths in DMSO with a slit width of 5 nm. It is obvious that the intensity emission at 335 nm was much higher than that at

293 nm and the emission peak positions were maintained in the same position. The Co-c-CNC1 displayed an intensive emission between 350 – 550 nm with the maximum peak at λ_{max} = 422 nm located in the violet – blue – cyan spectral range. Similarly, to carbazole quenching, a set of concentrations were measured and as can be seen in Figure 4.7.10a, upon increasing the concentration, the fluorescence intensity also increases up to 0.2 mg/mL, after which it starts to decrease indicating quenching effect (Figure 4.7.10b).

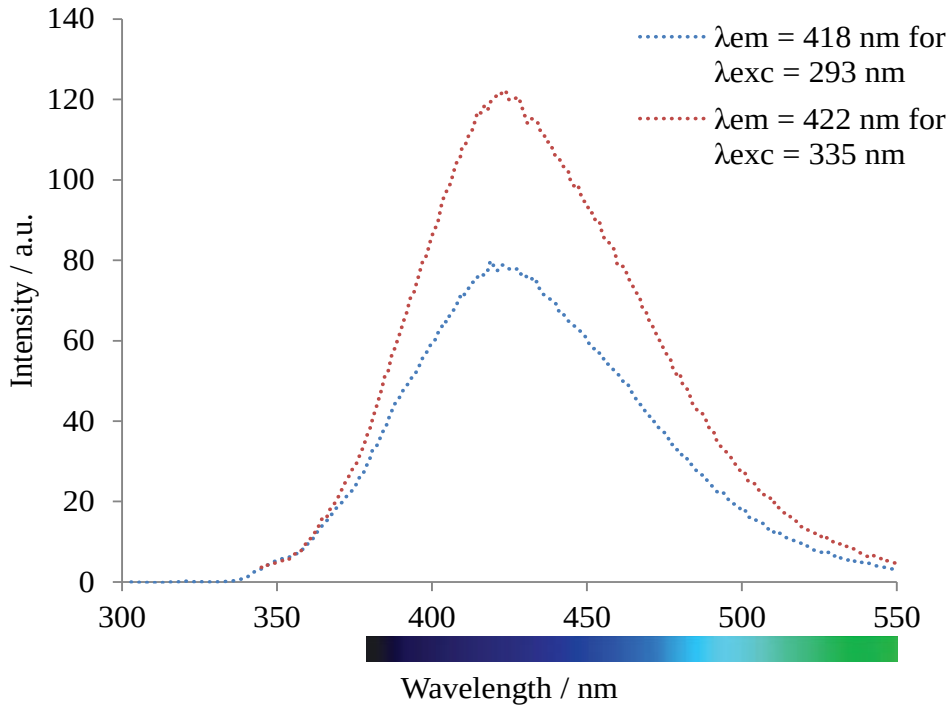


Figure 4.7.9 Fluorescence emission spectrum of coumarin-3-carboxylate cellulose (Co-c-CNC1) (0.2 mg/ml) when excited at the two absorption bands

As compared to carbazole-modified cellulose, the coumarin modification (Co-c-CNC1) requires a double concentration to reach the maximum fluorescence before quenching and 10 times more when compared to the coumarin-3-carboxylic acid (Co-c-a) (Figure 4.7.11).

Coumarin-3-carboxylate cellulose quenching with acrylonitrile was also probed and no significant intensity loss was observed (Figure 4.7.12). Even if an amount of up to 0.12 mol/L quencher was used, no quenching was observed. Thus it is considered that acrylonitrile is not a quencher for coumarin-3-carboxylate cellulose although coumarin-3-carboxylic acid and coumarin-3-carboxylate cellulose present their own quenching effects.

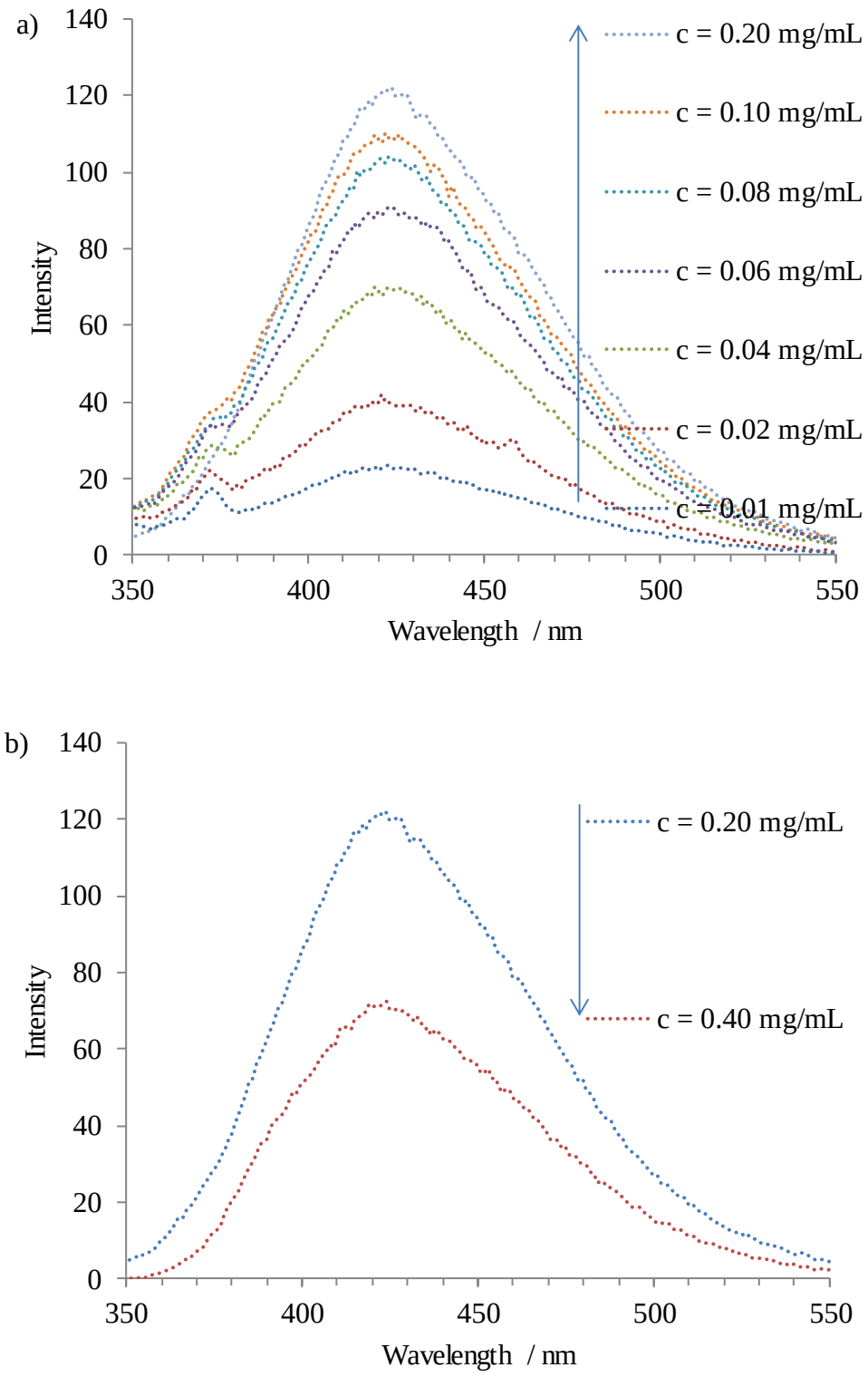


Figure 4.7.10 Fluorescence spectrum of Co-c-CNC1 in DMSO with varying concentrations 0-0.2 mg/mL (a) and 0.2-0.4 mg/mL (b) when λ_{exc} = 335 nm

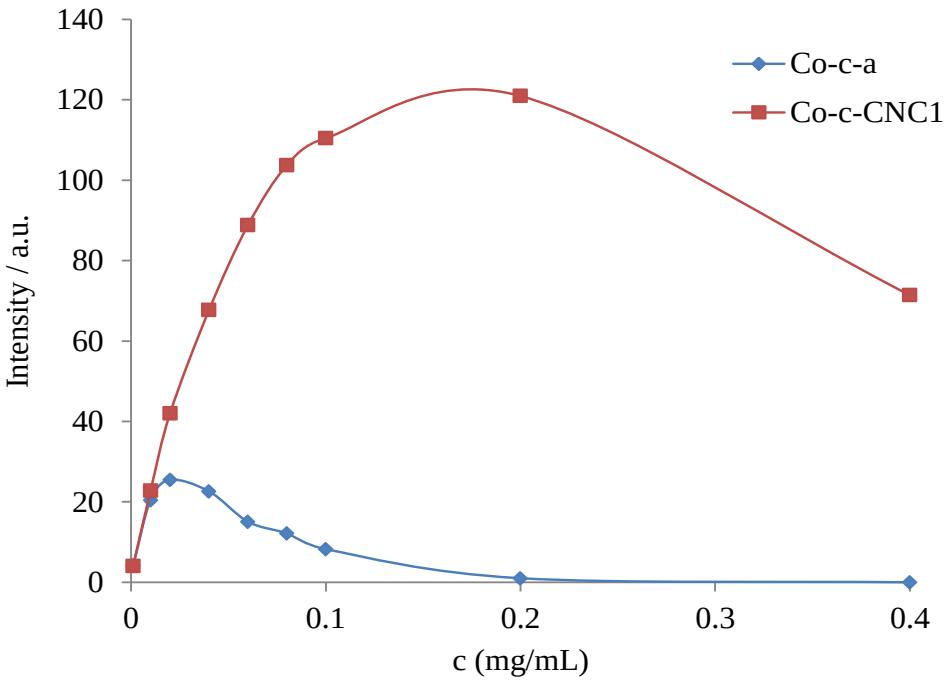


Figure 4.7.11 Fluorescence intensity of coumarin-3-carboxylate cellulose (Co-c-CNC1) and coumarin-3-carboxylic acid at the λmax = 420 nm in DMSO

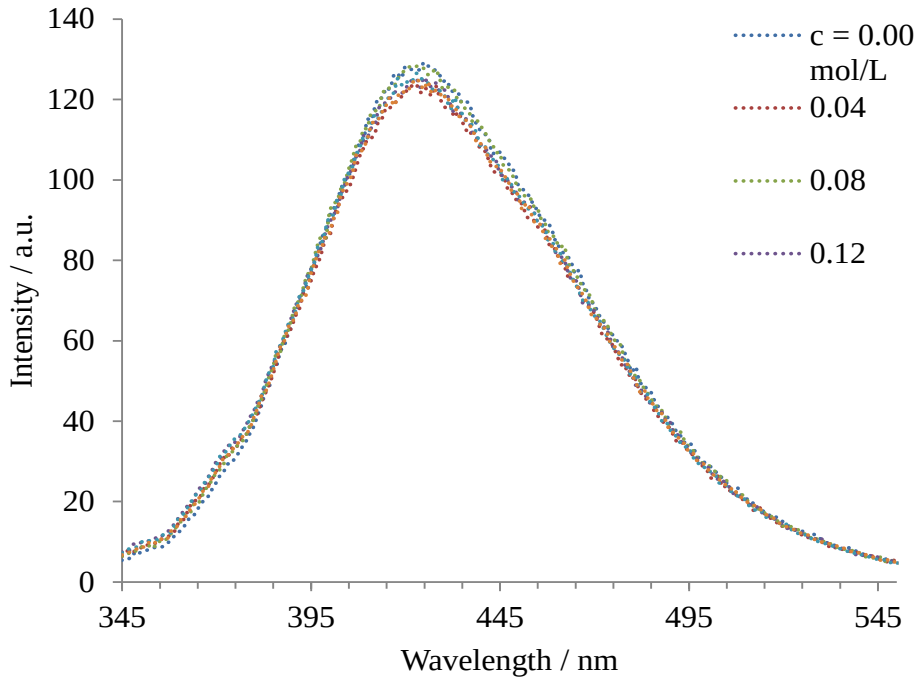


Figure 4.7.12 Emission spectrum of Co-c-CNC1 in DMSO (0.2 mg/mL) with varying concentrations of acrylonitrile

Thus, it was proven that the fluorescently modified cellulose nanocrystals displayed the expected fluorescence properties and the quenching effect significantly influenced the determination of the degree of substitution calculated using the number of moles of modification especially upon increasing the degree of substitution. In the next section an application for the fluorescently modified cellulose is proposed.

4.8 OLEDs preparation procedure

Fluorescent cellulose derivatives that use carbazole modifications to introduce optical and semi-conducting properties was proven to function as a hole transporting material (upon oxidation, organic materials lose an electron which creates a hole – a positive charge – on aromatic structures where it is a lot of delocatization) in the preparation of Organic Light Emitting Diodes (OLEDs) as described by Karakawa *et al.*[160] In their experiment, 6-O-p-Methoxytrityl cellulose was used as a starting material and prepared from microcrystalline cellulose under homogeneous reaction conditions using an earlier published literature procedure.[261] In this context, in the present research, OLED fabrication was carried out by using the grafted carbazole on CNC following an adapted methodology described by Karakava *et al.*[160]

Similar to a Light Emitting Diode (LED), an OLED is a solid state semiconductor device of about 100-500 nm thickness and can have either two layers or three layers of organic material as shown in Figures 4.8.1 and 4.8.2. An OLED is assembled from the substrate (clear plastic, glass, usually FTO (Fluorine doped Tin Oxide) or ITO (Indium Tin Oxide)), an electrically conductive glass or foil, followed by deposition of a transparent anode that removes the electrons/creates holes when a current is passed through, and organic layers: a conducting layer (transports the holes from the anode – Hole Transporting Layer (HTL)) and an Emissive Layer (EML) which is the place where the light is formed as a result of the combination of electrons transported from the cathode (through an intermediate layer (Electron Transporting Layer (ETL)) or without it) and the holes from the conducting layer with energy

release in the form of a photon. The last layer is the cathode that can be transparent or not and it injects the electrons when a current is applied. Usually, the EML is a light emitting dye or dopant and is dispersed in a host material/matrix often the same HTL or ETL.

In order to fabricate OLEDs in which carbazole-modified cellulose is used as a host/hole transporting material, at The University of Nottingham, I initial attempted to carried out the manufacturing by adapting the procedure described by Karakawa *et al.* when a three organic layers structure was designed as follows (Figure 4.8.1): conducting layer FTO / PDOT:PSS [(Poly(3,4-ethylenedioxythiophene) : Polystyrene sulfonate)] / emissive layer in matrix Alq3 [(Tris (8–hydroxyquinoline)–aluminium)] : Cz-a-CNC / electron transporting layer tBu-PBD [(2-(4-tert-Butylphenyl)-5-(4-biphenylyl)-1,3,4-oxadiazole)] / Au cathode where the 1% suspension in chloroform was respecting the ratio of 4% : 46% : 50% (Alq3 : Cz-a-CNC : tBu-PBD) (Figure 4.8.2).

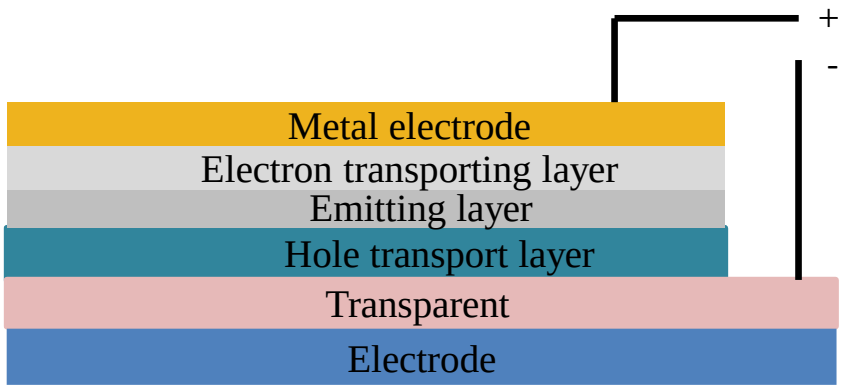


Figure 4.8.1 General representation of an OLED

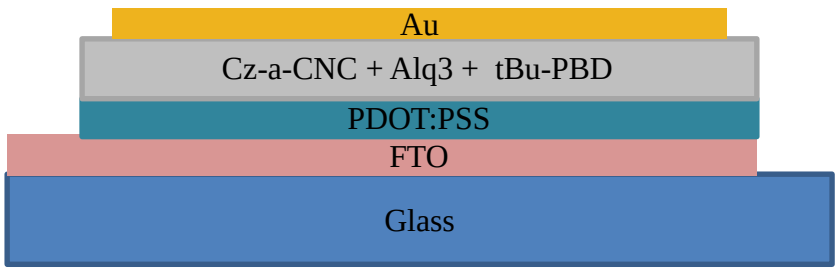


Figure 4.8.2 Structure of attempted OLED using carbazole modified CNC

Due to the lack of a proper fabrication environment, the work was continued and carried out in an inert environment for OLED fabrication by Dr. Enrique Pérez Gutiérrez at Group of Optical Properties of Materials (GPOM), Photonics Division Centro de Investigaciones en Óptica A.C. Guanajuato, Mexico as follows:

One wt% solutions in solvent were prepared by mixing the carbazole modified cellulose as the host material with the fluorescent compound (Alq3) as emissive layer in a ratio of 1:0.25 Cz-a-CNC: Alq3. In order to obtain a good dispersibility and possible solubility of cellulose compounds, chlorobenzene (CB) and CB-DMF (*N*,*N*-Dimethylformamide) mixture were used as solvent.

In the first approach, 10 mg of cellulose compound was suspended in 1 ml of chlorobenzene and kept overnight under stirring at 45 °C, which improved the solubility of the compound. The solution was filtered to eliminate agglomerates and then 2.5 mg of Alq3 were added and in this case Alq3 works also as an emitting material as well as electron transport material and therefore it was not necessary to use tBu-PBD. The solution looked homogeneous, yellow and highly fluorescent (under UV light). In order to analyse the morphology and fluorescence, the films were deposited by spin-coating onto a glass substrate. Figure 4.8.3 shows the fluorescence of the deposited film optical microscopy image.

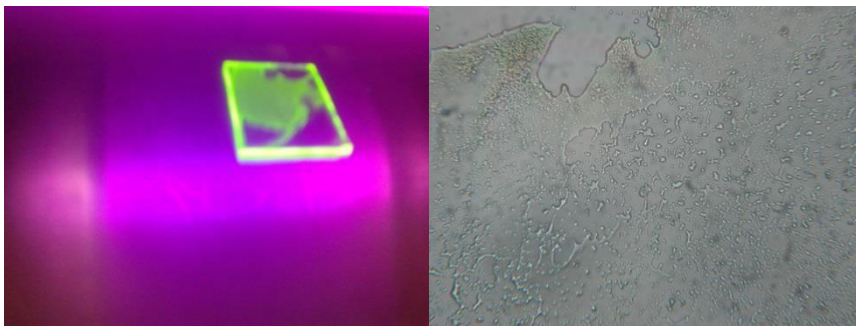


Figure 4.8.3 Fluorescence under UV-light (left) and optical image of deposited films (right)

In spite of the homogeneous apparent aspect of the film, the microscope image shows a non-homogeneous surface with a discontinuous phase and holes. Also,

some aggregates can be observed. Due to the poor solubility of the cellulose derivative compounds in CB, a mixture of CB-DMF was also tried as a solvent. The solution behaviour was similar, the compound was poorly soluble and the deposited films were non-homogeneous. Therefore, the morphology of deposited films indicates that the resulting films were less suitable for these organic electronic devices; however, OLED preparation was nonetheless attempted.

ITO or FTO glass was used as anode and substrate. As hole transport layer we used a PEDOT:PSS layer (50 nm). The emissive layer was deposited on top of the PEDOT:PSS layer by the spin-coating technique. Evaporated gold was used as a cathode and also the eutectic alloy known as Field´s metal (32.5% Bi, 51% In, 16.5% Sn, m.p. = 65°C) was used, where this metal alloy was melted and dropped on top of the active layer. The devices with the evaporated contact showed an ohmic behaviour that could be due to a direct contact between the metal and the PEDOT:PSS layer through the empty places in the active layer. When Field´s metal was used, a very dim emission was observed. Owing to surface tension of the melted drop, Field´s metal did not fall in the empty sites of active layer and the injection of charge carriers was done directly in the active layer. Due to the poor solubility of cellulose derivative compounds in non-polar solvents, it was not possible to obtain homogeneous films suitable for organic light emitting diodes. The insertion of longer aliphatic chains in the cellulose compounds could help to improve their use as a matrix for OLEDs.

4.9 Conclusions

Reactions of cellulose with carbazole-9-yl-acetic acid (Cz-ac-a) carried out in Chapter 4 with their reaction conditions and degrees of modification are presented in Table 4.9.1.

Based on the previously developed methods (TsCl/Py and DIC/DMAP), two new fluorescent CNC esters were synthesised here. Initially, the carbazole-9-yl-acetic acid was synthesised in 2 steps starting from carbazole.

Table 4.9.1 Summary of Chapter 4

Entry	Modified Surface	Acid	Molar ratio CNC:Acid:TsCl	Reaction Conditions			DS_{surf}(N)
1	CNC	Cz-ac-a	1:3:3:0.03	DIC	DMAP	DCM	0.09
2	CNC	Cz-ac-a	1:5.5:5.5:0.03	DIC	DMAP	DCM	0.10
3	CNC	Cz-ac-a	1:0.66:0.66	TsCl	Py		0.39
4	CNC	Cz-ac-a	1:1.33:1.33	TsCl	Py		0.72
5	CNC	Cz-ac-a	1:2:2	TsCl	Py		1.03
6	CNC	Cz-ac-a	1:2.66:2.66	TsCl	Py		1.60
7	CNC	Cz-ac-a	1:3.33:3.33	TsCl	Py		1.55

Considering the much lower acquisition price, the second fluorescent molecule, coumarin-3-carboxylic acid, was used as received from the supplier. The carbazole-9-yl-acetic acid was initially grafted onto the cellulose nanocrystal surface by DIC/DMAP methodology with a molar excess of 1:3:3:0.03 and 1:5.5:5.5:0.03 OH:Acid:DIC:DMAP and resulted in a low degree of substitution, from DS_{surf} = 0.09 to DS_{surf} = 0.1. Therefore, increasing the molar excess in the case of carbazole-9-yl-acetic acid did not bring significant improvement. Subsequently, TsCl/Py methodology was applied with a varying equimolecular excess as follow: 1:0.66:0.66; 1:1.33:1.33; 1:2:2; 1:2.66:2.66; 1:3.33:3.33 for CNC:Acid:TsCl. According to the EA, the DS_{surf} were as follow in order of increasing molar excess: 0.39, 0.72, 1.03, 1.6 and 1.55. Therefore, a molar excess of 1:2:2 would be considered sufficient in order to not exceed the maximum surface available hydroxyl groups without determining a loss of crystallinity due to internal modification of the nanocrystal.

The FT-IR analysis indicates a shift to higher wavenumbers of the carbonyl band from 1744 cm^{-1}, mainly in the case of the last two modifications, and therefore it is thought that some unreacted carbazole-9-yl-acetic acid is left on the cellulose surface and hence the theoretical maximum degree of substitution is only slightly exceeded. The crystallinity loss is determined by the degree of modification and non-grafted material. In addition, a similar situation is found in the case of TsCl/Py esterification of coumarin-3-carboxylic acid with cellulose surface. Between the two molar excess used (1:1.83:1.83 and 1:2.66:2.66 CNC:Acid:TsCl), the first one has a DS_{surf} = 1.33 while the second

slightly exceeds this maximum theoretical value (DS_{surf} = 1.56) which could actually be in the margin of error. Thus, once again, the efficiency of the reaction is dependent on the nature of the acid and on the molar excess. If in the case of carbazole-9-yl-acetic acid a molar excess of 1:2:2 gives a DS_{surf} = 1.03, in the case of coumarin-3-carboxylic acid, a lower molar excess than 1:2:2 (1:1.83:1.83) results in a DS_{surf} = 1.33, so a slightly higher modification. Thus, coumarin-3-carboxylic acid is more reactive than carbazole-9-yl-acetic acid (pKa for carbazole-9-yl-acetic acid is 3.5 while pKa for coumarine-3-carboxylic acid is 1.5) and even more than acrylic acid (pKa of acrylic acid is 4.25), which for the same molar excess (1:2:2) showed only a DS_{surf} = 1.10.

Furthermore, TEM and AFM characterization was carried out for the reaction products and the micrographs display lengths between 100 and 300 nm and widths ranging 5 to 15 nm, which are in agreement with literature data.[45]

Optical properties of fluorescently modified CNC were used to determine the amount of carbazole and coumarin grafted on the surface, initially by measuring UV-Vis spectroscopy followed by fluorescence measurements. The experiments showed that very high amount of dye were grafted on the surface of cellulose when compared with the literature. Furthermore, emission properties and quenching studies of carbazole modifications presented good results. OLED fabrication was attempted but without successful results as constrained by the formation of a homogeneous films.

5 Cationized materials based on cellulose nanocrystals

Cationized nanoparticles were introduced and described in section 1.7.3 and this chapter describes new contributions to this field. In cationization reactions, positive charges are grafted onto cellulose. As discussed earlier, cationized cellulose has been applied in the papermaking, textile and dyeing industries and it has been suggested for applications in drug delivery and cosmetics.[262] However, cationization of the surface of CNC has been reported only a few times in the literature because the required conditions generally result in crystal destruction. In addition, most methodologies include several synthesis steps and lead to a very low degree of substitution whenever the conditions were made more benign. Therefore, the interest in finding straightforward, more rapid methods with a high extent of modification without loss of cellulose I_β allomorph crystallinity is high. In short, Hasani e*t al.* were the first to introduce cationized CNC which involved the surface cationization of H_2SO_4 hydrolysed CNC using epoxy-propyltrimethylammonium chloride (EPTMAC) to introduce quaternary ammonium salts.[93] Although successful cationization was achieved, this method led to a low decrease in the total surface charge density as compared to the initial charge density of sulphated CNC. The degree of substitution (DS) was found to be 0.02 per bulk AGU and a surface charge density of +0.26 *e* nm^{-2} as compared to –0.41 *e* nm^{-2} for the starting sulphated CNC. Later, Eyley *et al*. developed a three-step cationization reaction consisting of initial chlorination of nanocrystalline cellulose followed by azidation. Cationization was then achieved by synthesising an alkyne-terminated imidazolium salt that was reacted with the azidated cellulose through a copper(I) mediated azide-alkyne cycloaddition reaction. As this synthesis route involved 3 steps, it could be considered difficult for commercial applications but it did result in a significantly higher degree of substitution than the previously reported surface modifications (DS of 0.36) and the cationized

surface charge increased up to +0.56 *e* nm^{-2}. Later Zaman *et al.* published a method comparable with the one adopted by Hasani *et al.* They reported on a cationic surface modification performed using glycidyltrimethylammonium chloride (GTMAC) based on a semi-dry method.[95] The most recently reported method by Jasmani *et al.* describes a one-pot route to produce pyridinium-grafted CNC using 4-(1-bromoethyl/ bromomethyl) benzoic acid where a DS of up to 1.1 could be achieved without loss of CNC crystallinity.[96]

In this chapter, two new synthesis methods involving two different alkylation agents and two ionic liquid precursors are presented together with their characterization and ion exchange capabilities.

5.1 Introduction to cationized materials

Based on the already existing literature on cationized nanoparticles as detailed in the introduction chapter, this chapter expands on the previous work. In order to give a wider variety of grafted molecules and methodologies, two alkylation agents (bromoacetic acid and bromoacetyl bromide) were used and different esterification methods were applied. Cationization of the cellulose nanoparticles could then be carried out at the same time as the esterification step or could be done sequentially to the esterification. Pyridine and 1-methylimidazole, which are two well-known amine used in the synthesis of ionic liquids (Figure 5.1.1), were used as the nucleophiles to create the cationic grafts (Figure 5.1.2-5.1.6) building on the work of Jasmani *et al.* in which she used pyridine and on the work of Morandi *et al.* on the esterification with bromoisobutyryl bromide in DMF under Et_3N catalysis.[64,96] The grafting of these two molecules by this esterification procedure had not been applied before.

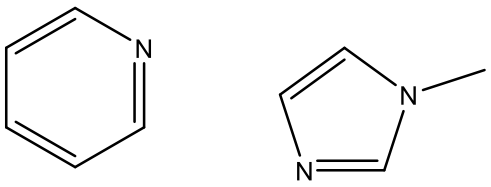


Figure 5.1.1 Structure of Pyridine (left) and 1-Methylimidazole (right)

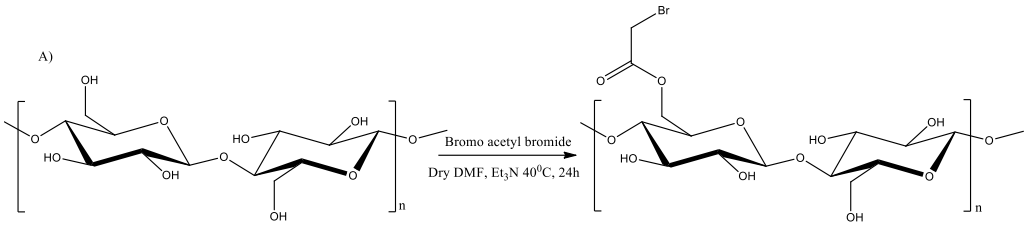


Figure 5.1.2 First step in order to obtain cationized cellulose nanoparticles – nucleophilic substitution of cellulose nanoparticles with bromoacetyl bromide for bromoacetate cellulose ester synthesis

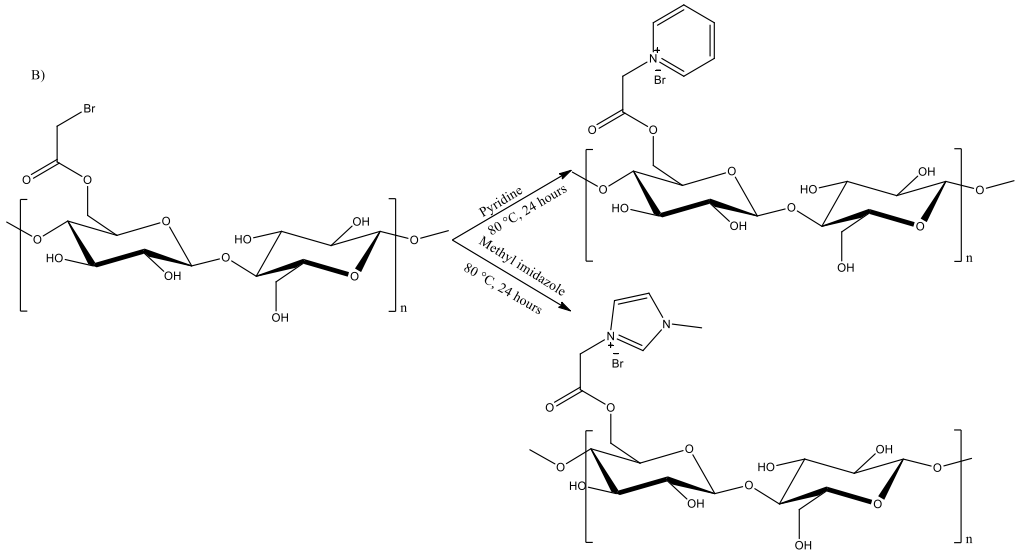


Figure 5.1.3 Second step in order to obtain cationized cellulose nanoparticles – cationization reaction of the bromoacetate cellulose nanoparticles with pyridine and 1-methylimidazole respectively

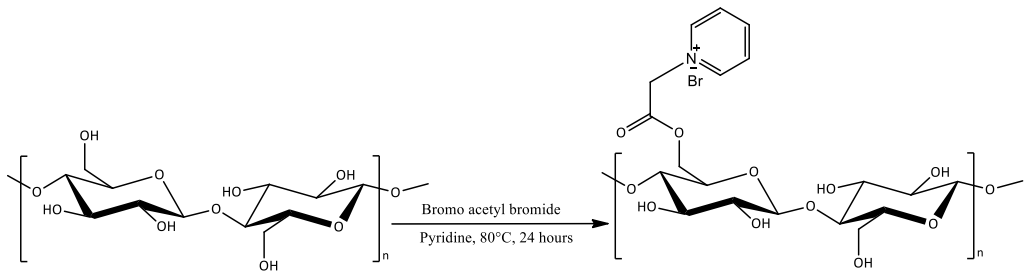


Figure 5.1.4 Synthesis reaction of single step pyridinium acetate cellulose bromide 2[Br][PyAc]-*g*-CNC

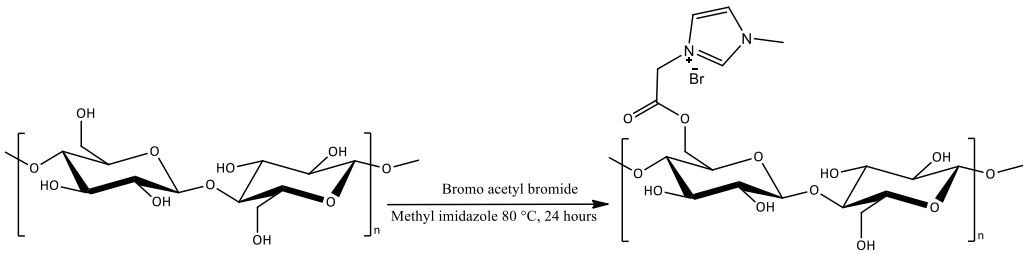


Figure 5.1.5 Synthesis reaction of single step methyl imidazolium acetate cellulose bromide 2[Br][MeImAc]-*g*-CNC

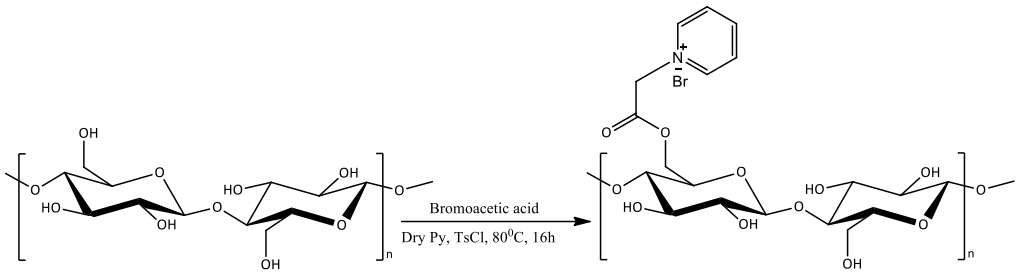


Figure 5.1.6 Synthesis of pyridinium acetate cellulose bromide using TsCl/Py methodology

An advantage for characterization is that both nucleophiles have a nitrogen atom allowing an easier determination of the degree of substitution via EA.

As mentioned before, the desired modification should be as easy and straightforward as possible, ideally in one-step. In order to find the optimum reaction conditions with the highest reaction yield, the research efforts also involved a two-step synthesis as this approach gave valuable results. The first method involved a two-step procedure with sequential esterification and nucleophilic attack, in which the bromoacetate cellulose, initially synthesised under different reaction conditions, is used in a separate cationization reaction with pyridine or 1-methylimidazole. The second method included a one-step reaction in which the esterification and the nucleophilic attack happened simultaneously in the vessel to create cationized cellulose nanoparticles.

The third esterification attempt was based on the work by Jasmani *et al.*[96] and is then applied to an optimised one-step method involving the esterification of bromoacetic acid instead of bromoacetyl bromide and the pyridinium formation in a one-step reaction using a TsCl/Py system.

5.2 Two steps synthesis towards cationized nanoparticles

The first attempted esterification procedure involves a two-step synthesis (A – Figure 5.1.2 and B – Figure 5.1.3). Esterified bromoacetate cellulose (A) is used to react with pyridine and 1-methylimidazole in the second step (B) to create cationic grafts. The methodology described by Morandi *et al.,* in which 2-bromoisobutyryl bromide was used to introduce initiating sites for atom transfer radical polymerization (ATRP), was adapted to introduce bromoacetyl esters onto the CNC surface and prepare the esterified bromoacetate cellulose (A).[64]

Due to a consistent reduction in crystallinity of the cellulose nanoparticles, the procedure described by Morandi *et al.* was slightly modified by reducing the reaction temperature from 70 °C to 40 °C and doubling the volume of the reaction solvent. This led to a much better homogenization of the reaction mixture, significantly increased the ease of purification of the reaction product, and also increased the total extent of modification. As shown in Figure 5.1.2, the nucleophilic acyl substitution reaction of CNC with bromoacetyl bromide was carried out in dry *N*,*N*-dimethylformamide and triethylamine as a catalyst and HBr scavenger at 40 °C for 24 hours. During the reaction, a large amount of triethylamine hydrogen bromide salt is formed and for the purification stage several trials were attempted to remove this salt and other physically adsorbed molecules on the surface of CNC. Intensive washing with DCM was the main step followed by additional acetone and water washes, acetone and DCM or EtOH and an additional subsequent DCM Soxhlet extraction. When intensive THF, DCM, acetone, acetone/water washes followed by Soxhlet extraction with EtOH and DCM were applied, the final surface degree of substitution was reduced by half which may indicate a possible trans-esterification reaction of EtOH with the already formed ester on the surface of cellulose although a 0.2 % nitrogen was still present on the surface. Therefore, the adopted method for purification was by Soxhlet extraction with DCM used in addition to cold solvent washes to avoid any possible unwanted reactions.

As expected, the highly reactive acyl bromide used for esterification results in a high degree of grafting and one can see a clearly visible absorption band at 1745 cm^{-1} in the infrared spectrum (Figure 5.2.1) that is attributed to C=O ester stretching. Another expected C–Br absorption band in the fingertip region is not visible as it overlaps with other characteristic absorption bands of cellulose.

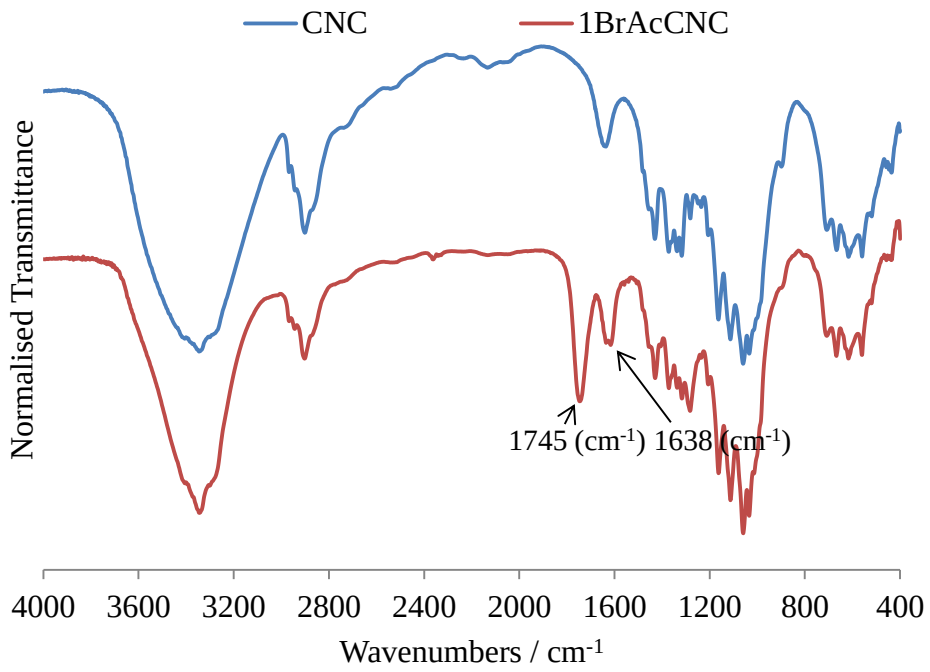


Figure 5.2.1 FT-IR Spectrum of CNC and bromoacetate cellulose 1BrAcCNC

In order to determine the true extent of modification, EA was used to calculate the surface degree of substitution using the Br content giving a DS_{surf} of 1.36 (Table 5.2.1). This indicates that more than two hydroxyl groups present on each AGU were modified. Comparing the Br content of 15.7 wt. % with the highest value found by Morandi *et al.* (9.5 wt.%)[64], I obtained a significantly higher conversion (almost double) of surface hydroxyl groups.

Table 5.2.1 Elemental analysis results for bromoacetate cellulose 1BrAcCNC

Sample	C (%)	H (%)	N (%)	Br (%)	DS_{surf}(Br)
CNC	42.38	6.15	0.00	-	-
1BrAcCNC	39.58	4.91	0.91	15.7	1.36

At the same time the EA results also indicate some nitrogen content which can be attributed to different factors and therefore XPS analysis is used to evaluate their chemical environments to get a better idea of the chemical states they are present in. The increased degree of esterification could be due to the slightly different methodology employed such as the change in reaction temperature and amount of solvent.

The crystalline structure of the reaction product needs to be verified as the high degree of substitution and the reagents may affect the nanoparticle crystallinity.

X-ray diffraction of the product (Chapter 5 Appendix, Figure 10.3.1) clearly indicates the maintenance of the cellulose I_β crystal structure and the calculated crystallinity is χ_C^R = 0.458, representing a significant drop of 33.78 % of crystallinity when compared with the crystallinity of the unmodified cellulose (χ_C^R = 0.796). Calculating the addition of amorphous material as a direct result of the esterification, determined from the EA, one finds 27.11 %. The discrepancy between the two values can be due to the presence of the non-crystalline materials in the form of the triethylammonium hydrogen bromide trapped on the CNC surface as a consequence of the extensive molar excess used or could be due to partial solubilisation of the highly modified cellulose surface chains.

XPS analysis revealed the presence of C, O and Br as expected but also the presence of N (Chapter 5 Appendix, Figure 10.3.2), in agreement with EA. The high resolution C1s scan (Figure 5.2.2 a) clearly shows the presence of a large component peak at 289.72 eV, corresponding to an ester carbonyl carbon which once again confirms esterification.[228]

Simultaneously, the high resolution O1s scan indicates the presence of an O–C=O component peak at a BE of 530.87 eV (Chapter 5 Appendix, Figure 10.3.3) (Table 5.2.2). Further evidence of successful nucleophilic acyl substitution of cellulose with bromoacetyl bromide comes from the high resolution scan of Br3d (Figure 5.2.2 b) which reveals the presence of two bromide environments, Br3d 5/2 at 67.85 eV and Br3d 5/2 at 70.85 eV. The chemical environment found at 70.85 eV corresponds to the C–Br alkyl chain

(77.13 %) as in the bromoacetate cellulose and the second environment at 67.85 eV corresponds to anionic bromine (22.87 %).[244,263] The anionic bromine environment is believed to be due to ionic bromine from triethylammonium hydrogen bromide (Et_3NHBr) remaining adsorbed onto the surface of cellulose.

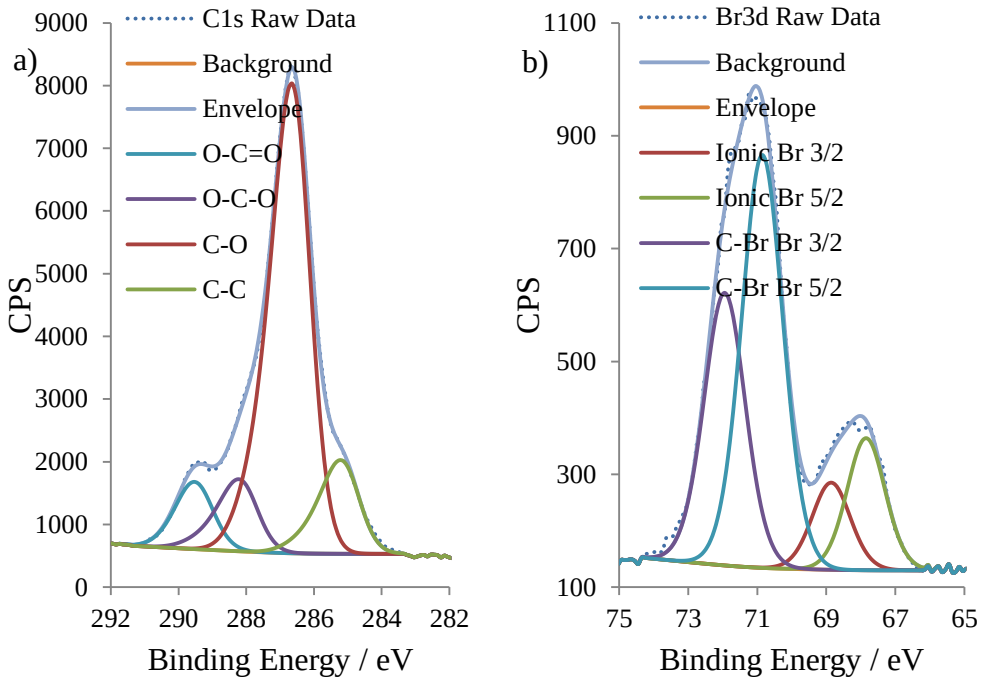


Figure 5.2.2 a) C1s high resolution XPS spectrum and b) Br 3d high resolution scan composed of two Br environments, the C-Br characteristic for bromoacetate cellulose 1BrAcCNC

This is confirmed by the N1s high resolution scan presenting a positively charged nitrogen chemical environment at 402.47 eV.[244] However, a second N environment at 400.87 eV in a ratio of about 1:4 to cationic N (Chapter 5 Appendix, Figure 10.3.4) is also found, believed to be due to TEA.

It has to be noted that although this reaction product was intensively washed with several solvents (acetone, water, EtOH, DCM) followed by either DCM and EtOH Soxhlet extraction or only DCM Soxhlet extraction, none of these purifications led to complete removal of the nitrogen containing by-products. However, the synthesised bromoacetate cellulose was still used in the second step towards the synthesis of cationized cellulose nanoparticles step B, Figure

5.1.3 as XPS could be used to quantify the reactive Br amount in the esterified product.

Table 5.2.2 Detailed XPS data of bromoacetate cellulose 1BrAcCNC

Orbital	Component	BE / eV	FWHM /eV	Rel.A/%[a]	at%
C1s	C–C	285.07	1.13	16.52	10.10
	C–O	286.50	1.13	70.73	43.23
	O–C–O	288.13	1.13	10.49	6.41
	O–C=O	289.72	1.13	2.27	1.39
				100.00	61.13
O1s	O–C=O	530.87	1.521	2.47	0.85
	C–O–H	532.53	1.521	65.03	22.50
	O–C–O	533.13	1.521	32.5	11.25
				100.00	34.60
N1s	C–N=	400.87	1.37	80.93	1.23
	$(C–)_4N^+$	402.47	1.37	19.07	0.29
				100.00	1.52
Br3d	Br^- 3/2	68.86	1.30	9.09	0.25
	Br^- 5/2	67.85	1.30	13.78	0.38
	C–Br 3/2	71.94	1.40	30.67	0.84
	C–Br 5/2	70.85	1.40	46.46	1.28
				100.00	2.75

[a] Relative area = component area×100/sum area of same orbital

5.2.1 Pyridinium acetate cellulose bromide

Pyridine was the first reagent used for the synthesis of cationized cellulose nanoparticles. Bromoacetate cellulose ester was used as previously synthesised and after three repeat cycles of vacuum-argon flushing in order to remove humidity, the modified cellulose nanoparticles were immersed in extra dry pyridine over molecular sieve and left to react at 80 °C for 24 hours. Initial attempts of this reaction proved that the desired reaction product was not obtained if the modified cellulose nanoparticles were simply flushed with argon. Furthermore, only reactions carried out at 80 °C were successful whereas reactions carried out at 40 °C did not result in cationic nanocrystals.

A first evaluation of the reaction product was done by FT-IR analysis and in Figure 5.2.3 the existence of a peak at 1755 cm^{-1} characteristic of carbonyl bond stretching that is slightly higher than the value of C=O peak in bromoacetate cellulose (1745 cm^{-1}) it can be seen. This shift could be due to the presence of C=N in the same region, and another two peaks at 1636 and 1490 cm^{-1}, attributed to C=C of the aromatic ring absorption bands.

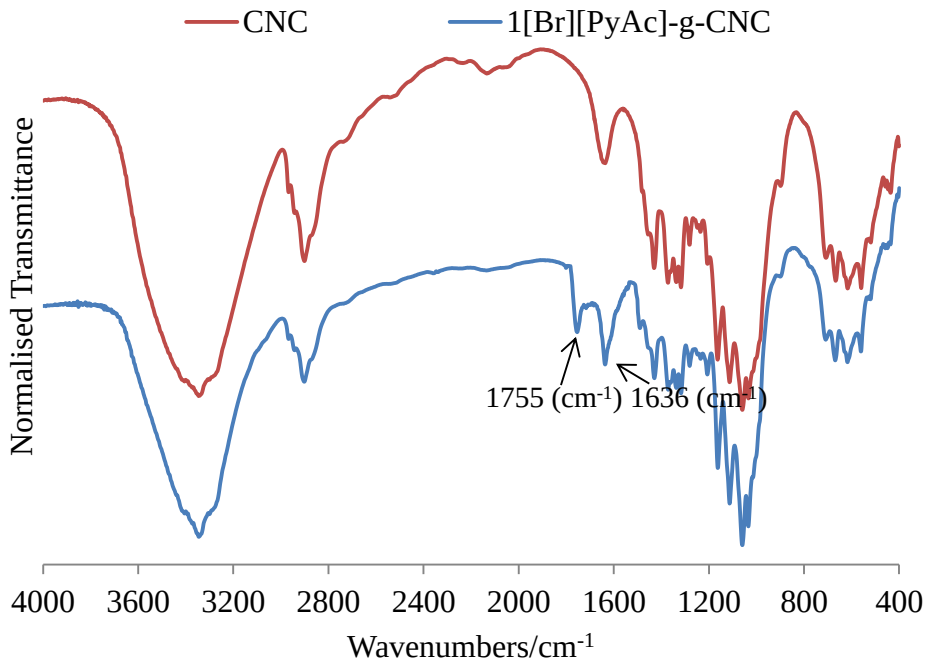


Figure 5.2.3 FT-IR Spectrum of CNC and pyridinium acetate cellulose bromide 1[Br][PyAc]-*g*-CNC

The high conversion of bromoacetate cellulose into pyridinium acetate cellulose is also confirmed by EA (Table 5.2.3) which displays a significant bromine and nitrogen content and an increase in carbon content from 39.58 wt.% (bromoacetate cellulose) to 42.91 wt.% for pyridinium acetate cellulose.

Table 5.2.3 Elemental analysis results for 1[Br][PyAc]-*g*-CNC

Sample	C (%)	H (%)	N (%)	Br (%)	DS_{surf}(N)
CNC	42.38	6.15	0.00	-	-
1[Br][PyAc]-*g*-CNC	42.91	5.38	2.24	10.2.	1.11

The presence of all these peaks indicates that the desired modification took place, i.e. giving pyridinium acetate cellulose bromide 1[Br][PyAc]-*g*-CNC.

The X-ray diffraction pattern confirmed that the crystalline structure was retained (Chapter 5 Appendix, Figures 10.3.5). The crystallinity index calculated for 1[Br][PyAc]-*g*-CNC is χ_C^R = 0.35, which represents a crystallinity drop of 44.6% with respect to the initial cellulose crystallinity (χ_C^R = 0.796). The expected modification determined from EA based on the nitrogen content is 34.87 %. The 9.73 % discrepancy between the two values can be due to a slight degradation of the CNC crystallinity as the cationization reaction is the second one performed on the same nanocrystal. Another possible explanation is related to the existence of unremoved triethylammonium hydrogen bromide which could contribute to the final amorphous material.

In order to identify the chemical environments, present in the reaction product, XPS analysis is used. Wide scan analysis confirms the presence of very well identified C, O, N, and Br elements, as expected (Chapter 5 Appendix, Figures 10.3.6). The C1s high resolution scan (Figure 5.2.4 a) displays the existence of the required O–C=O ester component at a BE of 289.38 eV (Table 5.2.4). This environment is also present in the oxygen high resolution scan (Chapter 5 Appendix, Figure 10.3.7). The C–C component overlaps with the C=C component at a BE of 284.96 eV and increased significantly from 10.10 at% before cationization (Table 5.2.2) to 17.11 at% after reaction with pyridine (Table 5.2.4), indicating the presence of the pyridinium aromatic ring.

Focussing on the N1s spectrum, the presence of the pyridinium species is confirmed through the existence of an N1s component present at a BE of 402.49 eV (Chapter 5 Appendix, Figures 10.3.8), representing 75.24 % of the total nitrogen present (Table 5.2.4), the other peak found at a BE of 400.6 eV, counted for uncharged pyridine adsorbed on the surface.

Pyridinium formation is further confirmed by the Br3d high resolution scan (Figure 5.2.4 b) through the conversion of 88.03 % (53.03+35.00 relative area, Table 5.2.3) of the C–Br chemical environment to anionic bromine at a BE of Br3d 5/2 = 67.79 eV. The remaining uncharged Br3d environment (Br3d 5/2 at 70.57 eV) is thought to be unconverted bromoacetate cellulose.

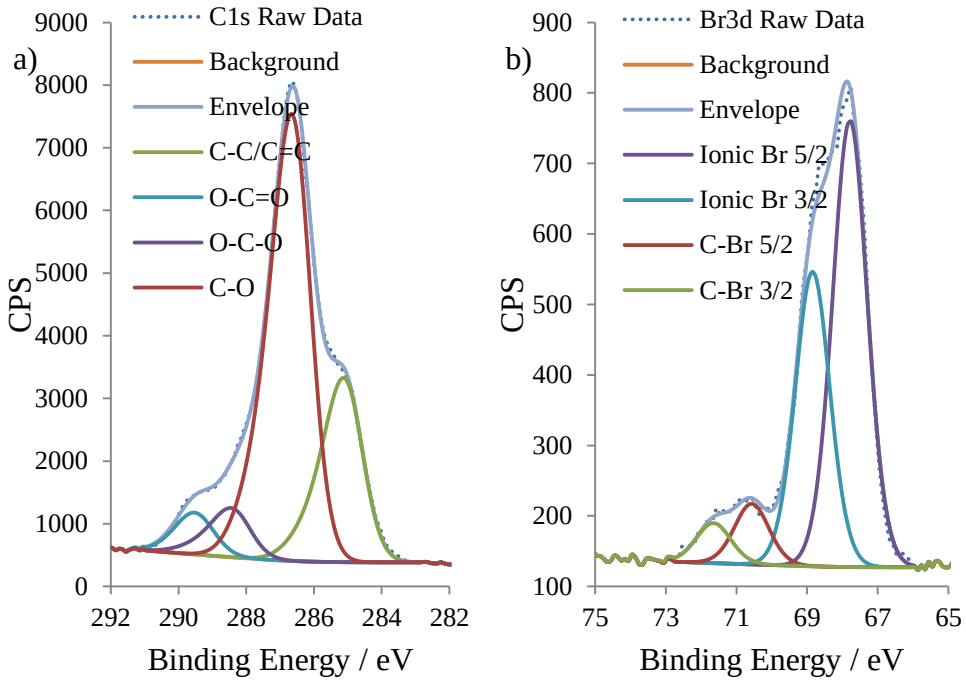


Figure 5.2.4 a) C1s high resolution XPS spectrum of pyridinium acetate cellulose bromide 1[Br][PyAc]-*g*-CNC and b) Br3d high resolution scan composed of the anionic bromide characteristic for charged nanoparticles and C-Br environment

There must be a correlation between XPS relative area percentages of nitrogen and bromine and the EA determined nitrogen and bromine contents. The EA gives a 10.2 wt% Br that results in a DS_{surf}(Br) = 0.83. Considering that 88.03 % (53.03 + 35.00 Rel. at% - Table 5.2.4) of the XPS-detected Br environment in 1[Br][PyAc]-*g*-CNC represents anionic bromine, then this would correspond in EA to a DS_{surf}(Br) = 0.72 for pyridinium species. If the same calculations are applied to nitrogen, where the positively charged N1s has an XPS percentage of 75.24 % (Table 5.2.4) and the DS_{surf}(N) = 1.11 (Table 5.2.3) then a DS_{surf}(N) = 0.84 is found for nitrogen in pyridinium species.

Therefore, it can be considered that both values stay consistent and give a substantial modification. The same calculations could be applied to 1BrAcCNC and so for a C–Br environment present in an XPS percentage of 77.13 (46.46 + 30.67 relative areas/% Table 5.2.2) it would result in an actual DS_{surf}(Br) = 1.05. So, the newly grafted pyridinium species present a slight decrease in

modification from the initial starting material, showing that not all C-Br species were converted into pyridinium grafts.

Table 5.2.4 Detailed XPS data of pyridinium acetate cellulose 1[Br][PyAc]-*g*-CNC

Orbital	Component	BE / eV	FWHM/eV	Rel.A/%[a]	at%
C1s	C–C/C=C	284.96	1.31	25.67	17.11
	C–O	286.50	1.31	62.22	41.48
	O–C–O	288.29	1.31	6.82	4.55
	O–C=O	289.38	1.31	5.29	3.53
	All			100.00	66.67
O1s	O–C=O	530.94	1.48	5.91	1.75
	C–O–H	532.52	1.48	62.74	18.55
	O–C–O	533.12	1.48	31.35	9.27
	All			100.00	29.57
N1s	C–N=	400.64	1.18	24.76	0.55
	$(C–)_4N^+$	402.49	1.18	75.24	1.67
	All			100.00	2.22
Br3d	Br^- 5/2	67.79	1.15	53.03	0.82
	Br^- 3/2	68.84	1.15	35.00	0.54
	C–Br 5/2	70.57	1.15	7.21	0.11
	C–Br 3/2	71.65	1.15	4.76	0.07
	All			100.00	1.54

[a] Relative area = component area×100/sum area of same orbital

5.2.2 Methyl imidazolium acetate cellulose bromide

Cationized nanoparticles were prepared using 1-methyl imidazole. Similar to the synthesis of 1[Br][PyAc]-*g*-CNC, 1-methylimidazolium acetate cellulose was prepared in the same manner through reaction of 1BrAcCNC with 1-methyl imidazole. The purification consisted of the same DCM Soxhlet extraction followed by drying under vacuum.

FT-IR characterization (Figure 5.2.5) show the appearance of a carbonyl stretching band at 1751 cm^{-1} and a very prominent new peak at 1634 cm^{-1} in addition to peaks at 1580 and 1518 cm^{-1} all of which are attributed to C=C absorption bands and aromatic ring vibrations. This is all indicative of the

expected product formation, i.e. methyl imidazolium acetate cellulose bromide, 1[Br][MeImAc]-*g*-CNC.

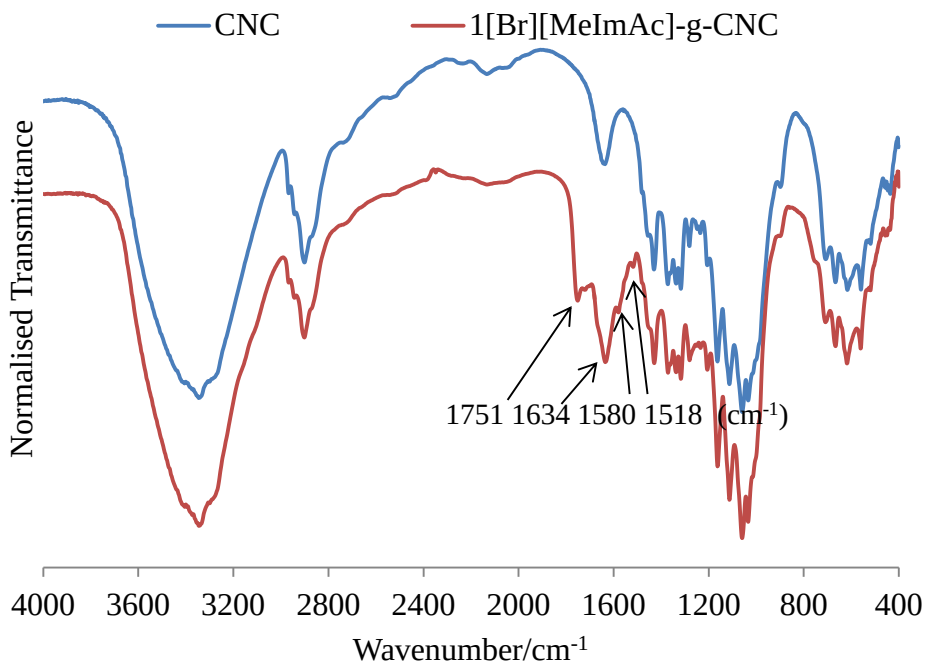


Figure 5.2.5 FT-IR Spectrum of CNC and methyl imidazolium acetate cellulose bromide 1[Br][MeImAc]-*g*-CNC

EA (Table 5.2.5) indicates the presence of a significant amount of N and Br, a decrease in H and a slight increase in C content as expected with a DS_{surf}(N) = 0.97. 1[Br][MeImAc]-*g*-CNC displayed a crystallinity index χ_C^R = 0.386 (Chapter 5 Appendix, Figures 10.3.9) representing a crystallinity drop of 41 % with respect to the starting material (χ_C^R = 0.796) and the expected modification based on EA nitrogen content is 31.80 %.

Similar to the previous cationization reactions, the disagreement between the two values can be attributed to some other undesired surface products which contribute to the total amorphous material and thus decreased crystallinity. Also, a further degradation of the CNC crystallinity could be admitted as the cellulose nanocrystals were subjected to the second synthesis.

Table 5.2.5 Elemental analysis results of methyl imidazolium acetate cellulose bromide 1[Br][MeImAc]-*g*-CNC

Sample	C (%)	H (%)	N (%)	Br (%)	DS_{surf}(N)
CNC	42.38	6.15	0.00	-	-
1[Br][MeImAc]-*g*-CNC	42.96	5.71	3.82	5.65	0.97

XPS analysis was used to determine successful nucleophilic substitution of the alkyl bromide. In the wide scan spectra of 1[Br][MeImAc]-*g*-CNC, C, O, N, and Br species were identified as expected (Chapter 5 Appendix, Figures 10.3.10). The C1s high resolution spectrum shows the presence of an O–C=O component (Figure 5.2.6 a) and also a component present at a BE of 284.98 eV (Table 5.2.6) which is attributed to C–C and C=C. This component peak is higher (12.84 at%, Table 5.2.6) than the C–C component of BrAcCNC (10.10 % Table 5.2.2) but not to the same extent as for 1[Br][PyAc]-*g*-CNC (17.11 at%, Table 5.2.4).

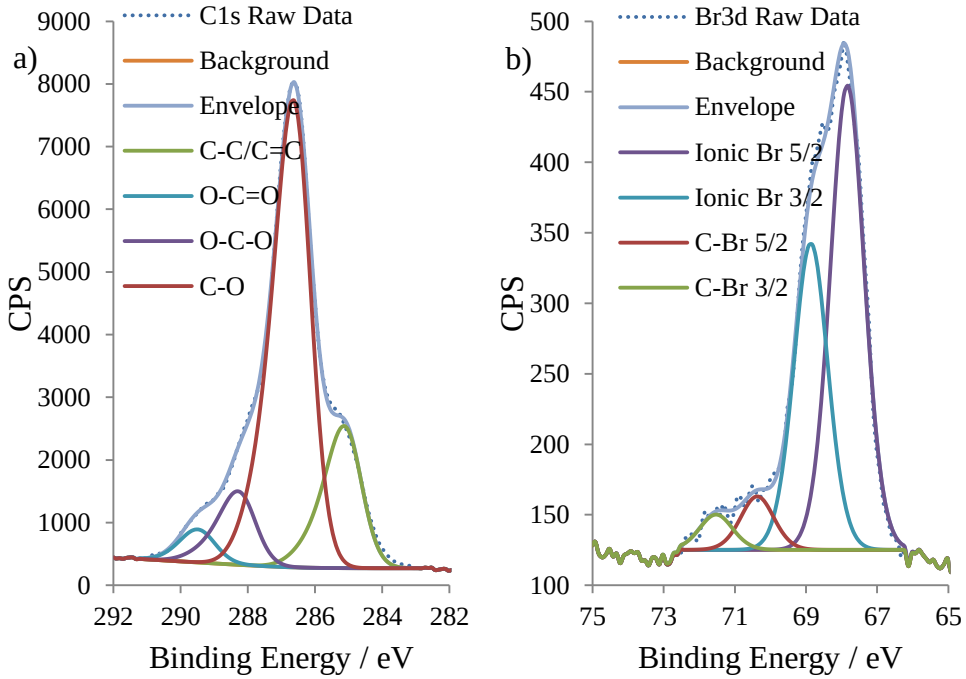


Figure 5.2.6 a) C1s and b) Br 3d high resolution scan of methyl imidazolium acetate cellulose bromide, 1[Br][MeImAc]-*g*-CNC, composed of an anionic Br component and a neutral C-Br environment

The Br3d and N1s high resolution scans (Figure 5.2.6 b and Chapter 5 Appendix, Figure 10.3.11 respectively) show that 89.91 % of the Br on the cationic species is anionic bromine while 72.93 % of the present nitrogen is a quaternary nitrogen, $(C–)_4N^+$ (Table 5.2.6). Considering the bromine at.% (0.64) much lower than the nitrogen at.% (4.21), a possible explanation for this is given by the well-known fact of XPS degradation of Br and therefore a lower final Br content.[65] These observations confirm the presence of the esterified cellulose also strengthened by the presence of an O–C=O oxygen component in O1s high resolution scan (Chapter 5 Appendix, Figure 10.3.12) and the existence of positively charged methyl imidazolium acetate CNC.

Table 5.2.6 Detailed XPS data of methyl imidazolium acetate cellulose bromide 1[Br][MeImAc]-*g*-CNC

Orbital	Component	BE / eV	FWHM /eV	Rel.A/%[a]	at%
C1s	C–C/C=C	284.98	1.213	19.94	12.84
	C –O	286.50	1.213	65.55	42.19
	O–C–O	288.14	1.213	10.29	6.62
	O–C=O	289.36	1.213	4.22	2.71
	All			100.00	64.36
O1s	O–C=O	531.20	1.282	9.5	2.92
	C–O–H	532.57	1.282	60.35	18.58
	O–C–O	533.17	1.282	30.16	9.29
	All			100.00	30.79
N1s	C–N=	400.33	1.312	27.07	1.14
	$(C–)_4N^+$	401.98	1.312	72.93	3.07
	All			100.00	4.21
Br3d	Br^- 5/2	67.84	1.128	54.16	0.35
	Br^- 3/2	68.86	1.128	35.75	0.23
	C–Br 5/2	70.37	1.101	6.08	0.04
	C–Br 3/2	71.53	1.101	4.01	0.03
	All			100.00	0.64

[a] Relative area = component area×100/sum area of same orbital

EA indicates a $DS_{surf}(N) = 0.97$ but considering that not all the N is cationic nitrogen (only 72.93% from the total XPS detected), and applying the same correction as for pyridinium acetate cellulose bromide, the degree of cationic substitution present on the surface is $DS_{surf}(N) = 0.71$. Similarly, to this,

considering only the $DS_{surf}(Br) = 0.43$ and the degree of substitution calculated only for anionic Br will give a $DS_{surf}(Br) = 0.38$.

The nucleophilic substitution of bromoacetate cellulose with 1-methyl-imidazole is lower than the one performed with pyridine and at the same time, the calculated degree of substitution based on bromine is inconsistent with the degree of substitution calculation based on nitrogen. One possible explanation for this observation could be attributed to the different solubility of the bromoacetate cellulose in pyridine and methyl imidazole. Considering the degree of substitution for the two modifications, it results that the cationization reaction is much more successful for pyridine when compared to 1-methylimidazole.

Pyridinium acetate cellulose bromide and methyl imidazolium acetate cellulose bromide were synthesised as confirmed. To further prove their cationic nature, their zeta potential was measured: 1[Br][PyAc]-*g*-CNC indicated a potential of + 31.8 mV with + 28.5 mV for 1[Br][MeImAc]-*g*-CNC. These potentials indicate the possibility to obtain colloidal stable nanoparticle dispersions. As the zeta potential is calculated assuming the particles to be spherical and greater than 0.2 microns in polar media, the determined zeta potentials can only be used for qualitative estimation instead of quantitative analysis.[234]

5.3 Modification of the two step cationic nanoparticles synthesis

Although the synthesis of cellulose nanocrystals bearing initiating sites for ATRP that involved the use of 2-bromoisobutyryl bromide in DMF was reported by Morandi *et al.* and in THF by Li Gang *et al.*, both papers do not give a clear indication on the purity of the reaction products.[64,264]

Therefore, in order to find the best methodology to synthesise bromoacetate cellulose with minimum impurities, the methodology that uses a solvent with a lower polarity than DMF was also attempted. The initial experiments were carried out with the methodology described by Li Gang *et al*. (1.6:33.33:33.33 CNC:TEA:acid chloride in THF).[106] Similarly to the results published by them,

this work used bromoacetyl bromide and led to very poor results with a calculated $DS_{surf}(Br) = 0.15$. Doubling the molar excess did not highly improve grafting. However, with an excessive molar excess of 1:100:115 CNC:TEA:bromoacetyl bromide, the amount of modification was markedly improved when left to react for 24 hours at 40 °C.

The FT-IR spectrum of this reaction product displayed the appearance of a strong absorption band at 1737 cm^{-1}, attributed to the carbonyl absorption band and indicating the formation of an ester (Figure 5.3.1). Therefore, this product was identified as the second bromoacetate cellulose, 2BrAcCNC.

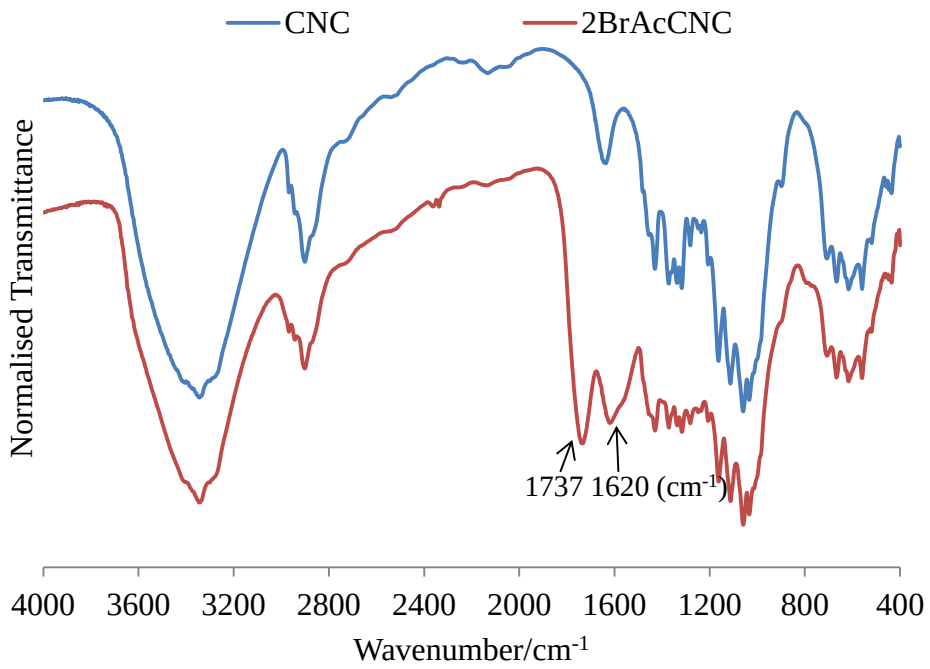


Figure 5.3.1 FT-IR spectrum of CNC and bromoacetate cellulose 2BrAcCNC, reaction product synthesised in THF

The EA results (Table 5.3.1) support successful esterification with Br = 12.4 wt%, which represents a $DS_{surf}(Br) = 1.02$, i.e. two hydroxyl groups per AGU were modified. Although EA also determines N content, this content is less (0.59 wt%) than in 1BrAcCNC (0.91 wt.%) and is going to be identified with the help of XPS.

Table 5.3.1 Elemental analysis results for the bromoacetate cellulose synthesised in THF

Sample	C (%)	H (%)	N (%)	Br (%)	DS_{surf}(Br)
CNC	41.96	6.00	0.00	-	-
2BrAcCNC	42.33	4.76	0.59	12.4	1.02

The examination of the X-ray diffraction pattern of 2BrAcCNC indicated the retention of the crystalline cellulose I_β allomorph (Chapter 5 Appendix, Figures 10.3.13) and the crystallinity was determined as χ_C^R = 0.333 similar to the one of 1BrAcCNC (χ_C^R = 0.327). The crystallinity loss is determined to be 46.3 % with respect to the initial starting material (χ_C^R = 0.796) while the extent of modification based on EA gives a 21.4 %. The difference could be explained with a further degradation of crystalline CNC and the existence of non-crystalline materials in the form of a possible triethylammonium hydrogen bromide trapped on the CNC surface as a consequence of the extensive molar excess used, similar to the previous bromoacetate cellulose product.

The XPS wide scan shows the expected oxygen, carbon, bromine and nitrogen but also a little peak of fluorine (fluorine element is counted as a contamination during the XPS experiment) (Figure 5.3.2 a). The C1s spectrum (Chapter 5 Appendix, Figures 10.3.14) shows the presence of an O–C=O component at a BE of 289.03 eV, a component that is also found in the O1s spectrum at a BE of 531.59 eV (Chapter 5 Appendix, Figure 10.3.15) (Chapter 5 Appendix, Table 10.3.1).

Furthermore, the wide scan of Br3d (Figure 5.3.2 b) displays a well-defined bromine environment with a BE of Br3d 5/2 of 70.55 eV that is attributed to C–Br and represents concrete proof that esterification also works very well in THF for the mentioned molar excess and results in less secondary products than the previous synthesised bromoacetate cellulose (Figure 5.2.2 b). Indeed, only a very small secondary bromine environment is present at a BE of 67.38 eV, attributed to ionic bromide.

This ionic bromide component accounts for only 2.66 % of the total present bromine, and matches the positively charged N1s identified in the high

resolution scan (Chapter 5 Appendix, Figures 10.3.16) at a BE of 402.28 eV, showing the presence of a small amount of triethylamine hydrogen bromide, despite an intensive purification by DCM and EtOH Soxhlet extraction. Similar to 1BrAcCNC, this synthesised bromoacetate cellulose presents two nitrogen chemical environments in its XPS spectrum. For 1BrAcCNC, N1s present at a BE of 400.87 eV was attributed to physically absorbed Et_3N. Here, N1s present at a BE of 400.04 eV, slightly lower than the previously mentioned value, could actually be correlated with the F1s found at a BE of 690.5 eV which are representative components of the anion bis(trifluoromethane-sulfonyl)imide (bistriflimide anion – Tf_2N).[265]

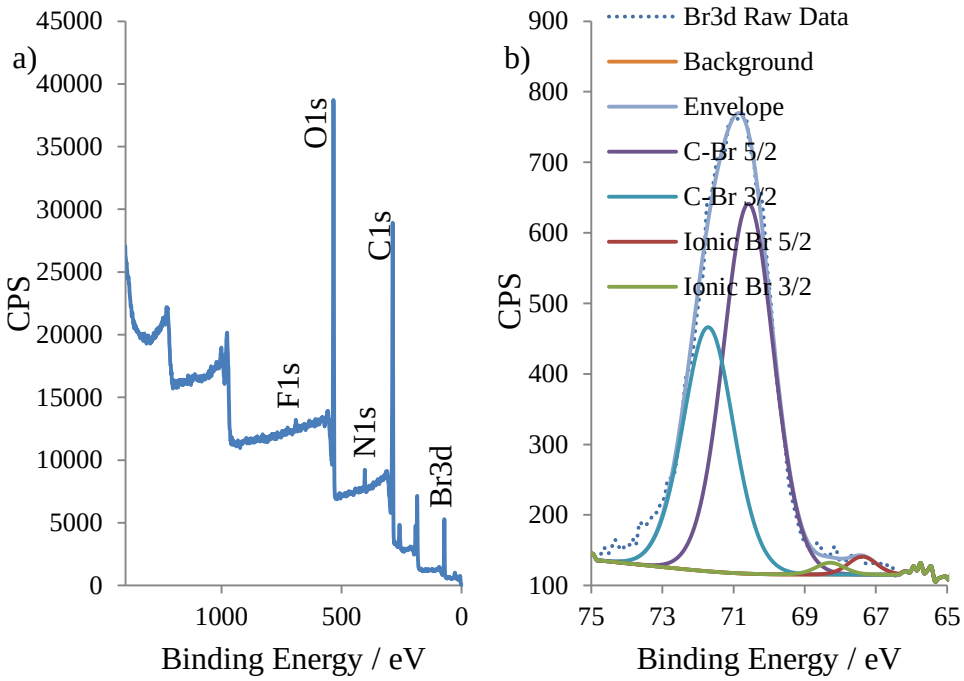


Figure 5.3.2 a) XPS wide scan of bromoacetate cellulose 2BrAcCNC synthesised in THF; b) Br3d high resolution scan of 2BrAcCNC that encompasses mainly the neutral C–Br environment

Considering the fact that the XPS service also runs analysis on ionic liquids containing bistriflimide anions and presently modified cellulose nanoparticles are positively charged, it is expected that the bistriflimide contamination was attracted to the surface of cellulose during the sample preparation or loading. The anion may have exchanged with bromide anion in the triethylamine

hydrogen bromide salt. The presence of a small C–F component peak in C1s at BE of 291.47 eV also supports this finding, in addition to other analyses carried out by the XPS service for our group. From the Br3d high resolution scan, it is found that 97.34 % of the total bromine content is found in a C–Br environment. Using this to correct the DS found from EA, the corrected $DS_{surf}(Br)$ = 0.99. Therefore, this methodology of synthesizing bromoacetate cellulose in THF is an improved one when compared with the previous method of using DMF as a solvent.

5.4 Influence of the solvent

In section 5.3 it was mentioned that there could be a possible influence of DMF on the already modified cellulose. Therefore, to check the effect of DMF on the reaction of bromoacetyl bromide with CNC by excluding it and carrying out the reaction in triethylamine only for 24 hours at 40 °C followed by DCM and EtOH Soxhlet extraction and *vacuo* drying. The EA results for the reaction product of this reaction gave a very small amount of bromine and no nitrogen with a $DS_{surf}(Br)$ = 0.03 (Table 5.4.1).

Table 5.4.1 Elemental analysis results for bromoacetate cellulose 3BrAcCNC synthesised as a reaction of the catalyst/solvent (triethylamine) with bromoacetyl bromide

Sample	C (%)	H (%)	N (%)	Br (%)	$DS_{surf}(Br)$
CNC	41.77	5.91	0.00	-	-
3BrAcCNC	42.18	6.28	0.00	0.5	0.03

The crystallographic diffraction pattern was determined (Chapter 5 Appendix, Figures 10.3.17) and the crystallinity of the reaction product showed a drop in crystallinity of 6.5 % with respect to the initial crystallinity of cellulose nanocrystals of χ_C^R = 0.663. This value is significantly higher than the reduction predicted based on the value of the EA-calculated modification (0.86 %). Thus, this can be explained as a loss of crystallinity in the crystalline cellulose although the benign reaction conditions are not expected to effect

such a decrease. An alternative explanation could be attributed to the disordered nature of the adsorbed species on the modified cellulose surface that contributes to the amorphous background on the XRD pattern.

Therefore, more information can be gleaned from the XPS analysis wide scans (Chapter 5 Appendix, Figures 10.3.18) in which carbon, oxygen, nitrogen and bromine were identified as well as some fluorine and silicon (coming from adhesive silicon tape) contamination. In the C1s spectrum (Chapter 5 Appendix, Figures 10.3.19), a O–C=O component is seen, indicating successful esterification. This is further confirmed by the O1s spectrum in which O–C=O is visible (Chapter 5 Appendix, Figures 10.3.20). Thus, the product of this reaction was identified as being bromoacetate cellulose denominated as 3BrAcCNC. Further confirmation comes from the Br3d high resolution spectrum where two bromine environments were identified, Br3d 5/2 at a BE of 70.74 eV representative of a C–Br component and Br3d 5/2 at a BE of 68.11 eV attributed to anionic Br (Figure 5.4.1 a, Table 5.4.2).

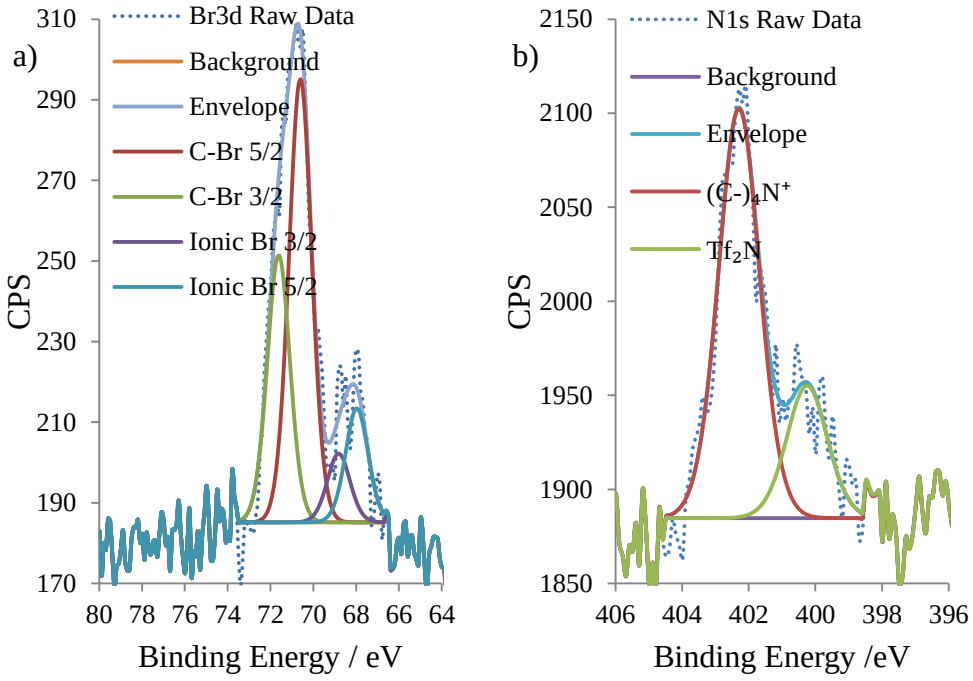


Figure 5.4.1 a) Br 3d high resolution scan composed of anionic Br characteristic for charged nanoparticles and neutral C-Br environment; b) N1s high resolution scan of bromoacetate cellulose 3BrAcCNC composed of

cationic N1s environment and nitrogen component of bistriflimide contamination, Tf_2N.

Table 5.4.2 Detailed XPS data of bromoacetate cellulose synthesised as a side reaction of bromoacetyl bromide with triethylamine, the catalyst

Orbital	Component	BE / eV	FWHM / eV	Rel.A/%[a]	at%
C1s	C–C	284.58	1.21	19.64	11.60
	C–O	286.50	1.21	66.09	39.04
	O–C=O	289.49	1.21	1.91	1.13
	O–C–O	288.23	1.21	11.61	6.86
	C–F	292.27	1.21	0.75	0.44
				100.00	59.07
O1s	O–C=O	531.77	1.14	14.47	5.29
	C–O–H	532.67	1.14	57.03	20.85
	O–C–O	533.27	1.14	28.5	10.42
				100.00	36.56
N1s	Tf_2N	400.45	1.37	22.71	0.08
	$(C–)_4N^+$	402.43	1.37	77.29	0.29
				100.00	0.37
Br3d	Br^- 5/2	68.11	1.23	12.25	0.03
	Br^- 3/2	68.92	1.23	7.37	0.02
	C–Br 5/2	70.74	1.23	50.18	0.11
	C–Br 3/2	71.74	1.23	30.20	0.07
				100.00	0.22
F1s	-[b]	689.5	1.99	100.00	1.46
Si2p	-[b]	102	1.82	100.00	2.32

[a] Relative area = component area×100/sum area of same orbital
[b] Data available from low resolution wide scan

The N1s spectrum includes a cationic N1s environment that matches the anionic bromine which confirms the formation of triethylammonium hydrogen bromide and also the existence of a nitrogen component of a bistriflimide contamination, Tf_2N (Figure 5.4.1 b). The reagents are well-dispersed in both solvents (DMF and Et_3N) and the reactants behave through the same mechanism of bromoacetate cellulose synthesis where Et_3N captures the HBr. As it was identified in the EA, Br was found in a very low concentration while N it couldn't be found in the EA. Due to the very low concentrations, neither Br3d or N1s high resolution scans presented peaks that could be readily identified from the noise.

5.5 One-pot reaction towards pyridinium cationized nanoparticles

After the synthesis of cationized nanoparticles in two steps as earlier described for 1[Br][PyAc]-*g*-CNC and 1[Br][MeImAc]-*g*-CNC, their synthesis in one single step was also attempted. The single step production of cationized cellulose nanoparticle involves the reaction of cellulose nanoparticles with bromoacetyl bromide directly immersed in the nucleophile which also acts as the solvent. This mixture is then left to react for 24 hours at 80 °C followed by water washing, and EtOH and DCM Soxhlet extraction. The schematic representation of the proposed reaction in which pyridine was selected as the nucleophile and solvent is given in Figure 5.1.4.

EA confirms the fact that the reaction was not as effective as expected with the cellulose poorly modified (Table 5.5.1). A nitrogen content of 0.91 wt.% was measured, representing a $DS_{surf}(N) = 0.37$.

Table 5.5.1 Elemental analysis results for pyridinium acetate cellulose bromide 2[Br][PyAc]-*g*-CNC synthesised in single step

Sample	C (%)	H (%)	N (%)	Br (%)	$DS_{surf}(N)$
CNC	41.77	5.91	0.00	-	-
2[Br][PyAc]-*g*-CNC	42.87	5.87	0.91	1.8	0.37

The X-ray diffractogram of this reaction product confirmed the preservation of the crystal structure of cellulose I_β (Chapter 5 Appendix, Figures 10.3.21) and subsequent calculations of the crystallinity indicated a χ_C^R = 0.620 which correspond to a loss of crystallinity of 17.6 % when compared with the crystallinity of the cellulose nanocrystals (χ_C^R = 0.796). This is in agreement with the mass of modification in the sample ($C_7H_8O_2NBr$) from the nitrogen content based on EA corresponding to 14.16 % amorphous modification.

The FT-IR spectrum of the reaction product (Figure 5.5.1) indicates the presence of an absorption band at 1735 cm^{-1} representative of the carbonyl stretch. The sharp peak present at 1636 cm^{-1} shows an overlap of ν(C=C) with

the water absorption band and further confirms the presence of the pyridine ring as the desired modification.

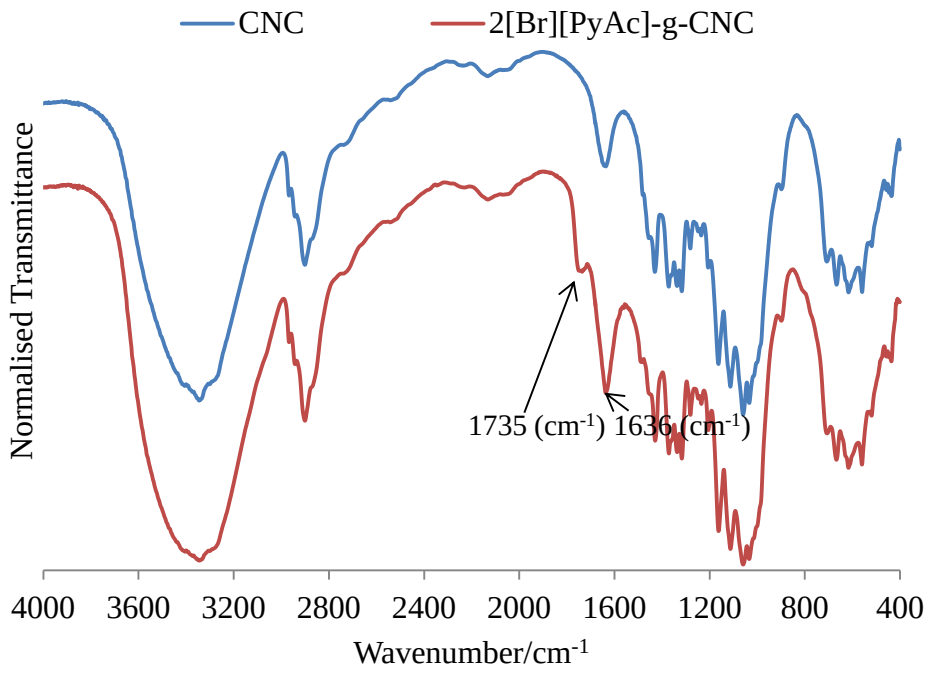


Figure 5.5.1 FT-IR Spectrum of CNC and pyridinium acetate cellulose bromide 2[Br][PyAc]-*g*-CNC

Further analysis of the reaction product is given by XPS analysis, which reveals the presence of carbon, oxygen, nitrogen and bromine in the wide scan (Chapter 5 Appendix, Figures 10.3.22). The O1s spectrum (Chapter 5 Appendix, Figures 10.3.23) and the C1s spectrum (Chapter 5 Appendix, Figures 10.3.24) showed the existence of an O–C=O component at a BE of 531.45 eV and 289.78 eV respectively (Table 5.5.2).

The formation of pyridinium is confirmed by the N1s peak at a BE of 402.18 eV (Figure 5.5.2 a), being attributed to a positively charged nitrogen environment.[263] At the same time, pyridinium formation is seen also by the Br3d 5/2 peak at a BE of 68.05 eV, corresponding to anionic bromine (Figure 5.5.2 b). The second bromine environment Br3d 5/2 found at a BE of 70.83 eV is attributed to the C–Br and this can be associated with a little amount of bromoacetate cellulose still left un-converted to cationic species (Table 5.5.2).

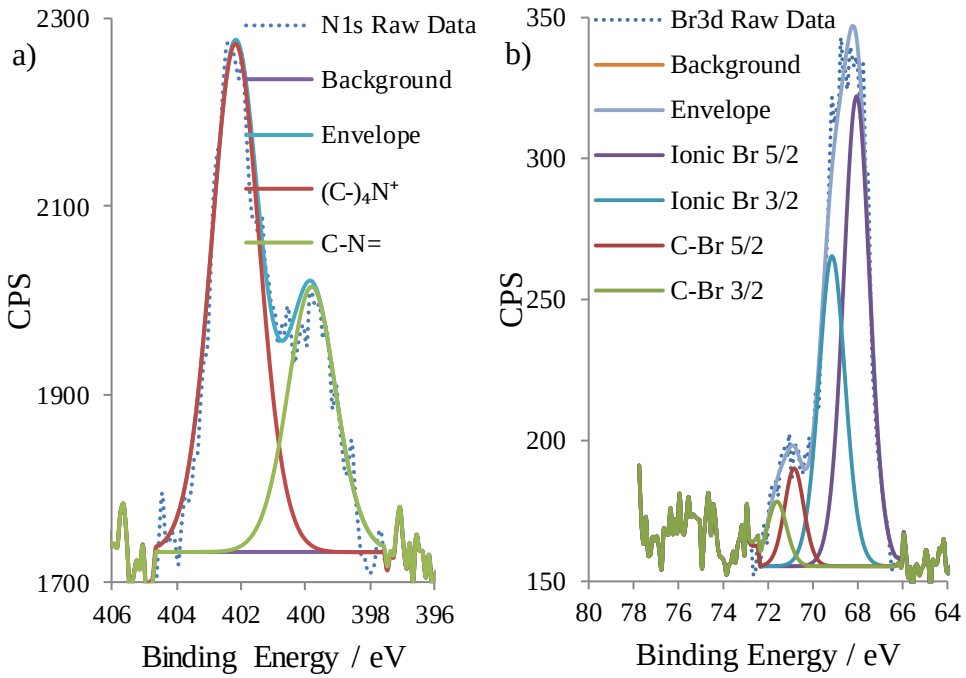


Figure 5.5.2 a) N1s high resolution scan of pyridinium acetate cellulose bromide 2[Br][PyAc]-*g*-CNC composed of a cationic N1s environment and a neutral nitrogen environment; b) Br 3d high resolution scan composed of anionic Br characteristic for charged nanoparticles and a neutral C-Br environment

This peak is difficult to be distinguished from the noise because of the low signal but could still be attributed to the chemical environment due to the expected position. Anionic bromine makes up 86.7% of the total bromine content. This indicates that the esterification reaction is the faster of the two and that the nucleophilic attack is significantly slower. As 65.79 % of the total nitrogen is cationic nitrogen content the surface modification is actually only $DS_{surf}(N) = 0.25$. The same calculations can be applied for 86.7 % anionic bromine which results in a $DS_{surf}(Br) = 0.10$. The discrepancy between the Br and N XPS environemnts and therefore the resulting calculations, could be again attributed to the degradation of Br in XPS run. Also, Br attribution is unreliable because of the low signal to noise ratio as it was displayed in Figure 5.2.2 b. Further explanation for the discrepancy between the calculated DS_{surf}, could be due to an Br^- anion exchange with HO^- during water washing

purification and hence increased disagreement between the nitrogen and bromine.

Table 5.5.2 Detailed XPS data of pyridinium acetate cellulose bromide 2[Br][PyAc]-*g*-CNC synthesised in a single step

Orbital	Component	BE / eV	FWHM / eV	Rel.A/%[a]	at%
C1s	C–C/C=C	284.98	1.14	16.29	10.202
	C–O	286.50	1.14	70.85	44.373
	O–C–O	288.19	1.14	11.7	7.328
	C–O=C	289.78	1.14	1.02	0.639
	C–F	292.4	1.14	0.14	0.088
				100.00	62.629
O1s	O–C=O	531.45	1.16	6.12	2.166
	C–O–H	532.65	1.16	62.59	22.156
	O–C–O	533.25	1.16	31.29	11.076
				100.00	35.398
N1s	C–N=	399.80	1.76	34.21	0.495
	$(C–)_4N^+$	402.18	1.76	65.79	0.953
				100.00	1.448
Br3d	Br^- 5/2	68.05	1.37	52.25	0.153
	Br^- 3/2	69.15	1.37	34.45	0.101
	C–Br 5/2	70.83	1.01	8.01	0.023
	C–Br 3/2	71.60	1.01	5.29	0.015
				100	0.292
S2p	3/2	168.73	0.88	66.72	0.060
	1/2	169.91	0.88	33.28	0.030
				100	0.090
F1s	F1s	689.5	1.66	100	0.143

[a] Relative area = component area×100/sum area of same orbital

The purification of this reaction product consisted in water washing, EtOH and DCM Soxhlet extraction, but there was still a N signal visible in the XPS of the CNC surface (BE 399.8 eV). Considering the BE of the nitrogen and the at.% (0.495) as compared to positively charged nitrogen (0.953 at.%), this is more likely to be due to some CNC surface adsorbed pyridine and not with bistriflimide contamination of the XPS chamber (as the amount of N1s agrees with the F1s signal and with the S2p (Chapter 5 Appendix, Figure 10.3.25).

It is worth mentioning that despite the very high reactivity of bromoacetyl bromide and of pyridine and a very high stirring rate, the reaction between the two reagents is hampered by the formation of a reaction mixture difficult to stir. It is believed that the formation of the ionic liquid occurs first as insoluble components were noticed forming during the reaction and consequently could have a low solubility in pyridine resulting in a low esterification as a second step. These results are comparable with 1[Br][MeImAc]-g-CNC where an inconsistency between DS_{surf}(Br) and DS_{surf}(N) was noticed. In the case of 1[Br][MeImAc]-g-CNC, the purification consisted in DCM Soxhlet extraction, whereas for 2[Br][PyAc]-g-CNC purification consisted of water washing, EtOH and DCM Soxhlet extraction. Additional understanding of the lower calculated DS_{surf} for bromine could be due to an anion exchange of Br^- with HO^- during water washing purification as it was mentioned earlier as well.

5.6 One-pot reaction towards methyl imidazolium cationized nanoparticles

The same type of one-pot reaction as the previously described reaction with pyridine under the same reaction conditions was carried out but this time 1-methylimidazole was used instead of pyridine (Figure 5.1.5).

FT-IR analysis of the reaction product of this synthesis is given in Figure 5.6.1 which displays the appearance of a prominent band at 1732 cm^{-1}, attributed to carbonyl stretch absorption, and two other bands at 1633 cm^{-1} and 1576 cm^{-1}, both attributed to C=C absorption. Both types of absorption bands indicate the formation of the ester and the existence of the double bonds specific of imidazole, confirming the formation of methyl imidazolium acetate cellulose bromide, 2[Br][MeImAc]-*g*-CNC.

The XPS wide scan (Chapter 5 Appendix, Figure 10.3.26) of the product displays the presence of carbon, oxygen, a relatively large nitrogen peak, and a bromine signal. The esterification is confirmed through the appearance of an O–C=O component at a BE of 289.22 eV in the C1s spectrum (Chapter 5

Appendix, Figure 10.3.27) and in the O1s spectrum (Chapter 5 Appendix, Figure 10.3.28) at a BE of 531.16 eV. Also, in the C1s spectrum the component present at 284.79 eV attributed to the C=C bond and overlapping with C–C clearly increased (17.81 at%) when compared to unmodified cellulose (4.56 at%) (Table 5.6.1).

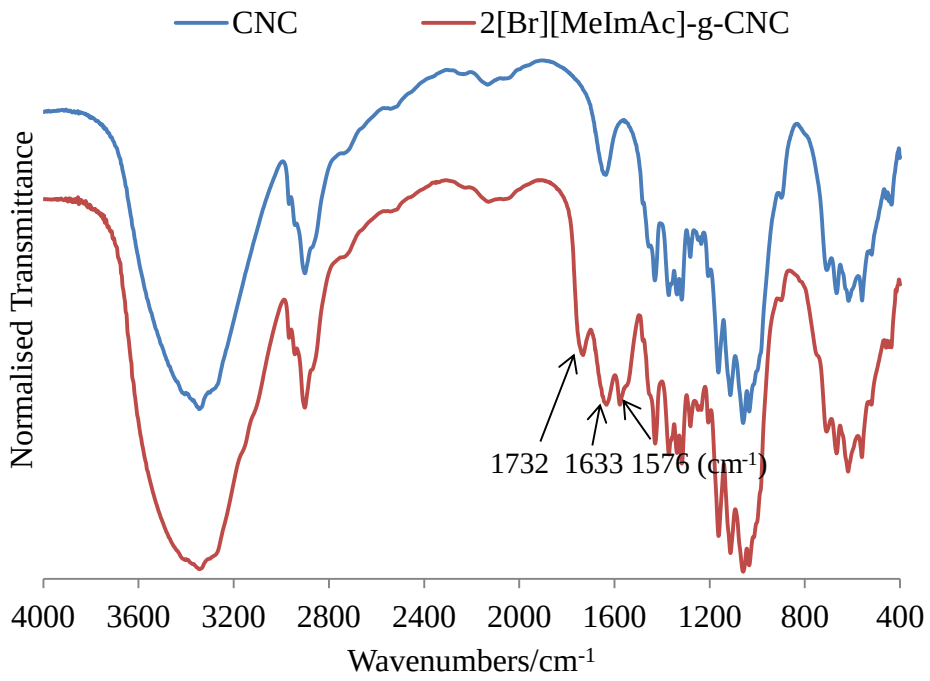


Figure 5.6.1 FT-IR Spectrum of CNC and methyl imidazolium acetate cellulose bromide 2[Br][MeImAc]-*g*-CNC

Furthermore, the N1s spectrum presents a single component present at a BE of 401.8 eV and this corresponds to positively charged nitrogen (Figure 5.6.2 a). At the same time, the Br3d spectrum shows a single component of Br3d 5/2 at a BE of 67.73 eV attributed to ionic bromine (Figure 5.6.2 b). Therefore, the reaction product of this synthesis is clean and without secondary products measurable by XPS analysis. The crystal structure of 2[Br][MeImAc]-*g*-CNC was further determined (Chapter 5 Appendix, Figure 10.3.29) and the crystallographic I_β allomorph was identified with a calculated crystallinity of χ_C^R = 0.434, representing a loss of crystallinity of 36.2 % (with initial cellulose crystallinity of χ_C^R = 0.796). Furthermore, considering the mass of nitrogen incorporated into the grafted methyl imidazolium acetate ($C_7H_8O_2NBr$) (Table

5.6.2), the amount of modification is expected to be 34.97 %, giving a good agreement between DS based on EA of nitrogen and XRD analysis. However, when calculating the amount of modification based on Br content (EA), one finds only 16.91 % expected modification. Expressing this in degree of substitution, $DS_{surf}(Br) = 0.42$ which is less than half the degree of substitution calculated for N, $DS_{surf}(N) = 1.06$.

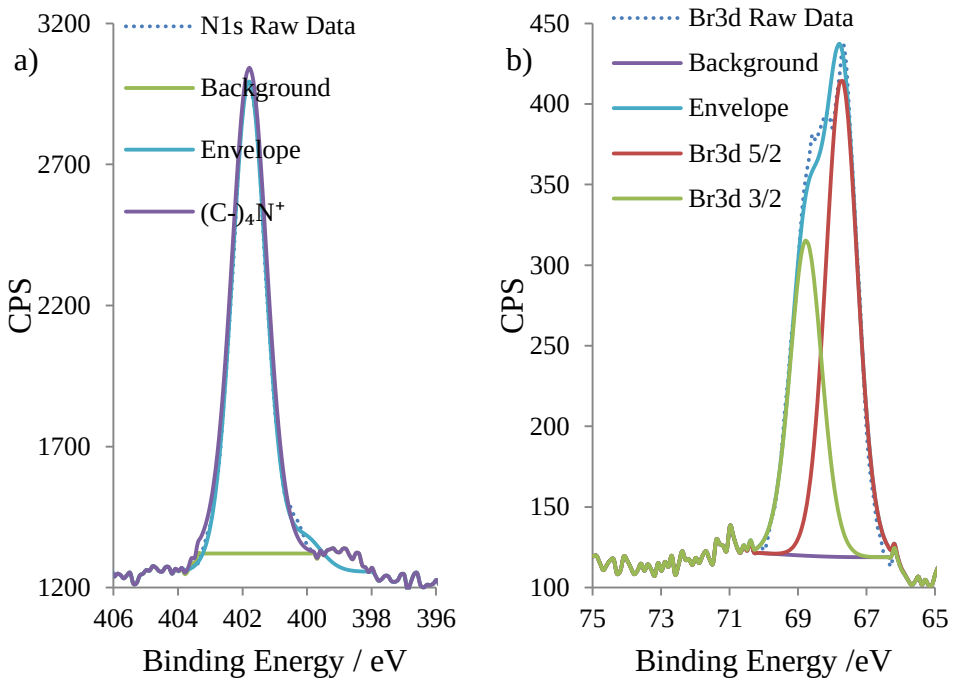


Figure 5.6.2 a) N1s high resolution scan and b) Br3d high resolution scan of 2[Br][MeImAc]-g-CNC showing only cationic N and anionic Br respectively

As confirmed by the Br3d and N1s high resolution, there are no other forms of nitrogen and bromine than the expected ones. Thus, the slightly lower than expected EA bromine amount is explained by some Br^- exchange with HO^- during water washing purification. Repetitions of the same reaction lead to the same results with a deficit of bromine. As mentioned in section 5.5, in the synthesis of 2[Br][PyAc]-*g*-CNC, where the same purification procedure was applied as for 2[Br][MeImAc]-*g*-CNC, the ionic bromine content is also found to be half the expected one. It could be concluded that the ionic bromine has been ion exchanged during purification, as research in our group has also proven.[65]

Table 5.6.1 Detailed XPS data of methyl imidazolium acetate cellulose bromide 2[Br][MeImAc]-*g*-CNC synthesised in a single step

Orbital	Component	BE / eV	FWHM / eV	Rel.A/%[a]	at%
C1s	C–C/C=C	284.79	1.15	26.84	17.81
	C–O	286.35	1.15	62.00	41.15
	O–C–O	288.05	1.15	9.67	6.42
	O–C=O	289.22	1.15	1.49	0.99
				100.00	66.37
O1s	O–C=O	531.16	1.25	8.11	2.24
	C–O–H	532.4	1.25	61.26	16.95
	O–C–O	533.00	1.25	30.63	8.48
				100.00	27.67
N1s	$(C–)_4N^+$	401.8	1.28	100.00	3.96
				100.00	3.96
Br3d	Br 5/2	67.73	1.09	60.26	0.42
	Br 3/2	68.77	1.09	39.74	0.27
				100.00	0.69
Si2p	-[b]	102	1.68	100.00	1.32

[a] Relative area = component area×100/sum area of same orbital
[b] Data available from low resolution wide scan, Si comes from adhesive tape

Table 5.6.2 Elemental analysis results for methyl imidazolium acetate cellulose bromide 2[Br][MeImAc]-*g*-CNC synthesised in a single step

Sample	C (%)	H (%)	N (%)	Br (%)	DS_{surf}(N)
CNC	41.77	5.91	0.00	-	-
2[Br][MeImAc]-*g*-CNC	43.95	5.70	4.20	5.80	1.06

It is clear that there is a difference between the degrees of substitution for the 1-methylimidazolium and pyridinium reaction products of the one-pot esterification and cationization step. It is worth mentioning that this is also visually observed that 1-methylimidazole is a much better cationization agent/solvent as it reacts with bromoacetyl bromide and CNC conferring a very homogeneous reaction medium while in the case of pyridine, the reaction mixture aggregates and sediments at the beginning of reaction despite intensive stirring.

The zeta potential of the prepared CNCs offers further confirmation of successful synthesis of cationized nanoparticles with 2[Br][PyAc]-*g*-CNC giving ζ= +37.42 mV and 2[Br][MeImAc]-*g*-CNC ζ= +37.89 mV, both of which lead to positive stable colloidal nanoparticles.

As a conclusion, by comparing the one step methodology with the one in two steps, it is evident that [Br][MeImAc]-*g*-CNC is more easily synthesised in the one step reaction, giving an excellent $DS_{surf}(N)$ = 1.06 while [Br][PyAc]-*g*-CNC gives better results when the synthesis is performed in two steps with a $DS_{surf}(N)$ = 0.84 meaning that almost two hydroxyl groups are modified on every surface AGU.

5.7 One-pot synthesis towards pyridinium cationized cellulose nanoparticles using TsCl/Py conditions

The last investigated pathway involved the esterification of bromoacetic acid onto CNC with simultaneous nucleophilic attack of pyridine onto the C–Br bond (Figure 5.1.6), whereas previously bromoacetyl bromide has been used. This was an attempt to improve the performance of the one-pot reaction to create pyridinium-modified CNC. A TsCl/Py system was used here for the esterification of surface hydroxyl groups with bromoacetic acid acting through the activation of acid by *p*-toluenesulfonyl chloride while the grafted C–Br bond undergoes a nucleophilic attack by pyridine to incorporate the pyridinium ions together with the bromine counter ion. CNC were reacted together with bromoacetic acid and tosyl chloride in a ratio of 1:2.75:2.75 in pyridine, at 80 °C for 16 hours followed by extensive purification by Soxhlet extraction with DCM and EtOH.

Esterification was confirmed by examination of the FT-IR spectrum of the reaction product which shows the appearance of an absorption band at 1755 cm^{-1}, attributed to the carbonyl peak (Figure 5.7.1). The aromatic C=C stretching vibration at 1637 cm^{-1}, which overlaps with the bending vibration of water at the same position, can also be seen. The band at 1491 cm^{-1} could be

attributed to pyridinium nitrogen (C–N^+=) while the very small peak present at 750 cm^{-1} can be attributed to C–Br stretching or to an out–of–plane C–H mono–substituted aromatic system as found in pyridinium. These two observations suggest that nucleophilic substitution of the alkyl bromide by pyridine took place as expected, and 3-pyridinium acetate cellulose bromide was the reaction product (3-[PyAc]-*g*-CNC]).

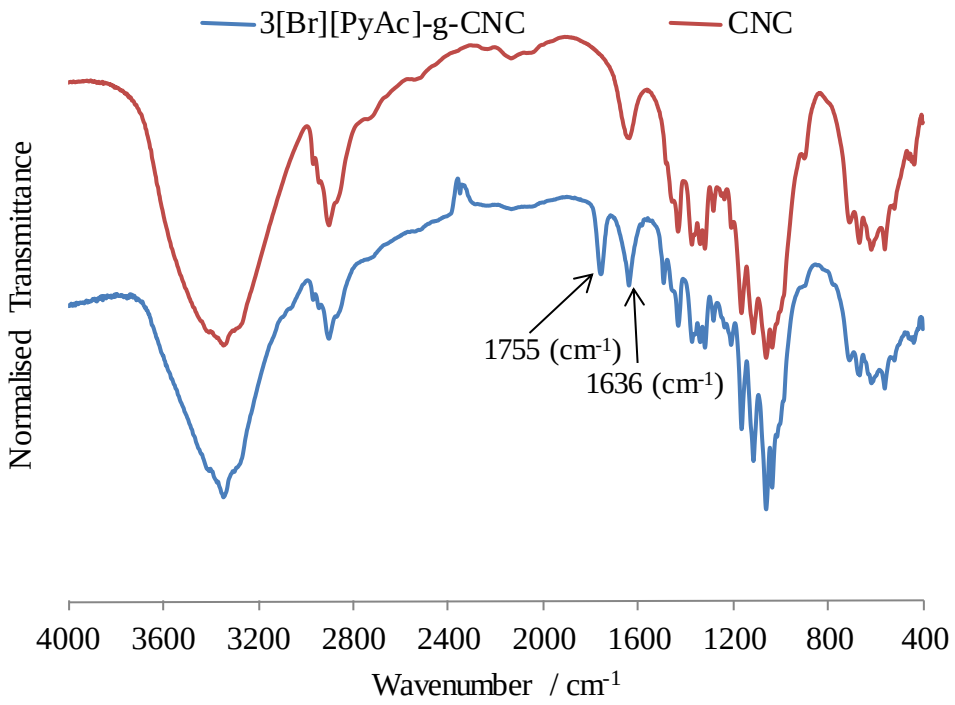


Figure 5.7.1 FT-IR Spectrum of CNC and 3-pyridinium acetate cellulose bromide synthesised through TsCl/Py methodology

This observation is strengthened by EA results that showed a content of 0.9 % N and 4.6 % Br contents which correspond to a DS_{surf} = 0.35 calculated for N and DS_{surf} = 0.31 calculated for Br. The values agree well and are consistent suggesting that alkyl bromide was converted to the pyridinium salt although the difference could be counted for a small Br^- replacement with HO^- during purification (Table 5.7.1). This degree of substitution indicates that less than one hydroxyl groups per AGU on the surface of the CNC was modified during the reaction. At the same time, the influence of the pyridine volume in the reaction was checked. It was observed that, for the same ratio of reactants, doubling the volume of pyridine (from 25 mL to 50 mL) increased the DS_{surf}

from 0.24 to 0.35, an observation which supports the idea that a higher volume of pyridine induces a better solubilisation of the acid and so a higher grafting efficiency.

Table 5.7.1 Elemental analysis results for 3-pyridinium acetate cellulose bromide produced using TsCl/Py methodology and for cellulose nanocrystals

Sample	C (%)	H (%)	N (%)	Br (%)	DS_{surf}(N)
CNC	41.77	5.91	0.00	-	-
3[Br][PyAc]-*g*-CNC	42.55	5.80	0.90	4.60	0.35

Investigation of the reaction product with the DS_{surf}(N) = 0.35 by XRD (Chapter 5 Appendix, Figure 10.3.30) indicates a loss in crystallinity of 17.91 % considering the initial crystallinity of cellulose of χ_C^R = 0.796. Counting on EA values, the N % and Br % in EA were divided by the percentage of nitrogen and bromine respectively in the modification ($C_7H_8NO_2Br$) in order to determine the percentage mass of modification. The calculated values are 14.01 % for N and 12.55 % for Br. These values stay consistent with each other but are less than the determined crystallinity. In the second experiment carried out for only 25 mL of pyridine, the calculated loss of crystallinity was of 17.3 % while the calculated expected modification for N is 9.34 % and for Br is 9.27 %. This disagreement between the values could be explained by pyridine acting as a swelling agent that may have induced some degradation of the crystallinity of the CNC crystalline core. Wide scan XPS analysis (Chapter 5 Appendix, Figure 10.3.31) revealed the presence of carbon, oxygen, nitrogen, and bromine as expected but also traces of fluorine and sulfur. Evidence of the esterification was found in the C1s high resolution spectrum (Figure 5.7.2 a) through the presence of an O–C=O component at a BE of 289.73 eV and in the O1s high resolution spectrum at a BE of 531.61 eV (Figure 5.7.2 b). Confirmation of nucleophilic substitution of the alkyl bromide by pyridine comes from the presence of an $(C–)_4N^+$ signal in the N1s high resolution scan with a BE of 402.3 eV (Chapter 5 Appendix, Figure 10.3.32),[244,263,265] and from the Br 3d 5/2 signal with a BE of 67.9 eV corresponding to ionic bromine (Figure 5.7.3)[244,265]

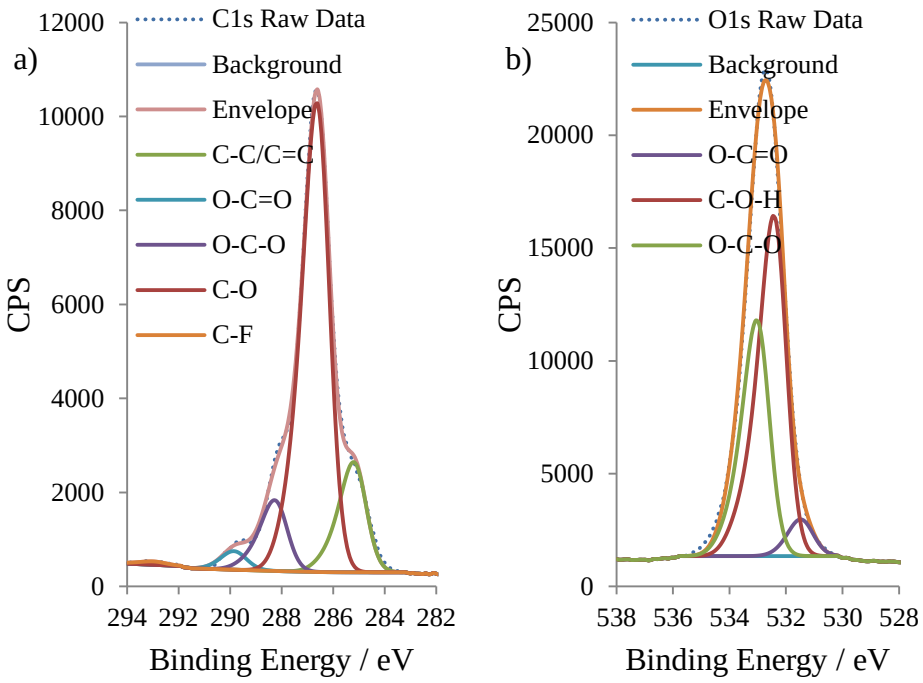


Figure 5.7.2 a) C1s and b) O1s high resolution XPS spectrum of 3-pyridinium acetate cellulose bromide synthesised through TsCl/Py methodology

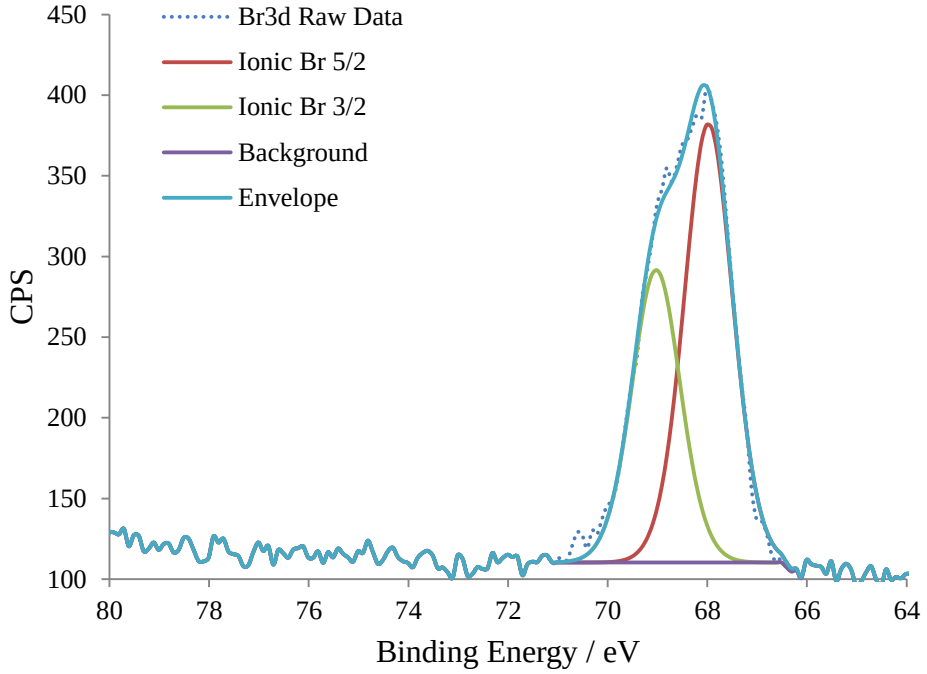


Figure 5.7.3 Br high resolution XPS spectrum of 3-pyridinium acetate cellulose bromide 3[Br][PyAc]-*g*-CNC showing ionic bromine formation as a counter ion of pyridinium synthesised through the TsCl/Py methodology

Detailed information about the reaction product composition based on XPS wide scan along with high resolution scans is given in Table 5.7.2.

Table 5.7.2 Detailed XPS data of 1-pyridinium acetate cellulose bromide 3[Br][PyAc]-*g*-CNC

Orbital	Component	BE / eV	FWHM /eV	Rel.A/%[a]	at%
C1s	C–C	285.07	1.14	16.46	10.38
	C–O	286.50	1.14	70.01	44.17
	O–C–O	288.14	1.14	10.53	6.64
	O–C=O	289.73	1.14	2.51	1.58
	C–F	292.85	1.14	0.49	0.31
				100.00	65.20
O1s	O–C=O	531.61	1.04	5.38	1.77
	C–O–H	532.56	1.04	56.78	18.69
	O–C–O	533.16	1.04	37.84	12.45
				100.00	32.91
Br3d	Br 3d 5/2	67.98	1.15	60.02	0.41
	Br 3d 3/2	69.03	1.15	39.98	0.27
				100.00	0.68
N1s	Tf_2N	399.82	1.27	13.43	0.22
	$(C–)_4N^+$	402.53	1.27	86.57	1.44
				100.00	1.66
F1s	-[b]	688.5 [b]	0.68 [b]	100.00	1.38
S2p	- [b]	168.0 [b]	2.69 [b]	100.00	0.29

[a] Relative area = component area×100/sum area of same orbital
[b] Data available from low resolution wide scan

The low resolution wide scan (Chapter 5 Appendix, Figure 10.3.31) revealed the presence of S2p at a BE of 168 eV, F1s at a BE of 688.5 eV and also another N1s environment at a BE of 399.82 eV, values that correspond with the BE found for component bis(trifluoromethanesulfonyl) imide (bistriflimide anion – Tf_2N^-) as described in the literature (Chapter 5 Appendix, Figure 10.3.32),[265] and coming from contamination of the XP chamber due to analysis of bistriflimide containing ionic liquids.

The zeta potential of these charged nanoparticles was measured and resulted a value of (ζ) = +41.47 mV and (ζ) = +33.22 mV for the less substituted one, which supports that cationization took place indeed. Both cationized CNC resulted in the formation of stable dispersions.

5.8 Adsorption of dye on the cationized cellulose nanoparticles

Up to now, five charged materials were synthesised, three pyridinium salts and two imidazolium salts. As charged nanoparticles, these materials have the capacity to exchange the counter anion (Br^-) with other anions in the environment. Therefore, as a second method to determine the substitution of cellulose, these materials were tested for ion exchange with the anion of Orange II dye sodium salt **(**4-(2-Hydroxy-1-naphthylazo) benzenesulfonic acid sodium salt (Figure 5.8.1).

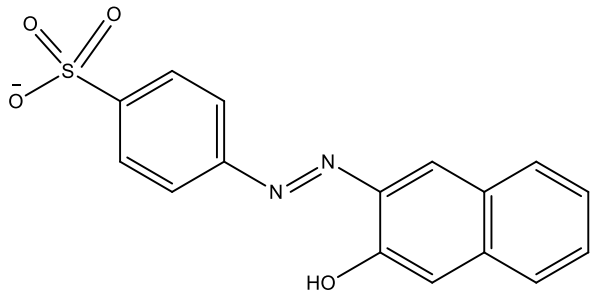


Figure 5.8.1 Structure of Orange II dye anion

Orange II dye is an azo mono-anionic dye, and one of the most common types of dye in the textile, pulp and paper industries. It has already been used for spectrophotometric determination of quaternary ammonium surfactants with which they reacts in a 1:1 stoichiometry.[266,267] The selection of the adsorption dye is essentially related to the size of the molecule which in comparison with the usual halides anions and sulphates should be large enough in order to be adsorbed only onto the surface of the cellulose nanoparticles without penetrating the crystal.[268]

Since the evaluation of the adsorption capacity of the five ion exchange products involves the use of Orange II as a reference in UV-Vis spectroscopy, determination of the absorption coefficient (ε) of the dye was initially performed. Figure 10.3.33 in the Appendix for Chapter 5 presents the UV-Vis spectra of Orange II dye solutions of increased concentrations in the range 1.5 – 50 μM in ultrapure water. These spectra were measured on a PerkinElmer

Lambda 25 UV-Vis Spectrophotometer operated by Lambda 25 software and using a quartz cell with a path length of 1 cm in the 190 – 600 nm range with 1 nm resolution.

The absorbance intensity of each solution at the maximum of 484 nm was plotted against the concentration of the solution (Figure 10.3.34, Chapter 5 Appendix) in order to determine the molar absorption coefficient (ε) by using the Beer-Lambert law ($A = \varepsilon cl$). The obtained value is ε = 23 349 L mol^{-1} cm^{-1} (R^2 = 0.9995), slightly higher than the literature reported value of 22000 L $mol^{-1}cm^{-1}$.[269]

Following the determination of the absorption coefficient, the evaluation of the adsorption capability (and thus the surface charge density) of each of the five modified CNCs was carried out by suspending each of the samples in 50 μM of Orange II sodium solution of a known concentration, previously calculated to match the absorption range. Each sample was sonicated before filtration through a Ministar-Plus 0.2 um cellulose acetate/glass microfibre syringe filter.

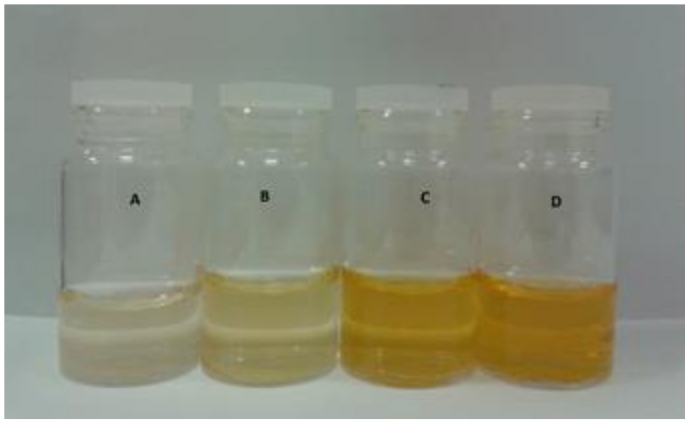


Figure 5.8.2 Adsorption of Orange II dye of: A - 1[Br][PyAc]-*g*-CNC, B - 1[Br][MeImAc]-*g*-CNC, C - CNC and D - Orange II dye D. Orange colour of C and D indicates no adsorption.

After filtration, the nanoparticles and absorbed dye are removed and the translucent permeate (Figure 5.8.2) was used to determine the UV-Vis spectrum. The amount of ion-exchanged dye can then be calculated from the difference of concentration of Orange II dye solutions (Figure 5.8.3). The detailed measurements and calculations are presented in Table 5.8.1.

As a comparison, the highest amount of anionic dye exchanged by a pyridinium modified CNC is achieved by 1[Br][PyAc]-*g*-CNC giving 0.615 mmol/g and a surface charge of 1.103 *e* nm^{-2} and for the corresponding modification with methyl imidazolium it is 2[Br][MeImAc]-*g*-CNC giving 0.883 mmol/g and a surface charge of 1.638 *e* nm^{-2} respectively.

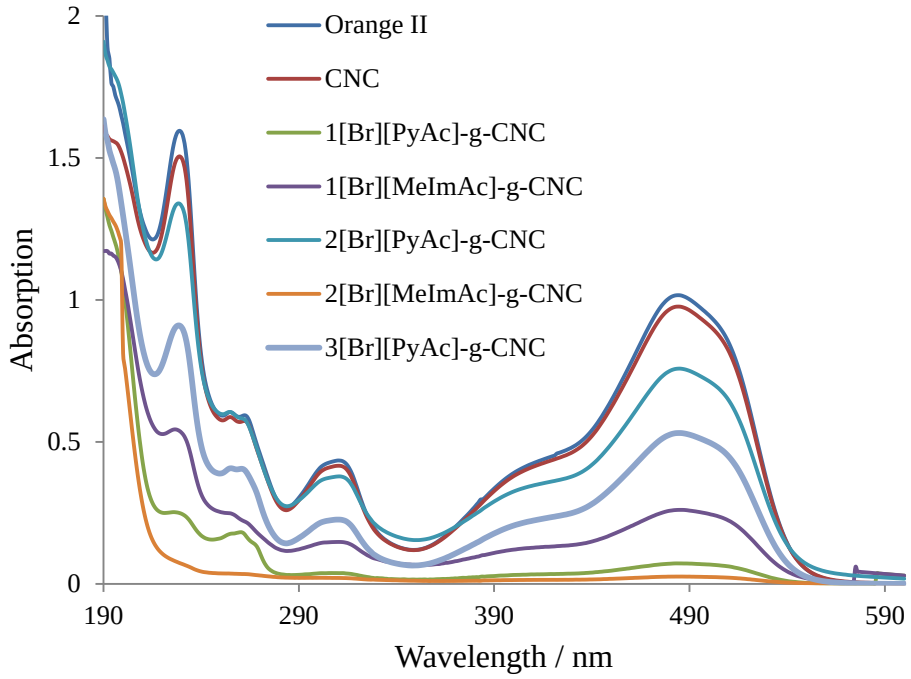


Figure 5.8.3 UV-Vis spectrum of Orange II dye, CNC and modified CNC solutions after filtration

These results situate themselves in between the current published data when considering the amount of dye absorbed per CNC surface (Figure 5.8.4) which can indicate that ion exchange can be used to determine DS. So, the values are around the amount of dye reported by Eyley *et al.* of 0.53 mmol/g for $DS_{surf}(N)$ of 0.36 and the values determined by Jasmani *et al*. 0.82 mmol/g for a $DS_{surf}(N)$ = 1.1 and 0.49 for a $DS_{surf}(N)$ = 0.38 when α-methylbenzyl pyridinium-*g*-CNC was synthesised. [94,96,193]

Table 5.8.1 Detailed results of the adsorption experiments with orange II dye

Product	Mass /mg	V(dye) /ml	Δ A [a]	ν [b] /mmolg^{-1}	σ [c] / *e* nm^{-2}
Filter	-	20	0	-	-
CNC	2.09	20	0.04	0.016	0.028
1BrAcCNC	1.36	20	0.17	0.107	0.182
1[Br][PyAc]-*g*-CNC	1.32	20	0.95	0.615	1.103
1[Br][MeImAc]-*g*-CNC	1.03	20	0.76	0.631	1.203
2[Br][PyAc]-*g*-CNC	1.84	20	0.26	0.121	0.219
2[Br][MeImAc]-*g*-CNC	0.96	20	1.00	0.883	1.638
3[Br][PyAc]-*g*-CNC	2.02	20	0.49	0.208	0.377

[a] Difference between the adsorption intensity of Orange II dye filtrated solution and filtrated solutions of cellulose or modified cellulose nanocrystals

[b] Number of moles of dye adsorbed per gram

[c] Surface charge density

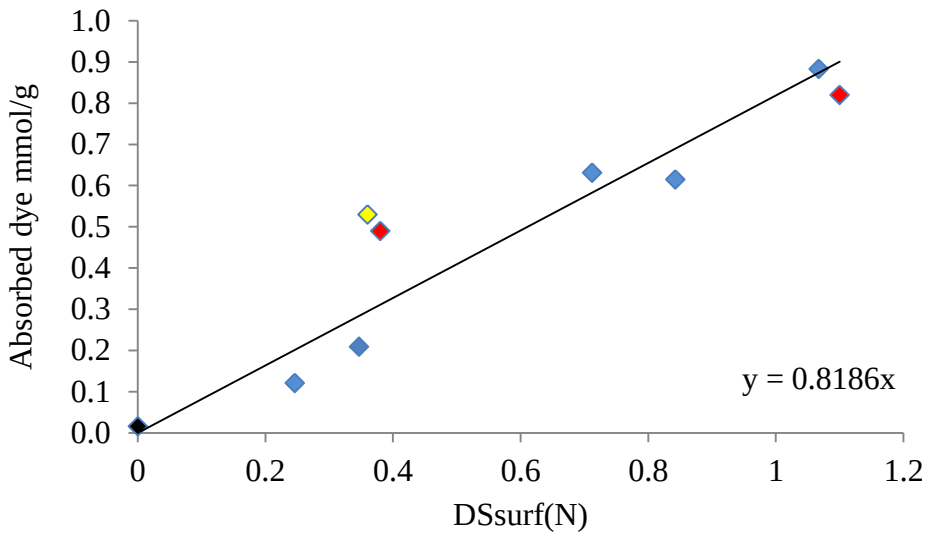


Figure 5.8.4 Degree of substitution based on nitrogen versus adsorption of dye for the 5 cationized nanoparticles (blue square), CNC (black square) and values obtained by Jasmani *et al.* (red squares)[96] and Eyley *et al.* (yellow square)[94], for comparison.

5.9 Conclusions

Reactions of cellulose with bromoacetyl bromide, bromoacetic acid, pyridine and 1-methyl imidazole carried out in Chapter 5 with their reaction conditions and degrees of modification are presented in Table 5.9.1.

Table 5.9.1 Summary of Chapter 5

	Modified Surface	Reagent	Reaction Product	Reaction Conditions	$DS_{surf}(N)$
1	CNC	Bromoacetyl bromide	1BrAcCNC	Et_3N/DMF /40°C/24h	1.36
2	1BrAcCNC	Py	1[Br][PyAc]-g-CNC	80°C/24h	0.84
3	1BrAcCNC	MeIm	2[Br][MeImAc]-g-CNC	80°C/24h	0.71
4	CNC	Bromoacetyl bromide	2BrAcCNC	Et_3N/THF/ 40°C/24h	1.02
5	CNC	Bromoacetyl bromide	3BrAcCNC	Et_3N/40°C /24h	0.03
6	CNC	Py	2[Br][PyAc]-g-CNC	80°C/24h	0.25
7	CNC	MeIm	2[Br][MeImAc]-g-CNC	80°C/24h	1.06
8	CNC	Bromoacetic acid	3[Br][PyAc]-g-CNC	80°C/16h	0.35

Thus, three methodologies were used to synthesise five cationic modified CNC. The first methodology involved a two-step synthesis in which bromoacetate cellulose was initially synthesised after which pyridine and 1-methyl imidazole were used as cationization agents in the second step. This pathway indicated a better pyridine nucleophilic substitution of bromoacetate cellulose ($DS_{surf}(N)$ = 0.84) as compared with nucleophilic substitution of bromoacetate cellulose with 1-methyl imidazole ($DS_{surf}(N)$ = 0.71). This observation could be explained by the different solubility of the bromoacetate cellulose in pyridine and 1-methyl imidazole.

The second methodology involved a single step in which CNC are reacted in one pot with bromoacetyl bromide in the desired cationization reagent. This method favoured the formation of 1-methylimidazolium acetate cellulose bromide ($DS_{surf}(N)$ = 1.06) as the 1-methylimidazole is more nucleophilic then

pyridine ($DS_{surf}(N) = 0.25$) (1-methylimidazole with its two nitrogen atoms is more basic then pyridine with one nitrogen atom[20]).

Additionally, the influence of the solvent on the reaction efficiency was verified. Therefore, when THF was used instead of DMF to synthesise bromoacetate cellulose, a slightly lower degree of substitution ($DS_{surf}(N) = 1.02$) was obtained for THF when compared with the synthesis in DMF ($DS_{surf}(N) = 1.36$), although less secondary by-products were identified by XPS analysis in THF. Also, it was proven that bromoacetate cellulose is also synthesised when the reaction is carried out in triethylamine only to a very low degree of substitution ($DS_{surf}(N) = 0.03$) and the N1s spectrum confirms the formation of triethylammonium hydrogen bromide, a component that was also identified in the other bromoacetate cellulose syntheses.

A third method using the one-pot approach with TsCl/Py-bromoacetic acid, instead of bromoacetyl chloride/Et_3N was applied only to the synthesis of pyridinium based cationic species and this also gave a satisfactory $DS_{surf}(N) = 0.35$. This methodology also reduces the required high molar excess and thus excludes secondary products that may appear and are difficult to be removed from the reaction products.

In addition, all the modified CNC were tested for their surface charge by measuring the zeta potential which proved to have highly positive values required for stable colloidal particles (> +30 mV). At the same time, the ion exchange capability of the cationic modified cellulose nanoparticles was tested through ion exchange with Orange II dye for all the cationized nanoparticles indicating good adsorption properties comparable with previously reported literature values.

6 Thiol-Ene click chemistry based on cellulose nanocrystals

This chapter extends the rapidly growing field of "click chemistry", which has been only a few times applied to the surface modification of cellulose nanocrystals. The advantages of this approach is that (a) it enlarges the range of functional groups that can be introduced onto the surface of cellulose, (b) the modifications can normally be achieved for very short reaction times, (c) without formation of by-products and (d) achieving very high yields. At the end of the chapter, novel modified nanocellulose based on click chemistry is presented, with possible applications as switchable nanoparticles in adjustable Pickering emulsions.

6.1 Click chemistry applied to cellulose nanocrystals

As it was presented in the Introduction Chapter, section 1.7.8, there are only a few studies on the surface modification of cellulose using "click chemistry" approaches. In short, the first attempt to apply "click" chemistry by using the copper-catalysed Huisgen reaction on polysaccharide cellulose was performed by Liebert *et al.* in 2006, who functionalized a cellulose surface through the introduction of functional groups using a triazole-spacer in a chemoselective and highly modular route.[192] Further applications of azide-alkyne click chemistry were performed in our group in order to synthesise cationized CNC as a support medium for ion exchange systems, catalysts, and for electron-conducting surface modified CNC.[94] Later on in 2010, Zhao *et al*. reported the first example of environmental friendly benign heterogeneous modification of cellulose in its native solid state by Thiol-Ene click chemistry activated by an organocatalyst being described as highly modular and completely metal-free.[191]

In 2010, similar research from our group was published on modified cellulose nanowhiskers using a Michael type addition resulting in attachment of analyte-sensitive fluorophores with applications as pH-sensing materials.[197]

In this work however, I investigated the efficiency and optimization of the modification of cellulose with Thiol-Ene click chemistry while also expanding the range of thiols used in order to increase the applicability of the modification strategy. Therefore, a new approach to efficiently functionalize the solid cellulose substrate is presented with nanowhiskers first organocatalytically modified with acids containing an ene functionality, as presented in Chapter 3, followed by the introduction of the thiol functional group through Thiol-Ene click chemistry. With this aim, thiol-Michael addition reactions were initiated with either an amine (hexylamine) or with a strong base (NaOH) which were added separately as a catalyst, or the reaction was self-catalysed when using an amino-terminated thiol as in the case for cysteamine. The addition of thiols to an electron-deficient C=C bond, also called hydrothiolation of an activated C=C bond or Michael addition, is from a traditional standpoint readily accomplished under base catalysis and the accepted mechanism is given in Figure 6.1.1.

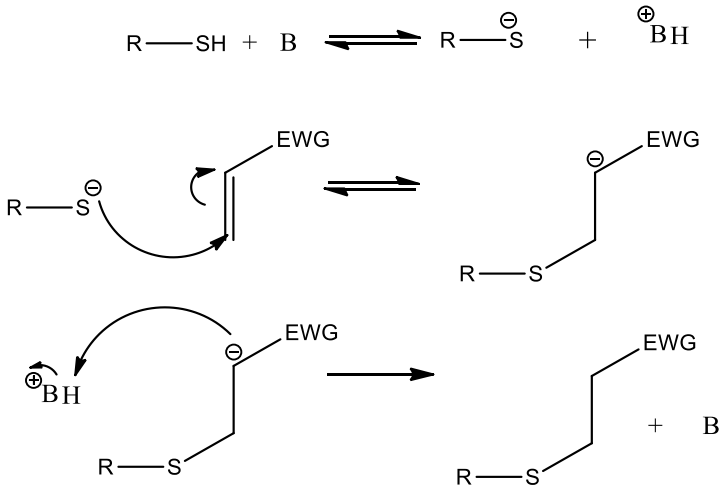


Figure 6.1.1 The base (B) catalysed hydrothiolation of an activated C=C bond close to an electron withdrawing group (EWG)[270]

The base, B, deprotonates the thiol generating a thiolate anion, RS^-, and its conjugate acid, BH^+. The electrophilic β carbon of the C=C bond is attacked by

the strong nucleophilic thiolate anion, generating the carbon centred intermediate, which itself is a strong base and deprotonates the conjugate acid, generating the thiol-Michael addition product and simultaneously regenerating the base catalyst.[270] A newer powerful catalytic approach is given by the use of nucleophilic catalyst such as a primary or secondary amine as well as tertiary phosphines. In the proposed reaction mechanism (Figure 6.1.2), the nucleophile undergoes addition to the electron deficient C=C bond resulting in a strong intermediate carbanion which then deprotonates the thiol. The created thiolate anion enters in an anionic chain process in which the thiolate anion undergoes direct thiol-Michael addition by regenerating the strong carbanion that continues to deprotonate more thiols with the simultaneous generation of the thiol-Michael product.[270]

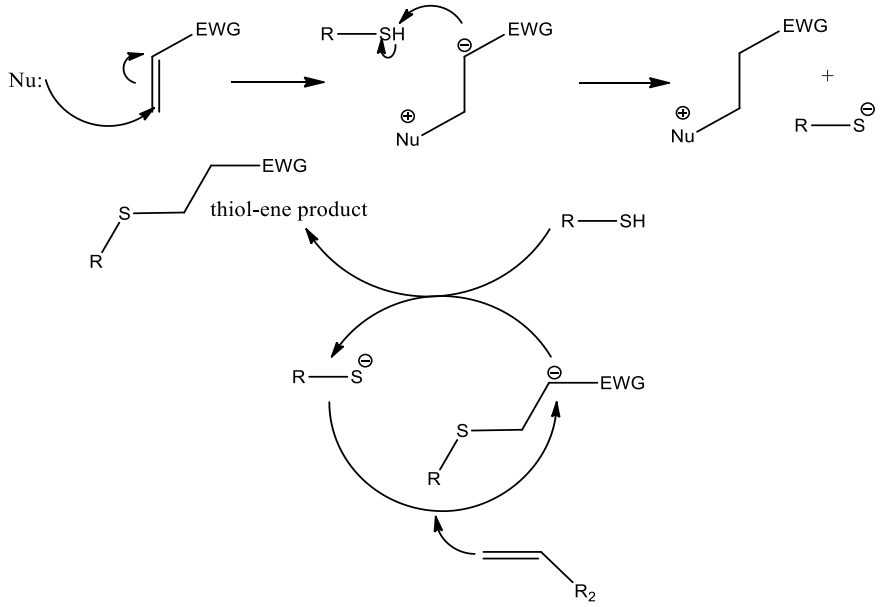


Figure 6.1.2 Proposed mechanism for the nucleophile (Nu:) -mediated hydrothiolation of an activated C=C bond close to an electron withdrawing group (EWG)[270]

Thus, ene-functionalized cellulose nanocrystal derivatives synthesised in Chapter 3, cellulose acrylate and cellulose methacrylate which contain non-sterically hindered terminal enes and offer spatial and temporal control of the structure, are further functionalized by introducing a range of selected alkyl thiols (Figure 6.1.3). In brief, Thiol-Ene click chemistry was carried out for a

series of reactions (Figures 6.1.4 and 6.1.5) in which CNC were mixed with the respective thiols and suspended in solvent under air, for a specified amount of time and at room temperature, followed by purification as it is described for each of them in the synthesis section.

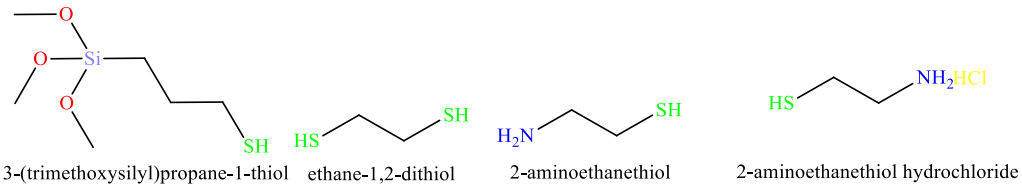


Figure 6.1.3 Chemical structures of thiols employed in Thiol-Ene reactions

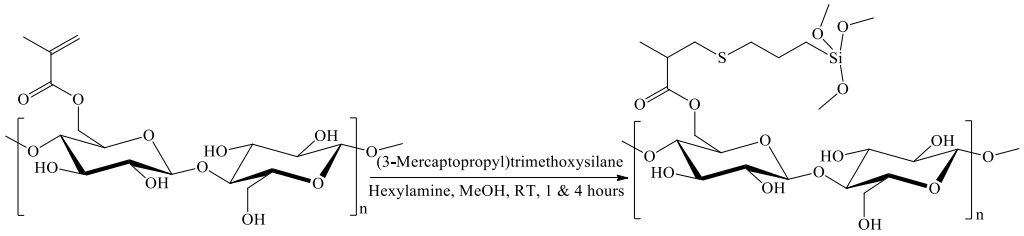


Figure 6.1.4 CNC thiol derivative based on cellulose methacrylate

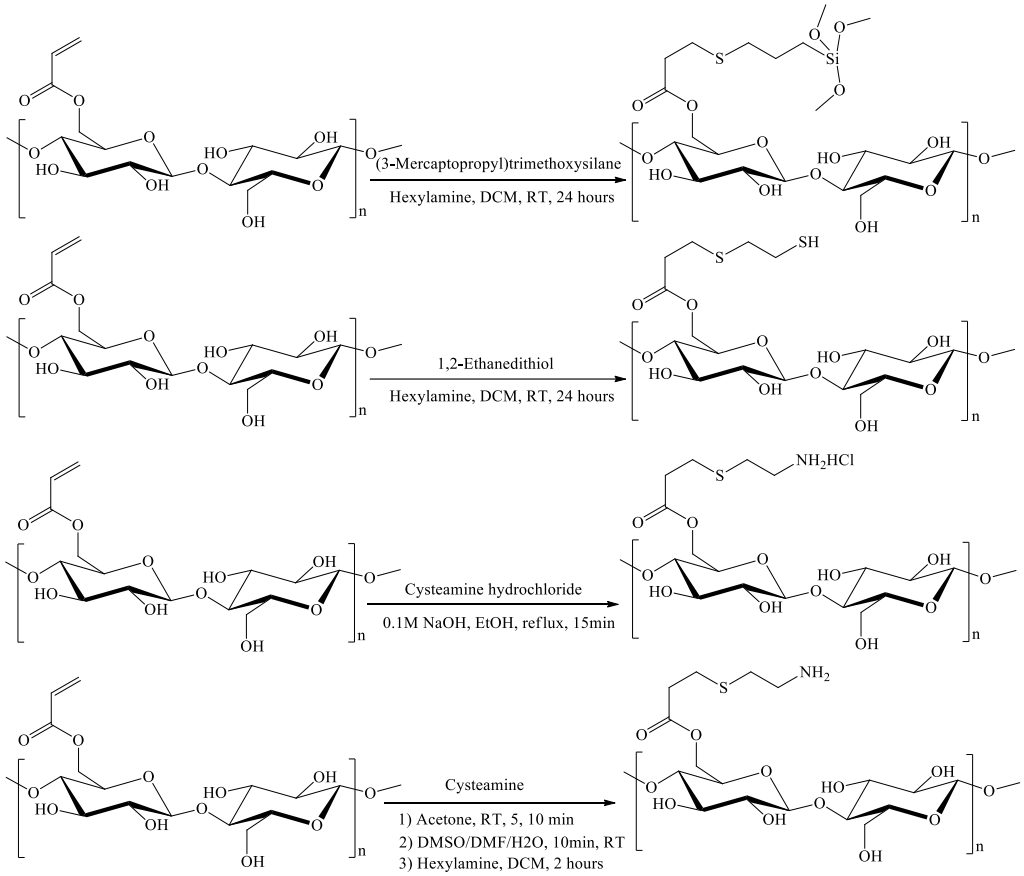


Figure 6.1.5 CNC thiol derivatives based on cellulose acrylate

6.2 Thiol-Ene click modified cellulose nanocrystals

The first attempted Thiol-Ene click reaction involves the reaction between cellulose methacrylate (1-MACNC) with a DS_{surf}(C) = 0.52 and 3-mercaptopropyl-trimethoxysilane in MeOH for 1-hour reaction time. Initial characterization consisted in the determination of the infrared spectrum which actually did not present any significant differences from the infrared spectrum of cellulose methacrylate (1-MACNC). At the same time the crystallinity determined from the XRD spectrum (Chapter 6 Appendix, Figure 10.4.1) was χ_C^R = 0.826, representing a crystallinity loss of 5.7 % compared to the original unmodified CNC (χ_C^R = 0.883) and a crystallinity increase of 6.3 % when compared with the cellulose methacrylate, the starting material in this second reaction over CNC, values that indicate an overall cellulose crystallinity increase, thus less amount of amorphous material on the surface. Moreover, EA did not show any sulfur present and an expected modification based on sulfur (the element that is different from the initial composition) could not be calculated. Still, the XPS wide scan spectrum (Chapter 6 Appendix, Figure 10.4.2) indicate the presence of carbon and oxygen as expected, as well as small peaks of sulfur and silicon. The C1s high resolution spectrum (Chapter 6 Appendix, Figure 10.4.3) shows the existence of the methacrylate ester through the presence of a carbon O–C=O peak at a BE of 289.44 eV and also of an oxygen O–C=O peak in the O1s high resolution spectrum (Chapter 6 Appendix, Figure 10.4.4) at a BE of 531.88 eV. But, at the same time, the fraction of O–C=O in the C1s high resolution spectrum has decreased in comparison with the initial cellulose methacrylate, which could mean that some methacrylate functionality has been removed from the surface of CNC. However, from the sulfur and silicon high resolution scans (Figure 6.2.1), it was observed that the S2p 3/2 peak is present at a BE of 163.5 eV which corresponds to the C–S–C bond meaning that the Thiol-Ene click reaction did in fact take place.[271,272] Moreover, the Si2p 3/2 component peak is found at a BE of 102.3 eV, an energy at which poly(dimethyl silicon) usually shows up in XPS (Table 6.2.1).[273]

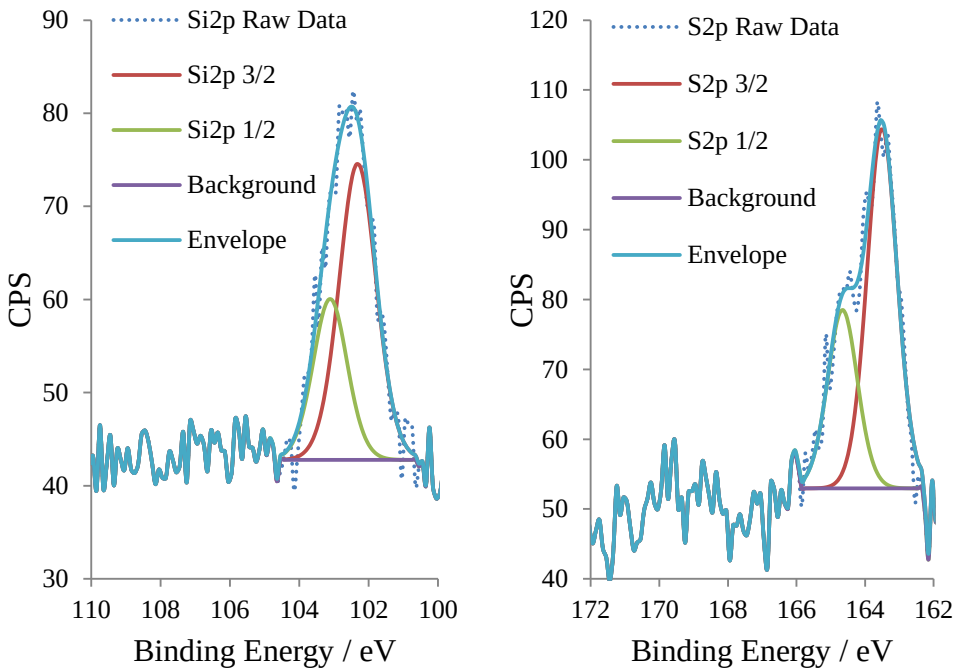


Figure 6.2.1 Si2p and S2p high resolution spectra of 1 hour click reaction

Table 6.2.1 2-methyl-3-((3-trimethoxysilyl)propyl)thio)propanoare XPS data

Orbital	Component	BE / eV	FWHM / eV	Rel.A/%[a]	at%
C1s	C–C/C–H	285.03	1.09	13.88	8.39
	C–O	286.50	1.09	72.14	43.61
	O–C–O	288.18	1.09	12.87	7.78
	O–C=O	289.44	1.09	1.11	0.67
				100.00	60.45
O1s	O–C=O	531.77	1.01	7.15	2.76
	C–O–H	532.57	1.01	55.71	21.48
	O–C–O	533.17	1.01	37.14	14.33
				100.00	38.58
Si2p	3/2	102.32	1.259	66.68	0.37
	1/2	103.11	1.158	33.32	0.19
				100.00	0.56
S2p	3/2	163.50	1.033	66.91	0.27
	1/2	164.66	1.033	33.09	0.13
				100.00	0.40

[a] Relative area = component area×100/sum area of same orbital

As a consequence, although a degree of substitution based on EA could not be calculated as a result of very low amounts of sulfur present, i.e. under the detection limit, the XPS proved the existence of S2p and Si2p at the binding

energies that correspond to the formation of cellulose 2-methyl-3-((3-trimethoxysilyl) propyl)thio)propanoate after 1-hour reaction.

An increase in the reaction time from 1-hour to 4-hours gave similar results as for the 1-hour reaction. So, no significant changes were seen in the infrared spectrum and the sulfur content was below the detection limit for EA determination. The XRD spectrum (Chapter 6 Appendix, Figure 10.4.5) indicate a crystallinity of χ_C^R = 0.785 which represents a crystallinity loss of 9.8 % when compared with the unmodified cellulose (χ_C^R = 0.883) and an increase of crystallinity of 2.2 % when related to the cellulose methacrylate, thus giving similar results with the reaction carried out for 1 hour. However, the only possible way to determine any characteristics of Thiol-Ene reaction was through XPS analysis. The wide scan resolution spectrum (Chapter 6 Appendix, Figure 10.4.6) indicated the presence of carbon, oxygen, sulfur and silicon as expected for a successful Thiol-Ene click reaction. Figure 6.2.2 presents the high resolution scan of Si2p and S2p where, similar to the previous case, S2p 3/2 was found at a BE corresponding to C-S-C bond and Si was found in the same chemical environment as in the thiol graft.[271-273] Table 6.2.2 shows the at% values for sulfur and silicon that did not differ very much and therefore no significant increase in functionalization when increasing the reaction time from 1-hour to 4-hours was noted. The presence of the methacrylate ester was confirmed in the C1s (Chapter 6 Appendix, Figure 10.4.7) and O1s (Chapter 6 Appendix, Figure 10.4.8) high resolution spectra. In short, the Thiol-Ene click reaction was thus proven to work for very short reaction times (1-hour to 4-hours) although the reaction could not be quantified through EA and the degree of substitution was minimal.

In order to improve the efficiency of the reaction, cellulose acrylate (1-ACNC) was reacted with the same thiol – 3-mercaptopropyltrimethoxysilane, but in DCM and for 24 hours. The crystallinity of the reaction product checked by X-ray diffraction (Chapter 6 Appendix, Figure 10.4.9) confirmed the cellulose I_β allomorph structure, with a crystallinity loss of 4.45 % (χ_C^R = 0.838) when related to the unmodified CNC (χ_C^R = 0.883) and a crystallinity increase of 6.3 % when compared with the cellulose acrylate crystallinity (χ_C^R = 0.775).

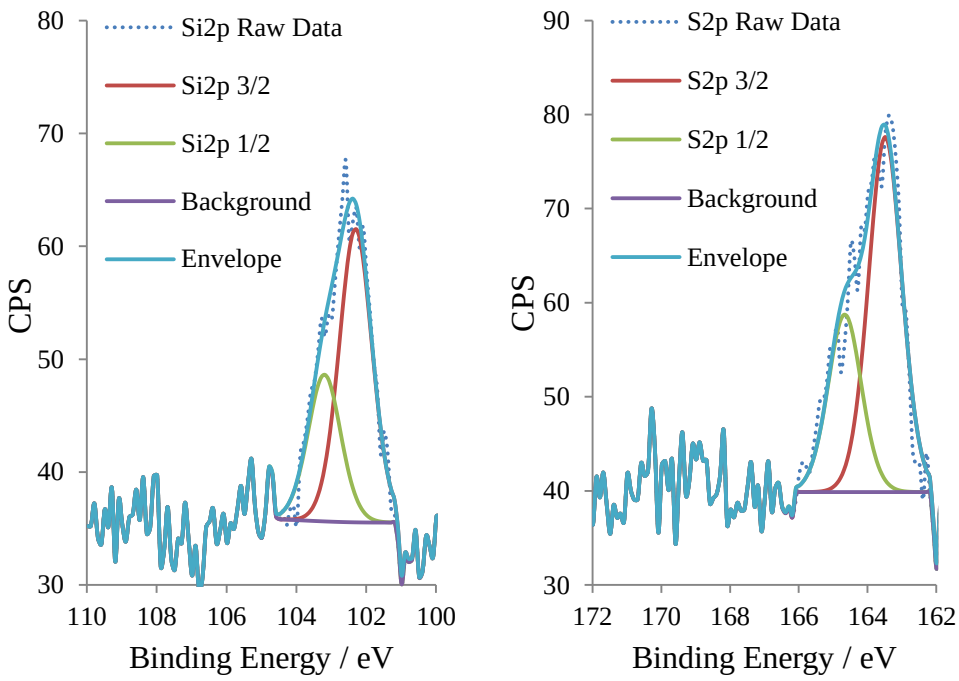


Figure 6.2.2 Si2p and S2p high resolution spectra of 4 hour click reaction

Table 6.2.2 2-methyl-3-((3-trimethoxysilyl)propyl)thio)propanoate XPS data

Orbital	Component	BE / eV	FWHM / eV	Rel.A/%[a]	at%
C1s	C–O	286.50	1.10	70.11	42.28
	C–C/C–H	285.02	1.10	15.29	9.22
	O–C–O	288.15	1.10	12.98	7.83
	O–C=O	289.43	1.10	1.62	0.98
				100.00	60.31
O1s	O–C=O	531.90	0.95	10.21	3.95
	C–O–H	532.66	0.95	59.27	23.19
	O–C–O	533.26	0.95	29.93	11.59
				100.00	38.73
Si2p	3/2	102.3	1.11	66.68	0.31
	1/2	103.2	1.11	33.32	0.16
				100.00	0.47
S2p	3/2	163.49	1.14	66.70	0.33
	1/2	164.66	1.14	33.30	0.16
				100.00	0.49

[a] Relative area = component area×100/sum area of same orbital

The crystallinity loss value is slightly lower than the expected calculated modification based on sulfur wt% in EA, which is 8.67 %, but within an acceptable difference and so it is concluded that the determined crystallinity is

due to the extent of modification. EA (Table 6.2.3) of the product revealed a visible functionalization with a calculated $DS_{surf}(S)$ = 0.19, which was also consistent with the increase in carbon content and decrease in hydrogen content.

Table 6.2.3 Elemental analysis results for CNC and cellulose 3-((3-trimethoxysilyl)propyl)thio) propanoate (T-24-CNC-DCM)

Sample	C (%)	H (%)	N (%)	S (%)	$DS_{surf}(S)$
CNC	41.96	6.00	0.00	-	-
T-24-CNC-DCM	42.42	5.87	0.43	1.04	0.19

Analogous to cellulose methacrylate reaction, the infrared spectrum of this modification did not present any visible changes. The wide scan XPS spectrum (Chapter 6 Appendix, Figure 10.4.10) displayed the presence of carbon, oxygen, sulfur and silicon as well as traces of nitrogen and fluorine. Considering the low resolution data, the N1s and F1s binding energies could indicate bistriflimide contamination during the XPS analysis process,[265] coming from the XPS chamber contamination. Figure 6.2.3 shows the high resolution scans Si2p and S2p, which are present at similar BE as for the methacrylate reaction, and therefore cellulose 3-((3-trimethoxysilyl)propyl)thio)propanoate (T-24-CNC-DCM) was indeed the reaction product. Also, the C1s and O1s high resolution scans (Chapter 6 Appendix, Figure 10.4.11 and 10.4.12) confirmed the existence of the acrylate ester linkage at 289.43 eV in C1s and at 531.79 eV in O1s respectively (Table 6.2.4). It is worth mentioning that the starting point for this Thiol-Ene click chemistry was based on the work of Nielsen *et al.* where methacrylate CNC were reacted with cysteamine in MeOH for 24 hours, resulting in a low DS.[147] Although, the full characterization of that reaction product is not presented here, repetition of that reaction led to a low $DS_{surf}(S)$ = 0.08.

Thus, by comparison with the two click reactions carried out up to now, increasing the reaction time from 1 hour to 24 hours, in the same solvent (MeOH), led to only half of the modification achieved than when DCM was used as a solvent for the same reaction time.

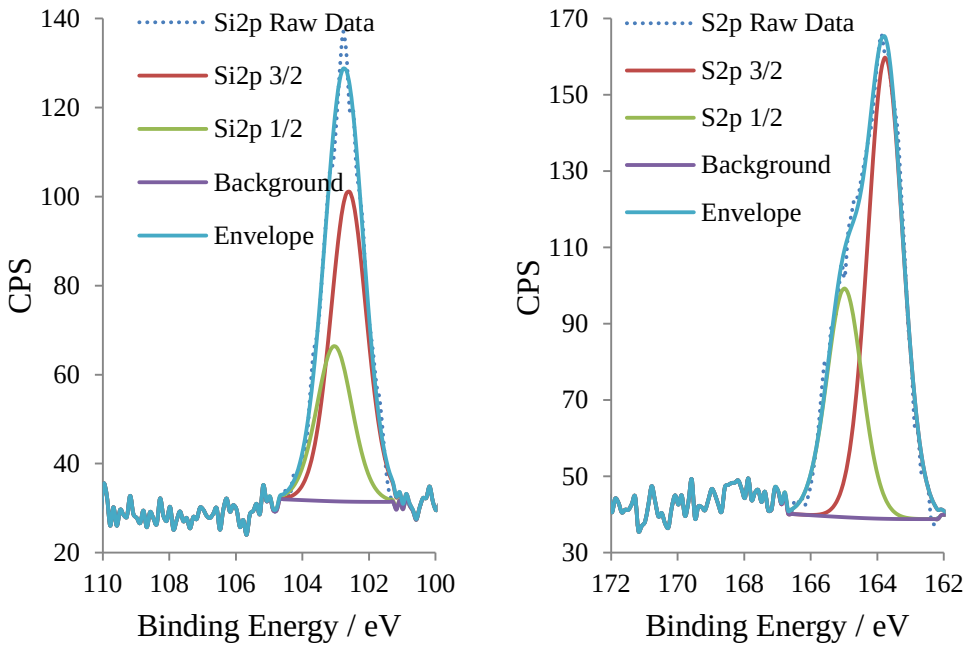


Figure 6.2.3 Si2p and S2p high resolution spectra of 24 hour click reaction

Table 6.2.4 cellulose 3-((3-trimethoxysilyl)propyl)thio) propanoate XPS data

Orbital	Component	BE / eV	FWHM / eV	Rel.A/%[a]	at%
C1s	C–C/C=C	285.03	1.20	29.05	17.76
	C–O	286.50	1.20	58.87	35.98
	O–C–O	288.25	1.20	10.06	6.15
	O–C=O	289.43	1.20	2.02	1.23
				100.00	61.12
O1s	O–C=O	531.79	1.11	10.21	3.38
	C–O–H	532.62	1.11	59.86	19.84
	O–C–O	533.22	1.11	29.93	9.92
				100.00	33.14
Si2p	3/2	102.61	1.26	66.67	1.42
	1/2	103.04	1.26	33.33	0.71
				100.00	2.13
S2p	3/2	163.76	1.25	66.71	1.26
	1/2	164.98	1.26	33.29	0.63
				100.00	1.89
F1s	-[b]	689.5	2.36	100.00	0.74
N1s	-[b]	401.4	3.75	100.00	0.97

[a] Relative area = component area×100/sum area of same orbital

[b] Data available from low resolution wide scan

In order to develop more insight into the reaction, a di-thiol was then used. Shortly, cellulose acrylate (1-ACNC), 1,2-ethanedithiol and hexylamine were suspended in DCM at room temperature and this time for an even longer period of time (48 hours).

Crystallinity of the reaction product was verified (Chapter 6 Appendix, Figure 10.4.13) leading to a determined crystallinity increase of 2 % ($\boldsymbol{\chi_C^R}$ = 0.795) from the crystallinity of the cellulose acrylate used as starting material ($\boldsymbol{\chi_C^R}$ = 0.775) and a loss of crystallinity of 8.8 % from the initial unmodified cellulose nanocrystal ($\boldsymbol{\chi_C^R}$ = 0.883). The expected calculated modification based on sulfur EA is 6.67 %. Thus, the loss of crystallinity determined by these two steps of modification perfectly matches the crystallinity loss determined by powder X-ray diffraction when compared with the unmodified cellulose crystallinity.

EA (Table 6.2.5) clearly indicated an increase in carbon content and a more than double amount of sulphur when compared to the silane-thiol modification based on the two sulfur atoms present in the current graft. The actual degree of substitution corresponds to a $DS_{surf}(S)$ = 0.24, slightly higher than T-24-CNC-DCM despite a doubling in the reaction time. Therefore, it can be considered that 1,2–dithiol is less reactive than 3-mercaptopropyl trimethoxysilane under the same conditions. The infrared spectrum again did not present any characteristic bands such as those specific for C–S bond which usually appears in the fingertip region as maybe overlapped by the characteristic CNC absorption bands and thus it is not shown here. Only for a very high degree of modification, the signal would appear in the 710 – 570 cm^{-1} spectrum region.

Table 6.2.5 Elemental analysis results for CNC and cellulose 3-((2-mercaptoethyl)thio)propanoate (DT-CNC-DCM)

Sample	C (%)	H (%)	N (%)	S (%)	$DS_{surf}(S)$
CNC	41.96	6.00	0.00	-	-
DT-CNC-DCM	43.88	6.01	0.13	2.59	0.24

The XPS wide scan (Figure 6.2.4) displayed the presence of only O1s, C1s and S2p as expected for the di-thiol modification.

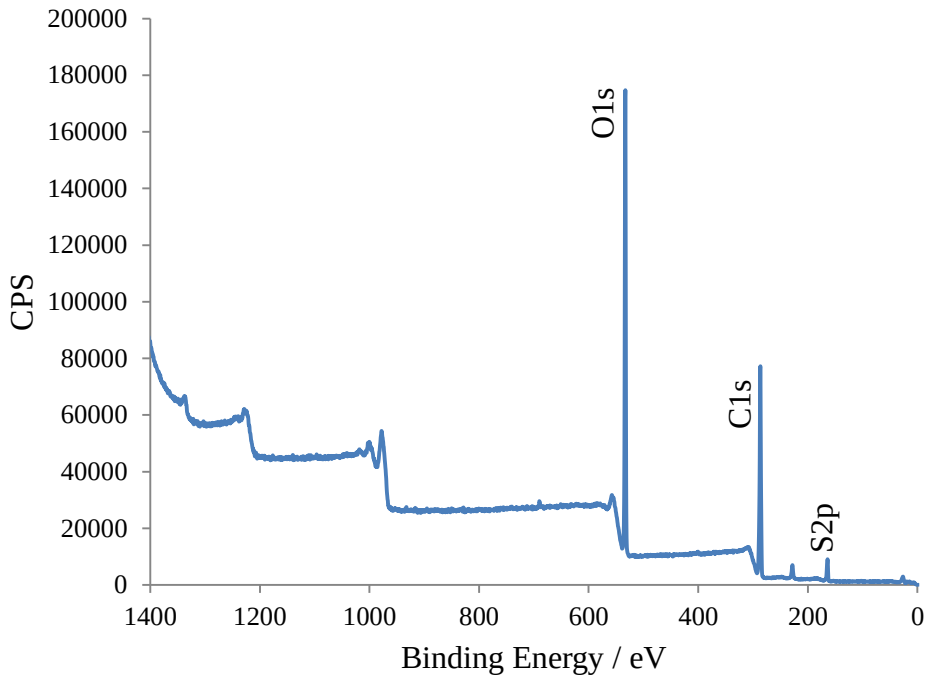


Figure 6.2.4 Wide scan XPS spectrum of cellulose 3-((2-mercaptoethyl)thio)propanoate

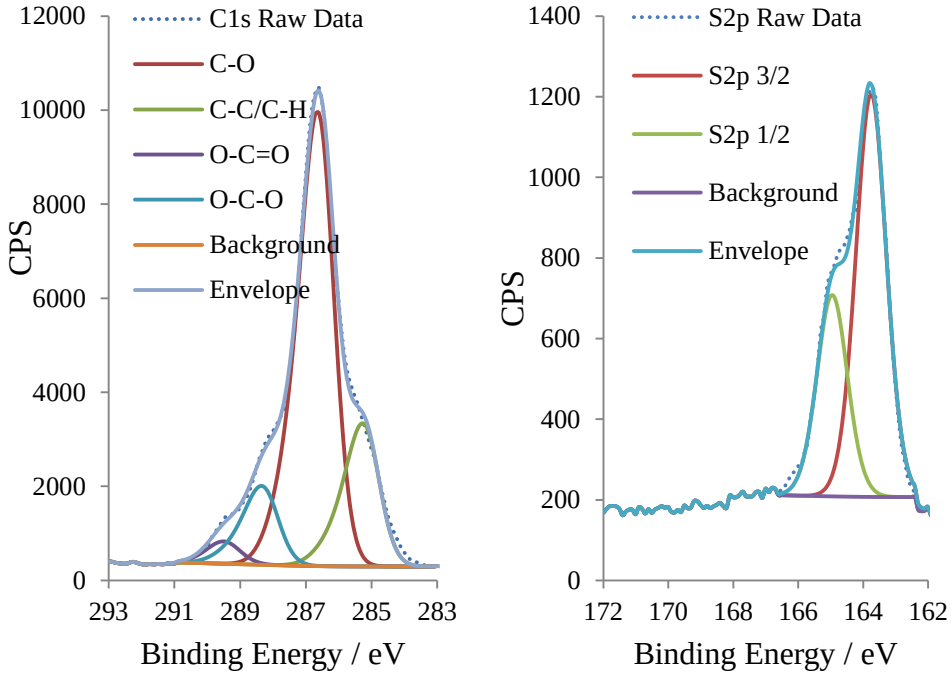


Figure 6.2.5 C1s (left) and S2p (right) high resolution spectra of cellulose 3-((2-mercaptoethyl)thio)propanoate (DT-CNC-DCM)

Confirmation of the acrylate ester linkage presence is indicated by the C1s (Figure 6.2.5 - left) and also O1s high resolution spectra (Chapter 6 Appendix, Figure 10.4.14) where the O–C=O bond is found at a BE of 289.37 eV in the C1s and 532.01 eV in the O1s spectrum (Table 6.2.6).

The presence of the thiolate bond is indicated by the position of the S2p 3/2 component at 163.76 eV (Figure 6.2.5 - right), which is maintained at the same position as for the previous modification with the silane-thiol and therefore confirming the formation of the desired reaction product identified as cellulose 3-((2-mercaptoethyl)thio)propanoate (DT-CNC-DCM).[271,272]

Table 6.2.6 Detailed XPS data of cellulose 3-((2-mercaptoethyl)thio) propanoate

Orbital	Component	BE / eV	FWHM / eV	Rel.A/%[a]	at%
C1s	C–C/C=C	285.12	1.17	20.56	12.51
	C–O	286.50	1.17	65.22	39.70
	O–C–O	288.20	1.17	11.30	6.88
	O–C=O	289.37	1.17	2.92	1.78
				100.00	60.87
O1s	O–C=O	532.01	1.09	9.78	3.56
	C–O–H	532.82	1.09	60.16	21.92
	O–C–O	533.42	1.09	30.06	10.95
				100.00	36.44
S2p	3/2	163.76	1.11	66.69	1.79
	1/2	164.95	1.11	33.31	0.90
				100.00	2.69

[a] Relative area = component area×100/sum area of same orbital

Besides nucleophilic catalysis with hexylamine, base catalysis was also attempted in order to diversify and improve the methodology developed here. Therefore, cellulose acrylate nanocrystals (1-ACNC) and cysteamine hydrochloride were suspended in EtOH and stirred to reflux before addition of a 0.1 M NaOH solution. The reaction was continued for another 10 minutes and 15 minutes respectively, followed straight away by filtration and thorough washing with EtOH. This modification was synthesised based on the method described by Kaasjager *et al.* for the preparation of 1-(2'-pyridyl)-3-thia-5-aminopentane, a methodology that was also adopted by Mountford *et al*. for the

same purpose.[274,275] The obtained nanoparticles were dryed *under vacuo* and dyalized against dionized water for 5 days.

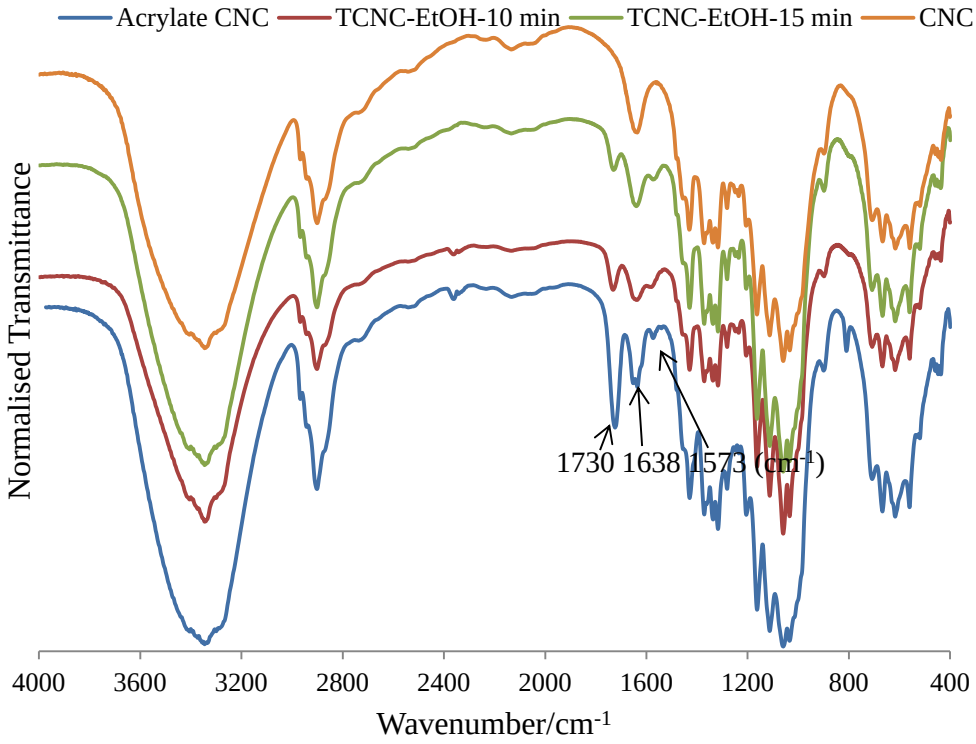


Figure 6.2.6 FT-IR spectrum of cellulose acrylate, cellulose 3-((2-aminoethyl)thio) propanoate hydrochloride for 10 and 15 minutes and CNC

The infrared spectra of the two reaction products together with the cellulose acrylate-starting material and CNC are presented in Figure 6.2.6. The evolution in time of the reaction indicates the decrease of the ester link present at around 1730 cm^{-1} and also the same trend for the C=C stretching band present at 1638 cm^{-1}. The reaction performed for 15 minutes with a molar excess 10 times higher than the one used for the 10 minutes reaction showed even higher reduction of the carbonyl peak which could indicate a possible removal of ester functionality from the surface.

The X-ray diffraction patterns of the two modifications (Chapter 6 Appendix, Figure 10.4.15) were consistent with the cellulose I_β allomorph. The crystallinity reductions in the modified products were calculated to be 7.3 % and 3.2 % for 10 and 15 minutes reaction time, respectively, when compared with the unmodified cellulose (χ_C^R = 0.883). If related to the cellulose acrylate,

there are slight increases of crystallinity, i.e. 3.5 % for 10 min reaction and 7.6 % for the 15 min reaction time, indicating an even lower amount of amorphous material present on the surface of cellulose and thus a higher crystallinity of the overall product. EA (Table 6.2.7) of the two reaction products revealed little modification but consistent for sulfur and nitrogen. As can be seen, there was a drop by half of the extent of modification for the second product although the reaction time was 50% longer and the molar excess was 10 times higher in the less modified product. Using sulfur to determine the extents of modification, one finds 5.44 % and 2.77 % respectively, values that are consistent with the loss of crystallinity determined from XRD.

Table 6.2.7 Elemental analysis results for CNC and 10 and 15 min TCNC-EtOH

Sample	C (%)	H (%)	N (%)	S (%)	$DS_{surf}(S)$
CNC	41.96	6.00	0.00	-	-
TCNC-EtOH-10 min	42.87	5.95	0.42	0.94	0.15
TCNC-EtOH-15 min	42.41	5.90	0.29	0.48	0.07

The XPS wide scans of the products (Chapter 6 Appendix, Figure 10.4.16) indicate the presence of the expected elements: carbon, oxygen, nitrogen and sulfur. The undesired presence of silicon found at a BE of 102 eV could be attributed only to the silicon coming from adhesive tape as there is no incoming source of silicon in these reactions and is in agreement with the BE of polydimethylsiloxane, the silicone oil found in silicon grease.[276]

Figure 6.2.7 presents the S2p high resolution spectra for the two modifications. In agreement with Table 6.2.8, these S2p high resolution spectra indicate an intensity decrease from one spectrum to another for the sulfur environment. S2p 3/2 component is identified at a BE of 163.7 eV consistent with the cellulose 3-((2-mercaptoethyl)thio)propanoate and cellulose 3-((3-trimethoxysilyl)propyl)thio) propanoate modifications and attributed to the C-S functionality of the product.

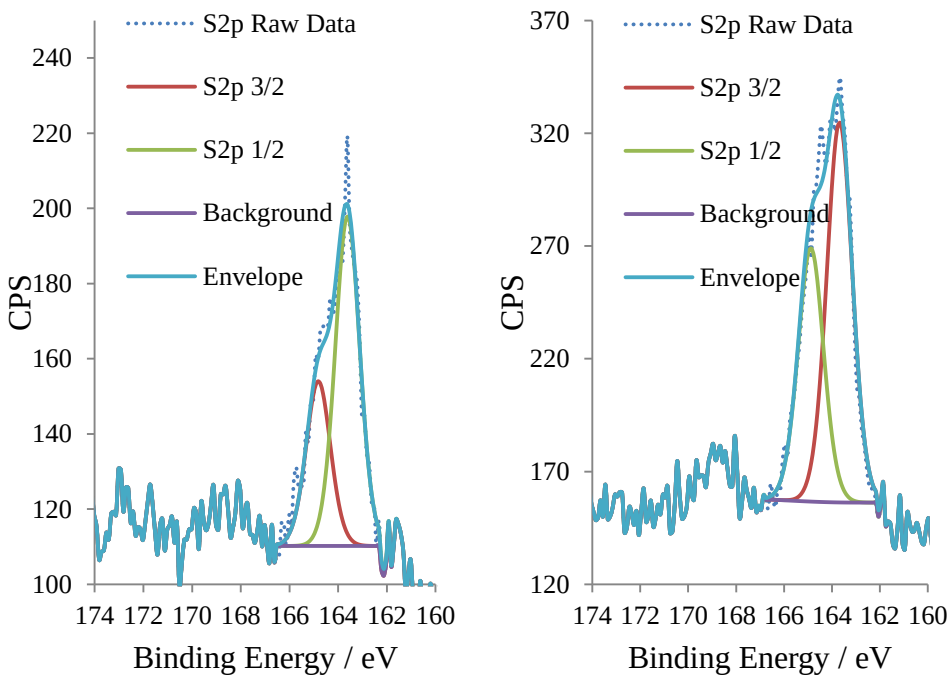


Figure 6.2.7 S2p high resolution spectra for 10 (left) and 15 min reaction time (right) of 3-((2-aminoethyl)thio)propanoate hydrochloride synthesised in EtOH

Table 6.2.8 presents the detailed XPS data for each of the high resolution element scans. The carbon, sulfur and nitrogen at% can be seen to decrease from TCNC-EtOH-10 min modification to TCNC-EtOH-15 min and therefore, a reduced grafting efficiency in the case of TCNC-EtOH-15 min that presents a $DS_{surf}(S) = 0.07$. A possible explanation for this decrease, correlated with the infrared spectrum and calculated $DS_{surf}(S)$, could be due to the fact that cysteamine can form a lactam by reaction of the amino head group of cysteamine (assuming the cysteamine hydrochloride is de-protected and HCl dissociated), with the electrophilic carbonyl carbon of the ester link (aminolysis) and so removal from the surface through a cyclisation of the grafted functionality.

Table 6.2.8 Detailed XPS data of 10/15 minutes reaction of cellulose 3-((2-aminoethyl)thio) propanoate hydrochloride in EtOH

Orbital	**C1s**					**O1s**					**S2p**					**N1s**			
	Co.	BE / eV	FWHM / eV	Rel.A /%[a]	at%	Co.	BE / eV	FWHM / eV	Rel.A /%[a]	at%	Co.	BE / eV	FWHM / eV	Rel.A /%[a]	at%	Co.	BE / eV	FWHM / eV	Rel.A /%[a]	at%
TCNC-EtOH-10 min	C=C	284.87	1.24	16.79	9.68	O–C =O	531.68	1.17	8.21	3.31	3/2	163.68	1.25	60.03	0.26	$–NH_2$	399.96	1.77	61.51	0.50
	C–O	286.50	1.24	67.57	38.97	C–O–H	532.64	1.17	61.20	24.70	1/2	164.88	1.25	39.97	0.18	$–NH_3^+$	401.92	1.77	38.49	0.32
	O–C=O	289.49	1.24	1.76	1.01	O–C–O	533.24	1.17	30.59	12.35				100	**0.44**				100	**0.82**
	O–C–O	288.16	1.24	13.88	8.00				100	**40.36**										
				100	**57.67**															
	Si 2p[b]	102.00	1.74	100	0.44															
TCNC-EtOH-15 min	C=C	284.84	1.14	18.63	10.70	O–C=O	531.79	1.02	11.38	4.66	1/2	163.61	1.18	66.69	0.21	$–NH_2$	400.02	1.76	70.16	0.41
	C–O	286.50	1.14	67.24	38.61	C–O–H	532.62	1.02	59.09	24.20	3/2	164.81	1.18	33.31	0.10	$–NH_3^+$	401.94	1.76	29.84	0.17
	O–C–O	288.14	1.14	12.78	7.34	O–C–O	533.22	1.02	29.53	12.09	3/2			100	**0.31**				100	**0.58**
	O–C=O	289.50	1.14	1.35	0.78				100	**40.95**	1/2									
				100	**57.42**															
	Si 2p[b]	102.00	1.82	100	0.74															

[a] Relative area = component area×100/sum area of same orbital

[b] Data available from low resolution wide scan

The two component peaks in the N1s spectrum are centred at around 400 eV and 401.3/401.9 eV and could be assigned to a free amino group ($–NH_2$) and a protonated amine/positively charged nitrogen, ($–NH_3^+$), as appears in the cysteamine hydrochloride.[277]

The possible secondary reaction is presented in Figure 6.2.8 forming 1,4-thiazepan-5-one upon cyclization and removal from the nanocellulose surface. This assumption is supported by the work of Jakob and Schlack (1963) who synthesised 5-oxo-1-thia-4-aza-cycloheptane from the reaction of cysteamine and methyl acrylate catalysed by a base in methanol (MeOH).[278] Subsequently, increasing the molar excess 10 times contributed to faster cyclization of the reaction, and in this case, de-grafting of the surface modification.

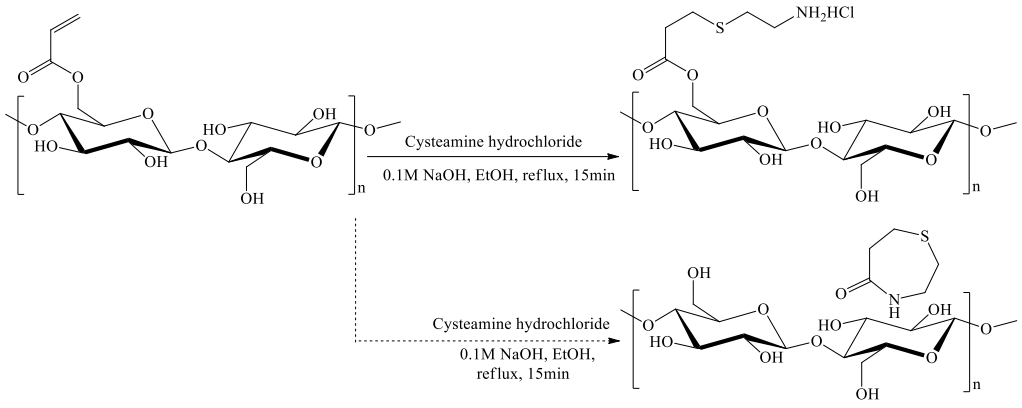


Figure 6.2.8 Thiol-Ene click reaction of cellulose acrylate with cysteamine hydrochloride and side reaction (aminolysis)

Earlier in this chapter, the work by Nielsen *et al.* in which cysteamine was reacted with cellulose methacrylate in MeOH was mentioned.[147] Therefore, it is proposed to carry out the reaction of cysteamine with cellulose acrylate (2-ACNC) for only 5-10 minutes in acetone (polar aprotic solvent with similar dielectric constant to MeOH), in order to give the cyclization reaction less time to occur. Determination of the crystallinity of the reaction product (Chapter 6 Appendix, Figure 10.4.17) confirmed the cellulose I_β structure that initially had a crystallinity of χ_C^R = 0.796, together with an increase in the crystallinity index from the cellulose acrylate, the starting material (χ_C^R = 0.738) with 7.9 % (χ_C^R = 0.817) for TCNC-Acetone-5 min and 1.2 % (χ_C^R = 0.750) for TCNC-Acetone-

10 min respectively. These increases of crystallinity values are proportional with the calculated expected modification based on EA (Table 6.2.9) 2.23 % and 1.84 % respectively. Thus, this increase of crystallinity may indicate the existence of a less amorphous material on the CNC surface and so a high amount of crystalline material, as it is confirmed also by the EA and the evolution of degree of substitution. If the cellulose acrylate has a $DS_{surf}(C)$ = 1.10, the Thiol-Ene product (TCNC-Acetone-5 min) has less than one tenth the amount of modification of the starting material. The calculated modifications indicate very close values for the two reactions. A $DS_{surf}(S)$ = 0.08 for 5 min reaction and $DS_{surf}(S)$ = 0.06 for 10 min reaction may be just identical as they stay within the accepted standard deviation of 0.4 % of EA.

Table 6.2.9 Elemental analysis results for CNC and 5/10 min TCNC-Acetone

Sample	C (%)	H (%)	N (%)	S (%)	$DS_{surf}(S)$
CNC	41.32	6.07	0.00	-	-
TCNC-Acetone-5 min	44.38	6.12	0.40	0.48	0.08
TCNC-Acetone-10 min	44.85	6.11	0.39	0.39	0.06

The wide scan XPS spectrum (Chapter 6 Appendix, Figure 10.4.18) identified only the expected elements, i.e. carbon, oxygen, sulfur and nitrogen. The detailed XPS analysis of these elements is given in Table 6.2.10. A decrease of O–C=O content from the cellulose acrylate 2.83 at%, (Table 3.3.2) to 1.78 and 1.98 at% for TCNC-Acetone-5 and TCNC-Acetone-10 min respectively was noticed in the C1s high resolution. The sulfur and nitrogen at% indicated a slight decrease from 10 min to 15 min reaction time, consistent with the EA results. The N1s high resolution spectrum also showed the presence of two N1s environments, a similar observation as in TCNC-EtOH-10 and 15 min. Fitting the N1s spectrum, the two component peaks centred at around 400 eV and 401.3/401.9 eV could be assigned to a free amino group ($–NH_2$) and a protonated amine/positively charged nitrogen, ($–NH_3^+$), that can be formed due to moisture presence.[277] The presence of the S2p 3/2 component peak at a BE

Table 6.2.10 Detailed XPS data for 5/10 minutes reaction of cellulose 3-((2-aminoethyl)thio) propanoate in acetone

Orbital	**C1s**					**O1s**					**N1s**					**S2p**			
	Co.	BE / eV	FWHM / eV	Rel.A /%[a]	at%	Co.	BE / eV	FWHM / eV	Rel.A /%[a]	at%	Co.	BE / eV	FWHM / eV	Rel.A /%[a]	at%	Co.	BE / eV	FWHM / eV	Rel.A /%[a]	at%
TCNC-Acetone-5 min	C=C	285.10	1.18	15.85	8.59	O–C =O	531.85	1.07	9.18	4.11	$–NH_2$	399.94	1.92	85.46	0.54	3/2	163.75	1.22	66.69	0.27
	C–O	286.50	1.18	68.38	37.06	O–C–O	532.65	1.07	60.56	27.11	$–NH_3^+$	401.97	1.92	14.54	0.09	1/2	164.95	1.22	33.31	0.13
	O–C–O	288.17	1.18	12.49	6.77	C–O–H	533.25	1.07	30.26	13.55				100	**0.63**				100	**0.40**
	O–C=O	289.41	1.18	3.28	1.78				100	**44.77**										
				100	**54.20**															
TCNC-Acetone-10 min	C=C	285.11	1.21	14.64	8.53	O–C=O	531.81	1.14	7.89	3.22	$–NH_2$	399.78	1.73	74.08	0.43	3/2	163.79	1.25	66.69	0.25
	C–O	286.50	1.21	68.46	39.88	C–O–H	532.64	1.14	61.42	25.06	$–NH_3^+$	401.31	1.73	25.92	0.15	1/2	164.94	1.25	33.31	0.12
	O–C–O	288.13	1.21	13.50	7.86	O–C–O	533.24	1.14	30.69	12.52				100	**0.58**				100	**0.37**
	O–C=O	289.39	1.21	3.40	1.98				100	**40.80**										
				100	**58.25**															

[a] Relative area = component area×100/sum area of same orbital

of 163.75 eV indicated the thiolate bond formation and therefore synthesis of the desired components TCNC-Acetone-5 min and TCNC-Acetone-10 min respectively which proves that the Michael addition of cysteamine to a α, β unsaturated carbonyl compound works even for a 5-minutes reaction time. Previously in the literature it has been shown that Thiol-Ene click reactions conducted in highly polar solvents with a high dielectric constant (i.e. DMF) for the surface functionalization of thiol-capped nanoparticles with water-soluble linear acrylate-based copolymers required no catalyst.[279]

Therefore, the same reaction of cysteamine with acrylate cellulose (2-ACNC) was carried out in solvents with a high dielectric constant such as DMF, DMSO and H_2O, in order to determine the most suitable solvent for these reactions. It also has to be noted that CNC disperse easier in these solvents. Infrared spectra (Figure 6.2.9) of the three modifications compared with the starting material showed slight differences from reactions carried out in DMSO, to DMF and H_2O. The three modifications present a consistent C=O band at around 1733 cm^{-1}, 10 cm^{-1} higher than the C=O peak position in cellulose acrylate, while the C=C peak shifts from 1635 cm^{-1} in the starting material to 1652 cm^{-1} in the modified products, which could be attributed to hydrothiolation of the C=C. The XPS wide resolution scan (Chapter 6 Appendix, Figure 10.4.19) of these three modifications identified the presence of carbon, oxygen, sulfur and nitrogen (Table 6.2.11). Although there is an increase in at% of O–C=O component from the modification in DMSO (1.07 at%) to modification in DMF (1.24 at%) and in H_2O (1.53 at%) in the C1s high resolution, this does not happen in the S2p at% evolution. The highest concentration of sulfur is found in the reaction product synthesized in DMF (0.76 at%) even if the difference between the S2p at% in the three modified products is very small it is still higher than in the products synthesized in acetone (10 min). Fitting the N1s spectrum indicates the presence of two component peaks centred at around 399.8 eV and 402 eV, which can be assigned to a free amino group ($–NH_2$) and to a protonated amine/positively charged nitrogen, ($–NH_3^+$) respectively. The positively charged nitrogen can be formed due to moisture as the reaction excludes inert conditions and use

analytical reagent grade solvents.[277] The crystal structure determination (Chapter 6 Appendix, Figure 10.4.20) showed loss of crystallinity for TCNC-DMSO, TCNC-DMF, and TCNC-H_2O as follows: 13.5 % (χ_C^R = 0.748), 12.41 % (χ_C^R = 0.759), 11 % (χ_C^R = 0.773) when compared with the unmodified CNC (χ_C^R = 0.883) and very small crystallinity increase when related to the starting material as follows: 1% for TCNC-DMSO, 2.1 % for TCNC-DMF, and 3.5 for TCNC-H_2O. Considering the sulfur content from EA, the estimated modification corresponds to 5.33 %, 5.59 % and 3.69 % respectively, values that only slightly match with their corresponding loss of crystallinity. These higher losses could be due to some damage of the crystal structure of nanocellulose as a result of the use of cellulose swelling solvents.

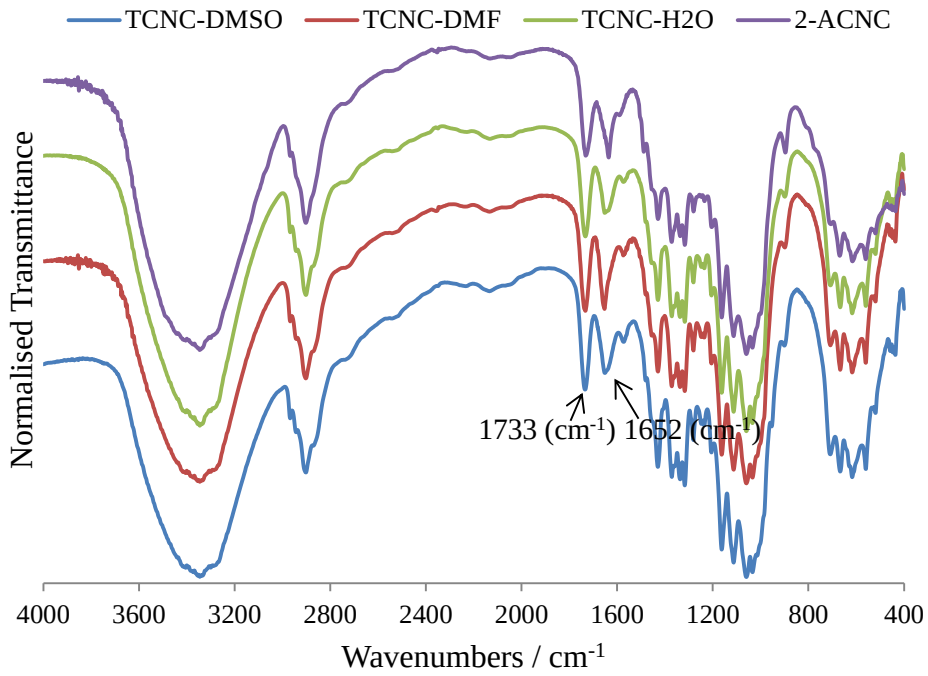


Figure 6.2.9 FT-IR spectrum of cellulose acrylate (2-ACNC) and 10 minutes reaction of cellulose 3-((2-aminoethyl)thio)propanoate in DMSO(TCNC-DMSO)/DMF(TCNC-DMF)/H_2O(TCNC-H_2O)

Table 6.2.11 Detailed XPS data for 10 minutes reaction of cellulose 3-((2-aminoethyl)thio) propanoate in DMSO/DMF/H_2O

Orbital	**C1s**					**O1s**					**S2p**					**N1s**			
	Co.	BE / eV	FWHM / eV	Rel.A /%[a]	at%	Co.	BE / eV	FWHM / eV	Rel.A /%[a]	at%	Co.	BE / eV	FWHM / eV	Rel.A /%[a]	at%	Co.	BE / eV	FWHM / eV	Rel.A /%[a]	at%
TCNC-DMSO	C=C	285.14	1.11	14.35	8.23	O–C =O	531.77	1.01	8.99	3.66	3/2	163.72	1.18	66.69	0.49	$–NH_2$	399.97	1.70	80.70	1.01
	C–O	286.50	1.11	70.53	40.44	C–O–H	532.67	1.01	60.68	24.67	1/2	164.90	1.18	33.31	0.25	$–NH_3^+$	402.06	1.70	19.30	0.24
	O–C–O	288.17	1.11	13.25	7.60	O–C–O	533.27	1.01	30.32	12.33				100	**0.74**				100	**1.25**
	O–C=O	289.55	1.11	1.87	1.07				99.99	**40.66**										
				100	**57.34**															
TCNC-DMF	C=C	285.18	1.09	14.18	8.15	O–C=O	531.83	1.00	8.89	3.62	3/2	163.72	1.10	66.69	0.51	$–NH_2$	399.82	1.62	74.50	0.80
	C–O	286.50	1.09	70.38	40.43	C–O–H	532.67	1.00	60.75	24.73	1/2	164.91	1.10	33.31	0.25	$–NH_3^+$	401.54	1.62	25.50	0.28
	O–C–O	288.17	1.09	13.28	7.63	O–C–O	533.27	1.00	30.36	12.36				100	**0.76**				100	**1.08**
	O–C=O	289.53	1.09	2.16	1.24				100	**40.70**										
				100	**57.45**															
TCNC-H_2O	C=C	285.15	1.11	14.29	8.28	O–C=O	531.80	1.03	8.37	3.38	3/2	163.74	1.24	66.69	0.43	$–NH_2$	399.79	1.61	78.47	0.82
	C–O	286.50	1.11	70.11	40.61	C–O–H	532.66	1.03	61.10	24.67	1/2	164.98	1.24	33.31	0.21	$–NH_3^+$	401.99	1.61	21.53	0.23
	O–C–O	288.16	1.11	12.96	7.51	O–C–O	533.26	1.03	30.53	12.33				100	**0.64**				100	**1.05**
	O–C=O	289.51	1.11	2.64	1.53				100	**40.38**										
				100	**57.93**															

[a] Relative area = component area×100/sum area of same orbital

EA results (Table 6.2.12) indicated a substantial increase in the sulfur content and consequently an increase in the surface degree of substitution, especially for the thiol-click reactions performed in DMSO and DMF and only a $DS_{surf}(S)$ = 0.13 for the reaction in water. Therefore, increasing the polarity of the solvents has brought about a good increase with the highest DS obtained in DMF – a solvent with the lowest dielectric constant of these three solvents.

Table 6.2.12 Elemental analysis results of the cellulose 3-((2-aminoethyl)thio)propanoate synthesised in DMSO/DMF/H_2O

Sample	C (%)	H (%)	N (%)	S (%)	$DS_{surf}(S)$
CNC	41.32	6.07	0.00	-	-
TCNC-DMSO	42.50	6.14	0.63	1.15	0.20
TCNC-DMF	44.45	6.23	1.08	1.20	0.21
TCNC-H_2O	44.28	6.14	0.56	0.79	0.13

However, the reaction performed in water – a green solvent – was proven to work and to have a good substitution considering the 10-minutes reaction time and room temperature conditions without any additional catalyst. This is quite remarkable for a heterogeneous reaction. Thus, reactions performed for longer reaction times could be planned in order to observe the evolution of the click chemistry, as part of the future work from the current research.

Michael-addition reactions developed until now were mainly based on cellulose acrylate or cellulose methacrylate synthesised in TsCl/Py or DIC/DMAP for either very short reaction time (5 and 10-minutes) or up to 1-2 days at room temperature. Therefore, in order to increase the DS_{surf}, a subsequent modification on cellulose acrylate (3-ACNC), cysteamine and hexylamine, suspended in DCM, at 50 °C, for 2 hours and catalysed by hexylamine was carried out. The purification was performed by Soxhlet extraction with DCM 24 hours and EtOH 48 hours followed by *vacuo* drying.

Considering the first round of extensive modification of cellulose acrylate 3-ACNC, the current reaction product maintains the X-ray diffractogram of the cellulose I_β allomorph (Chapter 6 Appendix, Figure 10.4.21) with a crystallinity loss of 24.2 % (χ_C^R = 0.554), a value that includes the previous loss

of crystallinity of cellulose acrylate of 21.4 % with respect to the initial cellulose crystallinity (χ_C^R = 0.796). The calculated expected modification based on sulfur content in EA is 16.55 %. Thus, the measured loss of crystallinity in the product is mainly caused by the extent of amorphous modification, although the determined amount of modification is slightly lower than the value indicated by XRD, which indicates the existence of some additional amorphous material in the reaction product, other than the sulfur containing material. A possible explanation for the amorphous material could be degradation of the crystalline CNC core during the acrylation, shown by the higher decrease in crystallinity than expected from EA for the acrylate product.

EA (Table 6.2.13) provides a very good indication of successful conjugate addition of cysteamine to α, β-unsaturated acrylate cellulose with a $DS_{surf}(S)$ = 0.68, which covers more than one OH hydroxyl group per AGU for a reaction of 2 hours and at 50°C.

Table 6.2.13 Elemental analysis results of the cellulose 3-((2-aminoethyl)thio)propanoate synthesised in DCM (TCNC-DCM)

Sample	C (%)	H (%)	N (%)	S (%)	$DS_{surf}(S)$	$DS_{surf}(N)$
CNC	41.31	6.15	0.00	-	-	
TCNC-DCM	45.47	6.18	1.54	3.55	0.68	0.68

When compared to all the previous modifications, this click chemistry approach gives the highest modification considering the reaction temperature and reaction time. The infrared spectrum presented in Figure 6.2.10 shows that the carbonyl stretch is found at 1735 cm^{-1} while a C=C absorption band is still found at 1647 cm^{-1} which indicate that there are still unmodified C=C bonds present. This is consistent with the EA DS_{surf} calculation where the Thiol-Ene click DS_{surf} was significantly lower than the DS_{surf} for the acrylation reaction. Therefore, an increase in the reaction time could possibly result in an even higher DS. In order to clarify the characterization of this modification, XPS was used and the wide scan of the reaction product (Figure 6.2.11) clearly indicated nitrogen and sulfur peaks, in addition to carbon and oxygen.

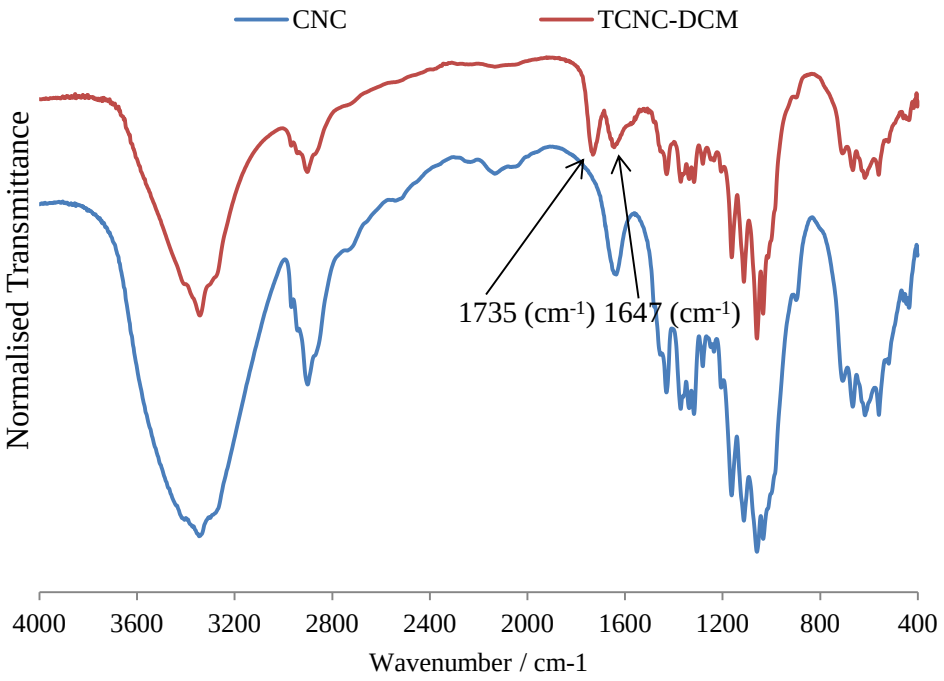


Figure 6.2.10 FT-IR spectrum of cellulose nanocrystals and 3-((2-aminoethyl)thio)propanoate synthesised in DCM for 2 hours at 50 °C (TCNC-DCM)

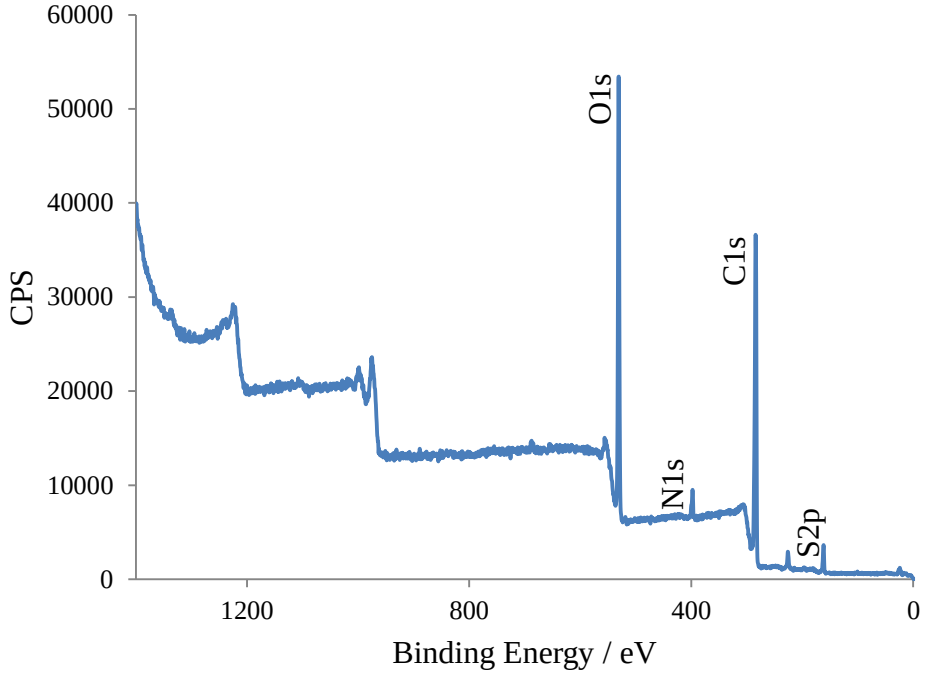


Figure 6.2.11 XPS wide scan of cellulose 3-((2-aminoethyl)thio)propanoate synthesised in DCM for 2, at 50 °C

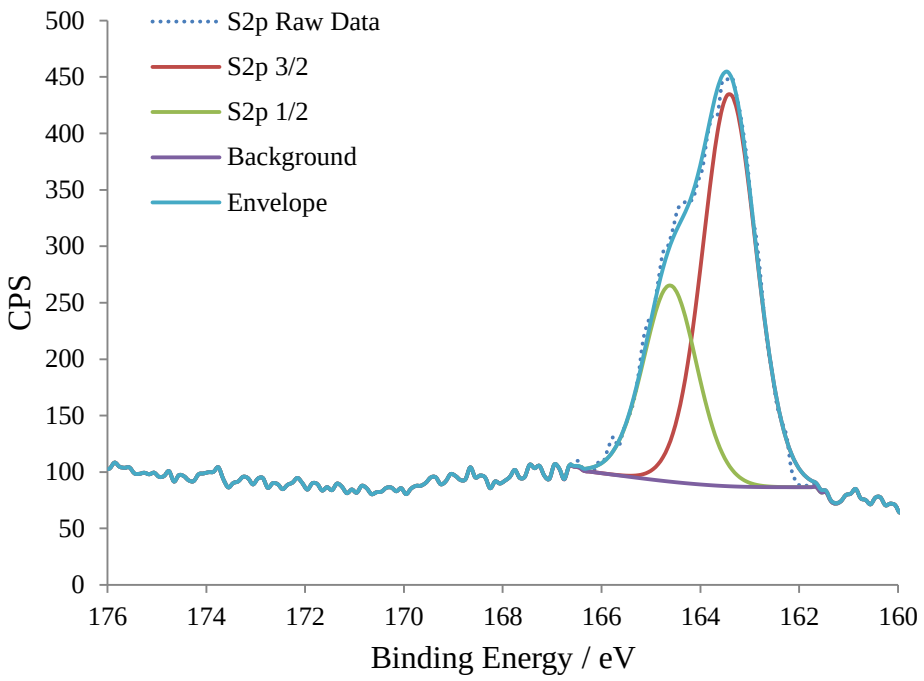


Figure 6.2.12 S2p high resolution scan of cellulose 3-((2-aminoethyl)thio)propanoate synthesised in DCM for 2 hours at 50 °C, TCNC-DCM

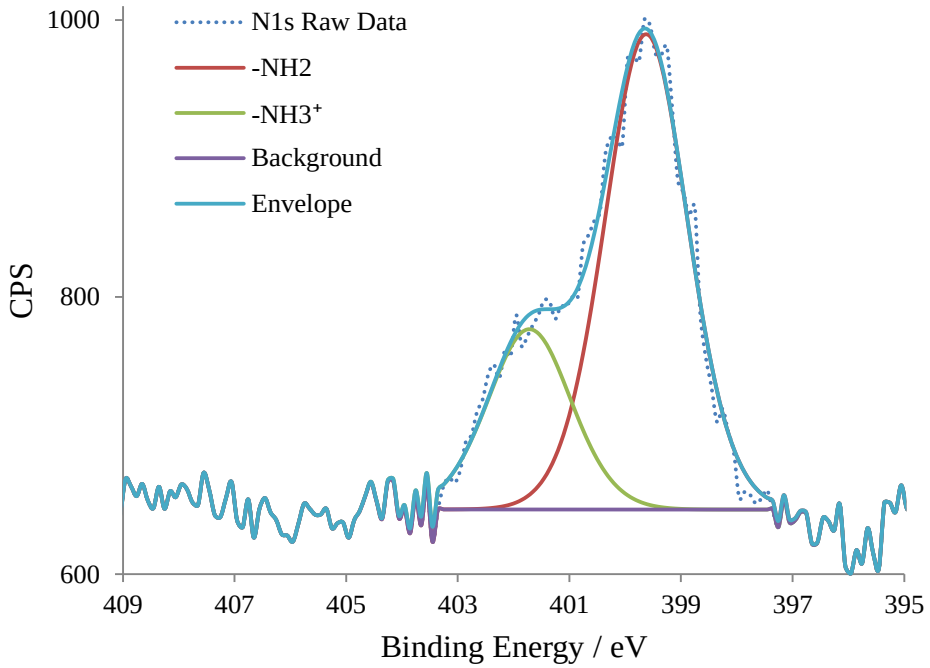


Figure 6.2.13 N1s high resolution spectrum of TCNC-DCM

Table 6.2.14 Detailed XPS data of TCNC-DCM

Orbital	Component	BE / eV	FWHM / eV	Rel.A/%[a]	at%
C1s	C–C/C=C	284.85	1.442	47.36	33.22
	C–O	286.26	1.442	38.94	27.32
	O–C–O	287.99	1.442	10.88	7.63
	O–C=O	289.07	1.442	2.82	1.98
				100.00	70.15
O1s	O–C=O	530.94	1.483	13.88	2.84
	C–O–H	532.31	1.483	57.42	11.74
	O–C–O	532.91	1.483	28.70	5.87
				100.00	20.45
N1s	$–NH_2$	399.62	1.761	72.51	1.81
	$–NH_3^+$	401.72	1.761	27.49	0.69
				100.00	2.50
S2p	3/2	163.41	1.274	66.69	1.30
	1/2	164.61	1.274	33.31	0.65
				100.00	1.95

[a] Relative area = component area×100/sum area of same orbital

The sulfur high resolution scan (Figure 6.2.12) presented only a sulfur environment found at a BE of 163.42 eV for S2p 3/2 indicating the formation of a thiolate bond giving the product cellulose 3-((2-aminoethyl)thio) propanoate (TCNC-DCM).

The C1s high resolution spectrum (Chapter 6 Appendix, Figure 10.4.22) indicated a decrease in the O–C=O carbon component from 4.64 at% in the starting material (Table 3.6.2) to 1.98 at% (Table 6.2.14) which could indicate some new contributions to the surface determining an overall at% decrease.

Also, C–C/C=C displayed a reduction from 35.98 to 33.22 at% which is expected upon conversion of C=C bond in C-S. The N1s high resolution scan (Figure 6.2.13) displayed similar components with the ones displayed before which are the amino-head (NH_2) identified at a BE of 399.62 eV and the respective protonated amino group found at a BE of 401.72 eV.

6.3 Thiol-Ene click chemistry conclusions

It can thus be concluded that the Thiol-Ene reactions between a thiol and an α, β-unsaturated ene developed in this chapter occurs readily at the surface of CNC. Three types of catalysts (base, nucleophile and self-catalysed reaction by a nucleophile) have been used to initiate the thiol-Michael addition reaction. Tables 6.3.1 and 6.3.2 summarise all the reactions performed in this chapter by presenting the molar excesses used in reactions and indicating the catalyst, solvent, temperature, time and DS_{surf}(S) for the Thiol-Ene modifications and DS_{surf}(C) of the initial starting acrylate/ methacrylate cellulose used as support for Thiol-Ene click reactions.

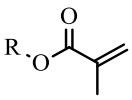
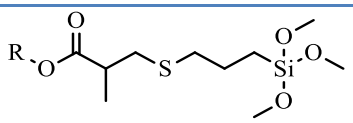
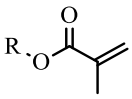
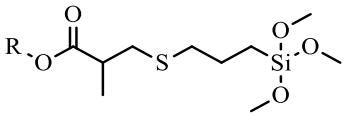
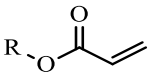
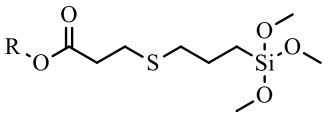
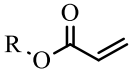
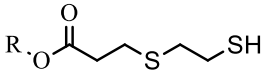
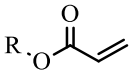
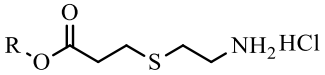
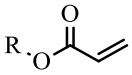
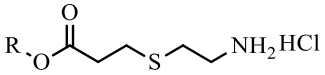
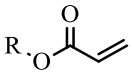
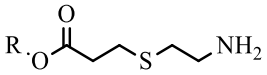
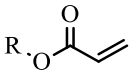
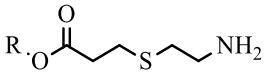
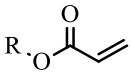
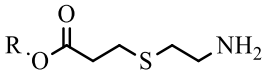
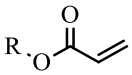
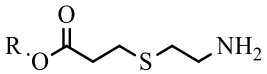
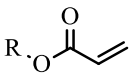
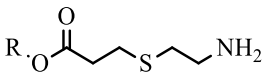
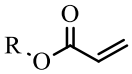
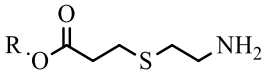
Table 6.3.1 Molar ratio used in Thiol-Ene click chemistry

Entry	CNC (mmol)	Thiol	Catalyst	DS_{surf}(S)	DS_{surf}(C) starting material
1	1	1.33	0.15[c]	-[a]	0.52
2	1	1.33	0.15 [c]	- [a]	0.52
3	1	1.66	1.66 [c]	0.19	0.94
4	1	39.73	2.52 [c]	0.24	0.94
5	1	0.5	0.5[d]	0.15	0.94
6	1	5	5 [d]	0.07	0.94
7	1	3	S.C.[b]	0.08	1.10
8	1	3	S.C. [b]	0.06	1.10
9	1	6.66	S.C. [b]	0.20	1.10
10	1	6.66	S.C. [b]	0.21	1.10
11	1	6.66	S.C. [b]	0.13	1.10
12	1	6.66	0.072 [c]	0.68	2.10

[a] DS_{surf}(S) could not be determined by EA
[b]S.C. = Self Catalysed reaction
[c] = hexylamine
[d] = sodium hydroxide

Entries 1 and 2 indicated the desired reaction only in the XPS spectrum but conversion was too low for EA analysis. Potential reasons for the low DS are steric hindrance of methacrylate compared with the acrylate and the aminolysis as secondary reaction.

Table 6.3.2 Thiol-click chemistry of cellulose acrylate/methacrylate modified developed in this chapter

	α, β-Unsaturated carbonyl compound	C[a]	Product	Temp (°C)	Time (min)	Solvent	DS_{surf} (S)
1		Yes		R.T.	60	MeOH	-[b]
2		Yes		R.T.	240	MeOH	-[b]
3		Yes		R.T.	1440	DCM	0.19
4		Yes		R.T.	2880	DCM	0.24
5		No		R.T.	10	EtOH	0.15
6		No		R.T.	15	EtOH	0.07
7		No		R.T.	5	Acetone	0.08
8		No		R.T.	10	Acetone	0.06
9		No		R.T.	10	DMSO	0.20
10		No		R.T.	10	DMF	0.21
11		No		R.T.	10	H_2O	0.13
12		Yes		50 °C	120	DCM	0.68

[a] C = Catalyst

[b] DS_{surf}(S) could not be determined by EA

Increasing the molar excess in entries 3 and 4 for reactions performed in DCM for 1 up to 2 days brought about a significant improvement and clearly successful substitution. As the aim was to get to short reaction times, entries 5 and 6 display the results for reactions of 10 up to 15 minutes in EtOH and 10 times excess in entry 6 as compared to entry 5, indicate that 5 mmol:1 mmol /

thiol:CNC would lead to a decreased in final DS based on too high molar ratio that would increasing aminolysis, the secondary reaction.

An equimolar amount of thiol and catalyst (entry 3 and 6) led to smaller DS values when compared to reactions where the thiol is predominant (entry 4 & 12). The entries 7 and 8 present only a very slight decrease of degree of substitution from 5 minutes ($DS_{surf}(S)$ =0.08) to 10 minutes ($DS_{surf}(S)$ =0.06), a decrease that is within the experimental error. Therefore, it is thought that if a maximum DS_{surf} happens before 5 min (entry 7) this could be monitored by Real-Time Fourier transform (RT-FT-IR).[280] Additional reactions that could help to understand the reaction evolution for such very short reaction time are also part of the future work.

The Thiol-Ene click self-catalysed reactions performed in more polar solvents (entries 9, 10 and 11) resulted in substantially increased substitution degrees compared with the reaction carried out in less polar solvents. When carrying out the reaction at higher temperature and catalysed by hexylamine, one notices a significant increase in DS ($DS_{surf}(S)$ = 0.68). The self-catalysed reactions (entries 7-11) performed in Acetone/DMSO/DMF/H_2O indicated that increasing the amino-thiol excess would be beneficial to increase the final DS_{surf}.

Table 6.3.1 further shows that the conversion of cellulose acrylate/methacrylate into a thiol-modified product varies between 5 % for entry 8 and a satisfactory 32 % for entry 12.

6.4 Surface Charge-Switchable Nanoparticles based on cellulose nanocrystals (Switch-CNC)

The ability to reversibly switch between phases or different aggregation states allows the development of a system that adapts its behaviour based on multiple inputs. There are different ways of introducing this switching aspect into supramolecular nano-assemblies such as light, temperature, concentration, solvent composition, external additives, and variation of charge.[281] Supramolecular self-assembly makes use of the ability of complementary systems that aggregate with a certain binding constant. Very little changes in the binding sites could have significant influence on the binding constant between functionalities with direct effects on aggregation that can then be trigged or destroyed.[281] This effect can be achieved by the creation of charges by oxidation or reduction or simply by changing the pH.[281] For example, carbon dioxide has been adopted for shuttling nanoparticles between phases.[282] Gold nanoparticles with widespread application in nanocomposites and thin film were synthesised and surface-modified to facilitate their dispersion in organic media. A gas expanded liquid precipitation technique based on CO_2 (as a green antisolvent for hydrophobic nanorods dispersed in toluene, hexane and cyclohexane) was used to effectively fractionate the gold nanoparticles. The advantage of gas expanded liquid media is given by their tunable solvent properties that facilitate the size-selective nanoparticle precipitation being easily controlled by this CO_2 antisolvent partial pressure.[282] Furthermore, Jessop *et al.* have reported a new kind of switchable solvents that behave as a hydrophobic phase with low water miscibility when in air but become hydrophilic and completely miscible with water when under a CO_2 atmosphere.[283] Along this line, they also developed long-chain alkyl amidine compounds that can be reversibly transformed into charged surfactants by exposure to carbon dioxide, thus stabilizing water/alkane emulsions or styrene in water.[284] This last work represents the starting point for the introduction of such switchable functionalities onto the surface of CNC and so expanding the field of nanocellulose. These switchable nanoparticles could be interesting

compounds to stabilise/de-stabilise Pickering emulsions. By definition, Pickering emulsions are emulsions that are stabilised by solid particles based on their property to adsorb at the interface between the phases.[285] This characteristic could make Pickering emulsions interesting for applications in industries spanning food, petroleum, biomedicine, pharmaceuticals, and cosmetics.[286] One current important Pickering emulsion application is in the oil-well drilling where they are used to alter the surface tension between water and oil in the reservoir, and so, mobilize oil which otherwise would remain in the reservoir as residual oil. There are many attempts to improve oil recovery through additives to water and surfactants but these are expensive and are required in large concentrations to stabilise the emulsions. Particles are recognized as effective emulsifiers and could lead to very stable emulsions based on sterical and electrostatic repulsions of the oil droplets and viscoelastic behaviour of the oil/water interface. Another distinct advantage of the particles is the fact that they achieve an equilibrium at high solution concentration which allows effective binding reversibility at the interface when compared to molecular surfactants.[286-289]

Currently, the work of Foster *et al.* recently claimed light-stimulated mechanically switchable photopatternable cellulose nanocomposites based on benzophenone derivatized cellulose nanocrystals (Bp-CNCs).[290] These Bp-CNCs are highly photoreactive and undergo radical-mediated reactions upon UV exposure and were tested for the development of materials with switchable mechanical properties. Beside this work, to the best of my current knowledge, there are no other publications regarding CNC with switchable properties in general or in colloidal systems in particular. For the system to be developed here, the switchable process consists in using benign gases (CO_2 and air) to promote the trigger to switch "on" and "off". The advantage of using CO_2 is given by the formation of carbonic acid (bicarbonate anion and a positively charged functional group) in water, which is easily switched off to the neutral state in comparison with the addition of acid and base which will result in salt accumulation with each cycle. The amidine functionality to be used reacts exothermically to form the bicarbonate or alkyl carbonate salt in water with

carbonic acid. The reversibility of the reaction can be achieved by bubbling N_2 or Ar through the net liquid salt or if the salt is a solid, through a solution, to remove CO_2.[284]

To achieve this surface energy change, the previously obtained cellulose 3-((2-aminoethyl)thio)propanoate synthesised in DCM for 2 hours, TCNC-DCM, were used as the starting material to introduce an amidine functionality by reaction of the amino end with *N*,*N*-dimethylacetamide dimethyl acetal by adaptation of a procedure for acetamidines. This method developed by Scoggins involves the heating of equimolecular amounts of primary amines with *N*,*N*-dimethylacetamide dimethyl acetal for a maximum of 20 minutes at 60 °C without solvent.[291] The adapted procedure for this reaction (Figure 6.4.1) consists in immersion of the modified CNC (TCNC-DCM) in an excess of *N*,*N*-dimethylacetamide dimethyl acetal in dry acetone (5 mL) under inert conditions. Considering the solid nature of CNC, the reaction is left to react for 24 hours at 60 °C followed by high-vacuum removal of the MeOH by-product and solvent and acetone intensive washing until the product was left clean and maintained their initial yellow colour.

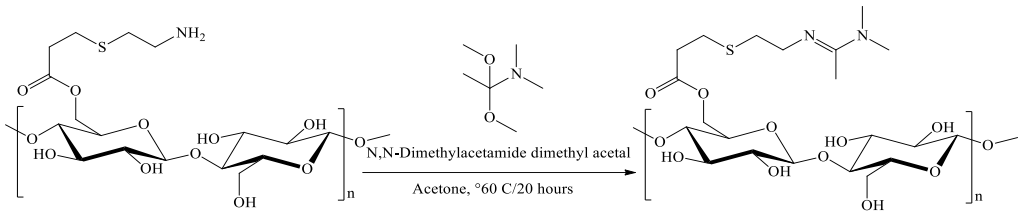


Figure 6.4.1 Proposed reaction for synthesis of switchable nanoparticles - 3-(2-(*N*,*N*-dimethylacetimideamide)ethyl)thio) propanoate cellulose nanocrystals

6.5 Switchable cellulose nanoparticles characterization

The infrared spectrum of the modification of cellulose 3-((2-aminoethyl)thio) propanoate (TCNC-DCM) with *N*,*N*-dimethylacetamide dimethyl acetal is compared with the previous two modifications in Figure 6.5.1. Beginning with the esterification in 3-ACNC, the carbonyl vibration stretch is significantly reduced in the next modification step and slightly decreased after the last

modification. Thus, the presence of ester link with an absorption stretch at 1731 cm^{-1} indicates the desired modification existence to a smaller degree, while the peak with a maximum at 1648 cm^{-1} can be some adsorbed surface water or can be attributed to some remaining unmodified C=C bonds as also found in TCNC-DCM.

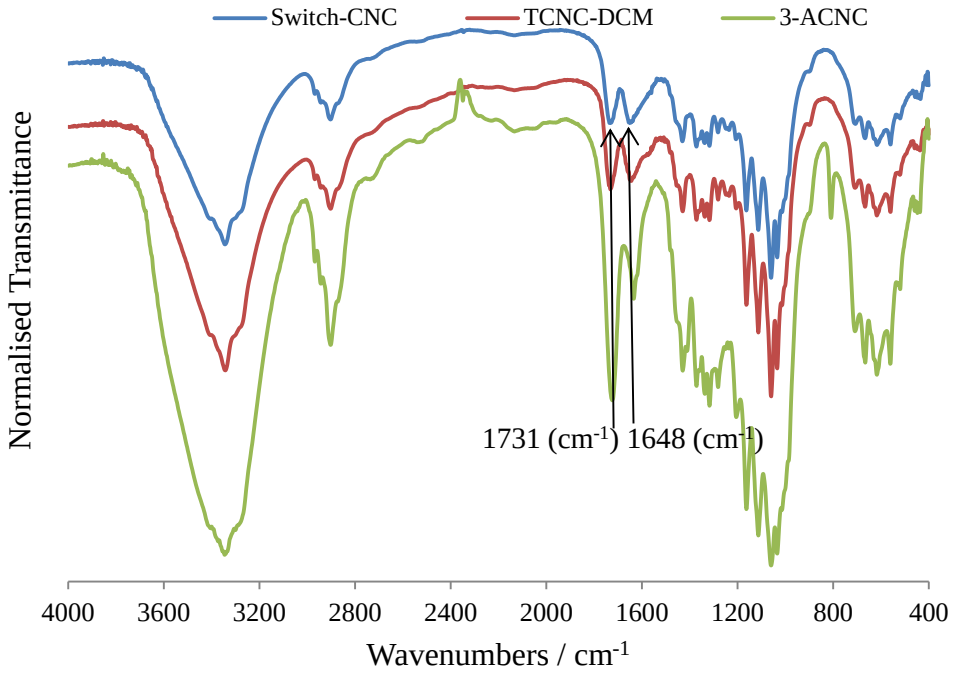


Figure 6.5.1 FT-IR spectrum of the initial acrylate cellulose (3-ACNC) nanocrystals, which were modified by a Thiol-Ene click reaction with cysteamine (TCNC-DCM) followed by their conversion in switchable nanoparticles (Switch-CNC).

Through observation of the XPS wide scan (Chapter 6 Appendix, Figure 10.4.24), it can be deduced that the expected carbon, oxygen, nitrogen and sulfur are present, and traces of silicon (Si2p) and zinc (Zn3d) are found. While the silicon contamination could be easily attributed to adhesive tape used in fixing the modified cellulose powder in XPS measurement support, the zinc contamination source is quite baffling. Repetition of the same reaction at different dates indicated the consistent appearance of this element, such that a possible contamination during the XPS measurement is excluded. The source for this Zn3d contamination could be attributed to contamination during

handling and transferring of dry acetone or *N*,*N*-dimethylacetamide dimethyl acetal by syringe or cannula, or initial contamination of the *N*,*N*-dimethylacetamide dimethyl acetal.

The C1s high resolution spectrum (Figure 6.5.2 a) is comparable with the C1s high resolution spectrum of cellulose 3-((2-aminoethyl)thio)propanoate (TCNC-DCM) and the presence of an O–C=O carbon environment at 289.03 eV. However, there was an increase in the C=C peak from 33.22 at% (in the starting material) to 37.54 at% (Table 6.5.1), indicating the presence of C–C/C–H bonds as part of the *N*,*N*-dimethylacetamide dimethyl acetal newly introduce on the surface.

Thus, the new modification is identified as 3-(2-(*N*,*N*-dimethylacetimideamide)ethylthio)propanoate cellulose nanoparticles, abbreviated as Switch-CNCs. Identification of O–C=O presence is also given by the O1s high resolution spectrum (Chapter 6 Appendix, Figure 10.4.25) at a BE of 531.48 eV as expected.

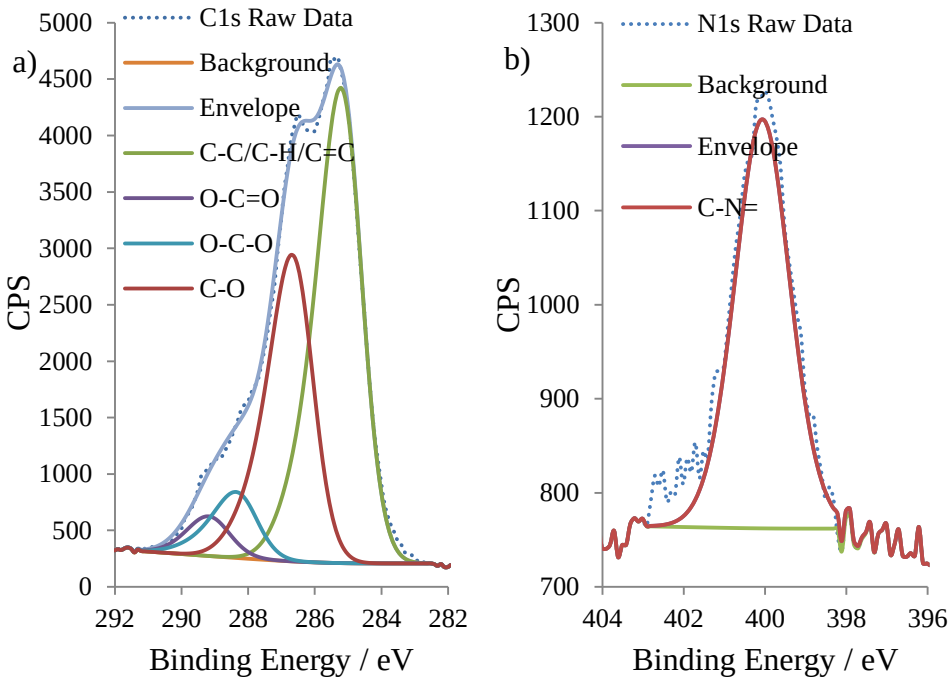


Figure 6.5.2 a) C1s high resolution XPS spectrum of 3-(2-(*N*,*N*-dimethylacetimideamide)ethylthio)propanoate cellulose nanoparticles; b) N1s high resolution XPS spectrum of switchable cellulose nanoparticles

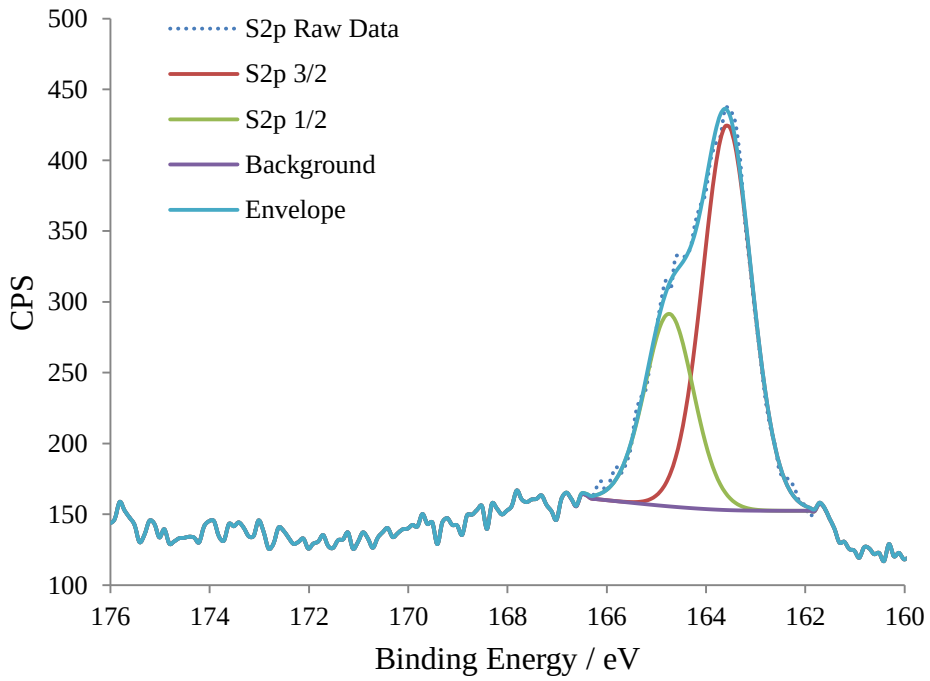


Figure 6.5.3 S2p high resolution XPS spectrum of Switch-CNC

Table 6.5.1 Detailed XPS data of the switchable nanoparticles

Orbital	Component	BE / eV	FWHM / eV	Rel.A/%[a]	at%
C1s	C=C/C–C	285.04	1.47	53.80	37.54
	C–O	286.50	1.47	34.67	24.19
	O–C–O	288.18	1.47	7.45	5.20
	C–O=O	289.03	1.47	4.08	2.85
				100.00	69.78
O1s	O–C=O	531.48	1.45	21.05	5.21
	C–O–H	532.53	1.45	52.64	13.03
	O–C–O	533.13	1.45	26.31	6.51
				100.00	24.75
N1s	C–N=	400.07	1.6	100.00	2.67
S2p	3/2	163.57	1.17	66.69	1.00
	1/2	164.74	1.17	33.31	0.50
				100.00	1.50
Si2p	-[b]	103	1.72	100.00	0.50
Zn3p	-[b]	90	5.16	100.00	0.81

[a] Relative area = component area×100/sum area of same orbital
[b] Data available from low resolution wide scan

The N1s high resolution spectrum (Figure 6.5.2 b) displayed a single peak at 400.07 eV, consistent with a neutral nitrogen environment specific for the 3-(2-(*N*,*N*-dimethylacetimideamide)ethylthio)propanoate cellulose nanoparticles

with two nitrogen atoms present in, with a 2.67 at% greater than in the starting material, (1.81 at%). More than this, the sulfur chemical environment (Figure 6.5.3) with its component S2p 3/2 present at 163.57 eV (Table 6.5.1), are kept at the same BE as in the cellulose 3-((2-aminoethyl)thio)propanoate (TCNC-DCM) where S2p 3/2 is found at a BE of 163.41 eV which confirms the presence of the thio-ether functionality in the modification.

Finally, the crystal structure was evaluated (Chapter 6 Appendix, Figure 10.4.24) and the loss of crystallinity was determined to be 22.30 % from unmodified CNCs of χ_C^R = 0.796. This current loss of crystallinity stays consistent with the loss of crystallinity of thiol-modified cellulose, TCNC-DCM, which is 24.2 % and therefore, from the previous modification step to this one, the crystallinity reduction is not significantly changed. The nitrogen content determined by EA (Table 6.5.2) resulted in a DS_{surf}(N) = 0.35 while the sulphur content reasonably displayed the same value, giving a perfect consistency and the finding stays consistent with the FT-IR as well.

Table 6.5.2 Elemental analysis results for CNC and Switch-CNC

Sample	C (%)	H (%)	N (%)	S (%)	DS_{surf}(N)	DS_{surf}(S)
CNC	41.77	5.91	0.00	-	-	-
TCNC-DCM	45.47	6.18	1.54	3.55	0.68	0.68
Switch-CNC	41.30	6.15	1.64	1.90	0.35	0.35

So, with the crystal structure retained after three subsequent modifications, the DS_{surf}(N) = 0.35 is a good result and therefore it is considered a successful reaction for its first synthesis. In order to test the switchable properties, the synthesised amidine–modified cellulose nanocrystals, 3-(2-(*N*,*N*-dimethylacetimideamide)ethylthio)propanoate cellulose nanoparticles (0.1 g) were suspended in 200 mL water to produce the amidinium bicarbonate salt by bubbling CO_2 (~1 atm) into the water while the pH was measured continuously. According to Figure 6.5.5, after only a few minutes the pH dropped off and was maintained at this value until the CO_2 bubbling was stopped and Ar was flushed into the solution.

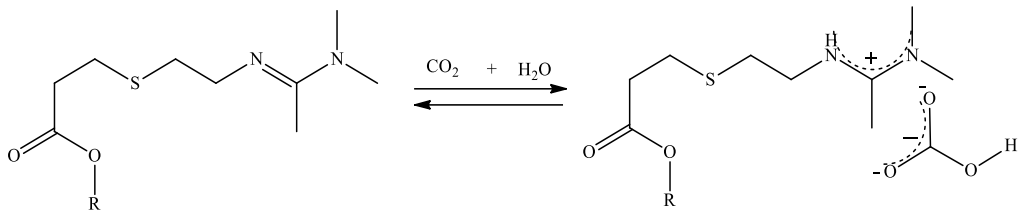


Figure 6.5.4 Switchable nanoparticles reaction with CO_2 in H_2O with formation of amidinium bicarbonate salt

Rapid decrease of the pH corresponds to carbonic acid dissolution and therefore the conversion of amidine modified cellulose to amidinium bicarbonate salt grafted CNC (the scheme given in Figure 6.5.4). Reversibility and repeatability is proved in the same figure for three cycles of CO_2/Ar on and off. In order to monitor the positive charge formation on the nanoparticles, zeta potential measurements were carried out in a similar experiment as the one described above.

Figure 6.5.6 describes the evolution of the zeta potential (purple rhombuses) upon pH (red triangles) variations as a result of CO_2 and Ar bubbling. Initial zeta potential measurement for the Switch-CNC was -15.6 mV, determined before starting the experiment.

Upon CO_2 bubbling, the zeta potential rose to a maximum value of + 37.5 mV after 4 hours, a value that was maintained until Ar flushing. It dropped down upon argon bubbling, leading to the initial state of nanoparticles negatively charged after 9 hours. Using the same nanoparticles, this first experiment was repeated on a second day (Figure 6.5.7) and was run for a shorter period of time (440 min) than the first one (560 min). The behaviour was very similar with the first experiment, proving the capacity of amidine modified CNC to be reversible/switchable and reusable.

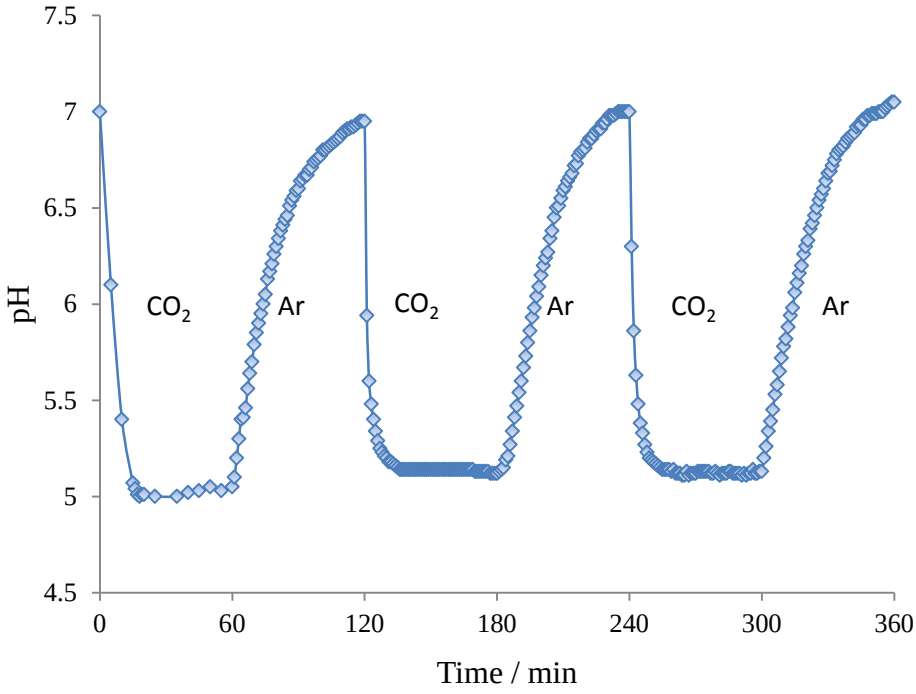


Figure 6.5.5 pH of solution during CO_2/Ar cycles in 100 mL H_2O containing 100 mg of switchable nanoparticles at 1 atm CO_2 and 1 atm Ar and 18 °C

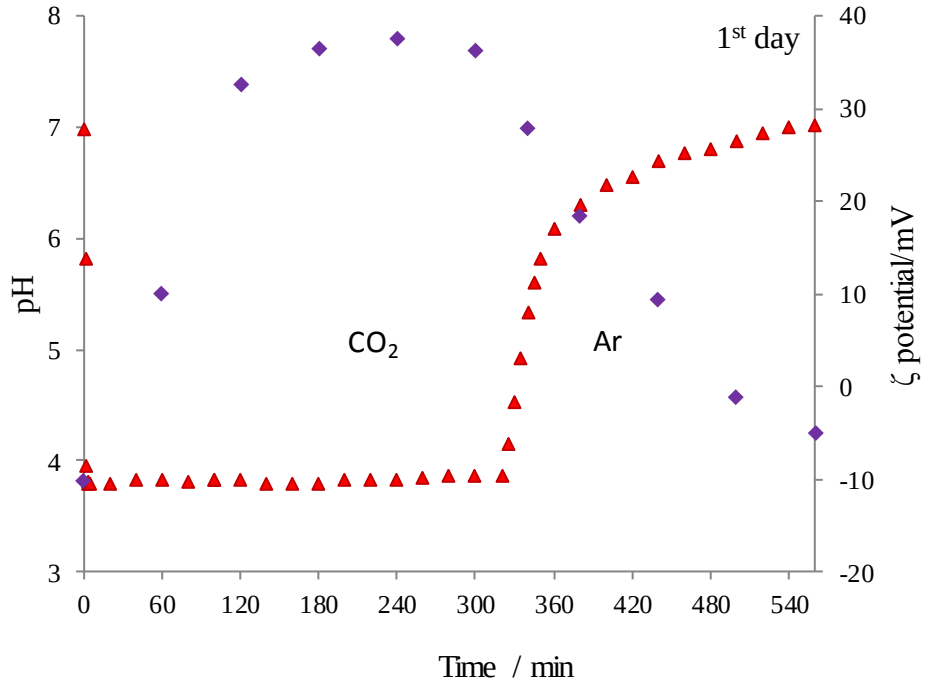


Figure 6.5.6 Zeta potential (purple rhombuses) measurements in H_2O under CO_2 and Ar bubbling concomitant with pH indication (red triangles) in the first day of experiment

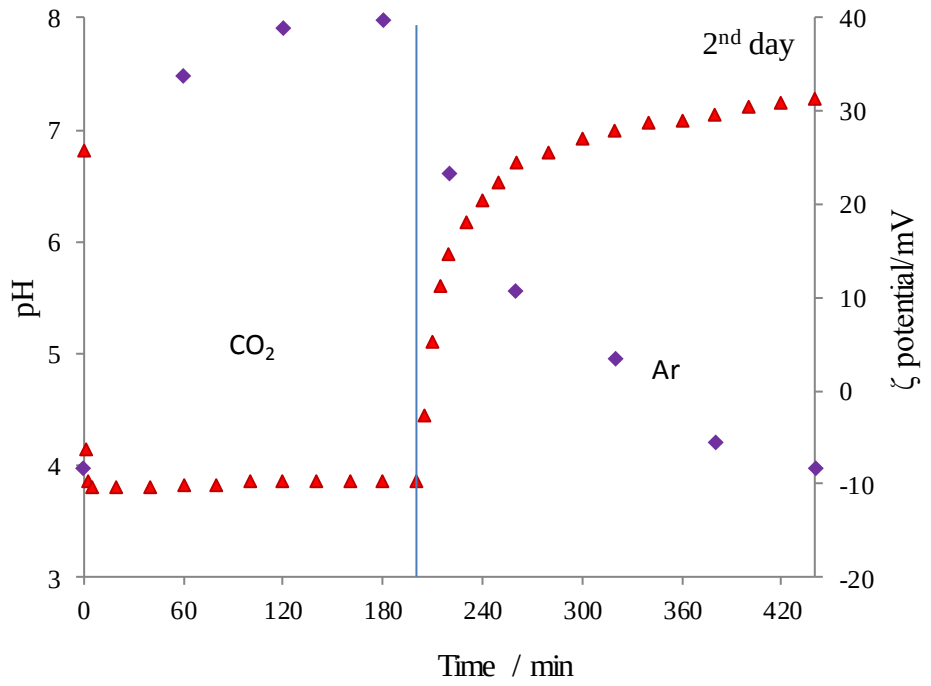


Figure 6.5.7 Zeta potential (purple rhombuses) measurements in H_2O under CO_2 and Ar bubbling concomitant with pH indication (red triangles) in the second day of experiment

6.6 Conclusions on switchable nanoparticles synthesis

In conclusion, amidine functionalised cellulose nanocrystals were synthesised based on previously obtained cellulose 3-((2-aminoethyl)thio)propanoate in a 24-hour reaction. The synthesis was an adapted method from the synthesis of switchable surfactants and it was successfully applied to CNC.

Furthermore, the behaviour of Switch-CNC was demonstrated in 2 experiments showing both reversibility and repeatability by measuring the zeta potential upon bubbling with CO_2 and flushing back with Ar. A possible application for these newly synthesised nanoparticles is in the field of Pickering emulsions.

7 Experimental

C, N, H analysis was carried out by the University of Nottingham Elemental Analysis service using a CE-440 Elemental Analyser manufactured by Exeter Analytical while S was determined on a Thermo Scientific 1112 Flash EA and halogen analysis were run by the University of Leeds on a CE Instruments Flash EA2000. Powder X-Ray diffraction was determined on a PANalytical X'Pert Pro multi-purpose Device. FT-IR spectra were recorded on a Thermo-Nicolet 380 FT-IR spectrometer in transmission mode from Thermo Electron Corporation using KBr disks. X-ray photoelectron spectroscopy spectra were recorded using a Kratos AXIS ULTRA with a mono-chromated Al kα X-ray source. ^{1}H Nuclear Magnetic Resonance measurements were run on a Bruker DPX300 NMR Spectrometer and Mass Spectrometry was performed on a Bruker MicroTOF (Time of Flight) mass spectrometer using Electron Spray Ionization (ESI).

7.1 Materials

Cellulose nanocrystals were prepared from cotton wool by acid hydrolysis as described in Chapter 2. Cotton wool together with Analytical Reagent Grade dichloromethane (DCM), ethanol (EtOH), *N*,*N*-Dimethylformamide (DMF), dimethyl sulfoxide (DMSO), MeOH and hydrochloric acid (36 %) (HCl), potassium carbonate (K_2CO_3), and potassium hydroxide (KOH) were purchased from Fisher Scientific. Acrylic acid (AA), methacrylic acid (MAA), *N,N'*- diisopropylcarbodiimide (DIC), triethylamine (Et_3N) and 1-methylimidazole, 3-mercaptopropyltrimethoxysilane (3-(trimethoxysilyl)-1-propanethiol) 95%, 1,2-ethanedithiol (ethane-1,2-dithiol), cysteamine (2-aminoethanethiol), cysteamine hydrochloride (2-aminoethanethiol

hydrochloride), hexylamine 99%, sodium hydroxide (NaOH), and *N*,*N*-dimethylacetamide dimethyl acetal 90% were purchased from Sigma Aldrich. 4-Dimethylaminopyridine (DMAP) was procured from Fluka. Extra dry 99.9 % DCM, extra dry 99.8% DMF, extra dry pyridine kept over molecular sieve 99.5% (Py), extra dry tetrahydrofuran (THF), carbazole (96 %) (Cz), methyl bromoacetate (99 %), bromoacetic acid 99%, bromoacetyl bromide 98+%, and orange II sodium salt (90% pure dye content) were procured from Acros Organics. *p*-Toluenesulfonyl chloride (98 %) (TsCl) was procured from Alfa Aesar and acryloyl chloride was procured from Merk. Cellulose extraction thimbles were purchased from VWR International. All chemicals were used as received.

7.2 Cellulose nanocrystals

Cellulose nanocrystals were prepared by acid hydrolysis of cotton wool (51.42 g) for 35 minutes in a 64 % H_2SO_4 at 45 °C solution bath under continuous stirring. The resulting nanowhisker suspension was diluted with deionized water and centrifuged three times at 10,000 rpm at 10 °C for 40 min, followed each time by replacing the supernatant with de-ionized water. Dialysis to neutrality of the nanowhisker suspension against tap water for 2 days was performed to remove residual free acid. For a homogeneous dispersion of the nanowhiskers in water, the suspension was sonified for 5 minutes at 15 % amplitude, at a maximum temperature of 35 °C using a Branson Sonifier. Then, the dispersion was filtered through a fritted glass filter No. 2 and ion-exchanged with Amberlite resin (100 g) for 24 h, to replace surface cations with protons. The stable suspension was filtered and sonicated once again, frozen in liquid nitrogen and freeze-dried on a Heto PowerDry PL600 apparatus. The purification of cellulose nanowhiskers was carried out with EtOH Soxhlet extraction for 3 days.[198] The nanowhiskers were dried *in vacuo* and were used as such for surface modification reactions. Found: C, 41.96; H, 6.00 %. Calculated for $(C_6H_{10}O_5)_n$: C, 43.43; H, 6.21 %. $\bar{\nu}_{max}$ (KBr) / cm^{-1} 3345 ν(O–H), 2900 ν(C–H), 1636 δ (H_2O), 1430 δ(C–O–H), 1337 δ(C–

O–H), 1317 δ(C–O–H), 1205 ν(C–O–C, glycosidic), 1163 ν(C–O–C, glycosidic, asym.), 1112 ν(C2–OH), 1059 ν(C3–OH), 1033 ν(C6–OH), 708 ω(C-OH), 666 ω(C-OH).

7.3 Synthesis of cellulose acrylate through the DIC/DMAP methodology

Cellulose nanocrystals (0.5 g, 1.5 mmol/g) and DMAP (0.005 g, 0.04 mmol) were suspended in dry DCM (30 ml) under argon atmosphere, before the DIC (1.29 ml, 8.25 mmol) and acrylic acid (0.56 ml, 8.25 mmol) were added. The reaction was conducted for 5 days at room temperature followed by filtration of the resulting white suspension through a cellulose Soxhlet extraction thimble and purification of the reaction product by Soxhlet extraction with DCM for 24 hours and EtOH for a further 24 hours. The resulting modified nanocrystals were dried in vacuo to a white solid (DS_{surf} = 0.94). Found: C, 43.97; H, 5.17; N, 0.15 %. Calc. for $C_{6.90}H_{10.9}O_{5.3}$: C, 43.99; H 5.76 %. $\bar{\nu}_{max}$ (KBr) / cm^{-1} 3345 ν(O–H), 2901 ν(C–H), 1726 ν(C=O), 1653 ν(C=C), 1636 ν(C=C), 1573 ν(C=C), 1429 δ(C–O–H), 1337 δ(C–O–H), 1317 δ(C–O–H), 1205 ν(C–O–C, glycosidic), 1162 ν(C–O–C, glycosidic, asym.), 1112 ν(C2–OH), 1059 ν(C3–OH), 1034 ν(C6–OH), 809 ω(C-OH), 708 ω(C-OH), 666 ω(C-OH).

7.4 Synthesis of cellulose methacrylate through the DIC/DMAP methodology

Cellulose nanocrystals (0.5 g, 1.5 mmol/g) and DMAP (0.005 g, 0.04 mmol) were suspended in dry DCM (30 ml) under an argon atmosphere, before the DIC (1.29 ml, 8.25 mmol) and methacrylic acid (0.69 ml, 8.25 mmol) were added. The reaction was carried out for 5 days at room temperature followed by the filtration of the resulting white suspension through a cellulose Soxhlet extraction thimble and purification of the reaction product by Soxhlet extraction with DCM for 24 hours and EtOH 24 hours. The resulting modified nanocrystals were dried *in vacuo* to give a white powder (DS_{surf} = 0.52). Found: C, 43.6; H, 6.04; N, 0.08 %. Calc. for $C_{6.65}H_{10.81}O_{5.16}$: C, 43.62; H 5.97

%. $\bar{\nu}_{max}$ (KBr) / cm^{-1}/ 3345 ν(O–H), 2901 ν(C–H), 1712 ν(C=O), 1636 ν(C=C), 1429 δ(C–O–H), 1337 δ(C–O–H), 1317 δ(C–O–H), 1205 ν(C–O–C, glycosidic), 1162 ν(C–O–C, glycosidic, asym.), 1112 ν(C2–OH), 1059 ν(C3–OH), 1034 ν(C6–OH), 707 ω(C–OH), 667 ω(C–OH).

7.5 Synthesis of cellulose acrylate through the TsCl/Py methodology

Cellulose nanocrystals (1 g) and TsCl (1.14 g) were suspended in Py (50 ml) before adding acrylic acid (0.41 ml). The reaction was left under stirring at 80 °C for 24 hours. The orange-red suspension was filtered through a cellulose Soxhlet extraction thimble and purified by Soxhlet extraction with DCM for 24 hours and EtOH 24 hours. The resulting modified nanocrystals were dried *in vacuo* to give slightly off-white solid nanoparticles (DS_{surf} = 1.10). Found: C, 43.25; H, 6.17; N, 0.56 %. Calc. for $C_{6.84}H_{10.84}O_{5.28}$: C, 43.23; H 5.86 %. $\bar{\nu}_{max}$ (KBr) / cm^{-1} 3345 ν(O−H), 2901 ν(C−H), 1723 ν(C=O), 1635 ν(C=C), 1573 ν(C=C) 1429 δ(C−O−H), 1336 δ(C−O−H), 1317 δ(C−O−H), 1205 ν(C−O−C, glycosidic), 1162 ν(C−O−C, glycosidic, asym.), 1112 ν(C_2−OH), 1059 ν(C_3−OH), 1034 ν(C_6−OH), 707 ω(C-OH), 667 ω(C−OH).

7.6 Synthesis of cellulose methacrylate through the TsCl/Py methodology

Cellulose nanocrystals (0.5 g) and TsCl (0.524 g) were suspended in Py (50 ml) under inert atmosphere, before adding methacrylic acid (0.23 ml). The reaction was left under stirring at 80 °C for 16 hours. After reaction, the orange-red suspension was filtered through a cellulose Soxhlet extraction thimble and purified by Soxhlet extraction with DCM for 24 hours and EtOH for 72 hours. The resulting modified nanocrystals were dried *in vacuo* to give slightly white-cream powder (DS_{surf} = 0.95). Found: C, 44.79; H, 5.71; N, 0.75 %. Calc. for $C_{7.23}H_{10.54}O_{5.30}$: C, 44.76; H 5.88 %. $\bar{\nu}_{max}$(KBr) / cm^{-1} 3345 ν(O−H), 2901 ν(C−H), 1714 ν(C=O), 1636 ν(C=C), 1429 δ(C−O−H), 1371 δ(C−O−H), 1317 δ(C−O−H), 12035 ν(C−O−C, glycosidic), 1162

ν(C−O−C, glycosidic, asym.), 1112 ν(C_2−OH), 1059 ν(C_3−OH), 1034 ν(C_6−OH), 707 ω(C-OH), 667 ω(C−OH).

7.7 Synthesis of cellulose acrylate through the TsCl/Et_3N methodology

Cellulose nanocrystals (0.5 g) and TsCl (0.524 g) were suspended in Et_3N (50 ml) before adding the acrylic acid (0.188 ml). The reaction was left under stirring at 80 °C for 16 hours. The suspension was filtered through a cellulose Soxhlet extraction thimble and purified by Soxhlet extraction with DCM for 24 hours and EtOH for 72 hours. The resulting modified nanocrystals were dried *in vacuo* to give a white powder. (DS_{surf} = 0.56). Found: C, 43.04; H, 6.10; N, 0.48 %. Calc. for $C_{6.56}H_{10.56}O_{5.18}$: C, 43.06; H 5.76 %. $\bar{\nu}_{max}$ (KBr) / cm^{-1} 3344 ν(O−H), 2901 ν(C−H), 1731 ν(C=O), 1634 ν(C=C), 1429 δ(C−O−H), 1336 δ(C−O−H), 1317 δ(C−O−H), 1205 ν(C−O−C, glycosidic), 1162 ν(C−O−C, glycosidic, asym.), 1112 ν(C_2−OH), 1058 ν(C_3−OH), 1034 ν(C_6−OH), 707 ω(C-OH), 666 ω(C−OH).

7.8 Synthesis of cellulose acrylate with acryloyl chloride through the Et_3N/DMF methodology

Cellulose nanocrystals (1 g) were suspended in dry DMF (150 ml) under inert atmosphere before Et_3N (32.05 ml) was added and acryloyl chloride (16.25 ml) was added dropwise through an addition funnel attached to the 3-neck round bottom flask, while the entire setup was placed into an ice bath. Once the acryloyl chloride addition started, Ar flow was maintained until all the acyl chloride was added. Once finished, the reaction flask was brought to room temperature and vigorously stirred. The reaction was left under stirring at 40 °C for 24 hours under a constant Ar atmosphere. The purification consisted of acetone and water centrifugation/washing steps and Soxhlet extraction with EtOH (24 hours) and DCM (24 hours). The resulting modified nanocrystals were dried *in vacuo* to give yellow solid nanoparticles (DS_{surf} = 2.11). Found:

C, 46.45; H, 5.95; N, 0.27 %. Calc. for $C_{8.0}H_{12.04}O_{5.58}$: C, 46.42; H 5.69 %. $\bar{\nu}_{max}$(KBr) / cm^{-1} 3345 ν(O−H), 2902 ν(C−H), 1728 ν(C=O), 1634 ν(C=C), 1430 δ(C−O−H), 1336 δ(C−O−H), 1317 δ(C−O−H), 1205 ν(C−O−C, glycosidic), 1162 ν(C−O−C, glycosidic, asym.), 1112 ν(C_2−OH), 1059 ν(C_3−OH), 1034 ν(C_6−OH), 707 ω(C-OH), 668 ω(C−OH).

7.9 Synthesis of methyl 2-(9*H*-carbazol-9-yl) acetate

9-*H*-carbazole (5.05 g, 30.2 mmol) was stirred with dry K_2CO_3 (11.12 g, 2.66 equiv.) in extra dry 99.8 % DMF (50 mL) under argon (Ar) for 45 min at 50 °C before methyl bromo acetate (8.5 mL, 3 equiv.) was added in aliquots over 3.5 hours. The reaction was then stirred at 50 °C for 14 hours, then quenched using cold water (100 mL) and stirred for another 1 hour on ice. The formed precipitate was filtered in a Buchner funnel and washed with cold water (200 mL). The product was dried under vacuum yielding a white crystalline powder. ^{1}H NMR (300 MHz, DMSO-d_6) ppm 3.68 (br. s., 3 H) 5.36 (br. s., 2 H) 7.23 (t, *J*=5.70 Hz, 2 H) 7.44 (t, *J*=6.92 Hz, 2 H) 7.55 (d, *J*=6.97 Hz, 2 H) 8.16 (d, *J*=5.46 Hz, 2 H); MS (ESI) m/z (%): 262 (M+Na, 100), 240 (M+H, 41), 180(33), 149(9).EA: Found: C, 74.75; H, 5.48; N, 5.48; Calculated: C, 75.30; H, 5.48; N, 5.85.

7.10 Synthesis of carbazole-9-yl-acetic acid

Methyl 9-*H*-carbazole-9-acetate (6 g, 25 mmol) and KOH solution (10%, 460 ml) were added into a large single-necked flask and heated to reflux for 5 hours under vigorous stirring. The mixture was cooled down in an ice bath and quenched with cold water (200 ml). The solution was acidified to a pH 4-5 with 10% diluted HCl (~260 ml). The formed precipitate was washed with water and dried *under vacuo*. The product was a white solid (yield 75 %). ^{1}H NMR (300 MHz, DMSO-d6) d ppm 5.22 (s, 2 H) 7.22 (t, J=7.21 Hz, 2 H) 7.43 (t, J=7.30 Hz, 2 H) 7.55 (d, J=7.91 Hz, 2 H) 8.15 (d, J=7.44 Hz, 2 H) MS (ESI)

m/z (%): 248 (M+Na, 100), 226(M+H, 33), 149(20), 116(11). EA: Found: C, 74.51; H, 4.87; N, 5.99. Calculated C, 74.65; H, 4.92; N, 6.22.

7.11 Synthesis of carbazole-9-yl-acetate cellulose through carbodiimide coupling

Cellulose nanocrystals (400 mg), carbazole-9-yl-acetic acid (1464 mg, 6.6 mmol) and 4-dimethylaminopyridine (5 mg, 41 μmol) were suspended in dry DCM (50 ml) under argon atmosphere, before *N,N'*- diisopropylcarbodiimide (1.03 ml, 6.6 mmol) was added. The reaction was conducted for 5 days at room temperature followed by the filtration of the resulting white-yellowish suspension through a cellulose Soxhlet extraction thimble and purification of the reaction product by Soxhlet extraction with DCM for 24 hours and EtOH for 24 hours. The resulting modified nanocrystals were dried *in vacuo* to give white solid nanoparticles (DS_{surf} = 0.1). Found: C, 43.67; H, 5.86; N, 0.23%. Calc. for $C_{6.42}H_{10.30}O_{5.03}N_{0.03}$: C, 43.68; H 6.06; N, 0.25 %. $\bar{\nu}_{max}$(KBr) / cm^{-1} 3345 ν(O−H), 2901 ν(C−H), 1744 ν(C=O), 1638 ν(C=C), 1485 ν(arom.), 1456 ν(arom.), 1429 δ(C−O−H), 1371 δ(C−N), 1336 δ(C−O−H), 1317 δ(C−O−H), 1206 ν(C−O−C, glycosidic), 1162 ν(C−O−C, glycosidic, asym.), 1112 ν(C2−OH), 1059 ν(C3−OH), 1034 ν(C6−OH), 751 ω(C-OH), 707 ω(C−OH), 665 ω(C−OH).

7.12 Synthesis of carbazole-9-yl-acetate cellulose through the TsCl/Py methodology

Cellulose nanocrystals (500 mg), carbazole-9-yl-acetic acid (450 mg, 2 mmol), and *p*-toluenesulfonyl chloride (381 mg, 2 mmol) were suspended in dry pyridine (50 ml) under argon atmosphere and heated at 80 °C for 24 hours. The solid product was filtered from the red suspension through a cellulose Soxhlet extraction thimble followed by the purification of the reaction product by Soxhlet extraction with DCM for 24 hours and EtOH for 72 hours. The resulting modified nanocrystals were dried in vacuo to give white-cream solid

nanoparticles (DS_{surf} = 0.72) Found: C, 51.42; H, 5.65; N, 1.57%. Calc. for $C_{9.38}H_{12.41}O_{5.24}N_{0.24}$: C, 51.03; H 5.60; N, 1.59 %. $\bar{\nu}_{max}$ (KBr) / cm^{-1} 3344 ν(O−H), 2900 ν(C−H), 1748 ν(C=O), 1627 ν(C=C), 1599 ν(C=C), 1485 ν(arom.), 1456 ν(arom.), 1428 δ(C−O−H), 1356 δ(C−N), 1324 δ(C−N), 1280 ν(C−O−C, glycosidic), 1161 ν(C−O−C, glycosidic, asym.), 1112 ν(C2−OH), 1059 ν(C3−OH), 1034 ν(C6−OH), 751 ω(C-OH), 722 ω(C-OH), 667 ω(C−OH).

7.13 Synthesis of coumarin-3-carboxylate cellulose through the TsCl/Py methodology

Cellulose nanocrystals (500 mg), coumarin-3-carboxylate (522 mg, 2.75 mmol), and *p*-toluenesulfonyl chloride (524 mg, 2.75 mmol) were suspended in dry pyridine (50 ml) under argon atmosphere and heated at 80 °C for 16 hours. The solid product was filtered from suspension through a cellulose Soxhlet extraction thimble followed by the purification of the reaction product by Soxhlet extraction with DCM for 24 hours and EtOH for 72 hours. The resulting modified nanocrystals were dried *in vacuo* to give white-cream solid nanoparticles (DS_{surf} = 1.33). Found: C, 50.00; H, 4.89%. Calc. for $C_{10.55}H_{12.27}O_{6.36}$: C, 50.02; H 4.65 %. $\bar{\nu}_{max}$(KBr) / cm^{-1} 3345 ν(O−H), 2901 ν(C−H), 1762 ν(C=O), 1609 ν(C=C), 1566 ν (arom.), 1455 ν (arom.) 1428 δ(C−O−H), 1335 δ(C−O−H), 1314 δ(C−O−H), 1246 ν(C–O–C), 1208 ν(C−O−C, glycosidic), 1162 ν(C−O−C, glycosidic, asym.), 1112 ν(C2−OH), 1059 ν(C3−OH), 1033 ν(C6−OH), 795 ω(C-OH), 763 ω(C-OH), 705 ω(C−OH), 666 ω(C−OH).

7.14 Synthesis of bromoacetate cellulose

In a three-necked round bottom flask equipped with an addition funnel and a condenser, cellulose nanocrystals (0.5 g) were initially flushed with argon before 100 ml of dry DMF were transferred into the reaction flask and another 20 ml added to the addition funnel. The flask was kept under an Ar atmosphere

for the duration of the reaction. Triethylamine (16 ml, 115 mmol) was added over the cellulose nanocrystal reaction mixture and bromoacetyl bromide (8.71 ml, 100 mmol) was added to the DMF in the addition funnel. The reaction flask was immersed in an ice bath before the bromoacetyl bromide solution was added dropwise. The reaction mixture was subsequently heated and left to react for 24 hours at 40 °C. The purification of the very dark brown reaction mixture was performed by filtration of the reaction suspension followed by washing with 500 ml DCM in order to dissolve formed triethylamine hydrogen bromide. The particles were then washed with acetone (100 ml), water (100 ml), and again acetone (100 ml), followed by Soxhlet extraction with DCM (24 hours) and *in vacuo* drying to give dark brown nanoparticles with a DS_{surf} = 1.36. Found: C, 39.58; H, 4.91; Br, 15.7; N, 0.91. Calc. for $C_{6.83}H_{10.41}O_{5.0}Br_{0.83}$: C, 36.52; H 4.82; Br 15.68 %. $\bar{\nu}_{max}$(KBr) / cm^{-1} 3344 ν(O−H), 2901 ν(C−H), 1745 ν(C=O), 1638 δ (H_2O), 1429 δ(C−O−H), 1336 δ(C−O−H), 1317 δ(C−O−H), 1280 ν(C−O−C, glycosidic), 1206 ν(C−O−C, glycosidic), 1162 ν(C−O−C, glycosidic, asym.), 1112 ν(C_2−OH), 1059 ν(C_3−OH), 1034 ν(C6−OH), 708 ω(C−OH), 666 ω(C−OH).

7.15 Synthesis of pyridinium acetate cellulose bromide - 1[Br][PyAc]-g-CNC

In a Schlenk tube, bromoacetate cellulose (1BrAcCNC) (100 mg) was vacuum-argon purged three times before pyridine (30 ml) was added over the nanocrystals and the mixture was left to react at 80 °C for 24 hours. The purification of the reaction product was performed by filtration of the reaction suspension into a cellulose thimble followed by Soxhlet extraction with DCM (24 hours) and *in vacuo* drying of the resulting brown nanoparticles with a DS_{surf} (N) = 0.84. Found: C, 42.91; H, 5.38; N, 2.24; Br, 10.02. Calc. for $C_{8.63}H_{12.63}O_{5.37}N_{0.37}Br_{0.37}$: C, 41.53; H 5.14; N, 2.12; Br 12.67 %. $\bar{\nu}_{max}$(KBr) / cm^{-1} 3344 ν(O−H), 2901 ν(C−H), 1755 ν(C=O), 1636 ν(C=C), 1490 ν(arom.), 1429 δ(C−O−H), 1337 δ(C−O−H), 1316 δ(C−O−H), 1280 ν(C−O−C, glycosidic), 1207 ν(C−O−C, glycosidic), 1162 ν(C−O−C, glycosidic, asym.),

1112 ν(C_2−OH), 1059 ν(C_3−OH), 1034 ν(C_6−OH), 709 ω(C−OH), 668 ω(C−OH).

7.16 Synthesis of methyl imidazolium acetate cellulose - 1[Br][MeImAc]-g-CNC

In a Schlenk tube, bromoacetate cellulose (1BrAcCNC) (100 mg) was vacuum-argon purged three times before 1-methylimidazole (30 ml) was added over the nanocrystals and the reaction was left to react at 80 °C for 24 hours. The purification of the reaction product was performed by filtration of the reaction suspension into a cellulose thimble followed by Soxhlet extraction with DCM (24 hours) and *in vacuo* drying of the resulting brown nanoparticles with a DS_{surf} (N) = 0.71 Found: C, 42.96; H, 5.71; N, 3.82; Br, 5.65. Calc. for $C_{7.81}H_{12.42}O_{5.30}N_{0.60}Br_{0.30}$: C, 39.82; H 4.39; N, 3.79; Br 10.85 %. $\bar{\nu}_{max}$(KBr) / cm^{-1} 3345 ν(O−H), 2901 ν(C−H), 1751 ν(C=O), 1634 ν(C=C), 1580 ν(arom.), 1518 ν(arom.), 1429 δ(C−O−H), 1337 δ(C−O−H), 1316 δ(C−O−H), 1280 ν(C−O−C, glycosidic), 1205 ν(C−O−C, glycosidic), 1162 ν(C−O−C, glycosidic, asym.), 1112 ν(C2−OH), 1059 ν(C3−OH), 1034 ν(C6−OH), 708 ω(C−OH), 666 ω(C−OH).

7.17 Synthesis of bromoacetate cellulose in THF

In a three-necked round bottom flask equipped with a condenser, cellulose nanocrystals (0.5 g) were flushed with argon before 50 ml of dry THF and triethylamine (16 ml, 115 mmol) were added to the reaction flask followed by dropwise addition of bromoacetyl bromide (8.71 ml, 100 mmol). The reaction flask was immersed in an ice bath before the bromoacetyl bromide solution was added dropwise and the reaction mixture was subsequently heated and left to react for 24 hours at 40 °C. The purification of the dark brown reaction mixture was performed by filtration of the reaction suspension, followed by THF (200 ml)/water (100 ml)/acetone (100 ml) washing and Soxhlet extraction

with DCM (24 hours) and EtOH (24 hours) and *in vacuo* drying of the resulting light brown nanoparticles with a DS_{surf} (Br) = 1.02. Found: C, 42.33; H, 4.76; N, 0.59; Br, 12.4. Calc. for $C_{6.61}H_{10.30}O_{5.0}Br_{0.61}$: C, 37.86; H 4.84; Br 12.42 %. $\bar{\nu}_{max}$(KBr) / cm^{-1} 3345 ν(O−H), 2901 ν(C−H), 1737 ν(C=O), 1620 δ (H_2O), 1429 δ(C−O−H), 1336 δ(C−O−H), 1316 δ(C−O−H), 1281 ν(C−O−C, glycosidic), 1206 ν(C−O−C, glycosidic), 1162 ν(C−O−C, glycosidic, asym.), 1112 ν(C2−OH), 1058 ν(C3−OH), 1033 ν(C6−OH), 706 ω(C−OH), 666 ω(C−OH).

7.18 Synthesis of bromoacetate cellulose in Et_3N

Cellulose nanocrystals (0.4 g) were flushed with argon and suspended in triethylamine (100 ml) before bromoacetyl bromide (5.22 ml, 60 mmol) was added dropwise and kept at 40 °C for 24 hours. The purification of the reaction product was performed by filtration of the reaction suspension through a cellulose thimble followed by Soxhlet extraction with DCM (24 hours) and EtOH (72 hours) and *in vacuo* drying of the resulting light brown nanoparticles with a DS_{surf} (Br) = 0.03. Found: C, 42.18; H, 6.28; N, 0.0; Br, 0.5. Calc. for $C_{6.02}H_{10.01}O_{5.0}Br_{0.02}$: C, 42.15; H 6.06; Br 0.52 %.

7.19 Synthesis of pyridinium acetate cellulose bromide 2[Br][PyAc]-g-CNC

Cellulose nanocrystals (0.4 g) were flushed with argon and suspended in dry pyridine (100 mL) before bromoacetyl bromide (5.22 ml, 60 mmol) was added dropwise and left to react at 80 °C for 24 hours. The purification of the reaction product was performed by filtration of the reaction mixture through a cellulose thimble followed by water washing, Soxhlet extraction with EtOH (72 hours) and DCM (24 hours), and *in vacuo* drying giving light brown nanoparticles with a DS_{surf}(N) = 0.25. Found: C, 42.87; H, 5.87; N, 0.91; Br, 1.8. Calc. for $C_{6.87}H_{10.87}O_{5.}12N_{0.12}Br_{0.12}$: C, 41.98; H 5.98; N, 0.93; Br 5.32 %. $\bar{\nu}_{max}$(KBr) /

cm^{-1} 3345 ν(O−H), 2900 ν(C−H), 1735 ν(C=O), 1636 ν(C=C), 1482 ν(arom.), 1428 δ(C−O−H), 1336 δ(C−O−H), 1317 δ(C−O−H), 1280 ν(C−O−C, glycosidic), 1205 ν(C−O−C, glycosidic), 1162 ν(C−O−C, glycosidic, asym.), 1112 ν(C2−OH), 1059 ν(C3−OH), 1034 ν(C6−OH), 706 ω(C−OH), 667 ω(C−OH).

7.20 Synthesis of methyl imidazolium acetate cellulose bromide 2[Br][MeImAc]-g-CNC

Cellulose nanocrystals (0.5 g) were flushed with argon and suspended in dry 1-methylimidazole (100 mL) before bromoacetyl bromide (8.71 ml, 100 mmol) was added dropwise and heated at 80 °C for 24 hours. The purification of the reaction product was performed by filtration of the reaction mixture through a cellulose thimble followed by washing with a water/EtOH mixture and Soxhlet extraction with EtOH (24 hours) and DCM (24 hours) and *in vacuo* drying giving brown nanoparticles with a DS_{surf} (N) = 1.06. Found: C, 43.95; H, 5.70; N, 4.20; Br, 5.80. Calc. for $C_{8.07}H_{12.76}O_{5.34}N_{0.69}Br_{0.34}$: C, 39.05; H 5.08; N, 4.16; Br 11.91 %. $\bar{\nu}_{max}$(KBr) / cm^{-1} 3345 ν(O−H), 2901 ν(C−H), 1732 ν(C=O), 1633 ν(C=C), 1576 ν(C=C), 1428 δ(C−O−H), 1336 δ(C−O−H), 1316 δ(C−O−H), 1280 ν(C−O−C, glycosidic), 1205 ν(C−O−C, glycosidic), 1162 ν(C−O−C, glycosidic, asym.), 1112 ν(C2−OH), 1059 ν(C3−OH), 1034 ν(C6−OH), 708 ω(C−OH), 666 ω(C−OH).

7.21 Synthesis of pyridinium acetate cellulose bromide 3[Br][PyAc]-g-CNC

Cellulose nanocrystals (0.5 g), bromoacetic acid (0.382 g, 2.75 mmol) and *p*-toluenesulfonyl chloride (0.524 g, 2.75 mmol) were flushed with argon and suspended in dry pyridine (50 mL) and left to react at 80 °C for 16 hours. The purification of the reaction product was performed by filtration of the reaction mixture through a cellulose thimble followed by Soxhlet extraction with DCM

(24 hours) and EtOH (72 hours). *In vacuo* drying gave light brown nanoparticles with a DS_{surf} (N) = 0.35. Found: C, 42.55; H, 5.80; N, 0.90; Br, 4.60. Calc. for $C_{6.86}H_{10.86}O_{5.12}N_{0.12}Br_{0.12}$: C, 41.98; H 5.49 N, 0.92; Br 5.28 %. $\bar{\nu}_{max}$(KBr) / cm^{-1} 3345 ν(O−H), 2901 ν(C−H), 1744 ν(C=O), 1638 ν(C=C), 1485 ν(arom.), 1456 ν(arom.), 1429 δ(C−O−H), 1336 δ(C−O−H), 1317 δ(C−O−H), 1280 ν(C−O−C, glycosidic), 1206 ν(C−O−C, glycosidic), 1162 ν(C−O−C, glycosidic, asym.), 1112 ν(C2−OH), 1059 ν(C3−OH), 1034 ν(C6−OH), 707 ω(C−OH), 665 ω(C−OH).

7.22 Synthesis of cellulose 2-methyl-3-((3-trimethoxysilyl)propyl)thio) propanoate

Cellulose methacrylate (synthesis 7.4 with a DS_{surf}(C) of 0.52) (0.2 g, 0.6 mmol), 3-mercaptopropyltrimethoxysilane (0.15ml, 0.8 mmol) and hexylamine (0.013 ml, 0.09 mmol) were suspended in MeOH (30 ml) in a round bottom flask. The reaction was left to react for 1 hour and 4 hours respectively at room temperature followed by the filtration of the resulting white suspension through a cellulose Soxhlet extraction thimble and purification of the reaction product by Soxhlet extraction with DCM for 24 hours and EtOH for further 24 hours. The resulting modified nanocrystals were dried *in vacuo* to give a white powder of solid nanoparticles. 1-hour reaction results - Found: C, 44.29; H, 6.12; N, 0.09, S 0 %. Calc. for $C_{6.0}H_{10.0}O_{5.0}S_{0.0}Si_{0.0}$: C, 44.44; H 6.21 S, 0.0; Si 0 %. $\bar{\nu}_{max}$(KBr) / cm^{-1} 3345 ν(O−H), 2901 ν(C−H), 1715 ν(C=O), 1637 ν(C=C), 1429 δ(C−O−H), 1317 δ(C−O−H), 1206 ν(C−O−C, glycosidic), 1162 ν(C−O−C, glycosidic, asym.), 1112 ν(C2−OH), 1059 ν(C3−OH), 1034 ν(C6−OH), 707 ω(C−OH), 667 ω(C−OH). 4-hour reaction results - Found: C, 43.52; H, 5.99; N, 0.07; S, 0 %. Calc. for $C_{6.0}H_{10.0}O_{5.0}S_{0.0}Si_{0.0}$: C, 44.44; H 6.21 S, 0.0; Si 0.0 %. $\bar{\nu}_{max}$(KBr) / cm^{-1} 3345 ν(O−H), 2901 ν(C−H), 1719 ν(C=O), 1637 ν(C=C), 1430 δ(C−O−H), 1371 δ(C−O–N), 1336 δ(C−O−H), 1317 δ(C−O−H), 1281 ν(C−O−C, glycosidic), 1163 ν(C−O−C, glycosidic, asym.), 1112 ν(C2−OH), 1059 ν(C3−OH), 1034 ν(C6−OH), 707 ω(C−OH), 665 ω(C−OH).

7.23 Synthesis of cellulose 3-((3-trimethoxysilyl)propyl)thio) propanoate

Cellulose acrylate (synthesis 7.3 with a $DS_{surf}(C)$ = 0.94) (0.5 g, 1.5 mmol), 3-mercaptopropyltrimethoxysilane (0.462 ml, 2.49 mmol) and hexylamine (0.329 ml, 2.49 mmol) were suspended in DCM (30 ml) in a round bottom flask. The reaction was left to react for 24 hours at room temperature followed by the filtration of the resulting white suspension through a cellulose Soxhlet extraction thimble and purification of the reaction product by Soxhlet extraction with DCM for 24 hours and EtOH for 24 hours. The resulting modified nanocrystals were dried *in vacuo* to give a white powder of solid nanoparticles ($DS_{surf}(S)$ = 0.19). Found: C, 42.42; H, 5.87; N, 0.43, S 1.04 %. Calc. for $C_{6.52}H_{11.11}O_{5.23}S_{0.05}Si_{0.05}$: C, 44.32; H 6.33 S, 1.06; Si 0.93 %. $\bar{\nu}_{max}$(KBr) / cm^{-1} 3345 ν(O−H), 2902 ν(C−H), 1736 ν(C=O), 1662 ν(C=C), 1572 ν(C=C), 1429 δ(C−O−H), 1371 δ(C−O–H), 1337 δ(C−O−H), 1317 δ(C−O−H), 1235 ν(C−O−C, glycosidic), 1162 ν(C−O−C, glycosidic, asym.), 1112 ν(C2−OH), 1059 ν(C3−OH), 1034 ν(C6−OH), 707 ω(C−OH), 667 ω(C−OH).

7.24 Synthesis of cellulose 3-((2-mercaptoethyl) thio) propanoate

Cellulose acrylate (synthesis 7.3 with a $DS_{surf}(C)$ = 0.94) (0.25 g, 0.75 mmol), 1,2-ethanedithiol (2.5 ml, 29.8 mmol) and hexylamine (0.25 ml, 1.89 mmol) were suspended in DCM (100 ml). The reaction was left to react for 48 hours at room temperature. The purification was carried out by Soxhlet extraction with DCM for 24 hours and EtOH for a further 24 hours. The resulting modified nanocrystals were dried *in vacuo* to give white solid nanoparticles ($DS_{surf}(S)$ = 0.24). Found: C, 43.88; H, 6.01; N, 0.13, S 2.59 %. Calc. for $C_{6.34}H_{10.62}O_{5.06}S_{0.13}$: C, 44.19; H 6.20 S, 2.56 %. $\bar{\nu}_{max}$(KBr) / cm^{-1} 3344 ν(O−H), 2902 ν(C−H), 1735 ν(C=O), 1650 ν(C=C), 1575 ν(C=C), 1429 δ(C−O−H), 1371 δ(C−O–H), 1337 δ(C−O−H), 1317 δ(C−O−H), 1205 ν

(C−O−C, glycosidic), 1162 ν (C−O−C, glycosidic, asym.), 1112 ν(C2−OH), 1059 ν(C3−OH), 1034 ν(C6−OH), 707 ω(C−OH), 666 ω(C−OH).

7.25 Synthesis of cellulose 3-((2-aminoethyl) thio) propanoate hydrochloride

Cellulose acrylate (synthesis 7.3 with a DS of 0.94) (0.1 g, 0.3 mmol) and 2-aminoethanethiol hydrochloride (0.017 g, 0.15 mmol) were suspended in EtOH (30 ml). The mixture was heated to reflux while stirring. Then 1.5 ml (0.15 mmol) of 0.1 M NaOH solution was added and the reflux was continued for 10 min followed by filtration of the reaction product through a Soxhlet extraction thimble and washing with 3×20 ml EtOH. The resulting modified nanocrystals were dialysed against deionised water for 5 days and dried *in vacuo* to give a white powder of solid nanoparticles. The same reactions were repeated for a reaction time of 15 min and with an increased molar equivalent of 10 times more than the initial excess. Ten min reaction results (DS_{surf}(S) = 0.15) - Found: C, 42.86; H, 5.95; N, 0.42, S 0.94 %. Calc. for $C_{6.29}H_{10.53}O_{5.04}S_{0.04}N_{0.04}Cl_{0.04}$: C, 44.21; H 6.21; N, 0.39 S, 0.91; Cl, 1.00 %. $\bar{\nu}_{max}$(KBr) / cm^{-1} 3345 ν(O−H), 2901 ν(C−H), 1731 ν(C=O), 1638 ν(C=C), 1585 ν(C=C), 1429 δ(C−O−H), 1371 δ(C−O–H), 1337 δ(C−O−H), 1317 δ(C−O−H), 1205 ν(C−O−C, glycosidic), 1162 ν(C−O−C, glycosidic, asym.), 1112 ν(C2−OH), 1059 ν(C3−OH), 1034 ν(C6−OH), 707 ω(C−OH), 667 ω(C−OH). Fifteen min reaction results (DS_{surf}(S) = 0.7) - Found: C, 42.41; H, 5.90; N, 0.29, S 0.48 %. Calc. for $C_{6.15}H_{10.28}O_{5.02}S_{0.02}N_{0.02}Cl_{0.02}$: C, 44.31; H 6.21; N, 0.21 S, 0.50; Cl, 0.55 %. $\bar{\nu}_{max}$(KBr) / cm^{-1} 3345 ν(O−H), 2901 ν(C−H), 1729 ν(C=O), 1639 ν(C=C), 1573 ν(C=C), 1429 δ(C−O−H), 1371 δ(C−O–H), 1336 δ(C−O−H), 1317 δ(C−O−H), 1205 ν(C−O−C, glycosidic), 1162 ν(C−O−C, glycosidic, asym.), 1112 ν(C2−OH), 1059 ν(C3−OH), 1034 ν(C6−OH), 707 ω(C−OH), 666 ω(C−OH).

7.26 Synthesis of cellulose 3-((2-aminoethyl)thio) propanoate in acetone

Cellulose acrylate (synthesis 7.5 with a DS = 1.10) (0.2 mg, 0.6 mmol) and cysteamine (0.46 g, 0.6 mmol) were suspended in acetone (50 ml) at room temperature. After 5 minutes half of the reaction suspension is filtered through a Soxhlet extraction thimble and thoroughly washed with EtOH. After 10 minutes, the rest of the reaction suspension was filtered and washed in the same manner as before through a second thimble. The resulting modified nanocrystals were dried *in vacuo* to give a white powder of solid nanoparticles. Five min reaction results ($DS_{surf}(S) = 0.08$) - Found: C, 44.38; H, 6.11; N, 0.40, S 0.48 %. Calc. for $C_{6.13}H_{10.26}O_{5.02}S_{0.02}N_{0.02}$: C, 44.46; H 6.24; N, 0.22 S, 0.50 %. $\bar{\nu}_{max}$(KBr) / cm^{-1} 3346 ν(O−H), 2902 ν(C−H), 1735 ν(C=O), 1646 ν(C=C), 1579 ν(C=C), 1427 δ(C−O−H), 1373 δ δ(C−O−H), 1317 δ(C−O−H), 1207 ν(C−O−C, glycosidic), 1162 ν(C−O−C, glycosidic, asym.), 1112 ν(C2−OH), 1058 ν(C3−OH), 1034 ν(C6−OH), 707 ω(C−OH), 665 ω(C−OH). Ten min reaction results ($DS_{surf}(S) = 0.06$) - Found: C, 44.84; H, 6.11; N, 0.39, S 0.38 %. Calc. for $C_{6.10}H_{10.20}O_{5.02}S_{0.02}N_{0.02}$: C, 44.46; H 6.23; N, 0.17 S, 0.40 %. $\bar{\nu}_{max}$(KBr) / cm^{-1} 3344 ν(O−H), 2901 ν(C−H), 1732 ν(C=O), 1651 ν(C=C), 1574 ν(C=C), 1429 δ(C−O−H), 1371 δ(C−O−H), 1336 δ(C−O−H), 1317 δ(C−O−H), 1206 ν(C−O−C, glycosidic), 1163 ν(C−O−C, glycosidic, asym.), 1112 ν(C2−OH), 1059 ν(C3−OH), 1034 ν(C6−OH), 708 ω(C−OH), 665 ω(C−OH).

7.27 Synthesis of cellulose 3-((2-aminoethyl)thio) propanoate in DMF/DMSO/H_2O

Cellulose acrylate (synthesis 7.5 with a DS = 1.10) (0.1 g, 0.3 mmol) and cysteamine (0.15, 2 mmol) were suspended in DMF, DMSO, or H_2O (30 ml) at room temperature and each was left to react for 10 minutes, followed by filtration through a Soxhlet extraction thimble and thorough washing with EtOH. The resulting modified nanocrystals were dried *in vacuo* to give a white

powder of solid nanoparticles. Reaction in DMSO results (DS_{surf}(S) = 0.20) - Found: C, 42.50; H, 6.14; N, 0.63, S 1.15 %. Calc. for $C_{6.29}H_{10.59}O_{5.05}S_{0.05}N_{0.05}$: C, 44.49; H 6.28; N, 0.49 S, 1.12 %. $\bar{\nu}_{max}$(KBr) / cm^{-1} 3345 ν(O−H), 2902 ν(C−H), 1734 ν(C=O), 1651 ν(C=C), 1527 ν(C=C), 1429 δ(C−O−H), 1371 δ(C−O−H), 1336 δ(C−O−H), 1317 δ(C−O−H), 1205 ν(C−O−C, glycosidic), 1162 ν(C−O−C, glycosidic, asym.), 1112 ν(C2−OH), 1059 ν(C3−OH), 1034 ν(C6−OH), 708 ω(C−OH), 665 ω(C−OH). Reaction in DMF results (DS_{surf}(S) = 0.21) - Found: C, 44.45; H, 6.23; N, 1.08, S 1.20 %. Calc. for $C_{6.31}H_{10.62}O_{5.06}S_{0.06}N_{0.06}$: C, 44.49; H 6.28; N, 0.51 S, 1.17 %. $\bar{\nu}_{max}$(KBr) / cm^{-1} 3345 ν(O−H), 2902 ν(C−H), 1733 ν(C=O), 1653 ν(C=C), 1558 ν(C=C), 1429 δ(C−O−H), 1371 δ(C−O−H), 1336 δ(C−O−H), 1317 δ(C−O−H), 1205 ν(C−O−C, glycosidic), 1162 ν(C−O−C, glycosidic, asym.), 1112 ν(C2−OH), 1059 ν(C3−OH), 1034 ν(C6−OH), 708 ω(C−OH), 666 ω(C−OH). Reaction in H_2O results (DS_{surf}(S) = 0.13) - Found: C, 44.28; H, 6.14; N, 0.56, S 0.79 %. Calc. for $C_{6.21}H_{10.42}O_{5.04}S_{0.04}N_{0.04}$: C, 44.47; H 6.26; N, 0.35 S, 0.81 %. $\bar{\nu}_{max}$(KBr) / cm^{-1} 3345 ν(O−H), 2901 ν(C−H), 1732 ν(C=O), 1652 ν(C=C), 1573 ν(C=C), 1429 δ(C−O−H), 1371 δ(C−O−H), 1336 δ(C−O−H), 1317 δ(C−O−H), 1205 ν (C−O−C, glycosidic), 1162 ν (C−O−C, glycosidic, asym.), 1112 ν(C2−OH), 1059 ν(C3−OH), 1034 ν(C6−OH), 707 ω(C−OH), 667 ω(C−OH).

7.28 Synthesis of cellulose 3-((2-aminoethyl) thio) propanoate in DCM

Cellulose acrylate (synthesis 7.8 with a DS of 2.11) (0.645 g, 1.935 mmol), cysteamine (0.995 g, 12.9 mmol) and hexylamine (0.018 ml, 0.14 mmol) were suspended in DCM (60 ml) in a round bottom flask. The reaction was left to react for 2 hours at 50 °C followed by filtration of the resulting white suspension through a Soxhlet extraction thimble and purification of the reaction product by Soxhlet extraction with DCM for 24 hours and EtOH for 48 hours. The resulting modified nanocrystals were dried *in vacuo* to give a white powder of solid nanoparticles (DS_{surf}(S) = 0.68 DS_{surf}(N) = 0.68). Found:

C, 45.47; H, 6.18; N, 1.54, S 3.55 %. Calc. for $C_{7.07}H_{12.15}O_{5.21}S_{0.21}N_{0.21}$: C, 44.59; H 6.42; N, 1.58 S, 3.62 %. $\bar{\nu}_{max}$(KBr) / cm^{-1} 3346 ν(O−H), 2902 ν(C−H), 1735 ν(C=O), 1647 ν(C=C), 1585 ν(C–N), 1429 δ(C−O−H), 1371 δ(C−O−H), 1336 δ(C−O−H), 1317 δ(C−O−H), 1206 ν(C−O−C, glycosidic), 1162 ν(C−O−C, glycosidic, asym.), 1112 ν(C2−OH), 1059 ν(C3−OH), 1034 ν(C6−OH), 709 ω(C−OH), 669 ω(C−OH).

7.29 Synthesis of switchable nanoparticles based on cellulose nanoparticles – 3-(2-(*N*,*N*-dimethylacetimideamide)ethylthio) propanoate cellulose nanoparticles

Cellulose 3-((2-aminoethyl)thiopropanoate (synthesis 7.28, DS_{surf}(N) = 0.68) (0.2 g, 0.6 mmol) and *N*,*N*-Dimethylacetamide dimethyl acetal (0.832 ml, 5.69 mmol) were suspended in dry acetone (5 ml) in a round bottom flask under inert atmosphere. The reaction is left to react for 24 hours at 60 °C followed by solvent and MeOH by-product removal under high-vacuum, and subsequent washing of the resulting yellow suspension with acetone and deionised water, filtration through a cellulose Soxhlet extraction thimble, and purification by Soxhlet extraction with EtOH for 24 hours. The resulting modified nanocrystals were dried *in vacuo* to give a yellow powder of solid nanoparticles (DS_{surf}(N) = 0.35 with the starting material DS_{surf}(N) = 0.68). Found: C, 46.30; H, 6.15; N, 1.64, S, 1.90 %. Calc. for $C_{6.99}H_{11.87}O_{5.11}S_{0.11}N_{0.22}$: C, 45.56; H 6.49; N, 1.67 S, 1.92 %. $\bar{\nu}_{max}$(KBr) / cm^{-1} 3343 ν(O−H), 2900 ν(C−H), 1731 ν(C=O), 1648 ν(C=C), 1430 δ(C−O−H), 1371 δ(C−O−H), 1336 δ(C−O−H), 1317 δ(C−O−H), 1206 ν(C−O−C, glycosidic), 1162 ν(C−O−C, glycosidic, asym.), 1112 ν(C2−OH), 1059 ν(C3−OH), 1034 ν(C6−OH), 709 ω(C−OH), 665 ω(C−OH).

PART III

Conclusions and Future Work

8 Conclusions and Future Work

This chapter represents an overview of the entire thesis by presenting the important results from each individual chapter and by recommending further work that could be carried out later to answer remaining questions or questions raised by the work in this thesis. Starting from the main aim of this thesis, the current work adds a substantial contribution to the field of surface modification of cellulose nanocrystals by adapting several esterification methodologies and developing new strategies and syntheses.

The current thesis starts with a substantial Introduction Chapter which introduces cellulose from AGU to supramolecular structure, continues with the morphology of cellulose fibrils and production and description of cellulose nanocrystals and later describes a wide range of surface cellulose nanocrystals modifications, part of which was applied in this thesis. Chapter 2 describes the different characterisation techniques (XRD, FT-IR, EA, XPS, AFM, TEM, UV-Vis, Fluorescence and Zeta potential) that were instrumental in the investigations carried out during this work. The following four chapters (Chapter 3, Chapter 4, Chapter 5 and Chapter 6) discuss the development and investigation of different esterification strategies and esterified CNC products. Chapter 7 presents the Experimental description of each reaction carried out in this thesis. Finally, Chapter 8 presents the Conclusions and Future Work resulted from this thesis as it is presented in here.

Chapter 3 starts with the development of a first esterification reaction applied to cellulose nanocrystals in this thesis, based on a literature method in which carbodiimide is used as a coupling agent in Steglich esterification.[136] Initially developed in my group as a simple method for the grafting of methacrylic acid, it gave a low degree of substitution ($DS_{surf}(C) = 0.2$).

Thus, the mild methodology which used *N*,*N*'-diisopropylcarbodiimide as a coupling agent, recently applied to cellulose nanocrystals, was tested. The esterification of cellulose nanocrystals with this reagent, catalysed by 4-dimethylaminopyridine was successfully applied to the synthesis of cellulose acrylate (DS_{surf}(C) = 0.94) and cellulose methacrylate (DS_{surf}(C) = 0.52) giving lower modifications when compared with the tosyl chloride methodology, but providing white crystalline materials and with potential applications for further modifications. Using the *N*,*N*'-diisopropylcarbodiimide/4-dimethylamino-pyridine methodology, white powder modified cellulose nanocrystals are obtained with an esterification efficiency dependent on the molar excess used and on the nature of the grafted acid. The DS_{surf} (C) = 0.94 for acrylate cellulose is almost double than for methacrylate cellulose modification (DS_{surf}(C) = 0.52) Considering the less reactive nature of methacrylic acid than the corresponding acrylic acid, as a result of electron-donating effect and the steric hindrance of α-methyl group, the difference between cellulose acrylate and cellulose methacrylate substitution degrees is unsurprising. A similar higher grafting efficiency of acrylic acid relative to methacrylic acid has also been seen under the tosyl chloride/pyridine reaction conditions with a grafting difference between the two modifications as it is indicated below.

Apart from carbodiimide mediated esterification, *p*-toluenesulfonyl chloride/pyridine, *p*-toluenesulfonyl chloride/triethylamine and esterifications with acryloyl chloride were also applied and compared in Chapter 3.

It was proven that for a relatively inert cellulose surface, esterification of cellulose nanocrystals with acrylic and methacrylic acid in *p*-toluenesulfonyl chloride/pyridine conditions requires a substantially lower excess of reagents (only an excess of two to three times considering 3 mmol/g OH groups) when compared with the traditional acryloyl chloride methodology.

Esterifications using *p*-toluenesulfonyl chloride/pyridine for the synthesis of methacrylate cellulose gave a degree of substitution of DS_{surf}(C) = 0.95 while for acrylate cellulose nanocrystals DS_{surf}(C) = 1.10, which shows this esterification methodology is a very efficient and straightforward method.

In addition to this, an esterification methodology of cellulose nanocrystals with tosyl chloride in triethylamine, intended to minimize the formation of secondary by-products and to avoid side reactions specific to the tosyl chloride/pyridine system, was proposed. Thus, in comparison with the slightly-coloured tosyl chloride/pyridine product, a purer white product was obtained. However, the obtained $DS_{surf}(C) = 0.56$ indicates a lower modification compared to *p*-toluenesulfonyl chloride/pyridine conditions, but this methodology is recommended whenever a white product is required, for example in optical applications. Considering the reactions in pyridine, the esterification of cellulose acrylate in triethylamine has also resulted in a lower decrease of crystallinity that could indicate that triethylamine is less of a swelling solvent for crystalline cellulose.

The final esterification methodology described in Chapter 3 was the traditional acyl halide esterification that was also applied to cellulose nanocrystals and involved the use of acryloyl chloride to obtain cellulose acrylate ($DS_{surf}(C) = 2.11$). As well, this methodology was used with bromoacetyl bromide to synthesise bromo acetate cellulose ($DS_{surf}(C) = 1.05$) in Chapter 5. The $DS_{surf}(C) = 2.11$ is indicative of primary and secondary hydroxyl groups surface modification and therefore a degree of substitution that exceeds the theoretical maximum degree of surface substitution of 1.5. With a crystallinity drop of 21 % considering the initial cellulose nanocrystals crystallinity of $\chi_C^R = 0.796$, acryloyl chloride cellulose nanocrystals esterification is a reaction in which the loss of crystallinity can be attributed on one hand to the very high extent of modification and therefore an increase of non-crystalline material on the surface of cellulose and on the other hand, this reaction also gave modification of some internal hydroxyl groups and so inherently a partial destruction of the crystallinity of the cellulose core. As a consequence of the very high molar excess used in this methodology and despite intensive purifications involved, the reaction products still contained some traces of by-products that are very difficult to remove, and may be trapped inside the CNC core. Therefore, as part of future work recommendations, further purification methods are still required to be investigated in this esterification strategy.

The acrylic and methacrylic acids and also the very reactive acryloyl chloride were specifically selected for their functional groups that later on were used for click-chemistry modification in Chapter 6.

The carbodiimide mediated esterification methodology and the esterification involving the intermediary formation of anhydrides using *p*-toluenesulfonyl chloride and pyridine were extended to graft carbazole-9-yl acetic acid and coumarin-3-carboxylic acid to CNC in Chapter 4 and to graft bromoacetic acid to CNC in Chapter 5 with successful synthesis of carbazole-9-yl-acetate cellulose, coumarin-3-carboxylate cellulose and bromo acetate cellulose as it is further concluded.

Thus, in Chapter 4, fluorescently labelled CNCs were obtained by grafting carbazole-9-yl-acetic acid onto the cellulose nanocrystal surface by carbodiimide mediated esterification and resulted in a low degree of substitution, between DS_{surf} = 0.09 and 0.1 upon increasing molar excess from 1:3:3:0.03 to 1:5.5:5.5:0.03 for OH:Acid:DIC:DMAP. Subsequently, the tosyl chloride/ pyridine methodology was applied as well, resulting in an increase in DS_{surf} of 0.39, 0.72, 1.03, 1.6 and 1.55 with increasing equimolecular excess as follows: 1:0.66:0.66; 1:1.33:1.33; 1:2:2; 1:2.66:2.66; 1:3.33:3.33 for CNC:Acid:TsCl. Therefore, a molar excess of 1:2:2 (resulting in DS_{surf}(N) = 1.03) was found to be sufficient to limit the reaction to the surface as this is equivalent to the maximum amount of surface available hydroxyl groups without any noticeable destruction of the crystalline hydrogen bonded network in the CNC core.

The second fluorescently labelled cellulose nanocrystals with coumarin-3-carboxylic acid used only the most efficient tosyl chloride/pyridine results of carbazole-modifications and two molar excesses were applied (1:1.83:1.83 and 1:2.66:2.66 CNC:Acid:TsCl) resulting in a DS_{surf}(C) = 1.33 and DS_{surf} (C) = 1.56, respectively. Once again, the efficiency of the reaction is dependent on the nature of the acid and on the molar excess. As coumarin-3-carboxylic acid is more reactive than carbazole-9-yl-acetic acid, for the same molar excess (1:2:2), this esterification showed a DS_{surf}(C) = 1.10 which is slightly higher

than the modification degree of carbazole-9-yl-acetate cellulose, $DS_{surf}(N)$ = 1.03. TEM and AFM characterization were carried out for fluorescently modified cellulose and the micrographs display lengths between 100 and 300 nm and widths ranging from 5 to 15 nm in agreement with the literature data and dimensions for the unmodified nanocrystals.[45]

All the fluorescently labelled cellulose nanocrystals exhibited the expected absorption and emission properties. Experiments showed that a very high amount of dye was grafted on the cellulose surface compared to other publications. The absorption spectra of the carbazole–modified celluloses exhibited three absorption bands at around 294, 327 and 339 nm, and the modifications presented double fluorescence emission intensities between 335–450 nm, for emission maxima at 347 and 362 nm as a result of excitation at 294 nm, when compared with the other two wavelengths. Coumarin-3-carboxylate cellulose exhibited two absorption bands at 293 nm and at approximately 335 nm and emitted in the visible region at around 420 nm. Fluorescence properties upon increasing concentration (0.001-0.5 mg/mL) of carbazole and carbazole-modified cellulose were also evaluated. At a concentration of 0.1 mg/mL of carbazole-modified cellulose with a substitution of two functional groups per AGU, a response sensitive to the concentration was measured by registering a fluorescence decrease with a further increase in concentration. A similar behaviour was shown by modification with three carbazole functionalities grafted per AGU but at a lower concentration (0.04 mg/mL). This behaviour is explained by the fact that distance between the carbazole molecules decreased with increasing concentration and beyond a certain concentration the carbazole groups start interacting with each other and thus fluorescence quenching occurs. All the carbazole and coumarin modified cellulose also exhibited self-quenching properties, while the addition of acrylonitrile as an electron acceptor for charge transfer properties quenched the emission spectra of only carbazole modified cellulose. The type of molecular interactions that cause fluorescence quenching (static quenching through a ground state complex formation and dynamic quenching due to short range collisions between the quencher molecules and excited molecules)[162] were not

determined due to unavailability to measure the fluorescence life time (by applying the Stern-Volmer equation) and therefore is part of future work. OLED fabrication based on modified cellulose was attempted but without successful results as deposited films were too non-homogeneous despite numerous attempts.

In Chapter 5 several approaches were taken to synthesise cationic CNC. Acyl halide esterification of cellulose nanocrystals with bromoacetyl bromide represents the first step used to introduce the C-Br bond needed to synthesise four different cationic modified cellulose nanocrystals. Additionally, an esterification of cellulose nanocrystals with bromoacetic acid was also attempted and the cationized nanoparticles were synthesised in the same step.

The first methodology involved a two-step synthesis in which bromoacetate cellulose was initially synthesised followed by a reaction with pyridine and 1-methylimidazole as cationization agents in the second step. This pathway showed a better nucleophilic substitution of bromoacetate cellulose by pyridine ($DS_{surf}(N)$ = 0.84) when compared with nucleophilic substitution of bromoacetate cellulose with 1-methylimidazole ($DS_{surf}(N)$ = 0.71). This observation is based on different solubilities of the bromoacetate cellulose in pyridine and 1-methylimidazole and consequently different degrees of substitution.

The second methodology involved a single step procedure. Cellulose nanocrystals were reacted in one pot with bromoacetyl bromide in the desired cationization reagent. This strategy favoured the formation of 1-methylimidazolium acetate cellulose bromide with a $DS_{surf}(N)$ = 1.06 much higher than the one of pyridinium acetate cellulose bromide synthesis ($DS_{surf}(N)$ = 0.25) due to the more nucleophilic character of 1-methylimidazole than pyridine and consequently a better reaction rate.

The third method used a one-pot approach to react bromoacetic acid with cellulose nanocrystals with TsCl/Py system. It was applied only to the synthesis of pyridinium-based cationic species which also gave a satisfactory $DS_{surf}(N)$ = 0.35. This methodology does not use very high molar excess and

thus reduces the formation of secondary products that may form and were found to be difficult to remove throughout the whole work carried out in this thesis.

The modified cellulose nanocrystals were tested for their stability and surface charge by measuring the zeta potential which was found to be highly positive (1[Br][PyAc]-*g*-CNC indicated a ζ = +31.8 mV with ζ = +28.5 mV for 1[Br][MeImAc]-*g*-CNC, 2[Br][PyAc]-*g*-CNC giving ζ = +37.42 mV and for 2[Br][MeImAc]-*g*-CNC ζ = +37.89 mV while 3[Br][PyAc]-*g*-CNC indicated a ζ = + 41.47 mV). Furthermore, the ion exchange capability of the cationic modified cellulose nanoparticles was proven by ion exchange with Orange II dye for all the cationized nanoparticles indicating good adsorption properties as follows: 1[Br][PyAc]-g-CNC = 0.615 $mmolg^{-1}$, 1[Br][MeImAc]-g-CNC = 0.631 $mmolg^{-1}$, 2[Br][PyAc]-g-CNC = 0.121 $mmolg^{-1}$, 2[Br][MeImAc]-g-CNC – 0.883 $mmolg^{-1}$ and 3[Br][PyAc]-g-CNC = 0.208 $mmolg^{-1}$, values that are comparable with the previously reported values.

Chapter 6 is allocated to Thiol-Ene Michael-addition as a click-chemistry reaction that was carried out on the surface of cellulose nanocrystals. The synthesised cellulose acrylates and methacrylates in Chapter 3, bearers of an α, β-unsaturated ene, were used as starting material in the reaction with four alkyl thiols. Three types of catalysts (base, nucleophile and self-catalysed reaction by a nucleophile) were used to initiate the thiol-Michael addition reaction. Initial click reactions of cellulose methacrylate with 3-mercaptopropyl trimethoxysilane in MeOH carried out for one up to four hours were proven to work only by XPS due to the low level of grafting. Using the same thiol with acrylate cellulose in DCM for 24 hours resulted in a satisfactory $DS_{surf}(S)$ = 0.19. Doubling the reaction time, cellulose acrylate reaction with 1,2-ethane-dithiol, in the same solvent resulted in a slightly higher $DS_{surf}(S)$ = 0.24.

The efficiency of thiol-click chemistry of acrylate cellulose was further tested for very short reaction times. Cellulose acrylate was reacted with cysteamine hydrochloride in EtOH catalysed by NaOH for 10 to 15 minutes, with an increased molar excess from 1:0.5:0.5 to 1:5:5 for CNC:Thiol:Catalyst. The

reaction led to a decrease in the final DS from one reaction to another upon increase of molar reagents equivalents. Possibly, the high molar ratio contributes to a side reaction that removes the grafted functionality from the surface (aminolysis) thus giving a decrease in modification from $DS_{surf}(S)$ = 0.15 to $DS_{surf}(S)$ = 0.07 (reaction carried out with a molar excess of 1:5:5 OH:Thiol:Catalyst). A slight decrease in the molar excess from 1:5 to 1:3 in a self-catalysed reaction by cysteamine in acetone for even shorter reaction times, gave a $DS_{surf}(S)$ = 0.08 and $DS_{surf}(S)$ = 0.06 for 5 and 10 minutes respectively, which may be the shortest reaction time for a click-chemistry on nanocellulose surfaces to the best of my knowledge. Considering that there is only a slight difference between the two modifications, it can be assumed that a maximum DS happens before 5 minutes reaction time as it is followed by a decrease of the DS for the 10 minutes reaction due to reaction conditions, or the measured difference is merely due to experimental error. As an alternative, these reactions could be monitored by Real-Time Fourier Transform Infrared (RT-FT-IR) to have a better evaluation of the reaction evolution and these are proposed as future work.

Reactions of cellulose acrylate with cysteamine in DMSO/DMF/H_2O for 10 minutes and at room temperature resulted in a satisfactory substitution as follows: $DS_{surf}(S)$ = 0.20 for DMSO, $DS_{surf}(S)$ = 0.21 for DMF and $DS_{surf}(S)$ = 0.13 for H_2O. Thus it was proven that the Thiol-Ene click-chemistry reaction works under very mild reaction conditions (room temperature), in an environmentally friendly solvent (H_2O) and without extra catalyst. Thus, more polar solvents increase the rate of reaction and are consistent with the previous reactions carried out in DCM.

Therefore, it was proven that click-chemistry applied to ene-modified cellulose nanocrystals works from very short reaction times such as 5-10 minutes, at room temperature, in different solvents including the environmental-friendly reaction in water, and the degree of substitution is satisfactory.

Once a higher temperature was used there was a noticeable increase in DS ($DS_{surf}(S)$ = 0.69) for a reaction carried out in DCM, for a longer reaction time

(2 hours) and catalysed by hexylamine. This last Thiol-Ene click product (cellulose 3-((2-aminoethyl)thio) propanoate) was used to synthesise an amidine functionalised cellulose nanocrystal product with *N,N* dimethylacetamide dimethyl acetal in acetone for 24 hours. The synthesis was an adapted method for the synthesis of switchable surfactants and therefore is the first synthesised amidine modified cellulose of its kind. It was demonstrated in 3 experiments that the switchable behaviour of amidine modified cellulose is reversible and repeatable by measuring the pH and zeta potential upon bubbling with CO_2 and flushing back with argon. These newly synthesised nanoparticles have potential applications in the field of Pickering emulsions.

Further research in the field of cellulose nanocrystals can be continued based on the work developed in this thesis. Here, the esterification reaction was investigated for five different acids and two acyl halides providing a launching platform for further investigations into the surface modification of CNC and thus, the development of new applications for these surface modified materials.

The two fluorescently labelled cellulose nanocrystals newly synthesised in this thesis can have potential use in biomedical applications such as bioimaging, as biosensors or as photodynamic therapy. However, the characterization by further fluorescent techniques of these carbazole- and coumarin-modified nanocellulose could be further continued in order to contribute to the interesting work about the life time and quenching effects.

Synthesised bromoacetate cellulose can be further used to convert hydrophilic cellulose nanocrystals into hydrophobic cellulose nanocrystals by grafting with i.e. methyl methacrylate (MMA), by using activators regenerated by electron transfer (ARGET) atom transfer radical polymerization (ATRP)[264] or by grafting polystyrene chains through surface-initiated atom transfer radical polymerization (SI-ATRP)[64].

Cationized nanoparticles were synthesised using pyridine and methyl imidazole by two different synthesis routes where the reaction efficiency is determined by the nature of the reagent used. Beside this, considering the variety of negatively

charged nanoparticles and the current developed positively charged nanoparticles, future work can focus on self-assembly through the mixing of positively and negatively charged nanoparticles which would result in layered nano-structures with controlled properties.

Thiol-Ene click chemistry can be further developed through a more in-depth time-evolution reaction by carrying out more reactions or by Real-Time Fourier Transform Infrared (RT-FT-IR) monitoring. Thiol-Ene chemistry could be further used in the formation of cross-linked networks with applications in hydrogels with distinctive properties for cell delivery materials, thin films with a uniform cross-linked matrix and lithographic applications, the current synthesised Thiol-Ene nanocrystals and ene-bearer nanocrystals are proposed to be applied in the same matrix to form cross-coupled structures with applications in the hydrogels-aerogels and the other mentioned applications.[188-190] In this thesis, the synthesis of switchable cellulose nanoparticle was achieved. Future work could focus on effective testing of these nanoparticles to stabilise/de-stabilise Pickering emulsions.

9 References

(1) Habibi, Y.; Lucia, L. A.; Rojas, O. J. *Chemical Reviews* **2010**, *110*, 3479-3500.

(2) McKendry, P. *Bioresource Technology* **2002**, *83*, 37-46.

(3) Klemm, D.; Heublein, B.; Fink, H.-P.; Andreas, B. *Angewandte Chemie International Edition* **2005**, *44*, 35.

(4) Cao, X.; Dong, H.; Li, C. M. *Biomacromolecules* **2007**, *8*, 899-904.

(5) Azizi Samir, M. A. S.; Alloin, F.; Sanchez, J.-Y.; El Kissi, N.; Dufresne, A. *Macromolecules* **2004**, *37*, 1386-1393.

(6) Eichhorn, S. J.; Dufresne, A.; Aranguren, M.; Marcovich, N. E.; Capadona, J. R.; Rowan, S. J.; Weder, C.; Thielemans, W.; Roman, M.; Renneckar, S.; Gindl, W.; Veigel, S.; Keckes, J.; Yano, H.; Abe, K.; Nogi, M.; Nakagaito, A. N.; Mangalam, A.; Simonsen, J.; Benight, A. S.; Bismarck, A.; Berglund, L. A.; Peijs, T. *Journal of Materials Science* **2010**, *45*, 1-33.

(7) Payen, A. *Comptes rendus hebdomadaires des seances de l'Academie des science* **1838**, *7*, 1052.

(8) Samyn, P. *Journal of Materials Science* **2013**, *48*, 6455-6498.

(9) Costa, S. M.; Mazzola, P. G.; Silva, J. C. A. R.; Pahl, R.; Pessoa Jr, A.; Costa, S. A. *Industrial Crops and Products* **2013**, *42*, 189-194.

(10) Fakrul Alam, A. B. M.; Mondal, M. I. H. *Journal of Applied Polymer Science* **2013**, *128*, 1206-1212.

(11) Radu, C.-D.; Salariu, M.; Avadanei, M.; Ghiciuc, C.; Foia, L.; Lupusoru, E. C.; Ferri, A.; Ulea, E.; Lipsa, F. *Carbohydrate Polymers* **2013**, *95*, 479-486.

(12) Bhattacharya, M.; Malinen, M. M.; Lauren, P.; Lou, Y.-R.; Kuisma, S. W.; Kanninen, L.; Lille, M.; Corlu, A.; GuGuen-Guillouzo, C.;

Ikkala, O.; Laukkanen, A.; Urtti, A.; Yliperttula, M. *Journal of Controlled Release* **2012**, *164*, 291-298.

(13) Adel, A. M.; Abd El-Wahab, Z. H.; Ibrahim, A. A.; Al-Shemy, M. T. *Carbohydrate Polymers* **2011**, *83*, 676-687.

(14) Oppermann, W. *Papier* **1995**, *49*, 765-769.

(15) Arancibia, C.; Bayarri, S.; Costell, E. *Food Biophysics* **2013**, *8*, 122-136.

(16) Kamel, S. *Express Polymer Letters* **2008**, *2*, 758-778.

(17) Wertz, J.-L.; Bedue, O.; Marcier, J. P. *Cellulose science and technology*; EPFL Press, Lausanne, 2010.

(18) Helbert, W.; Sugiyama, J.; Ishihara, M.; Yamanaka, S. *Journal of Biotechnology* **1997**, *57*, 29-37.

(19) Praly, J. P.; Lemieux, R. U. *Canadian Journal of Chemistry* **1987**, *65*, 213-223.

(20) Clayden J.; Greeves N.; Warren S.; Wothers P. *Organic Chemistry*; Oxford University Press: Oxford, 2001.

(21) Nishikawa S.; Ono S *Proceeding of Tokyo Mathematico-Physical Society* **1913**, *7*, 131-138.

(22) Nishiyama, Y.; Sugiyama, J.; Chanzy, H.; Langan, P. *Journal of the American Chemical Society* **2003**, *125*, 14300-14306.

(23) Sugiyama, J.; Persson, J.; Chanzy, H. *Macromolecules* **1991**, *24*, 2461-2466.

(24) Langan, P.; Nishiyama, Y.; Chanzy, H. *Biomacromolecules* **2001**, *2(2)*, 410-416.

(25) Wada, M.; Chanzy, H.; Nishiyama, Y.; Langan, P. *Macromolecules* **2004**, *37*, 8548-8555.

(26) Hayashi, J.; Sufoka, A.; Ohkita, J.; Watanabe, S. *Journal of Polymer Science: Polymer Letters Edition* **1975**, *13*, 23-27.

(27) Atalla, R. H.; VanderHart, D. L. *Solid State Nuclear Magnetic Resonance* **1999**, *15*, 1-19.

(28) O'Sullivan, A. *Cellulose* **1997**, *4*, 173-207.

(29) Sugiyama, J.; Okano, T.; Yamamoto, H.; Horii, F. *Macromolecules* **1990**, *23*, 3196-3198.

(30) Koyama, M.; Helbert, W.; Imai, T.; Sugiyama, J.; Henrissat, B. *Proceedings of the National Academy of Sciences of the United States of America* **1997**, *94*, 9091-9095.

(31) Sugiyama, J.; Vuong, R.; Chanzy, H. *Macromolecules* **1991**, *24*, 4168-4175.

(32) Nishiyama, Y.; Langan, P.; Chanzy, H. *Journal of the American Chemical Society* **2002**, *124*, 9074-9082.

(33) Park, H.; Park, K.; Shalaby, W. S. W. *Biodegradable Hydrogels for Drug Delivery*; Taylor & Francis, 2011.

(34) Bledzki, A. K.; Gassan, J. *Progress in Polymer Science* **1999**, *24*, 221-274.

(35) Satyanarayana, K. G.; Sukumaran, K.; Mukherjee, P. S.; Pavithran, C.; Pillai, S. G. K. *Cement and Concrete Composites* **1990**, *12*, 117-136.

(36) Dufresne, A. In *Monomers, polymers and Composite from Renewable Resources*; Elsevier, Oxford, UK 2008, Cellulose-based composites and nanocomposites pp 401-418.

(37) Lu, J.; Askeland, P.; Drzal, L. T. *Polymer* **2008**, *49*, 1285-1296.

(38) Siqueira, G.; Bras, J.; Dufresne, A. *Polymers* **2010**, *2*, 728-765.

(39) Rånby, B. G. *Acta Chemica Scandinavia* **1949**, *3*, 649-650.

(40) Ranby, B. G. *Discussions of the Faraday Society* **1951**, *11*, 158-164.

(41) Habibi, Y.; Chanzy, H.; Vignon, M. *Cellulose* **2006**, *13*, 679-687.

(42) Battista, O. A. *Industrial & Engineering Chemistry* **1950**, *42*, 502-507.

(43) Battista, O. A.; Coppick, S.; Howsmon, J. A.; Morehead, F. F.; Sisson, W. A. *Industrial & Engineering Chemistry* **1956**, *48*, 333-335.

(44) Araki, J.; Wada, M.; Kuga, S. *Langmuir* **2000**, *17*, 21-27.

(45) Elazzouzi-Hafraoui, S.; Nishiyama, Y.; Putaux, J.-L.; Heux, L.; Dubreuil, F.; Rochas, C. *Biomacromolecules* **2007**, *9*, 57-65.

(46) Sadeghifar, H.; Filpponen, I.; Clarke, S.; Brougham, D.; Argyropoulos, D. *Journal of Materials Science* **2011**, *46*, 7344-7355.

(47) Filpponen, I.; Argyropoulos, D. S. *Biomacromolecules* **2010**, *11*, 1060-1066.

(48) Dong, X. M.; Kimura, T.; Revol, J.-F.; Gray, D. G. *Langmuir* **1996**, *12*, 2076-2082.

(49) Miriam de Souza Lima, M.; Borsali, R. *Macromolecular Rapid Communications* **2004**, *25*, 771-787.

(50) Favier, V.; Chanzy, H.; Cavaille, J. Y. *Macromolecules* **1995**, *28*, 6365-6367.

(51) Terech, P.; Chazeau, L.; Cavaille, J. Y. *Macromolecules* **1999**, *32*, 1872-1875.

(52) Garcia de Rodriguez, N. L.; Thielemans, W.; Dufresne, A. *Cellulose* **2006**, *13*, 261-270.

(53) Siqueira, G.; Bras, J.; Dufresne, A. *Biomacromolecules* **2008**, *10*, 425-432.

(54) Habibi, Y.; Goffin, A.-L.; Schiltz, N.; Duquesne, E.; Dubois, P.; Dufresne, A. *Journal of Materials Chemistry* **2008**, *18*, 5002-5010.

(55) Raquez, J. M.; Murena, Y.; Goffin, A. L.; Habibi, Y.; Ruelle, B.; DeBuyl, F.; Dubois, P. *Composites Science and Technology* **2012**, *72*, 544-549.

(56) Beck-Candanedo, S.; Roman, M.; Gray, D. G. *Biomacromolecules* **2005**, *6*, 1048-1054.

(57) Revol, J. F. *Carbohydrate Polymers* **1982**, *2*, 123-134.

(58) Hirai, A.; Inui, O.; Horii, F.; Tsuji, M. *Langmuir* **2008**, *25*, 497-502.

(59) Araki, J.; Kuga, S. *Langmuir* **2001**, *17*, 4493-4496.

(60) Helbert, W.; Nishiyama, Y.; Okano, T.; Sugiyama, J. *Journal of Structural Biology* **1998**, *124*, 42-50.

(61) Hanley, S.; Revol, J.-F.; Godbout, L.; Gray, D. *Cellulose* **1997**, *4*, 209-220.

(62) Moon, R. J.; Martini, A.; Nairn, J.; Simonsen, J.; Youngblood, J. *Chemical Society Reviews* **2011**, *40*, 3941-3994.

(63) Filpponen, I.; Argyropoulos, D. S. *Biomacromolecules*, *11*, 1060-1066.

(64) Morandi, G.; Heath, L.; Thielemans, W. *Langmuir* **2009**, *25*, 8280-8286.

(65) Eyley, S. *Surface Modification of Cellulose Nanocrystals* PhD Thesis, The University of Nottingham, UK, 2012.

(66) Dong, X. M.; Revol, J.-F.; Gray, D. G. *Cellulose* **1998**, *5*, 19-32.

(67) Roman, M.; Winter, W. T. *Biomacromolecules* **2004**, *5*, 1671-1677.

(68) Klemm, D.; Kramer, F.; Moritz, S.; Lindström, T.; Ankerfors, M.; Gray, D.; Dorris, A. *Angewandte Chemie International Edition* **2011**, *50*, 5438-5466.

(69) Heinze, T.; Liebert, T. *Progress in Polymer Science* **2001**, *26*, 1689-1762.

(70) Glasser, W. G. *Macromolecular Symposia* **2004**, *208*, 371-394.

(71) Balser, K.; Hoppe, L.; Eicher, T.; Wendel, M.; Astheimer, A.-J. In *Ullmanns Encyclopedia of Industrial Chemistry*; 5th Edition ed.; VCH, W., Ed.; Gerhartz, W., Yamamoto, Y.S., Champbell, F.T., PfefferKorn, R., Rounsaville, J.F., : New York, 1986 Cellulose esters pp 419.

(72) Eyley, S.; Thielemans, W. *Nanoscale* **2014**, *6*, 7764-7779.

(73) Heux, L.; Chauve, G.; Bonini, C. *Langmuir* **2000**, *16*, 8210-8212.

(74) Bonini, C.; Heux, L.; International Patent WO 2000/077088, 2000.

(75) Bonini, C.; Heux. L.; International Patent WO 2000/077088 2000.

(76) Bonini, C.; Heux, L.; Cavaillé, J.-Y.; Lindner, P.; Dewhurst, C.; Terech, P. *Langmuir* **2002**, *18*, 3311-3314.

(77) Bondeson, D.; Oksman, K. *Composite Interfaces* **2007**, *14*, 617-630.

(78) Kim, J.; Montero, G.; Habibi, Y.; Hinestroza, J. P.; Genzer, J.; Argyropoulos, D. S.; Rojas, O. J. *Polymer Engineering & Science* **2009**, *49*, 2054-2061.

(79) Zhou, Q.; Brumer, H.; Teeri, T. T. *Macromolecules* **2009**, *42*, 5430-5432.

(80) Coseri, S.; Biliuta, G.; Simionescu, B. C.; Stana-Kleinschek, K.; Ribitsch, V.; Harabagiu, V. *Carbohydrate Polymers* **2013**, *93*, 207-215.

(81) Bragd, P. L.; van Bekkum, H.; Besemer, A. C. *Topics in Catalysis* **2004**, *27*, 49-66.

(82) Shibata, I.; Isogai, A. *Cellulose* **2003**, *10*, 151-158.

(83) de Nooy, A. E. J.; Besemer, A. C.; van Bekkum, H. *Recueil des Travaux Chimiques des Pays-Bas* **1994**, *113*, 165-166.

(84) Saito, T.; Okita, Y.; Nge, T. T.; Sugiyama, J.; Isogai, A. *Carbohydrate Polymers* **2006**, *65*, 435-440.

(85) Fujisawa, S.; Isogai, T.; Isogai, A. *Cellulose* **2010**, *17*, 607-615.

(86) Montanari, S.; Roumani, M.; Heux, L.; Vignon, M. R. *Macromolecules* **2005**, *38*, 1665-1671.

(87) Ho, T. T. T.; Zimmermann, T.; Hauert, R.; Caseri, W. *Cellulose* **2011**, *18*, 1391-1406.

(88) Gruber, E.; Granzow, C.; Ott, T. In *Cellulose Derivatives*; American Chemical Society, 1998; Vol. 688; pp 94-106.

(89) Abbott, A. P.; Bell, T. J.; Handa, S.; Stoddart, B. *Green Chemistry* **2006**, *8*, 784-786.

(90) Geary, N. W.; Peffly, M. M.; Staudigel, J. A.; Google Patents, 2004.

(91) Roy, D.; Knapp, J. S.; Guthrie, J. T.; Perrier, S. *Biomacromolecules* **2007**, *9*, 91-99.

(92) Song, Y.; Sun, Y.; Zhang, X.; Zhou, J.; Zhang, L. *Biomacromolecules* **2008**, *9*, 2259-2264.

(93) Hasani, M.; Cranston, E. D.; Westman, G.; Gray, D. G. *Soft Matter* **2008**, *4*, 2238-2244.

(94) Eyley, S.; Thielemans, W. *Chemical Communications* **2011**, *47*, 4177-4179.

(95) Zaman, M.; Xiao, H.; Chibante, F.; Ni, Y. *Carbohydrate Polymers* **2012**, *89*, 163-170.

(96) Jasmani, L.; Eyley, S.; Wallbridge, R.; Thielemans, W. *Nanoscale* **2013**, *5*, 10207-10211.

(97) Zhao, B.; Brittain, W. J. *Progress in Polymer Science* **2000**, *25*, 677-710.

(98) Ljungberg, N.; Bonini, C.; Bortolussi, F.; Boisson, C.; Heux, L.; Cavaillé *Biomacromolecules* **2005**, *6*, 2732-2739.

(99) Felix, J. M.; Gatenholm, P. *Journal of Applied Polymer Science* **1991**, *42*, 609-620.

(100) Vignon, M.; Montanari, S.; Habibi, Y.; (Centre National de la Recherche Scientifique CNRS, F. F., Ed., 2004

(101) Mangalam, A. P.; Simonsen, J.; Benight, A. S. *Biomacromolecules* **2009**, *10*, 497-504.

(102) Cao, X.; Habibi, Y.; Lucia, L. A. *Journal of Materials Chemistry* **2009**, *19*, 7137-7145.

(103) Chen, G.; Dufresne, A.; Huang, J.; Chang, P. R. *Macromolecular Materials and Engineering* **2009**, *294*, 59-67.

(104) Lin, N.; Chen, G.; Huang, J.; Dufresne, A.; Chang, P. R. *Journal of Applied Polymer Science* **2009**, *113*, 3417-3425.

(105) Pranger, L.; Tannenbaum, R. *Macromolecules* **2008**, *41*, 8682-8687.

(106) Yi, J.; Xu, Q.; Zhang, X.; Zhang, H. *Polymer* **2008**, *49*, 4406-4412.

(107) Zoppe, J.; Habibi, Y.; Rojas, O. J. In *Abstracts of papers of the American Chemical Society* American Chemical Society,Washington, USA, 2008; Vol. 235.

(108) Zoppe, J.; Habibi, Y.; Efimenko, K.; Genzer, J.; Rojas, O. J. In *Abstract of papers of the American Chemical Society* American Chemical Society, Washington, USA, 2009; Vol. 237.

(109) Mattoso, L., H., C.,; Medeiros, E., S.,; Baker, D. A.; Avloni, J.; Wood, D. F.; Orts, W. J.; American Scientific Publishers, May 2009; Vol. 5, Number 5; pp 2917-2922.

(110) Sassi, J.-F.; Chanzy, H. *Cellulose* **1995**, *2*, 111-127.

(111) Klemm, D.; Philipp, B.; Heinze, T.; Heinze, U.; Wagenknecht, W. *Comprehensive Cellulose Chemistry: Functionalization of Cellulose*; Wiley-VCH Verlag GmbH: Weinheim, Germany, 2004; Vol. 2.

(112) Cerqueira, D. A.; Filho, G. R.; Meireles, C. d. S. *Carbohydrate Polymers* **2007**, *69*, 579-582.

(113) Lin, N.; Huang, J.; Chang, P. R.; Feng, J.; Yu, J. *Carbohydrate Polymers* **2011**, *83*, 1834-1842.

(114) J. Clyden, N. G., S. Warren, P. Wothers *Organic Chemistry*; Oxford University Press, 2001.

(115) Boufi, S.; Belgacem, M. *Cellulose* **2006**, *13*, 81-94.

(116) Heinze, T.; Liebert, T.; Pfeiffer, K.; Hussain, M. *Cellulose* **2003**, *10*, 283-296.

(117) Sealey, J. E.; Samaranayake, G.; Todd, J. G.; Glasser, W. G. *Journal of Polymer Science Part B: Polymer Physics* **1996**, *34*, 1613-1620.

(118) Krouit, M.; Bras, J.; Belgacem, M. N. *European Polymer Journal* **2008**, *44*, 4074-4081.

(119) Vaca-Garcia, C.; Borredon, M. E. *Bioresource Technology* **1999**, *70*, 135-142.

(120) Brewster, J. H.; Ciotti, C. J. *Journal of the American Chemical Society* **1955**, *77*, 6214-6215.

(121) Thiebaud, S.; Borredon, M. E. *Bioresource Technology* **1995**, *52*, 169-173.

(122) Kwatra, H. S.; Caruthers, J. M.; Tao, B. Y. *Industrial & Engineering Chemistry Research* **1992**, *31*, 2647-2651.

(123) Maim, C. J.; Mench, J. W.; Kendall, D. L.; Hiatt, G. D. *Industrial & Engineering Chemistry* **1951**, *43*, 684-688.

(124) Samaranayake, G.; Glasser, W. G. *Carbohydrate Polymers* **1993**, *22*, 1-7.

(125) Tome, L. C.; Freire, M. G.; Rebelo, L. P. N.; Silvestre, A. J. D.; Neto, C. P.; Marrucho, I. M.; Freire, C. S. R. *Green Chemistry* **2011**, *13*, 2464-2470.

(126) Freire, C. S. R.; Silvestre, A. J. D.; Neto, C. P.; Belgacem, M. N.; Gandini, A. *Journal of Applied Polymer Science* **2006**, *100*, 1093-1102.

(127) Wang, P.; Tao, B. Y. *Journal of Applied Polymer Science* **1994**, *52*, 755-761.

(128) Baiardo, M.; Frisoni, G.; Scandola, M.; Licciardello, A. *Journal of Applied Polymer Science* **2002**, *83*, 38-45.

(129) Junior de Menezes, A.; Siqueira, G.; Curvelo, A. A. S.; Dufresne, A. *Polymer* **2009**, *50*, 4552-4563.

(130) Berlioz, S.; Molina-Boisseau, S.; Nishiyama, Y.; Heux, L. *Biomacromolecules* **2009**, *10*, 2144-2151.

(131) Hubbard, P.; Brittain, W. J. *The Journal of Organic Chemistry* **1998**, *63*, 677-683.

(132) Xu, Q.; Yi, J.; Zhang, X.; Zhang, H. *European Polymer Journal* **2008**, *44*, 2830-2837.

(133) Majoinen, J.; Walther, A.; McKee, J. R.; Kontturi, E.; Aseyev, V.; Malho, J. M.; Ruokolainen, J.; Ikkala, O. *Biomacromolecules* **2011**, *12*, 2997-3006.

(134) Gräbner, D.; Liebert, T.; Heinze, T. *Cellulose* **2002**, *9*, 193-201.

(135) Hasani, M.; Westman, G. *Cellulose* **2007**, *14*, 347-356.

(136) Neises, B.; Steglich, W. *Angewandte Chemie International Edition in English* **1978**, *17*, 522-524.

(137) Honeyman, J. *Journal of the Chemical Society (Resumed)* **1947**, 168-173.

(138) Rahn, K.; Diamantoglou, M.; Klemm, D.; Berghmans, H.; Heinze, T. *Die Angewandte Makromolekulare Chemie* **1996**, *238*, 143-163.

(139) McCormick, C. L.; Dawsey, T. R.; Newman, J. K. *Carbohydrate Research* **1990**, *208*, 183-191.

(140) Petzold-Welcke, K.; Michaelis, N.; Heinze, T. *Macromolecular Symposia* **2009**, *280*, 72-85.

(141) Ballistreri, F. P.; Cantone, A.; Maccarone, E.; Tomaselli, G. A.; Tripolone, M. *Journal of the Chemical Society, Perkin Transactions 2* **1981**, 438-441.

(142) Lyashchuk, S. N.; Skrypnik, Y. G.; Besrodnyi, V. P. *Journal of the Chemical Society, Perkin Transactions 2* **1993**, 1153-1159.

(143) Gericke, M.; Schaller, J.; Liebert, T.; Fardim, P.; Meister, F.; Heinze, T. *Carbohydrate Polymers* **2012**, *89*, 526-536.

(144) Feese, E.; Sadeghifar, H.; Gracz, H. S.; Argyropoulos, D. S.; Ghiladi, R. A. *Biomacromolecules* **2011**, *12*, 3528-3539.

(145) Wang, N.; Ding, E.; Cheng, R. *Frontiers of Chemical Engineering in China* **2007**, *1*, 228-232.

(146) Goussé, C.; Chanzy, H.; Excoffier, G.; Soubeyrand, L.; Fleury, E. *Polymer* **2002**, *43*, 2645-2651.

(147) Nielsen, L. J.; Eyley, S.; Thielemans, W.; Aylott, J. W. *Chemical Communications* **2010**, *46*, 8929-8931.

(148) Bosch, P.; Catalina, F.; Corrales, T.; Peinado, C. *Chemistry – A European Journal* **2005**, *11*, 4314-4325.

(149) Basabe-Desmonts, L.; Reinhoudt, D. N.; Crego-Calama, M. *Chemical Society Reviews* **2007**, *36*, 993-1017.

(150) Mori, H.; Tando, I.; Tanaka, H. *Macromolecules* **2010**, *43*, 7011-7020.

(151) Lai, M.-H.; Tsai, J.-H.; Chueh, C.-C.; Wang, C.-F.; Chen, W.-C. *Macromolecular Chemistry and Physics* **2010**, *211*, 2017-2025.

(152) Dong, S.; Roman, M. *Journal of the American Chemical Society* **2007**, *129*, 13810-13811.

(153) Jung, S.; Angerer, B.; Löscher, F.; Niehren, S.; Winkle, J.; Seeger, S. *ChemBioChem* **2006**, *7*, 900-903.

(154) Knölker, H.-J.; Reddy, K. R. In *The Alkaloids: Chemistry and Biology*; Geoffrey, A. C., Ed.; Academic Press, 2008; Vol. 65; pp 3-158.

(155) Brace, L. *The American journal of medical technology* **1983**, *49*, 457-463.

(156) Lake, B. G. In *Disease, Metabolism and Reproduction in the Toxic Response to Drugs and Other Chemicals*; Chambers, P., Preziosi, P., Chambers, C., Eds.; Springer Berlin Heidelberg, 1984; Vol. 7; pp 16-29.

(157) Yuen, S. H. *Analyst* **1978**, *103*, 842-850.

(158) Hagan, E. C.; Hansen, W. H.; Fitzhugh, O. G.; Jenner, P. M.; Jones, W. I.; Taylor, J. M.; Long, E. L.; Nelson, A. A.; Brouwer, J. B. *Food and Cosmetics Toxicology* **1967**, *5*, 141-157.

(159) Helgeland, L. I. V. *Biochemical Education* **1980**, *8*, 66-69.

(160) Karakawa, M.; Chikamatsu, M.; Nakamoto, C.; Maeda, Y.; Kubota, S.; Yase, K. *Macromolecular Chemistry and Physics* **2007**, *208*, 2000-2006.

(161) Karakawa, M.; Chikamatsu, M.; Yoshida, Y.; Azumi, R.; Yase, K.; Nakamoto, C. *Macromolecular Rapid Communications* **2007**, *28*, 1479-1484.

(162) Zhang, L.; Zhou, J.; Zhang, L. *Macromolecular Chemistry and Physics* **2012**, *213*, 57-63.

(163) Xu, Z.-K.; Xu, Y., -Y.,; Wang, M. *Journal of Applied Polymer Science* **1998**, *69*, 1403-1408.

(164) Yatsue, T.; Miyashita, T. *The Journal of Physical Chemistry* **1995**, *99*, 16047-16051.

(165) Ito, S.; Ohmori, S.; Yamamoto, M. *Macromolecules* **1992**, *25*, 185-191.

(166) Seufert, M.; Fakirov, C.; Wegner, G. *Advanced Materials* **1995**, *7*, 52-55.

(167) Löscher, F.; Ruckstuhl, T.; Jaworek, T.; Wegner, G.; Seeger, S. *Langmuir* **1998**, *14*, 2786-2789.

(168) Xiao, Y.; Ritcey, A. M. *Langmuir* **2000**, *16*, 4252-4258.

(169) Mao, L.; Ritcey, A. M. *Thin Solid Films* **1994**, *242*, 263-266.

(170) Moylan, C. R. *The Journal of Physical Chemistry* **1994**, *98*, 13513-13516.

(171) Geng Zhang, F.; Lian Yu, C. *Journal of Applied Physics* **1987**, *62*, 49-50.

(172) Jones, G.; Rahman, M. A. *The Journal of Physical Chemistry* **1994**, *98*, 13028-13037.

(173) Kostova, I. *Current Medicinal Chemistry -Anti-Cancer Agents* **2005**, *5*, 29-46.

(174) Kostova, I. *Mini Reviews in Medicinal Chemistry* **2006**, *6*, 365-374.

(175) Huang, J.-L.; Li, C.-J.; Gray, D. G. *ACS Sustainable Chemistry & Engineering* **2013**, *1*, 1160-1164.

(176) Biyani, M.; Weder, C.; Foster, E. J. *Polymer Chemistry* **2014**.

(177) Kolb, H. C.; Finn, M. G.; Sharpless, K. B. *Angewandte Chemie International Edition* **2001**, *40*, 2004-2021.

(178) Binder, W. H.; Sachsenhofer, R. *Macromolecular Rapid Communications* **2008**, *29*, 952-981.

(179) Johnson, J. A.; Finn, M. G.; Koberstein, J. T.; Turro, N. J. *Macromolecular Rapid Communications* **2008**, *29*, 1421-1421.

(180) Lundberg, P.; Hawker, C. J.; Hult, A.; Malkoch, M. *Macromolecular Rapid Communications* **2008**, *29*, 998-1015.

(181) Enders, C.; Tanner, S.; Binder, W. H. *Macromolecules* **2010**, *43*, 8436-8446.

(182) Posner, T. *Berichte der deutschen chemischen Gesellschaft* **1905**, *38*, 646-657.

(183) Kade, M. J.; Burke, D. J.; Hawker, C. J. *Journal of Polymer Science Part A: Polymer Chemistry* **2010**, *48*, 743-750.

(184) Pounder, R. J.; Stanford, M. J.; Brooks, P.; Richards, S. P.; Dove, A. P. *Chemical Communications* **2008**, 5158-5160.

(185) Sukumaran, S. C.; Sunitha, K.; Mathew, D.; Reghunadhan Nair, C. P. *Journal of Applied Polymer Science* **2013**, *130*, 1289-1300.

(186) Hansell, C. F.; Espeel, P.; Stamenović, M. M.; Barker, I. A.; Dove, A. P.; Du Prez, F. E.; O'Reilly, R. K. *Journal of the American Chemical Society* **2011**, *133*, 13828-13831.

(187) Sumerlin, B. S.; Vogt, A. P. *Macromolecules* **2009**, *43*, 1-13.

(188) Nuttelman, C. R.; Rice, M. A.; Rydholm, A. E.; Salinas, C. N.; Shah, D. N.; Anseth, K. S. *Progress in Polymer Science* **2008**, *33*, 167-179.

(189) Clark, T.; Hoyle, C.; Nazarenko, S. *Journal of Coatings Technology and Research* **2008**, *5*, 345-351.

(190) Campos, L. M.; Meinel, I.; Guino, R. G.; Schierhorn, M.; Gupta, N.; Stucky, G. D.; Hawker, C. J. *Advanced Materials* **2008**, *20*, 3728-3733.

(191) Zhao, G.-L.; Hafrén, J.; Deiana, L.; Córdova, A. *Macromolecular Rapid Communications* **2010**, *31*, 740-744.

(192) Liebert, T.; Hänsch, C.; Heinze, T. *Macromolecular Rapid Communications* **2006**, *27*, 208-213.

(193) Eyley, S.; Thielemans, W. *Chemical Communications*, *47*, 4177-4179.

(194) Li, M.; De, P.; Gondi, S. R.; Sumerlin, B. S. *Journal of Polymer Science Part A: Polymer Chemistry* **2008**, *46*, 5093-5100.

(195) Chan, J. W.; Hoyle, C. E.; Lowe, A. B. *Journal of the American Chemical Society* **2009**, *131*, 5751-5753.

(196) Kakwere, H.; Perrier, S. b. *Journal of the American Chemical Society* **2009**, *131*, 1889-1895.

(197) Nielsen, L. J.; Eyley, S.; Thielemans, W.; Aylott, J. W. *Chemical Communications*, *46*, 8929-8931.

(198) Labet, M.; Thielemans, W. *Cellulose* **2011**, *18*, 607-617.

(199) Habibi, Y.; Hoeger, I.; Kelley, S. S.; Rojas, O. J. *Langmuir* **2009**, *26*, 990-1001.

(200) Thygesen, A.; Oddershede, J.; Lilholt, H.; Thomsen, A. B.; Ståhl, K. *Cellulose* **2005**, *12*, 563-576.

(201) Bragg, W. H.; Bragg, W. L. *The Crystalline State: A general survey, by W. L. Bragg*; G. Bell and Sons, 1954.

(202) Clegg, W. *Crystal Structure Analysis: Principles and Practice*; International Union of Crystallography, 2001.

(203) Hammond, C. *The basics of crystallography and diffraction*; Oxford University Press, 2009.

(204) Segal, L.; Creely, J. J.; Martin, A. E.; Conrad, C. M. *Textile Research Journal* **1959**, *29*, 786-794.

(205) Klug, H. P.; Alexander, L. E. *X-Ray Diffraction Procedures: For Polycrystalline and Amorphous Materials*; Wiley, 1974.

(206) Rietveld, H. *Journal of Applied Crystallography* **1969**, *2*, 65-71.

(207) Ifuku, S.; Nogi, M.; Abe, K.; Handa, K.; Nakatsubo, F.; Yano, H. *Biomacromolecules* **2007**, *8*, 1973-1978.

(208) Salajkova, M., Royal Institute of Technology, KTH, 2012.

(209) Iwamoto, S.; Nakagaito, A. N.; Yano, H. *Applied Physics A* **2007**, *89*, 461-466.

(210) Saito, T.; Hirota, M.; Tamura, N.; Kimura, S.; Fukuzumi, H.; Heux, L.; Isogai, A. *Biomacromolecules* **2009**, *10*, 1992-1996.

(211) Viëtor, R. J.; Newman, R. H.; Ha, M.-A.; Apperley, D. C.; Jarvis, M. C. *The Plant Journal* **2002**, *30*, 721-731.

(212) Wada, M.; Heux, L.; Nishiyama, Y.; Langan, P. *Biomacromolecules* **2008**, *10*, 302-309.

(213) Maréchal, Y.; Chanzy, H. *Journal of Molecular Structure* **2000**, *523*, 183-196.

(214) The University of Nottingham: Chemistry School Intranet, CHN Microanalysis Instrument 2014.

(215) de la Motte, H.; Hasani, M.; Brelid, H.; Westman, G. *Carbohydrate Polymers* **2011**, *85*, 738-746.

(216) Siegbahn, K. *Electron Spectroscopy for Atoms, Molecules and Condensed Matter*; Inst. of Physics, Univ., 1981.

(217) Niemantsverdriet J. V. *Spectroscopy in Catalysis*; 2nd ed.; Wiley-VCH: Weinheim, 2000.

(218) Briggs, D.; Seah, P. *Practical Surface Analysis, Auger and X-ray Photoelectron Spectroscopy*; Wiley, 1990.

(219) Hüfner, S. *Photoelectron Spectroscopy: Principles and Applications*; Springer, 2003.

(220) Briggs D.; T., G. J. *Surface analysis by Auger and x-ray photoelectron spectroscopy* IMP Publications, Chichester, UK and Surface Spectra: Manchester, UK, 2003.

(221) Briggs, D. *Surface and Interface Analysis* **1981**, *3*, v-v.

(222) Taylor, A. *Electrochemistry in vacuo*; PhD Tesis, The university of Nottingham: Nottingham, UK, 2010.

(223) Villar-Garcia, I. J. *X-ray Photoelectron Spectroscopy of ionic liquids*; PhD Thesis,The University of Nottingham, Nottingham, 2009.

(224) Cros, A. *Journal of Electron Spectroscopy and Related Phenomena* **1992**, *59*, 1-14.

(225) BS ISO; 19318:2004 "Surface chemical analysis - X-ray photoelectron spectroscopy - Reporting of methods used for charge control and charge correction," 2004.

(226) Walton, J. *Peak Fitting with CasaXPS: A Casa Pocket Book*; Acolyte Science, 2010.

(227) Beamson, G.; Briggs, D. *High Resolution XPS of Organic Polymers: The Scienta ESCA300 Database*; Wiley, 1992.

(228) Beamson G.; Briggs D. *XPS of polymers database*; SurfaceSpectra: Manchester, 2000.

(229) Powell, C. J.; Jablonski, A. *Journal of Electron Spectroscopy and Related Phenomena* **2010**, *178–179*, 331-346.

(230) Lahiji, R. R.; Xu, X.; Reifenberger, R.; Raman, A.; Rudie, A.; Moon, R. J. *Langmuir* **2010**, *26*, 4480-4488.

(231) www.lifetechnologies.com: Introduction to Fluorescence 2014.

(232) Sauer, M.; Hofkens, J.; Enderlein, J. *Handbook of Fluorescence Spectroscopy and Imaging: From Single Molecules to Ensembles*; Wiley-VCH, Weinheim, GER, 2010.

(233) McNaught, A. D.; Wilkinsom, A. *IUPAC. Compendium of Chemical Terminology, 2nd ed. (the "Gold Book")*; Blackwell Scientific Publications, Oxford, UK, 1997.

(234) Malvern Instruments Ltd; Malvern; UK *Technical Note: Zeta Potential An Introduction in 30 Minutes* **2012**.

(235) O'Brien, R. W.; Midmore, B. R.; Lamb, A.; Hunter, R. J. *Faraday Discussions of the Chemical Society* **1990**, *90*, 301-312.

(236) Hanaor, D.; Michelazzi, M.; Leonelli, C.; Sorrell, C. C. *Journal of the European Ceramic Society* **2012**, *32*, 235-244.

(237) Stadler, A.; Kappe, C. O. *Tetrahedron* **2001**, *57*, 3915-3920.

(238) Spectral Database for Organic Compounds SDBS, 2013.

(239) Chowdhury, S. R.; Sabharwal, S. *Journal of Materials Chemistry* **2011**, *21*, 6999-7006.

(240) Briggs, D. *Surface Analysis of Polymers by XPS and Static SIMS*; Cambridge University Press: Cambridge, 1998.

(241) Liang, S.-S.; Chen, S.-L.; Chen, S.-H. *Chemical Communications* **2011**, *47*, 8385-8387.

(242) Marsano, E.; De Paz, L.; Tambuscio, E.; Bianchi, E. *Polymer* **1998**, *39*, 4289-4294.

(243) Heuser, E.; Heath, M.; Shockley, W. H. *Journal of the American Chemical Society* **1950**, *72*, 670-674.

(244) Wagner, C. D.; Riggs, W. M.; Devis, L. E.; J.F., M.; G.E., M. *Handbook of X-ray Photoelectron Spectroscopy*; Perkin-Elmer Corporation, Physical Electronics Division: Eden Prairie, Minnesota, 1979.

(245) Shao, H.; Chen, X.; Wang, Z.; Lu, P. *Journal of Luminescence* **2007**, *127*, 349-354.

(246) Webb, M. R.; Corrie, J. E. T. *Biophysical Journal*, *81*, 1562-1569.

(247) Hannig, E.; Schobess, B. *Archiv Der Pharmazie Und Berichte Der Deutschen Pharmazeutischen Gesselschaft* **1963**, *296*, 536-&.

(248) Conn, M. M.; Deslongchamps, G.; de Mendoza, J.; Rebek, J. *Journal of the American Chemical Society* **1993**, *115*, 3548-3557.

(249) Guo, D.-C.; Li, P.-L.; Wang, X.; Wang, L.-Y.; Wu, P.-L. *Synthetic Communications* **2010**, *40*, 3315-3321.

(250) He, Y.-J.; Xie, M.-H.; Zou, P.; Liu, Y.-L.; Wang, H.-Y. *Acta Crystallographica Section E* **2009**, *65*, o1136.

(251) Xie, M.-H.; Zou, P.; He, Y.-J.; Liu, Y.-L.; Huang, B. *Acta Crystallographica Section E* **2009**, *65*, o2860.

(252) Allen, F. H.; Kennard, O.; Watson, D. G.; Brammer, L.; Orpen, A. G.; Taylor, R. *Journal of the Chemical Society, Perkin Transactions 2* **1987**, S1-S19.

(253) He, Y. J.; Xie, M. H.; Zou, P.; Liu, Y. L.; Wang, H. Y. *Acta Crystallogr Sect E Struct Rep Online* **2009**, *65*, o1136.

(254) Dobson, A. J.; Gerkin, R. E. *Acta Crystallographica Section C* **1996**, *52*, 3081-3083.

(255) Lahaye, J.; Nansé, G.; Bagreev, A.; Strelko, V. *Carbon* **1999**, *37*, 585-590.

(256) Chekunov, A. V.; Polyakova, I. A. *Journal of Applied Spectroscopy* **1969**, *10*, 523-525.

(257) Sawicki, E.; Hauser, T. R.; Stanley, T. W.; Elbert, W.; Fox, F. T. *Analytical Chemistry* **1961**, *33*, 1574-1579.

(258) Cisse, L.; Djande, A.; Capo-Chichi, M.; Delatre, F.; Saba, A.; Tine, A.; Aaron, J.-J. *Spectrochimica Acta Part A: Molecular and Biomolecular Spectroscopy* **2011**, *79*, 428-436.

(259) Lowen, S. V.; Buschek, J.; Mastantuono, R.; Holden, D. A.; Kovacs, G. J.; Loutfy, R. O. *Macromolecules* **1990**, *23*, 3242-3249.

(260) Lakowicz, J. R. *Principles of Fluorescence Spectroscopy*; 2nd Edition ed.; Plenum Press New York, 1999.

(261) Gömez, J. A. C.; Erler, U. W.; Klemm, D. O. *Macromolecular Chemistry and Physics* **1996**, *197*, 953-964.

(262) Hasani, M.; Westman, G.; Potthast, A.; Rosenau, T. *Journal of Applied Polymer Science* **2009**, *114*, 1449-1456.

(263) Lovelock, K. R. J.; Villar-Garcia, I. J.; Maier, F.; Steinrück, H.-P.; Licence, P. *Chemical Reviews* **2010**, *110*, 5158-5190.

(264) Gang, L.; Haipeng, Y.; Yixing, L. *Advanced Materials Research* **2011**, *221*, 5.

(265) Kolbeck, C.; Cremer, T.; Lovelock, K. R. J.; Paape, N.; Schulz, P. S.; Wasserscheid, P.; Maier, F.; Steinrück, H. P. *The Journal of Physical Chemistry B* **2009**, *113*, 8682-8688.

(266) Abramian, L.; El-Rassy, H. *Chemical Engineering Journal* **2009**, *150*, 403-410.

(267) Scott, G. V. *Analytical Chemistry* **1968**, *40*, 768-773.

(268) In *Ion Exchange: Theory and Practice (2)*; Harland, C. E., Ed.; The Royal Society of Chemistry, 1994; pp 39-48.

(269) Petrova, S. N.; Volodarskii, M. V.; Makarov, S. V.; Li, L. *Russian Journal of Applied Chemistry* **2008**, *81*, 1573-1577.

(270) Hoyle, C. E.; Lowe, A. B.; Bowman, C. N. *Chemical Society Reviews* **2010**, *39*, 1355-1387.

(271) Kelemen, S. R.; George, G. N.; Gorbaty, M. L. *Fuel* **1990**, *69*, 939-944.

(272) Wei, C.; Chen, M.; Tao, J.; Wu, X.; Khan, M.; Liu, D.; Huang, N.; Li, L. *Polymer Chemistry* **2014**.

(273) Briggs, D.; Seah, M. P. *D. Briggs, & M. P. Seah,(Editors), John Wiley & Sons, Chichester 1983, xiv+ 533* **1983**.

(274) Kaasjager, V. E.; Puglisi, L.; Bouwman, E.; Driessen, W. L.; Reedijk, J. *Inorganica Chimica Acta* **2000**, *310*, 183-190.

(275) Mountford, S. J.; Campi, E. M.; Robinson, A. J.; Hearn, M. T. W. *Tetrahedron* **2011**, *67*, 471-485.

(276) Briggs, D.; Seah, P. *Practical Surface Analysis: Auger and X-ray photoelectron spectroscopy*; Wiley, 1990.

(277) Maria Chong, A. S.; Zhao, X. S. *The Journal of Physical Chemistry B* **2003**, *107*, 12650-12657.

(278) Jakob, F.; Schlack, P. *Chemische Berichte* **1963**, *96*, 88-92.

(279) Kakwere, H.; Perrier, S. *Journal of the American Chemical Society* **2009**, *131*, 1889-1895.

(280) Cramer, N. B.; Bowman, C. N. *Journal of Polymer Science Part A: Polymer Chemistry* **2001**, *39*, 3311-3319.

(281) Fenske, T.; Korth, H.-G.; Mohr, A.; Schmuck, C. *Chemistry – A European Journal* **2012**, *18*, 738-755.

(282) Von White, G.; Provost, M. G.; Kitchens, C. L. *Industrial & Engineering Chemistry Research* **2012**, *51*, 5181-5189.

(283) Jessop, P. G.; Phan, L.; Carrier, A.; Robinson, S.; Durr, C. J.; Harjani, J. R. *Green Chemistry* **2010**, *12*, 809-814.

(284) Liu, Y.; Jessop, P. G.; Cunningham, M.; Eckert, C. A.; Liotta, C. L. *Science* **2006**, *313*, 958-960.

(285) Pickering, S. U. *Journal of the Chemical Society, Transactions* **1907**, *91*, 2001-2021.

(286) Tang, J.; Quinlan, P. J.; Tam, K. C. *Soft Matter* **2015**, *11*, 3512-3529.

(287) Binks, B. P.; Fletcher, P. D. I. *Langmuir* **2001**, *17*, 4708-4710.

(288) Kralchevsky, P. A.; Ivanov, I. B.; Ananthapadmanabhan, K. P.; Lips, A. *Langmuir* **2005**, *21*, 50-63.

(289) French, D. J.; Taylor, P.; Fowler, J.; Clegg, P. S. *Journal of Colloid and Interface Science* **2015**, *441*, 30-38.

(290) Biyani, M. V.; Jorfi, M.; Weder, C.; Foster, E. J. *Polymer Chemistry* **2014**, *5*, 5716-5724.

(291) Scoggins, M. W. *Journal of Chromatographic Science* **1975**, *13*, 146-148.

10 Appendix

10.1 Appendix for chapter 3

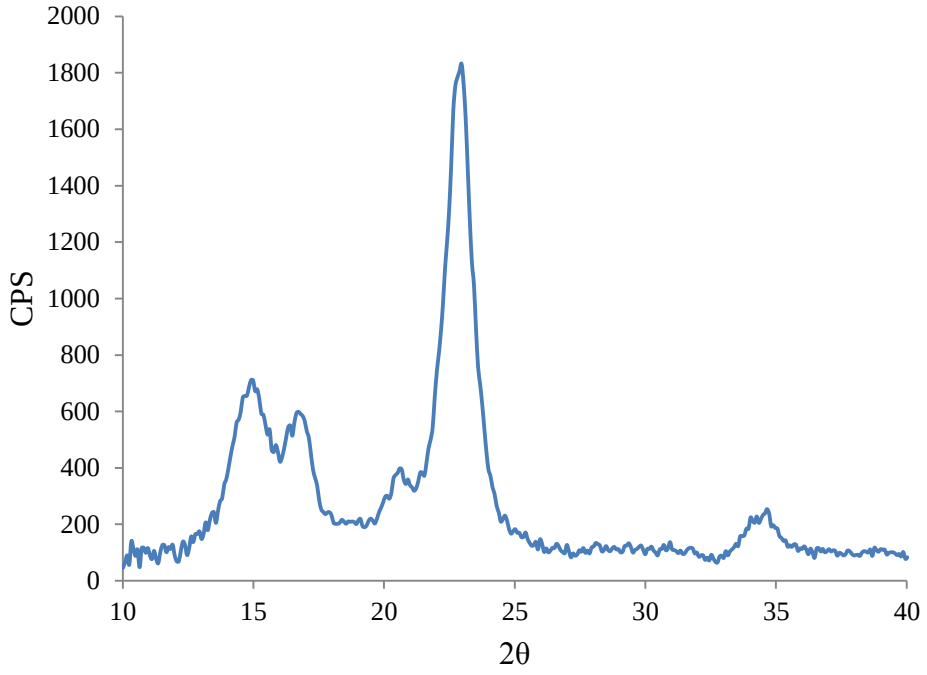


Figure 10.1.1 X-ray diffractogram of acrylate cellulose (1-ACNC) synthesised through DIC/DMAP

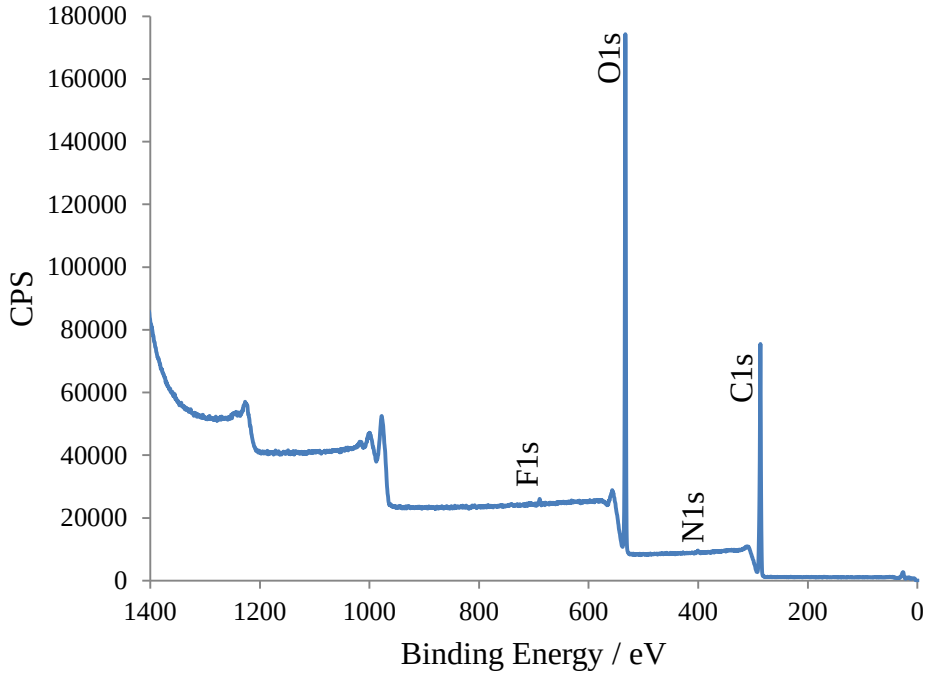


Figure 10.1.2 XPS wide scan of acrylate cellulose (1-ACNC)

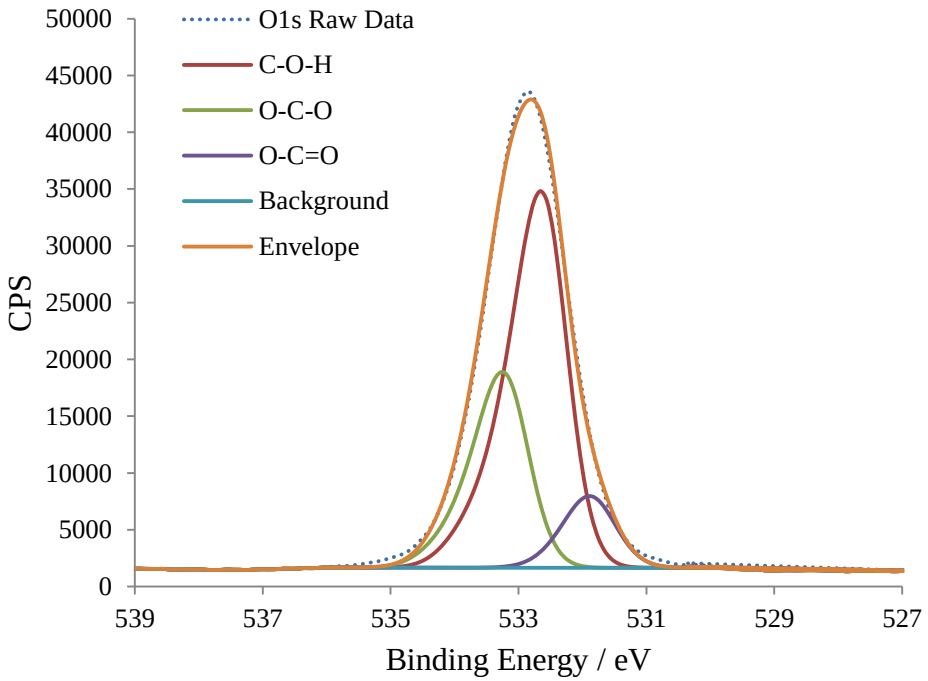


Figure 10.1.3 O1s high resolution scan of cellulose methacrylate (1-MACNC)

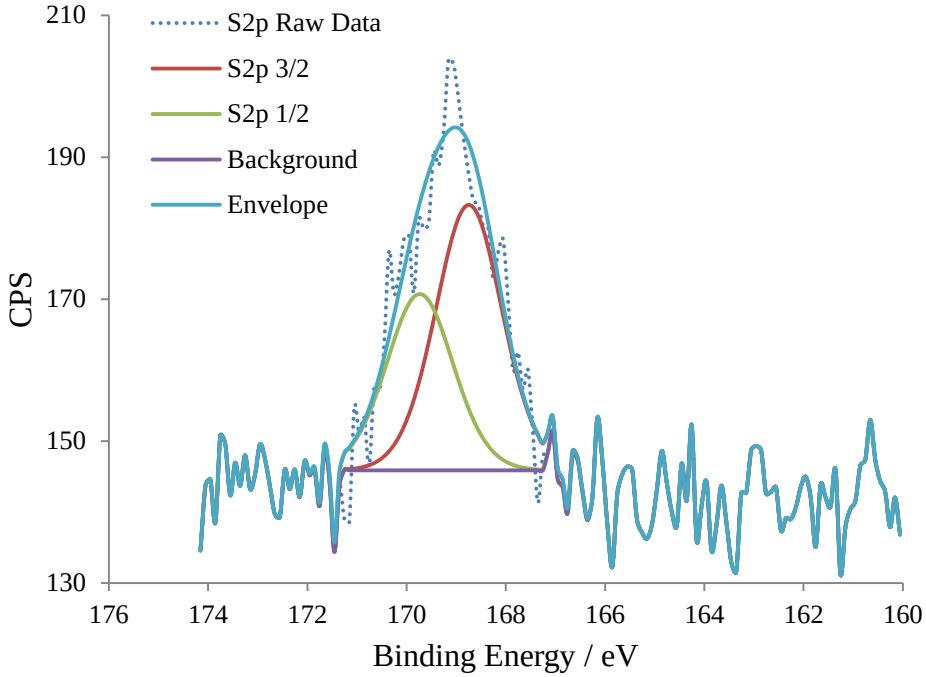


Figure 10.1.4 S2p high resolution scan of cellulose methacrylate (1-MACNC)

Table 10.1.1 Detailed XPS data of cellulose methacrylate (1-MACNC) synthesised through DIC/DMAP methodology

Orbital	Component	BE /eV	FWHM	Rel. A / % [a]	at%
C1s	C–C/C=C	284.83	1.14	8.05	4.82
	C–O	286.50	1.14	72.59	43.50
	O–C–O	287.93	1.14	17.68	10.59
	O–C=O	289.08	1.14	1.68	1.01
				100.00	59.92
O1s	O–C=O	531.78	0.94	10.04	4.01
	C–O–H	532.53	0.94	59.98	23.96
	O–C–O	533.13	0.94	29.98	11.98
				100.00	39.95
S2p	3/2	168.75	1.58	60.04	0.08
	1/2	169.73	1.58	39.96	0.05
				100.00	0.13

[a] Relative area = component area×100/sum area of same

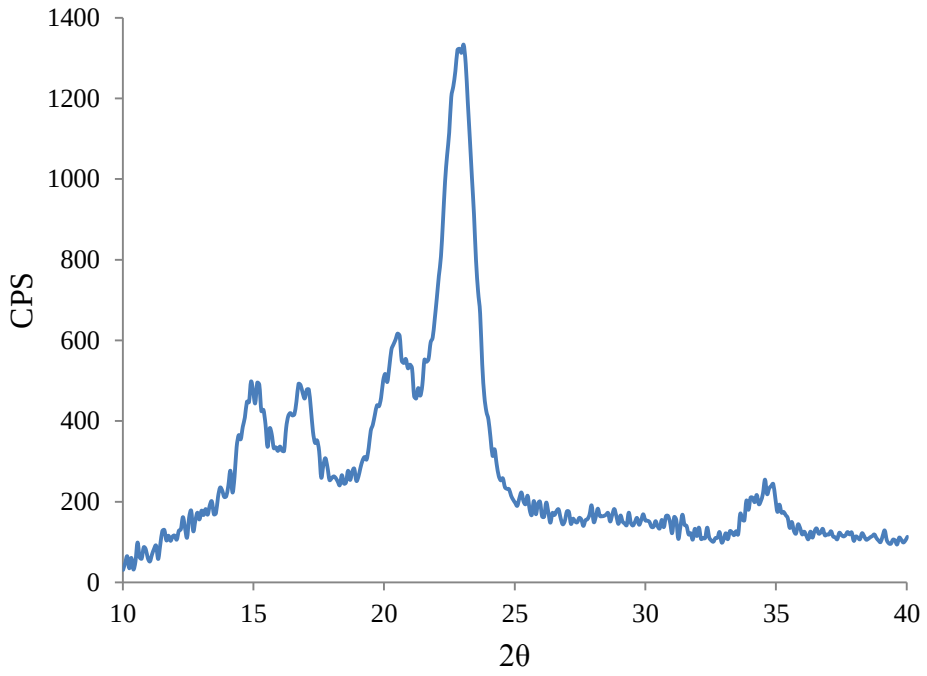


Figure 10.1.5 X-ray diffractogram of acrylate cellulose (2-ACNC) synthesised through TsCl/Py

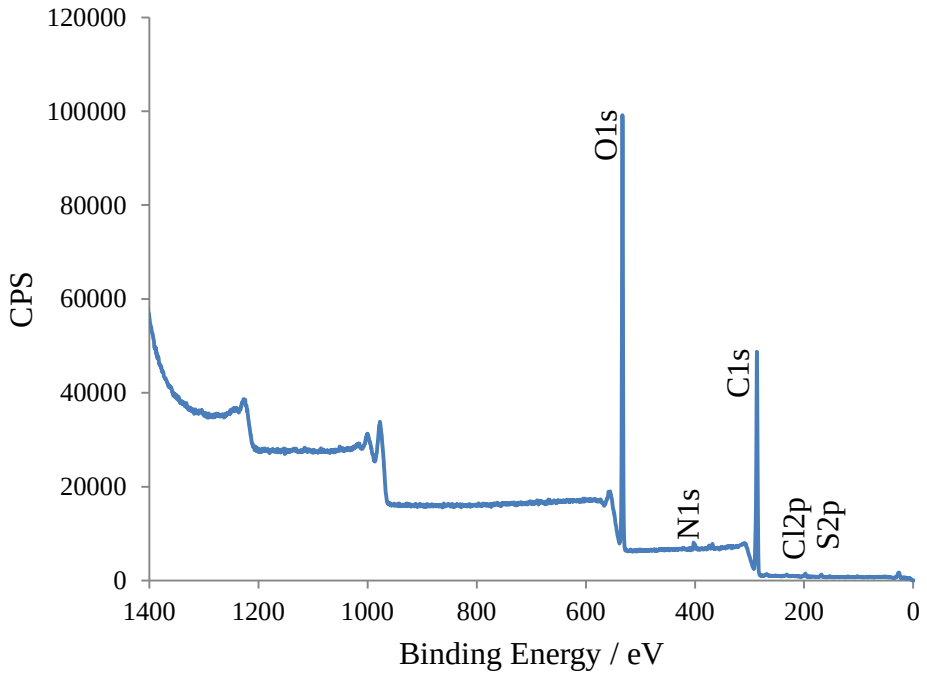


Figure 10.1.6 XPS spectrum of acrylate cellulose (2-ACNC) synthesised through TsCl/Py

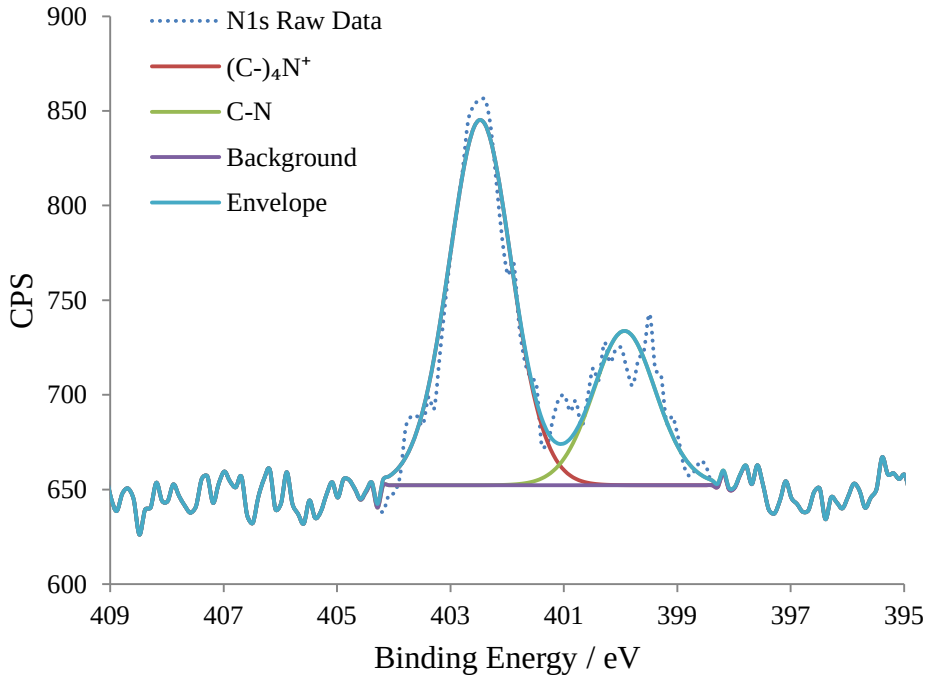


Figure 10.1.7 N1s high resolution scan of acrylate cellulose (2-ACNC) synthesised through TsCl/Py methodology

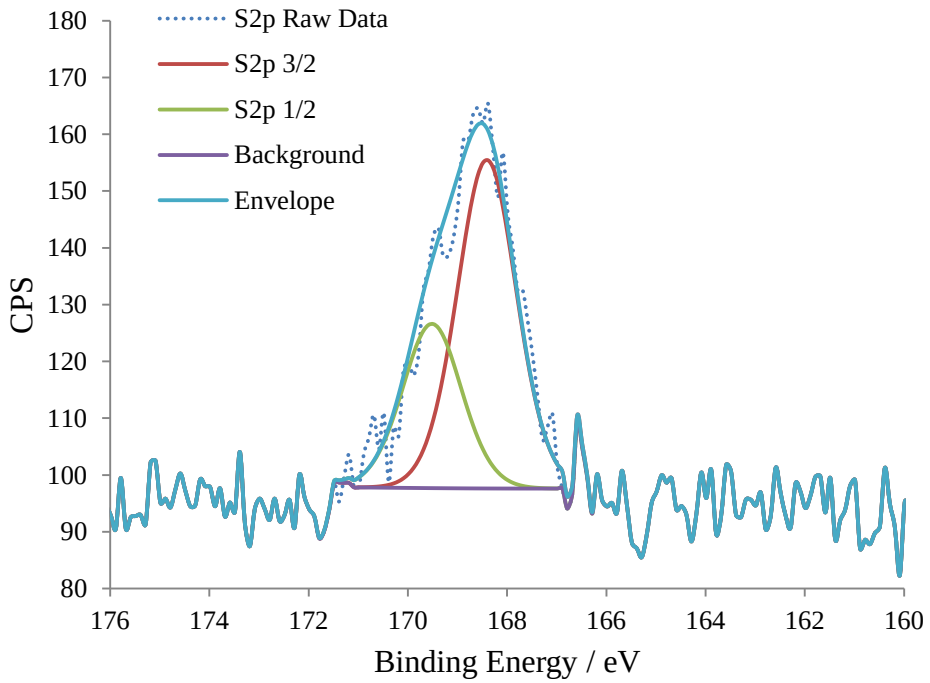


Figure 10.1.8 S2p high resolution scan of acrylate cellulose (2-ACNC) synthesised through TsCl/Py methodology

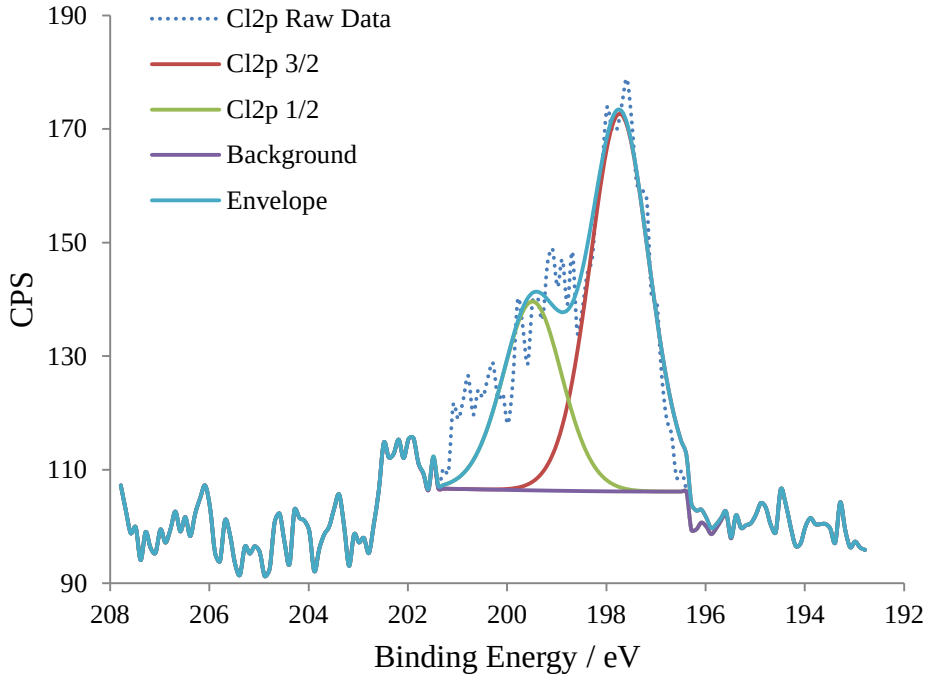


Figure 10.1.9 Cl2p high resolution scan of acrylate cellulose (2-ACNC) synthesised through TsCl/Py methodology

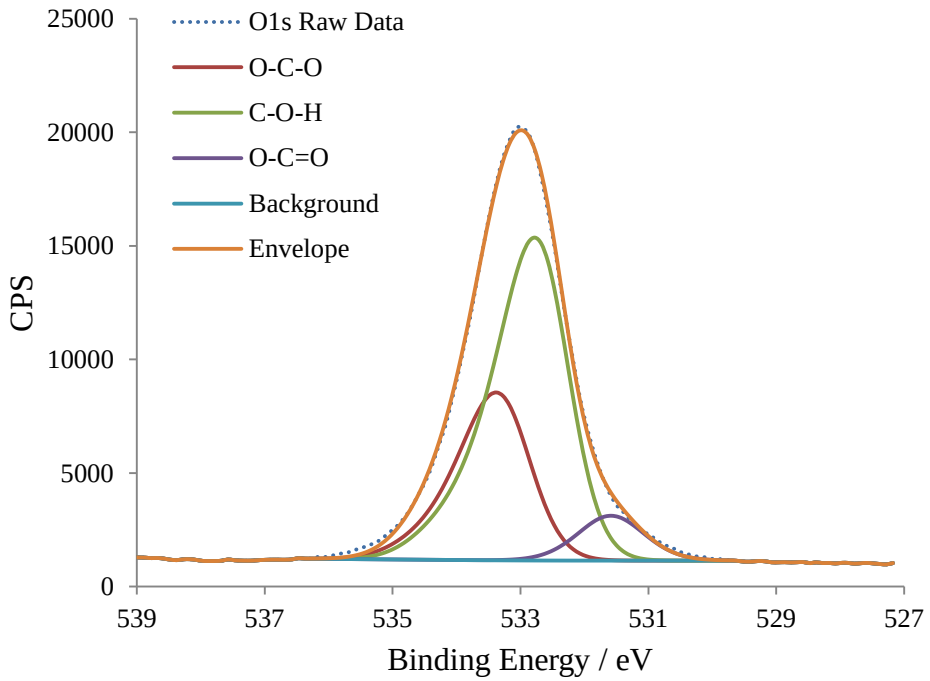


Figure 10.1.10 O1s high resolution spectrum of methacrylate cellulose (2-MACNC) synthesised through TsCl/Py methodology

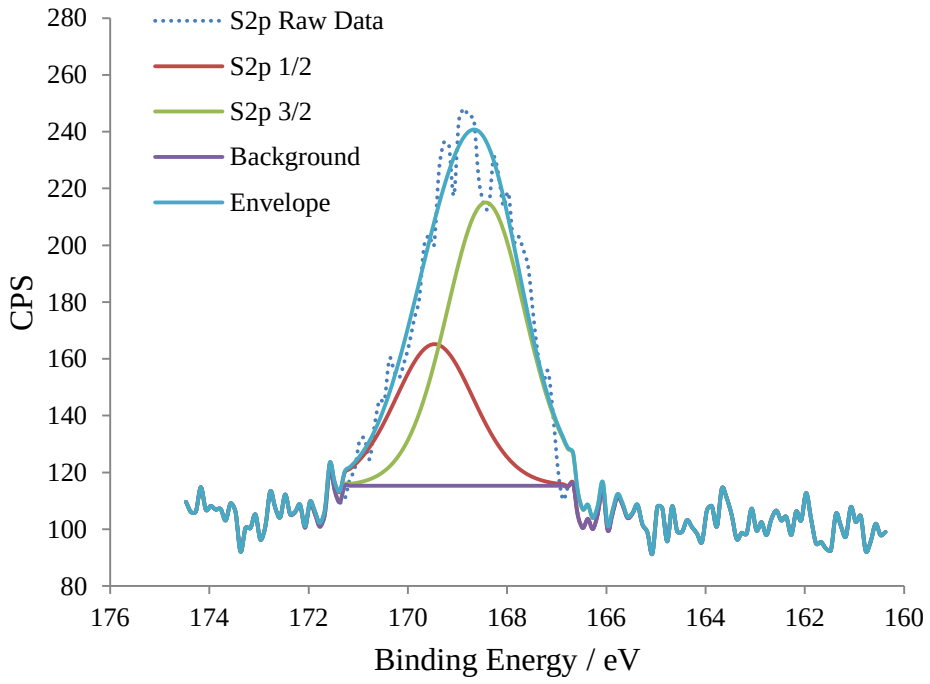


Figure 10.1.11 S2p high resolution scan of methacrylate cellulose (2-MACNC) synthesised through TsCl/Py methodology

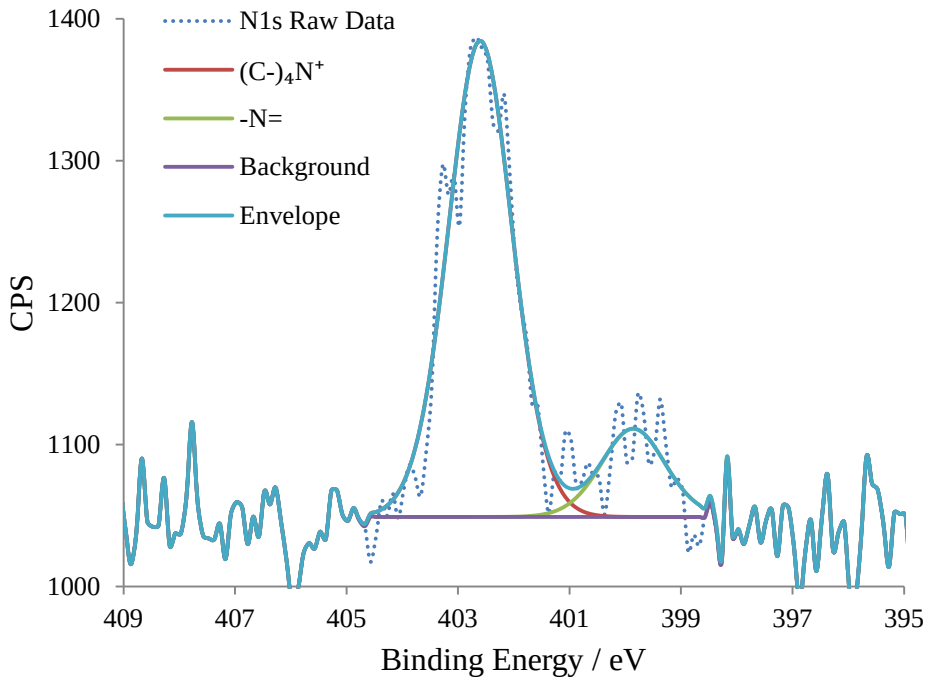


Figure 10.1.12 N1s high resolution scan of methacrylate cellulose (2-MACNC) synthesised through TsCl/Py methodology

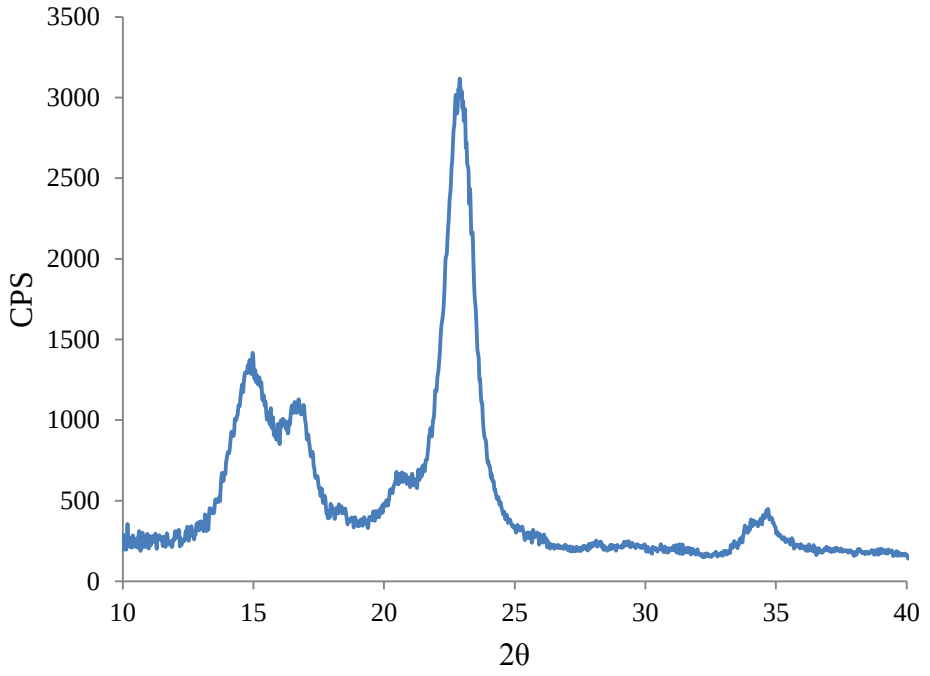


Figure 10.1.13 X-ray diffractogram of acrylate cellulose (2-ACNC(Et_3N)) synthesised through TsCl/Et_3N

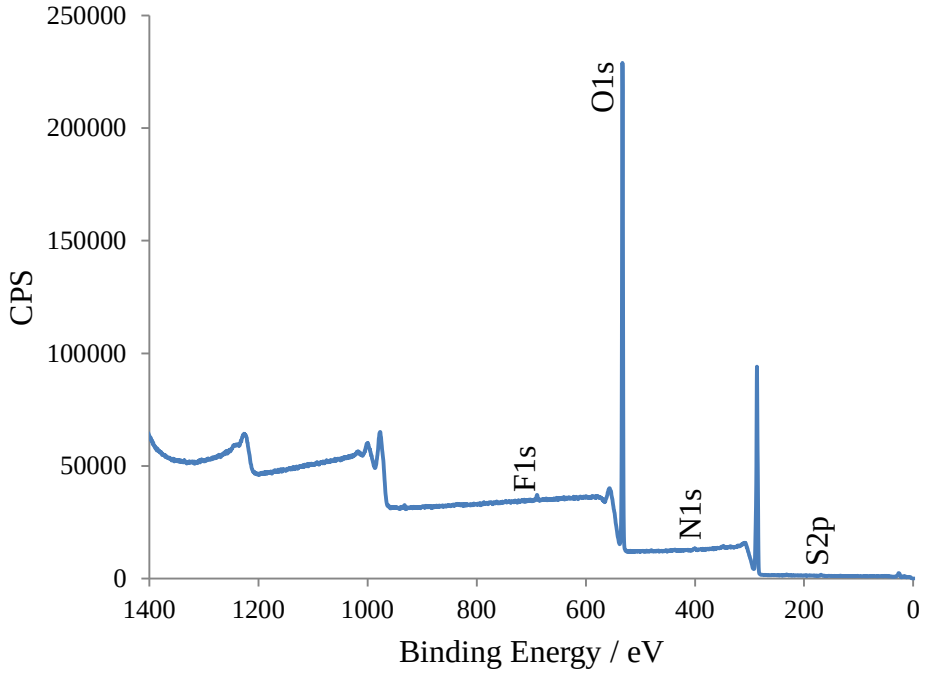


Figure 10.1.14 XPS spectrum of acrylate cellulose (2-ACNC(Et_3N)) synthesised through TsCl/Et_3N

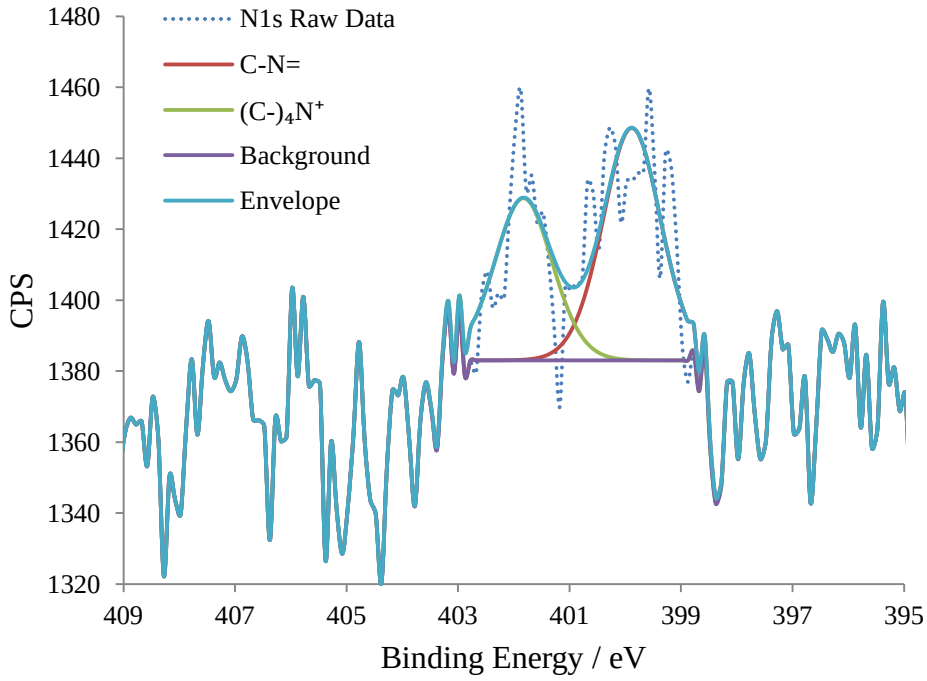


Figure 10.1.15 N1s high resolution scan of acrylate cellulose (2-ACNC(Et_3N)) synthesised through TsCl/Et_3N methodology

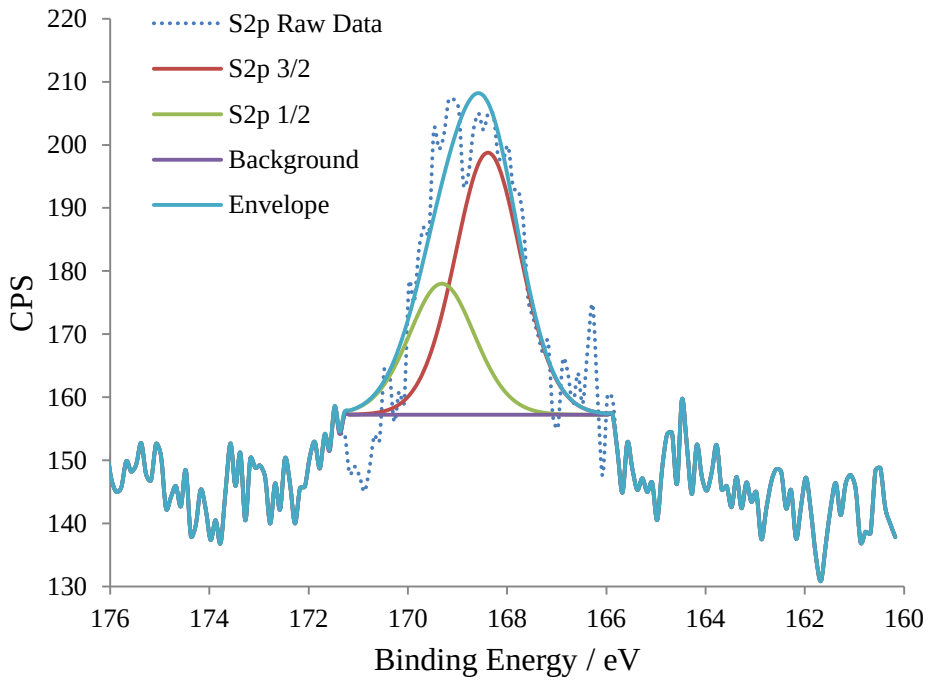


Figure 10.1.16 S2p high resolution scan of acrylate cellulose (2-ACNC(Et_3N)) synthesised through TsCl/Et_3N methodology

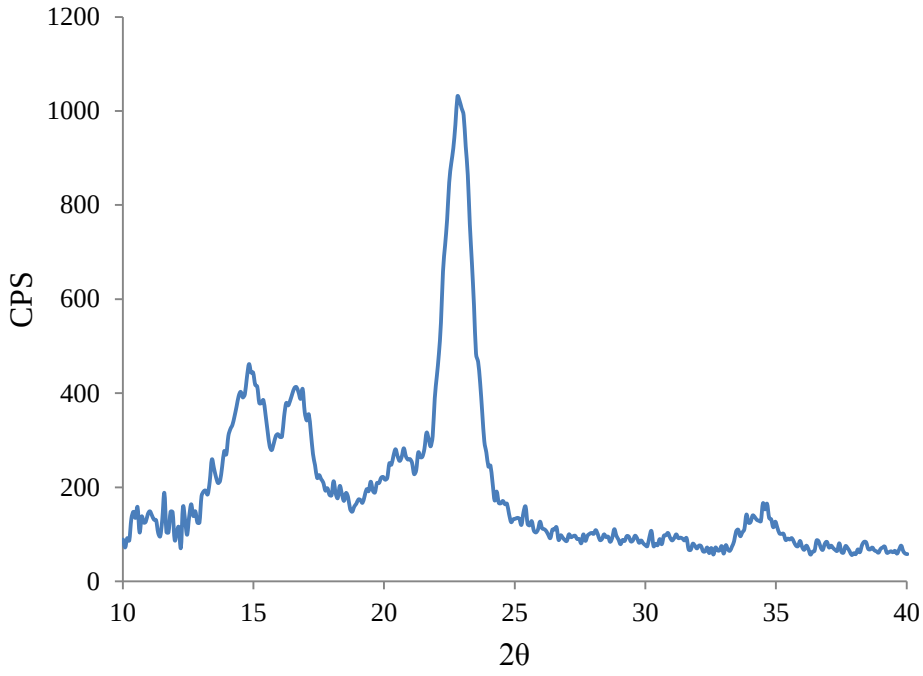


Figure 10.1.17 X-ray diffractogram of acrylate cellulose (3-ACNC) synthesised through the alkylation of acryloyl chloride in Et_3N/DMF system

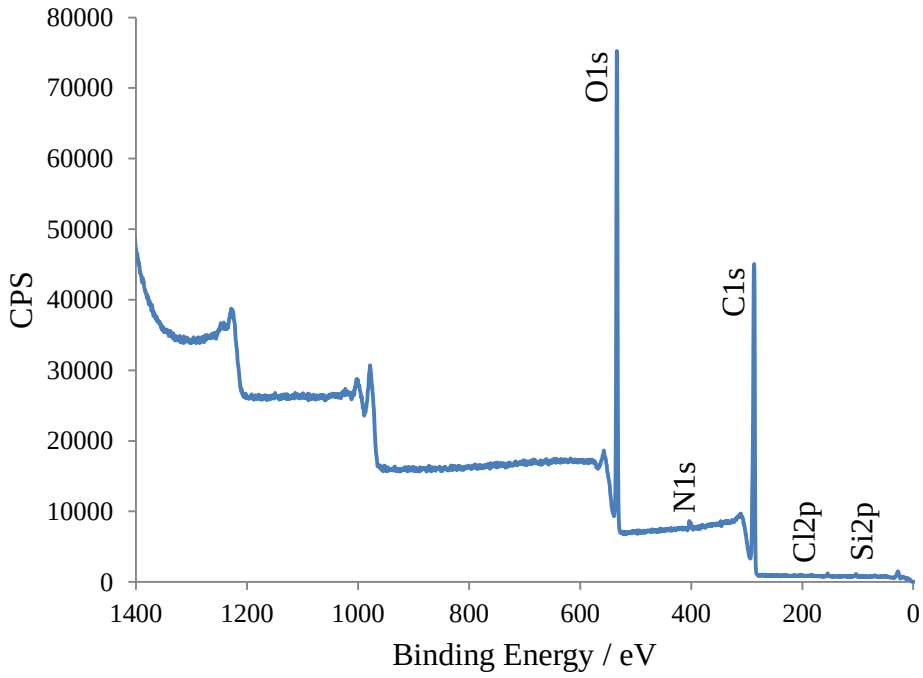


Figure 10.1.18 XPS spectrum of acrylate cellulose (3-ACNC) synthesised through the alkylation of acryloyl chloride in Et_3N/DMF system

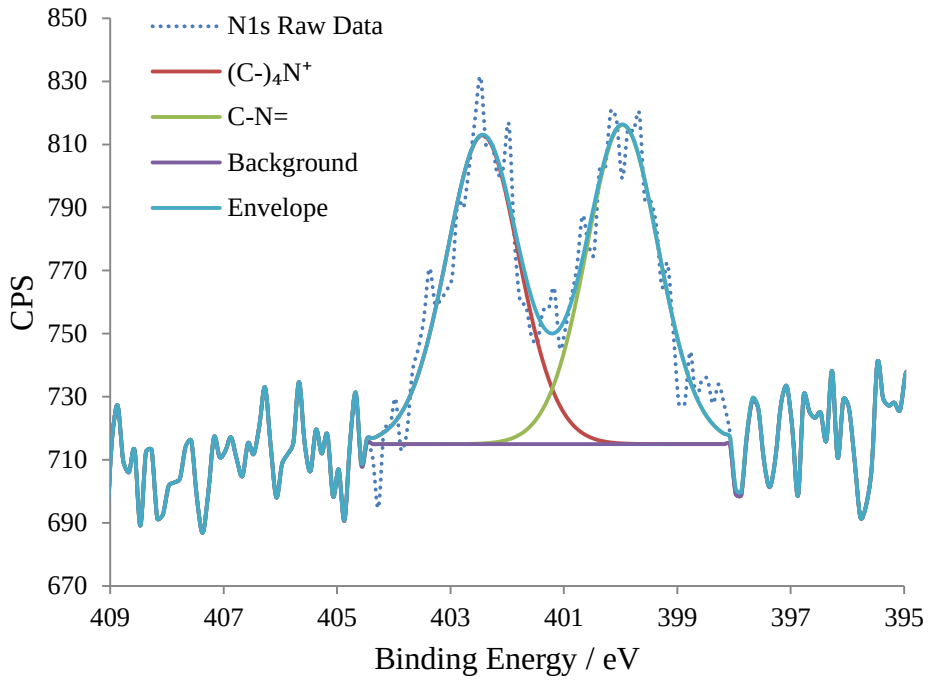


Figure 10.1.19 N1s high resolution scan of acrylate cellulose (3-ACNC) synthesised through the alkylation of acryloyl chloride in Et_3N/DMF system

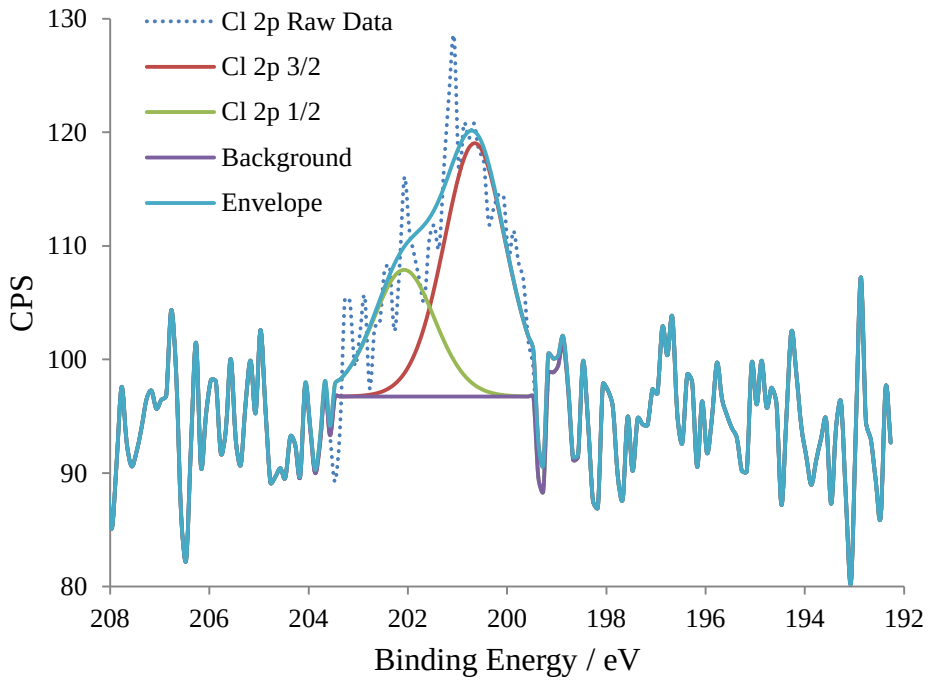


Figure 10.1.20 Cl2p high resolution scan acrylate cellulose (3-ACNC) synthesised through the alkylation of acryloyl chloride in Et_3N/DMF system

10.2 Appendix for chapter 4

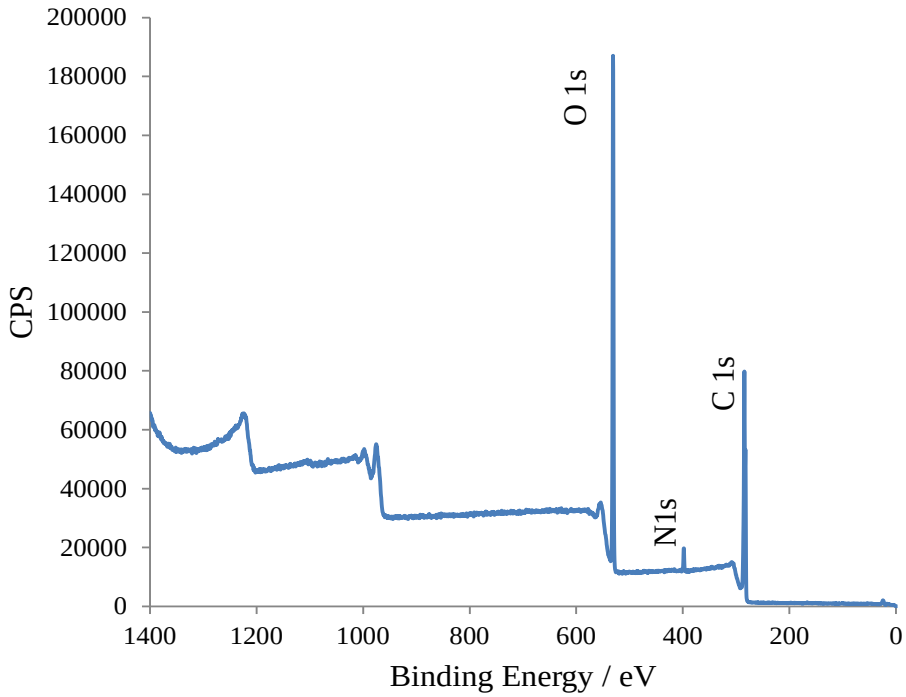


Figure 10.2.1 XPS wide scan of carbazole-9-yl-acetate cellulose synthesised through DIC/DMAP

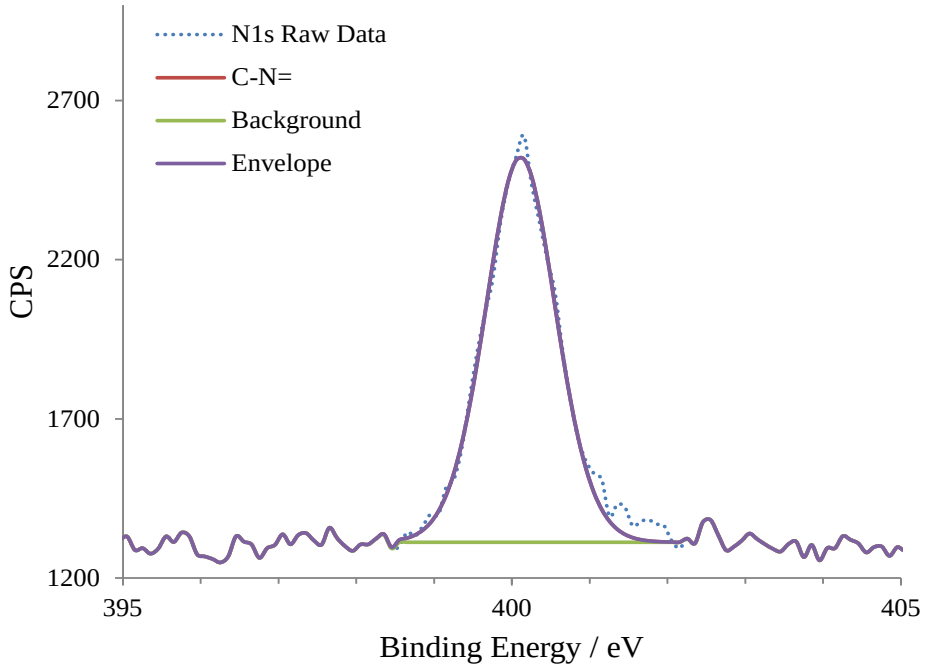


Figure 10.2.2 N1s high resolution scan of carbazole-9-yl-acetate, Cz-a-CNC-M2, synthesised through DIC/DMAP

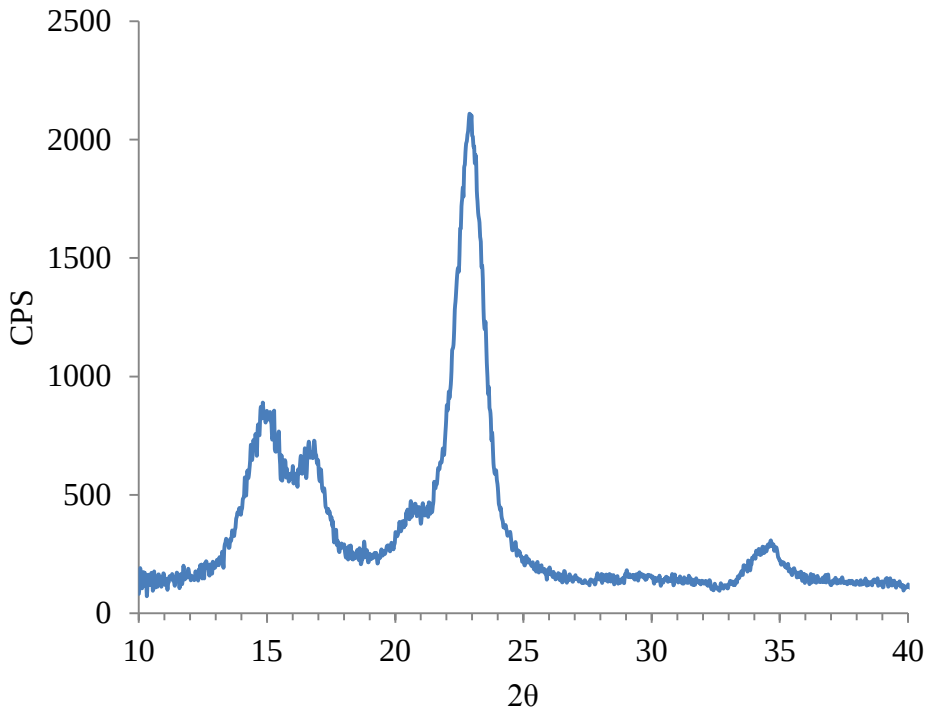


Figure 10.2.3 X-ray diffractogram of carbazole-9-yl-acetate cellulose synthesised through DIC/DMAP

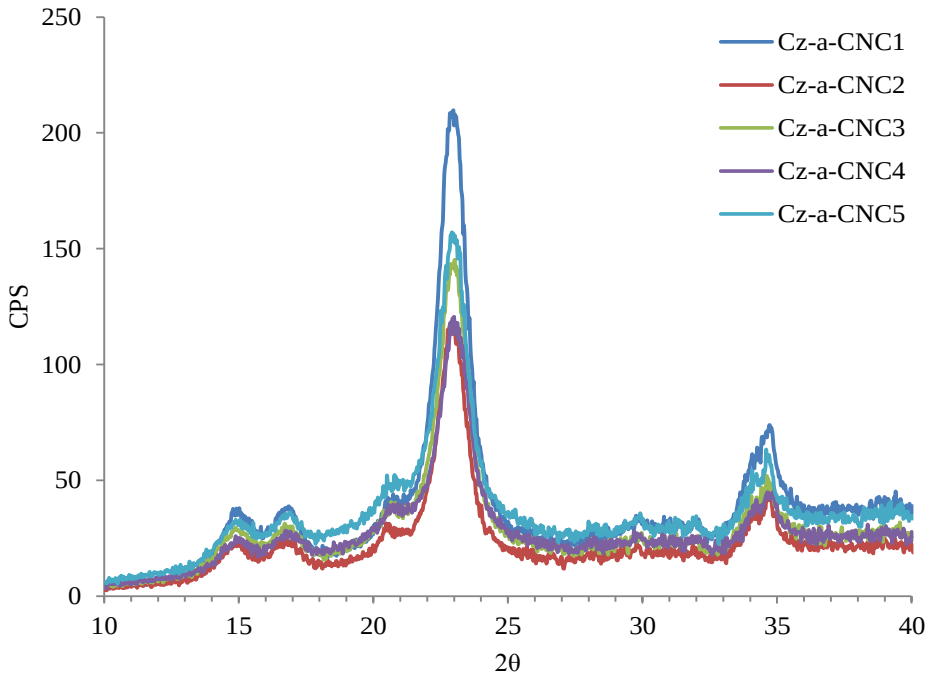


Figure 10.2.4 X-ray diffractogram of the five carbazole-9-yl-acetate cellulose synthesised through TsCl/Py

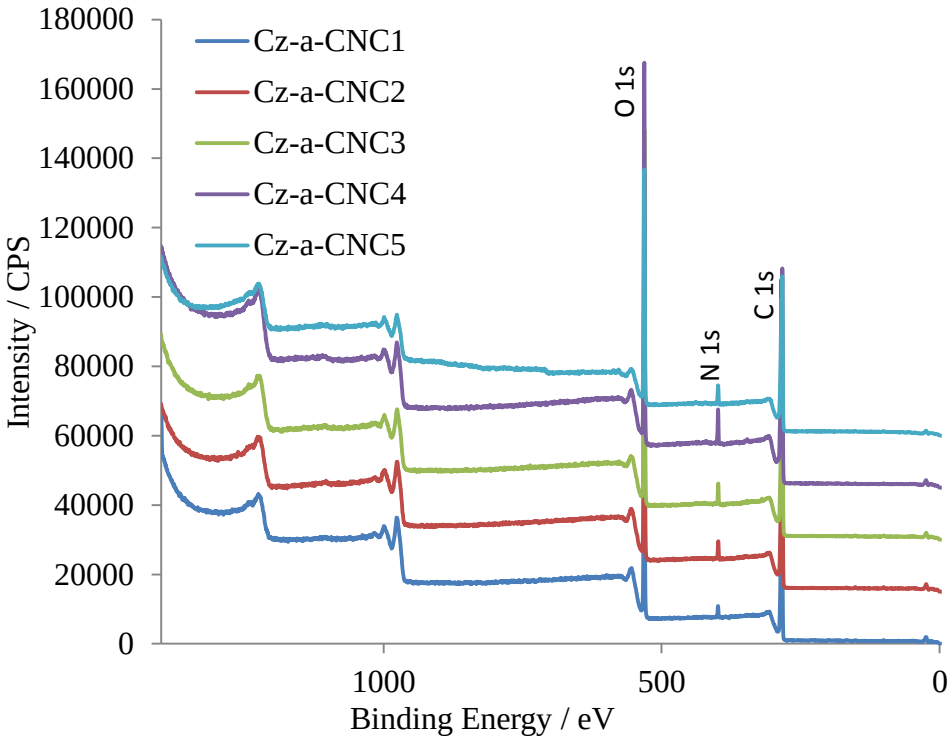


Figure 10.2.5 XPS wide scan of carbazole-9-yl-acetate cellulose synthesised through TsCl/Py

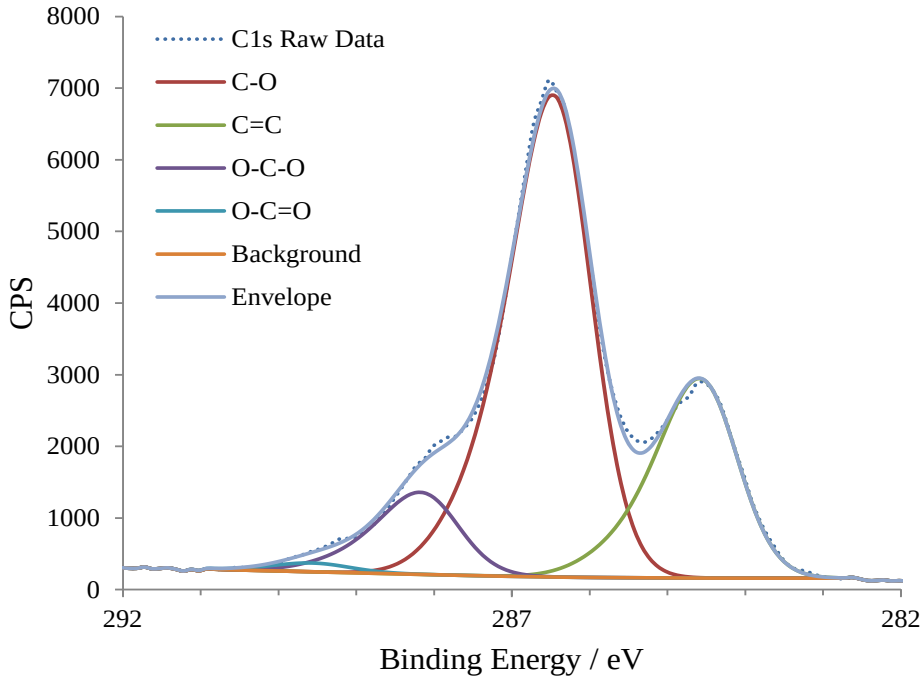


Figure 10.2.6 XPS high resolution spectrum of C1s peak of Carbazole-9-yl-acetate cellulose, Cz-a-CNC1, synthetized through TsCl/Py

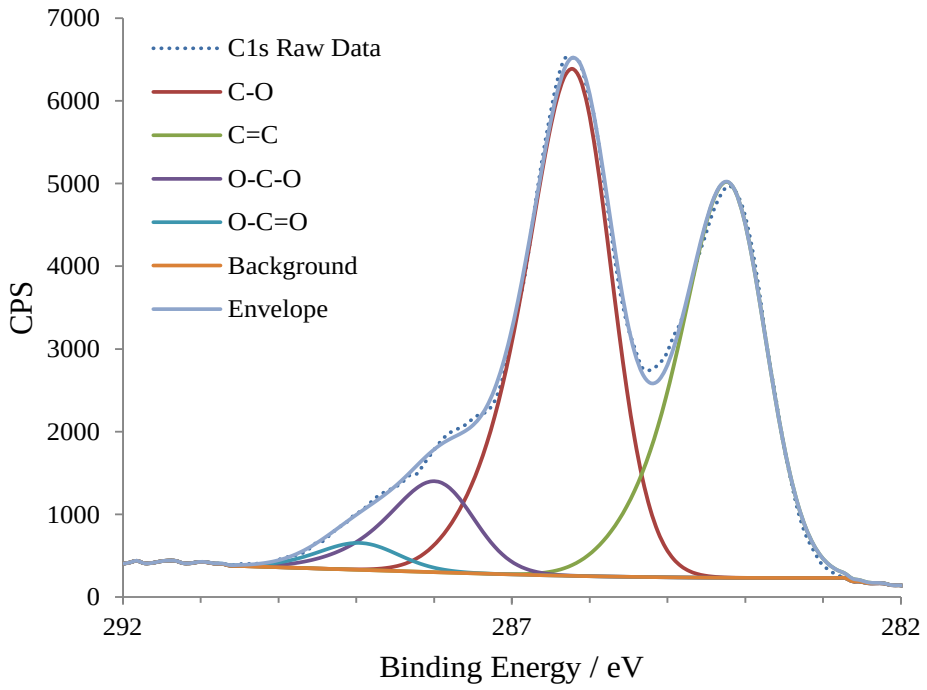


Figure 10.2.7 XPS high resolution spectrum of C1s peak of Carbazole-9-yl-acetate cellulose, Cz-a-CNC2, synthetized through TsCl/Py

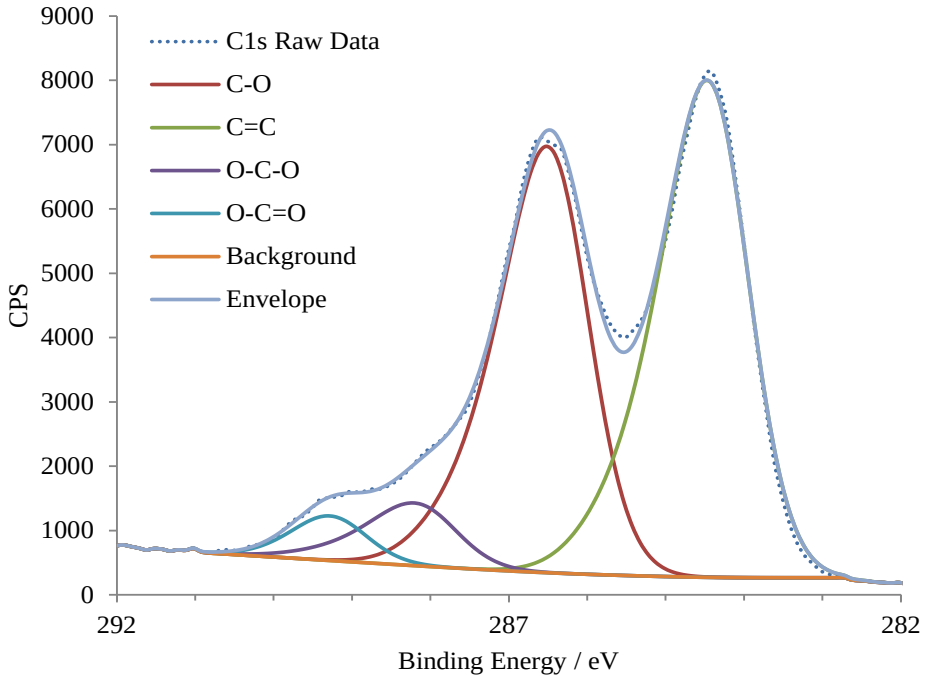


Figure 10.2.8 XPS high resolution spectrum of C1s peak of Carbazole-9-yl-acetate cellulose, Cz-a-CNC4, synthetized through TsCl/Py

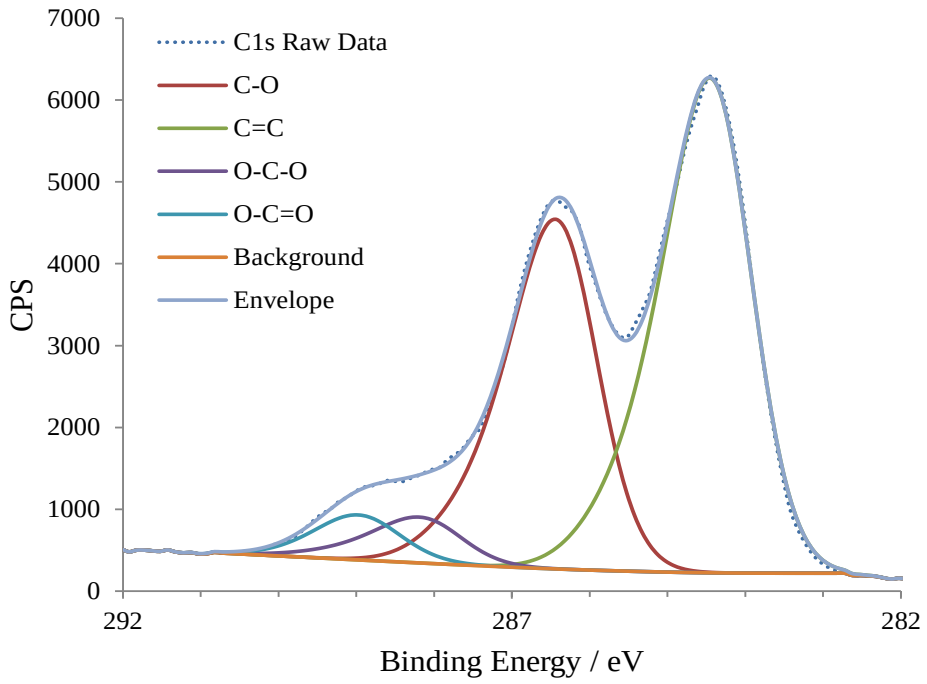


Figure 10.2.9 XPS high resolution spectrum of C1s peak of Carbazole-9-yl-acetate cellulose, Cz-a-CNC5, synthetized through TsCl/Py

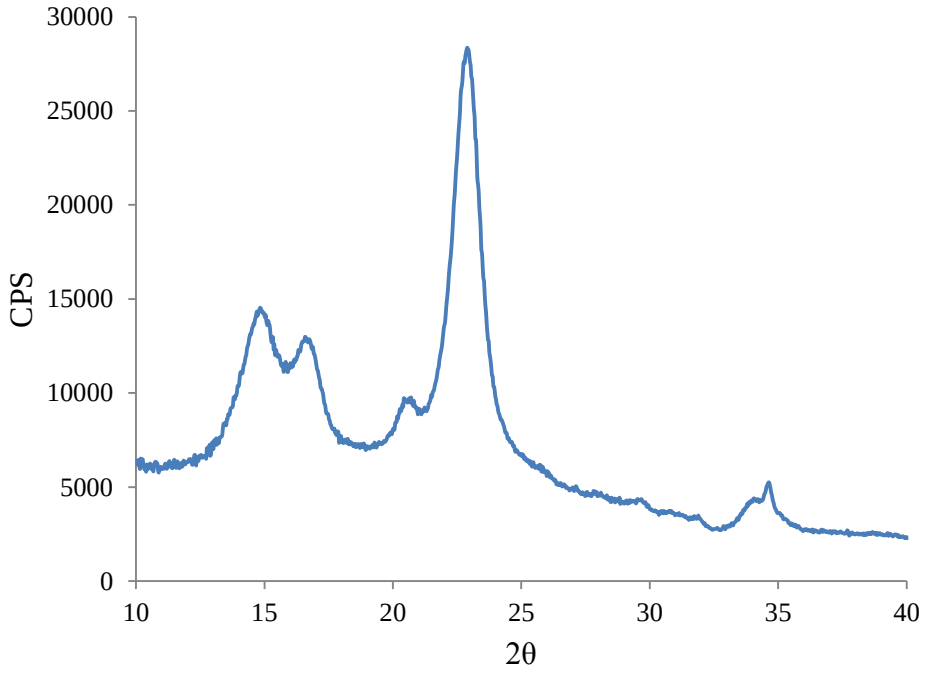


Figure 10.2.10 X-ray diffractogram of the coumarin-3-carboxylate cellulose Co-c-CNC1, synthesised through TsCl/Py

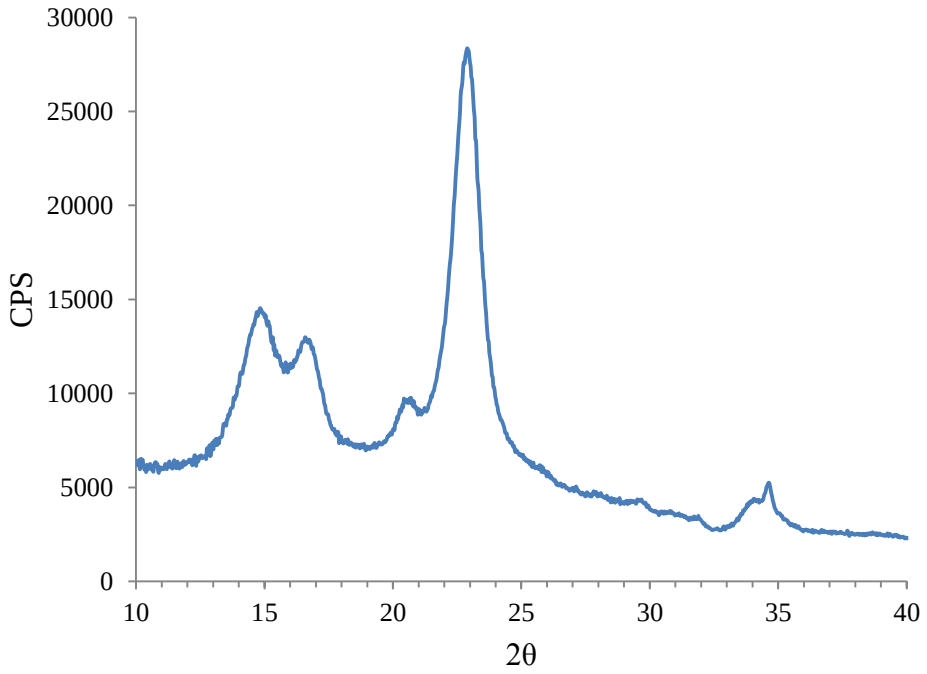


Figure 10.2.11 X-ray diffractogram of coumarin-3-carboxylate cellulose Co-c-CNC2, synthesised through TsCl/Py

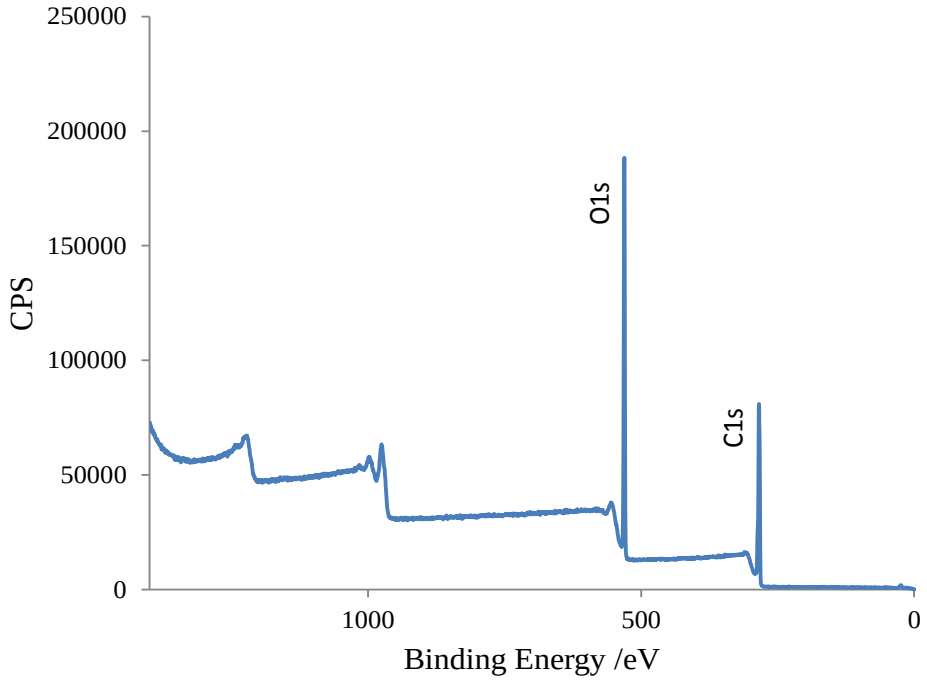


Figure 10.2.12 XPS wide scan of Co-c-CNC1 coumarin-3-carboxylate cellulose synthesised through TsCl/Py methodology

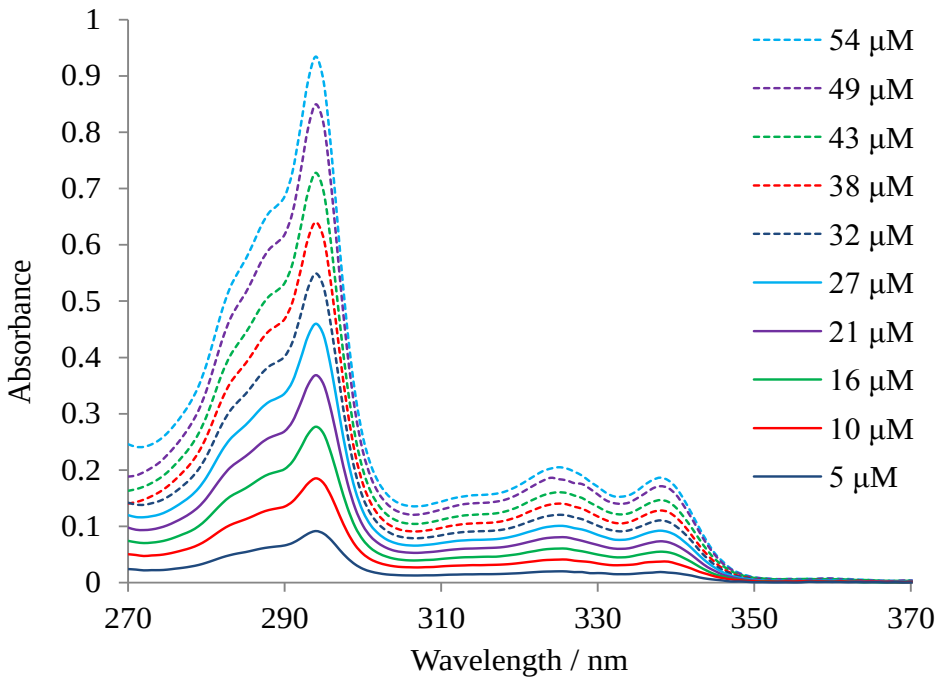


Figure 10.2.13 UV-Vis spectra for calibration of carbazole absorptivity in DMSO

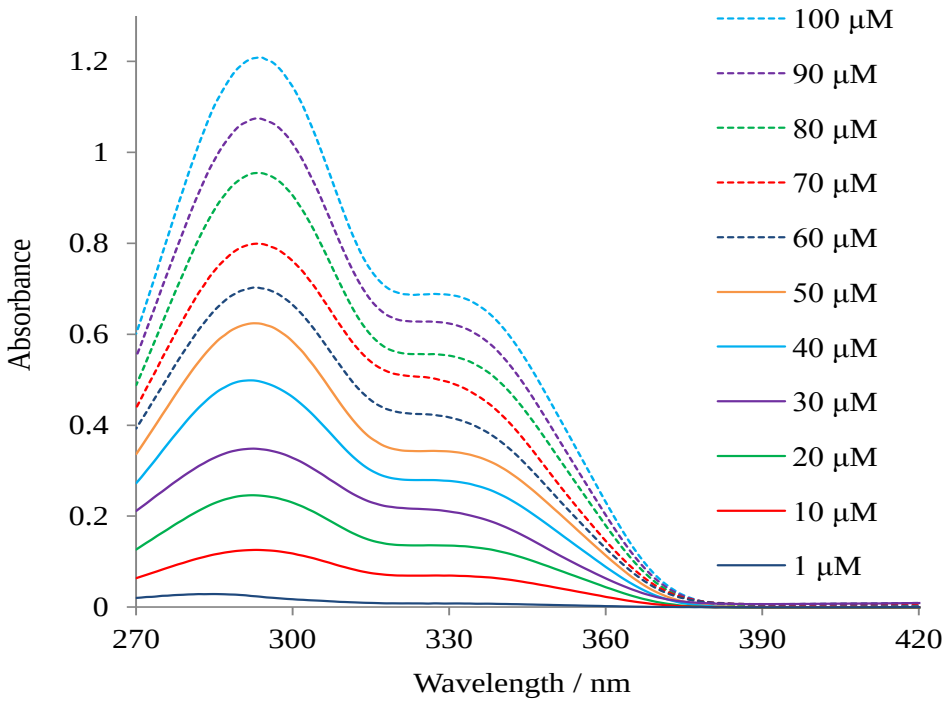


Figure 10.2.14 UV-VIS spectrum of coumarin-3-carboxylic acid absorptivity in DMSO

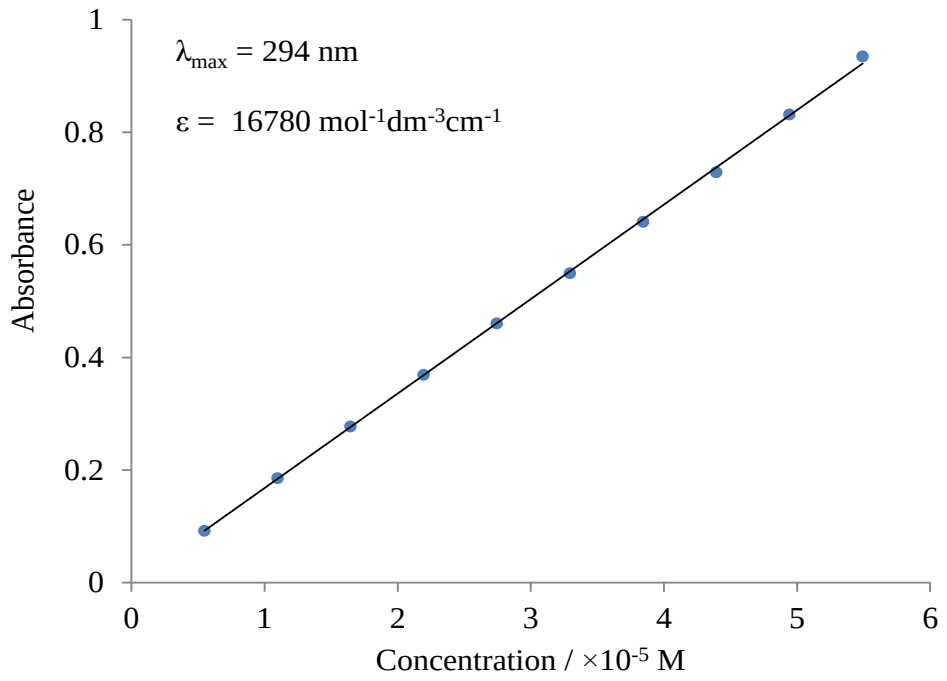


Figure 10.2.15 Calibration curve for carbazole in DMSO where the slope is the equivalent of the molar absorption coefficient, ε

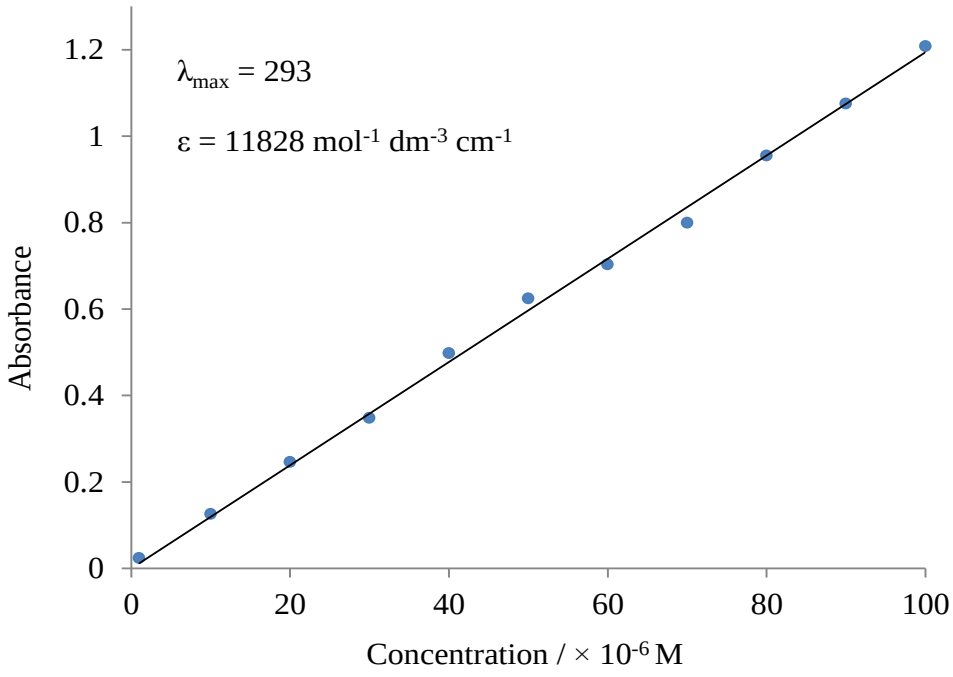


Figure 10.2.16 Calibration curve for coumarin carboxylic acid in DMSO where the slope is equal to the molar absorption coefficient, ε

10.3 Appendix for chapter 5

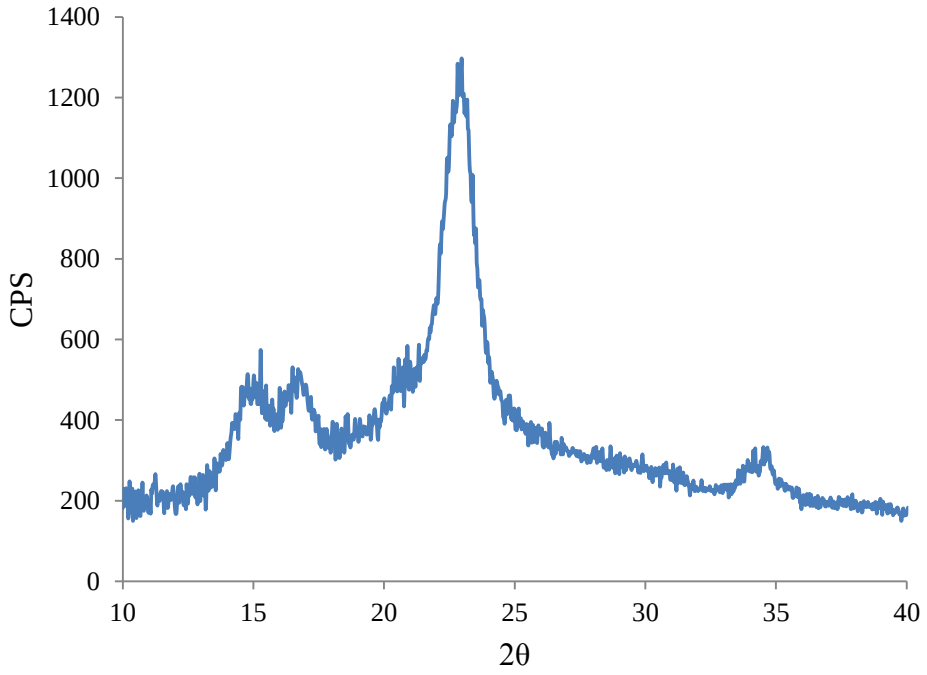


Figure 10.3.1 X-ray diffractogram of bromoacetate cellulose 1BrAcCNC

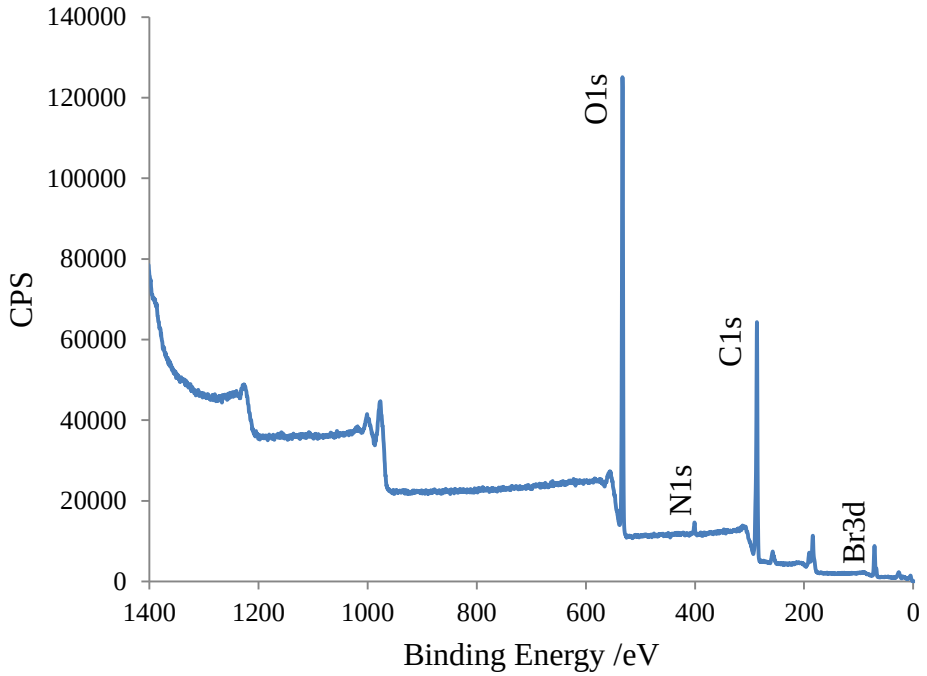


Figure 10.3.2 XPS wide scan of bromoacetate cellulose 1BrAcCNC

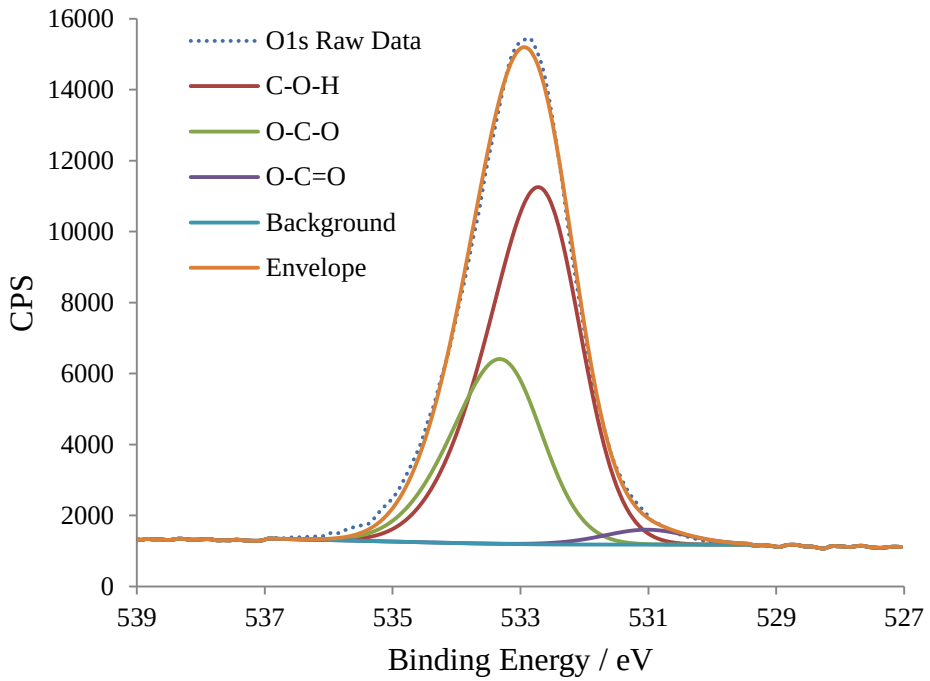


Figure 10.3.3 XPS high resolution spectrum of O1s peck of bromoacetate cellulose 1BrAcCNC

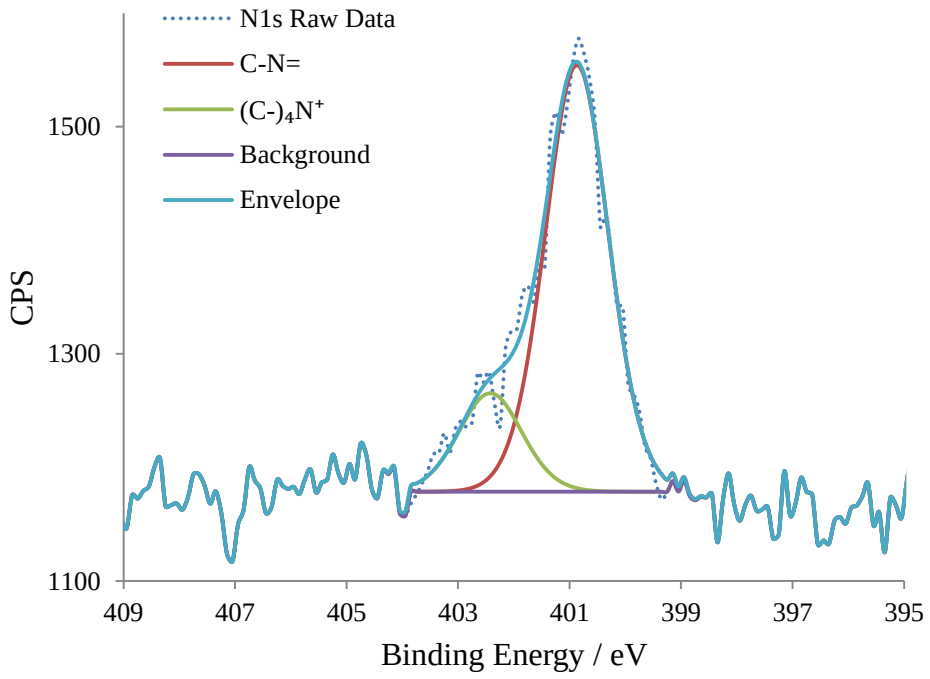


Figure 10.3.4 N1s high resolution scan of bromoacetate cellulose 1BrAcCNC with the two N1s environments, cationic nitrogen and neutral nitrogen

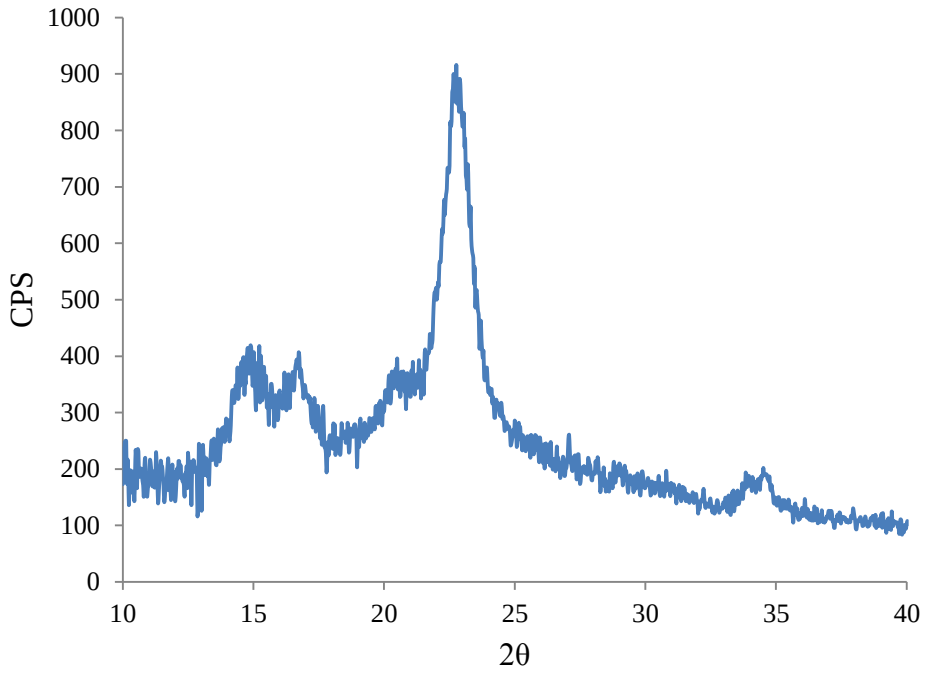


Figure 10.3.5 X-ray diffractogram of pyridinium acetate cellulose bromide 1[Br][PyAc]-*g*-CNC

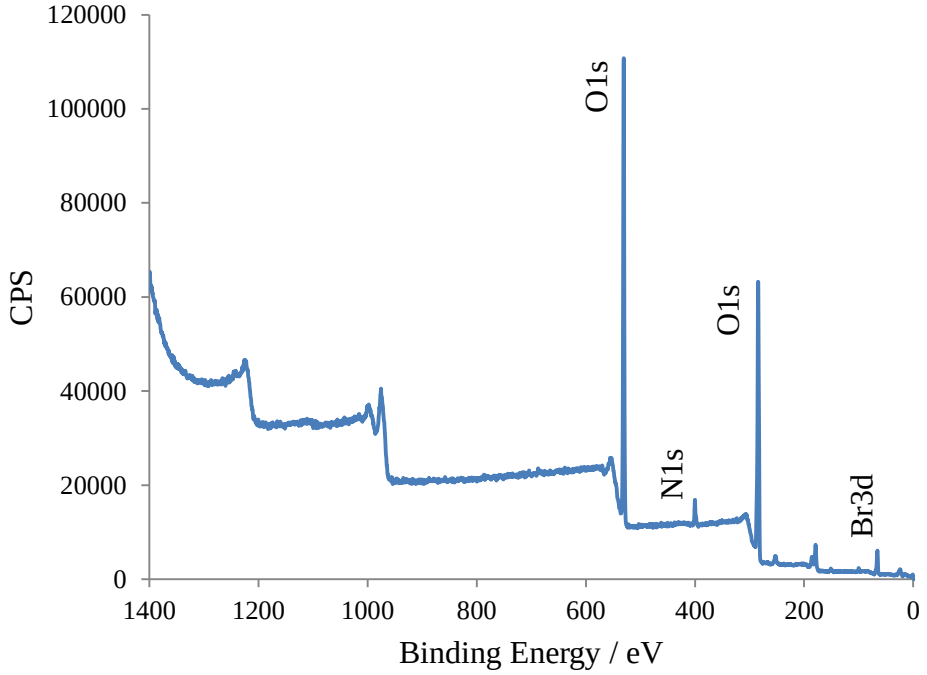


Figure 10.3.6 XPS wide scan of pyridinium acetate cellulose bromide 1[Br][PyAc]-*g*-CNC

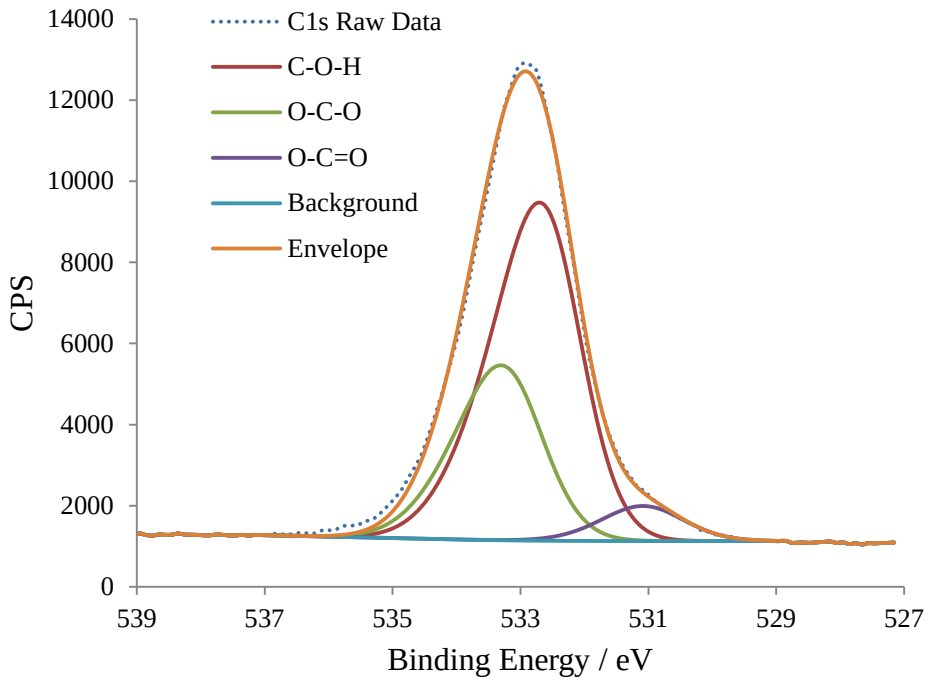


Figure 10.3.7 O1s high resolution XPS spectrum of pyridinium acetate cellulose bromide 1[Br][PyAc]-*g*-CNC

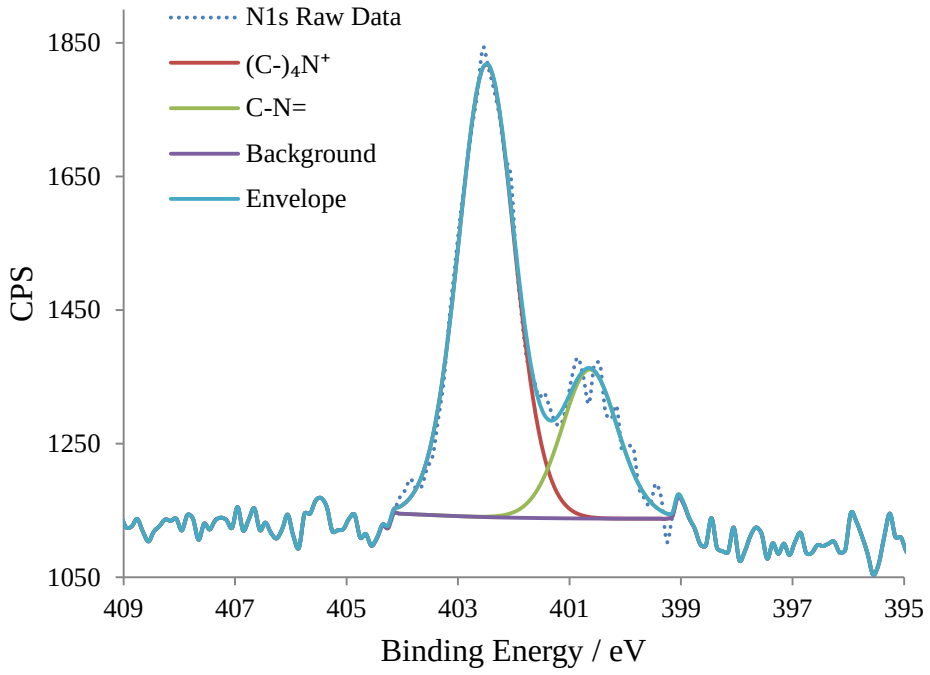


Figure 10.3.8 N1s high resolution scan of pyridinium acetate cellulose 1[Br][PyAc]-*g*-CNC with cationic N1s environment and neutral nitrogen

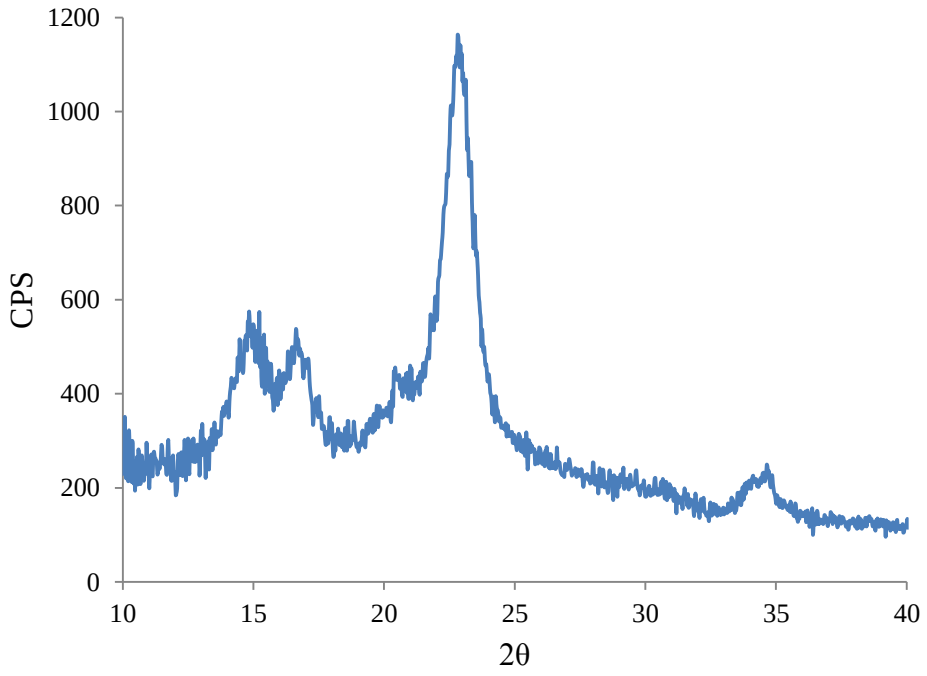


Figure 10.3.9 X-ray diffraction of methyl imidazolium acetate cellulose bromide 1[Br][MeImAc]-g-CNC

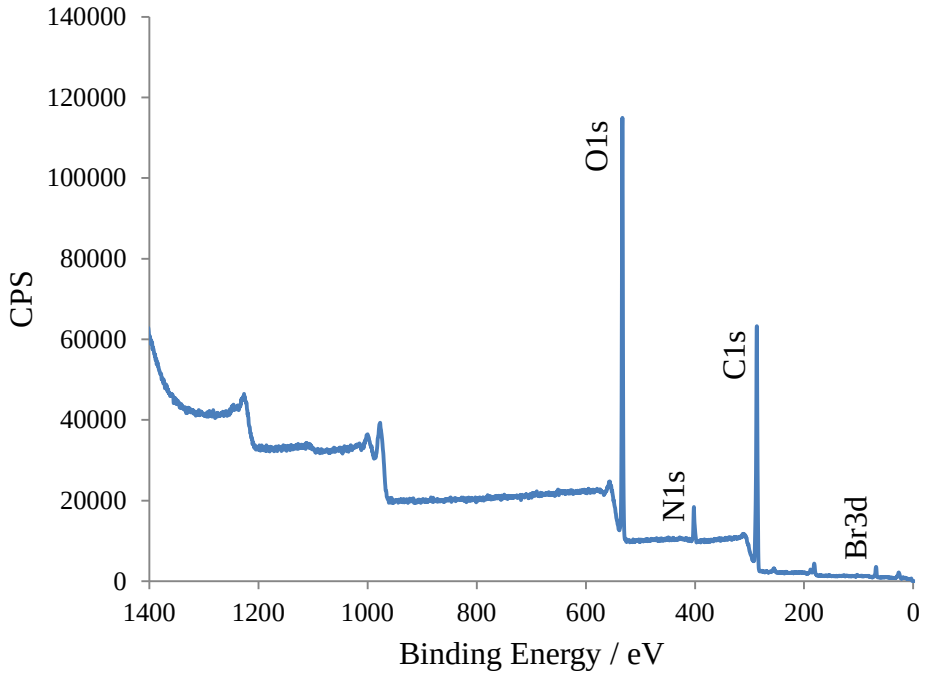


Figure 10.3.10 XPS wide scan of methyl imidazolium acetate cellulose bromide 1[Br][MeImAc]-g-CNC

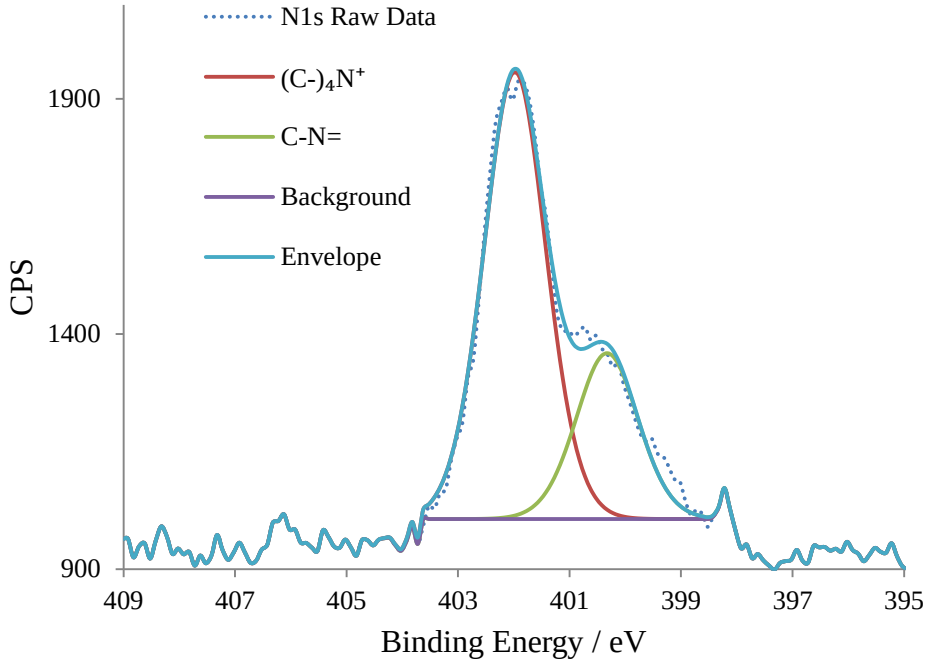


Figure 10.3.11 N1s high resolution scan of methyl imidazolium acetate cellulose 1[Br][MeImAc]-g-CNC composed of cationic N1s environment and neutral nitrogen

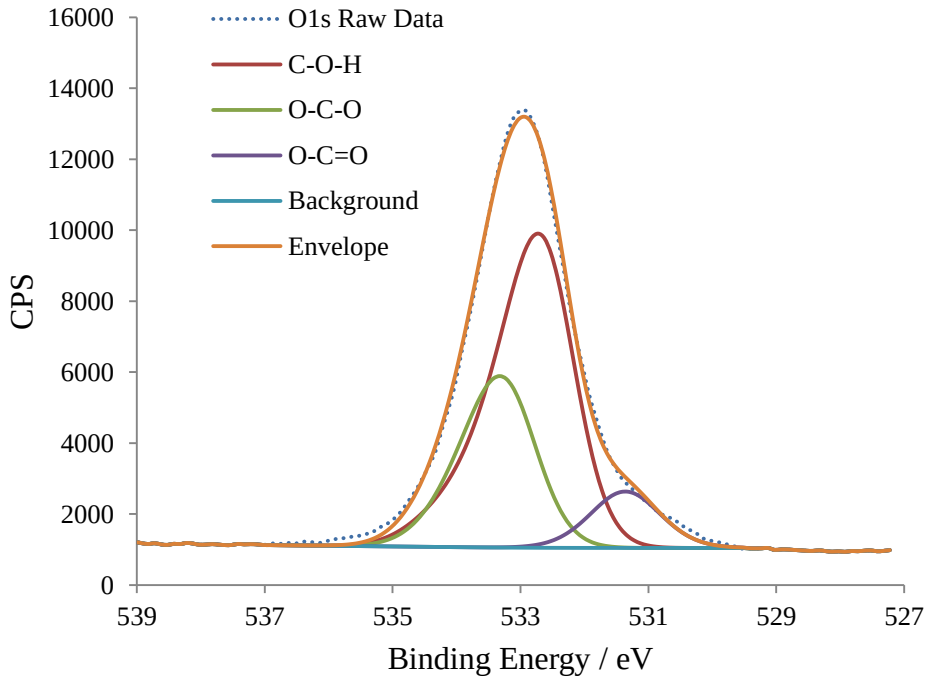


Figure 10.3.12 O1s high resolution XPS spectrum of methyl imidazolium acetate cellulose bromide 1[Br][MeImAc]-*g*-CNC

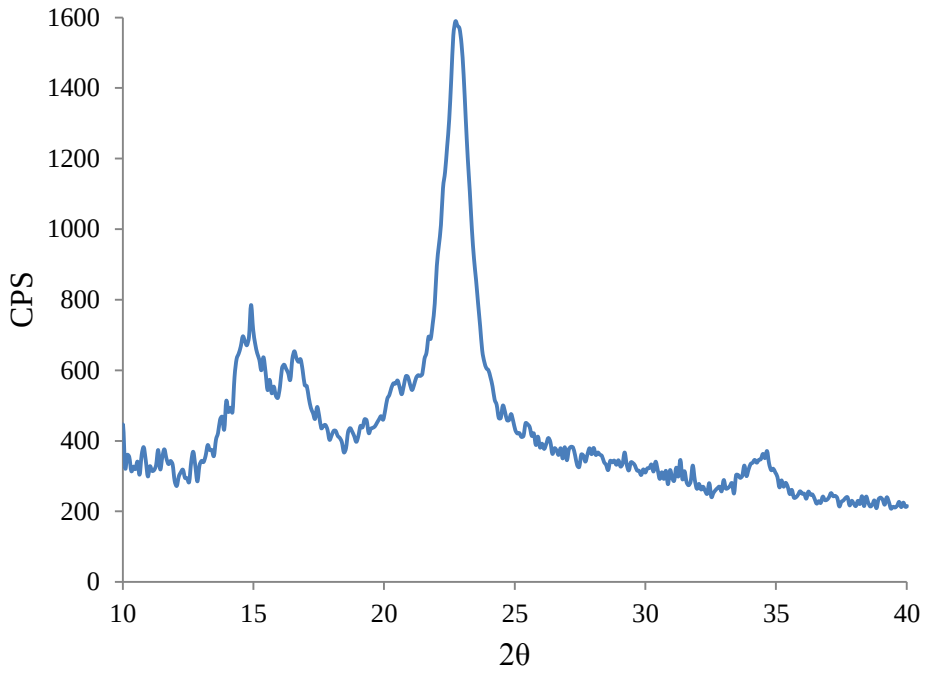


Figure 10.3.13 X-ray diffraction of bromoacetate cellulose, 2BrAcCNC, synthesised in THF

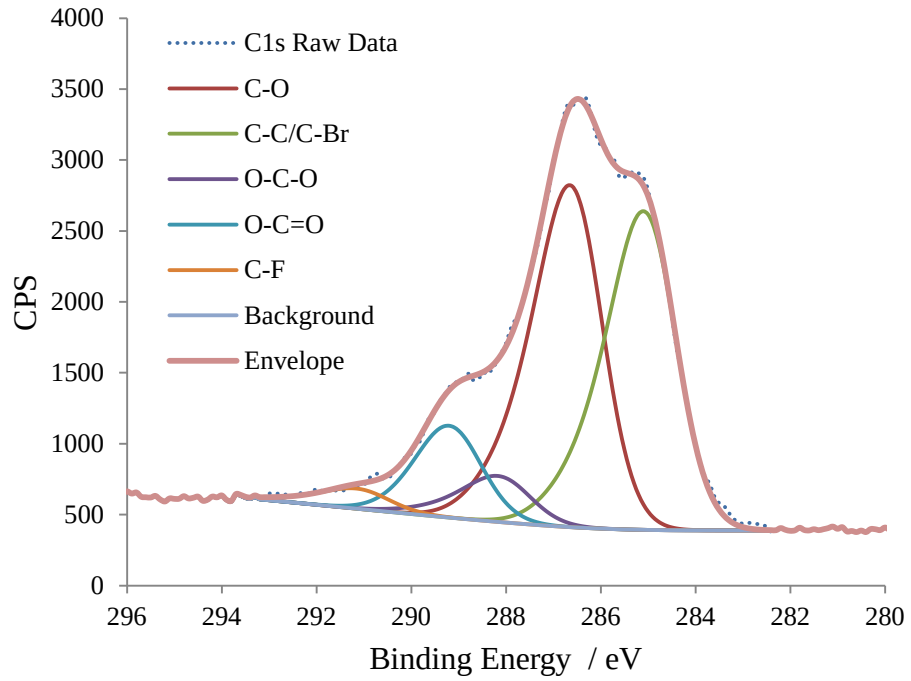


Figure 10.3.14 C1s high resolution XPS spectrum of bromoacetate cellulose, 2BrAcCNC

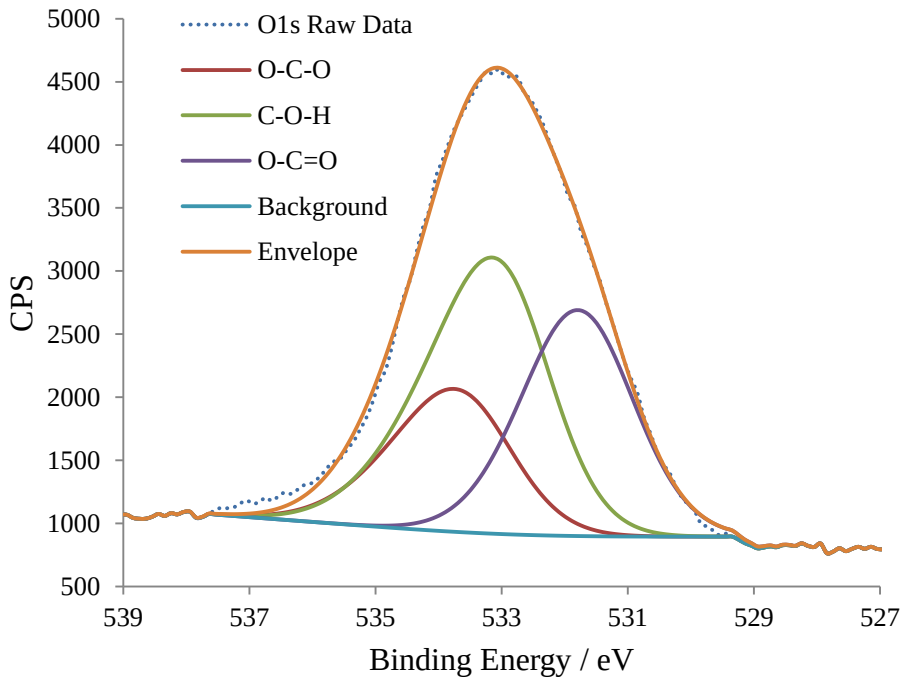


Figure 10.3.15 O1s high resolution XPS spectrum of bromoacetate cellulose 2BrAcCNC synthesised in THF as an alternative methodology -N^{-}-

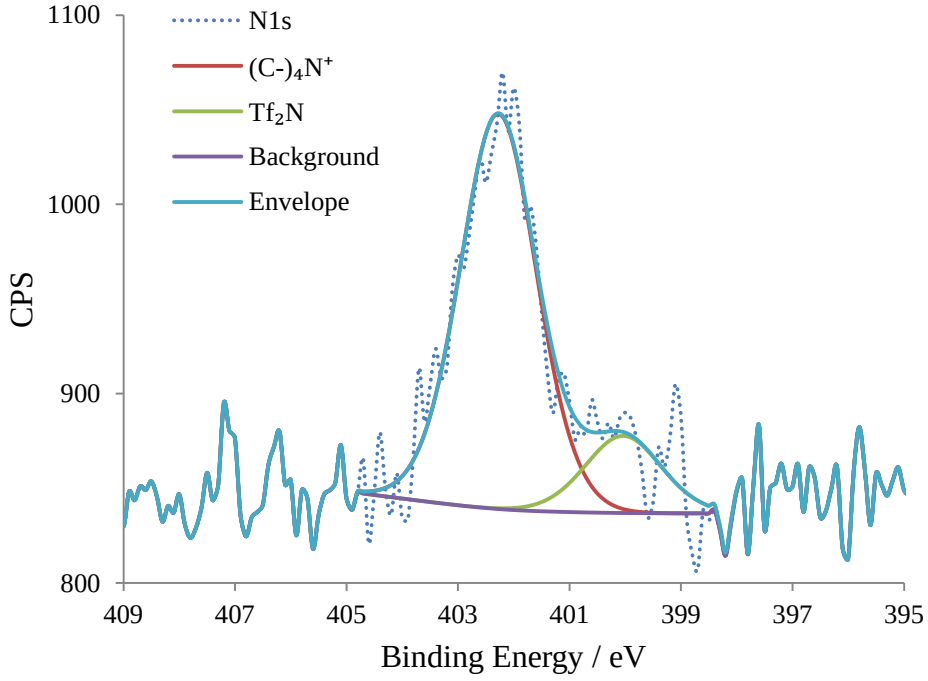


Figure 10.3.16 N1s high resolution scan of bromoacetate cellulose 2BrAcCNC composed of cationic N1s environment and bistriflimide contamination

Table 10.3.1 Detailed XPS data of bromoacetate cellulose synthesised in THF

Orbital	Component	BE / eV	FWHM /eV	Rel.A/%[a]	at%
C1s	C–C/C–Br	284.94	1.60	39.31	27.46
	C–O	286.50	1.60	42.16	29.46
	O–C–O	287.99	1.60	5.61	3.92
	O–C=O	289.03	1.60	11.39	7.96
	C–F	291.47	1.60	1.54	1.08
				100.00	69.87
O1s	O–C=O	531.59	2.06	33.12	8.57
	C–O–H	532.9	2.06	44.59	11.54
	O–C–O	533.5	2.06	22.29	5.77
				100.00	25.89
N1s	C–N= / N^-	400.04	1.61	16.32	0.14
	$(C–)_4N^+$	402.28	1.61	83.68	0.71
				100.00	0.85
Br3d	Br^- 5/2	67.38	0.94	1.60	0.05
	Br^- 3/2	68.28	0.94	1.06	0.03
	C–Br 5/2	70.55	1.54	58.62	1.79
	C–Br 3/2	71.66	1.54	38.72	1.18
				100.00	3.06
F1s	F–C[b]	690.5	2.556	100.00	0.32

[a] Relative area = component area×100/sum area of same orbital
[b] Data available from low resolution wide scan

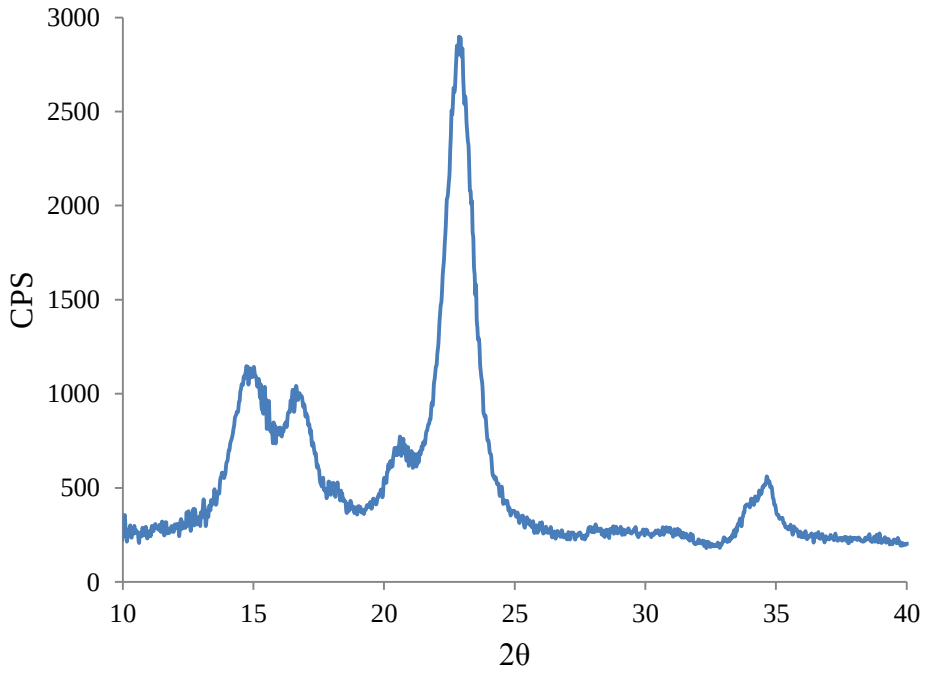


Figure 10.3.17 X-ray diffractogram of bromoacetate cellulose obtained by reaction of cellulose, bromoacetyl bromide and triethylamine only, 3BrAcCNC

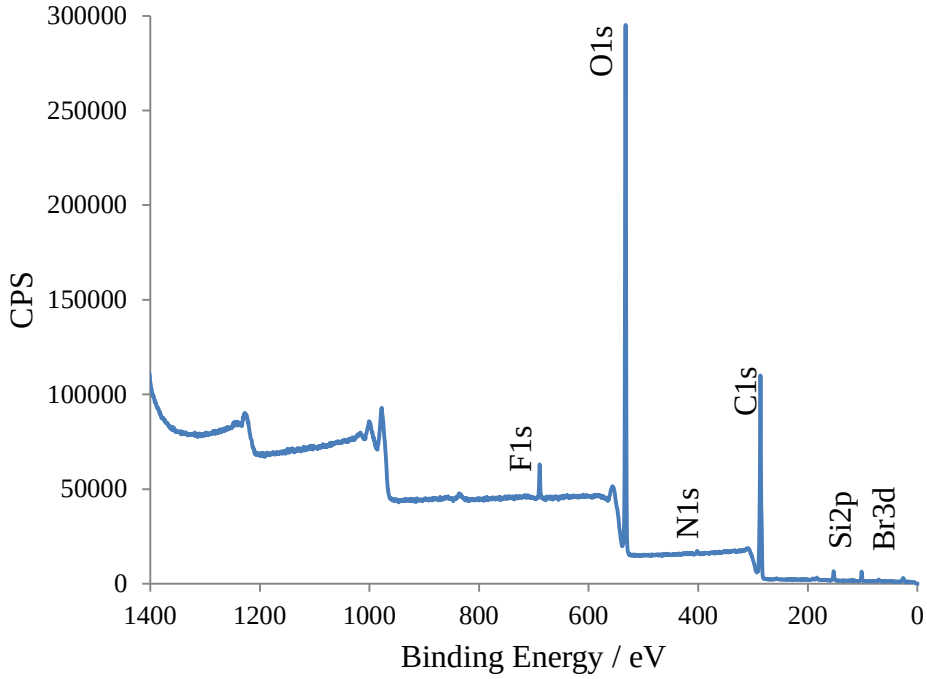


Figure 10.3.18 X-ray diffractogram of bromoacetate cellulose 3BrAcCNC with bistriflimide and silicon adhesive tape contamination

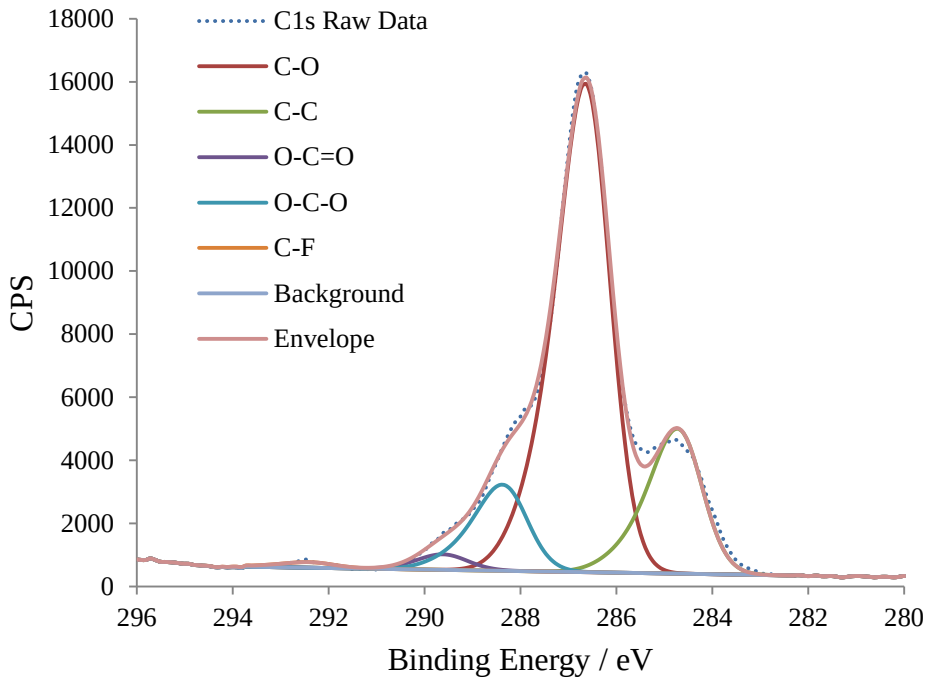


Figure 10.3.19 C1s high resolution XPS spectrum of bromoacetate cellulose 3BrAcCNC synthesised as a side reaction of the catalyst (triethylamine) with bromoacetyl bromide

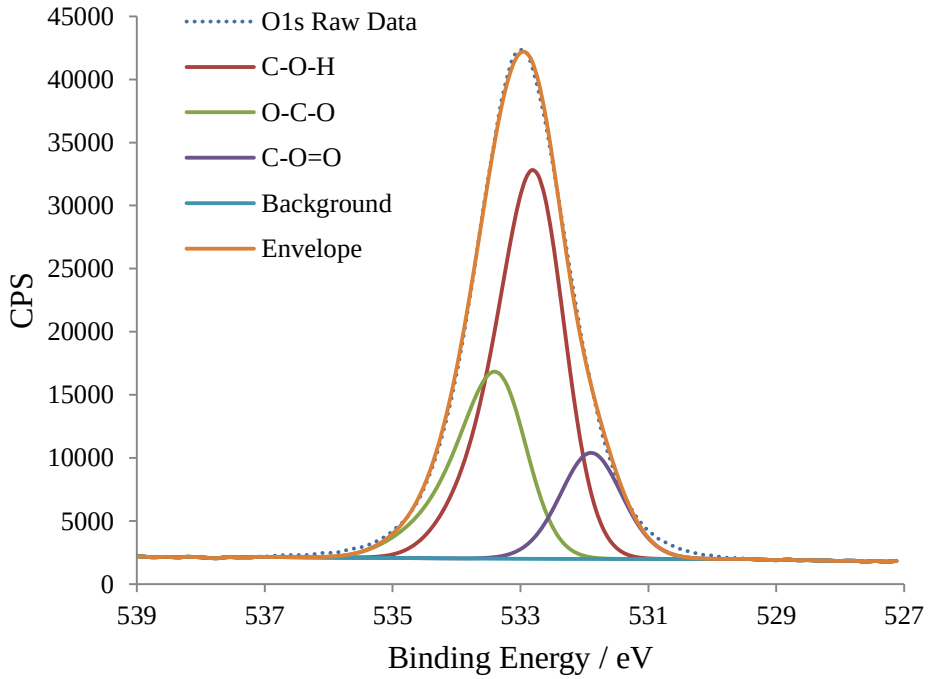


Figure 10.3.20 O1s high resolution scan of bromoacetate cellulose 3BrAcCNC

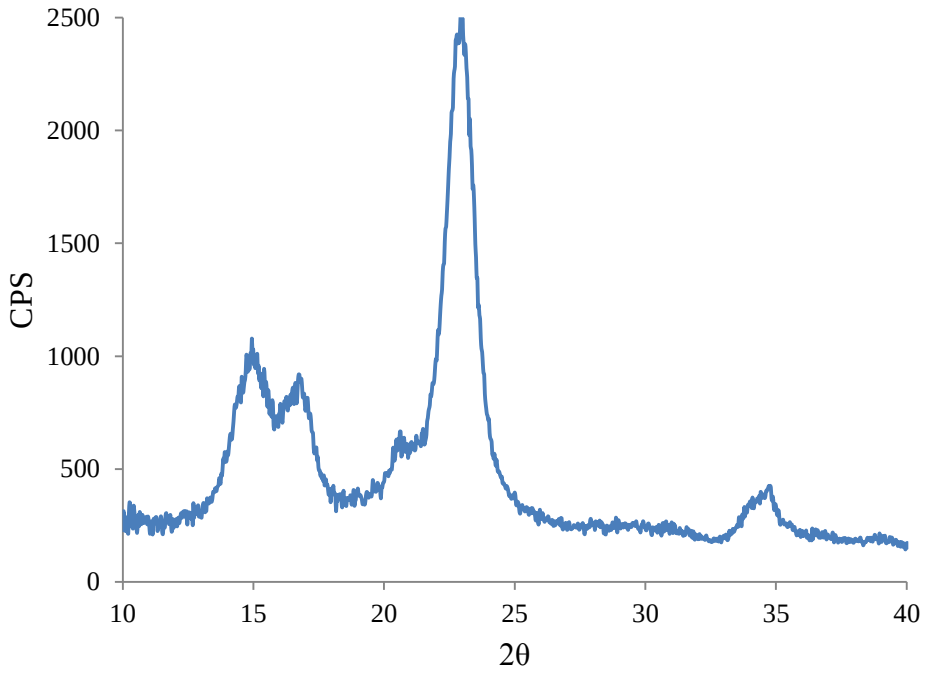


Figure 10.3.21 X-ray diffractogram of pyridinium acetate cellulose bromide 2[Br][PyAc]-*g*-CNC

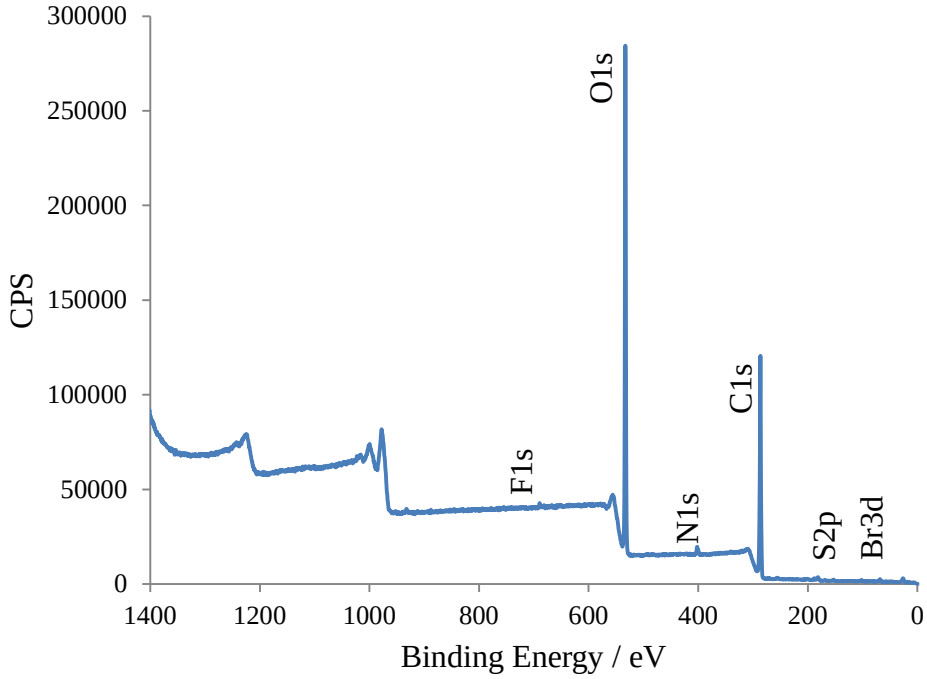


Figure 10.3.22 X-ray diffractogram of pyridinium acetate cellulose bromide 2[Br][PyAc]-*g*-CNC

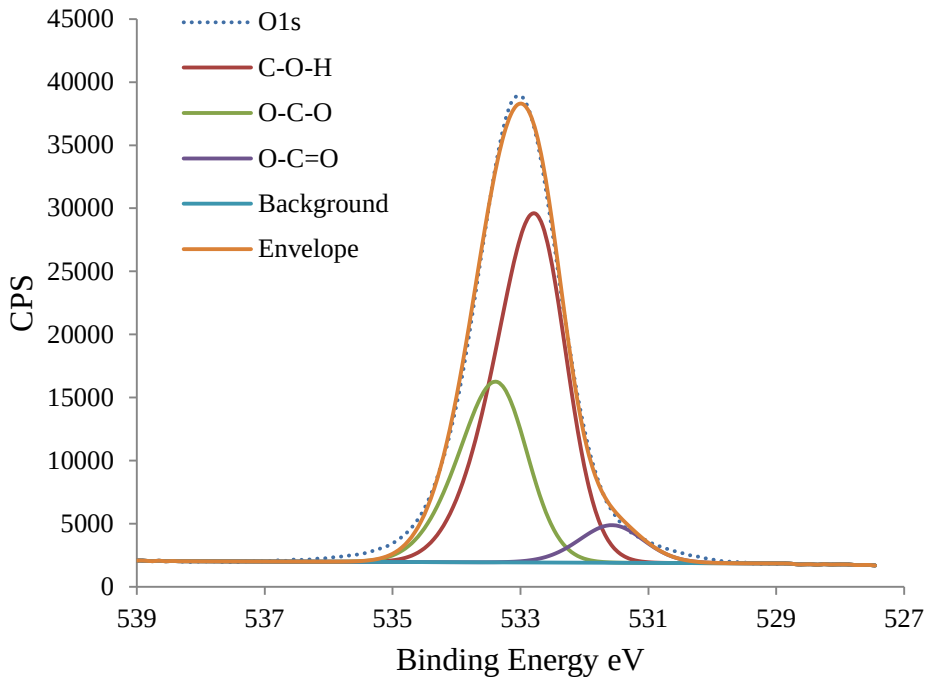


Figure 10.3.23 O1s high resolution scan of pyridinium acetate cellulose bromide 2[Br][PyAc]-*g*-CNC

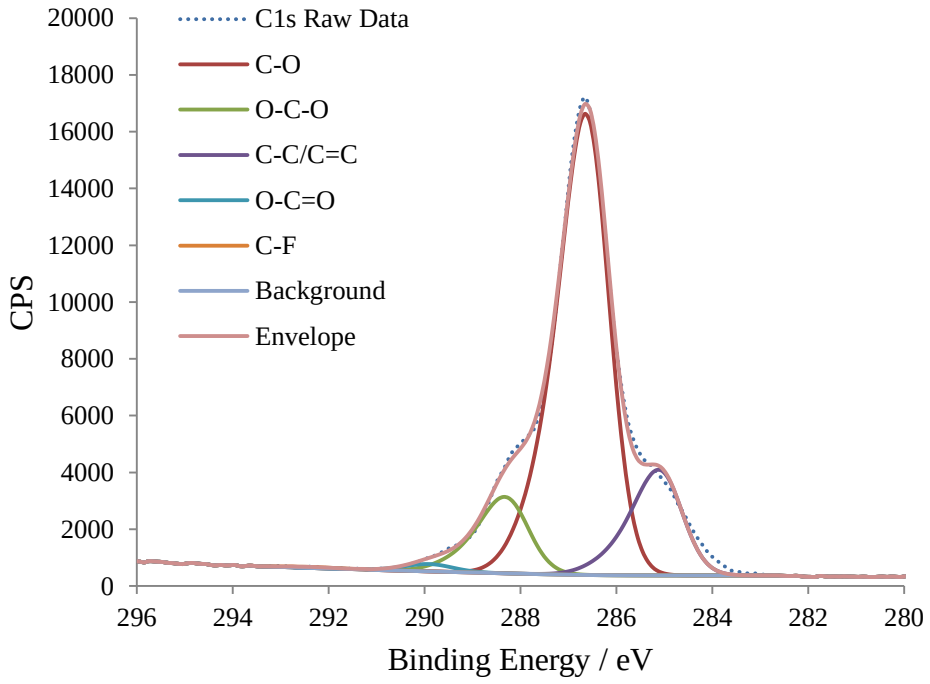


Figure 10.3.24 C1s high resolution XPS spectrum of pyridinium acetate cellulose bromide 2[Br][PyAc]-*g*-CNC

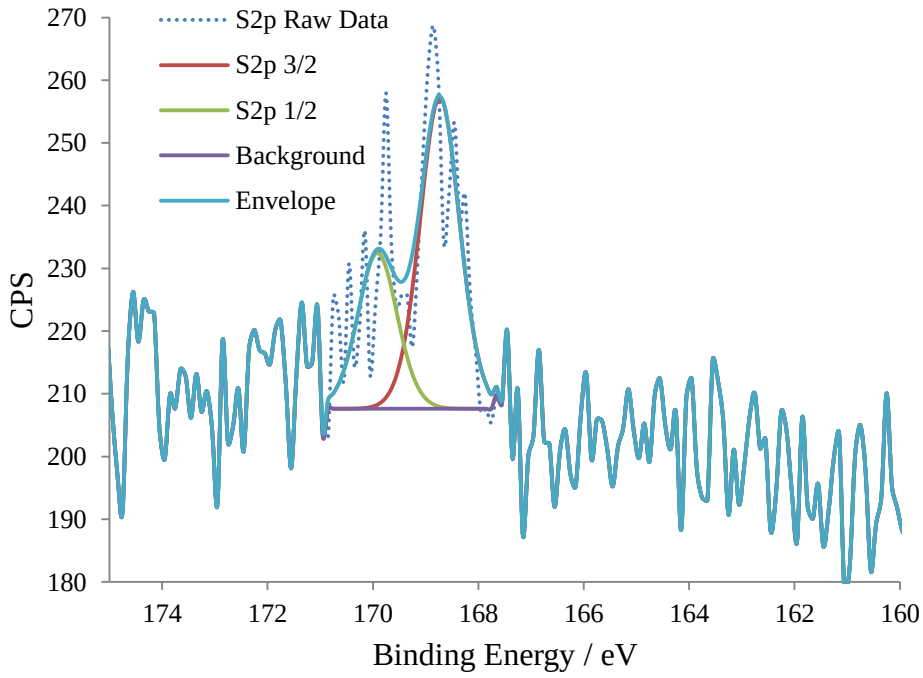


Figure 10.3.25 S2p high resolution XPS spectrum of pyridinium acetate cellulose bromide 2[Br][PyAc]-*g*-CNC

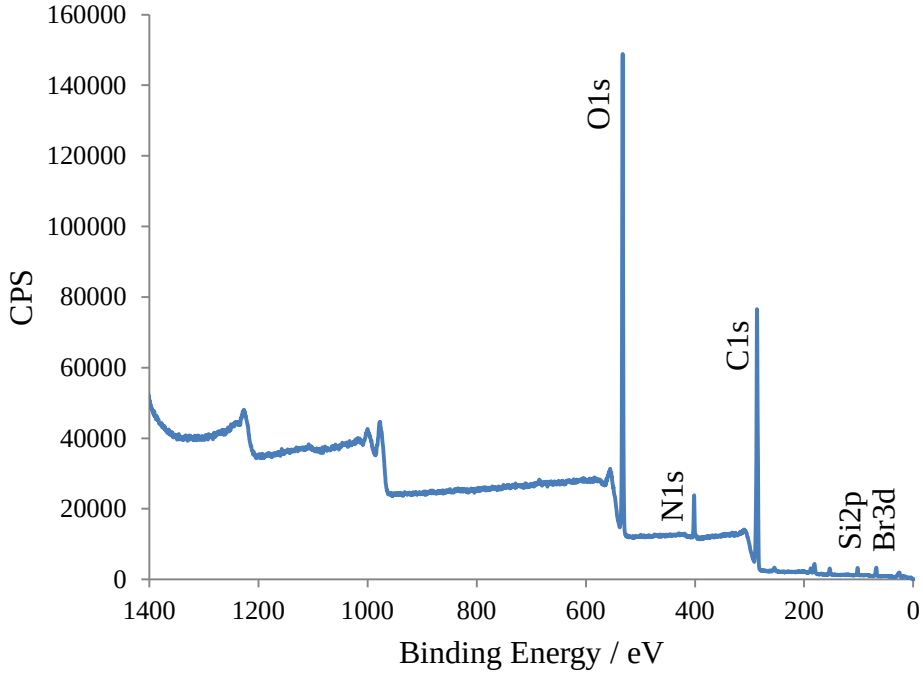


Figure 10.3.26 X-ray diffractogram of methyl imidazolium acetate cellulose bromide 2[Br][MeImAc]-g-CNC with Si contamination (adhesive tape)

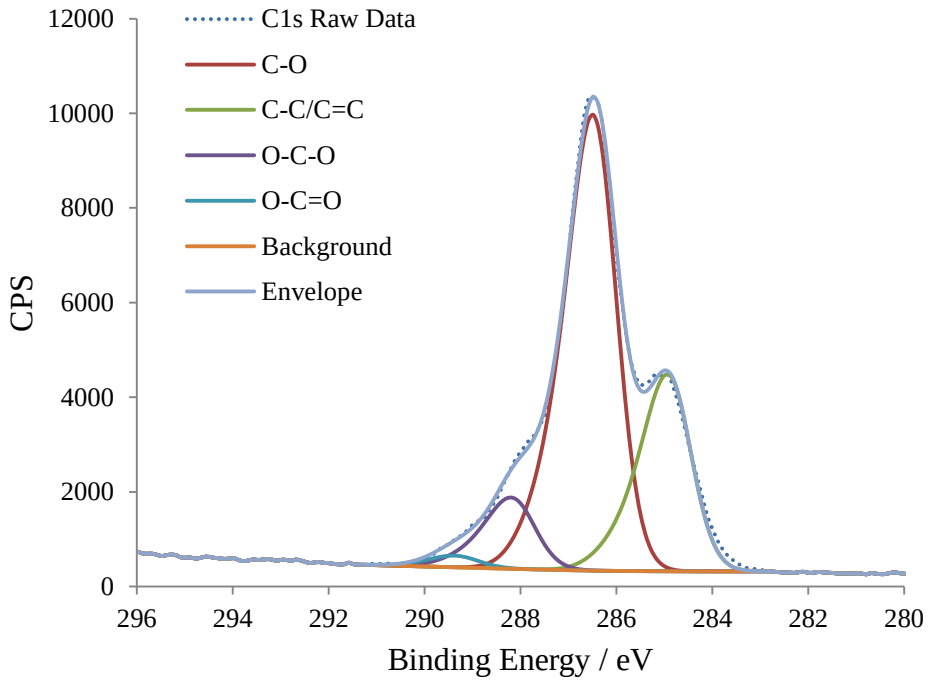


Figure 10.3.27 C1s high resolution XPS spectrum of methyl imidazolium acetate cellulose bromide 2[Br][MeImAc]-g-CNC

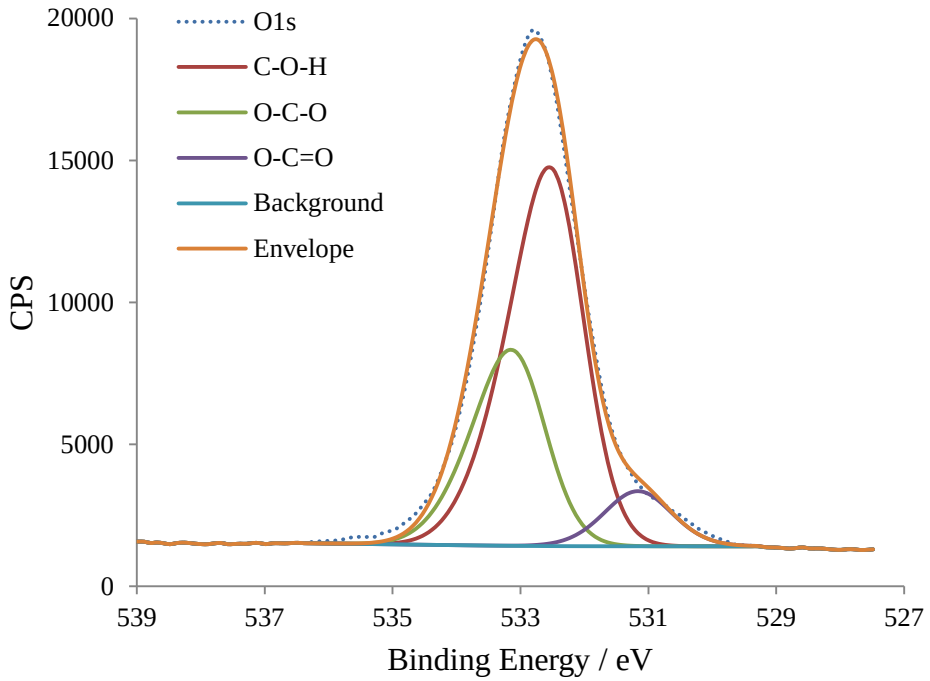


Figure 10.3.28 O1s high resolution XPS spectrum of methyl imidazolium acetate cellulose bromide 2[Br][MeImAc]-*g*-CNC

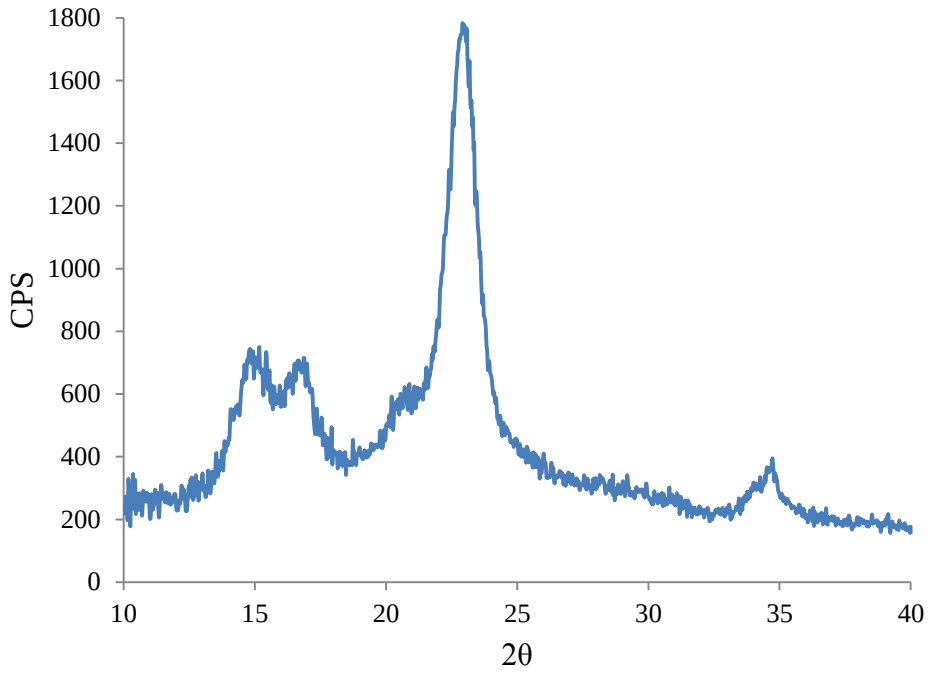


Figure 10.3.29 X-ray diffraction of methyl imidazolium acetate cellulose bromide 2[Br][MeImAc]-g-CNC

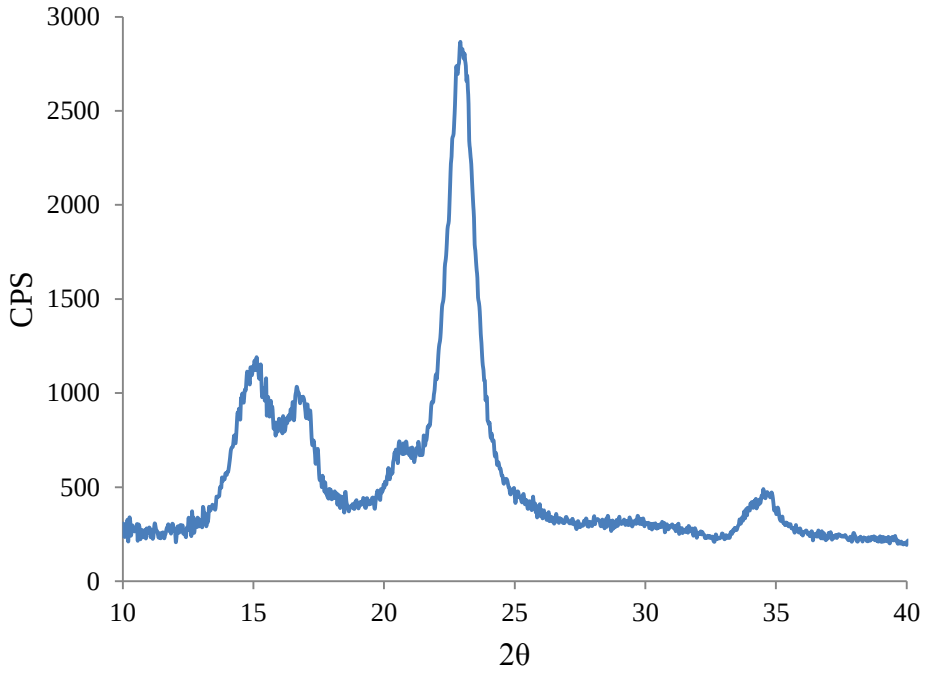


Figure 10.3.30 X-ray diffractogram of pyridinium acetate cellulose bromide 3[Br][PyAc]-*g*-CNC

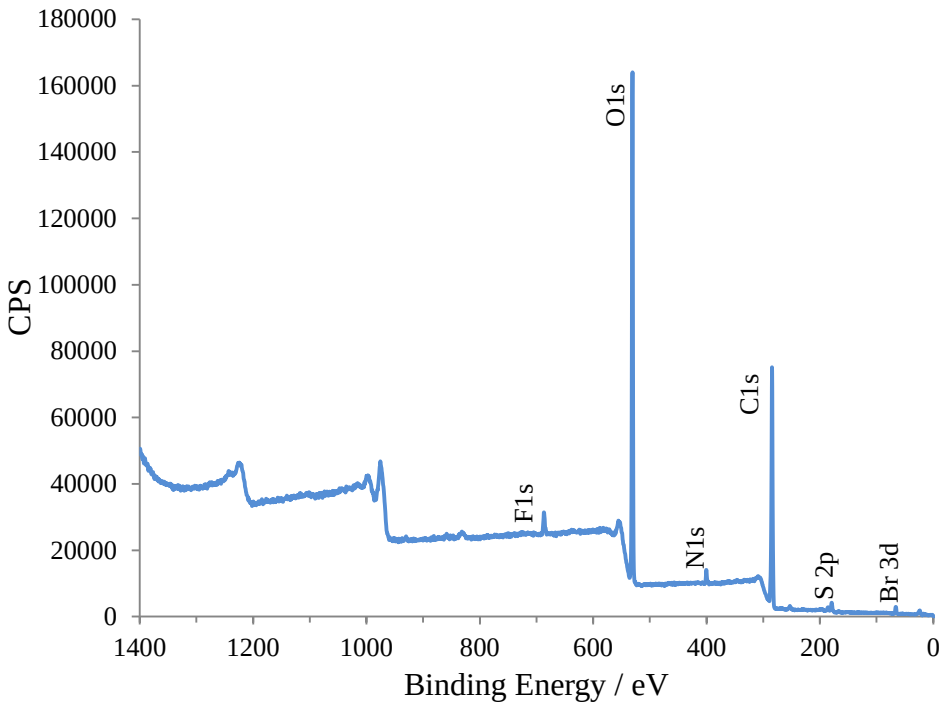


Figure 10.3.31 Wide scan XPS spectrum of 3-pyridinium acetate cellulose bromide 3[Br][PyAc]-*g*-CNC

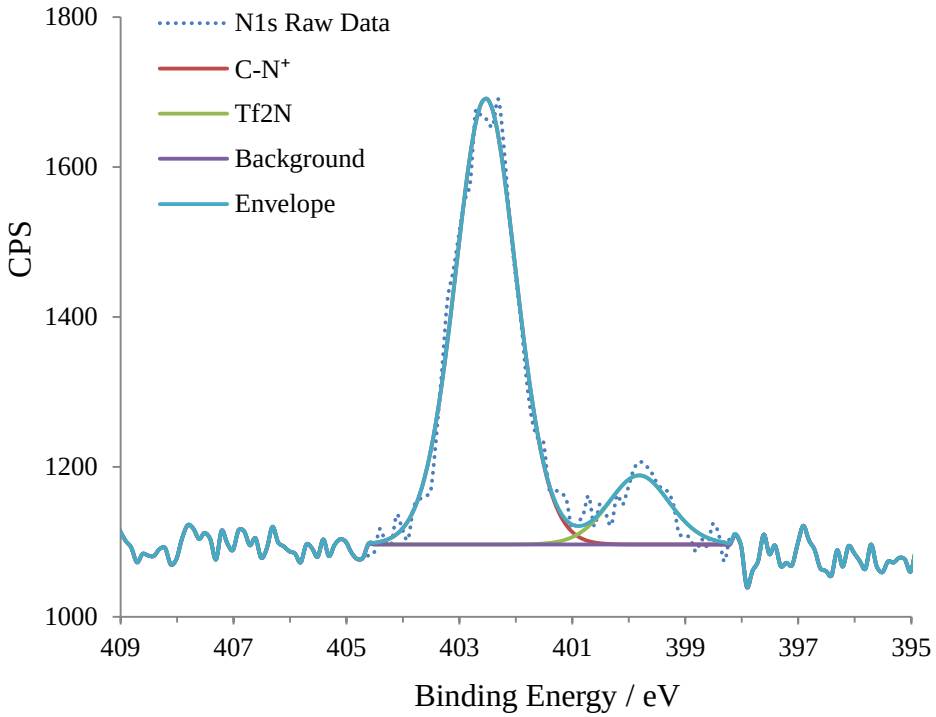


Figure 10.3.32 N 1s high resolution XPS spectrum of 1-pyridinium acetate cellulose bromide 3[Br][PyAc]-*g*-CNC showing pyridinium formation and bistriflimide contamination.

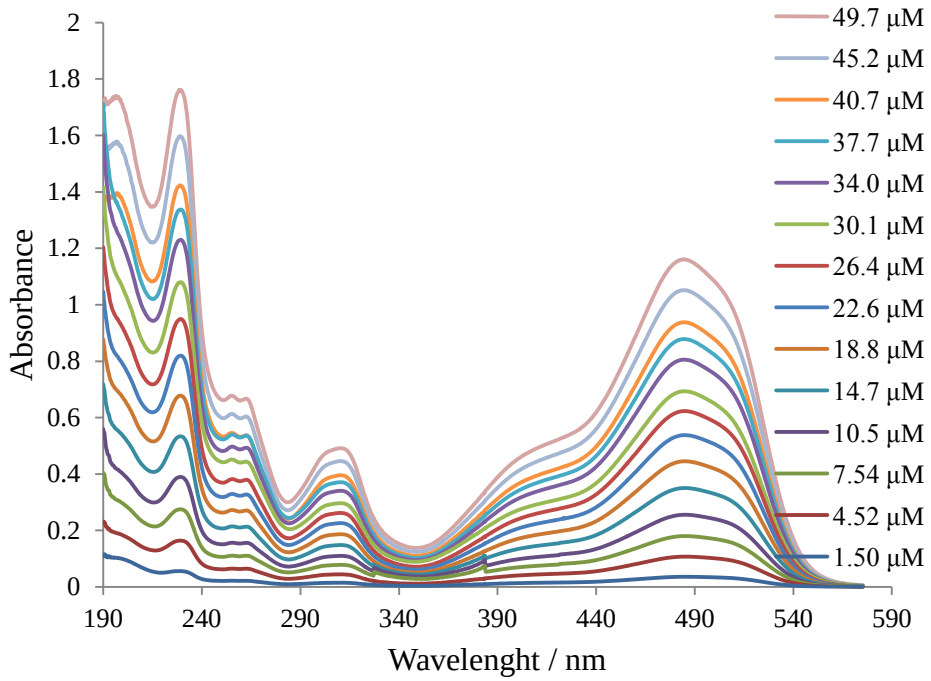


Figure 10.3.33 UV-Vis spectra of Orange II dye sodium salt at increased concentrations

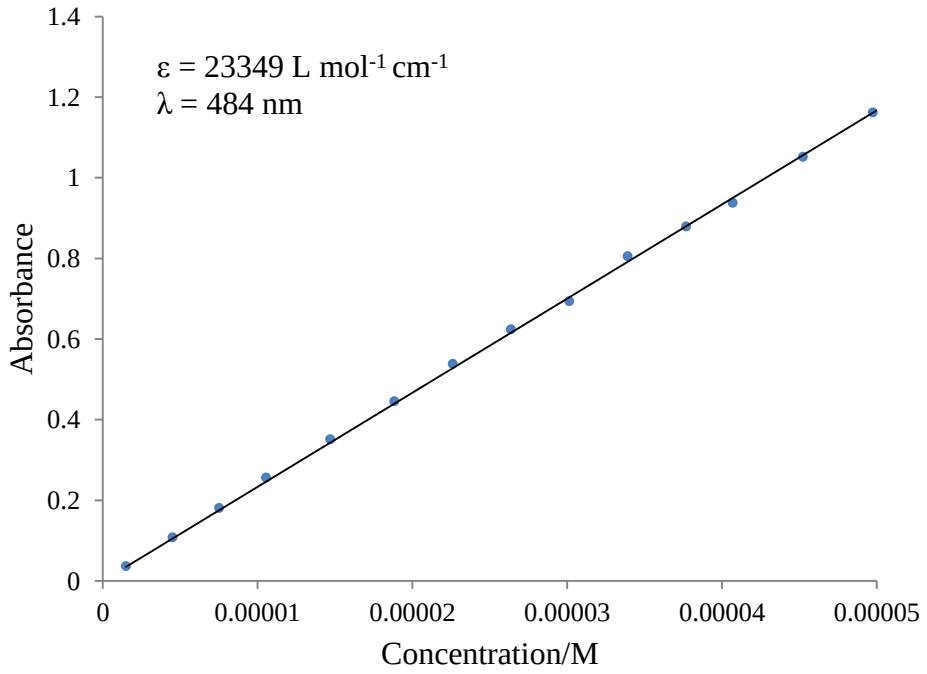


Figure 10.3.34 Calibration curve for Orange II dye sodium salt where the slope is the molar absorption coefficient

10.4 Appendix for chapter 6

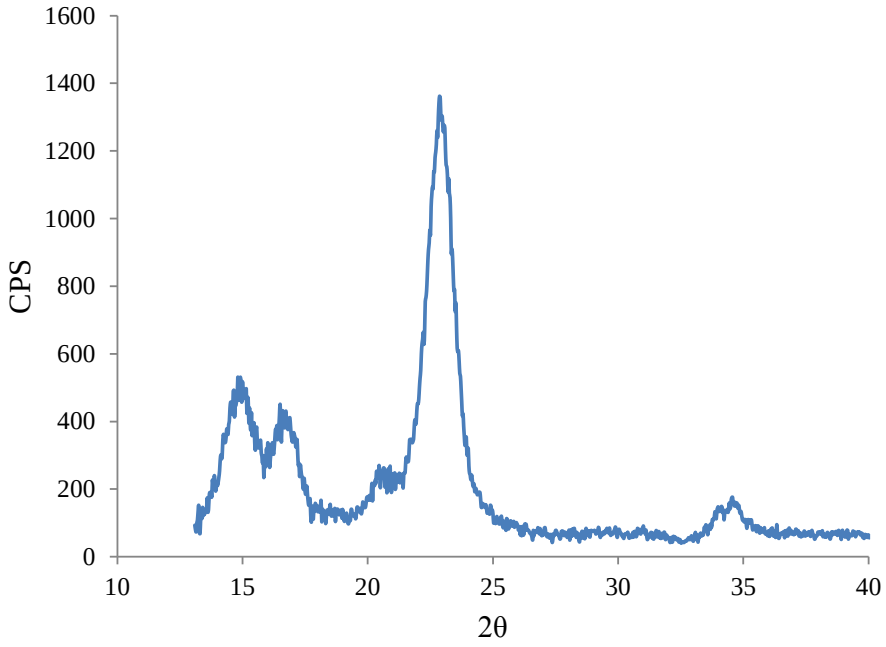


Figure 10.4.1 X-ray diffractogram of 1-hour synthesised cellulose 2-methyl-3-((3-trimethoxysilyl)propyl)thio) propanoate

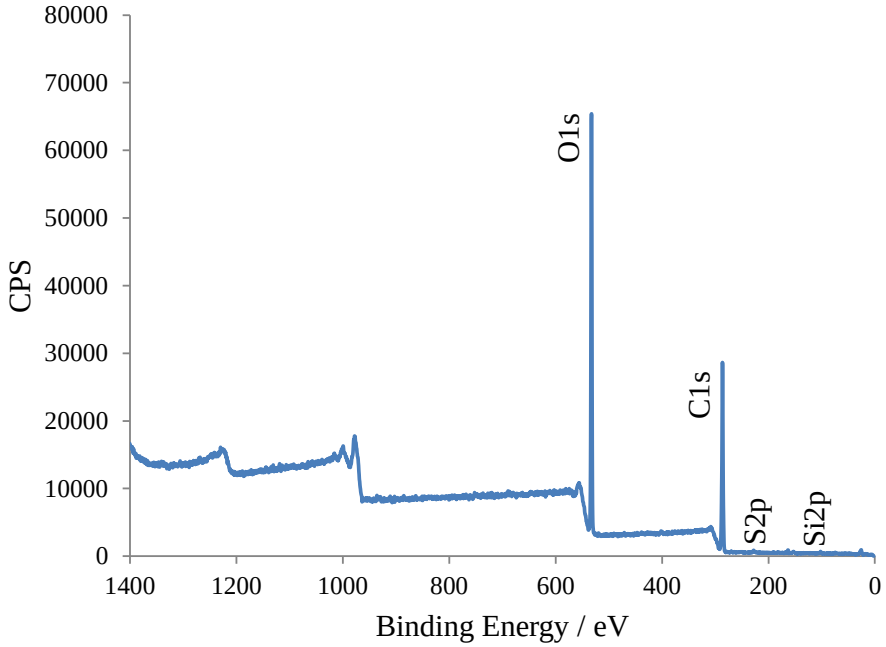


Figure 10.4.2 XPS wide scan of 1-hour synthesised cellulose 2-methyl-3-((3-trimethoxysilyl)propyl)thio) propanoate

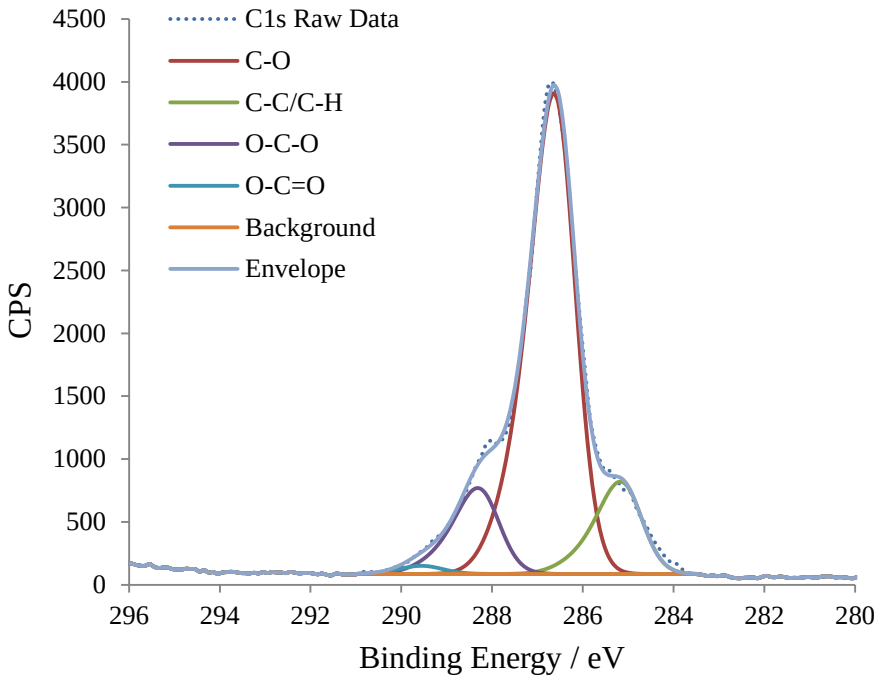


Figure 10.4.3 C1s high resolution spectrum of 1-hour synthesised cellulose 2-methyl-3-((3-trimethoxysilyl)propyl)thio)propanoate

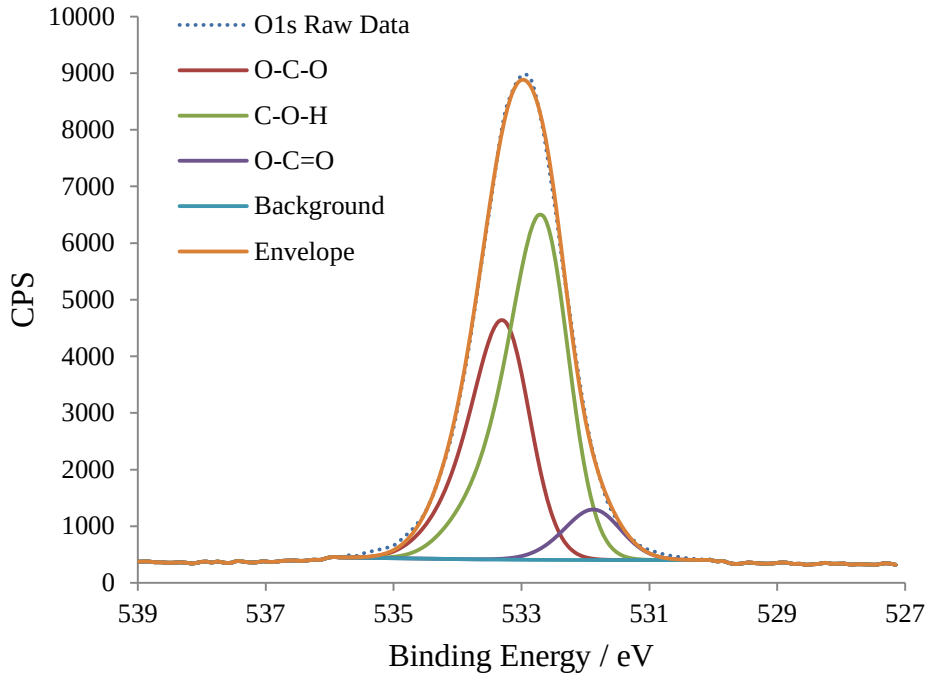


Figure 10.4.4 O1s high resolution spectrum of 1-hour synthesised cellulose 2-methyl-3-((3-trimethoxysilyl)propyl)thio) propanoate

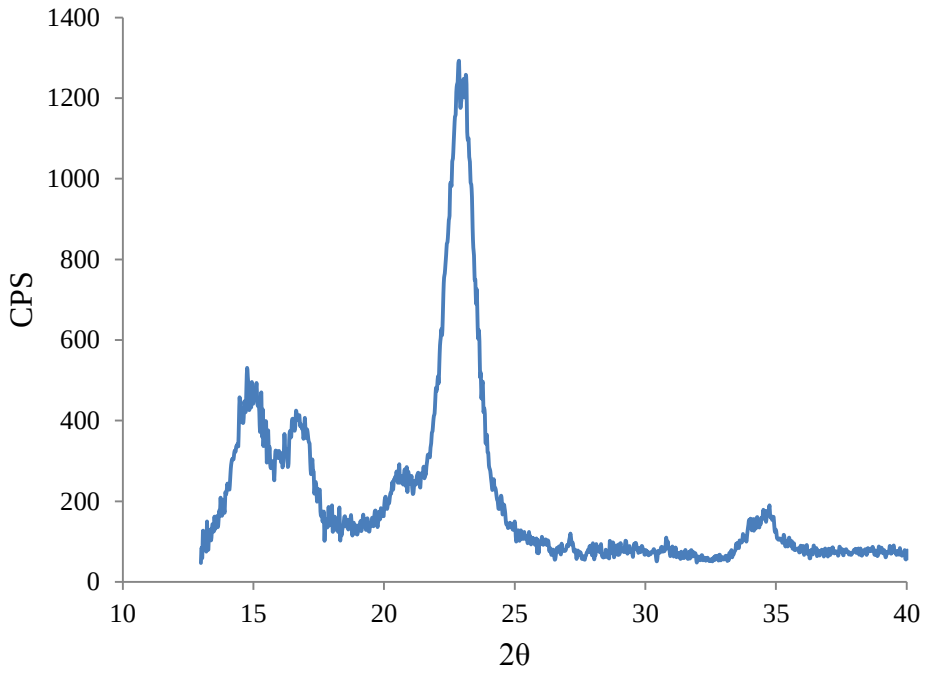


Figure 10.4.5 X-ray diffractogram of 4 hours synthesised cellulose 2-methyl-3-((3-trimethoxysilyl)propyl)thio) propanoate

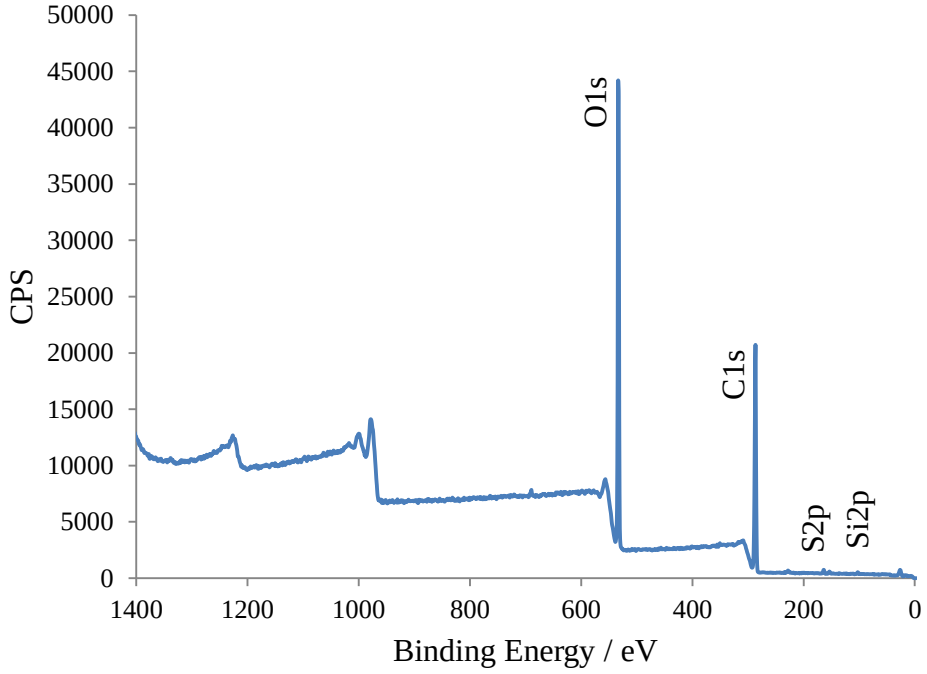


Figure 10.4.6 XPS wide scan of 4 hours synthesised cellulose 2-methyl-3-((3-trimethoxysilyl)propyl)thio) propanoate

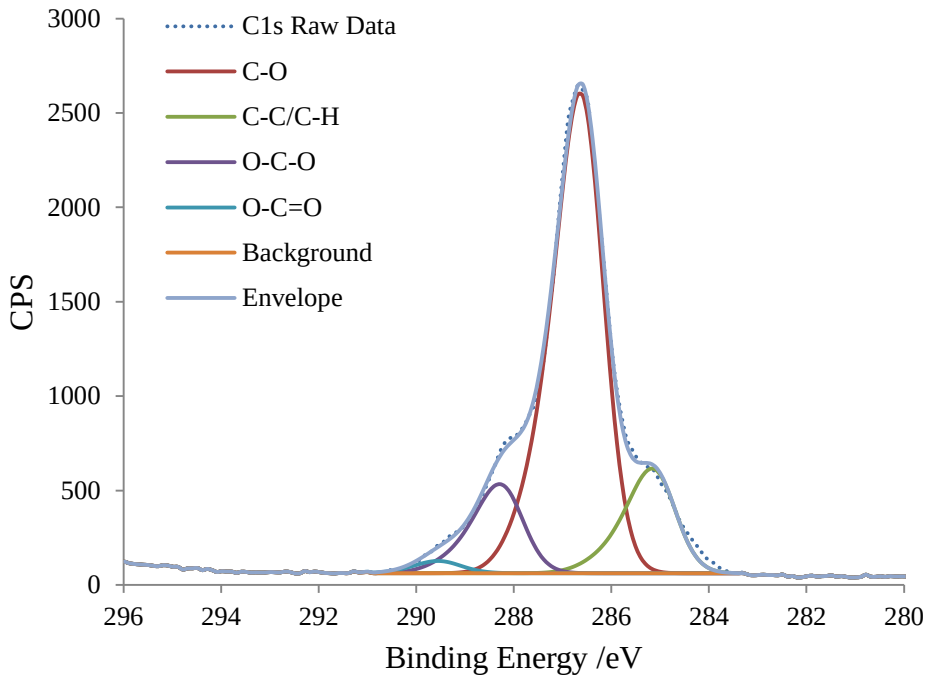


Figure 10.4.7 C1s high resolution scan of 4 hours synthesised cellulose 2-methyl-3-((3-trimethoxysilyl)propyl)thio) propanoate

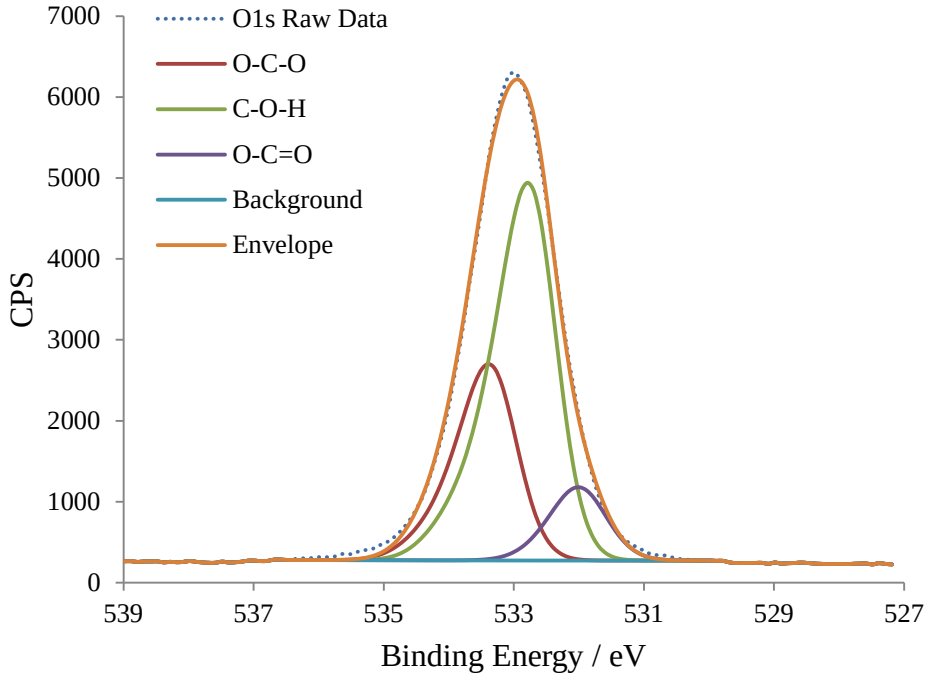


Figure 10.4.8 O1s high resolution scan of 4 hours synthesised cellulose 2-methyl-3-((3-trimethoxysilyl)propyl)thio) propanoate

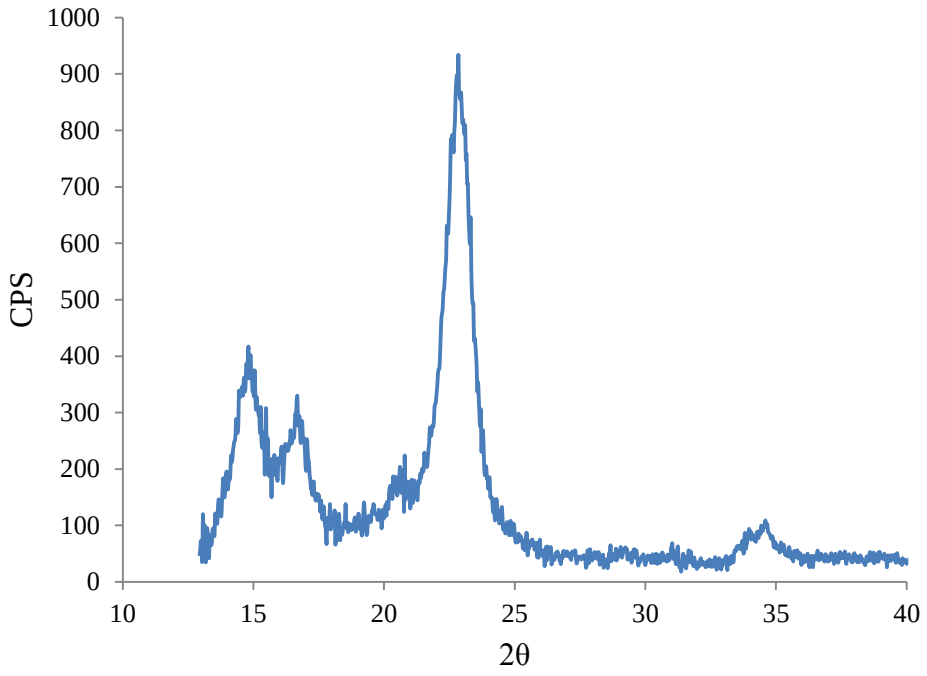


Figure 10.4.9 X-ray diffractogram of 3-((3-trimethoxysilyl)propyl)thio) propanoate

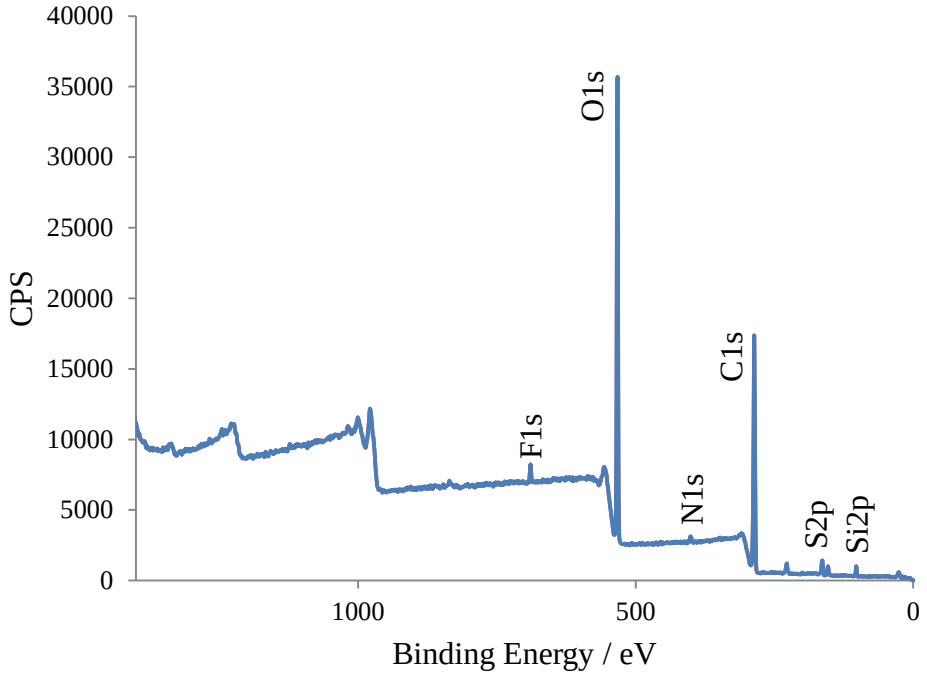


Figure 10.4.10 XPS wide scan of 3-((3-trimethoxysilyl)propyl)thio) propanoate

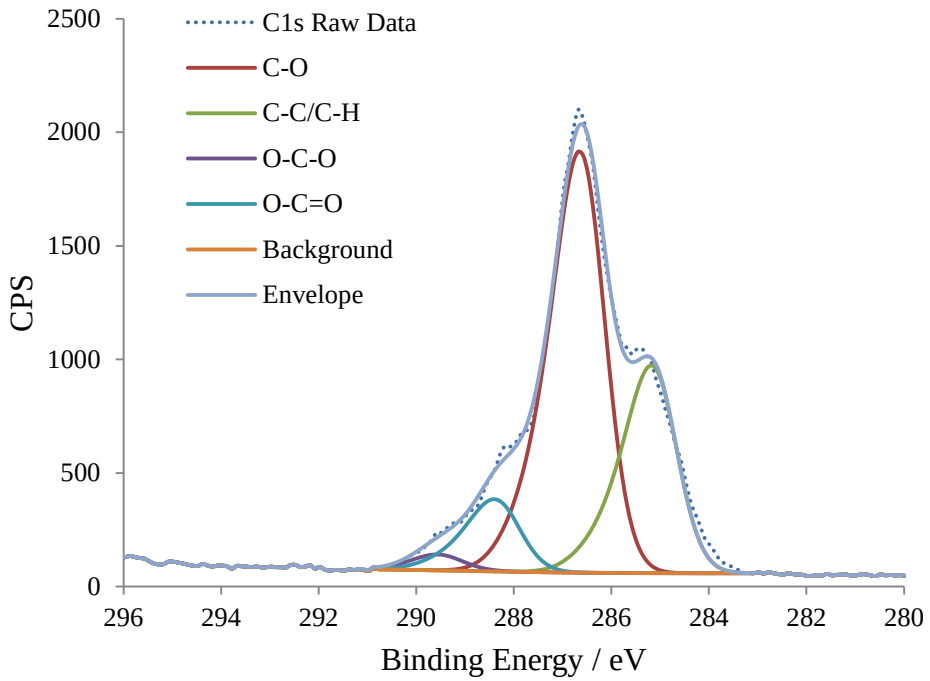


Figure 10.4.11 C1s high resolution scan of 3-((3-trimethoxysilyl)propyl)thio) propanoate

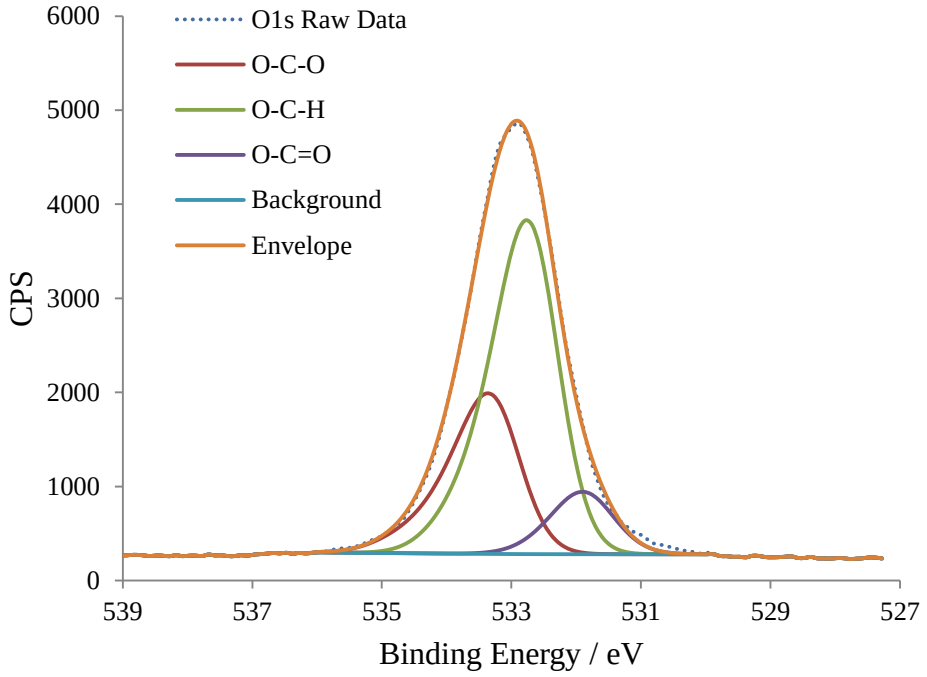


Figure 10.4.12 O1s high resolution scan of 3-((3-trimethoxysilyl)propyl)thio) propanoate

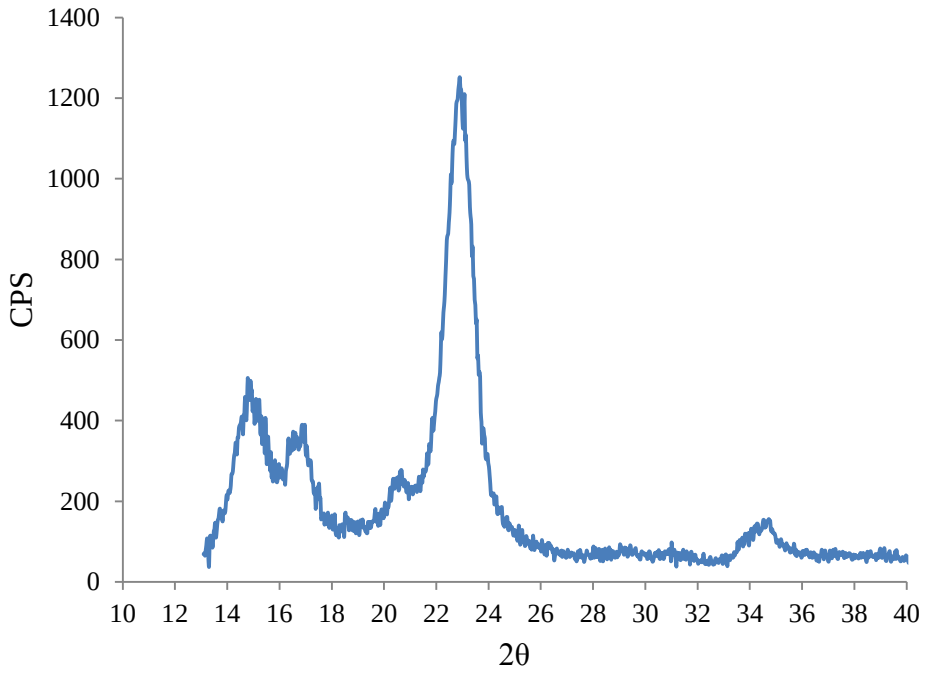


Figure 10.4.13 X-ray diffractogram of cellulose 3-((2-mercaptoethyl)thio) propanoate

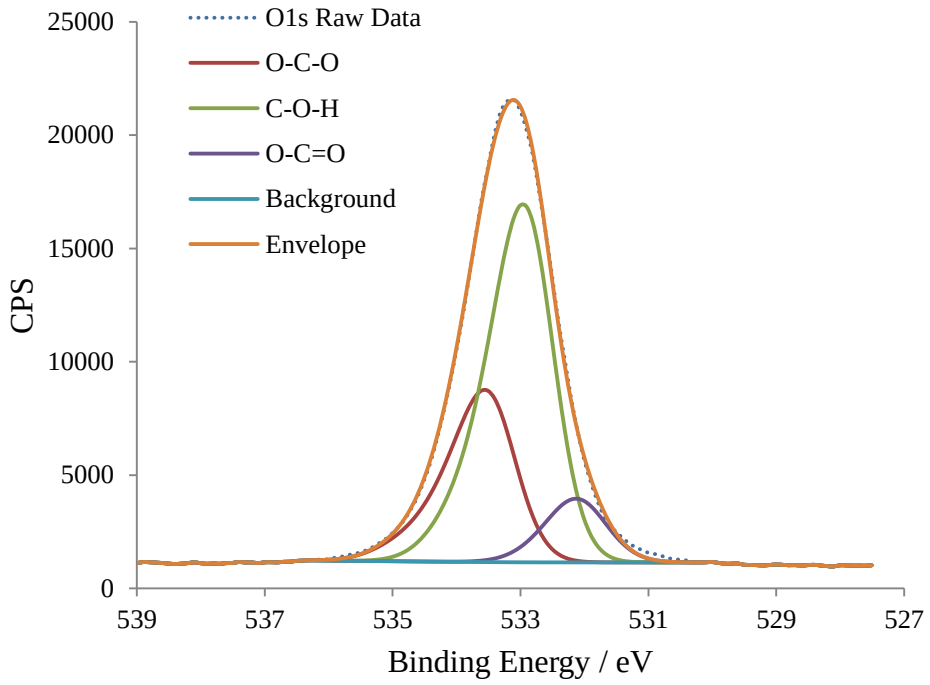


Figure 10.4.14 O1s high resolution spectrum of cellulose 3-((2-mercaptoethyl)thio) propanoate

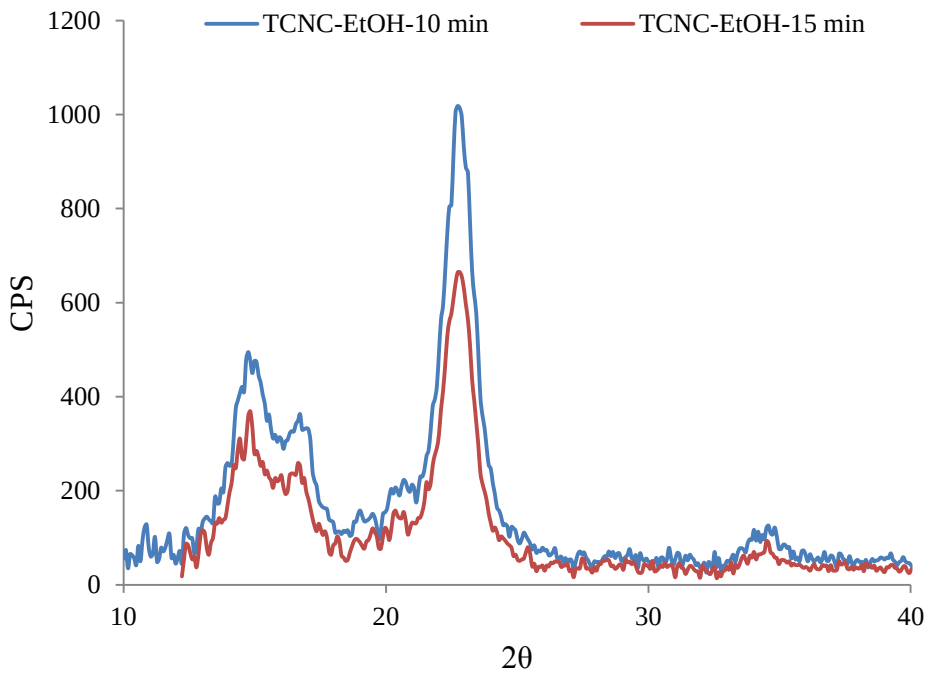


Figure 10.4.15 X-ray diffractogram of cellulose 3-((2-aminoethyl)thio) propanoate hydrochloride synthesised in EtOH for 10 and 15 minutes

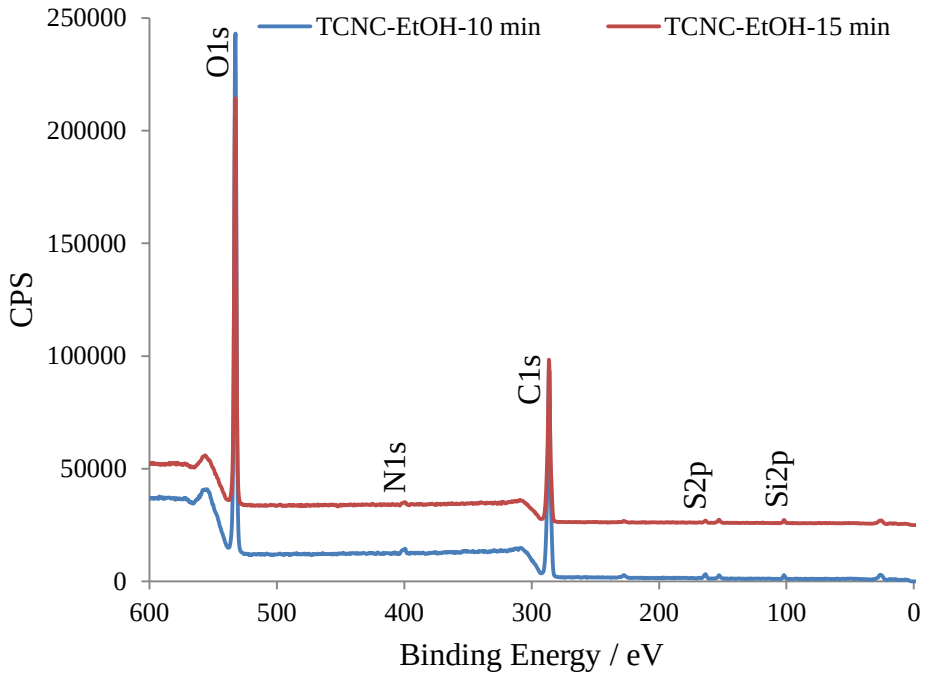


Figure 10.4.16 XPS wide scan of cellulose 3-((2-aminoethyl)thio) propanoate hydrochloride synthesised in EtOH for 10 and 15 minutes

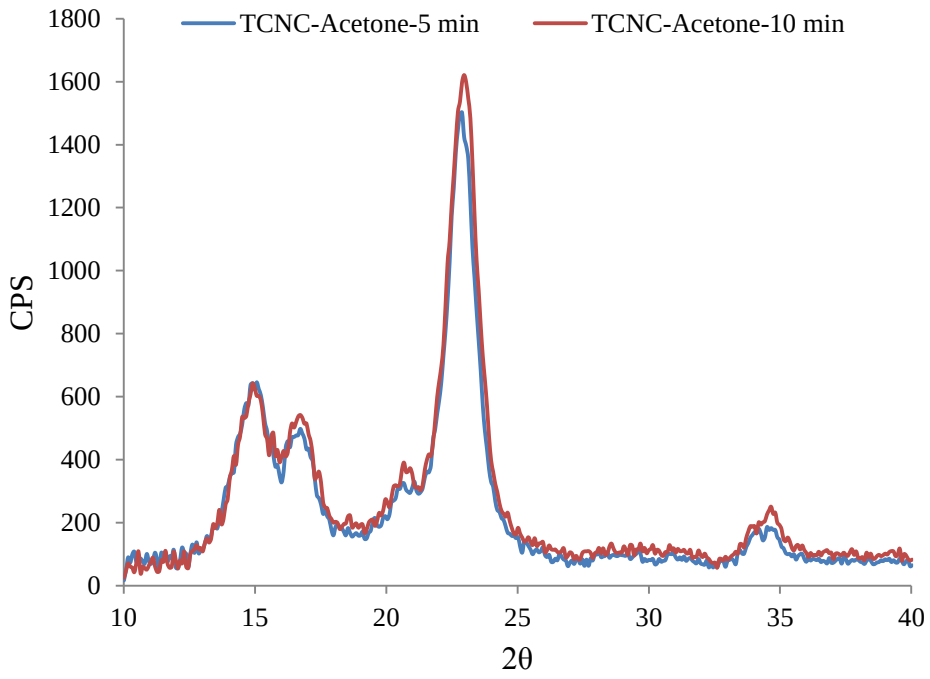


Figure 10.4.17 X-ray diffractogram of cellulose 3-((2-aminoethyl)thio) propanoate synthesised in acetone for 5 and 10 minutes

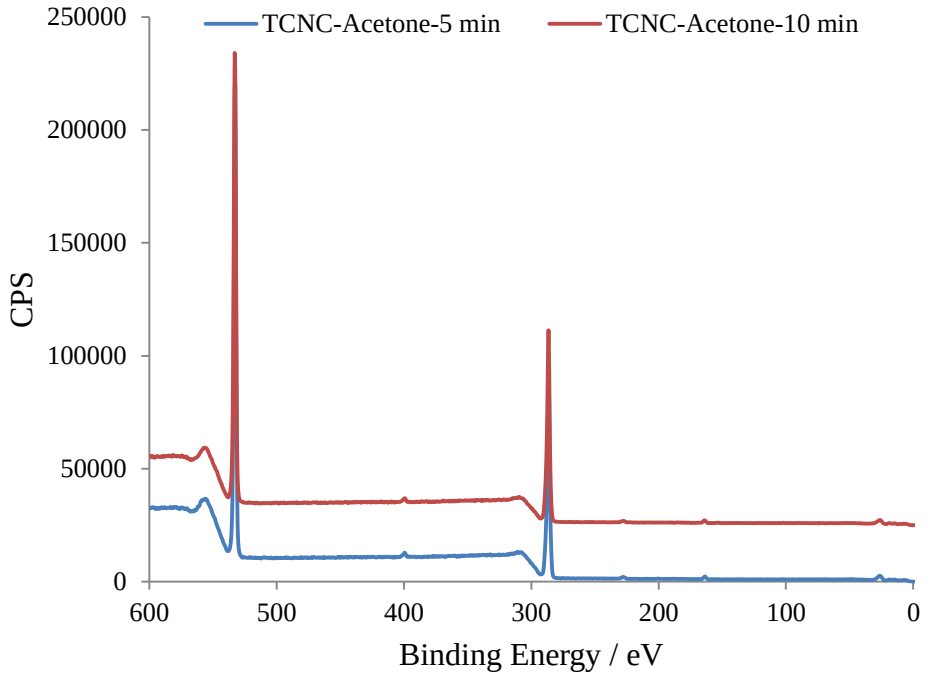


Figure 10.4.18 XPS wide scan of cellulose 3-((2-aminoethyl)thio) propanoate synthesised in acetone for 5 and 10 minutes

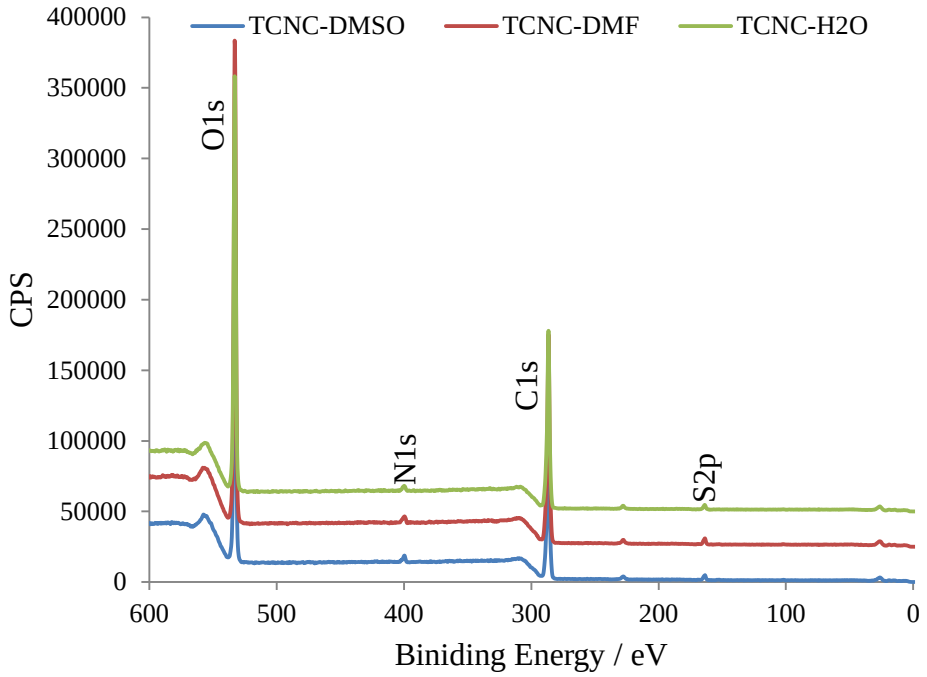


Figure 10.4.19 XPS wide scan of cellulose 3-((2-aminoethyl)thio) propanoate synthesised in DMSO/DMF/H_2O

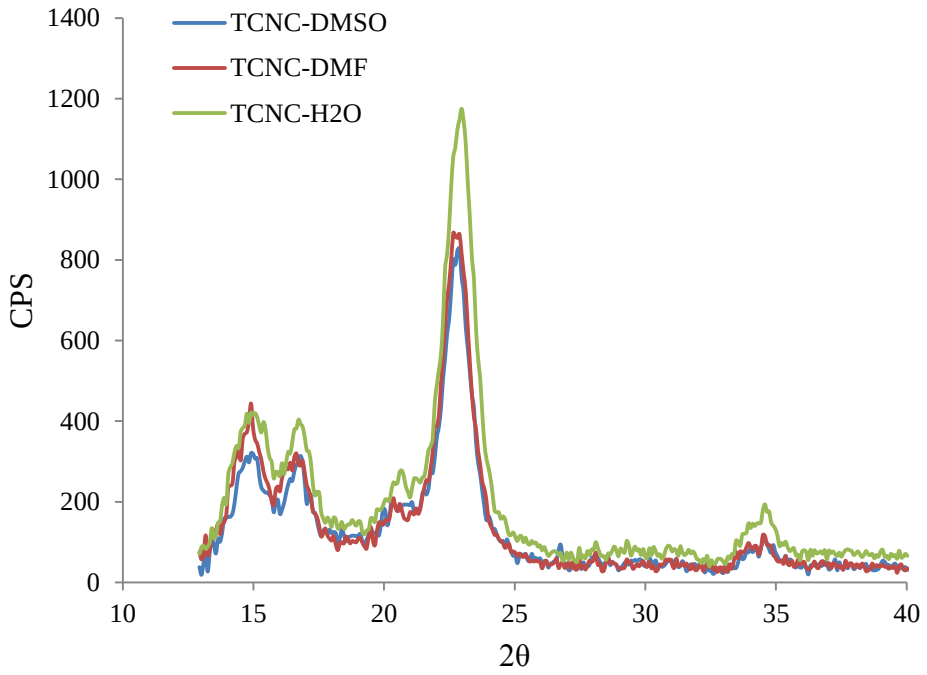


Figure 10.4.20 X-ray diffraction pattern of cellulose 3-((2-aminoethyl)thio propanoate synthesised in DMSO/DMF/H_2O

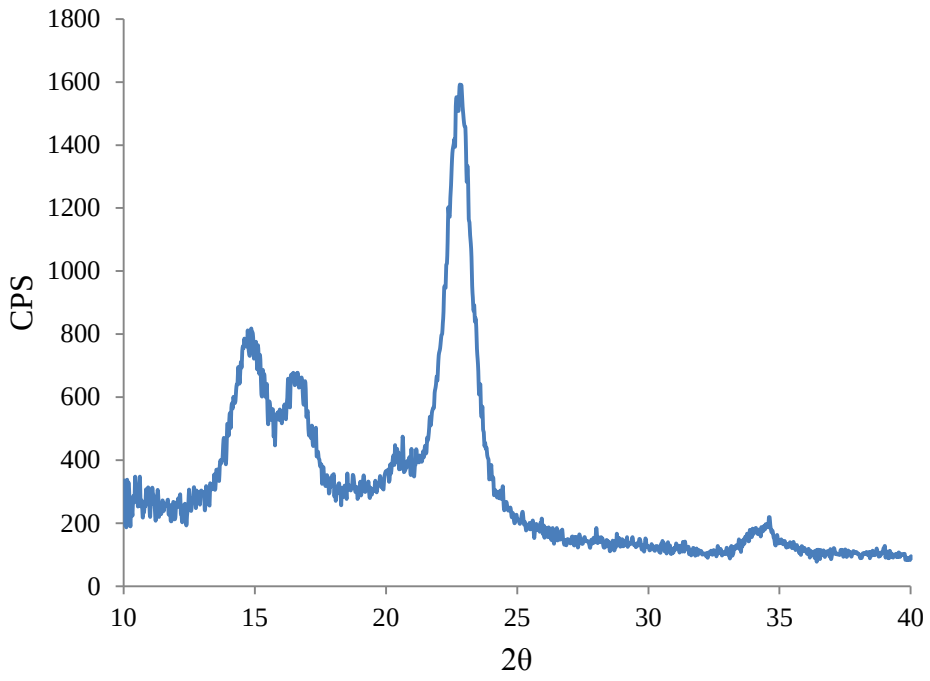


Figure 10.4.21 X-ray diffractogram of cellulose 3-((2-aminoethyl)thio) propanoate synthesised in DCM for 2 hours

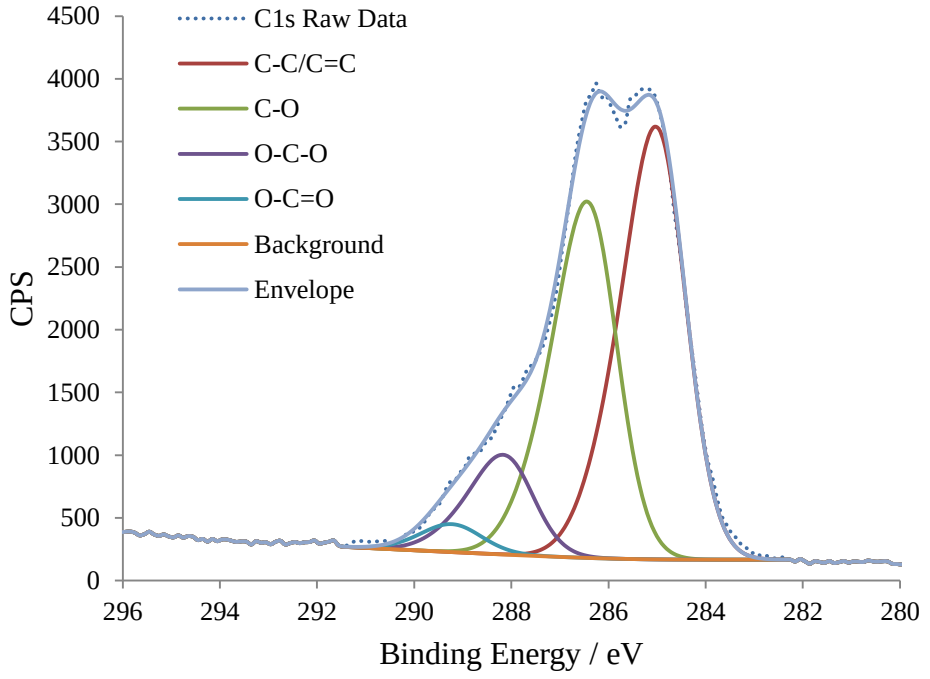


Figure 10.4.22 C1s high resolution spectrum of cellulose 3-((2-aminoethyl)thio) propanoate synthesised in DCM for 2 hours

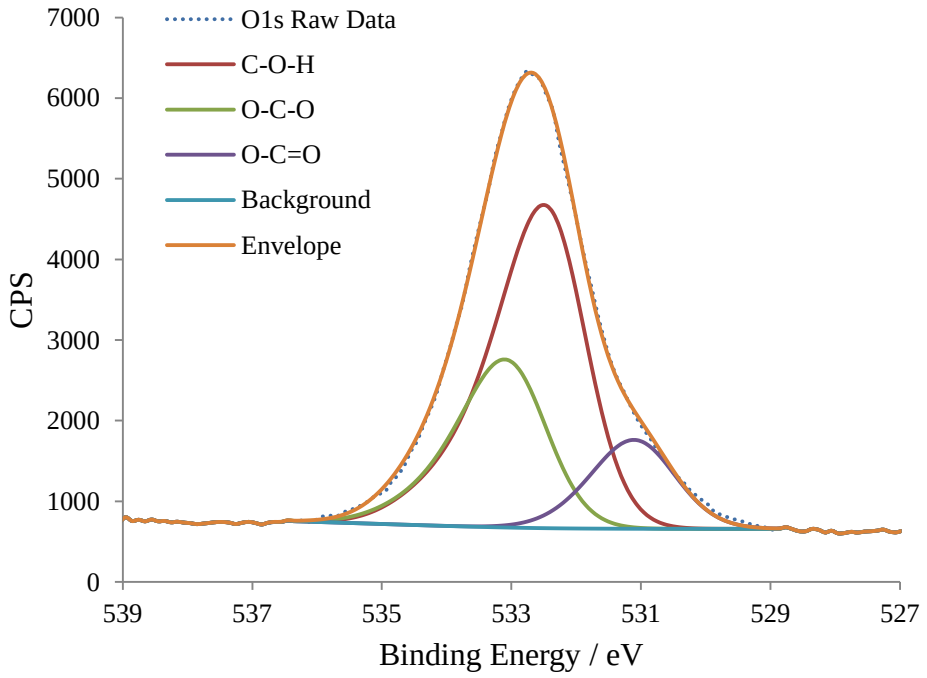


Figure 10.4.23 O1s high resolution spectrum of cellulose 3-((2-aminoethyl)thio) propanoate synthesised in DCM for 2 hours

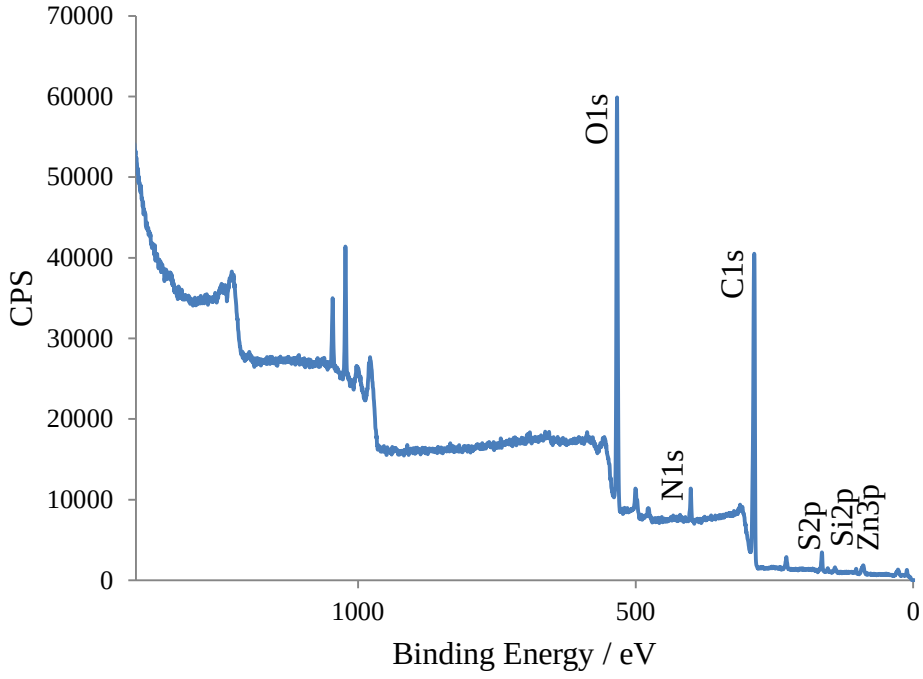


Figure 10.4.24 XPS wide scan of switchable cellulose nanoparticles, Switch-CNC

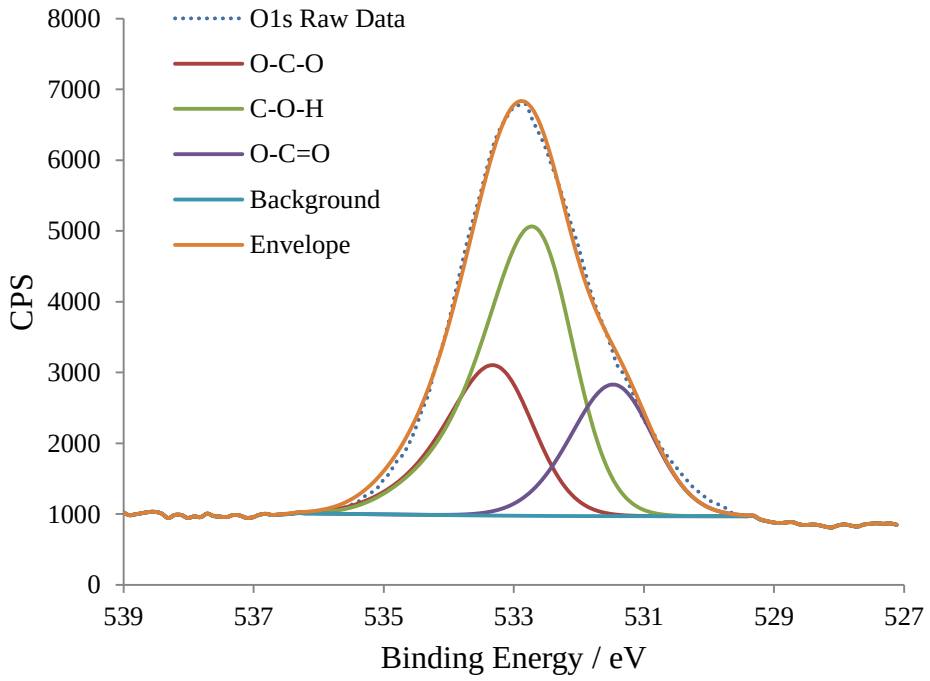


Figure 10.4.25 O1s high resolution XPS spectrum of switchable cellulose nanoparticles, Switch-CNC

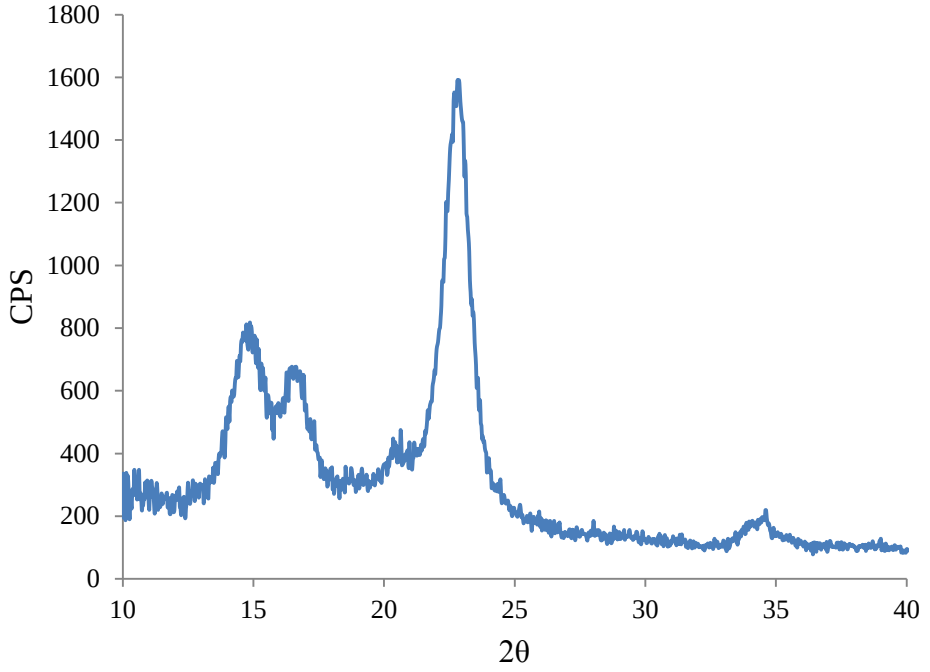


Figure 10.4.26 X-ray diffraction of Switch-CNC, 3-(2-(*N*,*N*-dimethylacet-imideamide)ethyl)thio) propanoate cellulose nanoparticles